

MODEL PATHWAYS IN LIGNIN THERMOLYSIS

by

Michael Tully Klein

BScE , University of Delaware  
(1977)

SUBMITTED IN PARTIAL FULFILLMENT  
OF THE REQUIREMENTS FOR THE  
DEGREE OF

DOCTOR OF SCIENCE

at the

MASSACHUSETTS INSTITUTE OF TECHNOLOGY

January 1981

© Massachusetts Institute of Technology 1981

Signature of Author \_\_\_\_\_  
Department of Chemical Engineering  
January 1981

Certified by \_\_\_\_\_  
Preetinder S. Virk  
Thesis Supervisor

Accepted by \_\_\_\_\_  
Glenn C. Williams, Chairman  
Departmental Committee on Graduate Theses

ARCHIVES  
MASSACHUSETTS INSTITUTE  
OF TECHNOLOGY

AUG 20 1981

LIBRARIES

# MODEL PATHWAYS IN LIGNIN THERMOLYSIS

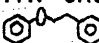
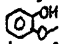

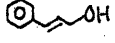
by

MICHAEL TULLY KLEIN

Submitted to the Department of Chemical Engineering  
on February 3, 1981 in partial fulfillment of the  
requirements for the Degree of Doctor of Science

## ABSTRACT

A fundamental description of lignin thermolysis was attempted.

Analysis of the chemical topology of lignin suggested likely reaction pathways of import to lignin pyrolysis. In turn, 20 model compound pyrolysis substrates were selected to mimic the important reactive functional groups present in whole-lignin thermolysis. The more salient models were: phenethyl phenyl ether (PPE) , which depicts the most prevalent lignin interunit linkage, guaiacol , model of the predominant aromatic methoxyl, and saligenol  and cinnamyl alcohol , models of important propanoid side chains.

Detailed pathway and kinetic analyses and determination of reaction Arrhenius parameters provided mechanistic insights into the model compound pyrolyses. Several pericyclic reaction mechanisms, hitherto not mentioned in the lignin pyrolysis literature, were suggested. In particular, PPE likely pyrolyses via a concerted retro-ene mechanism, whereas guaiacol and saligenol may respectively eliminate methane and water by concerted group transfers.

A statistical interpretation of the lignin substrate coupled with the experimental model compound pyrolyses allowed simulation of whole-lignin thermolysis. The simulations were in substantial agreement with experimental pyrolyses reported in the literature in regard to overall gas, methane, carbon monoxide, individual phenols, and carbonaceous residue yields. Weight loss kinetics deduced from the time dependency of the latter yield also accorded well with the experimental literature.

Thesis Supervisor: Dr. Preetinder S. Virk

Title: Associate Professor of Chemical Engineering

Department of Chemical Engineering  
Massachusetts Institute of Technology  
Cambridge, Massachusetts 02139

Professor Jack P. Ruina  
Secretary of the Faculty  
Massachusetts Institute of Technology  
Cambridge, Massachusetts 02139

Dear Professor Ruina:

In accordance with the regulations of the Faculty, I herewith submit a thesis entitled "Model Pathways in Lignin Thermolysis" in partial fulfillment of the requirements for the degree of Doctor of Science in Chemical Engineering at the Massachusetts Institute of Technology.

Respectfully submitted,

*Michael Tully Klein*

Michael Tully Klein

## Acknowledgements

It is with sincere gratitude that I acknowledge the efforts of my thesis supervisor, Preetinder S. Virk. I am indebted for his patience, dedication, and demanding rigor, although the latter was often cursed throughout my tenure at MIT. More than guidance to successful completion of this thesis, I am particularly grateful for exposure to an overall approach to science and engineering.

With pleasure I acknowledge my colleague, friend and general sounding board, Mary Jane Garry, who really did have that one good idea.

Acknowledgements to Ka Cheung Yu and Regina Murphy for their efforts in closely related work.

I would like to thank Professors J.P.Longwell and C.G.Vayenas and Dr. W.A. Peters for valuable discussions.

Among the personal friends who have directly or indirectly contributed to this effort are John Nenniger, Gina Shuck, Glenn and Karen Hong, Tom Hastings and Mark Zacharias.

My final gratitudes are reserved for family, particularly my wife, Bitsy. Her love and understanding provided inspiration throughout both the good and bad. I am indebted to my parents for overall support, direction and freedom. My brothers and sisters are gratefully acknowledged for support. A true bonus in my marriage to Bitsy was the accompanying set of in-laws. An eternal debt to 'both' families for their help in the preparation of this thesis. Special acknowledgements to my mother-in-law, Ellen Thompson, for incredible efforts in typing and literally assembling this thesis.

The author gratefully acknowledges financial support from the MIT Energy Lab and the US DOE.

## TABLE OF CONTENTS

	Page
List of Figures	7
List of Tables	10
1.0 Summary	11
1.1 Introduction.....	11
1.2 Motivation.....	11
1.3 Lignin.....	12
1.4 Previous Pyrolyses.....	15
1.4.1 Previous Lignin Pyrolyses.....	15
1.4.2 Previous Model Compound Pyrolyses.....	18
1.4.3 Limitations of Previous Work.....	20
1.5 Present Approach.....	21
1.5.1 Analysis of Lignin Structure.....	21
1.5.2 Selection of Model Compounds.....	23
1.5.3 Simulation of Lignin Thermolysis.....	24
1.6 Experimental Methods.....	27
1.7 Experimental Results.....	29
1.7.1 Phenethyl Phenyl Ether(PPE) Pyrolysis.....	29
1.7.2 Summary of Experimental Results.....	37
1.8 Implications of Experimental Results.....	44
1.9 Simulated Lignin Thermolysis.....	46
1.10 Discussion.....	51
1.10.1 The Mechanism of PPE Pyrolysis.....	51
1.10.2 Comparison Between Simulated and Experimental Lignin Pyrolyses.....	56
1.11 Summary and Conclusions.....	64
2.0 Introduction.....	67
3.0 Lignin.....	72
3.1 Lignin Chemistry.....	73
3.2 The Isolation of Lignin.....	97
3.3 Relationship Between Lignin and Coal.....	119
4.0 Previous Pyrolyses.....	133
4.1 Previous Lignin Pyrolyses.....	134
4.2 DTA and Other Thermal Treatments.....	159
4.3 Effects of Additives on Lignin Pyrolysis.....	166
4.4 Brief Comparison With Coal Pyrolyses.....	173
4.5 Previous Model Compound Pyrolyses.....	174

5.0	Present Approach .....	209
5.1	Limitations of Previous Lignin Investigations.....	209
5.2	Analysis of Lignin Structure.....	213
5.3	Formal Pathways in Lignin Thermolysis: Selection of Model Compounds.....	223
5.4	Simulation of Lignin Thermolysis.....	235
6.0	Experimental Methods.....	250
6.1	Chemicals Used.....	250
6.2	Apparatus.....	254
6.3	Chemical Analysis.....	257
7.0	Experimental Results.....	261
8.0	Implications and Applications of Experimental Results to Lignin Thermolyses.....	411
8.1	Implications to Lignin Moieties and Functional Groups: Pathway Interrelationships.....	411
8.2	Whole-Lignin Considerations.....	431
8.3	Simulation.....	436
8.4	Simulation Rate Constants.....	455
8.5	Differential Equations.....	467
9.0	Simulation Results.....	470
10.0	Discussion.....	490
10.1	Model Compound Pyrolyses.....	490
10.2	Simulation Predictions.....	578
10.3	Optimization and Modification Strategies.....	612
11.0	Conclusions.....	620
12.0	Suggestions for Future Research.....	625
13.0	References.....	631
14.0	Appendices.....	641
15.0	Nomenclature.....	824

## LIST OF FIGURES

Figure No.		Page
3.1	Production of aromatics from carbohydrates via the shikimic acid pathway	75
3.2	Production of esters of lignin cinnamic acids	76
3.3	Resonance forms of coniferyl alcohol radical	78
3.4	Typical lignification lignols	80
3.5	Freudenberg lignin structural model	83
3.6	Completion of Freudenberg structure as used in the present investigation	88
3.7	Distribution of lignin methoxyphenols as found in the Freudenberg model	90
3.8	Distribution of 3-carbon side chains as found in the Freudenberg model	92
3.9	Matrix of dilignols arising from coupling of coniferyl alcohol radical forms R <sub>A</sub> -R <sub>D</sub>	94
3.10	Typical Sulfate pulping reaction as presented by Rydholm	109
3.11	Structural model for typical Kraft lignin	112
3.12	Structural models for Sulfite lignins	116
3.13	Ternary diagram due to Stephens	126
3.14	Coal structural schematics due to Wender	128
3.15	Hill and Lyon structural model for coal	130
3.16	Coal model due to Given	131
4.1	Schematic of overall lignin pyrolysis product spectrum	135
4.2	Schematic coke structure of Gillet & Urlings	158
5.1	Aromatic unit grid: Freudenberg structure	218
5.2	Aromatic unit grid: Present approach	221
5.3	Simulation kinetic approach	242
6.1	PPE NMR Trace	253
6.2	Schematic of experimental tubing bomb reactor	256
6.3	Schematic of experimental procedures	258
7.1	Experimental Strategy for Model Compound Pyrolyses	262
7.1.1	Major products from neat PPE pyrolysis	268
7.1.2	Product relationships in neat PPE pyrolysis	270
7.1.3	PPE pyrolysis kinetics at 400 C	272
7.1.4	Variation of k <sub>1</sub> PPE with initial PPE concentration	273
7.1.5	Arrhenius diagram for PPE pyrolysis	275
7.1.6	Product relationships in PPE pyrolysis, T=400 C	277
7.1.7	Major products from PPE pyrolysis in tetralin at 400 C; C <sub>E</sub> =0.25, S=1.48	280

LIST OF FIGURES (cont.)

Figure No.		Page
7.1.8	Product relationships as function of substrate conversion for PPE pyrolysis in tetralin at 400 C	282
7.1.9	PPE pyrolysis kinetics, in tetralin	283
7.2.1	Guaiacol pyrolysis product evolution	286
7.2.2a-c	Product relationships in guaiacol pyrolysis	287
7.2.3	Guaiacol pyrolysis kinetics at 350 C	292
7.2.4	Catechol appearance at 350 C	294
7.2.5	Arrhenius diagram for guaiacol pyrolysis	295
7.3.1	Arrhenius diagram for methoxyphenol pyrolysis	299
7.4.1	Anisole pyrolysis product evolution	300
7.4.2a-c	Product relationships in Anisole pyrolysis	302
7.4.3a-c	Anisole pyrolysis kinetics at 450 C	306
7.4.4	Arrhenius diagram for Anisole pyrolysis	309
7.5.1a-c	Veratrole pyrolysis product spectra	311
7.5.2	Product relationships in veratrole pyrolysis	314
7.5.3	Arrhenius diagram for veratrole pyrolysis	317
7.5.4	Comparison of 'model' and experimental veratrole pyrolysis	319
7.6.1	Saligenol pyrolysis kinetics	321
7.6.2	Product relationships in saligenol pyrolysis	322
7.7.1	Benzaldehyde pyrolysis product evolution, T=400 C	324
7.7.2	Product relationships in benzaldehyde pyrolysis	325
7.7.3	Benzaldehyde pyrolysis kinetics at 400 C	327
7.7.4	Arrhenius diagram for benzaldehyde pyrolysis	328
7.8.1	Vanillin pyrolysis product evolution	330
7.8.2	Product relationships in vanillin pyrolysis	331
7.8.3	Arrhenius diagram for vanillin pyrolysis	333
7.9.1	Acetophenone pyrolysis product evolution	334
7.9.2	Product relationships in acetophenone pyrolysis	336
7.9.3a-c	Acetophenone kinetics at T=550 C	337
7.9.4	Arrhenius diagram for acetophenone pyrolysis	341
7.10.1	Cinnamaldehyde pyrolysis product evolution	343
7.10.2a-b	Product relationships in cinnamaldehyde pyrolysis	344
7.10.3a-b	Global cinnamaldehyde pyrolysis kinetics	347
7.10.4a-c	Variation of product mol fraction with initial cinnamaldehyde concentration	350
7.10.5	Arrhenius diagram for cinnamaldehyde pyrolysis	353
7.10.6	Arrhenius diagram for carbonyl R1 pathways, all carbonyls	355
7.11.1a-e	Cinnamyl alcohol pyrolysis product spectra	357
7.11.2	Arrhenius diagram for cinnamyl alcohol pyrolysis	365
7.12.1a-d	OHD pyrolysis product evolution	367
7.12.2	Product relationships in OHD pyrolysis	372



## LIST OF FIGURES (cont.)

Figure No.		Page
7.12.3	Arrhenius diagram for OHD pyrolysis	373
7.13.1a-d	Phenyl ether pyrolysis product spectra	375
7.13.2	Product relationships in phenyl ether pyrolysis	379
7.13.3	Arrhenius diagram for phenyl ether pyrolysis	381
7.14.1	Benzene appearance from biphenyl pyrolysis at T=587 C	383
7.16.1a-c	Product evolution from cinnamic acid pyrolysis	384
7.16.2a-b	Product relationships in cinnamic acid pyrolysis	388
7.16.3	Arrhenius diagram for cinnamic acid pyrolysis	390
7.17.1a-d	CO <sub>2</sub> evolution in ferulic acid pyrolysis	392
7.17.2	Arrhenius diagram for carboxylic acid pyrolyses	396
7.18.1a-c	CO <sub>2</sub> evolution from 1- and 2- naphthonic acids	398
8.1	Model pathway for lignin pyrolysis	433
8.2	3-carbon side chain reactions as in simulation	438
8.3	Comprehensive methoxyphenol reaction network	448
8.4	Simplified methoxyphenol reaction network	452
8.5	Simulation differential equations	468
9.1a-c	Model predictions	471
9.2	Comparison of simulation weight loss predictions with the experimental data of Iatridis and Gavalas	488
10.1.1	Guaiacol pyrolysis pathways	504
10.1.2	Overall veratrole reaction network	520

## LIST OF TABLES

Table No.		Page
1.7.1	Summary of Reaction Pathways and Kinetic Parameters	30
1.7.2	Styrene Pyrolysis Kinetics	35
3.1	Analytical data for Conifer lignin	86
3.2	Wood pulping processes	105
3.3	Lignin related coal residues	122
3.4	Lignin related coal residues	124
4.1	Representative products from lignin pyrolysis	136
4.2	Lignin pyrolysis product spectra of Iatridis and Gavalas	139
4.3	Products from wood pyrolysis	143
4.4	Components of lignin thermolysis tar	147
4.5	Phenols reported from lignin thermolysis	150
4.6	Phenols from lignin pyrolysis	152
4.7	DTA data of Domburg, et al.	161
4.8	DTG data of Domburg and Sergeeva	163
4.9	Lignin pyrolysis with additives	168
4.10	Previous Model Compound Pyrolyses	175
4.11	Products from $\beta$ -ether pyrolysis	180
5.1	Model compounds to be pyrolysed	224
6.1	Experimental grid for model compound pyrolyses	251
7.1.1	Representative product spectra from PPE pyrolysis	267
8.1a-b	Simulation rate constants	456
10.1.1	Summary of thermochemical parameters for model pathways	565
10.1.2	Thermochemical parameters for model molecular species	568
10.2.1	Literature references relevant for comparison with simulation predictions	580
10.2.2	Quantitative simulation-literature comparison grid	584

## 1. Summary

### 1.1 Introduction

This thesis attempts a fundamental description of lignin thermolysis. A series of 20 different lignin model compounds were pyrolysed in the experimental portion of this work. A mathematical lignin thermolysis model was developed, based on both the experimental model pathways and a theoretical interpretation of lignin structure.

The investigation comprised three major components. First a critical examination of lignin and lignin chemistry was undertaken, aimed at discerning likely thermolysis reaction pathways. On the basis of this theoretical analysis, model compounds mimicking the essential reactive units of the whole-lignin substrate were selected and pyrolysed. The reaction pathways suggested by the model compound pyrolyses were then coupled with the structural analysis of whole-lignin to formulate a mathematical simulation model for whole-lignin thermolysis. Hence, the experimental model compound results were coupled with the theoretical analysis in an effort to describe the essential features of whole-lignin thermolysis.

### 1.2 Motivation

The increased utilization of biomass and coal resource bases must be accompanied by an enhanced understanding of the fundamental events effecting their thermal processing. The elucidation of these fundamentals should greatly assist in the selection of catalysts, solvents, and process operating conditions for optimal substrate conversion, as well as provide insight into the expected results of operating in regions devoid of experimental details. The objective of this investigation is an elucidation of the important reaction pathways and mechanisms involved in lignin pyrolysis, with an aim toward providing a rationalization and prediction

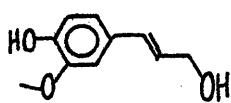
of observed lignin pyrolysis products and kinetics.

Lignin is a major component of biomass, accounting for up to about 36% of wood by weight. The U. S. coal reserve is composed of predominantly lignite, subbituminous, and bituminous coals, the respective percentages being 28%, 27%, and 43%.<sup>2</sup> In view of the evolutionary linkage of lignin to low rank coal, the high percentage of low rank bituminous and lignitic coals suggests that lignin thermolysis may be relevant to many aspects of coal pyrolysis.

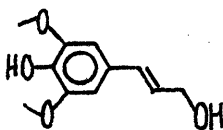
Both coal and lignin are ill-defined refractory substrates which lack unequivocal chemical structures. Their pyrolyses yield complex and poorly characterized product spectra. Thus, the reaction pathways and mechanisms involved in the pyrolyses of these complex substrates have remained obscure. This motivated the use of model compounds, where the products from pyrolysis of a well defined substrate may be used to infer reaction pathways, kinetics, and mechanisms.

### 1.3 Lignin

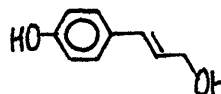
Pure lignin is a natural phenolic polymer composed of carbon, hydrogen, and oxygen. The ultimate lignin precursors are carbon dioxide and water, biosynthetic fixation of which<sup>4</sup> produces coumaryl, coniferyl, and sinapyl alcohols, shown below. These three alcohols are the sole



CONIFERYL



SINAPYL



COUMARYL

monomeric precursors to lignin, with coniferyl alcohol predominant.

Natural lignification can be artificially duplicated by the enzymatic, oxidative dehydrogenation of coniferyl alcohol, which eventually yields an amorphous polymer very similar to conifer lignin. The mechanisms

and pathways of lignin growth have been ascertained by the isolation of intermediates, termed lignols, of this process. According to Freudenberg<sup>4</sup>, the classic reference on the subject, lignification proceeds thus.

Under the action of enzymes like laccase, the phenolate anion of coniferyl alcohol is converted to a phenoxy radical. This radical enjoys a half life of about 45 seconds<sup>5</sup>, being stabilized by resonance as depicted in Figure 3.3. The major lignification growth mechanism is the coupling of these free-radical species, the most important coupling mode being the combination of an  $R_a$  and  $R_b$  radical. This is shown in Figure 3.4. The resulting quinonmethide (IV) will generally add water in a nucleophilic manner to yield the guaiacyl-glycerol- $\beta$ -coniferyl ether (V). This  $\beta$ -ether is the most prevalent link in the lignin macromolecule. However, the nucleophilic component of this reaction can be varied considerably. For example, guaiacyl-glycerol- $\alpha,\beta$ -diconiferyl diether (VI) represents the addition of coniferyl alcohol to the quinonemethide. Plant sugars and polysaccharides also compete for addition to the quinonemethide, representing the main pathway for formation of lignin-carbohydrate covalent bonds. Similar coupling reactions of each radical form  $R_a$ - $R_d$ , as well as coupling of the higher lignols, accounts for the molecular weight increase attending lignification.

Of direct importance to this investigation is a representation of the types and proportions of the moieties and bonds which constitute lignin. This information is conveyed in the classic schematic structural representation of Freudenberg<sup>4</sup>, shown in Figure 3.5. This formula is not to be interpreted as a literal, unequivocal chemical structure for lignin, but rather as a schematic depiction of the structural insights gleaned from experiment. Harkin<sup>5</sup> draws an analogy between lignin and playing cards,

emphasizing the existence of a broad statistical distribution of well known but also well shuffled chemical structures that cannot possibly be represented in one formula. Only in the limit of infinite statistical sampling, or infinite schematic formula size can lignin structure truly be realized. This emphasizes the importance of bond and moiety types and their frequency distributions in lignin description. Note, for example, that the linkages between units 1-4, 4-5, 5-6, 7-8, 10-11, 12-15, and 15-16 in Figure 3.5 are all of the  $\beta$ -ether type. This is clearly the single most predominant interunit linkage.

For the present purposes the best characterization of Freudenberg's structure was effected in terms of the phenolic units and the propanoid side chains of each monomer. Figure 3.7 schematically represents the types of methoxyphenol units in Figure 3.5. The three monomer alcohols are divided into two types, those with etherified hydroxyls and those with free phenolic hydroxyls. The former category is further subdivided according to ether type. Because of the large percentage of coniferyl alcohol monomer incorporated into the lignin macromolecule, guaiacols, either free or  $\beta$ -etherified, account for the largest proportion of the methoxyphenol units in a spruce lignin. The propanoid side chains occurring in Figure 3.5 are shown in Figure 3.8. Despite the apparent complexity of the Freudenberg structure, there exist but eight side chain types. The most prevalent of these is the  $\beta$ -etherified guaiacyl-glycerol moiety, which occurs, e.g., as the side chain to unit 6. The mechanisms of lignification suggest that while the side chain of one aromatic unit may be involved in a lignin linkage with the guaiacyl moiety of another monomeric unit, it cannot be involved in bonding with its own guaiacyl moiety. With regard to the Freudenberg structure, this point implies that the side chain shown for

unit 6, for example, might be associated with any of the methoxyphenol moieties shown for units 6, 7, 8, and 3, in proportions related to the probabilities of the given methoxyphenol and side chain unit derived from Figures 3.7 and 3.8.

#### 1.4 Previous Work

A major goal of the present work was elucidation of the fundamental reaction pathways involved in lignin pyrolysis. This section will consider previous pyrolyses of lignin and lignin model compounds.

##### 1.4.1 Previous Lignin Pyrolyses

Figure 4.1 is a summary of major lignin pyrolysis products and Table 4.1 is a representative listing of the major pyrolysis products reported in the literature.

Gases  
As illustrated in Table 4.1, total gas yields average 15% by weight of lignin pyrolysed, the major product gases being  $\text{CH}_4$ ,  $\text{CO}$ ,  $\text{CO}_2$ , and ethane. Heuser and Skioldebrand<sup>23</sup> obtained a gas consisting of 50.9%  $\text{CO}$ , 37.5%  $\text{CH}_4$ , 9.6%  $\text{CO}_2$ , and 2% ethane from pyrolysis of an HCl spruce lignin, while Gladkova, et al.<sup>25</sup>, reported 25%  $\text{CO}$ , 48%  $\text{CH}_4$ , and 11%  $\text{CO}_2$  in the product gas from pyrolysis of a hydrolysis hardwood lignin. In both cases the high contents of  $\text{CO}$  and  $\text{CH}_4$ , and the rather low content of  $\text{CO}_2$ , are noteworthy. Iatridis and Gavalas<sup>26</sup> pyrolysed a Douglas fir Kraft lignin; the major gaseous products were  $\text{CH}_4$ ,  $\text{CO}$ , and  $\text{CO}_2$ , with minor amounts of other hydrocarbon gases also. The ratio  $\text{CO}/\text{CH}_4$  exhibited an interesting variation with temperature. At 400 C,  $\text{CO}/\text{CH}_4$  was approximately 2.3 while at 500 C this ratio dropped to roughly 0.85, and finally at 550 through 650 C the ratio climbed to values approaching 2. The relatively large  $\text{CO}_2$  content, typically 6%, observed by these authors is inconsistent with previous literature citations, and likely arose from modification of

their lignin during Kraft pulping.

#### Aqueous Distillate Products

Aqueous distillate yields from pyrolysis amount to roughly 20% by weight of the lignin charged. Its main constituents are water, methanol, acetic acid and acetone.

Methanol is formed in yields ranging from 0.3% to 3% of the lignin; this corresponds to about 10% of the lignin methoxyl content.<sup>19</sup> Klason<sup>24</sup> pyrolysed wood from birch, beech, pine and spruce and found the yield of methanol from the former two hardwoods twice as high as that from the latter two softwoods. Other observations<sup>23,31</sup> also show that hardwood lignins yield more methanol than softwood lignins. Because hardwood lignins incorporate a larger proportion of dimethoxylated sinapyl alcohol monomer units than do softwoods, Allan and Matilla<sup>30</sup> have suggested that methanol originates from methoxyl moieties in lignin.

The acetic acid and acetone produced from lignin pyrolysis presumably originate in the three carbon phenylpropane unit. Allan and Matilla<sup>30</sup> report that the yields of acetic acid from hardwoods are significantly higher than those from softwoods. This is attributed to the hardwoods possessing a less condensed lignin polymer than the softwoods. In general, as seen in Table 4.1, acetone yields are considerably lower than those of acetic acid and methanol. The data of Iatridis and Gavalas<sup>26</sup> show significant yields of methanol and acetone, but do not include acetic acid.

Water is the major component of the aqueous distillate fraction; water yields of 10%-20% of the lignin are typical, as shown in Table 4.1. Extensive hydrogen bonding between hydroxyl groups and other oxygen moieties in lignin is likely responsible for the rather facile loss of



water during pyrolysis. However, the mechanistic aspects of water release are poorly understood. Also, interpretation of water yield data is complicated by the inevitable presence of physically bound water in lignin samples.

### Tars and Oils

The tar fraction resulting from lignin pyrolysis has received considerable attention due to the high proportion of valuable phenols in it. As seen in Table 4.1, the tar yield is typically 15%-20% by weight of the lignin. The lignin isolation method exerts a significant influence on tar yields<sup>34,39</sup>. Thus pyrolysis of alkali, HCl, and H<sub>2</sub>SO<sub>4</sub> lignins<sup>34</sup> yielded 17.7%, 7.5%, and 7.4% tar yields, respectively. In the rapid thermolysis of alkali, HCl, and H<sub>2</sub>SO<sub>4</sub> lignins<sup>39</sup>, the alkali lignin yielded the largest proportion of phenols; it was also noteworthy that lignins from different woods isolated by the same method were much more similar than lignins from the same wood isolated by different methods.

Table 4.5 is a representative listing of phenols identified in the tar product. The phenols detected mirror the constituent lignin monomers. Thus, guaiacol and catechol derivatives predominate, with sinapyl and coumaryl units in evidence as well. The singly oxygenated phenols likely arise from reactions of the guaiacyl and sinapyl moieties and also from degradation of coumaryl alcohol monomers. Phenol substitution is invariably in the para position, and often includes all three carbons of the original propanoid side chain.

### The Carbonaceous Residue

A carbonaceous residue is a prevalent lignin pyrolysis product. Chemical analysis of this product has rarely been effected, though Gillet and Urlings<sup>48</sup> found that coke from a Brauns and from an ethanolysis lignin

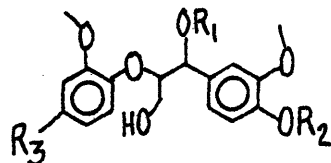
each had an elemental composition similar to that of a Rhenish lignite. Their elemental formula of  $(C_{40}H_{30}O_{11})_2$  is represented in Figure 4.2 by their speculative coke structure.

#### 1.4.2 Previous Model Compound Pyrolyses

Previous model compound studies may be organized into three groups: the lignin interunit linkages, the methoxyphenols, and the 3-carbon side chain units.

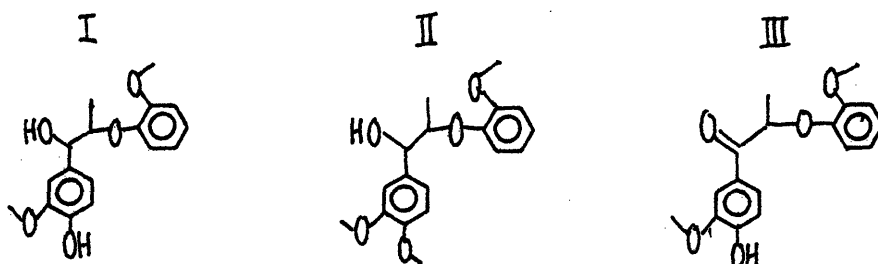
##### Lignin Interunit Linkages

The most prevalent lignin interunit linkage is the  $\beta$ -ether linkage, which can be represented, in the lignin, as:



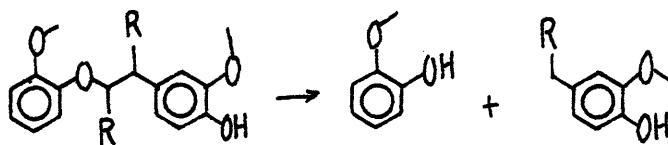
The thermal behavior of these  $\beta$ -ether linkages has been studied by two investigators<sup>75,76</sup>. Domburg<sup>75</sup> studied the substituted  $\beta$ -ethers I, II, and III.

The temperature for 50% weight loss for each of these were reported, from Differential Thermal Analysis (DTA) experiments conducted at 12C/min, as

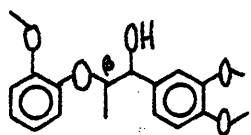


I(280 C)<II(310 C)<III(365 C). Activation energies of 16, 15, and 82 kcal/mol were also reported for I, II, and III respectively. The product spectra consisted of guaiacol, methyl-, ethyl-, and propyl-guaiacols, cis- and trans-isoeugenol, vanillin and acetovanillone, the latter two forming in much larger quantities from III than either I or II. The large predominance of guaiacol products appears indicative of a formal scission of the  $\beta$ -carbon

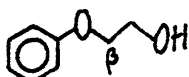
oxygen linkage:



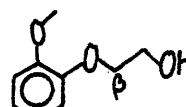
Savinykh<sup>76</sup> probed the effect of methoxyl and phenyl substituents on the thermal behavior of lignin  $\beta$ -ethers. They heated compounds II, IV and V to 500 C at a rate of 5C/min. The temperatures for 10% weight loss were



II



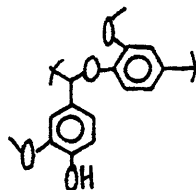
IV



V

II(300C)<<V(380C)<IV(400C). The most pronounced effect is that of veratryl substitution(cf V,II); compound II also differs from V in methyl substitution at the  $\beta$  carbon of II, but this is likely a minor factor in comparison with the veratryl substituent.

Another prevalent link in the lignin macromolecule is the  $\alpha$  aryl ether bond, as in:



The decomposition of  $\alpha$ -aryl alkyl ether bonds, as in benzyl phenyl ether (BPE), appears to be a rather facile process for the conditions of interest here<sup>79,80,81</sup>. A conversion of 31% at 320 C and 30 minutes holding time was reported<sup>79</sup>, with phenol, toluene, and benzylphenol as predominant products.

### Methoxyphenols

The aromatic methoxyl unit is a characteristic moiety of lignin. Pyrolyses of several related model compounds have been reported, including

guaiacol<sup>91,92,93,94</sup> and veratrole<sup>91,92</sup> which model free hydroxylic and etherified methoxyphenols, respectively. Pyrolyses have also been reported for anisole<sup>91,95,96,97,82</sup> and 2,6-dimethoxyphenol(DMP)<sup>91</sup>. In these previous pyrolyses of veratrole, anisole and guaiacol, demethylation, demethoxylation, and isomerization reactions have been found to occur. In the temperature range 400-600 C, demethylation seems modestly predominant for guaiacol and veratrole, but overwhelmingly predominant for anisole. However, the literature pyrolyses have been effected at rather high conversions, which permit significant secondary reactions and thus provide product spectra little indicative of reaction pathways.

#### Side Chain Units

Previous experiments relating to lignin side chain unit pyrolyses arise both from lignin-related and other experiments. In general, hydroxylic side chain units appear to undergo dehydration<sup>99,100,101</sup> and isomerization reactions<sup>100</sup>, with reactivity dependent upon the structure of the side chain and substituent groups. Carbonyl side chains are reported to undergo decarbonylation with evolution of CO; e.g., benzaldehyde yields CO and benzene at temperatures of 400-500C, by a mechanism quite likely molecular in nature.<sup>98,82</sup>

#### 1.4.3 Limitation of previous work

Previous lignin pyrolyses provide little fundamental insight into the mechanisms and pathways of degradation. This is due, in part, to the wide range of lignin types, lignin isolation methods, and lignin pyrolysis reactors employed. Further, the complex product spectra obtained have thus far defied efforts to unequivocally elucidate the origins of individual products.

Previous model compound pyrolyses provide some insight into possible

lignin pyrolysis reactions, but fail to detail either product spectra or primary reaction pathways. Few kinetic parameters are reported. Further, many studies employ non-isothermal DTA and DTG techniques, the latter being particularly difficult to interpret since chemical transformations, e.g. isomerizations, need not be attended by weight loss. Finally, it is significant that previous model compound studies have never hitherto been applied to describe whole-lignin pyrolysis.

### 1.5 Present Approach

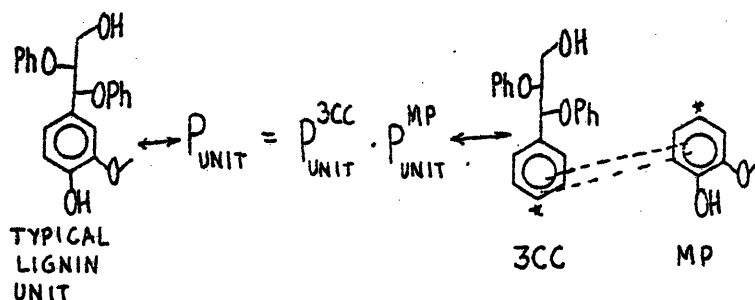
The present approach involved analysis of the lignin to suggest formal reaction pathways for lignin thermolysis. This permitted development of a list of model compounds to be experimentally pyrolysed. Pyrolysis results, combined with the earlier lignin structural analysis, then allowed a mathematical simulation of whole-lignin thermolysis in a manner comparable with available experiments.

#### 1.5.1 Analysis of Lignin Structure

Lignin is a random co-polymer of coniferyl, sinapyl and coumaryl alcohol monomers. The single ring aromatic units in lignin possess, at positions 1, 3, and 4, respectively, a 3-carbon chain, methoxy, and phenol substituents. These aromatic units are connected by interunit linkages of (in descending prevalence)  $\beta$ -ether,  $\alpha$ -ether, diphenylmethane, diarylether, diaryl, pinosresinol, and phenylcoumaran types. Thus lignin is simply an ensemble of single ring aromatic units, linked by seven types of interunit bonds.

An essential feature of lignin constitution, noted earlier, is that while the methoxyphenol of a given aromatic unit may be involved in bonding with the 3-carbon chain or methoxyphenol of an adjacent unit, it is never involved in bonding with the 3-carbon chain of the same aromatic

unit. Thus the nature of methoxyphenol substitution on a given aromatic unit is independent of the nature of 3-carbon side chain substitution on the same unit. Thus, as illustrated below, the probability of the occurrence in lignin of a given aromatic unit must be equal to the prob-



ability of the proper side chain multiplied by the probability of the proper methoxyphenol. This is the probability of the simultaneous occurrence of two independent events, namely the product of the individual probabilities, i.e.,  $P_A$  and  $B = P_A \times P_B$ .

The present probabilistic interpretation of the Freudenberg lignin structure can now be elaborated. Figure 5.1 is a numerical summary of the types of aromatic units present in the Freudenberg structure of Figure 3.5. The grid points in Figure 5.1 show the 18 aromatic unit types depicted in the Freudenberg structure, and are positioned in the grid so as to represent the appropriate match of methoxyphenol and 3-carbon side chain substituents. The present interpretation of the Freudenberg structure is schematized in Figure 5.2. Using the distributions of 3-carbon side chains and methoxyphenols detailed in Figures 3.7 and 3.8, a grid of 18 total aromatic units has been generated by multiplying all possible methoxyphenol types against all possible 3-carbon side chain substituent types. Thus, many of the grid points with zero entries in Figure 5.1 now have non-zero entries in Figure 5.2;

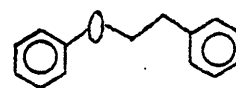
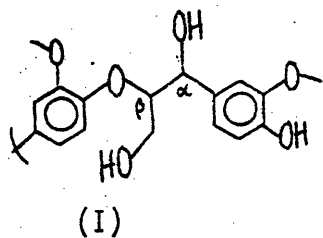
correspondingly, the proportions of certain overemphasized aromatic units in Figure 5.1 have been reduced.

This investigation will use the preceding statistical matching approach to describe whole lignin.

### 1.5.2 Formal Pathways in Lignin Thermolysis: Selection of Model Compounds

At the temperatures of interest in most lignin thermolyses, the aromatic units will persist. Thus, the essential reactivity of whole-lignin will be that of the methoxyphenols, 3-carbon side chains, and interunit linkages. Consideration of such units present in the Freudenberg structure generated a set of compounds capable of describing the essential features of lignin pyrolysis. Table 5.1 lists these model compounds. A complete discussion of the logic used to arrive at this list is presented on the main text of this thesis.

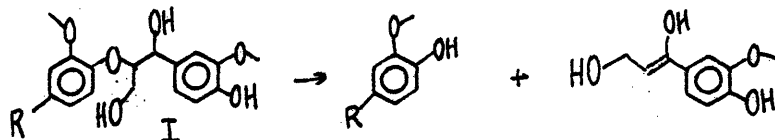
The prevalent guaiacyl  $\beta$ -ether link, structure I, was modelled as phenethyl phenyl ether (PPE), compound 1. PPE contains the essential  $\beta$ -ether carbon-oxygen link but does not possess the  $\alpha$ -hydroxy,  $\beta$ -methylol and guaiacyl substituents present in the actual lignin moiety. The effects of these substituents (which can be accounted for theoretically and experimentally) should be of second order importance<sup>75,76</sup> as compared to the basic reactivity of the  $\beta$ -ether link.



(1) phenylethyl-phenylether, PPE.

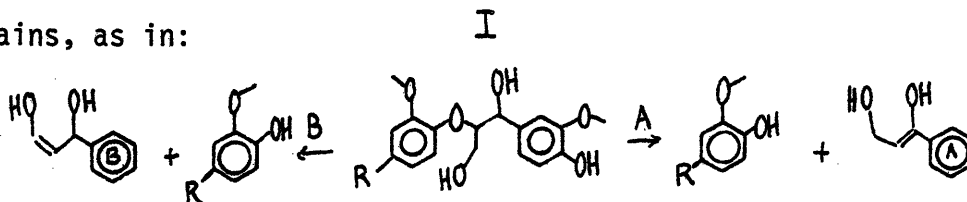
Of particular significance are the reactions of the  $\beta$ -ether. Formal reversion of the guaiacyl-glycerol- $\beta$ -ether may generate a guaiacol type

methoxyphenol from a veratrole type unit, as in:

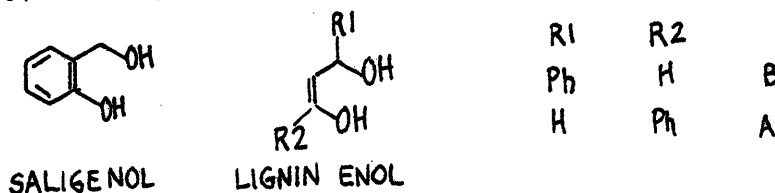


Hence, the relative reactivities of veratrole and guaiacol are of interest.

Reversion of ether I might result in the formation of hydroxy enol side chains, as in:



The hydroxy enol type moiety, IA or IB, is modelled by saligenol, as indicated below:

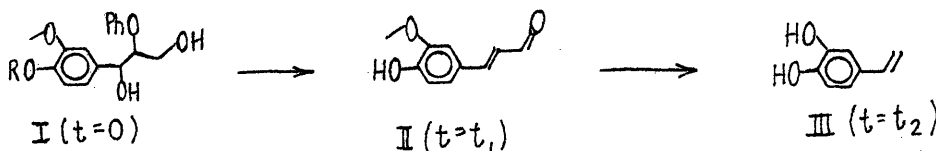


To summarize, the selection of model compounds was effected in two ways. First, compounds which mimic the functionalities and moieties known to exist in the unreacted lignin substrate were selected. The second method of selection was to choose compounds reflecting likely pyrolysis intermediates.

### 1.5.3 Simulation of Lignin Thermolysis

Whole lignin pyrolysis was modelled using the experimental results obtained from the model compound pyrolyses. The task involved depiction of the lignin substrate in terms of the model moieties, followed by delineation of the consecutive and parallel reactions of this substrate in terms of the model pathways. Finally, the products obtained in the model compound pyrolyses had to be related to those of whole-lignin.

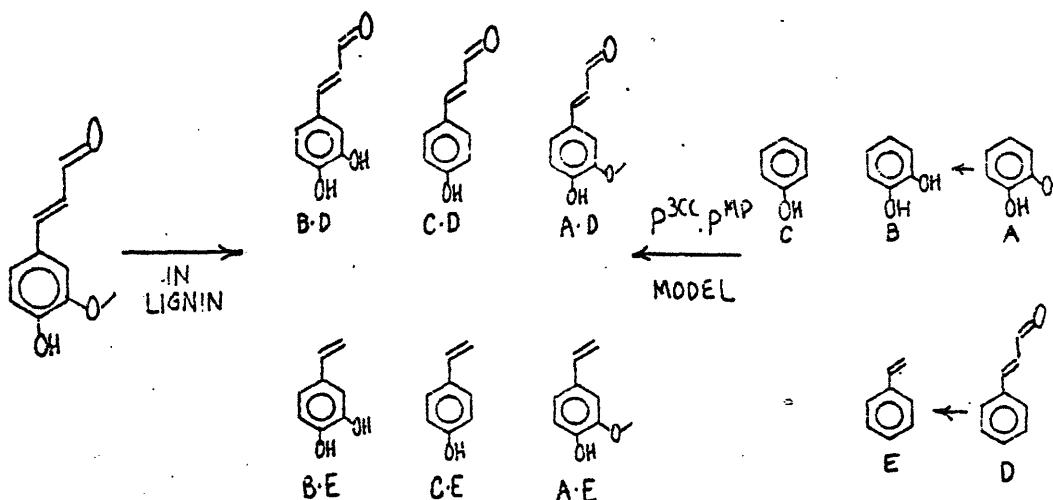
Each aromatic unit in lignin was assigned a 3-carbon side chain and methoxyphenol substituent. Consider the structural transformations:





Unit I depicts a typical aromatic unit as found in lignin. Reversion of the  $\beta$ -ether on the side chain followed by subsequent side chain dehydration and methoxyphenol ether cleavage may alter the aromatic unit to II. The original hydroxyl and ether substituents are no longer considered as part of the 3-carbon chain or methoxyphenol, but are either in separate stable products or associated with the 3-carbon chains or methoxyphenol of another aromatic unit. Further reaction could alter the aromatic unit to III. Thus, while the aromatic unit remains intact, changes in the 3-carbon side chain and methoxyphenol substituents chronicle lignin pyrolysis.

The pyrolysis products were then found from a statistical matching of the corresponding products from methoxyphenol and 3-carbon side chain pyrolyses, dictated by the kinetics of each reaction. For example, guaiacol pyrolysis might yield phenol and catechol, whereas cinnamaldehyde might yield styrene. Thus a coniferaldehyde lignin aromatic unit might be expected to yield all of the products shown below. The proportions B:D, C:D, A:D, B:E, C:E, and A:E are dictated by the individual yields of products A through E in experimental pyrolyses of the models guaiacol and cinnamaldehyde. Integration (summation) over the entire distribution of aromatic



units should then describe the products from whole-lignin pyrolysis.

### Mathematics of the Simulation

Ordinary linear differential equations describing the variation with time of each methoxyphenol and 3-carbon side chain moiety were used to describe a constant volume batch pyrolysis. The rate of change of each product was, in general, proportional to the number of mols of each other product, or in vector form,

$$\frac{d\vec{X}}{dt} = \underline{\underline{K}}\vec{X} \quad ; \quad \frac{d\vec{Y}}{dt} = \underline{\underline{L}}\vec{Y} \quad \vec{X}(t=0) = \vec{X}_0$$

$$\vec{Y}(t=0) = \vec{Y}_0$$

where the vector  $X$  represents all methoxyphenol products, and  $Y$  is the 3-carbon side chain product vector. The equations were numerically integrated forward in time via a fourth order Runge-Kutta technique. The initial conditions required for the solution of these equations were obtained from the distribution of methoxyphenols and 3-carbon side chains depicted in the Freudenberg structure for spruce lignin, given in Figure 5.2. These conditions reflect the molar, or moiety, fraction of each methoxyphenol or 3-carbon chain in the initial lignin structure. Note that the initial conditions are a function of lignin origin. As light gases, water, and MeOH are evolved in pyrolysis, total simulation mols are not conserved. However, the total number of methoxyphenol and 3-carbon side chain moieties is conserved while being chemically altered in pyrolysis; total aromatic units are also conserved. Formation of single ring aromatic products necessitates that all interunit linkages of the side chain and the methoxyphenols be cleaved. Two types of substituents arise, those entirely free of interunit linkages, designated as S, and those involved in interunit bonding, designated M. Since a single ring aromatic will form only when an S-type 3-carbon chain and an

S-type methoxyphenol are formed, the probability of single ring aromatic formation from lignin,  $P_S^{LIG}$ , is  $P_S^{LIG} = P_S^{MP} \cdot P_S^{3CC}$ . Any other combination involving  $P_M^{MP}$  or  $P_M^{3CC}$  represents the formation of a multiple aromatic ring product.

In summary, the simulation numerically solved a set of first order differential equations which described the variation with time of the number of each type of 3-carbon side chain and methoxyphenol moiety per unit weight of lignin substrate. The initial concentration of each moiety was obtained from the distributions depicted in the Freudenberg structural model for lignin. Statistical matching of methoxyphenol and 3-carbon side chain substituents at any time then described the products expected from whole-lignin thermolysis.

## 1.6 Experimental Methods

Table 6.1 is a summary detailing the range of operating conditions for the experimental pyrolyses. Listed are the model compound, structure, purity, and the temperature, time and concentration range studied. The experimental details are conveniently grouped into three categories, namely, the source of the chemicals used for pyrolysis, the actual apparatus used to effect the pyrolyses, and the chemical analysis system used for product characterization.

### Chemicals Used

All but one of the compounds were available commercially and were used as received. PPE was not commercially available and this substrate was synthesized by the method of Mademov and Khydyrov<sup>164</sup>. Structural details of the synthesis product were confirmed by NMR. Analysis by GC on OV-17 showed the ether to be 95% pure, with phenol, the main impurity, amounting to 1%.

### Apparatus

A batch reactor system was employed for all pyrolyses. The batch reactors were stainless steel "tubing bombs" fashioned from Swagelok components. Four different size reactors were used, having volumes of 0.2, 0.6, 3.5, and 10.6 cm<sup>3</sup>. Kinetic studies were confined to the reactors of 0.2 and 0.6 cm<sup>3</sup> in an effort to minimize the effect of heat-up time. The larger reactors were used for quantitative gas and liquid stoichiometry studies.

The batch reactors were either loaded and sealed in a glove box maintained with a nitrogen or argon inert atmosphere, or were externally loaded and slowly purged with an inert flow before closure. The inert served as an internal standard for later gas analyses. Loaded reactors were then immersed in a constant temperature fluidized sand bath for the duration of reaction, and finally quenched in an ice-water bath. After quenching, the reactors were dried, opened, and septum-capped in a helium environment for GC gas analysis. The liquid and solid products were then solvent-collected for later GLC/GC analyses.

### Chemical Analysis

The pyrolysis products were identified and analysed by Gas Chromatography. Gases were separated by either molecular sieve(10'), silica gel(6'), or porapak Q(6') columns. Analysis for light liquids, such as H<sub>2</sub>O, MeOH, EtOH, and up to about toluene and phenol was effected on porapak Q and principally porapak P(6') columns. The heavier compounds, including alkylbenzenes, phenols and the model compounds were separated on an OV-17 column (6'). Product identification was primarily by GC with standard coinjection. Quantitative product mol fractions were determined from calibration factors obtained from standard samples of known composi-

tion.

## 1.7 Experimental Results

For each model compound, it was desired to:

1. Characterize and quantify pyrolysis product spectra
2. Develop product relationships and stoichiometries
3. Identify likely reaction pathways
4. Determine reaction orders
5. Measure reaction kinetics and derive Arrhenius parameters.

Experimental results are described for each compound, listed in order of descending importance. Detailed description is limited to Phenethyl Phenyl Ether (PPE) pyrolysis. Kinetic parameters and reaction pathways for each pyrolysis are summarized in Table 1.7.1.

### 1.7.1 Phenethyl Phenyl Ether (PPE)

The pyrolyses were effected over the range of operating conditions detailed in Table 6.1. The experiments were conducted at temperatures from 300-550 C, with holding times of 1-240 minutes. Substrate conversions were generally held to less than 30% in an effort to emphasize primary reactions; however, kinetic data were obtained at conversions as high as 90%. Initial substrate concentrations ranged from 0.083 to 1.66 mol/l in the gas phase.

PPE was also pyrolysed in tetralin at 350, 400, and 450 C, at substrate concentrations of 0.25mol/l. The effect of tetralin was examined in detail at 400 C, where the mol ratio of tetralin to PPE, called S, was varied from 0.245 to 9.8.

Care was taken to monitor material balance closure, quantified by the determination of the parameter  $\langle M \rangle$ , physically the average molecular weight of the pyrolysis products, defined below. In this expression  $X_i$  is

Table 17.1 Summary of Reaction Pathways and Kinetic Parameters

Substrate	Pathway:Products	$\log_{10}A(s^{-1})$	$E^*$ (kcal/mol)
PPE	R1: PhOH + St	11.1	45.0
St	: PhH, Tol, EB	5	22
OHD	R1: Tol + PhOH	9.6	43.4
PE	R1: PhH + PhOH	14.8	72.1
BP	R1: 2PhH	-	-
BPhOH	N.R.	-	-
GUA	R1: CAT + CH <sub>4</sub>	10.9	43.7
	R2: PhOH + CO	11.5	47.4
I	R1: PC + CH <sub>4</sub>	10.8	42.9
	R2: PP + CO	11.3	46.2
DMP	R1: MC + CH <sub>4</sub>	10.4	42.2
	R2: GUA + CO	11.1	45.5
VA	R1 <sub>CH<sub>4</sub></sub> : DHB + CH <sub>4</sub>	12.2	47.3
	R1 <sub>CO</sub> : GUA + CO	10.2	38.5
VE	R3: GUA + CH <sub>4</sub>	13.9	55.9
	R3': PhOH + CO + CH <sub>4</sub>	14.1	58.4
	R4: AN + CO	14.8	60.1
	R5: oC + CO	11.2	49.2
AN	R3: PhOH + CH <sub>4</sub>	13.0	54.7
	R4: PhH + CO	14.5	61.0
	R5: oC	7.9	40.5
CAL	R1: CAD	14.2	21.8
SAL	R1: QM + H <sub>2</sub> O	13.4	33.4
BA	R1: PhH + CO	9.5	41.5
AP	: Tol	10.9	56.4
	: PhH	9.6	50.5
CAD	R1: St + CO	12.1	48.2
	R2: Phenols	8.5	34.5
	R3: Dimers	8.6	33.7
CA	R1: St + CO <sub>2</sub>	8.0	31.0
FA	R1: VG + CO <sub>2</sub>	5.2	19.8
1-NA	R1: N + CO <sub>2</sub>	4.5	24.0
2-NA	R1: N + CO <sub>2</sub>	7.9	36.5

$$\langle M \rangle \equiv \frac{\sum_{i=2}^n X_i M_i}{\sum_{i=2}^n X_i}$$

n = total number of products, including PPE  
i = 1 = PPE

the mol fraction and  $M_i$  the formula weight of product  $i$ . Thus only true products are considered in the  $\langle M \rangle$  calculation, with unreacted ether excluded. An ideal production of two product mols from each ether substrate mol would thus yield  $\langle M \rangle = 198/2 = 99$ . The 157 experimental PPE pyrolyses yielded a mean value  $\langle M \rangle = 100.5 \pm 3.98$  as a quantitative measure of pathway closure to two product mols. Carbon, hydrogen and oxygen atom balances were effected and the ratios H/C and O/C were within  $\pm 3.2\%$  and  $\pm 11.7\%$  of those for the unreacted substrate; the latter provide a measure of overall material balance. The results will be described in two parts, neat pyrolyses and pyrolyses in tetralin.

### Neat Pyrolysis

#### A. Primary Products

The products from representative pyrolyses at various temperatures and times are listed in Table 7.1.1. Two striking observations emerge. First, while 13 pyrolysis products were detected and quantified, the major products were limited to phenol and the hydrocarbons styrene, ethylbenzene, toluene, and benzene. The remaining products, in sum total, amounted to at most 6% of the ether converted. Of the hydrocarbons, styrene was predominant at low conversions, with increasing amounts of toluene as conversion increased. Secondly, the details of the product spectra were relatively insensitive to temperature, and showed a slight dependence on initial substrate concentration and a strong dependence on substrate

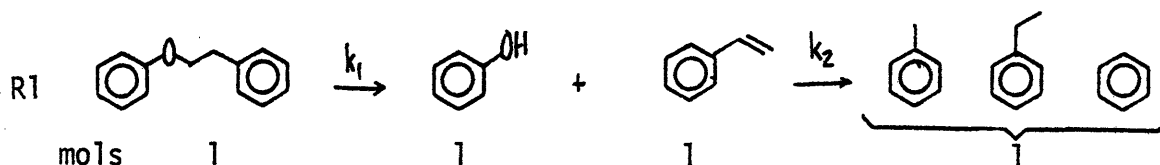
conversion. The latter two observations are reflected most strongly in the relative proportions of major hydrocarbon product.

The time variation of substrate and major product proportions, in mols per initial mol of ether for pyrolysis at 400 C and initial ether concentration of 0.25 mol/l, are depicted in Figure 7.1.1. The slopes of the phenol appearance and ether disappearance are suggestive of a stoichiometric production of phenol from substrate. Figure 7.1.1 further shows the styrene product produced stoichiometrically with phenol at  $t=5$  minutes and reaching a maximum at 25 minutes. The maximum yield of styrene, coupled with apparent initial slopes of zero for toluene and ethylbenzene production is suggestive of secondary reactions of the styrene to other products, including toluene, ethylbenzene, and benzene.

The stoichiometric implications of Figure 7.1.1 are further developed in Figure 7.1.2, where product selectivities, i.e., the mol yields of phenol, styrene, and the hydrocarbon sum (styrene+ethylbenzene+toluene+benzene)=(HC) per mol of decomposed substrate, are plotted as a function of substrate conversion. The constant ordinate of unity for phenol at all conversions in Figure 7.1.2 shows that for each mol of ether decomposed a mol of phenol was always produced. For styrene the ordinate decreases monotonically with increasing conversion, from about 0.8 at a fractional conversion of 0.1 to about 0.2 at fractional conversions of 0.8. Thus, at low substrate conversions, one mol of styrene is observed per mol of ether decomposed, but this styrene selectivity decreases with increasing conversion. This is indicative of secondary styrene degradation. Finally, it is observed in Figure 7.1.2 that the hydrocarbon sum HC is essentially unity at all substrate conversions. In summary, then, Figure 7.1.2 shows that decomposition of one mol of ether always yielded one mol of phenol and



one mol of total hydrocarbons. At low substrate conversions, the hydrocarbon is solely styrene, the primary product, which undergoes secondary reactions to the other hydrocarbons at higher conversions. The corresponding pathway for PPE decomposition is the of the type R1:



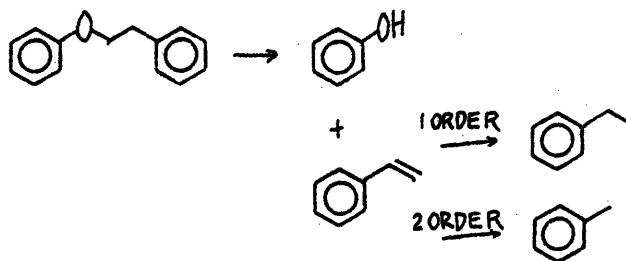
The order of reaction R1 was examined in a series of experiments at 400 C with initial substrate concentrations ranging from 0.083 to 1.66 mol per liter. Figure 7.1.3 plots the variation with time of  $-\ln E/E_0$  for each initial concentration studied, where E is an abbreviated symbol for PPE. A reaction with rate expression  $r = kE^\alpha$ , i.e., rate constant k and order  $\alpha$ , would yield an initial slope  $|\text{dln}(E/E_0)/\text{dt}|_{t \rightarrow 0} = kE_0^{\alpha-1}$ . The data of Figure 7.1.3 show no systematic dependence on  $E_0$  and are described by a single average slope, implying  $\alpha=1$ , i.e., first order kinetics. The linearity of  $-\ln E/E_0$  vs. t up to fractional conversions of 0.7 is further indicative of first order kinetics. First order rate constants separately determined from Figure 7.1.3 for each initial substrate concentration are plotted in Figure 7.1.4, as  $k(\text{s}^{-1})$  versus  $E_0(\text{mol/l})$  on doubly logarithmic coordinates. The rate constant is seen to be substantially independent of  $E_0$  over a twentyfold range of the latter.

Further pyrolyses at temperatures from 300-500 C revealed the activation parameters of the first order rate constant. These data are shown in Figure 7.1.5, an Arrhenius diagram with coordinates of  $\log_{10} k(\text{s}^{-1})$  vs  $\Theta^{-1}$ , where  $\Theta = 4.576 \times 10^{-3} T$ , with T in Kelvins. On these coordinates, an Arrhenius relationship is described by a straight line  $\log_{10} k = \log_{10} A - E^*/\Theta$ , where the pre-exponential factor A has units of the rate constant

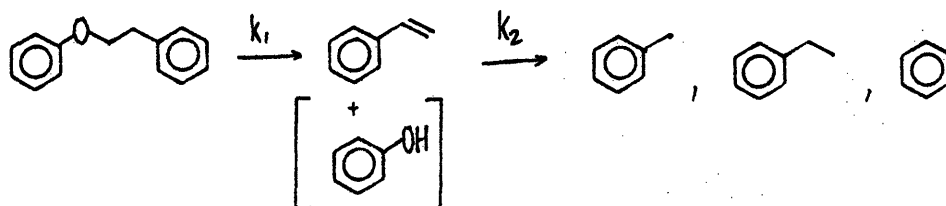
and the activation energy  $E^*$  is expressed in kcal/mol. It is evident from Figure 7.1.5 that  $\log_{10}k$  follows the Arrhenius relationship over a range of five orders of magnitude in  $k$ . The best fit of these data yields Arrhenius parameters ( $\log_{10}A(s^{-1}), E^*(kcal/mol)$ ) =  $(11.1 \pm 0.9, 45.0 \pm 2.7)$ .

### B. Secondary Products

Table 7.1.1 and Figures 7.1.1 and 7.1.2 suggested that ethylbenzene, toluene and benzene were secondary products from styrene degradation. The secondary reaction of styrene was concentration dependent, as depicted in Figure 7.1.6, a plot of product appearance vs. substrate conversion at 400 C for initial PPE concentration,  $E_0$ , ranging from 0.083 to 1.66 mol/l. While the ratios  $PhOH/(E_0-E)$  and  $HC/(E_0-E)$  were substantially unity, independent of  $E_0$  and substrate conversion, a definite trend of decreasing  $St/(E_0-E)$  with increasing  $E_0$  could be discerned at all conversion levels. This is indicative of reaction order in excess of unity for the overall secondary styrene reaction. From Table 7.1.1, the higher order reaction path can be linked with toluene production, which increases with increasing  $E_0$ ; in contrast, the ethylbenzene appearance was relatively insensitive to  $E_0$ . Thus, the pathways to secondary products appear to be of the type:



The rate for secondary styrene degradation was estimated from the consecutive reaction series:



An overall pseudo-first order rate constant  $k_2$  for secondary styrene degradation was obtained from the maximum concentration:

$$\frac{St_{MAX}}{E_0} = \frac{k_1}{k_2} (k_2 / (k_2 - k_1))$$

These calculations were made for all PPE pyrolyses where a styrene maximum was apparent, with the results given in Table 1.7.2.

Table 1.7.2 Styrene Pyrolysis Kinetics

T(C)	PPE <sub>0</sub> (mol/l)	k <sub>2</sub> /k <sub>1</sub>	k <sub>2</sub> (s <sup>-1</sup> )
400	0.083	4.42	0.00172
400	0.25	5.78	0.00310
400	0.25	5.78	0.00225
400	0.75	10.0	0.00585
400	0.83	11.0	0.0037
400	1.66	13.5	0.01
450	0.25	3.15	0.006
500	0.25	2.02	0.018
500	0.75	4.03	0.0655

At a given temperature of 400 C, the ratio  $k_2/k_1$  increased with increasing initial ether concentrations; this reflects the higher order character of styrene degradation relative to ether reversion. The increase in  $k_2/k_1$  with an increase in PPE<sub>0</sub> was also apparent at 500 C. Further, for a given initial ether concentration at 0.25 mol/l, comparison of the data at 400, 450 and 500 C showed that  $k_2$  increased with increasing pyrolysis temperature. The pseudo-first order rate constant  $k_2$  had apparent Arrhenius parameters  $(\log_{10} A, E^*) = (5, 22)$ ; thus, secondary styrene degradation was considerably less activated than the primary reversion of PPE.

#### Pyrolysis in Tetralin

The ether was pyrolysed in tetralin at temperatures of 350, 400 and 450 C. The primary product spectra were substantially similar to those

for neat ether pyrolysis, as illustrated in Figure 7.1.7, a plot of product yields as a function of reaction time at 400 C, initial tetralin to PPE ratio  $S=1.48$ , and initial ether concentration  $E_0 = 0.25$  mol per liter. The only significant change was in the secondary reaction of styrene, where the presence of tetralin shifted the secondary selectivity toward ethylbenzene. Product relationships were further examined in Figure 7.1.8, where the mol ratios  $PhOH/(E_0-E)$ ,  $St/(E_0-E)$  and  $HC/(E_0-E)$  are plotted as a function of ether conversion. As was the case with neat pyrolysis, both the ratio  $PhOH/(E_0-E)$  and  $HC/(E_0-E)$  were near unity for all conversions attained, while the ratio  $St/(E_0-E)$  dropped rapidly with conversion. Hence, the primary pathway for ether decomposition to phenol and styrene was unchanged. The rate of styrene decrease was higher in the presence of tetralin than in its absence. Thus, in Figure 7.1.8, the open circles depicting neat pyrolysis indicate a higher styrene concentration at each conversion than do the closed circles representing cases with  $S>0$ . This is characteristic of a higher order reaction of styrene and tetralin to ethylbenzene, earlier noted as the major secondary pathway for  $S>0$ .

The kinetics of ether pyrolysis in tetralin were examined for varying values of  $S$  at 350, 400, and 450 C. These data are presented in Figure 7.1.9, a plot of the first order rate constant vs. the mol ratio  $S$  for each temperature studied. A scale change in the abscissa of Figure 7.1.9 allows inclusion of the rate constant from neat pyrolysis for comparison. At 350 and 450 C rate data were obtained over two orders of magnitude of  $S$ . It is evident the rate constants were virtually independent of the presence and amount of tetralin. More comprehensive study at 400 C revealed a slight diminution of the rate constant with increasing

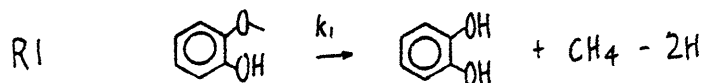
tetralin proportions, of the order of  $0.2 \log_{10} k$  units for the range  $S=0$  to  $S=9.8$ . Statistical analyses of the neat and tetralin pyrolyses for all  $S$  revealed that the difference in the means of each was less than the standard deviation of this difference. Further comparison of the neat and in-tetralin ether pyrolyses was presented in the Arrhenius diagram Figure 7.1.5. The dark circles representing data for pyrolysis in tetralin were identical with the neat values.

In summary, PPE was pyrolysed both neat and in the presence of tetralin. Neat ether pyrolysis resulted in the primary stoichiometric production of phenol and styrene, with secondary degradation of the latter. Overall ether pyrolysis was substantially first order, and was fit by Arrhenius parameters  $(\log_{10} A, E^*) = (11.1, 45.0)$ . Secondary pyrolysis of styrene was of reaction order greater than unity, and proceeded with apparent pseudo-first order Arrhenius parameters of  $(\log_{10} A, E^*) = (5 \pm 2, 22 \pm 3)$ . Pyrolysis in tetralin was similar to neat ether pyrolysis, the only significant difference arising as an increased selectivity of secondary styrene conversion to ethylbenzene. The kinetics of neat and in-tetralin pyrolyses were identical.

### 1.7.2 Summary of Experimental Results

#### Guaiacol

Two parallel pathways described guaiacol pyrolysis, these being demethanation to catechol and methane and demethoxylation to phenol and CO.



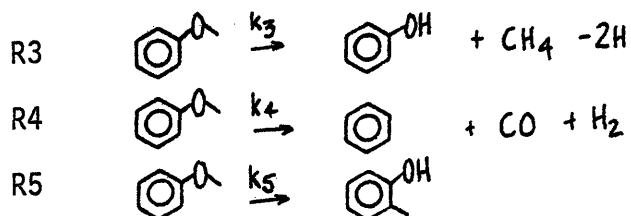
The former pathway was tenfold faster. The assignment of catechol as a direct pyrolysis product is as yet tentative. Both of the demethanation and

demethoxylation pathways were first order in substrate, with respective Arrhenius parameters  $(\log_{10} A, E^*) = (10.9 \pm 0.5, 43.7 \pm 1.4)$  and  $(11.5 \pm 0.5, 47.4 \pm 1.6)$ .

Substituted Guaiacols: 2,6-dimethoxyphenol (DMP), Isoeugenol, Vanillin  
 Pyrolyses of DMP, isoeugenol, and vanillin probed the respective effects of electron donating, conjugative, and electron withdrawing substitution on guaiacol reactivity. The substrates decomposed by pathways similar to R1 and R2 for guaiacol; vanillin underwent extensive decarbonylation as well. The kinetics of guaiacol demethanation and demethoxylation were virtually unaffected by substitution.

### Anisole

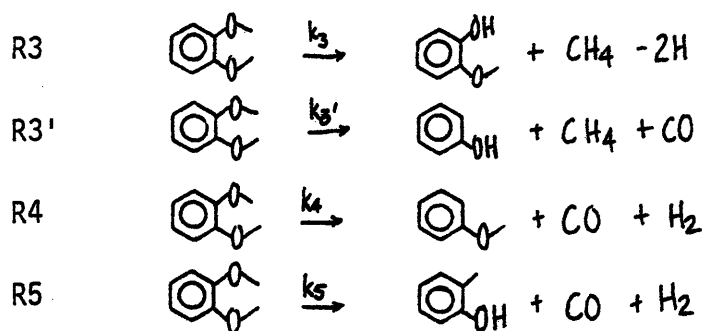
Anisole pyrolysis probed the effect of ortho-hydroxy substitution on the reactions of the guaiacol methoxyl group. The effect is marked, as overall anisole pyrolysis was typically at least an order of magnitude slower in rate than that of guaiacol. Three pathways described anisole pyrolysis, leading to the formation of phenol, benzene, and o-cresol:



Unequivocal relationships between gas and liquid phase products could not be discerned. First order Arrhenius parameters were  $(\log_{10} A, E^*) = (13.0 \pm 1.0, 54.7 \pm 3.1), (14.5 \pm 1.2, 61.0 \pm 4.0),$  and  $(7.9 \pm 1.5, 40.5 \pm 4.9)$  for R3, R4, and R5, respectively.

### Veratrole

Four primary reaction pathways were important in veratrole pyrolysis. These were similar to those previously described for anisole, and took the form listed below. The kinetics of pathways R3 and R5 were compar-



able to those for analogous R3 and R5 anisole pathways. Apparent first order Arrhenius parameters  $(\log_{10}A, E^*) = (13.9 \pm 1.3, 55.9 \pm 4.0), (14.1 \pm 1.0, 58.4 \pm 2.8), (14.8 \pm 1.8, 66.1 \pm 5.7)$  and  $(11.2 \pm 2.2, 49.2 \pm 7.1)$  for pathways R3, R3', R4, and R5, respectively.

#### Saligenol

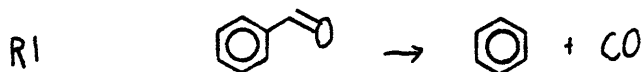
Saligenol underwent facile dehydration at temperatures as low as 175-225 C. Each mol of decomposed substrate yielded one product mol of water. Thus, a pathway of the type R1 was postulated, where:



The quinonemethide was not isolated, being a labile precursor to the only major pyrolysis co-product, an obscure higher molecular weight polymer. Apparent first order Arrhenius parameters for R1 were  $(\log_{10}A, E^*) = (13.4 \pm 2.9, 33.4 \pm 6.3)$ .

#### Benzaldehyde

The major pyrolysis route for benzaldehyde was first order degradation to stoichiometric amounts of CO and benzene, pathway R1:

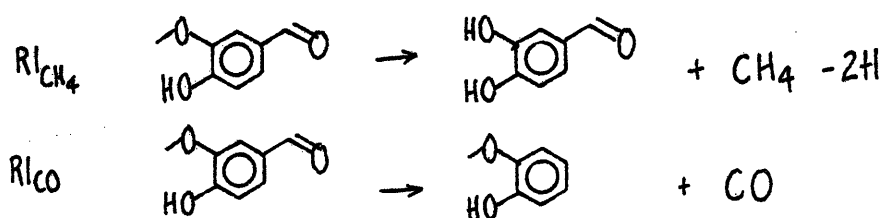


Kinetic description of R1 at temperatures from 300-500 C provided first

order Arrhenius parameters  $(\log_{10} A, E^*) = (9.5 \pm 0.8, 41.5 \pm 2.7)$ .

### Vanillin

Vanillin pyrolysis involved two major pyrolysis pathways, demethanation to dihydroxybenzaldehyde and decarbonylation to guaiacol; the latter pathway was faster by a factor of 10. Thus, vanillin pyrolysis pathways were of the type R1 previously delineated for each of guaiacol and benzaldehyde. Kinetic analysis of vanillin pyrolysis yielded de-



methanation parameters of  $(\log_{10} A, E^*) = (12.2 \pm 3.0, 47.3 \pm 8.6)$  and decarbonylation parameters of  $(10.2 \pm 2.1, 38.5 \pm 5.9)$ . Thus, guaiacol demethanation was essentially unaffected by carbonyl substitution, whereas benzaldehyde decarbonylation was markedly enhanced by guaiacyl substitution.

### Acetophenone

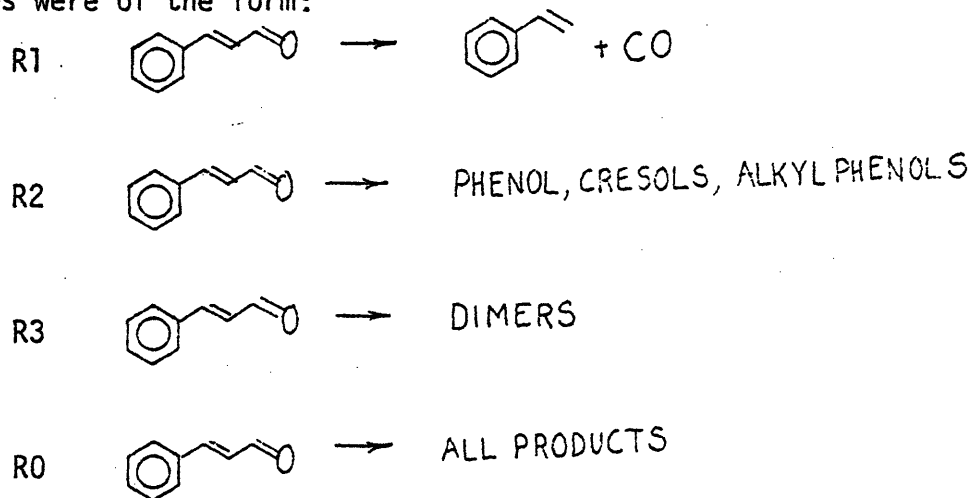
Acetophenone pyrolysis yielded CO, CH<sub>4</sub>, benzene and toluene as the major light products, along with appreciable amounts of alkylbenzenes, phenols and apparent dimers. Because of the complexity of the liquid product spectra, no clear link could be established between gaseous and condensed phase products. An apparent overall acetophenone decomposition reaction order of 1.2-1.3 was determined, with a reaction order of unity for toluene appearance and 1.5 for benzene appearance. Pseudo-first order Arrhenius parameters for overall acetophenone decomposition, benzene appearance and toluene appearance were  $(\log_{10} A, E^*) = (10.9 \pm 1.2, 52.1 \pm 4.1)$ ,  $(9.6 \pm 1.9, 50.5 \pm 6.7)$  and  $(10.9 \pm 2.2, 56.4 \pm 7.6)$ , respectively. Overall acetophenone pyrolysis was typically two orders of magnitude slower than benz-



aldehyde pyrolysis for the temperature range studied here.

### Cinnamaldehyde

Pyrolysis of cinnamaldehyde yielded styrene, phenols, apparent dimers, and CO as primary products, as well as toluene and ethylbenzene as secondary products. Styrene and CO were formed stoichiometrically at low substrate conversions. Overall cinnamaldehyde decomposition was described in two parts, a set of first and a set of second order reactions, of the form:  $-d(\text{CAD})/dt = k_1(\text{CAD}) + k_2(\text{CAD})^2$ , where  $k_1$  accounts for first order reactions and  $k_2$  the second order reactions. Styrene and phenol appearance were best described as first order, and dimer formation by a reaction order in excess of unity, likely two. The major cinnamaldehyde pyrolyses were of the form:

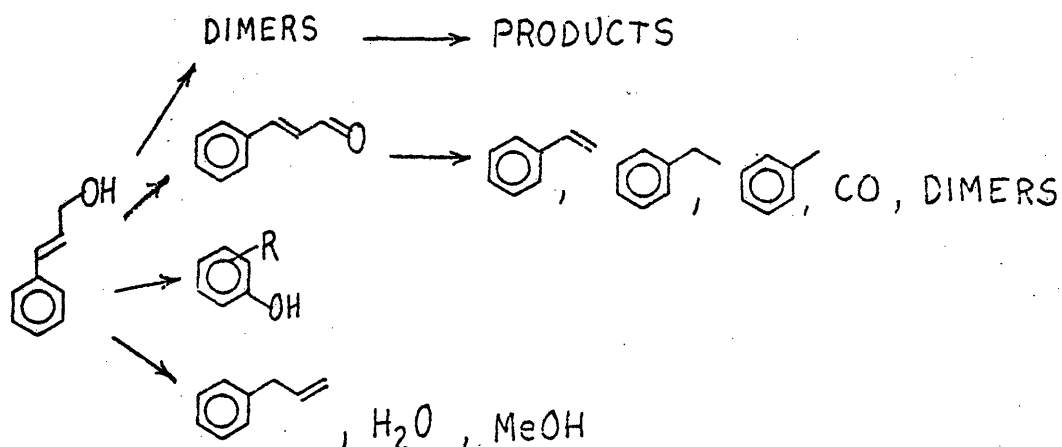


Pseudo-first order Arrhenius parameters for R1, R2, R3, and R0 were  $(\log_{10} A, E^*) = (12.1 \pm 0.4, 48.2 \pm 1.1), (8.5 \pm 0.4, 34.5 \pm 1.0), (8.6 \pm 1.4, 33.7 \pm 3.1)$  and  $(9.7 \pm 1.7, 35.4 \pm 4.6)$ , respectively.

### Cinnamyl Alcohol

The products from cinnamyl alcohol pyrolysis fell into one of four categories: a gas fraction, water soluble light liquids, monoaromatics, and a polymeric fraction. Significant products were CO, H<sub>2</sub>O, MeOH, cinnamaldehyde, styrene, phenols, allylbenzene, and apparent dimers. In spite of

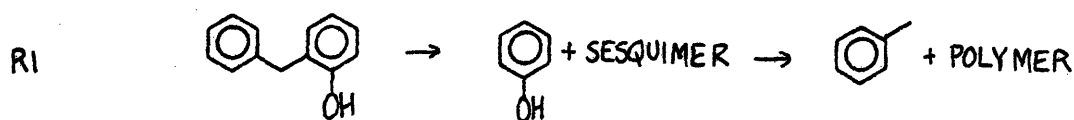
complex product spectra, several generalizations regarding cinnamyl alcohol pyrolysis were possible. Lower temperature pyrolysis data suggested that dimers, cinnamaldehyde, phenols, allylbenzene, water and methanol were primary products, whereas styrene, toluene, ethylbenzene, and CO likely arose from secondary pyrolyses. The reaction network was of the type:



Of the primary reactions, cinnamaldehyde, dimer and alkylphenol formation were the most facile, whereas methanol formation was typically two orders of magnitude slower in rate than overall alcohol decomposition.

#### Orthohydroxydiphenylmethane (OHD)

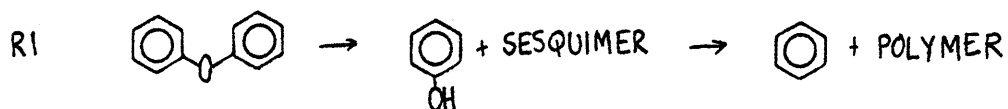
Pyrolysis of OHD resulted in phenol, toluene, and apparent triphenyl sesquimers as the major products. Of these, phenol and sesquimers were primary, the latter degrading by secondary pathways to toluene. OHD degradation pathways were of the type R1:



Apparent first order Arrhenius parameters for OHD pyrolysis were ( $\log_{10} A$ ,  $E^*$ ) = (9.6±0.4, 43.4±1.4).

#### Phenyl Ether

The pyrolysis of phenyl ether could be effected only at temperatures in excess of 500 C. The major pyrolysis products were phenol, benzene, and apparent sesquimers. Ether pyrolysis appeared to proceed via primary degradation to phenol and sesquimers, the latter capable of degradation to benzene and polymers. Thus, a pathway of the type R1 was suggested, where :



Apparent first order Arrhenius parameters were  $(\log_{10} A, E^*) = (14.8 \pm 1.3, 72.1 \pm 4.8)$ .

#### Biphenyl

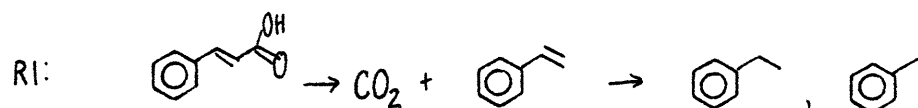
Pyrolysis of biphenyl to benzene occurred only at 587 C. Higher molecular weight materials, which were presumably formed to maintain hydrogen balance, went undetected in the present analysis. An apparent first order rate constant  $-\log_{10} k_{587 \text{ C}} = 3.82$  was determined.

#### Biphenol

Biphenol was pyrolysed to 500 C and 30 minutes holding time. The compound was quite stable, and no degradation to any light products could be discerned.

#### Cinnamic Acid

Pyrolysis of cinnamic acid over a temperature range of 300-400 C produced  $\text{CO}_2$  and styrene as major primary products, the latter capable of secondary degradation to toluene and ethylbenzene. The major cinnamic acid pathway was thus of the type R1, namely:



Apparent first order Arrhenius parameters of  $(\log_{10}A, E^*) = (8.0 \pm 1.8, 31.0 \pm 5.0)$  were determined.

#### Ferulic acid

Pyrolysis of ferulic acid from 200-350 C elucidated the effect of guaiacyl substitution on cinnamic acid decarboxylation. Initial rates of  $CO_2$  release were a hundred fold higher for ferulic acid than for cinnamic acid, showing substantial decarboxylation enhancement by guaiacyl substitution. Apparent first order rate data from the initial rates of  $CO_2$  formation yielded Arrhenius parameters of  $(\log_{10}A, E^*) = (5.2 \pm 2.0, 19.8 \pm 5.2)$ .

#### Napthoic Acids

The time evolution of  $CO_2$  from 1- and 2- napthoic acids was monitored from pyrolyses at 300, 400, and 500 C. The pyrolyses were modelled as a stoichiometric evolution of  $CO_2$  and naphthalene.  $CO_2$  release from 1-napthoic acid was faster than that from 2-napthoic acid. Apparent first order Arrhenius parameters of  $(\log_{10}A, E^*) = (4.5 \pm 1.4, 24.0 \pm 1.3)$  and  $(7.9 \pm 2.7, 36.5 \pm 8.1)$  were determined for 1- and 2- napthoic acids, respectively.

### 1.8 Implications of Experimental Results

The model compound pyrolysis pathways developed in the previous section allowed formulation of a primary reaction network to describe the essential features of lignin pyrolysis. The network is presented as Figure 8.1. For illustrative purposes, lignin has been depicted as the oligomeric unit I. The primary reactions used in Figure 8.1 are PPE reversion, BPE cleavage, guaiacol demethanation, and cinnamaldehyde decarbonylation. The veratrole methoxyls of aromatic units 1, 2, 3, and 4 are considered unreactive. Among the interunit linkages, the diphenyl-ether between units 4 and 5 is inert. Application of the facile guaiacol,

cinnamaldehyde, PPE, and BPE R1 pathways to structure I generates the structures shown as set II. The cinnamaldehyde reaction of unit I released CO and generated a styrene side chain. Reversion of PPE and BPE links resulted in guaiacol formation at units 1, 2, and 3, as well as a saligenol moiety on unit 2 and a cinnamyl alcohol on unit 4. Demethanation resulted in the formation of a diquinone at unit 5. The net release of gases and water is tabulated in Figure 8.1; one mol each of CO and CH<sub>4</sub> were formed in transformation of the lignin depicted as structure I to set II. The aromatics generated in set II are subject to further reactions, resulting in the products shown as set III. With regard to set III, unit 1 depicts guaiacyl demethanation as well as the degradation of styrene to toluene, ethylbenzene, and benzene. The products from whole-lignin pyrolysis, then, would be catechol, methylcatechol, and ethylcatechol precursors. Units 2 and 3 similarly depict guaiacyl demethanation, greatly facilitated by ether reversion. Water arose from dehydration of the saligenol moiety of unit 2, which generated the guaiacyl acrolein as well. Unit 4 depicts cinnamyl alcohol dehydrogenation to cinnamaldehyde; it also illustrates the relative stabilities of the phenyl ether link and thus of the associated veratrole methoxyl. Further application of the same kinds of reactions to set III generates the compounds of set IV, of which some may still further react. However, the veratrole methoxyl of unit 4 is relatively stable, and the diphenylether is essentially inert; both will thus concentrate in the carbonaceous residue.

The structural moieties and possible reactions of Figure 8.1 depict only a small number of the pathways involved in whole-lignin pyrolysis. A more accurate description of lignin pyrolysis must incorporate more of the structural details of the Freudenberg model as well as account for the

complex set of parallel and consecutive reactions likely important in lignin pyrolyses. For this purpose, a lignin pyrolysis simulation model was developed. This model combined the approach outlined in section 1.5 with the experimental model compound pyrolysis results. It possessed the same logic as displayed in Figure 8.1, but was considerably extended in scope.

### 1.9 Simulation Results

Spruce lignin pyrolysis was simulated at temperatures of 300, 400, 500, and 600 C, to holding times of  $10^4$ ,  $10^4$ ,  $10^2$ , and seven seconds, respectively. Figures 9.1a, b, and c are graphical presentations of selected product yields at each temperature studied. The present discussion will consider the more important aspects of these simulation results, which will be described in terms of the gas, light liquid, phenolic, and carbonaceous coke product fractions.

#### 1.9.1 Gas Evolution

The model presently accounts for methane and carbon monoxide release.



Simulated pyrolysis to  $10^4$  s produced methane in yields of 0.05% and 6.2% at 300 and 400 C, respectively. The greater yield at 400 C reflects not only guaiacol and veratrole activation, but also activation of the prevalent PPE linkage. At 500 C and 100 s, the simulation predicted a methane yield of 5.9%, whereas at 600 C and 7s, a yield of 6.1% was predicted. Thus, these increases in the pyrolysis temperature resulted in a sharp decrease in the time required to reach a nominal yield of 6%. These yields compare with a theoretical maximum of about 9%, obtained by assuming each aromatic unit could contribute one methane mol.

Simulation to  $10^4$ s at 300 and 400 C produced CO in yields of 0.037% and 3.5%, respectively. In both cases, these were less than the corresponding methane yield, yet initial rates of formation of CO at 400 C were faster than those for methane as seen at short times in Figure 9.1a. This early CO arises from the cinnamaldehyde side chains initially in lignin, which decarbonylate rather easily. At longer times, ether reversions generate further carbonyl and guaiacol units, the former through rapid saligenol dehydration. However, a large fraction of these carbonyls are of the acrolein type, which decarbonylate slower than cinnamaldehydes. Hence, CO release becomes slower than methane release as pyrolysis proceeds, the ratio  $\text{CH}_4/\text{CO}$  exceeding unity for modest conversions at 300 and 400 C. At the highest temperature of 600 C, however, CO again exceeds  $\text{CH}_4$  as seen in Figure 9.1c, where the respective yields of CO and  $\text{CH}_4$  are 9% and 6% at 7s. This occurs because CO producing pathways such as decarbonylation and demethoxylation are both more highly activated than the primary  $\text{CH}_4$  producing pathway of guaiacyl demethanation. In short, the ratio  $\text{CO}/\text{CH}_4$  is predicted to vary from greater than unity at low temperatures and low conversions, to less than one at low to modest temperatures and modest to long holding times, and back to greater than unity at high temperatures. This behavior originates in the dual sites for CO release and the relative kinetics of carbonyl, ether, and guaiacyl pyrolyses.

### 1.9.2 Liquid Products

The present version of the model accounts for only two components of the aqueous distillate, water and methanol. Simulation water formation occurs predominantly through saligenol-type unit dehydrations. Cinnamyl alcohol side chains provide less important precursors. Ultimate water yields were rather modest, amounting to 0.05%, 5.3%, 4.4%, and 4.4% at (300C,  $10^4$ s), (400C,  $10^4$ s), (500C,  $10^2$ s) and (600C, 7s), respectively.

Thus, the water yields predicted by the simulation are about 1/3 of the nominal  $15\pm 5\%$  reported in experimental investigations. This discrepancy is significant, and merits later discussion.

An ultimate methanol yield of only about 0.1% is predicted by the simulation model. The single methanol forming pathway simulated is through degradation of cinnamyl alcohol side chain units. These units are rather rare in whole-lignin and the methanol forming pathway of this unit was itself relatively minor. Thus, the simulation model generally underpredicted methanol yields of the order 0.28-1.5% reported in the literature.

### 1.9.3 Phenolic Products

The simulation predicts most of the thirty phenols reported in previous experimental pyrolyses; it also predicts several phenolic products not hitherto reported in the literature. Overall, the product yields are within the band of yields reported in the literature. The simulation predictions will be discussed by phenol types.

#### Guaiacols

Guaiacols arise in lignin pyrolysis through degradations of both the 3-carbon side chain and etherified methoxyphenol substituents. Thus the products coniferaldehyde, guaiacylacrolein, eugenol, propylguaiacol, vinylguaiacol, ethylguaiacol, methylguaiacol, and guaiacol represent various stages of 3-carbon chain degradation. Of these, coniferaldehyde and guaiacylacrolein are the most primary products, degrading to vinylguaiacols, which, in turn, yield methylguaiacols, ethylguaiacol, and guaiacol upon further pyrolysis. These trends are reflected in the simulation predictions. At 400C and 100s the ratios (coniferaldehyde:vinylguaiacol:methylguaiacol:guaiacol) were (0.68: 0.13: 0.088: 0.011), whereas at 500s the proportions were (0.096:0.02:0.26:0.034) and at  $10^4$ s (0.000128:



0.000218:0.03:0.0039). By  $10^4$  s, the data reflect not only 3-carbon side chain degradation of the aldehyde, but also secondary pyrolysis of guaiacols to catechols. Each guaiacol product is both formed and degraded during pyrolysis, and therefore attains maximal proportions at some time.

#### Syringols (2,6-dimethoxyphenols)

With two exceptions, the reactions of syringol compounds directly mimic those of guaiacol compounds. The more important difference is the reaction path degeneracy inherent in syringols, on account of the multiple methoxyl substitution. The second exception involves lignification steric effects, which prevent the formation of biphenyl and phenylcoumaran links in aromatic units arising from sinapyl alcohol monomers. However, the consecutive and parallel nature of the reaction paths generating syringol products is substantially as described above for guaiacols.

#### Catechols

Rather substantial amounts of catechols are predicted by the simulation model, due to the relatively facile demethanation of guaiacol and substituted guaiacols. The catechols are clearly secondary products, favored at long holding times. These generalizations are reflected in the data. At 400 C and 100 s, the proportions (catechol:methylcatechol:vinylcatechol), in weight percent, were  $(5 \times 10^{-4}:4 \times 10^{-4}:6 \times 10^{-3})$ , whereas for pyrolysis to  $10^4$  s the yields were (0.2:1.6:0.012). At 500 C and 10 s holding time the ratios were (0.02:0.15:0.16), changing to (0.38:3.03:0.19) at 100 s. Finally at 600 C the proportions were (0.069:0.54:1.2) at 1 s and (0.86:6.8:1.2) at 7s. Thus, the yields of catechol and methylcatechol increased dramatically with increasing holding time at all temperatures. Note that this contrasts with the corresponding guaiacol yields, which reached maxima at short holding times and decreased monotonically there-

after with increasing time.

### Phenols

Phenols arise from two sources, namely, aromatic units initially derived from incorporation of coumaryl alcohols during lignification, and from the demethoxylation reactions of guaiacol and syringol units. The statistical matching procedure demands that the phenol types be analogous to the guaiacols and syringols. Thus, simple phenol, cresol, ethylphenol, propylphenol, vinylphenol, allylphenol, coumaraldehyde, and hydroxyacrolein all arise as products. The simulated yields of phenol (PhOH) and para-cresols (pCR) were (PhOH,pCR) = ((0.00031, 0.0024), (0.067, 0.55), (0.16, 1.3), (0.39, 3.1)) at temperatures and times of ((300C,10<sup>4</sup>s), (400C,10<sup>4</sup>s), (500C,10<sup>2</sup>s), and (600C,7s). The absolute yields of phenols increased with increasing pyrolysis severity. the greater energy of activation for guaiacol demethoxylation relative to demethylation shifts the higher temperature selectivity toward phenols, even though absolute phenol yields were still lower than those of the corresponding catechols.

### Carbonaceous Residue

As depicted by the present model, the carbonaceous residue is comprised of all aromatic units involved in interunit bonding. It should be characterized by higher concentrations of the refractory phenylether and diphenylmethane linkages than the initial lignin. Further, its methoxyl content should be markedly reduced relative to lignin due to demethanation and demethoxylation of guaiacyl and veratryl units. Finally, catechol and diquinone moieties should concentrate in the residue.

Carbonaceous residue formation can be interpreted in kinetic terms. Most kinetic analyses of lignin pyrolysis focus upon substrate weight loss, a reasonable operational definition of global lignin reactivity. In

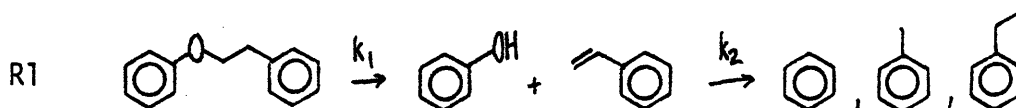
the present simulation, single ring aromatic units, light liquids, and gases can be designated as volatile, and multiple ring aromatics as non-volatile. If the latter group is considered to be 'unreacted lignin', the model then provides a measure of lignin 'conversion'. Figure 9.2 is a comparison between weight loss curves simulated in the present work and the experimental weight loss curves of Iatridis and Gavalas<sup>26</sup>. The experimental and simulated weight loss curves align best at 500 C, with a slight simulation overprediction at 600 C and underprediction at 400 C; overall agreement is within about  $\pm 10\%$  of the lignin.

### 1.10 Discussion

Two aspects of the present results merit discussion, namely the mechanisms of the experimental model compound pyrolyses and the application of the model pathways to simulate whole-lignin pyrolysis.

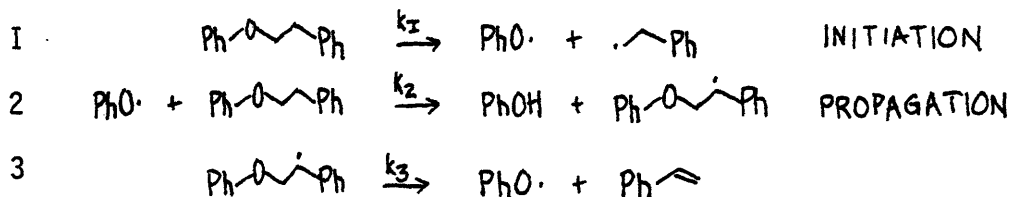
#### 1.10.1 The Mechanism of Phenethyl Phenyl Ether (PPE) Pyrolysis

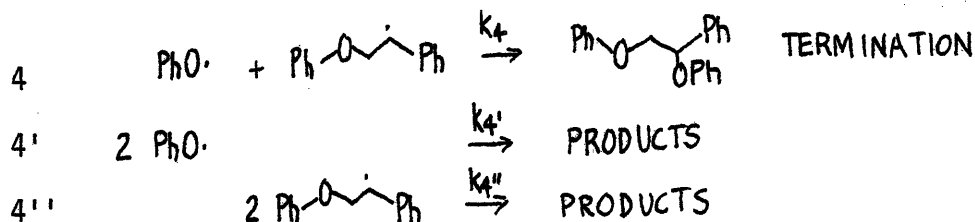
The relatively clean pyrolysis of PPE to phenol and styrene, earlier described in section 1.7.1, suggested an overall pathway of the type R1:



We attempt to interpret PPE pyrolysis in terms of both a free radical chain mechanism and a pericyclic retroene mechanism.

For neat PPE pyrolysis, a Rice-Herzfeld type of radical chain mechanism that yields the observed phenol and styrene products is:





Invoking the steady state hypothesis for the radical species<sup>175</sup>, and assuming long kinetic chain lengths, an overall PPE decomposition ex-

$$\begin{array}{l}
 5 \quad -dE/dt \approx k_2[\text{PhO}\cdot][E] = (2k_2k_3k_I/k_4)^{1/2} \cdot E \\
 5' \quad -dE/dt \approx k_2(2k_3/k_4)^{1/2} \cdot E^{3/2} \\
 5'' \quad -dE/dt \approx k_3(2k_I/k_4)^{1/2} \cdot E^{1/2}
 \end{array}$$

pression can be derived. The kinetic expressions (5) are seen to depend upon the dominant termination step assumed, with steps (4), (4)', and (4)'' respectively yielding decomposition orders of 1, 3/2, and 1/2 in PPE.

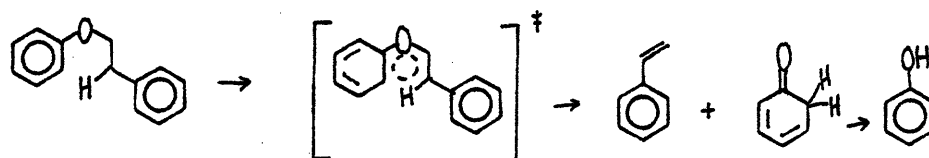
(Note  $E \equiv \text{PPE}$ ) The experimentally observed order of 1 in PPE would thus imply cross-coupling (4) to be the major termination step. If this is so, then, from (5), the observed rate constant should equal  $(2k_2k_3k_I/k_4)^{1/2}$ . Estimated thermochemical parameters<sup>169</sup> for the elementary reactions 1, 2, 3, and 4 are  $(\log_{10} A, E^*) = (17.0, 70.0), (9.0, 15.0), (13.0, 25.0)$  and  $(9.0, 0.0)$ , respectively. From them, the kinetic expression (5) provides first order Arrhenius parameters of (15, 55). These parameters differ significantly from the present experimental Arrhenius parameters of (11.1, 45.0), although at 400 C the estimated rate constant  $\log_{10} k = -2.9$  is within half an order of magnitude of the experimental value of  $\log_{10} k = -3.5$ .

Further, a free radical chain such as (1)-(4) should be affected by a hydrogen-donor such as tetralin. The tetralin could cap the chain carrier radicals, hindering propagation. In the limit of infinite PPE

dilution in tetralin, the 'chain' would essentially be reduced to one of initiation only, i.e., the unimolecular fission of PPE to phenoxy and ethylbenzene radicals as the rate determining step. Such a unimolecular fission should proceed with an activation energy at least as great as the bond strength, which is of order  $70 \pm 5 \text{ kcal/mol}$ ;<sup>169</sup> too, the accompanying transition state would be 'loose', resulting in  $\log_{10} A > 13.5$ . Experimentally, ether pyrolysis kinetics were unaffected by tetralin, and the observed Arrhenius parameters of  $(\log_{10} A, E^*) = (11.1, 45.0)$  were strongly different from those predicted for unimolecular ether fission.

In summary, the long chain free radical mechanism represented a plausible possibility that did not accord with the present experimental observations.

A concerted pericyclic mechanism for the observed pathway R1 is:



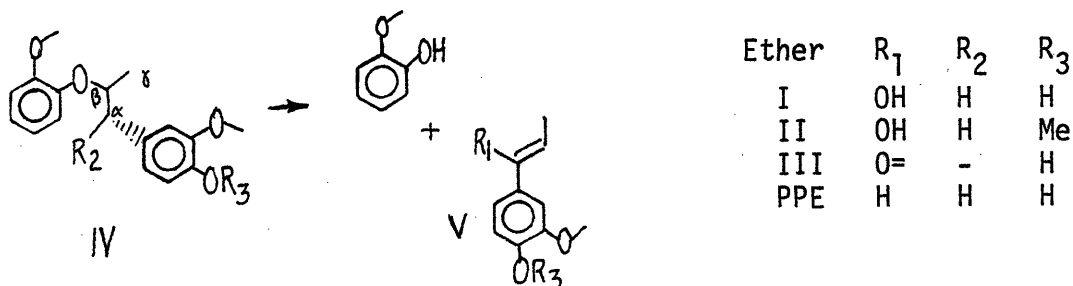
where a coiled form of the substrate PPE undergoes a retro-ene reversion; hydrogen tautomerism in the carbonyl intermediate fragment then regenerates the aromatic phenol. Such a PPE reversion to phenol and styrene should be unimolecular, exhibiting first order kinetics. The transition state of this pericyclic pathway should be 'tight', i.e., ordered, making  $\log_{10} A < 13.5$ . Further, as for most pericyclic reactions<sup>170</sup>, the decomposition should be relatively insensitive to solvent effects. Hence, tetralin should exert little overall effect on a PPE pyrolysis proceeding via a retro-ene mechanism. The experimental observations of the present work accord quite well with the postulated retro-ene mechanism.

By the principle of microscopic reversibility, the forward and re-

verse reactions must share a common transition state. If PPE reversion in fact occurs by the pericyclic mechanism postulated above, then the reverse reaction should occur with Arrhenius parameters characteristic of an ene cycloaddition. Estimation of thermochemical parameters for PPE<sup>169</sup>, coupled with those for phenol and styrene, yields thermochemical parameters of  $(\Delta H^{\circ}_R(\text{kcal/mol}), \Delta S^{\circ}_R(\text{cal/molK})) = (11.3, 33.8)$  for the reversion reaction. These may be combined with the experimentally determined forward activation parameters to yield the reverse cycloaddition parameters  $(\log_{10} A(1/\text{mol s}), E^*(\text{kcal/mol})) = (5.9, 35.9)$ . These reverse Arrhenius parameters agree well with those of typical bimolecular cycloaddition reactions<sup>167,171</sup>.

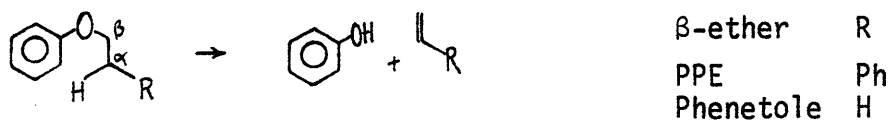
In summary, a pericyclic retro-ene mechanism accords with the present experimental results for PPE pyrolysis.

It is instructive to consider some previous  $\beta$ -ether pyrolyses<sup>75,76</sup> in light of the present experimental and mechanistic findings for PPE. The investigation of Domburg<sup>75</sup> was previously described in section 1.4.2. DTA pyrolysis of three substituted  $\beta$ -ethers, I, II, and III (see page 18) gave product spectra consisting of guaiacol, methyl-, ethyl-, and propyl-guaiacols, cis- and trans-isoeugenol, traces of eugenol, vanillin, and acetovanillone; the latter two formed in much larger quantities from III than from I. The large predominance of guaiacol product, in their case, is completely analogous to the large yields of phenol obtained from PPE, inasmuch as their reactions may be viewed as:



with appropriate modifications of structure V when emanating from ether III. Thus it is evident that guaiacol should predominate from pyrolysis of I-III, just as phenol was found from PPE. For pyrolysis of I and II, the co-product V can be visualized to suffer dehydration to yield the isoeugenols. For pyrolysis of III, co-product V can be envisioned as a facile precursor to vanillin and acetovanillone. Hence, formation of co-product V is rather analogous to the production of styrene from PPE. Further, the methyl-, ethyl-, and propylguaiacols can arise from V in much the same way that benzene, toluene, and ethylbenzene arose from secondary pyrolyses of styrene. Thus, the product spectra of Domburg can be almost completely accounted for by analogy to the present PPE results.

It should be further recalled that for Domburg's  $\beta$ -ethers, the temperatures for 50% weight loss were in the order I(280C)<II(300C)<<III(365C). The present work also provides a rationale for these observations. Thus, the pericyclic reversion mechanism is available to both I and II, but unavailable to III, for lack of an H substituent R<sub>2</sub> in III, which shifts in the retro-ene step. Thus, I and II may easily participate in a concerted retro-ene reaction of the type postulated for PPE, whereas an alternate, higher energy pathway is required for III. Possible higher energy pathways for III could involve direct scission of the  $\beta$ -carbon and oxygen atoms of structure IV, or a phenetole-type ether reversion involving the  $\gamma$ -carbon of structure IV. Phenetole is structurally similar to PPE, differing in phenyl substitution at the  $\alpha$  carbon, as shown below:



Phenetole degradation has been studied by Benjamin, et al.<sup>78</sup>, who report 5% substrate decomposition in tetralin after one hour at 400 C. Major

pyrolysis products included phenol, ethane, and ethylene. This conversion corresponds to an apparent first order rate constant of  $\log_{10}k(s^{-1}) = -4.85$ , which is over an order of magnitude lower than that for PPE at the same temperature. The  $\alpha$ -phenyl substituent evidently enhances ether reversion considerably. The data of Savinykh<sup>76</sup>, described earlier in section 1.4.2, also show that phenyl substitution enhances the pyrolysis of  $\beta$ -ethers.

### 1.10.2 Simulation of Lignin Pyrolysis

Discussion will begin with consideration of those literature citations which allow comparison with results of the present simulation. Overall yields of gas, liquid, phenolic and carbonaceous residue product fractions quoted in section 1.9 will be compared both with the literature yields and theoretical maximum limits. Individual product yields will also be discussed.

The matrix in Table 10.2.1 depicts items predicted by the present simulation which can be compared with previous literature. In the rows of this matrix, four major product fractions have been delineated in terms of overall and constituent component yields; the carbonaceous residue fraction subheading labeled 'kinetics' concerns the time dependency of overall lignin pyrolysis. The matrix has six columns, representing our model predictions and five sets of literature references. The latter include the collected reports of Table 4.1, the data of Iatridis and Gavalas<sup>26</sup>, of Kirshbaum<sup>41</sup>, of Domburg<sup>39</sup>, and the DTA/DTG data of Domburg and Sergeeva<sup>129</sup>. In each matrix element, a plus indicates that information relevant to that row was reported, whereas an 'X' implies that it was not. The present simulation provides entries for each row save CO<sub>2</sub> yield. The overall gas fraction is the sum of CO and CH<sub>4</sub>; these are by far the prevalent constituents of the lignin off-gas. The aqueous distillate was composed of water



and methanol only; acetone, acetic acid and other minor liquid products were not included in the simulation. The phenolic fraction was the molar sum of all single ring phenols; this overall yield should correspond best to the overall tar yield reported in pyrolysis experiments. Finally, the carbonaceous residue fraction is composed of all multiple ring aromatic units. The investigations collected in Table 4.1 provide detailed accounts of gas and aqueous distillate yields, and overall tar and char yields. Because detailed temperature-time information is lacking for many of these investigations, entries in this column are best considered the asymptotic, 'ultimate', yields of destructive distillations. The data of Iatridis and Gavalas<sup>26</sup> were obtained in a reactor designed to emphasize primary reactions, providing detailed temperature-time information and entries for all save overall aqueous distillate yields and water yields. Kirshbaum<sup>41</sup> provided overall gas, phenolics, and carbonaceous residue yields; detailed phenolic product spectra were provided also. Detailed descriptions of phenolic product spectra were also given by Domburg<sup>39</sup>. Finally, Domburg and Sergeeva<sup>129</sup> provide DTA/DTG weight loss information for lignin decomposition.

A numerical summary of the product yields predicted by the simulation and reported in the literature is presented as Table 10.2.2, a matrix completely analogous to that in Table 10.2.1. The discussion to follow considers each row of Table 10.2.2; note that all yields are in weight percent of original lignin substrate.

#### Gas Fraction

The simulated overall gas fraction rose steadily with increasing time and temperature and achieved a value of about 15% at 600 C. This compares favorably with the data of Table 4.1, where gas yields ranged

from about 10-20%. Iatridis and Gavalas report an overall yield as high as 23% at 650 C, but this included 7.2% CO<sub>2</sub>. As discussed below, this rather high CO<sub>2</sub> content may be due to their use of a Kraft lignin. Omitting CO<sub>2</sub>, their overall gas yield is 16%, in good agreement both with the simulation and earlier literature. Additionally, Kirshbaum reports total gas (and losses) yield of ~5% at 250 C and ~18% at 600 C.

Theoretically, the maximum overall gas yield should be a function of temperature. At low temperatures, methoxyphenols prevalently release methane gas; assuming an ideal release of one mol of methane per methoxy unit, a maximum methane yield of ~9% arises. Further, assuming a release of one mol of CO per side chain, a low temperature CO maximum of ~15% arises. At low temperatures, a maximum total gas yield of ~24% by weight of lignin is thus calculated, comprising CH<sub>4</sub> and CO in the ratio 2:3. With increasing temperature, methoxyphenol gas release selectivity shifts toward CO evolution, and thus in the limit of high temperatures, two mols of CO will be produced from each aromatic unit in lignin; a corresponding overall gas yield of ~30% thus arises, composed entirely of CO.



The simulated time-dependency of methane yield at several temperatures was earlier detailed in Figures 9.1a-c. Based on 15% average total gas yields from DTA and destructive distillation of lignin, Table 4.1 provides methane yields of 7.1%. This agrees quite well with our simulated yield of 6.2% at 400 C and 10<sup>4</sup>s. Iatridis and Gavalas reported methane yields of 2.21% at 500 C and 60 s, and 1.3% at 600 C and 10 s. The simulation predicted methane yields of 5.1% at 500 C and 60 s and 6.1% at 600 C and 7s. Thus our simulation overpredicted methane yield as compared to the data of Iatridis and Gavalas. This discrepancy likely arises be-

cause, on the one hand, the pyrolyser of Iatridis and Gavalas was designed to emphasize primary reactions, such that primary products could leave the 'reaction zone' without secondary pyrolysis. On the other hand, our simulation models a batch reactor, where primary products, such as guaiacols, were subjected to extensive secondary pyrolyses, yielding more catechols and methane. Also, Kraft lignins, used in this experiment, are known to have a lower methoxyl content than the simulated spruce lignin substrate; this contributes to the discrepancy between experimental and simulated methane yields.

#### CO

The simulation predicted CO evolution in yields of 0.037%, 3.5%, 4.4%, and 9% at (300C,10<sup>4</sup>s), (400C,10<sup>4</sup>s), (500C,60s), and (600C,7s), respectively. These yields are in substantial agreement with the literature citations noted in Table 4.1. As in the case of methane, simulated CO yields generally exceeded those reported by Iatridis and Gavalas. These workers report 1.2%, 2.1%, 2.7%, and 9.2% at (400C,120s), (500C,60s), (600C,10s), and (650C,120s), respectively, whereas simulated yields were 0.22%, 4.4%, and 9% at (400C,100s), (500C,60s), and (600C,7s), respectively. Interestingly, the experimental CO/CH<sub>4</sub> ratio varied from about 2.3 at 400 C to 0.88 at 500 C and 1.8 at 600 C, which closely accords with the behavior of this ratio in our simulation. This was earlier interpreted in terms of dual carbonyl and methoxyphenol sites for CO release from lignin.

#### Aqueous Distillate

Based on the sum of water and methanol yields, the simulation predicted an overall distillate yield of about 6%, rather lower than the yields of ~15% reported by the literature references in Table 4.1. Water is by far the most prevalent component of the overall aqueous distillate,

with methanol (0.3 to 2%), acetic acid (0.1 to 1.0%), and acetone (0.1 to 1.0%) as minor components. Theoretically, assuming the release of one  $H_2O$  mol per 3-carbon side chain, a maximum water yield of ~10% is calculated. However, aqueous distillate yields higher than 10% are reported in the literature (cf Table 4.1); these are likely due to physically associated water either extant in the plant lignin or introduced during lignin isolation. Another possible source of water is the carbohydrate impurity invariably present in lignin preparations.

#### $H_2O$

Our simulation predicted ultimate water yields of 6%. Absolute water yields have not often been experimentally measured. However, taking account of the minor components methanol, acetone, and acetic acid in the aqueous distillate, an average water yield of 12-13% can be estimated from Table 4.1. The experimental yield is significantly higher than predicted in our simulation, which suggests that the latter requires further sources for water formation in the lignin; kinetic limitations are precluded by the rapidity of saligenol dehydration. Physically adsorbed water and saturated hydroxyl groups are possible precursors for further water yields. The former has already been discussed. As for the latter, formal hydroxyl cleavage could conceivably produce two water mols from guaiacyl-glycerol- $\beta$ -ethers, and thus increase net water formation from lignin to as much as 13%.

#### MeOH

An ultimate methanol yield of 0.1% is predicted by the simulation. This is substantially less than the yields of 0.28 to 1.5% reported in Table 4.1 and the yield of 2% obtained by Iatridis and Gavalas. The reasons for our smaller methanol predictions are not yet clear, and could

involve both kinetic limitations and alternative lignin pathways. With regard to the former, the simulated pathway to methanol was through degradation of cinnamyl alcohol side chains. This reaction was subject to considerable experimental uncertainty and a greater rate constant would increase the predicted selectivity to methanol. Alternative methanol forming pathways, not delineated in the present model compound pyrolyses, may well operate in whole-lignin pyrolysis. This is an area for further experimental investigation. However the experimental results obtained here and reported in the literature<sup>91,96</sup> do indicate that methanol formation from methoxyphenols, the obvious moieties for demethoxylation, is not significant.

#### Phenolic Fraction

The predicted overall yield of single ring phenols ranged from 7-80%. These represent lignin aromatic units that were transformed into single ring aromatics during simulated pyrolysis. Included in this single ring phenol yield are substantial amounts of complex phenols, such as coniferaldehyde and guaiacyl vinyl ketone (or guaiacyl acrolein), which are not often reported with single ring phenols in experimental pyrolyses. Experimental overall phenolic fraction yields were 3 to 30% for Kirshbaum, and 0.2 to 14% for Domburg. These were lower than the simulation for two likely reasons. First, many complex phenols in the tar fraction were not experimentally identified. It is cogent to note that tar yields in excess of 50% have been reported<sup>71</sup>. Second, the simulation suppressed bimolecular condensation and polymerization reactions which would have lowered the yield of single ring phenols.

#### Individual Phenols

As noted earlier, the present simulation predicts most of the

thirty-odd phenols detected in the previous experimental pyrolyses. The accuracy of these individual phenol yield simulations is uncertain, on account of the wide range of lignin types, isolation methods, and reactor configurations employed in experimental studies. These provide a rather generous band for comparison with model predictions. In most cases the predicted and experimental yield data agreed to within a half-order of magnitude. Larger deviations, such as those related to guaiacol, catechol and syringol, could be reasonably explained by inherent differences between simulated and experimental conditions. In particular, it is noteworthy that deviations between the present simulation and experiment were no greater than deviations between individual experiments.

#### Carbonaceous Residue

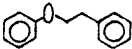
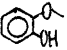
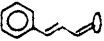
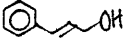
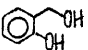
The simulated carbonaceous residue yields of 91% at 300 C and 10<sup>4</sup>s and 40% at 600 C and 7s compare favorably with the literature. In Table 4.1, ultimate tar yields from destructive distillation were 40 to 60% of lignin. Iatridis and Gavalas report weight losses of 20% and 53% at 400 and 600 C, respectively, corresponding to char yields of 80% and 47%. Kirshbaum reports a char yield of 91% at 250 C and only 26% at 600 C. In short, the present operational definition of residue as multiple ring aromatics provides simulated carbonaceous residue yields that are in good accord with the experimental literature.

#### Weight Loss Kinetics

The residue-forming kinetics implied by the time variation of the simulated yield of multiple ring aromatic units have earlier been compared in Figure 9.2 with the data of Iatridis and Gavalas. The simulated weight loss curves accorded well with the experimental weight loss curves, with modest deviations at the lowest and highest temperatures. Furthermore,

these deviations can reasonably be attributed to differences between the respective lignin substrates. Iatridis and Gavalas used a Douglas fir precipitated Kraft lignin, whereas the present simulation was based on Freudenberg's unperturbed "protolignin". Kraft pulping can alter the chemical nature of lignin substantially. It results in increased internal condensations, with the original reactive  $\alpha$ - and  $\beta$ -ether linkages transformed into less reactive diphenyl-methane, ethane, and ethylene linkages; it also introduces carboxylic acid units into the lignin macromolecule. The low temperature reactivity of a Kraft lignin might be expected to be greater than its protolignin counterpart because of facile  $\text{CO}_2$  evolution from the carboxylic acid units. At higher temperatures and conversions, however, the reactivity of a Kraft lignin may well be lower than that of the protolignin since relatively refractory diphenylmethane, ethane and ethylene units have replaced the original reactive  $\alpha$ - and  $\beta$ -ethers. In the light of these assertions it is interesting that Iatridis and Gavalas report  $\text{CO}_2$  yields of 5.9% at 400 C and 120s, and 4.1% at 600c and 10s. These suggest a constant number of easily decarboxylated acid sites in their substrate. Further, these authors' reported weight loss of 20% at 400 C and 120s exceeds our simulated weight loss of 13% by an amount substantially equal to their  $\text{CO}_2$  yield. At 600 C and 10s the experimental weight loss corrected for  $\text{CO}_2$  is ~50%, somewhat lower than our simulated value of 60% on account of the reduced reactivity of their Kraft lignin.

### 1.11 Summary and Conclusions

1. Theoretical analysis of Freudenberg's classical spruce lignin structure permitted the selection of model chemical compounds that would mimic the reactivity of lignin during its thermal degradation. Some of the model compounds chosen, and their attributes relevant to lignoid moieties, were: Phenethylphenylether (PPE) , for the prevalent  $\beta$ -ether linkage: Guaiacol, , for the aromatic methoxyphenol unit: Cinnamaldehyde  and Cinnamyl alcohol , for the propanoid side chain and saligenol, , for the hydroxy enol that might form in lignin following  $\beta$ -ether reversion.

2. Experimental pyrolyses of each of 20 model compounds were undertaken to determine hitherto unknown reaction pathways, kinetics, and activation parameters. The products from these model pyrolyses were closely analogous to those observed in actual lignin thermolysis, including methane (from guaiacol), carbon monoxide (from cinnamaldehyde), water (from saligenol), methanol (from cinnamyl alcohol), and phenol (from PPE).

3. Mechanistic interpretations of pyrolysis pathways were possible in at least five instances. For example, PPE reverted stoichiometrically to phenol plus styrene as primary products; at 400 C the reaction was first order in PPE over a twentyfold range of initial concentrations and unaffected by tetralin dilution; at temperatures from 300 to 500 C, the rate constant followed an Arrhenius relationship, with  $(\log_{10} A(s^{-1}), E^*$  (kcal/mol)) = (11.0 $\pm$ 0.9, 45.0 $\pm$ 2.7). These experimental data were well rationalized by a concerted, pericyclic retro-ene reaction mechanism. Similarly, methane elimination from guaiacol,  $(\log_{10} A, E^*) = (10.9, 43.7)$ , and water elimination from saligenol, (13.4, 33.4), could both be well interpreted as concerted, pericyclic group transfers.



4. It appears that the molecular topology of lignin is well suited to the occurrence of concerted pericyclic reactions, which have not hitherto been mentioned in the lignin pyrolysis literature. Likely examples of pericyclic pathways found in the present experiments included:

- (i) Retroene reversion of Phenethylphenylether.
- (ii) Group transfer demethanation of guaiacols and group transfer dehydration of saligenol.
- (iii) Sigmatropic methyl shifts in anisole and veratrole to o-cresol, the latter with subsequent retroene release of CO and H<sub>2</sub>. An analogous hydrogen shift for guaiacol demethoxylation is likely.
- (iv) Cheletropic extrusion of CO from benzaldehyde, vanillin, and cinnamaldehyde, with calculated reverse carbonylation Arrhenius parameters consistent with those of concerted cycloadditions.
- (v) Diels-Alder cycloaddition reactions for cinnamaldehyde and cinnamyl alcohol side chain units, of the type reported in the literature for styrene and acrolein.

5. Mathematical simulation of whole-lignin pyrolyses, at 300 to 600 C with holding times of 1 to 10<sup>4</sup> s, was achieved by combining a statistical interpretation of lignin structure with experimental results of the present model compound pyrolyses. The outcome of these simulations, expressed in terms of product fractions as a percent of initial lignin, was:

(i) Gas Fraction: Simulated overall gas, methane, and CO yields accorded with previous experimental lignin pyrolyses; respective ultimate yields typically 15%, 6%, and 9% were in quantitative agreement with the literature of Table 4.1. The simulated variation of (CH<sub>4</sub>/CO) ratio with time and temperature further agreed with that recently reported by Iatridis and Gavalas<sup>26</sup>.

(ii) Aqueous Fraction: Simulated water yields were typically about half the reported experimental yields of 12%. Simulated methanol yields were half an order of magnitude lower than the literature yields of 0.3-1.5 %.

(iii) Phenolic Fraction: Simulated overall phenolic yields were generally higher than the literature yields by a factor of two. The simulation accounted for more than thirty individual phenols reported in the literature. Simulated yields of simple guaiacols, catechols, syringols, and phenols, each nominally 2%, were within the band of values reported in the literature.

(iv) Carbonaceous Residue: Simulated curves of weight loss versus time at 400, 500, and 600 C were nearly coincident with the experimental curves due to Iatridis and Gavalas<sup>26</sup> for pyrolysis of a Kraft lignin. Also, the modest disagreements between these curves, at both low and high temperatures, were traced to structural differences between the respective lignin substrates.

## 2.0 Introduction

The increased utilization of biomass and coal resource bases must be accompanied by an enhanced understanding of the fundamental events effecting their processing. The elucidation of these fundamentals should greatly assist in the selection of catalysts, solvents, and process operating conditions for optimal substrate conversion, as well as provide insight into the expected results of operating in regions devoid of experimental details. The objective of this investigation is an elucidation of the important reaction pathways and mechanisms involved in lignin pyrolysis, with an aim toward providing a rationalization and prediction of observed lignin pyrolysis products and kinetics. Compounds selected to mimic the important functionalities and chemical moieties which constitute the lignin macromolecule will be pyrolysed to realize this goal. After a brief discussion of the need for increased biomass and coal utilization, this section will describe the motivation for the choice of the lignin substrate, the process of pyrolysis, and the employment of model compounds for pathway elucidation.

In 1970, the total energy consumption of the United States was about  $70 \times 10^{15}$  Btu, or 70 Q.<sup>1</sup> Of this, the contributions of oil, natural gas, coal, and wood were about 30 Q, 22 Q, 14 Q, and 0.8 Q respectively. Thus, in 1970 coal accounted for roughly 20% of the U.S. energy resource, a figure to be compared to 48% in 1947.<sup>2</sup> The decline in coal and wood use arose because of the appearance of the cleaner, more mobile, and more environmentally acceptable petroleum resource.

However, rising oil prices, turbulent world events, and in particular the 'oil crisis' of 1973 have emphasized the limitation and costs of oil as a feedstock for energy and chemicals. For example, the economically extractable portion of the U.S. oil reserves is presently estimated at 50 billion bbl,<sup>2</sup> which would supply the U.S. for about nine years at present consumption levels. Although economics are certainly variable and overall oil resources exceed 50 billion bbl, these figures emphasize the limited nature of domestic oil reserves and further project either a continual dependence on foreign petroleum or the need for the development of the huge coal and biomass reserves of the U.S. In contrast to oil, U.S. coal resources, approximately 20% of the total world resources, have an energy value equal to about 850 times the U.S. energy consumption of 1970, and those identified and economically recoverable resources total at least 55 times the 1970 consumption figure. Perhaps less certain but nevertheless indicative of a huge resource, Brink<sup>3</sup> estimates that  $5 \pm 3 \times 10^{18}$  Btu are stored annually by photosynthesis, equivalent to one-half the proved and currently available energy from natural gas, natural gas liquids, crude oil, and syncrude from oil. Of course, not all of this stored solar energy is recoverable, but the figure demonstrates the significance of the biomass resource.

Lignin is a major component of this biomass resource system, accounting for up to about 36% of wood by weight, and closer to 40% by enthalpic content. Further, lignin is a major by-product of pulping operations, which dissolved at least 16 million tons of the

substance in 1975. Of this, only a very small part was recovered, the large majority burnt in the pulping chemical recovery units. The combustion gains are marginal, however, as the lignin is associated with large amounts of water. Thus, even waste lignin, in addition to the huge amounts of lignin in U.S. forest reserves, can account for a significant resource.

The U.S. coal reserve is composed of predominantly lignite, subbituminous, and bituminous coals, with a small fraction of anthracite. For example, the respective percentages of these are approximately 28%, 27%, 43%, and 1.3%.<sup>2</sup> In view of the evolutionary linkage of lignin to coal, to be developed later, the high percentage of low rank bituminous and lignitic coals suggest that lignin thermolysis may be relevant to many aspects of coal pyrolysis. Since coal is a heterogeneous substrate, with lignin and lignitic residues intermixed with higher rank elements, the thermal behavior of even a nominally higher rank coal may be strongly influenced by the pyrolysis reactions important for lignin and thus, an elucidation of the pathways and mechanisms of lignin pyrolysis would likely find applications in both biomass and coal thermal processes.

The technologies for processing coal and biomass substrates include combustion, partial combustion, liquefaction, gasification and pyrolysis. Common to these is that chemical reactions are effected at elevated temperatures, where thermal degradation of the substrate can be appreciable and is in fact often an integral phase of the overall process. Thus, pyrolysis insights are applicable to not only

inert pyrolysis, but also combustion, partial combustion, gasification and liquefaction. In short, pyrolysis constitutes an important aspect of any process performed at elevated temperature, desired or not.

As will be developed in Section 3, both coal and lignin are ill-defined refractory substrates which lack an unequivocal chemical structure. Further, the pyrolysis of these yields complex and poorly characterized product spectra, which have eluded unequivocal qualitative or quantitative determination. Thus, it is not surprising that the reaction pathways and mechanisms involved in the pyrolysis of a complex substrate to a complex product spectrum have remained obscure. This motivated the use of model compounds, where the products from pyrolysis of a well defined substrate may be used to infer reaction pathways, kinetics and mechanisms. Even this ideal will not likely be realized in every case, but it is clear that more fundamental insights are to be gained as a result of this simplification.

This investigation will thus examine the thermal behavior of lignin through the selection and pyrolysis of compounds which mimic the essential functionalities and moieties comprising the substrate. Lignin pyrolysis is relevant to thermal processing of both the biomass and coal resource systems, which will likely be extensively utilized for chemicals and energy production as petroleum supplies increase in cost and decrease in quantity.

In particular, the investigation was comprised of three major components. The first of these was a critical examination of lignin and lignin chemistry, with an aim toward discerning likely thermolysis

reaction pathways. This theoretical analysis then suggested strategies for the remaining components. That is, on the basis of the lignin structure analysis, model compounds mimicking the essential reactive units of the whole-lignin substrate were selected and pyrolysed. The reaction pathways suggested by the model compound pyrolysis will then be coupled with the structural analysis of whole-lignin to formulate a mathematical simulation model for whole-lignin thermolysis. Hence, the experimental model compound results were superimposed as suggested by the theoretical analysis in an effort to describe the essential features of whole lignin thermolysis.

The present report is divided in 10 remaining sections. The first of these deals with the chemical and structural features of lignin. An understanding of the chemistry of lignin is indispensable in both the selection of model compounds as well as interpretation of likely reaction pathways. Further, as lignin exists intermixed with other biomass carbohydrates, separation techniques must be effected for lignin isolation. The elucidation of the possible chemical and structural modifications induced by these techniques is essential in interpreting previous lignin pyrolyses, as well as evaluating potential processes for utilization of various lignin types. The relationship between coal and lignin need also be developed, as lignin thermolysis will likely be relevant to thermal operations for coal processing.

The second remaining section will examine previous lignin and lignin model compound pyrolyses, as well as provide a brief comparison

with coal thermolysis. This section will be followed by a delineation of the present approach, which will examine the implications and limitations of the literature, as well as present the experimental and theoretical characteristics of this investigation. These will be followed by sections delineating the experimental and theoretical techniques and results. Finally, a discussion of these results will yield the major conclusions and recommendations for further research, as suggested by the present work.

In short, the investigation will contain theoretical and experimental analyses, results and conclusions, all directed toward describing the essential features of lignin pyrolysis. Each of these requires the development of certain background materials, to be considered next.

### 3.0 Lignin

The design and interpretation of lignin pyrolysis experiments requires an understanding of the chemical and structural details of the substrate. For example, the high proportion of phenols obtained in lignin pyrolysis is well rationalized by the phenolic nature of the substrate. With regard to the present analysis, the theoretical and experimental approach are both entirely dependent upon aspects of lignin chemistry and structure. Thus, this section will consider the principles of lignification as well as resulting lignin structural details, reflected in schematic formula models. The methods of lignin isolation, including those involved in pulping operations, are then



developed, as these generally effect chemical modifications that may be reflected in pyrolysis. Finally, this section will conclude with a consideration of the relationships between lignin and coal, as it is quite likely that the thermal behavior of the former material may shed considerable insight into the thermolysis of the latter.

### 3.1 Lignin Chemistry

The essential building blocks and chemical functionalities comprising lignin are rather well known. These have been elucidated through both laboratory synthesis and degradation studies. The former technique has been greatly enhanced by the isolation of various intermediate products in the lignin synthesis, which will be reviewed here in some detail. An understanding of the chemical moieties which constitute lignin is not only helpful in the interpretation and design of previous and future pyrolyses of lignin and its models, but is essential in the task of modelling or simulating whole-lignin thermal treatment. Additionally, a signal advantage in gleaning coal thermolysis insights from lignin pyrolysis rests in the better fundamental understanding of the chemistry of the latter substrate.

#### 3.1.1 Biosynthesis of Lignin Precursors

A natural phenolic polymer comprising up to 36% of wood, pure lignin is composed of only carbon, hydrogen and oxygen. The ultimate lignin precursors are carbon dioxide and water and this section will

consider the pathway from these to more complex lignin monomers. Carbohydrate production from carbon dioxide assimilation via photosynthesis is the first step in lignin formation. That  $\text{CO}_2$  is eventually incorporated into the lignin has been demonstrated in tracer studies exploiting  $^{14}\text{CO}_2$ , the tracer appearing in isolable lignin biosynthesis phenolic intermediates.<sup>4</sup> The carbohydrates are then converted to the phenylpropanoid amino acids, L-phenylalanine and L-tyrosine through the shikimic acid pathway. This production of aromatic compounds from carbohydrates is a key step in lignification, and is further delineated in Figure 3.1. Continuing, the L-phenylalanine and L-tyrosine are then converted into esters of coumaric, ferulic and sinapic acids, as described in Figure 3.2. These cinnamic acids are then enzymatically reduced to the corresponding alcohols, coumaryl, coniferyl and sinapyl, respectively, which are the 'monomers' of the lignin polymer. The proportion of each alcohol actually incorporated into the lignin varies with the type of lignin produced. Grass lignins are formed from chiefly coniferyl and coumaryl alcohols, whereas softwood or conifer lignins incorporate coniferyl, sinapyl and coumaryl alcohols in 80:6:14 proportions respectively. Hardwood lignins contain a larger fraction of sinapyl units, reflected in an increased methoxyl content.

### 3.1.2 Lignin Growth Mechanisms

Natural lignification can be artificially duplicated by the

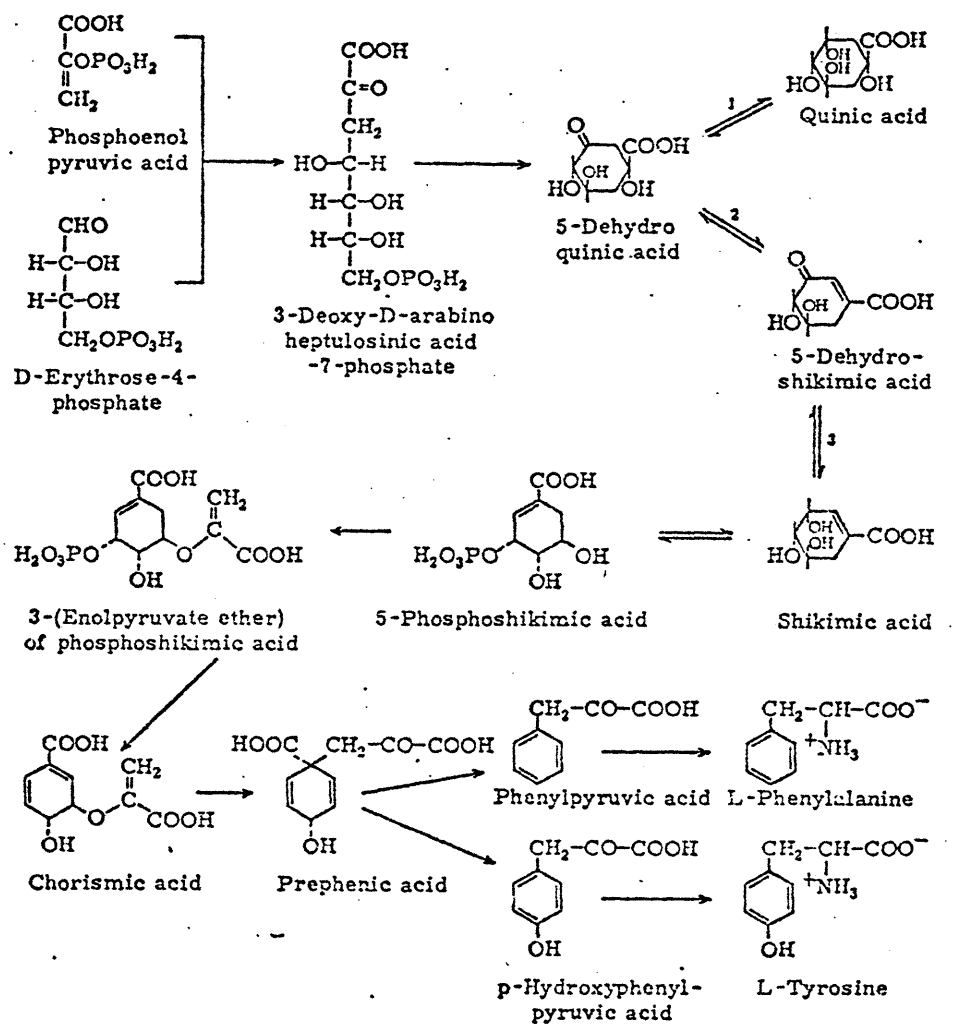


Figure 3.1 Production of aromatics from carbohydrates via the shikimic acid pathway. <sup>4</sup>

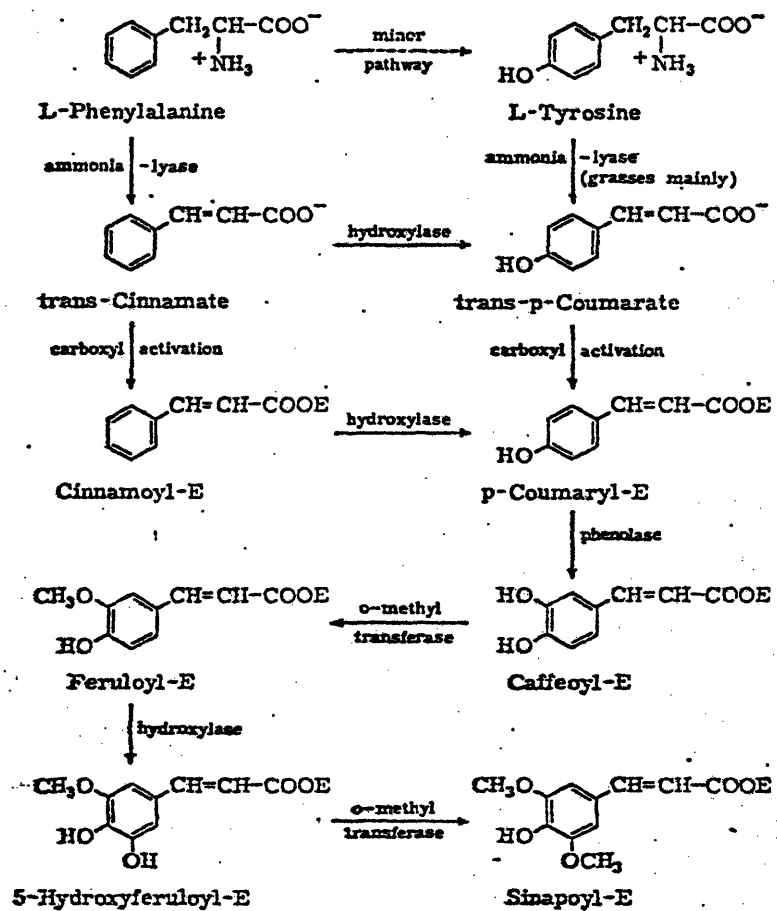


Figure 3.2 Production of esters of lignin cinnamic acids.<sup>4</sup>

enzymatic, oxidative dehydrogenation of the cinnamyl alcohols. The mechanisms and pathways of lignin growth have been ascertained by the isolation of intermediates, termed lignols, of this process. Although natural lignification incorporates all three alcohols to some extent, utilization of a mixture of these in laboratory studies yields an unwieldy set of lignols and is thus self-defeating in pathway studies. Coniferyl alcohol is the ideal monomer for laboratory lignification, since it is the most abundant of those precursors incorporated into the lignin. Additionally, sinapyl alcohol alone will not polymerize, and coumaryl alcohol lacks methoxyl groups. Thus, most of the principles of lignification and many lignin structural details have been gleaned through the interrupted polymerization of coniferyl alcohol. Coniferyl alcohol yields an amorphous polymer very similar to conifer lignin. Over 40 various lignols have been isolated and identified, providing conclusive evidence of the functional groups and bonds comprising lignin. The pioneering work of Freudenberg<sup>4</sup> serves as the classic reference to laboratory lignification.

Under the action of enzymes, likely peroxidase or laccase, the phenolic hydroxyl of a cinnamyl alcohol is converted to a phenoxy radical. Mechanistically, the actual process is the removal of an electron from a phenoxy anion. The radical thus generated enjoys a half life of about 45 seconds,<sup>5</sup> stabilized by resonance as depicted in Figure 3.3.

The major lignification growth mechanism is the coupling of these free-radical species, which yields covalently bonded lignols. However,

# CONFERYL ALCOHOL RADICAL

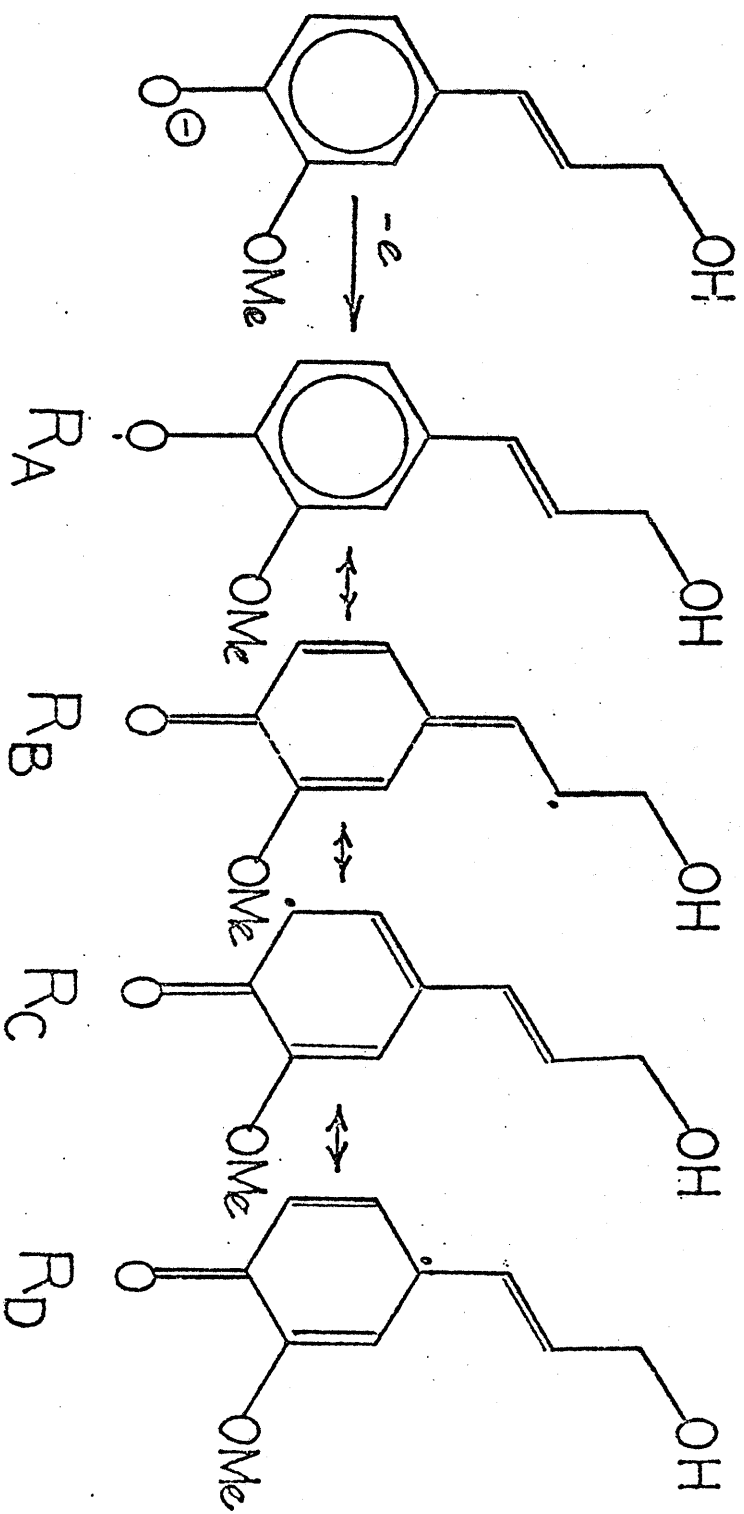


Figure 3.3 Resonance forms of conferyl alcohol radical.

by abstracting hydrogen atoms from other molecules, the radicals can also undergo radical disproportionation exchange reactions. These exchange reactions are the pathways to coniferaldehyde, ferulic acid and other oxidized lignin intermediates, which can in turn experience phenolic dehydrogenation and radical coupling and yield the aldehydic, carboxylic and lactonic groups in lignin. Harkin<sup>5</sup> further notes that the exchange reactions occur with polyphenols as well, and that this reaction must be considered one of the basic principles of lignification. The pathway to molecular weight increase, however, is principally free-radical coupling.

Figure 3.4 depicts some of the lignols isolated and identified from this mode of growth. Referring to the radical forms of Figure 3.3, the combination of an  $R_b$  and  $R_c$  radical yields, after proton tautomerism and phenoxide nucleophilic attack, the phenyl-coumaran structure dehydro-diconiferyl alcohol (I). The pinoresinol structure (II) arises from the combination of two  $R_b$  radicals, again after double prototropy of an intermediate double quinone methide. With respect to the previously mentioned exchange reactions, the dimer representing the formal addition of the  $R_b$  forms of coniferyl alcohol and ferulic acid has been isolated from the laboratory dehydrogenation of pure coniferyl alcohol alone.<sup>5</sup> The resulting structure contains a lactone ring (III), identified in other moieties as well.

A more frequent and perhaps the most important coupling made in lignin growth is the combination of an  $R_a$  and  $R_b$  radical. The resulting quinone methide (IV) does not undergo hydrogen tautomerism, but instead will generally add water in a nucleophilic manner to yield the

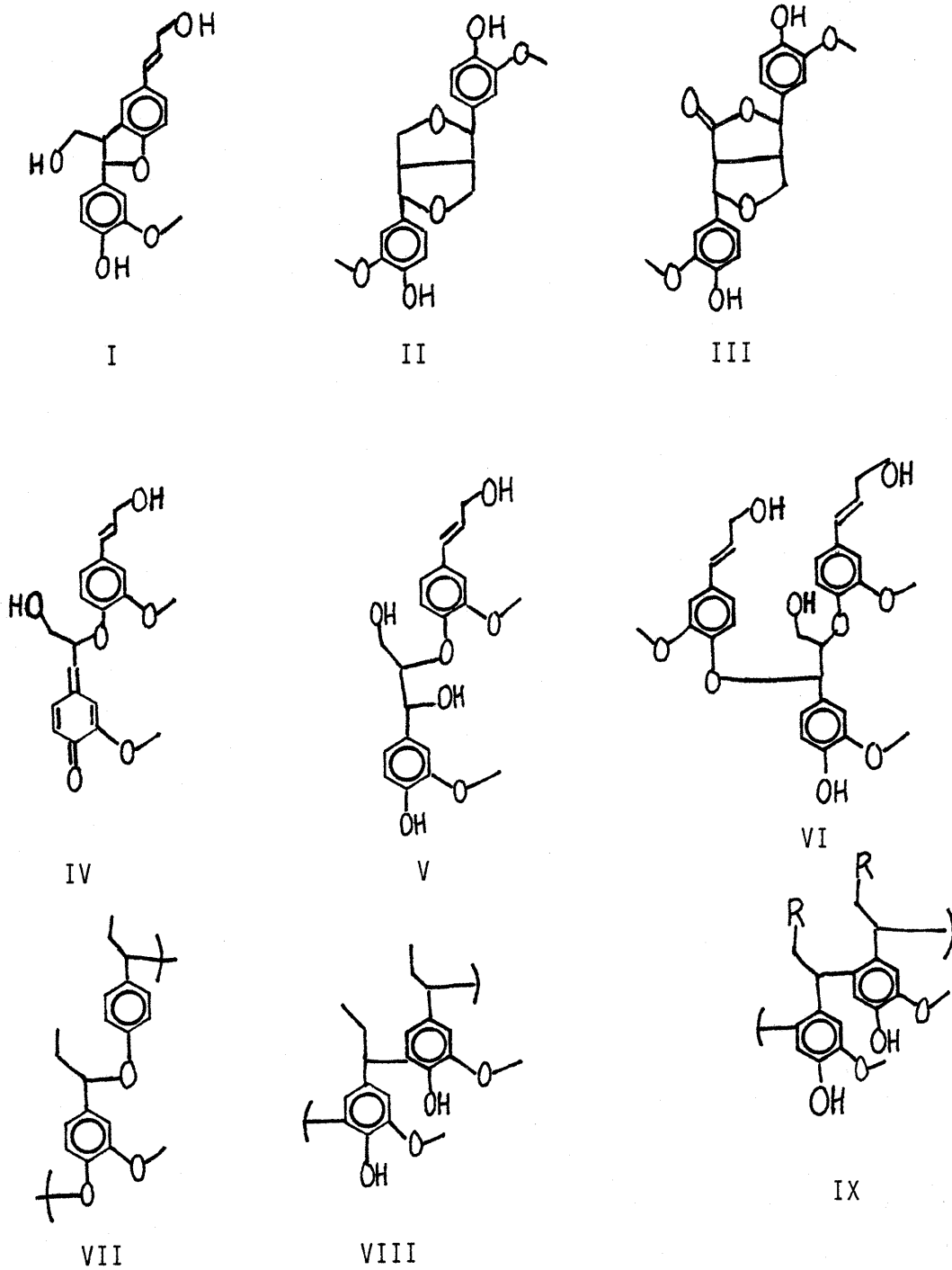


Figure 3.4 Typical lignification lignols.



guaiacyl-glycerol- $\beta$ -coniferyl ether (V). This  $\beta$ -ether bond is the most prevalent link in the lignin macromolecule. The nucleophilic component of this reaction can be varied considerably, ranging from water to the phenoxides of other monomer lignol units. Guaiacyl-glycerol- $\alpha,\beta$ -diconiferyl diether (VI) represents the addition of coniferyl alcohol to the quinonemethide, for example. Plant sugars and polysaccharides are sufficiently nucleophilic to compete for addition to the quinonemethide, representing what is considered to be a main pathway to the formation of lignin-carbohydrate covalent bonds. The linkages of the lignin with other wood moieties is considered in greater detail in a later section. These nucleophilic reactions also effect lignin molecular growth and thus represent a different lignification mechanism, likely the major pathway to branching in the lignin macromolecule.

Lignols involving biphenyl and phenyl ether bonds form as a result of the combination of two  $R_C$  radicals and an  $R_a$  and  $R_C$  radical, respectively. Although these structures are well established lignin moieties, they are rather modest in number when compared with the  $\beta$ -ether and nucleophilic substitution links.

Yet another lignin growth mechanism involves the linear polymerization of the quinonemethides. This polymerization yields the chains of benzyl aryl ethers depicted as structure VII in Figure 3.4. These  $\alpha$ -aryl ethers can rearrange to the diphenylmethane derivatives represented as VIII or IX, and account for a rather small portion of lignin interunit linkages.

### 3.1.3 Lignin Structural Details

Although only a fraction of the identified synthesis lignols have been listed, the major mechanisms of lignin growth have been delineated. More detailed accounts of lignin growth and the lignols involved can be found in the treatises of Freudenberg<sup>4</sup>, Sarkanen and Ludwig<sup>6</sup>, Pearl<sup>7</sup> and Harkin<sup>5</sup>. Of more direct importance to this investigation is a representation of the types and proportions of the moieties and bonds which constitute lignin. This information is conveyed in the schematic structural representation set forth by Freudenberg<sup>4</sup>, which attempts to assemble the information accrued from the synthesis studies with aspects of other lignin research, namely, degradation, elemental composition, and spectroscopic studies. Figure 3.5 is this formula. Not to be interpreted as a literal, unequivocal chemical structure, Figure 3.5 is rather a schematic depiction of the structural insights gleaned from experiment. Thus, while the isolated laboratory lignols are excellent representations of the lignin chemical building blocks, the exact juxtaposition of these is unclear. Harkin<sup>5</sup> draws an analogy between lignin and playing cards, emphasizing the existence of a broader statistical distribution of well known but also well shuffled chemical structures than can possibly be represented in one formula. Only in a limit of infinite statistical sampling, or infinite schematic formula size can the true details of lignin be depicted, and thus the important parameters are bond and moiety types and distributions. The Freudenberg structure describes these as can best be accomplished in 18 units, and is a reasonable account of the statistical and

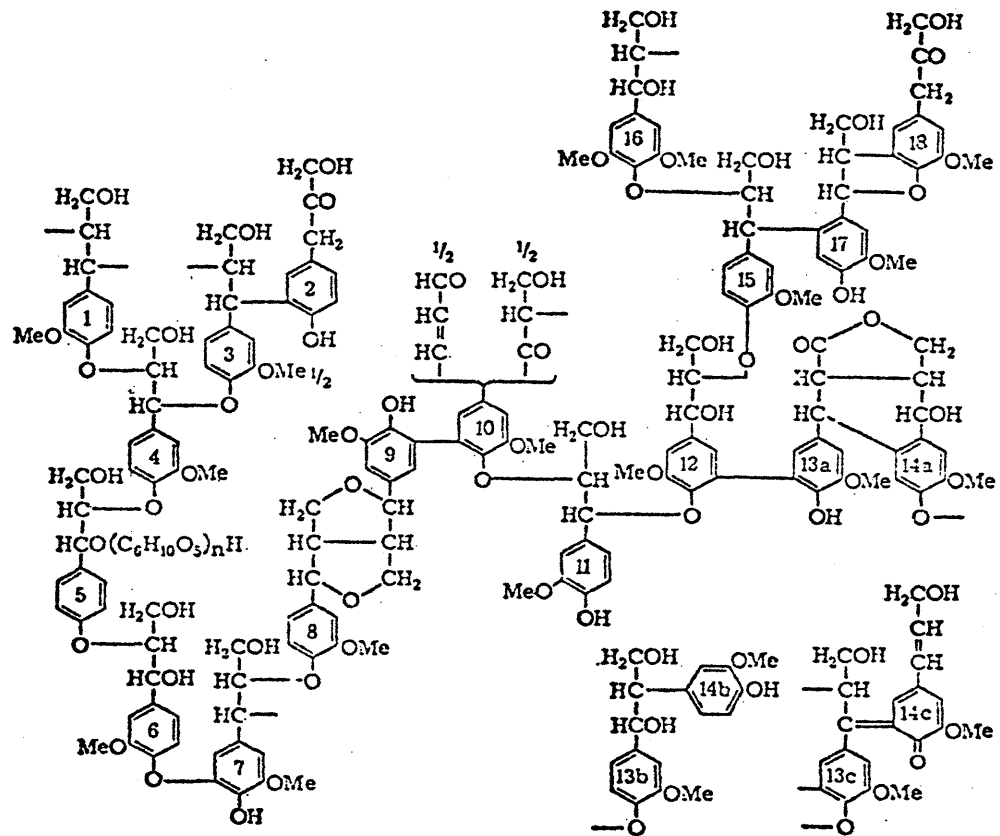


Figure 3.5 Freudentberg lignin structural model.<sup>4</sup>

experimental details, as will be developed below.

With regard to Figure 3.5, the linkage between units 1-4, 4-5, 5-6, 7-8, 10-11, 12-15 and 15-16 is of the  $\beta$ -ether type. This clearly is the single most predominant interunit linkage, in fact accounting for about 40% of the 18 principal linkages. The nucleophilic adducts to the quinonemethide include water (6,12), phenoxide (4,11,15) and the carbohydrate in Unit 5. Note that the bond type of Unit 15 is, in fact, of the diphenylmethane type, arising from the rearrangement of the phenoxide-produced  $\alpha$ -ether, as discussed earlier.

The  $\alpha$ -ether linkage is represented as the linkage between units 3-4 and 11-12, arising through phenoxide nucleophilic attack on the quinonemethide. The diphenylmethane linkage between 2-3, 13c-14c and 15-17, as previously mentioned, is again likely derived from rearrangement of the  $\alpha$ -ether linkage. As depicted in Figure 3.5, however, about 11% of the principal 18 linkages are of the  $\alpha$ -ether type.

Other interunit linkages represented in Figure 3.5 are the diphenyl aryl-aryl link, bonding units 9-10 and 12-13, the phenyl ether bond, depicted with reference to units 6-7, the phenyl-coumaran of 17-18 and the pinoresinol of units 8-9. Units 13a and 14a reflect the presence of lactone moieties in lignin, a conidendrin-type linkage shown here. All of these latter linkages occur in lignin in smaller proportions than the  $\beta$ -ether linkage, and in fact are likely overemphasized in the Freudenberg structure. However, their cumulative content is significant and must be accounted for as constituent moieties of lignin.

A structure such as that presented by Freudenberg invites comparison

with the chemical and elemental data for lignin. Table 3.1 presents the analytical data obtained for a conifer lignin, as well as the same data for coniferyl alcohol and coniferyl aldehyde. Also included in Table 3.1 is a comparison of the distribution of the non-methoxyl oxygen depicted in the Freudenberg structure (in parentheses) with that found directly or indirectly for the spruce lignin. As seen in Table 3.1, the average spruce lignin is closely akin to the coniferyl alcohol and aldehyde in proportions of C, H and O atoms. Further, the distribution of oxygen in the Freudenberg structure is remarkably analogous to the analytical data. Also incorporated into the Freudenberg structure is a coumaryl:coniferyl:sinapyl ratio of 13.9:80.6:5.5, much as suggested earlier for conifer lignins.

For the temperatures of general interest in both industrial and laboratory biomass thermolyses, the essential reactivity of lignin will be located at either the 3-carbon side chain or methoxyphenol units. The essence of this is to realize that below 700-800 C, ring opening reactions of the benzenoid nuclei will be negligible. Thus, while the types and proportions of lignin interunit linkages have been outlined above, important aspects of lignin reactivity lie in the types and proportions of the phenolic and propanoid units implied by these linkages. That is, as a result of lignification, many of the methoxyphenol units have undergone etherification, and the propanoid units have been changed from the cinnamyl alcohol side chain of the lignin monomers. In an attempt to consistently characterize the types and proportions of side chains and methoxyphenol units, Figure 3.6 is the result of a completion of the bond types left undelineated by

Table 3.1: Analytical data for Conifer lignin (4)

	C	H	O	OMe
Average spruce lignin $C_9H_{7.15}O_2(H_2O)_{.4}(OCH_3)_{.92}$	65.08	5.90	29.02	15.60
Coniferyl alcohol $C_9H_9O_2(OCH_3)_1$	66.65	6.71	26.64	17.22
Coniferyl aldehyde $C_9H_7O_2(OCH_3)_1$	67.41	5.66	26.94	17.42

## Distribution of oxygen, except methoxyl

1. On the benzene ring				1.0
2. Fraction of 1: free phenolic OH			0.32 (0.32)	
3. Fraction of 1: etherified phenol			0.66 (0.67)	
4. Fraction of 3: benzyl aryl ethers			0.17 (0.18)	
5. Fraction of 4: benzyl aryl ether, cyclic	0.09 (0.06)			
6. Fraction of 4: p-hydroxybenzyl aryl ether, not cyclic	0.02 (0.06)			
7. Fraction of 4: p-alkoxybenzyl aryl ether, not cyclic	0.06 (0.06)			
8. Fraction of 3: alkyl aryl ether, not benzyl			0.44 (0.39)	
9. Fraction of 3: diaryl ethers			0.06 (0.06)	
10. In the side chain				1.4
11. Fraction of 10: aliphatic hydroxyl			1.0 (1.01)	
12. Fraction of 11: primary hydroxyl			0.75 (0.81)	
13. Fraction of 11: secondary hydroxyl			0.25 (0.20)	
14. Fraction of 10: carbonyl			0.20 (0.19)	

## Distribution of oxygen, except methoxyl

15. Fraction of 14: aldehyde	0.03 (0.03)	
16. Fraction of 14: ketone	0.17 (0.16)	
17. Fraction of 10: lactone		0.04 (0.03)
18. Fraction of 10: dialkyl ethers		0.18 (0.11)
19. Total oxygen		2.4

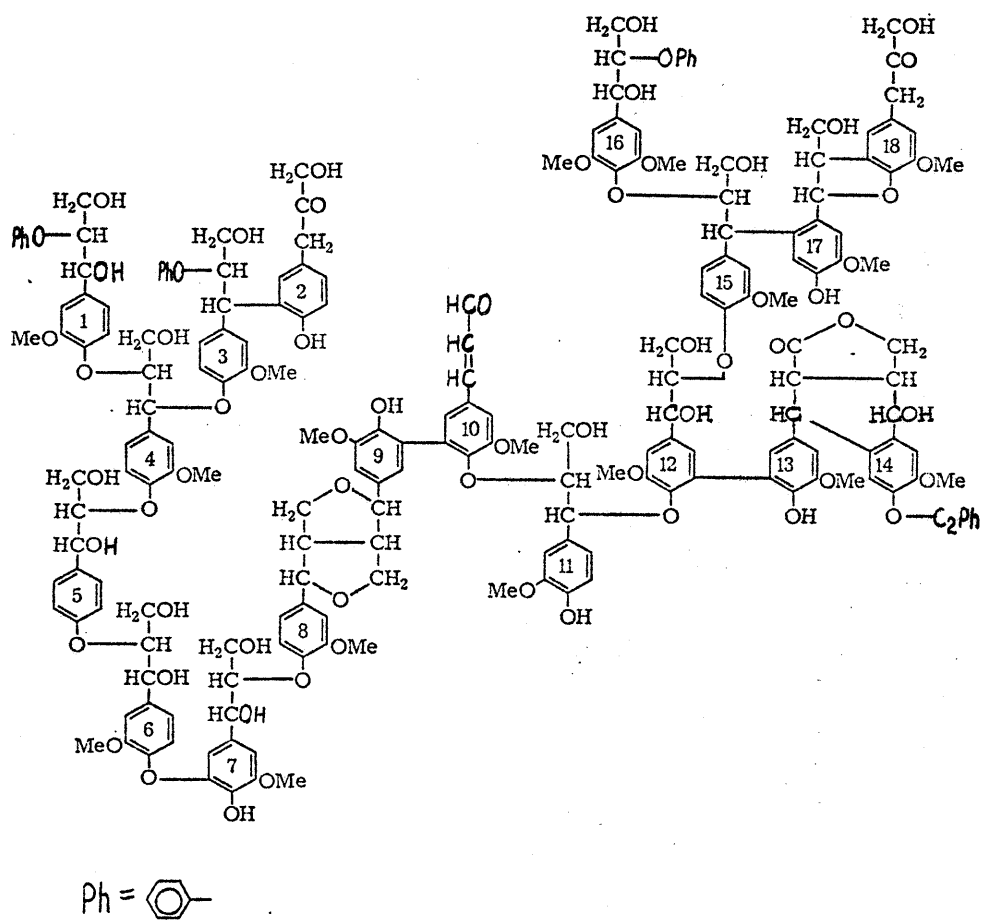


Figure 3.6 Completion of Freudenberg structure as used in the present investigation.



Freudenberg (c.f. units 1, 3, 16 in Figures 3.5 and 3.6), as effected by the present investigators. This introduces no fundamental errors, as the best representation of lignin is neither Figure 3.5 nor 3.6, rather a statistical distribution of propanoid and methoxyphenol types. The distribution of these will be discussed in terms of Figure 3.6, however, in order to provide a pictorial and statistical description together.

Figure 3.7 schematically represents the types of methoxyphenol units depicted in Figure 3.6. The three monomer alcohols are divided into two types, those with free phenolic hydroxyls, and those with etherified hydroxyls. The latter category is further subdivided according to ether type, these being  $\beta$ -ethers,  $\alpha$ -benzylphenyl ethers, phenyl ethers and phenylcoumarans, the latter possibility excluded for sinapyl substrates due to steric hindrance effects. Because of the large percentage of coniferyl alcohol monomer incorporated into the lignin macromolecule, it is clear that free and  $\beta$ -etherified guaiacols account for the largest proportion of the methoxyphenol units in a spruce lignin. The relative amounts of each of the methoxyphenol type depicted in Figure 3.7 will of course vary with lignin type. The most important aspect, however, is that a detailed account of the reactivity of the phenolic units must include not only the behavior of the free phenolic groups, but also the reactivity of  $\beta$ -ethers,  $\alpha$ -ethers, phenyl ethers and phenylcoumarans. The reactivity of these must be simultaneously modelled to integrate to the behavior of whole lignin.

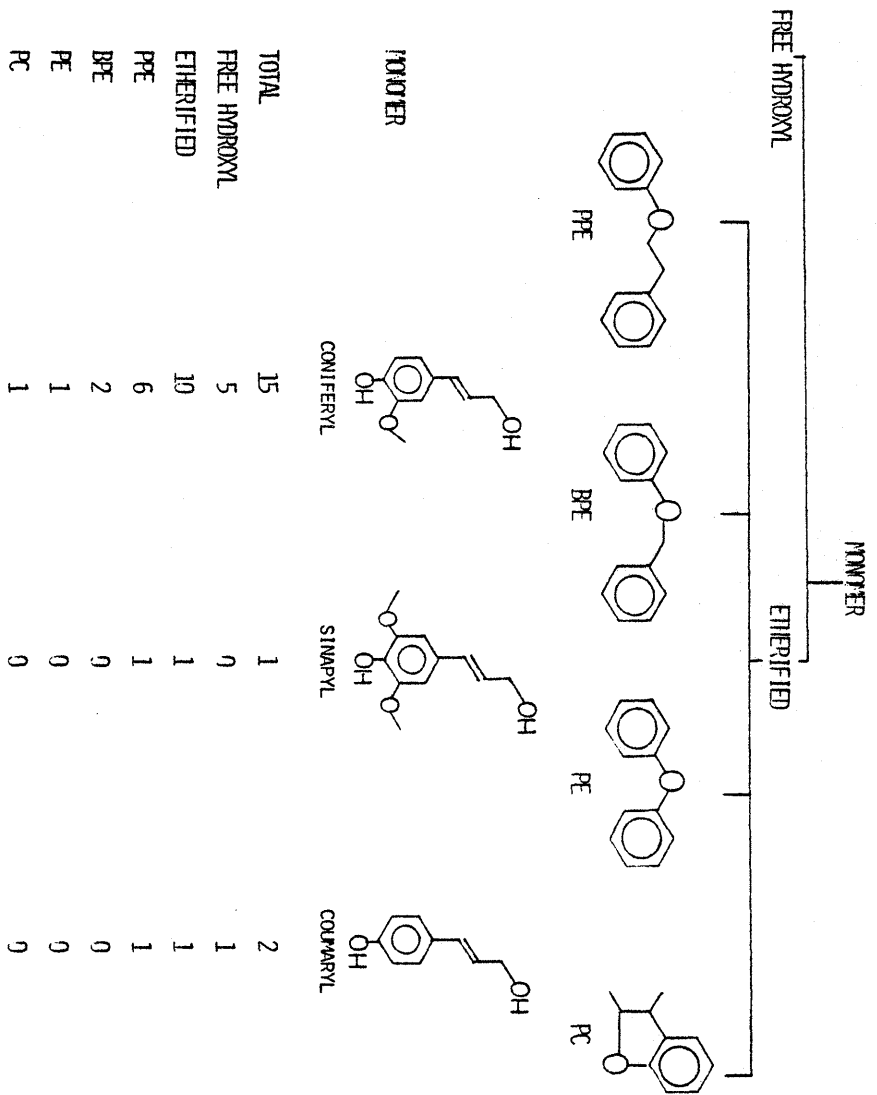


Figure 3.7 Distribution of lignin methoxyphenols as found in the Freudenberg model.

A similar schematic showing the breakdown of propanoid side chains is given as Figure 3.8. In spite of the apparent complexity of the Freudenberg structure, there exist remarkably few types of these side chains. The most prevalent of these is the  $\beta$ -etherified guaiacyl glycerol moiety, accounting for 33% of the units in Figure 3.6. This type of linkage is depicted as the side chain to unit 6, for example. As represented by Structure 2, the side chain reflecting phenoxide attack on the quinonemethide is the next largest in proportion. The resultant side chain is etherified in both the  $\alpha$  and  $\beta$  positions, with a primary hydroxyl on the  $\gamma$  position. As previously delineated, rearrangement of the  $\alpha$  ether link leads to structures of the type Structure 3, a diphenylmethane linkage. Side chains involving this structure are roughly 11% in proportion. Another lignin side chain is of the type Structure 4, a guaiacyl substituted acetone moiety, accounting also for 11% of the side chain units. Structure 5 of Figure 3.8, a free cinnamaldehyde unit, accounts for approximately 6% of the total side chain units. The remaining units are of the type phenylcoumaran and pinoresinol, structures 6 and 7 of Figure 3.8 respectively, the latter structure incorporating two side chain units into one moiety. In short, with small perturbations, the vast majority of the lignin side chain units are of the type represented in Structures 1-8 of Figure 3.8.

It is interesting to examine the methoxyphenol and 3-carbon side chain distributions of Figures 3.7 and 3.8 in light of the monomer radical forms of Figure 3.3. Since the coniferyl, coumaryl and

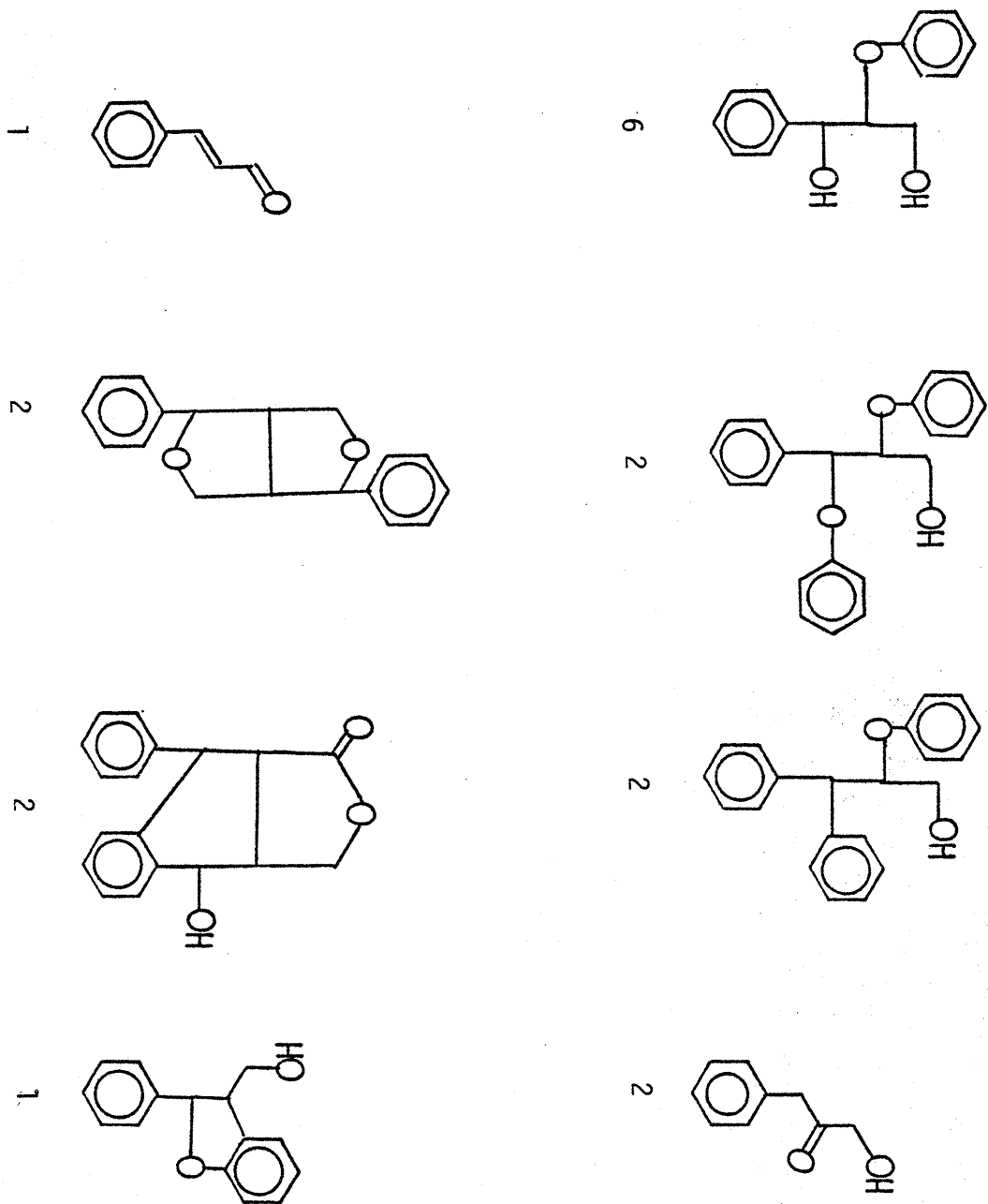
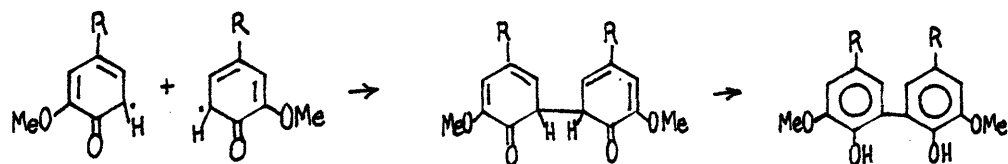


Figure 3.8 Distribution of 3-carbon side chains as found in the Freudenberg model.

sinapyl alcohols are the sole lignin monomer precursors, and the major lignification reaction was one of radical coupling, it is clear that the methoxyphenols and 3-carbon chains in whole lignin must also be described in terms of radical couplings. Figure 3.9 presents a matrix of dilignols formed from the formal coupling of each radical type.

With regard to the methoxyphenols, it is clear that coupling involving radical  $R_a$  will yield etherified methoxyphenols, such as the PPE link of the combination  $R_a-R_b$  or the PE link from  $R_a-R_c$  or  $R_a-R_d$ . Coupling via  $R_a-R_a$  yields the peroxide shown in Figure 3.9 and is not a significant lignin reaction. Thus, coupling involving radical form  $R_a$  is the only direct coupling mode to yield etherified methoxyphenols; however, coupling via  $R_b-R_c$ , followed by intramolecular hydrogen tautomerization, also yields an etherified methoxyphenol, of the phenylcoumaran type. Further, nucleophilic substitution or linear polymerization reactions can also yield BPE type methoxyphenols. However, with regard to direct radical coupling, radical  $R_a$  is the major precursor to etherified methoxyphenols. By difference, it is evident that the forms  $R_b$ ,  $R_c$  and  $R_d$  yield free phenolic methoxyphenols, generated by intramolecular hydrogen tautomerization of intermediate quinone. For example, coupling via  $R_c-R_c$  likely proceeds as shown here, where the



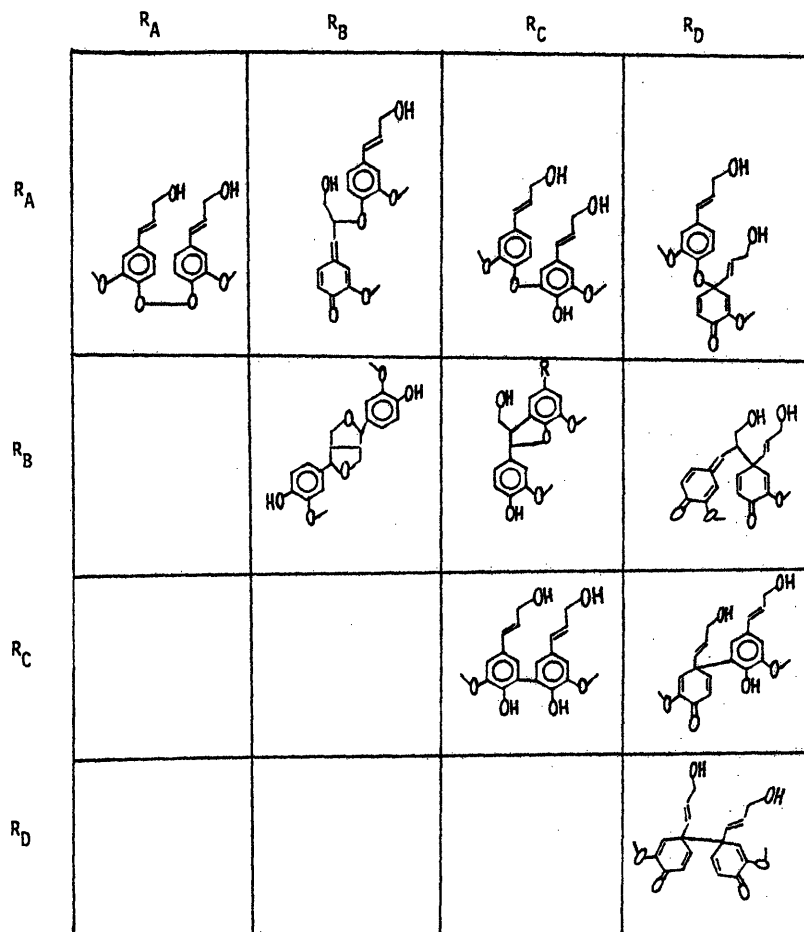


Figure 3.9 Matrix of dilignols arising from coupling of coniferyl alcohol radical forms  $R_A$ - $R_D$ .

biphenol linkage is that observed.

Turning next to 3-carbon side chain moieties, it is clear that radical coupling affects the propanoid side chain in only certain instances. The most important of these is the coupling  $R_a-R_b$ , which generates the quinonemethide, precursor to Units 1, 2, and 3 of Figure 3.8. Thus, nucleophilic hydroxylic attack of the  $R_a-R_b$  adduct yields the guaiacylglycerol- $\beta$ -ether Unit 1 of Figure 3.8, whereas phenoxide attack generates Unit 2. Further isomerization of Unit 2 produces the diphenylmethanes depicted by Unit 3 of Figure 3.8. Coupling of radical forms  $R_b-R_b$  and  $R_b-R_c$  yields the pinoresinol and phenylcoumaran units, respectively, shown in both Figure 3.8 and 3.9. The remaining possible radical combinations which involve the 3-carbon chain are those of  $R_a-R_d$ ,  $R_b-R_d$ ,  $R_c-R_d$  and  $R_d-R_d$ , shown in Figure 3.9. Of these  $R_b-R_d$  is notable, where elimination of the  $R_d$  side chain generates a diphenylethane moiety. However, this coupling mode is rather minor, depicted in very small amounts in the Freudenberg structure. The virtual absence of the other coupling forms involving  $R_a$  likely reflects the steric hindrance of the 3-carbon chain in  $R_d$  coupling. In short, the Freudenberg structure clearly demonstrates the importance of the  $R_a-R_b$  coupling mode, as the thus generated quinonemethide gives rise to structures 1, 2 and 3 of Figure 3.8, which amount to at least 55% of the side chains of Figure 3.6. In fact, this is likely an underrepresentation of the importance of the  $R_a-R_b$  coupling modes. Other coupling modes generate other 3-carbon side chain configurations in modest proportions, while those not involving

the 3-carbon chain generate dimers with intact cinnamyl alcohol units. Of course, these alcohol units are subject to disproportionation reactions, and the dimers themselves are capable of reactions similar to those delineated for the monomers.

A subtle point regarding the interrelationships of the side chain and methoxyphenol units of Figure 3.5 and 3.6 must be clarified. As can be deduced from the mechanisms of lignification, the synthesis reactions of the side chain of a given monomer unit are virtually independent of the synthesis reactions of the guaiacyl units. That is, while the side chain of one aromatic unit may be involved in a lignin linkage with the guaiacyl moiety of another different unit, it is not involved in bonding with a guaiacyl moiety on the same aromatic nucleus. With regard to the Freudenberg structure, this point implies that the side chain of Unit 6, for example, might be accompanied by the guaiacyl moiety of Unit 7, 8 or 3, as well as Unit 6, in proportions related to the probabilities of the given methoxyphenol and side chain unit. This rather random behavior of lignification is due to the availability of lignols as well as monomer alcohols as substrates for molecular growth, as well as the common nucleophilic mechanisms of water, phenoxide and carbohydrate attack on the quinonemethide. Thus, it is quite reasonable that a statistical representation of the available synthesis and chemical data of lignin should provide a complete depiction of the types and proportions of lignin functionalities and moieties.



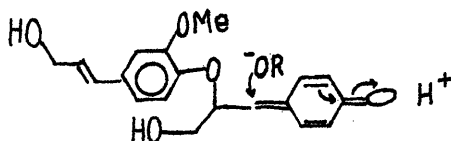
### 3.2 The Isolation of Lignin

Whether for purposes of scientific inquiry or commercial pulping, the goal of lignin isolation procedures is to effect a separation of lignin from the remaining wood constituents, principally cellulose and hemicellulose. This is somewhat distorted for commercial pulping, of course, where the actual goal is to recover the cellulose, not the lignin. The methods used for isolation of lignin are of two general types, those dissolving the lignin for later precipitational recovery or those dissolving the carbohydrate, leaving a lignin residue. Inherent in these methods are several shortcomings, including lignin yields of less than 100%, carbohydrate impurities in the product lignin, and chemical modification of the lignin effected by the isolation procedure. Thus, an interpretation of experimental lignin pyrolysis data or a proposal for use of lignin pulping residues must account for the effect of lignin isolation method. The various procedures for lignin isolation as well as the chemical modifications resulting from pulping operations need thus be considered. The essence of all isolation procedures is a disruption of the lignin-carbohydrate bonding forces, and it is therefore logical to consider the chemistry of the lignin-carbohydrate linkage prior to a discussion of the processes used to destroy it.

#### 3.2.1 The Lignin Carbohydrate Link

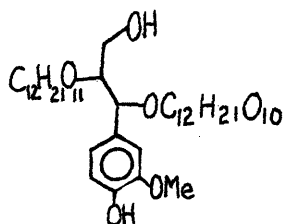
The exact nature of the bonding forces between lignin and carbohydrates is not unequivocally elucidated, yet it is reasonably well

confirmed that lignin is not only in an intimate physical admixture with carbohydrates, but that these are linked by actual covalent bonds as well. Hydrogen, acetal, ketal, ester and ether bonds are all generally believed to be present. As earlier discussed in regard to the mechanisms of lignification, a probable point of lignin-carbohydrate bonding is in the  $\alpha$ -position of the phenyl-propanoid side chain. The quinone methide structure (cf Fig.3.9) will not experience intramolecular hydrogen tautomerism, but rather suffers nucleophilic attack as demonstrated here:



The addition of water yields the common guaiacyl-glycerol structure, yet laboratory experiments have demonstrated that sugars and polysaccharides can add in this manner, providing a stable, covalent link.

Another type of lignin-carbohydrate bond obtained in model compound experiments is the guaiacylglycerol- $\alpha$ ,  $\beta$ -disucrose ether, with structure:



Isolation of this compound from coniferyl alcohol and sucrose alone is indicative of radical abstraction and exchange reaction.<sup>5</sup>

Other types of lignin-carbohydrate bonds are listed and discussed by Harkin<sup>5</sup>, who also notes that ester bonds between the lignin and

polysaccharides are likely formed through the nucleophilic addition of the carboxylic acid groups of plant uronic acid residues onto the p-quinonemethides.

The matter of the lignin-carbohydrate linkage is a subject of considerable uncertainty and debate. In short, it is likely that both physical and chemical forces are involved, the strongest of these being the quinonemethide-related ether bonds. Other weaker bonding forces are likely hydrogen, acetal, ketal and ester linkages. Disruption of these is the key to separation of lignin and carbohydrates, a non-routine task as evidenced by the preponderance of methods and recipes.

### 3.2.2 Lignin Isolation Methods

#### Milled Wood Lignin (MWL) or Bjorkman Lignin

Currently the best method of lignin isolation available, a process pioneered by Bjorkman<sup>179</sup> yields a product termed Milled Wood Lignin. Modifications of the original procedure have been suggested, but the essence of the process remains intact.

To achieve degradation of the cellulose microfibrils in the wood cell walls, wood meal is first ground dry, and then ball milled in a toluene milling medium. The wood is then stirred for two hours in a dioxane-water mixture to effect dissolution of the crude MWL. The preparation is then purified by precipitation of a 90% acetic acid solution into water. A final purification of the product is achieved by dissolving the MWL into a 1,2 dichloro-ethane or ethanol mixture followed by precipitation into ethyl ether.

The Bjorkman process nominally produces a MWL in up to about 50% yield of the plant lignin, with carbohydrate impurities ranging from 2% up to 8%. There is some question as to whether a product in 50% yield is entirely representative of the total lignin mass. Further, potential influence of the carbohydrates on lignin reactions must be accounted. A distinct advantage of the method, however, is that the lignin suffers little chemical modification of the type induced by strong mineral acids and bases.

#### Brauns Lignin

A precursor to MWL, the isolation procedure yielding a Brauns lignin is also referenced as a 'native' or 'soluble' lignin, due to the mild solvents used for separation. In this method, 100-150 mesh plant material is dissolved with 95% ethanol and precipitated by water. A final purification is achieved by precipitation of a dioxane solution of crude product into ethyl ether. Lignin yields range from 0.1 to 8% of the wood, and as with MWL, carbohydrate impurities are present. The major difference between the Brauns and MWL method is the duration of milling of the latter, as attempts to increase Brauns lignin yields by milling failed due to inadequate milling conditions. In spite of the yield difference the lignins isolated by Brauns and MWL procedures are similar.

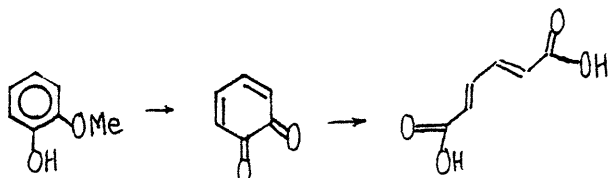
#### Enzymatically Liberated Lignin

A variation of the Brauns procedure involves the addition of brown rot fungus to effect a yield increase. The fungi presumably hydrolyse the lignin-carbohydrate links, increasing

yields to about 13% of the lignin mass.

#### Periodate Lignins

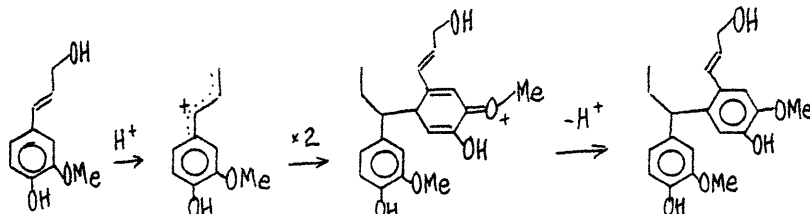
As with the previous solvolysis methods (Brauns and MWL), periodate lignin isolation procedures avoid the condensation alterations induced by strong mineral acids and alkali. However, oxidation reactions, and thus lignin modifications are encouraged. The method converts monosaccharide units to dialdehydes which are susceptible to hydrolysis in boiling water. At least six cycles of exposure to 4.5% aqueous  $\text{Na}_2\text{H}_2\text{IO}_6$  for 25 hours followed by 3 hours of boiling water are required. The lignin modifications are of the type:



with estimates that 20% of the lignin units are modified. Lignin yields approach 30% for spruce wood.<sup>18</sup>

#### Sulfuric Acid or Klason Lignins

The treatment of wood meal with 72% sulfuric acid yields a product termed Klason lignin. The use of mineral acids not only liberates the lignin, but causes further condensation reactions. These condensations proceed through carbonium ion intermediates, of the type,



The lignin product is dark brown due to extensive reactions of this type, and is very unreactive in most lignin reactions. As such it is of

little value in lignin research. However, a large extent of carbohydrate degradation is effected by the sulfuric acid, and large lignin yields are realized. In fact, the Klason isolation method is generally accepted as the standard for quantitative determination of lignin in plants and wood.

#### HCl or Willstatler Lignin

The treatment of wood meal with fuming hydrochloric acid in 40-43%, after hydrolysis, yields an HCl or Willstatler lignin product. The product lignin is lighter in color and less condensed than that from the Klason procedure, for reasons not well known. The HCl lignin has been used in lignin research, but is in fact still considerably modified by reactions of the type delineated for sulfuric acid lignins.

#### Cuoxam, Cuproxam Lignin

The treatment yielding a Cuoxam lignin utilizes the hydrolysing ability of sulfuric acid at milder conditions. The procedure involves alternative treatments of 1%  $H_2SO_4$  for 1 - 2 hours and copper ammonia for 12 hours, the latter removing the polysaccharide components of the wood. The copper ammonia is ineffective without at least partial polysaccharide hydrolysis, realized by the sulfuric acid addition. Reasonably unaltered, carbohydrate-free lignins can be recovered in yields of about 55-80%. As is the case with most lignin isolation methods, variation and modifications of the Cuoxam process abound.

#### Dioxane Acidolysis

A treatment similar to that of Cuoxam lignin involving the use of

dioxane and dilute HCl yields a so-called dioxane lignin. This procedure employs mild hydrolytic conditions in a good lignin solvent, namely a ratio of 9/1: dioxane/dilute HCl. In spite of reasonable yields the product lignins are generally inferior due to a combination of appreciable carbohydrate impurity, condensation reactions and chlorine uptake.

#### Mercapto Lignins

Treatment of wood with thioglycolic acid in boiling alcohol can, after extraction with alkali, yield a thioglycolic acid lignin in yields of 90% of the wood lignin. The product lignin contains appreciable amounts of combined thioglycolic acid groups. The reaction between wood and hydrogen sulfide yields a thiolignin, which is an important reaction in Kraft pulping. Other alkylmercaptans can be used to yield mercapto lignins as well.

#### Alkali Lignins

Only under rather severe conditions will alkali treatments isolate wood lignins. Typically, 5% NaOH at temperatures of 130-170C is used, and precipitation by acid yields a substantially modified lignin. The reaction has important implications in both soda and Kraft pulping processes. The procedure is better suited for grass lignins, applicable at room temperature and yielding therefore a less altered lignin.

#### Sulfite Lignins

Lignin can be extracted by wood digestion in acidic to neutral sulfite-bisulfite solutions. This extraction forms the basis for the sulfite and neutral sulfite pulping processes, and is generally effected at high temperature and pressure. The product lignin, generally

termed a liginosulfonate, will be discussed in greater detail in a consideration of the major pulping processes.

The methods of lignin isolation all involve compromise. Those methods effecting little change in the lignin structure suffer from yields of less than 100% and, generally, modest amounts of carbohydrate impurities. Questions arise as to the efficacy of the representation of these product lignins to the entire wood lignin. At the other extreme, methods yielding nearly 100% lignin product, such as the Klason procedure, generally are attended by massive condensation reactions rendering the product useless for further reaction. Coupling these effects with the variations of lignins with wood species, and even within a given plant, leaves the generic term 'lignin' devoid of scientific meaning. Thus, the specification of any lignin must include both lignin origin and isolation method, because of the profound structural variations possible. As a corollary to this, it is clear that model compound experiments, devoid of such difficulties, can be applied only in light of the specification of a given lignin, with possible structural variations accounted.

### 3.2.3 Lignin Reactions in Pulping

Table 3.2 is a classification of the processes used for the pulping of wood,<sup>20</sup> which provides on the order of 95% of the raw material for papermaking. While most pulp is in fact produced for the paper industries, a relatively small amount is used for the manufacture of artificial fibers. This pulp is designated dissolving



## Classification of pulping processes

Category	Pulping process	Chemical treatment	Mechanical treatment	Pulp yield, % unbleached
<i>Mechanical</i>				
Bolts	Groundwood, cold	None	Grinder	93-98
"	hot	"	"	93-98
Chips	Bauerite, Sprout-Waldron	None or bleach	Refiner	93-98
"	Isogrand	" " "	Defibrator	93-98
"	Asplund	Steam	Defibrator	92-95
"	Mason	"	Steam expansion	80-90
<i>Semichemical</i>				
Bolts	Groundwood, steamed	Steam	Grinder	80-90
"	Decker	Acid sulfite	"	—
"	Fish	Kraft	"	—
"	Chemigroundwood	Neutral sulfite	"	80-90
Chips	Water hydrolysis	Steam	Refiner	70-95
"	High yield sulfite	Acid sulfite	"	60-90
"	High yield bisulfite	Bisulfite	"	60-90
"	High yield kraft	Kraft*	"	55-70
"	Neutral sulfite, NSSC	Neutral sulfite	"	65-90
"	Cold caustic	Alkali	"	80-90
Straw	Mechanochemical	Alkali or kraft*	Hydrapulper	50-75
<i>Chemical</i>				
One-stage	Acid sulfite (Sulfite)	Acid sulfite	Opener or none	40-60
"	Bisulfite	Bisulfite	Opener or none	45-60
"	Kraft (Sulfate)	Kraft*	None	40-55
"	Soda	Alkali	"	40-55
"	Nitric acid (Delbay, etc.)	Nitric acid	"	40-60
"	Organo-solvent (dioxane, alcohols)	Acid in solvent	"	40-60
"	Hydrotropic	Hydrotropic solvents	"	40-60
Multistage	Neutralsulfite-acid sulfite	Neutral and acid sulfite	" (opener)	50-65
"	Bisulfite-acid sulfite	Bisulfite and acid sulfite	" "	40-60
"	Neutral sulfite-bisulfite	Neutral and bisulfite	" "	50-65
"	Bisulfite-carbonate	Bisulfite and carbonate	" "	40-50
"	Acid sulfite-carbonate	Acid sulfite and carbonate	"	30-45
"	Acid sulfite-kraft	Acid sulfite and kraft*	"	30-45
"	Prehydrolysis-kraft	Acid or water and kraft	"	30-45
"	Carbonate-kraft	Green liquor and kraft	"	40-55
Multistage (straw)	Celdecor (Pomilio)	Alkali and chlorine	"	35-45

\*Sodium hydroxide and sulfide.

Table 3.2 Wood Pulping Processes 20

pulp. In spite of the complexity of Table 3.2, those basic processes utilizing chemical action are quite few in number, with variations of the basic process accounting for the scope of the listings. Further, these few basic chemical processes accounted for at least 85% of the total pulp production of 1967, emphasizing their significance. These pulping processes are either soda, Kraft, or sulfite, the Kraft process dominant. In 1964, for example, of 27,722 million metric tons of pulp production, 20,884 were by the Kraft process, 5,093 by sulfite methods, and 1,745 was dissolving pulp.<sup>19</sup> However, the Kraft and sulfite processes each have specific uses and markets, and will likely both be significant future processes, worthy of discussion here.

The goal of any pulping process is to isolate fibrous cellulose by removing lignin and non-cellulosic materials. Chemical reactions are an essential feature of this separation, and of interest here is the effect of these on the lignin structure. The soda and Kraft processes are intimately related, and will be discussed simultaneously. This will then be followed by a consideration of the principles of sulfite pulping.

#### 3.2.3.1 Kraft and Soda Pulping

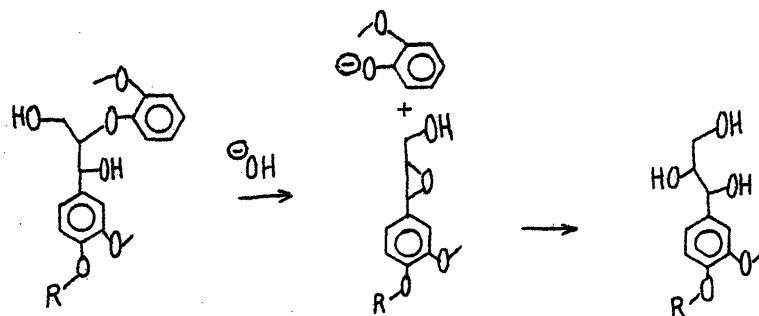
Soda pulping, also known as alkali pulping, effects the separation of lignin and cellulose by alkali cleavage of lignin alkyl-aryl ether bonds. This reaction produces phenoxide anions, which increase lignin solubility in the alkaline solution and thereby enhances lignin

dissolution. It has been observed that the presence of hydrosulfide moieties greatly facilitates these lignin reactions, at the same time effecting little change in the carbohydrate degradation. The resulting pulp is superior in quality, because of the sulfide induced rate increase, but also in part because the sulfur moieties decrease lignin condensation reactions. These decrease lignin solubility and produce a darker product pulp. This pulping process utilizing sulfur is known as the Kraft, or sulfate process. The term 'sulfate' arose because of sodium sulfate addition to the cooking liquor in order to compensate for chemical losses. The sodium sulfate is reduced to sodium sulfide during the combustion part of chemicals recovery. Thus, the essential difference between the Kraft (sulfate) and soda (alkali) processes is the presence of sulfur. The latter process utilizes sodium hydroxide with minor amounts of sodium carbonate, whereas the Kraft process utilizes, in addition to about 1% NaOH and small amounts of  $\text{Na}_2\text{CO}_3$ , sodium sulfide and sulfate, and other process-generated sulfur components.

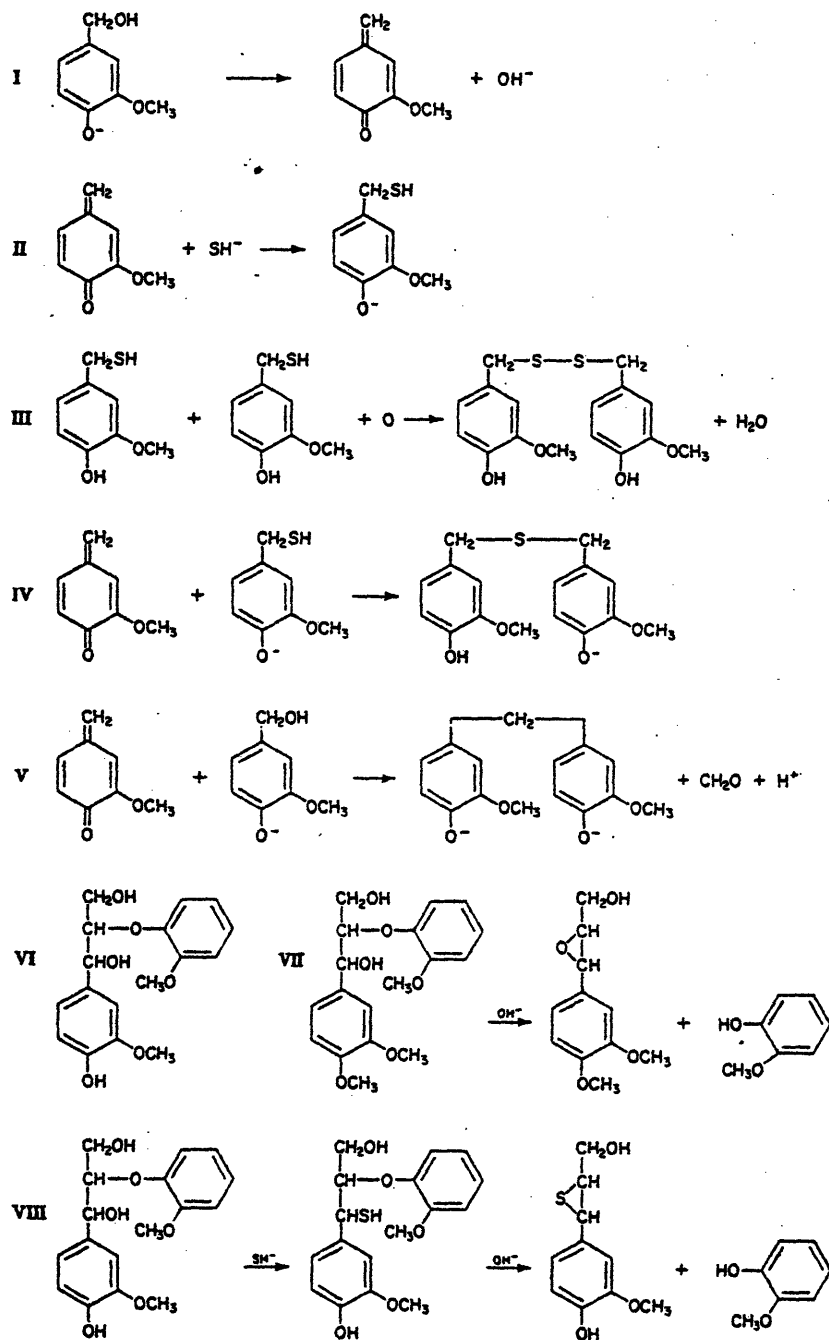
The addition of sulfur increases not only the rate of delignification, but also the eventual yield. This is presumably due to the sulfur induced hinderance of condensation reactions. For example, in a pure alkaline cook at 160 C, the pulp lignin content was reduced to about 5% in 10 hours, whereas the addition of sulfur (25%) lowered the lignin content to 3% in 8 hours.<sup>19</sup>

Model compound experiments have elucidated the major reactions involved in Kraft pulping, and these include alkaline hydrolysis,

mercaptation or sulfidation, condensations, hydrolysis, and demethylations. For example, model compound experiments have shown that guaiacylglycerol ethers with a free benzylic hydroxyl are split by alkali, likely through an epoxide intermediate, as in:



The presence of sodium sulfide resulted in complete cleavage of these units, while 2N NaOH alone effected only 30% rupture.<sup>19</sup> Further experiments demonstrated that the cleavage due to NaOH proceeded through methylene quinone and enol ether structures, while the reaction with sulfur occurred with the formation of sulfhydryl links. A more complete description of the reaction sequences is provided as Figure 3.10 due to Rydholm<sup>20</sup>. Reaction I depicts the formation of the quinone-methide, which in sequence II reacts with the hydrosulfide forming a mercaptan. When the pulping vessel is opened to the atmosphere, oxidation to the disulfide, reaction III, occurs. Sequence IV depicts the reaction of the mercaptan with the quinonemethide, yielding the vanillyl sulfide structure. Reaction IV is in competition with reaction V, the reaction of a benzylic alcohol group with the quinone-methide to yield the diphenylmethane derivative and formaldehyde. Reaction V is likely condensation pathway, and comparison to reaction IV demonstrates the condensation-blocking mechanism of sulfur. The



Model compound reactions illustrating the lignin reactions of alkaline cooking and the role of the sulfide in kraft cooking

Figure 3.10 Typical Sulfate pulping reaction as presented by Rydholm. 20

products of reaction IV are generally believed to regenerate the hydrosulfide and monomer units upon hydrolysis, a reaction very unlikely for a diphenylmethane derivative. Only those compounds with a p-hydroxybenzyl alcohol or alkyl ether reacted with the sulfide, as phenolic etherification rendered the alcohol or ether unreactive. Thus, while guaiacylglycerol- $\beta$ -guaiacyl ether (VI) was reactive toward hydrosulfide, the veratryl analogue (VII) was not.

Another reaction of the sulfide is the demethylation of guaiacyl units to catechol yielding also the corresponding methyl mercaptan. The analogous reaction to methanol and catechol is much slower from NaOH alone. Softwood Kraft lignins contain a methoxyl content indicative of a loss of roughly 0.1 methoxyl groups per monomer. Carbonyl and carboxylic acid groups arise also as a result of Kraft pulping, due likely to hydrolysis of oxidized species or exchange reactions.

Thus, a general mechanism for soda and Kraft pulping may be set forth. In the absence of sulfur, high temperature alkali cleavage of alkyl aryl ether links produce phenolate anions, which in turn increase the lignin solubility in alkaline. Condensation reactions may also occur at the benzyl alcohol groups, which serve to hinder delignification. With sulfide added, low temperature mercaptation occurs at the benzyl alcohol and alkyl ether groups of the lignin, contributing to the dissolution of lignin. Dibenzyl sulfide groups are formed with heating, which serve to inhibit eventual condensations. In the high temperature stage of the cook, alkaline hydrolysis of the 'thiolignin' regenerates the hydrosulfide ions and the hydroxyl degradation products, soluble in alkaline. There is little net sulfur uptake and in many

respects the sulfur acts as a catalyst for bond cleavage and an inhibitor of condensation.

The structural details of a softwood Kraft lignin have been summarized in an idealized schematic representation by Marton<sup>21</sup>. This structure, given as Figure 3.11, depicts the metamorphosis of a softwood lignin as effected by the Kraft process described above. The changes are best noted with respect to the lignin structure of Freudenberg, Figure 3.5. Most notably, Figure 3.11 depicts a sharp reduction in the  $\alpha$ - and  $\beta$ -ether content of lignin. This is a consequence of the alkaline ether cleavage effected for lignin dissolution. The structure is representative of likely condensation products, of the type diphenyl-methane or ethane. The methoxyl content is lower, and the presence of the catechol unit 8 is noted. The carboxylic acid content is much higher in the Kraft lignin, with ketonic carbonyls present as well. Finally, the low sulfur content of Kraft lignin, in the range of 1-3% sulfur or .07-.25/monomer unit is depicted in Unit 1.

In spite of the alterations listed here, the essential Freudenberg-type lignin structure is intact in the Kraft lignin. The structures of Marton and Freudenberg contain many identical moieties, with the basic phenolic monomer unit intact. Hence, with the appropriate structural modifications accounted, model compound pyrolyses should yield insight into the thermal behavior of even Kraft lignin. For example, the Kraft lignin would be expected to yield considerable quantities of  $\text{CO}_2$  as a result of the increased carboxylic acid content.

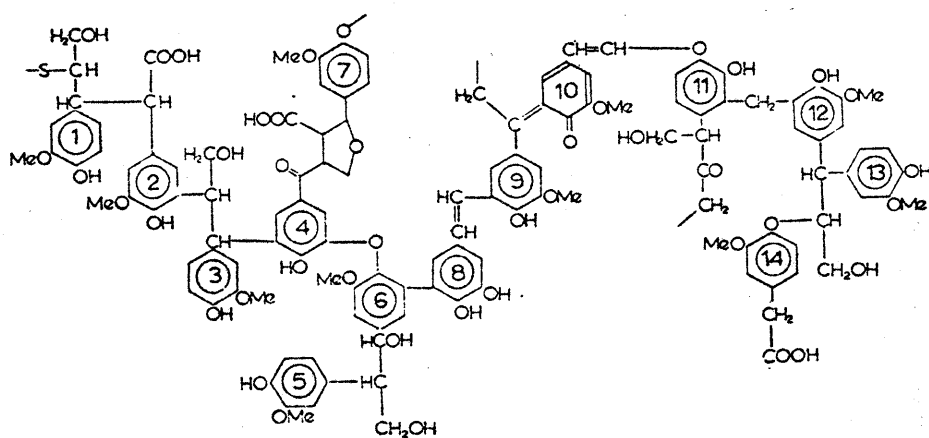


Figure 3.11 Structural model for typical Kraft lignin.<sup>21</sup>



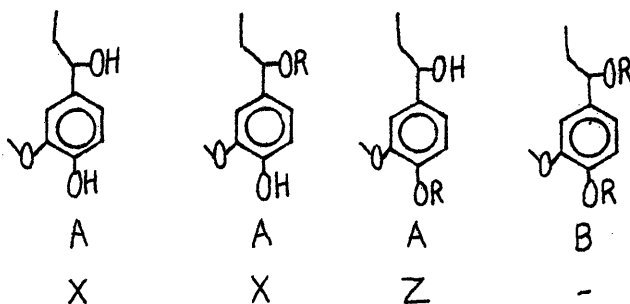
### 3.2.3.2 Sulfite Pulping

Once a predominant pulping method, the sulfite process has lost much ground to the Kraft process. The process effects a dissolution of lignin and other noncellulosic carbohydrates through the action of an important lignin reaction, sulfonation. Various side reactions can be appreciable, including condensation, which hinder lignin dissolution. Finally, the reactions actually effecting dissolution of the lignin are likely both hydrolysis and sulfitolysis.

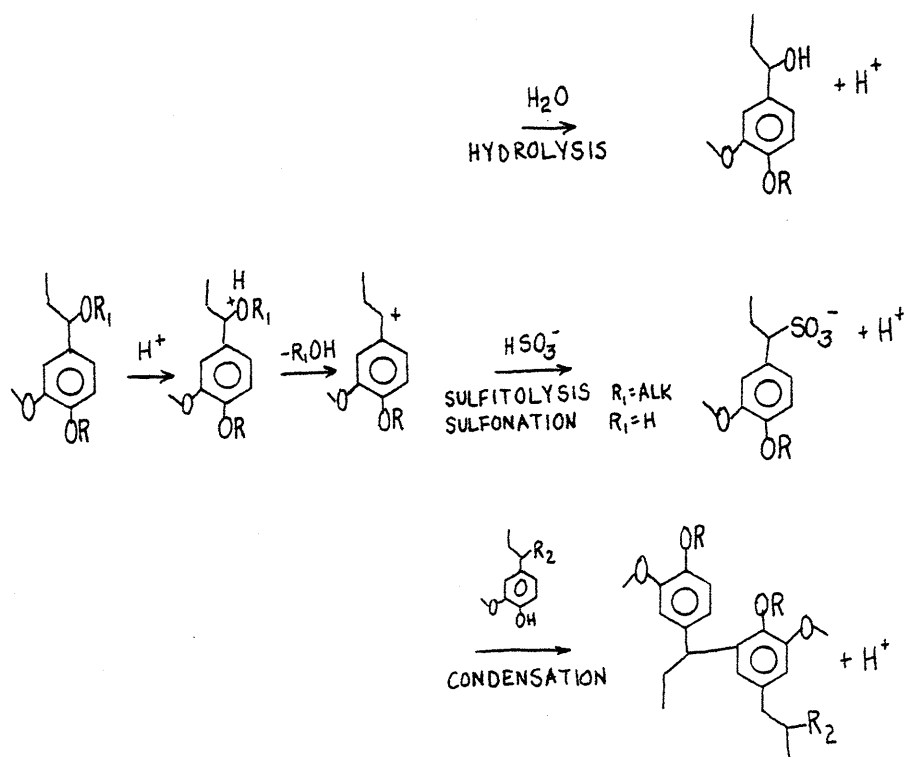
The sulfite cooking liquor is an acid solution of bisulfite in water, with an excess of dissolved sulfur dioxide, and is obtained by reacting a carbonate or hydroxide with  $\text{SO}_2$  and water. The carbonate cation is generally calcium, magnesium, sodium or ammonium. The  $\text{SO}_2$  is dissolved in the water in a hydrated form and accounts for the presence of sulfurous acid and bisulfite ions in the cooking liquor.

As was the case with sulfate pulping, it is generally the  $\alpha$  position of the phenylpropanoid side chain which is the site of sulfonation. These sites can be broadly broken into two groups, A and B sites. The A sites are sulfonatable by neutral sulfite solutions, to an extent reaching approximately 0.3 S/OCH<sub>3</sub>. Model compound experiments suggest that A groups are both 1) free benzylalcohol sites, as well as 2) those  $\alpha$ -ether sites activated by a free phenolic hydroxyl group on the same phenylpropane unit. The remainder of the sites are the B groups, characterized by an etherified phenolic oxygen in the same phenylpropane unit as an etherified  $\alpha$  hydroxyl.

These amount up to .7 S/OCH<sub>3</sub>. The B groups are sulfonatable by an acid cooking medium. If, after sulfonation by neutral sulfite, the wood is hydrolysed, the dissolved low-sulfonated lignin can be further sulfonated in either neutral or acid mediums in amounts up to 1S/OCH<sub>3</sub>. Those B groups made more reactive through hydrolysis are labeled B' groups. The A groups may be further subdivided into X and Z groups on the basis of reactivity. The X groups, about 0.5 in proportion, react very fast in neutral medium and are those  $\alpha$ -ethers and benzyl alcohols with a free phenolic hydroxyl, whereas the Z groups react more slowly and are the phenolic etherified free benzyl alcohol groups. This is made clear by considering the structures of each, namely

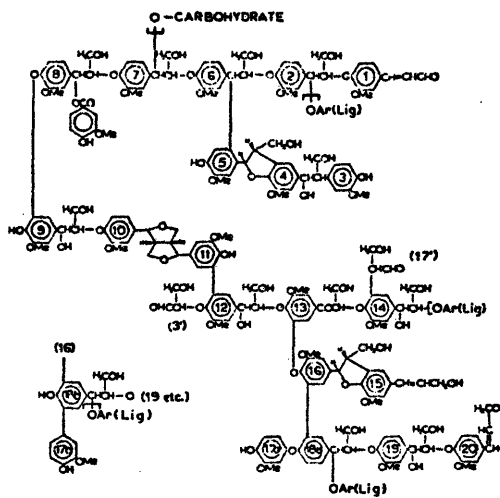


As suggested by the presence of B groups, sulfonation is enhanced by higher acidity. Thus, a likely mechanism for hydrolysis, sulfonation, sulfitolysis and condensation reactions all involve the addition of a proton to the  $\alpha$ -carbon oxygen, as in

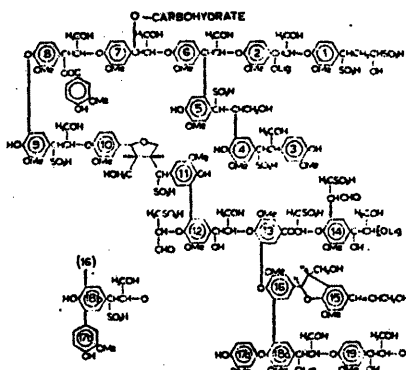


The proportion of each reaction product is a function the ion concentrations, water concentration, and proximity of condensable moieties. Not unexpectedly, a high bisulfite ion concentration decreases condensation selectivity, thereby increasing lignin dissolution. The lignin must be sulfonated to at least about 0.3 S/OCH<sub>3</sub> to become sufficiently hydrophilic for hydrolysis and sulfitolysis to effect dissolution.

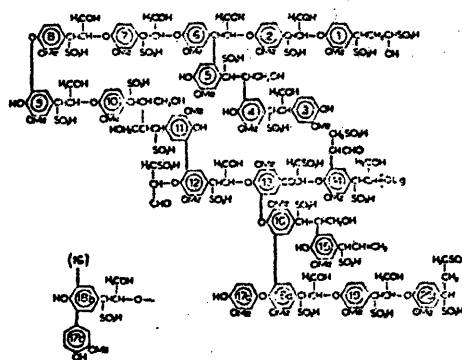
Although other pulping reactions are known to occur, such as the less important formation of loosely combined SO<sub>2</sub> and the thiosulfate reactions, it is not the purpose of this discussion to explore the details of sulfite pulping. Rather, of considerable interest is the effect on the lignin macromolecular of these reactions. Glennie<sup>21</sup>



a) Schematic structure for a segment of spruce lignin.



b) Structural sketch for insoluble lignin sulfonate, formed by sulfonation at pH 6 and 135°.



c) Structural sketch for extensively sulfonated lignin sulfonic acid.

Figure 3.12 Structural models for Sulfite lignins. 22

has presented structural schematics for an unperturbed spruce lignin, a neutral sulfonation lignosulfonate, and an extensively sulfonated lignin sulfonic acid. These are presented as Figure 3.12a, b and c, respectively. Comparison of these demonstrates the nature of neutral and acidic sulfite pulping. With regard to the former, Unit 1 of Figure 3.12b depicts the formation of a disulfonate from a cinnamaldehyde moiety, a reaction not specifically delineated before. The pinoresinol and tetrahydrofuran structures 10-11 and 4-5 have been sulfonated and ring opened. The A-type structures (9,4) are also readily sulfonated in neutral cooks, as has been previously discussed. Figure 3.12c reflects the lignin obtained in extensive sulfonation, indicative of reactions of both A and B units as well as disruption of the carbohydrate bond of Unit 7. The major distinguishing feature among structures 3.12a, b and 3 is simply the degree of sulfonation; the essential Freudenberg structure remains intact, with  $\beta$ -ether bonds, methoxyl groups, and primary hydroxyls in large proportions. This is to be contrasted to the Kraft lignin schematic of Marton, which had a low sulfur content, but depicted few  $\beta$ -ether bonds as well as evidence of significant condensation. Of course, the authors present these structures as schematics based on impressions rather than unequivocal structural information. As such, they are to be interpreted as suggestive of functional groups and chemical moieties likely present in the altered lignin. These impressions may still be exploited in predicting pyrolysis behavior from model compound results.

In summary, any method of lignin isolation, for purposes of experimental inquiry or commercial pulping, yields a lignin of questionable integrity. Generally, those methods associated with a high lignin yield produce the lignin in a highly modified state. Alternatively, those milder procedures effecting little change in the lignin structure produce a low-yield product that may not be representative of the plant lignin. Thus, the prediction or interpretation of the pyrolysis behavior of any lignin necessarily must account for not only the lignin type, but also the structural modifications attendant to the isolation procedure.

### 3.3 Relationships Between Lignin and Coal

Although commercial interest in biomass is reasonably high, economic thermal treatment of coal to obtain fuels and chemicals is of more immediate application. Hence, an important aspect of the elucidation of lignin pyrolysis pathways lies in the relationship of lignin to coal. The chemical constitution of coal is known with even less certainty than that of lignin, and the evolutionary link of biomass to coal suggests that lignin thermolysis insights may in fact be applicable to coals. In order to develop this link more clearly, aspects of coalification and coal models will be considered.

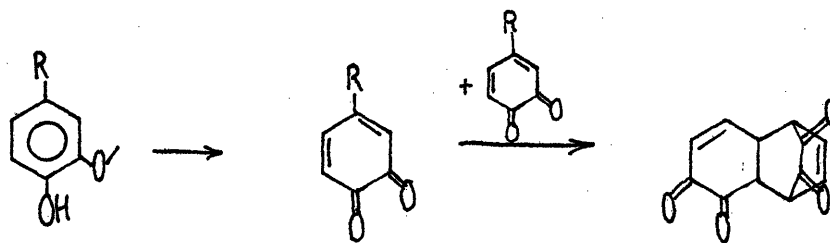
#### 3.3.1 Coalification

A detailed discussion of coalification is provided by van Krevelen<sup>8</sup>. Coal may be regarded as fossilized plant material, evolving from temperature and pressure effects over time. Peat from plant matter became buried under sedimentary matter and converted into lignite or brown coal. Under the influence of mainly thermal effects, the lignite was then converted into bituminous and anthracitic coal.

In 1922, Fischer and Schrader postulated that coal was formed exclusively from the plant lignin, the cellulose experiencing bacterial degradation.<sup>8</sup> As coal is highly aromatic, the phenolic nature of lignin and the non-aromatic nature of cellulose is further suggestive of this view. However, carbohydrate decomposition products, such as reactive keto acids, are thought to aromatize under coalification conditions, suggesting that cellulose may in fact partly function

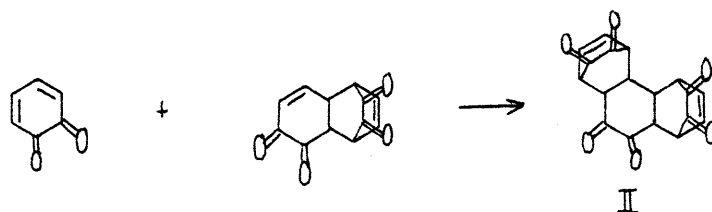
as a coal precursor. Lignin is more resistant to microbial attack and would thus likely concentrate. This is not meant to imply that either lignin or cellulose function as an exclusive coal precursor. Lignin is composed of only C, H and O, and coal contains small amounts of N and S, and in fact, traces of most of the periodic table. The nitrogen content of coal is likely derived from proteins, peptides, amino acids, ammonia and lipids, yet is in rather small concentration. These precursors thus likely influence overall coal reactivity little. Thus, while it would be unsubstantiated to claim that coal is simply transformed lignin, it is quite reasonable to expect features of coal reactivity to be analogous to lignin reactions.

A notable difference between coal and lignin is the existence of fused aromatic ring systems in the former, and only single unit phenols in the latter. A mechanism explaining the formation of fused aromatics from lignin during coalification has been proposed by Flaig<sup>9</sup>. After demethylation, potentially reactive diquinones dimerize through a Diels-Alder addition to yield fused ring products, as in,





An additional Diels-Alder addition would yield a phenanthrene backbone, of the type currently thought to exist in coal,<sup>10</sup>



Adduct II would likely decarbonylate, decarboxylate, or dehydrate in route to the C rich and H and O poor higher rank coals.

In addition to the plausibility of a pathway from lignin to coal, further evidence of the importance of lignin in coalification exists in the work of Raj<sup>11</sup> and Hayatsu, et.al.<sup>12</sup> These workers have identified lignin residues in coals. By oxidation of peat, lignitic, subbituminous and bituminous coals with performic acid, Raj has identified the list of lignin related residues listed in Table 3.3. The residues contain either or both of the characteristic lignin 3 carbon side chain or methoxyphenol units. From Table 3.3, Raj concludes that methoxyl groups are present in vitrinites in larger quantities than generally reported, and that the structure of vitrinites is quite similar to that of lignin. Hayatsu, et.al.<sup>12</sup>, have also identified lignin-like units in coals from alkaline cupric oxide oxidations. The organic acids identified in their studies are listed in Table 3.4. Of particular note is the identification of large quantities of benzoic acids which are hydroxy substituted in the para- or meta-positions, from both bituminous and lignitic coals. Of course, these

Compound	Sample Phenols and Acids Identified			
	Direct Humic Acid		Humic Acid from Oxidized Coals	
	Peaks	Microtiter	Microtiter	Rocky Mountain Province Coals
Acetic Acid	2	3	3	10
Propionic Acid	2	3	3	10
Phenol	2	3	3	10
p-Cresol	2	3	3	10
o-Isobutyl Phenol	2	3	3	10
m-Isobutyl Phenol	2	3	3	10
Hydroquinone	2	3	3	10
m-Hydroxy Benzoic Acid	2	3	3	10
Catechol	2	3	3	10

Phenols Identified Hawley's Biological Associations  
(Lignin and its Precursors; A-ring of Flavonoids)

Compound	Humic Acid from Oxidized Coals			
	Direct Humic Acid		Humic Acid from Oxidized Coals	
	Peaks	Microtiter	Rocky Mountain Province Coals	Interior Province Coals
Chromonic Acid	2	3	3	10
Chromonic Alcohol	2	3	3	10
Phenyl, 3-Pyruvic Acid	1	1	1	2
Phenyl, 3-Pyruvic Alcohol	2	3	3	10
p-Hydroxy benzoic Acid	2	3	3	10
p-Coumaric Acid	1	1	1	2
p-Hydroxy Phenyl, 3-Pyruvic Acid	1	1	1	2
p-Hydroxy Phenyl, 3-Treptonic Acid	2	3	3	10
Pyrogallol	2	3	3	10
Gallic Acid	2	3	3	10
Vanillin Alcohol	2	3	3	10
Vanillinic Acid	2	3	3	10
Acetovanillone	1	1	1	2
Ferulic Acid	1	1	1	2
Callicolic Acid	1	1	1	2
3-Methoxy, 4-Hydroxy Phenyl, 3-Pyruvic Alcohol	2	3	3	10
3-Methoxy, 4-Hydroxy Phenyl, 3-Pyruvic Acid	1	1	1	2
3-Methoxy, 4-Hydroxy Phenyl, 3-Treptonic Alcohol	1	1	1	2

Table 3.3 Lignin related coal residues II

Compound	Direct Humic Acid		Humic Acid from Oxidized Coals			
	2 Peats	3 Lignites	5 Lignites	15 Rocky Mountain Province Coals	10 Interior Province Coals	Eastern Province Coals
3-Methoxy, 4-Hydroxy Phenyl, 3-Propanol				1		
3-Methoxy, 4-Hydroxy Phenyl, 3-Glyceric Acid	1	1	1	3	1	
Dehydrovanillinone				2	1	
Syringic Aldehyde	1	1	1	5	3	2
Syringic Alcohol				3	2	4
Syringic Acid	2	1	1	7	5	3
3, 5-Dimethoxy, 4-Hydroxy Phenyl, 3-Pyruvic Aldehyde		2	1		1	4
3, 5-Dimethoxy, 4-Hydroxy Phenyl, 3-Propionic Acid				1		
3, 5-Dimethoxy, 4-Hydroxy Phenyl						
3-Glyceric Acid					1	
3, 5-Dimethoxy, 4-Hydroxy Phenyl						
3-Pyruvic Acid	1	1		2		
3, 5-Dimethoxy, 4-Hydroxy Cinnamic Acid				3	5	3
x, y-Dimethoxy Cinnamic Alcohol					1	
x, y-Dihydroxy Cinnamic Aldehyde					3	2

Table 3.3(cont)

Organic Acids Identified as Their  $d_3$ -methyl Esters by GC-MS and High Resolution MS

Peak No.	Compound
1	Succinic acid
2	$C_3$ -dibasic acid
3	Benzoic acid
4	Methylbenzoic acid
5	p-Hydroxybenzoic acid
6	Hydroxytoluic acid
7	1,2-Benzenedicarboxylic acid
8	1,4-Benzenedicarboxylic acid
9	1,3-Benzenedicarboxylic acid
10	Methylbenzenedicarboxylic acid
11	Dihydroxybenzoic acid
12	Pyridinedicarboxylic acid
13	3,4-Dihydroxybenzoic acid
14	Dimethylbenzenedicarboxylic acid (naphthoic acid, minor)
15	Hydroxybenzenedicarboxylic acid (4-hydroxy-1,3-benzenedicarboxylic acid, largest peak)
16	Methylhydroxybenzenedicarboxylic acid
17	1,2,4-Benzenetricarboxylic acid
18	1,2,3-Benzenetricarboxylic acid
19	1,3,5-Benzenetricarboxylic acid
20	Methylbenzenetricarboxylic acid
21	Pyridinetricarboxylic acid
22	Naphthalenedicarboxylic acid
23	Hydroxybenzenetricarboxylic acid
24	1,2,4,5-Benzenetetracarboxylic acid
25	1,2,3,4-Benzenetetracarboxylic acid
26	1,2,3,5-Benzenetetracarboxylic acid
27	Methylbenzenetetracarboxylic acid
28	Dihydroxy-diphenyldicarboxylic acid (T)
29	Hydroxynaphthalenedicarboxylic acid
30	Benzenepentacarboxylic acid

\* Indicates that identification is tentative.

$CrO_3$ -NaOH Oxidation of Model Compound at 200°C for 8-10 Hours

Compound	Type of Reaction	Major Product <sup>a</sup>	Yield wt %
4-Methylbenzyl alcohol	$-CH_2OH \rightarrow -COOH$	4-Methylbenzoic acid	93
β-Naphthyl methylcarbinol	$-CH_2OH \rightarrow -COOH$	β-Naphthoic acid	77
Benzaldehyde	$-CHO \rightarrow -COOH$	Benzoic acid	95
4-Methoxybenzaldehyde	$-CHO \rightarrow -COOH$	4-Hydroxybenzoic acid	89(4)
2,6-Dimethoxyphenol	$-OCH_3 \rightarrow -OH$	b	-
Syringaldehyde	$-CHO \rightarrow -COOH$	3,4,5-Trihydroxybenzoic acid	4,5 <sup>c</sup>
Dibenzylmethane	$-CO-CH_2- \rightarrow -COOH$	Benzoic acid	76
1,4-Naphthoquinone	$-CO-C \rightarrow -COOH$	Phthalic acid	91
Phorylacetic acid	$-CH_2-CO- \rightarrow -COOH$	Benzoic acid	68
Diphenyl ether	$-O- \rightarrow -OH$	Phenol	67
Dibenzyl ether	$-H_2C-O-CH_2- \rightarrow -COOH$	Benzoic acid	81
Diphenyl methane	$-C-C- \rightarrow -COOH$	Benzoic acid	11
Poly-(4-methoxystyrene)	$-C-C \rightarrow -COOH$	4-Hydroxybenzoic acid	6 <sup>d</sup>
1-Methylnaphthalene	$-C-C \rightarrow -COOH$	1-Naphthoic acid	3
2,4-Dimethoxytoluene	$-C-C \rightarrow -COOH$	2,4-Dihydroxybenzoic acid	5(5)
3,4-Dimethoxytoluene	$-C-C \rightarrow -COOH$	3,4-Dihydroxybenzoic acid	7(5)

<sup>a</sup> All products were derivatized with  $d_3$ -dimethylsulfate or diazomethane, and analyzed by GC/MS.

<sup>b</sup> About 16.9 wt % of the oxidation product was obtained under the same conditions (170°C for 8 hours) employed for plant materials, humic acids and marine sediments. The product consisted mainly of polymerized material. Very small amounts of trihydroxy compounds (2-3%) was detected by GC/MS.

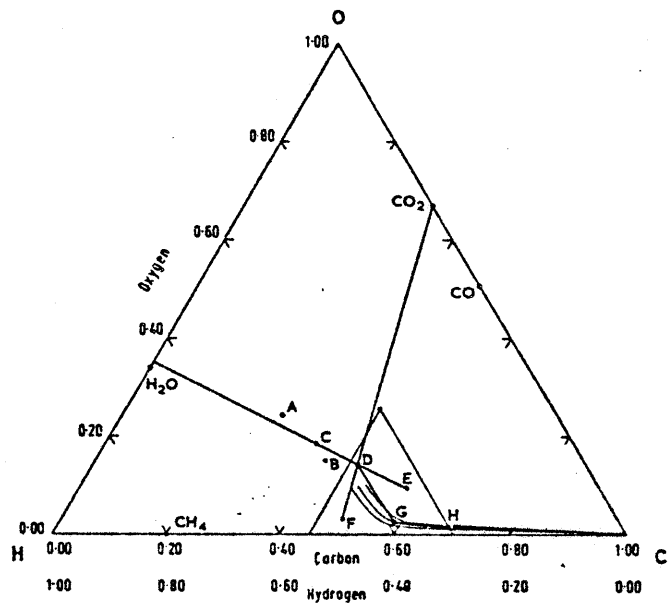
<sup>c</sup> Most of syringaldehyde was degraded.

<sup>d</sup> Shown as wt %.

Table 3.4 Lignin related coal residues<sup>12</sup>

hydroxysubstituents are again characteristic of the lignin monomer units.

Although the above arguments provide evidence as to the importance of lignin as a coal precursor, it is clear that while all functionalities present in lignin may have been incorporated into coals, the latter substrate contains many moieties not found in the former. Aside from the polymerization or condensation type reaction previously noted, the transformation of biomass to coal is attended by decarbonylation, decarboxylation, demethanation and dehydration reactions, or more generally, a decrease in oxygen and hydrogen content. Stephens<sup>13</sup> provides a convenient method for assessing the characteristics of a substrate by presenting a C-H-O ternary diagram for coal classification. This diagram is presented as Figure 3.13 and includes entries for H<sub>2</sub>O, CH<sub>4</sub>, CO<sub>2</sub>, CO, cellulose, lignin, peat, lignites and other coals. As Stephens notes and has been previously discussed, the formation of peat from plant matter is the first step in coalification. Point C in this diagram is at the position for peat, with A and B representing cellulose and lignin, respectively. That C lies between A and B indicates that both cellulose and lignin act as peat precursors; however the contribution from cellulose is less than from lignin as reflected in the relative proximities of A and B to C. Again, this is likely due to biological degradation of cellulose. Point D, an entry for lignite, is virtually colinear with the entry for peat and the entry for water, indicating a substantial dehydration in the metamorphosis from peat to lignite. In a similar manner, a vectoral



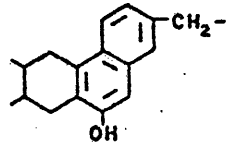
Ternary diagram with Seyler coalification band illustrating the chemistry of the formation and maturation of coals. A, cellulose; B, representative lignin; C, representative peat; D, representative brown coal/lignite; E, subhydrous (inertinite-rich) coal; F, perhydrous (exinite-rich coal); G, median (vitrinite-rich) coal; H, anthracite. Dehydration and decarboxylation reactions are indicated by the lines C D E and D F respectively. The small triangle about the Seyler coalification band is a convenient subsection of the full ternary diagram which is useful in a magnified form for studying coal chemistry in detail

Figure 3.13 Ternary diagram due to Stephens.<sup>13</sup>

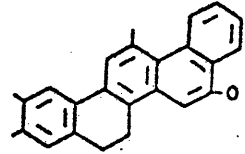
addition is indicative of the net metamorphosis reactions in traversing from one entry to another in Figure 3.13. Thus, for example, the line D-F represents decarboxylation. It is noteworthy that the line B-D formally represents a demethanation, likely due to methoxyl group loss in the metamorphosis from lignin to lignite. In short, the ternary diagram of Stephens provides a rapid assessment of the formal conversions in the metamorphosis of biomass to coals of any rank.

### 3.3.2 Coal Models

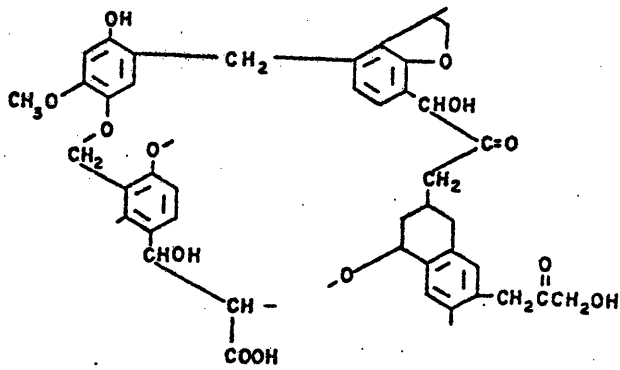
The actual chemical units believed to comprise coal are suitably discussed in terms of model structures for coal, similar in principle and goal to that presented for lignin by Freudenberg. Most structural models have been formulated for coals of at least bituminous in rank. Wender<sup>14</sup> provides an exception, listing structural scenarios for four different coal ranks, ranging from the plentiful lignites to a low volatile bituminous coal. These structures are presented as Figure 3.14, which includes the particularly significant lignite moiety. This lignite structure is remarkably similar to the Freudenberg model, Figure 3.5. Included in this lignite representation are phenolic hydroxyl, phenolic methoxyl, and propanoid side chain substituents. The lignite has a high oxygen content, and contains primarily single ring aromatic units. Two of the three interunit linkages are of the  $\alpha$ -aryl ether or diphenylmethane type, both occurring in lignin. The subbituminous coal retains a relatively high oxygen content, but



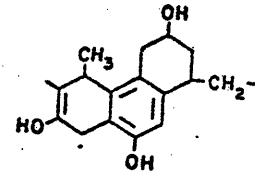
HIGH VOLATILE BITUMINOUS



LOW VOLATILE BITUMINOUS



LIGNITE



SUBBITUMINOUS

Figure 3.14 Coal structural schematics due to Wender.<sup>14</sup>



begins to differ from lignin in other respects. Wender's picture includes the phenolic and alkyl hydroxylic group, but excludes the aromatic methoxyl substituent. The onset of aromatic ring fusion is noticed at this stage of coalification as well. The higher rank coals are characterized by a decrease in hydrogen and oxygen content and an increase in the preponderance of fused aromatic rings.

A rather detailed description of a high volatile bituminous coal has been presented by Hill and Lyon<sup>15</sup>, shown as Figure 3.15. Important aspects reflecting the chemical and physical data accumulated on coal emerge. The 'chicken wire' representation of fused aromatic rings has been generally replaced by smaller aromatic groups in this model. This may in fact yet overestimate the degree of ring fusion, more popularly represented as phenanthrene units linked via methylene and/or ether linkages. Figure 3.15 also includes  $\beta$ -ether, phenyl ether, phenolic hydroxyl and diquinone structures, all either present in or closely related to lignin. The structure projects not only the chemical and physical data associated with coals, but also an awareness of the evolutionary link of coal and lignin, most singularly noted in the  $\beta$ -ether bonds.

Given has presented a model which compared favorably with properties observed for vitrinites<sup>10</sup>. His structure, Figure 3.16 was one of the first to rationalize the observations that while most of the carbon in coal is aromatic, most of the hydrogen is on non-methyl aliphatic carbons. A key feature of Given's model was the inclusion of structures

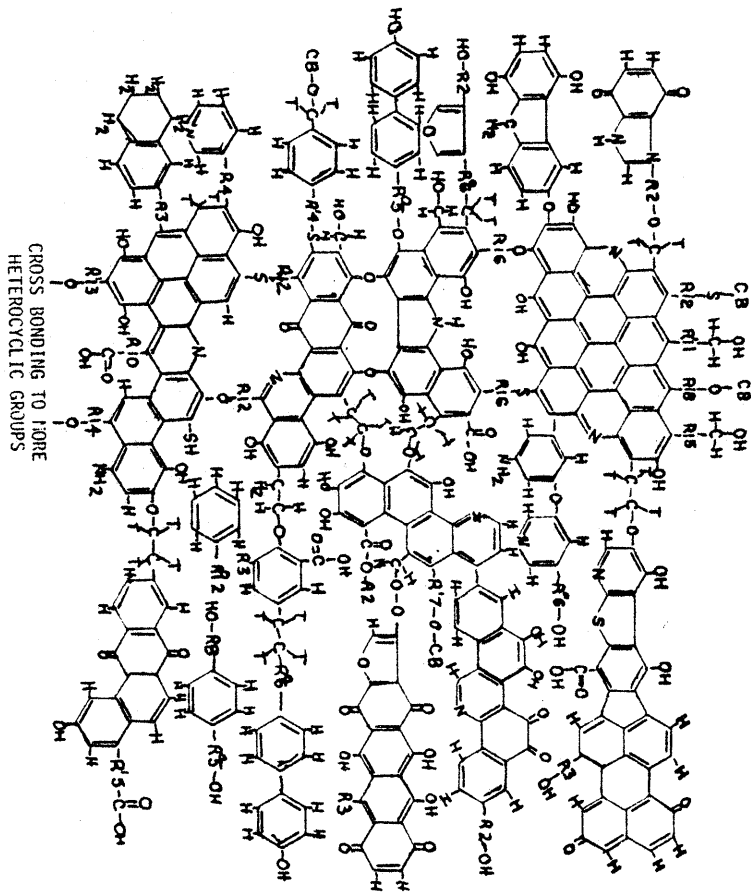


Figure 3.15 Hill and Lyon structural model for coal. 15

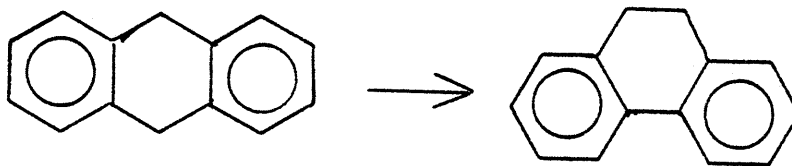
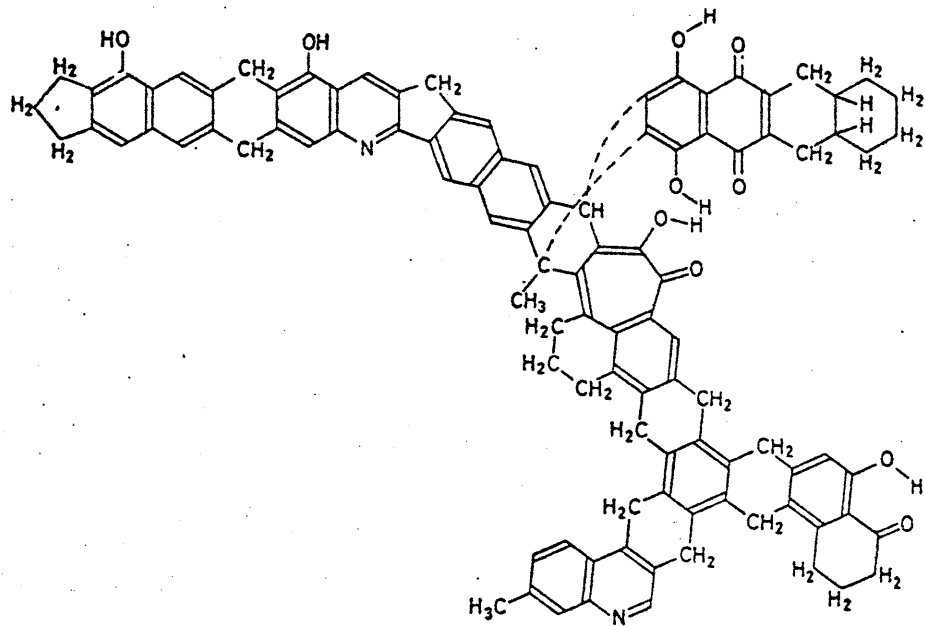
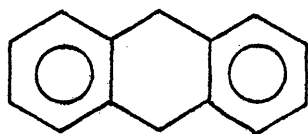
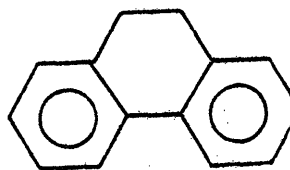


Figure 3.16 Coal model due to Given. <sup>10</sup>

of the type 9,10-dihydroanthracene.



9,10-dihydroanthracene



dihydrophenanthrene

This repeating unit was later amended to a dihydrophenanthrene unit, principally on the basis of NMR studies of coal extracts<sup>16</sup>. These studies did not contradict Given's general description of coal, consisting primarily of small groups of aromatic nuclei linked by hydroaromatic rings. Rather, these studies demonstrated that few  $-CH_2-$  groups were linked directly to two aromatic rings. Given's modification to the phenanthrene structure allowed the model of Figure 3.16 to accord not only with the distribution of hydrogen and carbon as previously noted, but also to later NMR data. Given also points to coal oxidation studies<sup>17</sup> in which both phenanthrene and diaryl units were discovered in quantities much larger than anthracene units. The phenanthrene backbone also accords with the successive Diels-Alder mechanism previously postulated for lignin-type coal precursors. In short, one of the more cogent aspects of Given's model was the presentation of coal as hydroaromatic units containing typically three or four aromatic nuclei, where very early models favored a 'chicken wire' structure resembling graphite.

These structural models provide insights into the important functional groups and reactive sites in coal. In many cases the bond and moiety types were similar to those in lignin, particularly true for the low rank models of

Wender and Hill and Lyon. For these, it is quite reasonable to expect that many essential elements of lignin reactivity will be mimicked in coal reactivity.

The heterogeneous nature of coal suggests further correspondence of lignin and coal. As previously discussed, a general coalification scheme can be represented by the series lignin → peat → lignite → higher rank coals. However, many nominal coal types are in fact believed to be mixtures of coals at various stages of coalification, and thus lignin - or lignite - type elements will contribute to the overall reactivity of a higher rank coal. Recall the works of Raj and Hayatsu, et.al., who have demonstrated the existence of lignin-related residues in higher rank coals. A consequence of this is that the low rank residues will be reactive even during the approach to a 400 or 800C coal liquefaction or gasification temperature.

Thus, the evolutionary link of lignin to coal is significant in two ways. As a coal precursor, many of the bond and chemical moiety types of lignin are reflected in coal. Secondly, coal is a rather heterogeneous substrate, and lignin related residues are likely present in even high rank coals. The global reactivity of any coal type should then demonstrate some elements of lignin reactivity.

#### 4.0 Previous Pyrolyses

The major goal of the present investigation is the elucidation of the fundamental reaction pathways involved in lignin pyrolysis. Thus, previous investigations of the thermal behavior of lignin and

lignin model compounds are relevant. This section will consider both. Whole lignin thermolyses include inert pyrolysis, DTA and DTG studies and pyrolysis in the presence of various additives. These will be briefly compared with lignite and coal pyrolysis, which should yield insights into the reactivity changes effected by coalification. Finally, a discussion of previous model compound studies is of particular interest, since the experimental section of the present investigation utilizes model substrates.

#### 4.1 Previous Lignin Pyrolyses

Active research dealing with lignin pyrolysis dates to at least 1920. These processes have been many and varied, ranging from destructive distillation at relatively modest temperature to rapid pyrolysis at 2500 C. The products from lignin pyrolysis are plentiful in number, without one dominating product. Further, reported product spectra vary from one investigation to another, reflecting differences in analytical chemistry capabilities (cf 1920), variances in lignin wood species, and lignin modifications due to isolation methods. However, a unifying feature is that the products from each of these thermolyses can be grouped into four categories, including a gas, aqueous distillate, tar, and carbonaceous coke fraction. Figure 4.1 is a schematic of these major lignin pyrolyses pathways and Table 4.1 is a representative listing of the major pyrolysis products reported in the literature. The previous lignin thermolyses are effectively discussed in terms of the products constituting each of the four

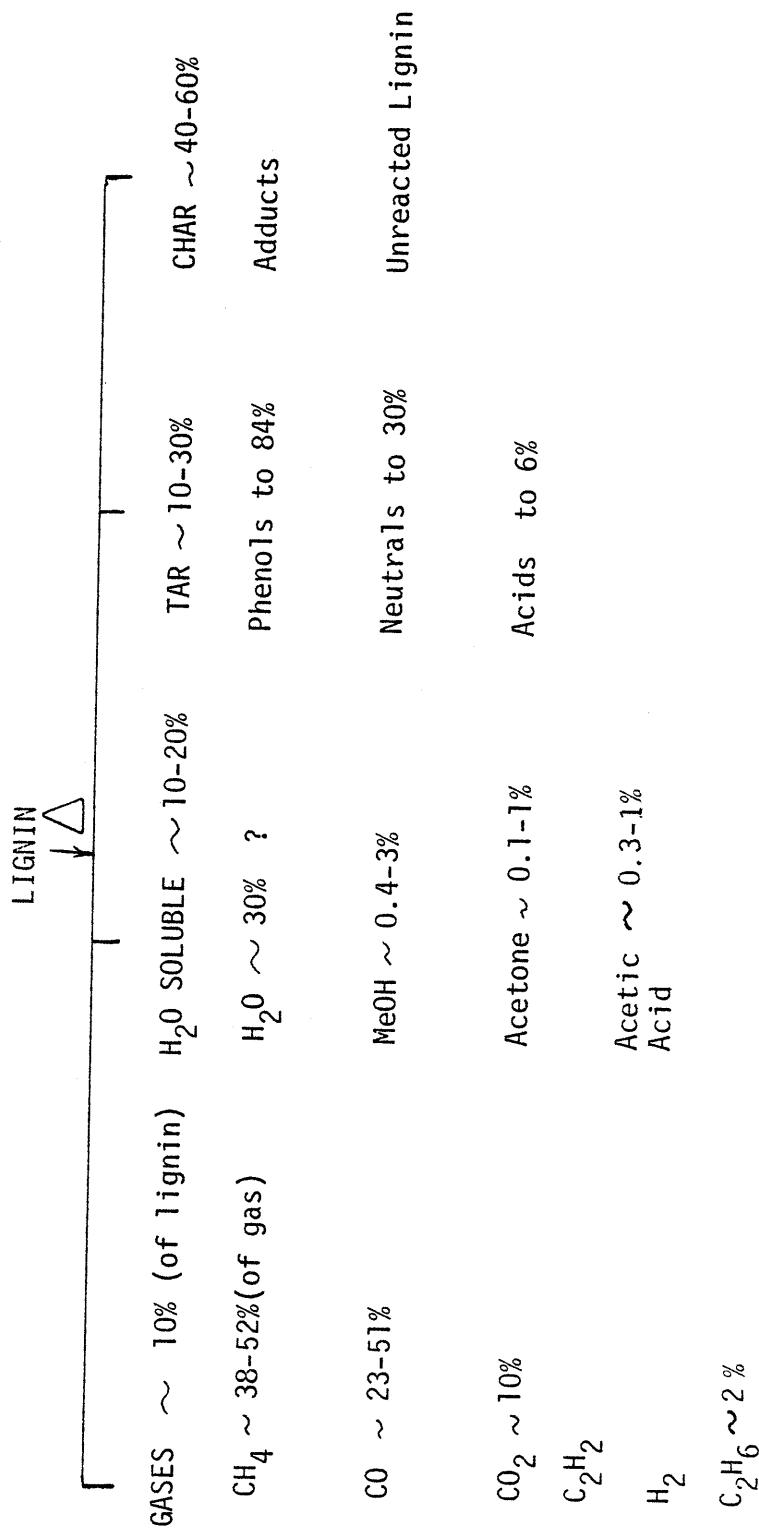


Figure 4.1 Schematic of overall lignin pyrolysis product spectrum

Reference	Material Pyrolysed	Char	Tar	Aqueous % of Lignin	MeOH	Acetone	Ac. Acid	Gas	CO	CH <sub>4</sub> % Gas	CO <sub>2</sub>	Other
(52)	1975 Lignin	63.5	7.2	16.4				12.9				
(35)	1938 Alk. corn stlk. Lig	57	19.5	11.8	.28	.28	.43	11.7				
(34)	1929 Alk. Lig	52.2	17.7	15.5	1.9	.13	.05	13.5				
	HCl Lig	58.5	7.5	15.1	.7	.57	1.1	19.1				
	H <sub>2</sub> SO <sub>4</sub> Lig	65.5	7.4	15.0	1.1	1.0	.9	11.5				
(31)	1928 Oak Lig	50.6	3		1.5	.21	1.3					
	Birch Lig	50.6	4		1.4	.18	1.3					
	Beech Lig	50.6	5		1.0	.22	1.3					
(23)	1919 Spruce Lig	50.6	13		.9	.19	1.1		50.9	37.5	9.6	C <sub>2</sub> H <sub>6</sub> 2.
(53)	1918 Aspen Lig	45.0	9.6		.7	.10	.64		32.4	3.12	62.9	C <sub>2</sub> H <sub>6</sub> 1.6
(24)	1907 Cellulose	34.9	6.3		0.0	.13	2.8		32.6	9.3	56.5	C <sub>2</sub> H <sub>6</sub> 1.7
	Wood	37.8	8.1		.96	.20	3.2					
(32)	1925 HCl Aspen	44.3	14.3		.87	.22	1.3		23.7	44.52	10.2	C <sub>2</sub> H <sub>2</sub> 18
(25)	1974 Hydr. Lig	40.5	14.2						+	+	+	
(29)	1975											
(27)	1932 Alk. corn	50.5	28.3	11.7	.65	.1	.3	9.3	+	+	+	
(54)	1920 HCl Lig	57.2	12.5	13.2				17.0				
(55)	1921 HCl spruce	53.8	10.2	14.2								
(56)	1923 HCl spruce	52.0	15	21								
(57)	1952 HCl	60	7	20				15				
(58)	1955 H <sub>2</sub> SO <sub>4</sub>	56		19				10.3				
(60)	1950 HCl	44.8	30	35.7				17.8				
(61)	1958	55.66	5.9	8.7								
(62)	1947	63.5	7.2	13.21	.4	.2	.3	12.9				
(52)	1970	54.7	7.4	16.4				17.4				
	400 C	51.0	7.6	20.4				20.4				
	500 C	51.0	7.6	22.1				20.4				
(63)	1970	42	21	22.1				20				
(26)	IATRIDS AND GAVVALS DETAILED SEPARATELY											

Table 4.1 Representative products from lignin pyrolysis.



major product fractions.

#### 4.1.1 Gases

The gases formed from lignin pyrolyses have often been neglected, and in fact, some of the gas yields shown in Table 4.1 are calculated by difference. An early exception to this trend was the work of Heuser and Skioldebrand<sup>23</sup>, who obtained a gas consisting of 50.9% CO, 37.5% CH<sub>4</sub>, 9.6% CO<sub>2</sub> and 2% C<sub>2</sub>H<sub>6</sub> from pyrolysis of an HCl spruce lignin. The high content of CO and CH<sub>4</sub>, and the rather low content of CO<sub>2</sub>, are noteworthy, especially upon comparison with the work of Klason<sup>24</sup>. This investigator pyrolysed a spruce wood and spruce cellulose, and obtained a product gas of CO:CH<sub>4</sub>:CO<sub>2</sub>:C<sub>2</sub>H<sub>6</sub> = 32.6:9.2:56.5:1.72 from the cellulose. The wood products more closely resembled those from the cellulose rather than those from the lignin. The low content of methane from cellulose and wood suggests that sites for methane release lie within the lignin. One possible set of precursors are the aromatic methoxyls, which are characteristic of and plentiful in the substrate. Gladkova, et al.<sup>25</sup>, report somewhat different percentages of CO, CH<sub>4</sub> and CO<sub>2</sub> in the product gas from pyrolysis of an hydrolysis lignin. These investigators report CO:CH<sub>4</sub>:CO<sub>2</sub> = 23-27:45-52:10-12. As was the case with Heuser and Skioldebrand, the CO<sub>2</sub> proportion was on the order 10% and the methane and CO predominated. The nature of the wood species studied by Gladkova, et al., is not clear, but many Russian lignin scientists will typically employ a hardwood, such as aspen. These incorporate higher proportions of sinapyl alcohol, the

dimethoxylated cinnamyl alcohol, than does a spruce wood. This reasoning is in accord with the earlier speculation of the lignin aromatic methoxyl as a methane precursor.

Recently, Iatridis and Gavalas<sup>26</sup> have pyrolysed a Douglas fir Kraft lignin and performed gaseous product by gas chromatography. Their data are presented in Table 4.2. Although five light hydrocarbons and CO and CO<sub>2</sub> are reported, the latter two and CH<sub>4</sub> again predominate. Of special note is the variation with temperature of the ratio CO/CH<sub>4</sub>. At 400C, this ratio is approximately 2.3 while at 500C, CO/CH<sub>4</sub> drops to roughly 0.85, and finally at 550 through 650C the ratio climbs to values approaching 2. This behavior might be interpreted in terms of multiple sites for CO release. A facile precursor might readily eliminate CO at 400C, with other, more activated sites becoming important at higher temperatures. Compared relative to a single site for methane release, these could account for the behavior of the CO/CH<sub>4</sub> ratio. The large CO<sub>2</sub> content is inconsistent with previous literature citations, and likely arises due to modification of the lignin structure during Kraft pulping. As has already been discussed, the addition of carboxylic acid groups, likely CO<sub>2</sub> precursors, is one modification due to Kraft pulping.

Mikulich, et al.<sup>27</sup>, have pyrolysed a lignin at the constant rate of 9 C/min from 20 to 900C. These workers report that the temperature of maximum lignin degradation, as well as the temperature of maximum CO<sub>2</sub> and CH<sub>4</sub> release, was 420C. The maximum evolution of CO and H<sub>2</sub> occurred at a higher temperature.

Product Distribution Yields from the Pyrolysis of a Precipitated Kraft Lignin

Product <sup>a</sup>	temp, °C																			
	400				500				550				600				650			
	20	60	120	180	30	60	120	180	30	60	120	180	30	60	120	180	30	60	120	180
CH <sub>4</sub>	0.22	0.52	0.52	0.80	1.70	2.21	1.00	2.30	2.60	2.70	1.33	2.34	1.80	3.06	4.42	4.83	3.06	4.42	4.83	4.83
C <sub>2</sub> H <sub>6</sub>	0.01	0.01	0.02	0.02	0.19	0.20	0.08	0.17	0.22	0.25	0.10	0.22	0.14	0.30	0.30	0.33	0.14	0.30	0.30	0.33
C <sub>2</sub> H <sub>4</sub>	0.01	0.01	0.01	0.017	0.02	0.18	0.10	0.12	0.16	0.18	0.10	0.21	0.19	0.24	0.30	0.35	0.19	0.24	0.30	0.35
C <sub>2</sub> H <sub>2</sub>	0.02	0.02	0.03	0.043	0.07	0.10	0.12	0.15	0.27	0.31	0.13	0.27	0.23	0.38	0.41	0.51	0.23	0.38	0.41	0.51
C <sub>3</sub> H <sub>8</sub>	0.09	0.09	0.10	0.037	0.10	0.12	0.05	0.12	0.30	0.32	0.08	0.38	0.11	0.47	0.55	0.60	0.11	0.47	0.55	0.60
CH <sub>3</sub> OH	1.65	2.04	2.24	1.12	2.00	2.34	1.40	2.08	2.46	2.58	1.71	2.21	1.90	2.36	2.85	2.95	1.90	2.36	2.85	2.95
CH <sub>3</sub> COCH <sub>3</sub>	0.11	0.33	0.66	0.26	0.32	0.47	0.20	0.52	0.74	0.77	0.32	0.66	0.46	0.67	0.81	0.81	0.46	0.67	0.81	0.81
G	0.14	0.90	1.10	0.10	0.44	0.98	0.29	0.54	1.03	1.15	0.49	0.63	0.52	0.70	1.15	1.18	0.52	0.70	1.15	1.18
AmG	0.12	0.74	0.76	0.12	0.40	1.01	0.27	0.73	1.07	1.20	0.30	0.78	0.34	0.60	1.05	1.12	0.34	0.60	1.05	1.12
PhOH	0.074	0.09	0.10	0.01	0.08	0.10	0.05	0.10	0.10	0.12	0.06	0.11	0.06	0.15	0.15	0.19	0.06	0.15	0.15	0.19
AcG	0.022	0.33	0.39	0.02	0.18	0.15	0.12	0.20	0.23	0.23	0.14	0.22	0.14	0.29	0.23	0.32	0.14	0.29	0.23	0.32
M-Cr	0.064	0.07	0.07	0.01	0.26	0.19	0.05	0.25	0.32	0.33	0.05	0.31	0.07	0.35	0.37	0.41	0.07	0.35	0.37	0.41
CO	0.50	1.20	1.20	0.50	1.50	2.05	1.20	2.35	3.18	3.6	2.53	4.45	4.50	6.30	6.70	9.20	4.50	6.30	6.70	9.20
C <sub>6</sub> H <sub>6</sub>	2.10	5.60	5.90	1.10	4.40	5.50	2.51	5.10	6.05	6.35	4.15	5.75	5.49	6.30	6.83	7.20	5.49	6.30	6.83	7.20
G <sub>1</sub> -C <sub>4</sub>	0.35	0.65	0.63	0.92	2.03	2.71	1.15	2.66	3.55	3.76	1.74	3.42	2.47	4.45	5.94	5.55	2.47	4.45	5.94	5.55
M <sub>1</sub> -A	1.76	2.57	2.70	1.31	2.32	2.91	1.60	2.60	3.20	3.35	3.03	2.87	2.36	3.03	3.66	3.76	2.36	3.03	3.66	3.76
PCC	0.23	2.13	2.41	0.26	1.35	2.44	0.73	1.83	2.75	3.09	1.04	2.05	1.13	2.20	2.93	3.22	1.13	2.20	2.93	3.22

<sup>a</sup> C<sub>1</sub>-C<sub>4</sub>: num of C<sub>1</sub>-C<sub>4</sub> hydrocarbons; M<sub>1</sub>-A: methanol and acetone; PCC: sum of phenol, guaiacol, 4-methylguaiacol, 4-ethylguaiacol, and m-cresol.

Table 4.2 Lignin pyrolysis product spectra of Iatridis and Gavaias<sup>26</sup>

Higher temperature pyrolysis seems to change the nature of the gaseous products. In a low temperature plasma (700-750C), Zaitsev, et al.<sup>28</sup>, obtained acetylene and carbon monoxide as the major gaseous components. Similarly, Goheen and Henderson<sup>29</sup> have pyrolysed a number of lignins at high temperatures and short residence times. Blowing a suspension of dry powdered lignin through an electric arc, with helium as the sweep gas, gave acetylene in a 14% yield. Other gases noted were CO<sub>2</sub> and CO. Use of a tungsten coil at 2000-2500C effected an increase in the acetylene yield to 23%, with small amounts of methane and ethylene produced as well. When spent liquor solids were pyrolysed, considerable amounts of H<sub>2</sub>S were detected also.

In summary, the product gas of lignin pyrolysis consists chiefly of CO, CH<sub>4</sub> and CO<sub>2</sub>, with the former two predominating. The pathways and precursors for the formation of these is not clear. Comparisons with cellulose pyrolysis, as well as possible product spectra variations with wood type, suggest that methane may be formed by demethanation of aromatic methoxyls. Further, inspection of the data of Iatridis and Gavalas suggests that CO may be formed by the degradation of more than one precursor. The method of lignin isolation likely exerts significant influence on the details of the gaseous product spectra as well.

#### 4.1.2 Aqueous Distillate Products

The aqueous distillate is formed from the pyrolysis of lignin in yields of roughly 20% of the lignin charged. In addition to water, the main constituents are methanol, acetone and acetic acid. Table 4.1

lists some of the yields of these products.

Methanol is formed in yields ranging from about 0.3 to 3% of the lignin. Allan and Mattila<sup>30</sup> report that the methanol presumably originates from the guaiacyl methoxyl unit. In support of this, they point to some observations<sup>23,31</sup> which show that hardwood lignins gave about twice the yield of methanol as did softwood lignins. Similarly, Klason<sup>24</sup> pyrolysed wood from birch, beech, pine and spruce and found the yield of methanol from the former two twice as high as that from the latter two. Although hardwood lignins incorporate a larger proportion of dimethoxylated sinapyl units than do softwoods, it is unlikely that the methoxyl content is twice as large, as implied by Allan and Mattila. It is also not universally true that hardwoods yield more methanol than softwood, as illustrated by a comparison of the data of Heuser and Brotz<sup>32</sup> and Heuser and Skioldebrand<sup>23</sup>. These investigators report virtually identical yields of methanol from aspen and spruce lignins isolated by the HCl method.

Klason also compared the pyrolysis of the birch, beech, pine and spruce woods to the pyrolysis of cellulose. In general, little, if any, methanol was formed from the cellulose, indicating that the lignin was the likely methanol precursor. Interestingly, the wood methanol yields were higher than those from the lignin, although lignin contains about three times the methoxyl content of wood. Brauns<sup>33</sup> feels that this is likely to be due to the changes in lignin effected during its isolation.

The work of Phillips<sup>34</sup> demonstrates that the method of lignin isolation can have a significant effect on the yield of methanol. He determined yields of 1.9%, 0.7% and 1.1% from corncob lignins isolated by alkali, HCl and H<sub>2</sub>SO<sub>4</sub> methods, respectively. These data support the aforementioned arguments of Brauns.

Considering that the modifications introduced by lignin isolation procedures are generally condensations involving the lignin side chains, and that the alkali method is the most likely of these to alter the guaiacyl methoxyl groups, these data also suggest that the guaiacyl methoxyl group may not be the sole site of methanol formation. Rather, primary alcohols in the lignin side chains may in fact be precursors to substantial methanol formation.

Overall, if the guaiacyl methoxyl groups were in fact responsible for the methanol produced from lignin pyrolysis, rather large amounts might be expected. Formation of one methanol mol from each aromatic unit predicts an ultimate yield of about 20%, by weight. However, the yields of methanol reported here, for both lignin and wood, correspond to only about 7 - 10% of the lignin methoxyl content<sup>19</sup>, a rather less than overwhelming correlation. Further, the effects of pyrolysis temperature and pressure reveal interesting insights into the pathways involved. Wenzyl<sup>19</sup> presents the data of Klason, who has studied birchwood pyrolysis at atmospheric, low vacuum and high vacuum pressure. These data are presented as Table 4.3. Under conditions of high vacuum, where volatiles are rapidly removed and secondary reactions are less significant, methanol and acetone were not reported,

DRY DISTILLATION OF BIRCHWOOD (MAXIMUM TEMPERATURE 400°C)<sup>a</sup>

Product	High vacuum 5 hr heating	Low vacuum 5 mm Hg 5 hr	Atmospheric pressure			
			3 hr heating	8 hr heating	16 hr heating	14 days heating
Charcoal	19.38	19.54	25.51	30.85	33.18	39.44
Tar	43.66	37.18	18.0	16.94	10.1	1.8
Acids <sup>b</sup>	10.20	10.05	7.42	7.57	7.30	6.91
Acetic acid	7.05	7.05	6.50	6.77	6.58	6.48
Formic acid	2.40	2.30	0.71	0.61	0.55	0.33
Methyl alcohol	—	1.20	1.49	1.47	1.50	1.41
Acetone	—	0.03	0.16	0.20	0.22	0.35
Formaldehyde	1.27	1.20	1.00	0.90	—	0.80

<sup>a</sup> Yields in percent of weight of dry wood on ash-free basis.

<sup>b</sup> Acids determined as acetic acid by titration.

Table 4.3 Products from wood pyrolysis<sup>19</sup>

and formic acid, formaldehyde and tars were obtained in maximum yields. An increase in pyrolysis pressure resulted in a decrease in tar, formaldehyde and formic acid, and an increase in charcoal, methanol and acetone. These data suggest that methanol may not even be a primary pyrolysis product, rather formed by secondary reactions, perhaps involving formic acid or aldehyde.

It is clear that the origin of the methanol is not well understood. Even less certain is the mechanism of its formation. The phenylmethoxyl bond strength is on the order 101 kcal/mol and homolytic fission would not be a very likely pathway to methanol at the temperatures reported here. Methanol might also arise from a reaction of a primary alcoholic group, also prevalent in lignin. In this case, the higher yield of methanol from hardwood lignins can be interpreted in terms of not a greater amount of precursor methoxyls, rather a smaller degree of condensation and side chain linkages in the lignin substrate because of steric effects of the methoxyls. Further, it has not been clearly demonstrated that methanol is a direct, primary pyrolysis product, and may in fact arise through the secondary reactions of formaldehyde or some other intermediate product.

The acetone and acetic acid produced from lignin pyrolysis presumably originate in the three carbon phenylpropane unit. Allan and Mattila<sup>30</sup> also report that the yields of acetic acid from hardwoods are significantly higher than those of softwoods. This is generally attributed to the blocking action of the methoxyl group yielding less condensation in the lignin polymer. In general, the acetone is



considerably less than the acetic acid and methanol, but this is not universally true<sup>35,34</sup>. Studies have shown that acetone can be formed from acetic acid<sup>36</sup>, and this is also suggested by the data on wood pyrolysis at different pressures presented by Wenzyl, previously discussed. However, the data of Iatridis and Gavalas<sup>26</sup> show significant yields of methanol and acetone, but do not include or report acetic acid.

The remaining distillate component, water, is in fact the major component of the lignin aqueous distillate fraction. The yield of water from wood pyrolysis has been reported at close to 30% of the oven dry wood<sup>19</sup>, and much water is, in fact, likely physically bound as well. Thus, pyrolysis of an 'as-received' wood or lignin will generally produce overwhelming amounts of water as the major product. This will hinder economic exploitation of biomass for at least two reasons. The first of these is the heat requirement introduced by such large amounts of water, and the second is that water is a very inefficient form for oxygen rejection from an already hydrogen poor substrate. The aim of biomass application in synthetic fuels production is to introduce hydrogen to produce interesting and useful product moieties, and as hydrogen is expensive to produce, loss of chemically bound hydrogen in the form of water is a serious disadvantage.

In lignin, the extensive hydrogen bonding between hydroxyl groups and other oxygen moieties is likely responsible for the rather facile loss of water in pyrolysis. The details of water release are poorly understood, and elucidation of these represent a major challenge to

the eventual commercial application of lignin and biomass thermal processes.

#### 4.1.3 Tars and Oils

The tar fraction resulting from lignin pyrolysis has received considerable attention, due in large part to the high proportion of valuable phenols obtained. As seen in Table 4.1, 15-20% is a representative figure for the tar yield. The phenolic compounds are many and varied, and this is the major obstacle confronting economic production of phenols from lignin. Even with the highest total yields, the product spectrum is complex and one phenol does not predominate.

The constituents of the thermolysis tar can be grouped into three main categories, including the phenols, acids, and neutral oils. These determinations have historically been made on the basis of solubility. For example, Bridger<sup>35</sup> notes that the separation of the tar components has been accomplished by successive extractions with bicarbonate and hydroxide solutions to dissolve the acidic and phenolic portions, respectively. The remaining insoluble tar is then classified as neutral. However, Morgan<sup>37</sup> has shown that this distinction may not be entirely accurate. Table 4.4 is a listing of the proportions of the components of the thermolysis tar as reported by a number of investigators.

It can be seen from Table 4.4 that the pyrolysis process, lignin wood type, and lignin isolation method all affect the tar yield and composition. For example, the alkali lignins seem to yield a high fraction of phenols.

TABLE 4.4 - COMPONENTS OF LIGNIN THERMOLYSIS TAR

REFERENCE	LIGNIN	TAR YIELD	PHENOL	NEUTRAL	ACIDS
(34)	Alkali	17.7	84	7.4	8.6
(25)	Hydrolysis	14-15	50-55	30-40	
(64)	Alkali	20	to 80		
(55)		12	34	13	
(56)	Hydrolysis	10.2	37.2		
(62)		5.2-8.9	27	25	6.1
(65)	Hydrolysis		53	35.6	4.3
(66)	Hydrolysis	38	29		
(67)	Hydrolysis	17.7	39.5		
(68)	Hydrolysis	19	50	21	
(69)	Spruce Hydroly	18	50	25	
(70)		22	52	32	
(71)	Aspen	51	13		
(72)	Hydrolysis	25.30	39.5	49.8	
(73)	Cotton Hull	30	43.3	53	2.8
(74)		17	50	33	

The pressure of pyrolysis has a significant effect on tar yields. Bridger<sup>35</sup> studied this effect on the pyrolysis of alkali lignin from cornstalks. He found a pressure of 5.5 in Hg and a temperature of at least 400C as optimal conditions for the production of tar. The phenol yield, however, was best at 2.2 in Hg, the lowest pressure he studied. Bridger speculates that the reduction in pressure led to an increase in product volatility as well as an increased rate of removal of vaporized products. The increased volatility and mobility of the products reduced the likelihood of complete decomposition to carbon or its oxides. Similarly, Domburg, et al.<sup>38</sup>, pyrolysed lignins at temperatures of 150-450C and at a pressure of 0.01 mm Hg and obtained yields of volatile products as high as 80%.

That the lignin isolation method exerts significant influence on tar yields was demonstrated by Phillips<sup>34</sup>. The pyrolysis of alkali, HCl and H<sub>2</sub>SO<sub>4</sub> lignins yielded 17.7%, 7.5% and 7.4% tar yields respectively. This accords well with the earlier described procedures for lignin isolation, where acid methods gave rise to considerable intra lignin condensation reactions. Domburg, et al.<sup>39</sup>, performed rapid thermolysis on alkalis, HCl, and H<sub>2</sub>SO<sub>4</sub> lignins as well. As was the case with Phillips, the alkali lignin yielded the largest proportion of phenols. Domburg, et al., report, in fact, that lignins from different woods isolated by the same method were much more similar than lignins from the same wood isolated by different methods.

The phenolic portion of the pyrolysis tar has received considerable attention. As previously noted, a rather small yield of a complex

mixture of phenols arises from lignin pyrolysis. The work of Domburg, et al.<sup>39</sup>, demonstrates the wide range of phenols obtained from pyrolysis, as these researchers report 24 different phenolic tar components.

Table 4.5, a representative listing of identifiable product phenols as reported in the literature, is evidence of the complexity of the product spectra. The most comprehensive quantitative investigations of the phenolic product spectra are those due to Kirshbaum<sup>41</sup>, Domburg<sup>39</sup> and Iatridis and Gavalas<sup>26</sup>. These workers report absolute yields of the individual phenols obtained from the pyrolysis of various lignin types. For comparison with Table 4.5, these data are presented as Table 4.6 for Kirshbaum and Domburg, Table 4.2 for Iatridis and Gavalas.

The phenols produced reflect the lignin cinnamyl alcohol monomers. Guaiacol and catechol derivatives predominate, and sinapyl and coumaryl units are evidenced as well. The singly oxygenated phenols likely arise from reactions of the guaiacyl and sinapyl moieties in addition to the incorporation of coumaryl alcohol monomers. In each case, phenolic substitution is invariably in the para position, and often includes all three carbons of the original propanoid side chain.

Panasyuk, et al.<sup>40</sup>, have demonstrated that the types of phenols obtained are dependent on the type of lignin, whereas the quantitative yield is sensitive to the method of lignin isolation. For example, guaiacols were found to predominate from the lignin of wood, while cresols were the main products from annual plant materials. Sunflower husks yielded 3% of the valuable m-cresol, while hydrolytic lignins of maize stumps gave about 25% o- and p- cresol, with little m-cresol.

Table 4.5 Phenols Reported From Lignin Thermolysis

	PHENOL	REFERENCE
1	Phenol	43,35,39,58,62,54, 42,41, 26
2	o-cresol	{43,40,35,39,42,58,62, 26,54,41
3	m,p-cresol	
4	m-ethylphenol	40
5	p-ethylphenol	43,49, 40
6	p-propylphenol	40
7	xlenols	40,35,58,62, 42,41
8	guaiacol	43,40,35, 41,39,58,62, 34,44, 42,26
9	p-methylguaiacol	35,39, 58,41,62, 44, 42,26
10	p-ethylguaiacol	30,58,62,44,26,41,42
11	p-propylguaiacol	39,54,41,42
12	eugenol	39,32,41
13	isoeugenol	39,41
14	vinylguaiacol	39,54,38,41
15	coniferaldehyde	38
16	vanillin	38,41,42
17	acetovanillone	39,42
18	propiovanillone	41
19	vanillic acid	41
20	catechol	39,38,65,41,54
21	p-methylcatechol	39,38,41
22	p-ethylcatechol	39
23	syringol (DMP)	39, 42,44, 41
24	p-methylsyringol	39,44, 41,42
25	p-ethylsyringol	42
26	p-propylsyringol	38,41,42
27	vinylsyringol	39,41
28	allylsyringol	39
29	syringaldehyde	38
30	acetosyringone	41
31	propiosyringone	41
32	methoxycatechol	38,41

SEE ACCOMPANYING ILLUSTRATION FOR CHEMICAL STRUCTURES

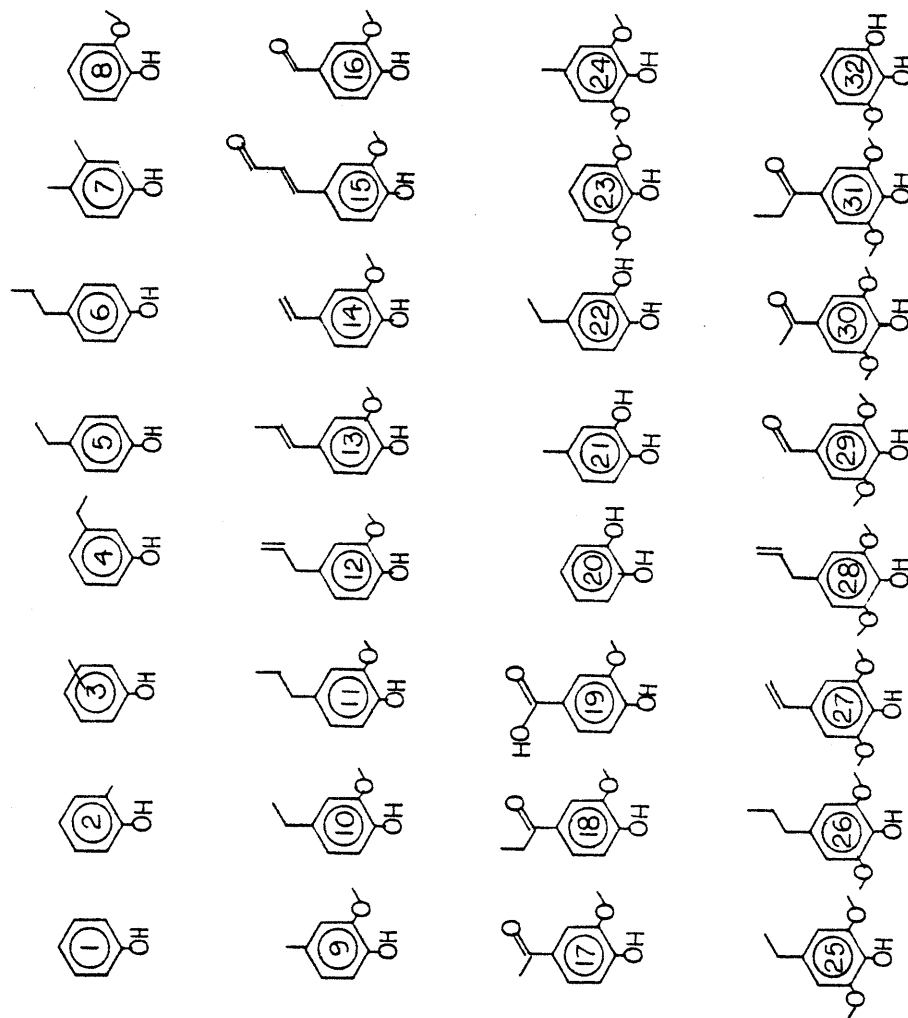


Table 4.5 (cont.) Chemical Formula key

RAPID THERMOLYSIS OF LIGNIN PREPARATIONS  
AT 475°. YIELD AND COMPOSITION OF DISTILLATE  
 (% on the basis of abs. dry lignin)

Products	Alkali lignin		Hydrochloric acid lignin		Sulphuric acid lignin
	aspen	spruce	aspen	spruce	of aspen
Distillate	56.50	49.80	53.70	47.70	37.30
Identified phenol compounds	14.50	13.00	9.20	11.30	3.30
among them:					
Phenol	0.05	0.10	1.40	0.10	0.80
o-,m-,p- Cresols	0.20	0.50	0.20	0.50	-
p-Ethylphenol	0.05	0.10	0.05	0.10	-
Pyrocatechol	0.40	0.80	0.60	1.00	-
Methylpyrocatechol	0.50	1.10	0.15	0.60	-
Ethylpyrocatechol	0.40	0.50	0.05	0.30	-
Guaiacol	0.80	1.40	0.50	1.80	0.40
Methylguaiacol	1.50	3.90	0.90	2.00	0.40
Ethylguaiacol	0.50	1.20	0.20	0.70	0.10
Propylguaiacol	0.10	0.10	0.05	0.10	0.05
Vinylguaiacol	0.50	1.10	0.10	0.90	0.05
Eugenol	0.10	0.20	0.10	0.20	-
cis-Isoeugenol	0.10	0.20	0.10	0.40	-
trans-Isoeugenol	0.15	0.50	0.15	1.30	-
Syringol	1.90	0.10	1.10	0.10	0.70
Methylsyringol	3.00	-	1.60	0.10	0.70
Ethylsyringol	1.00	absent	0.50	absent	0.05
Propylsyringol	0.10	absent	0.05	absent	-
Vinylsyringol	0.50	1.10	0.10	0.90	0.05
Allylsyringol	0.50	absent	0.20	absent	-
Vanillin	0.40	0.80	0.50	0.60	-
Acetovanillone	0.40	0.40	0.30	0.40	-
Syringylaldehyde	0.70	absent	0.10	absent	-
Monomethylpyro-gallol	0.70	0.05	0.40	0.10	0.05

Table 4.6 Phenols from lignin pyrolysis<sup>39</sup>



No. of peak	product	Temperature of pyrolysis, °C										Phenols remaining in solid residue of pyrolysate at 250°C	
		250	300	350	400	425	450	475	500	550	600		450
1	overall distillate	3.1	12.1	24.8	41.4	49.7	33.6	56.5	56.7	66.6	56.4	40.3	...
2	resin	...	...	...	14.4	19.9	29.4	29.4	32.6	29.9	...	...	...
3	solid residue	91.3	77.1	62.2	41.5	35.7	31.5	29.3	27.0	26.2	47.2	...	...
4	gases and losses (according to difference)	5.6	10.8	13.0	14.0	14.7	11.5	12.0	16.4	18.4	12.5	...	...
5	phenol	0.006	0.02	0.03	0.05	0.06	0.06	0.08	0.09	0.1	0.04	...	...
6	m, n cresol	...	...	...	0.03	0.08	0.08	0.09	0.1	0.1	0.05	...	...
7	1, 3, 5 Xylenol	...	...	...	...	...	...	...	...	...	...	...	...
8	n-ethylphenol	...	...	...	0.01	0.02	0.05	0.06	0.06	0.07	0.03	...	...
9	o-cresol	...	...	...	0.01	0.03	0.03	0.03	0.04	0.09	0.01	...	...
10	2, 5(2,4)-Xylenol	...	...	...	0.01	0.03	...	...	0.04	0.09	0.03	...	...
11	pyrocatechol	...	...	...	0.07	0.3	0.5	0.5	0.6	0.9	0.2	...	...
12	Methylpyrocatechol	...	...	...	...	...	0.2	0.4	0.4	0.4	0.2	...	...
13	Ethylpyrocatechol	...	...	...	...	...	...	...	...	...	...	...	...
14	Guaiacol	0.005	0.1	0.3	0.6	0.6	0.7	0.8	0.7	0.5	0.5	0.02	0.02
15	Methylguaiacol	0.003	0.1	0.3	0.9	1.0	1.2	1.3	1.1	0.7	0.7	0.01	0.01
16	Ethylguaiacol	0.002	0.07	0.3	0.4	0.4	0.5	0.5	0.5	0.5	0.4	0.007	0.007
17	Propylguaiacol	0.001	0.003	0.04	0.06	0.06	0.06	0.07	0.07	0.05	0.07	...	...
18	Pyrogallol	...	...	...	0.4	0.5	0.5	0.5	0.6	0.8	0.4	...	...
19	Monomethyl ether of pyrogallol	...	...	...	...	...	...	...	...	...	...	...	...
20	syrringol	0.02	0.4	1.1	1.8	2.1	2.1	2.3	1.8	1.0	1.7	0.06	0.06
21	Methylsyrringol	0.006	0.4	1.2	2.1	2.3	2.6	3.0	2.5	1.2	2.0	0.03	0.03
22	Ethylsyrringol	0.007	0.2	0.6	0.9	0.9	1.0	1.0	0.8	0.6	0.7	0.02	0.02
23	Propylsyrringol	0.002	0.02	0.1	0.1	0.1	0.1	0.1	0.08	0.03	...	...	...
24	Vinylguaiacol	0.002	0.03	0.07	0.1	0.3	0.4	0.4	0.4	0.3	0.04	0.02	0.02
25	Eugenol	0.001	0.006	0.02	0.03	0.05	0.06	0.05	0.05	0.01	0.08	...	...
26	cis-Isoeugenol	0.003	0.01	0.05	0.05	0.05	0.06	0.06	0.06	0.05	0.01	...	...
27	trans-Isoeugenol	0.002	0.01	0.05	0.05	0.04	0.1	0.1	0.1	0.06	0.04	0.01	0.01
28	Vinylsyrringol	0.04	0.1	0.1	0.2	0.3	0.4	0.4	0.4	0.2	0.3	0.1	0.1
29	Vanillin	0.01	0.04	0.1	0.1	0.2	0.3	0.3	0.2	0.2	0.3	0.1	0.1
30	Acetovanillin	0.01	0.07	0.07	0.1	0.1	0.1	0.1	0.1	0.09	0.04	0.06	0.06
31	Propiovanillin	0.04	0.3	0.3	0.5	0.7	0.7	0.9	0.9	0.5	0.4	0.3	0.3
32	Syringaldehyde	0.02	0.1	0.2	0.3	0.4	0.4	0.5	0.4	0.3	0.2	0.2	0.2
33	Acetosyringon	0.01	0.1	0.2	0.3	0.3	0.3	0.4	0.4	0.3	0.2	0.2	0.2
34	Propiosyringon	...	...	...	...	...	...	...	...	...	...	...	...
35	Vanillic acid	...	...	...	...	...	...	...	...	...	...	...	...
36	sum of GC-analyzable phenols in distillate	0.2	2.2	5.8	9.4	11.3	13.3	14.6**	12.7	10.1	8.8	...	...
37	sum of GC-determinable in solid residue	...	0.4	...	...	...	...	...	...	...	...	...	...

Table 4.6 (cont)<sup>41</sup>

The investigators note that actual phenol was found only in small quantities from the annual plant materials.

Domburg, et al.<sup>38</sup>, studied the nature of the phenols obtained from pyrolysis of different lignin preparations at reduced pressure. They found a substantial difference in the behavior of the different preparations. The lignins isolated by the HCl procedure were more stable than the alkali lignins. This behavior is likely due to the greater extent of lignin condensation reactions inherent in the HCl isolation method. A distinguishing feature of the products from the HCl lignin was the isolation of coniferyl aldehyde, the aldehydic form of the monomer coniferyl alcohol. Alkali lignins yielded catechols as part of the pyrolysis tar, arising from demethylation in either the pyrolysis or perhaps the isolation procedure. Not unexpectedly, the hardwood lignins yielded syringyl derivatives, such as syringaldehyde.

Kirshbaum, et al.<sup>41</sup>, studied the effect of heat-up rate on the yield of phenols from pyrolysis. They reported 475C as optimal for the production of phenols. The yields of distillates and phenols were lower from slow pyrolysis than those obtained at high heat-up rate. However, the composition of the phenolic fraction was rather insensitive to heat-up rate. It is interesting to note that these workers identified a total of 30 phenolic pyrolysis products.

Kirshbaum and Domburg<sup>42</sup> compared the rapid and slow pyrolysis of aspen alkali lignin. At 500C. the overall yield of phenols from rapid pyrolysis was at least 12%, as much as twice the yield of that obtained in slow pyrolysis. The low content of phenol, cresols and

xlenols in the products from rapid pyrolysis was indicative of the absence of secondary reactions. Thus, the lower yields from slow pyrolysis seem to result from secondary recombinations and polymerizations of primary products.

Iatridis and Gavalas<sup>26</sup> have pyrolysed a Douglas fir Kraft lignin in an apparatus designed to emphasize primary reactions. Their data are presented in Table 4.2. These investigators obtained single-ring phenols in yields of up to 3% of the dry lignin, yet in light of the work of the Russian investigators, Iatridis and Gavalas report rather few different phenols. The phenols listed are guaiacol, 4-methylguaiacol, phenol, 4-ethylguaiacol and m-cresol, which seem to indicate appreciable secondary reaction (cf phenol, cresol), even at 400C.

Vorher and Schweers<sup>43</sup> performed some interesting studies of phenol lignin, the organic matter formed during the phenol pulping of wood. As this lignin is sulfur-free, these workers thought it to be an excellent substrate for pyrolysis to obtain phenols and guaiacols. They pyrolysed a crude phenol lignin, an ether-soluble phenol lignin, an ether-insoluble phenol lignin, and the sodium lignophenolates of these obtained by stoichiometric conversion with 1N NaOH. The ether-soluble phenol lignin gave the highest yield of monomeric phenols, followed by the crude phenol lignin and then the ether-insoluble lignin. From the pyrolysis of the sodium lignophenolates they identified only phenol, o- and p- cresol, guaiacol, and ethyl phenol in reproducible amounts. Phenol was over 60% of the total phenolic yield. On the basis of this data, Vorher and Schweers feel a phenol pulping process could be

self-supporting in pulping chemicals, with the possibility of a surplus of phenols.

A pyrolysis of a synthetic lignin, of the type utilized by Freudenberg, was performed by Faix and Schweers<sup>44</sup>. These workers found a systematic dependence of the yields of the various types of phenols on the amounts of the guaiacyl and syringyl units actually incorporated into the synthetic polymers. For example, the yields of guaiacol and syringol correlated with the amounts of coniferyl and sinapyl alcohols used. They report that direct phenol production from coumaryl units was small, indicating that the degree of condensation of these units was high in the synthetic lignins studied.

Goldstein<sup>45</sup> feels that for the utilization of lignin conversion products to become economically feasible, the products other than the phenols must be used as well. He refers to the success of coal tar conversion, which depended on the use of the bulk of the material for economic feasibility. In 1940, chemicals were only 4.8% of the coal tar, and without utilization of the remaining 95% the industry would not have developed. An analogous use of the lignin materials could make production of phenols from lignin feasible.

In a similar vein, based on a 40% yield of a mixture of phenols and catechols obtained from lignin hydrogenation, Hellwig, et al.<sup>46</sup>, project a yield of 35% pure phenol from secondary reforming processes. Likewise, hydrocracking lignin tar has been shown to increase the yield of phenols.<sup>47</sup>

By way of summary, the tar fraction of lignin pyrolysis can be

obtained in high yields, depending on the lignin, lignin isolation method, and conditions of pyrolysis. Average yields range from about 15-20%, however. The components of the tar are divided into three groups, these being phenols, acids and neutrals. The phenolic portion has received considerable attention, but has eluded commercialization due to modest yields of complex mixtures. The phenols are characteristic of the three lignin monomer alcohols, but at even rather low pyrolysis temperature are indicative of secondary pyrolyses.

#### 4.1.4 The Carbonaceous Residue

The carbonaceous deposit is the predominant lignin pyrolysis product. Chemical analysis of this product has been rarely effected, however Gillet and Urlings<sup>48</sup> found that the coke of a Brauns and ethanolysis lignin had an elemental composition similar to that of a Rhenish lignite. Their elemental formula of  $(C_{40}H_{30}O_{11})_2$  is represented in Figure 4.2 as speculation of the coke structure.

Many investigators have found the pyrolysis residue suitable as an activated carbon precursor. Panasyuk and Maksimenko<sup>49</sup> have mixed lignin with anthracene oil and heated at various temperatures and pressures. The best activated carbon was that from a 45 minute pyrolysis at 380C and 200mm pressure.

A higher temperature work was performed by Zaitsev, et al.<sup>28</sup>, who pyrolysed hydrolysis lignins in a low temperature plasma. They found a direct proportionality between the power supplied and the yield of carbon black, and further determined an increase in the carbon surface

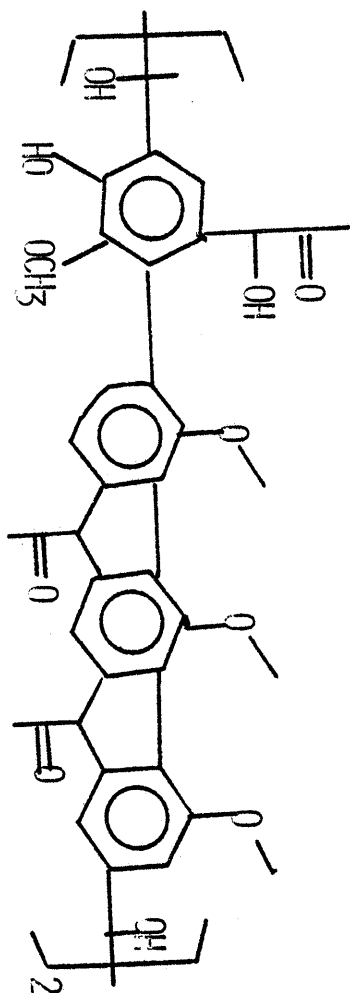


Figure 4.2 Schematic coke structure of Gillet & Urllings<sup>48</sup>

area with increasing power.

Skrigan, et al.<sup>50</sup>, believe the treatment of hydrolysis lignin to be economically feasible, as they describe a process to yield 250-280 kg of activated carbon along with valuable oils, phenols and gas from one ton of lignin.

#### 4.2 DTA and Other Thermal Treatments

With the advent of the DTA and DTG processes, a new line of research on the thermal behavior of lignin began. Much of the research done in this area is reported by the Russian workers, who have a particular incentive to develop processes for their vast forest resources. One major shortcoming of this research, however, is that the off-gases and volatiles are often not qualitatively or quantitatively analysed, a potential source of valuable mechanistic information. However, these DTA and DTG analyses do provide some insight into the behavior of lignins at high temperatures. Some aspects of DTA and DTG studies have been previously reported, yet they are conveniently organized into one section.

The thermal behavior of lignins of different woods isolated by different methods was studied by Domburg, et al.<sup>39</sup> These workers isolated lignin from aspen, birch, oak and spruce by the Bjorkman method, with DMS, alkali, alcohol, HCl and H<sub>2</sub>SO<sub>4</sub>. They found the DTA curves of different woods isolated by the same method much more identical than the curves of different preparations from the same wood species.

The sulfuric acid lignins were the most thermostable. Domburg, et al., report 400C as the temperature for bond rupture and devolatilization for these lignins. Because phenolic compounds with two and three carbon atom side chains were absent in the small yield of volatiles obtained, these workers claimed a paucity of aryl-alkyl ether linkages in the  $H_2SO_4$  lignins. They found these linkages intact in the Bjorkman, alcohol and HCl lignins.

The coniferous lignins were more thermostable than their deciduous counterparts. This is likely due, they propose, to the potential stable bond in the five position of the guaiacyl nucleus in the coniferous lignins, blocked in syringyl moieties.

From gravimetric data, Domburg, et al., obtained activation energy values for the degradation of these lignin preparations. The values ranged from 17.4 kcal/mol for an aspen sulfuric acid lignin to about 33 kcal/mol for an aspen alkali-methylated lignin. Only one other value was outside this interval, that of an aspen alkali lignin at 54.8 kcal/mol in the temperature range 340-370C. Their data are presented in Table 4.7.

In another study, Domburg and Sergeeva<sup>129</sup> investigated the thermal degradation of sulfuric acid lignins of hardwood. They proposed three stages for the pyrolysis of lignin in air. In the first, short side chains were assumed to be split from the primary nuclei. In the second, a stage they termed active pyrolysis, the bonds between the structural units were broken, resulting in a large quantity of volatile products. Radicals were formed in the solid phase, and their



Table 4.7 DTA Data of Domburg, et al.<sup>39</sup>

Lignin preparation	Wood species	Temperature range, C	Volatile products %	Activation energy, kcal/mol
Bjorkman lignin	aspen	180-290	14.6	22.8
		20-600	50.0	-
	spruce	180-270	10.4	18.3
		20-600	55.9	-
Dimethylsulphoxide lignin	aspen	160-200	4.0	31.2
		180-270	12.3	33.8
		20-600	68.8	-
	spruce	180-270	3.4	22.9
		20-600	41.4	-
Alcohol lignin	aspen	240-385	35.0	29.2
		20-600	54.0	-
	spruce	240-395	21.9	28.8
		20-600	65.5	-
Alkali lignin	aspen	250-290	22.4	28.9
		340-370	8.5	54.8
		20-600	48.3	-
	spruce	300-400	17.4	26.8
		20-600	48.3	-
Alkali methylated lignin	aspen	350-400	13.9	32.9
		20-600	67.2	-
	spruce	300-410	18.5	31.1
		20-600	56.3	-
Hydrochloric acid lignin	aspen	300-360	11.1	30.16
		20-600	52.0	-
	spruce	300-370	9.4	22.8
		20-600	42.3	-
Sulphuric acid	aspen	270-360	12.4	17.4
		20-600	36.1	-
	spruce	300-390	21.3	27.4
		20-600	32.3	-

subsequent recombination generated heat, overlapping with the endothermicity of bond breaking. The third stage was a series of destructive-condensation processes yielding volatiles and polynuclear aromatics.

The temperatures of decomposition were lower for acid insoluble lignins than that of acid soluble. The former began to decompose in the range 250-280, with a maximum rate at 290-340. The acid-soluble lignins decomposed at a maximum rate from 325-375.

The activation energies were once again rather low. Many values less than 20 kcal/mol were reported. Table 4.8 summarizes these data. These workers note that the range of activation energies found, 17.1-38.3, is in agreement with that found by other workers.<sup>130,131,132</sup>

In another study, Domburg and Sergeeva<sup>133</sup> subjected hydrotropic aspen lignin to thermal treatment at temperatures from 150 to 450C and examined the properties of the remaining solid residue. The lignins were held at the various temperatures for either one or 30 minutes. The yield of the residue dropped with increasing temperature and increasing duration of treatment. At low temperatures, the phenoxy, hydroxy, and carboxylic groups in the residue were reported to rise with increasing temperature of heat treatment, reaching a maximum near 250C. As the temperature of treatment increased further, the concentration of these groups dropped.

An interesting point in this research is the concentration of methoxy groups in the residue. Domburg and Sergeeva describe demethoxylation in terms of three stages. In the first, more than 3%

Table 4.8 DTG Data of Domburg and Sergeeva 129

Wood species	Lignin preparation	Temperature range, C	Weight loss	kcal/mol
when vapours and gases are removed				
Birch	acid-insoluble	200-290	10.2	25.8
	acid soluble	200-360	33.9	38.3
Aspen	acid-insoluble	200-320	11.1	24.5
	acid-soluble	200-365	15.2	17.8
Oak	acid-insoluble	200-320	12.1	26.1
	acid-soluble	200-355	16.4	18.6
in vapour-gas atmosphere				
Birch	acid-insoluble	200-385	18.5	19.6
	acid-soluble	200-390	18.3	24.0
Aspen	acid-insoluble	200-370	17.1	19.1
	acid-soluble	200-400	18.5	17.1

of the methoxyl groups were lost. This is attributed not to ether cleavage, but rather the loss of guaiacyl moieties, such as vanillin. In this range the investigators reported that the gases had an overwhelming smell of vanillin.

In the second stage, which is at temperatures from 200-250C, the methoxyl content remained constant. However, in the third stage, at 300C, there was a rapid, followed by more uniform, loss of methoxyl groups. They concluded that the methoxyl group was thermally stable, elimination by either cleavage occurring only at 300C and higher. They report that this is in agreement with the work of Andersen<sup>134</sup>, who found the aryl-methyl ether linkage stable to 235C.

In a continuing series of investigations, Domburg and Sergeeva<sup>135</sup> studied the change in the i-r spectra of the lignins after thermal treatment. Of particular interest in this study is the loss of a series of absorption bands attributed to methoxyl groups after thermal treatment to 350C. At 450C they noted a shift in some absorption bands and the appearance of new ones, which they linked to the development of additional carbon-carbon bonds and condensed benzene nuclei. They also reported changes in the i-r spectra with thermal treatment as low as 150-200C, indicating changes in the structure of the lignin macromolecule.

In yet another study<sup>136</sup>, the EPR spectra was recorded as the DTA was performed. The researchers recorded the concentration of paramagnetic centers with increasing temperature. The room temperature lignin had a PMC of the order of  $10^{16}$ , and each increase of temperature

by 100C increased the PMC by about one order of magnitude. They noted that the highest rate of PMC formation was before and after a period of exothermic reaction. The authors claimed a free radical mechanism for the thermal decomposition of lignin on the basis of this study. However, it is questionable as to whether the free radicals generated are all actually involved in the reaction sequences. The room temperature lignin had a PMC of  $10^{16}$ , indicating that the lignin radicals are relatively stable and may not be reactive.

The effect of methoxyl groups on the thermal action of lignin was studied by Domburg, et al.<sup>137</sup> They heated lignins from spruce and aspen wood and studied their thermal degradation by DTA. The study indicated that the presence of a second methoxyl group on the aromatic ring intensified the splitting of the aryl-alkyl ether bonds between lignin units. This was considered a factor in causing a high content of syringyl compounds to be identified in the volatiles of hardwood lignin pyrolysis. The DTA showed the splitting to occur at 150-320C. Interestingly, the replacement of the methoxyl group with a hydroxyl substituent lowered this temperature range to 150-200C.

Domburg, Sergeeva and Popov<sup>138</sup> have investigated the DTA behavior of lignins under conditions where gaseous products were variably removed. When the gaseous products were removed, active thermal degradation of the lignin began at 250-260C and peaked at 320C. In an atmosphere of the products, the degradation temperature range was widened and the main exothermic peak was shifted to a higher temperature. They note that the activation energy for the stage of increasing degradation rate

was higher for the case where gases were removed than where they were not, indicating a more intense free-radical combination process in the presence of gaseous products. In either case the activation energy was low, with a maximum value of 24.5 kcal/mol reported.

The DTA and DTG studies have generally indicated low activation energies, on the order 20-30 kcal/mol, for the pyrolysis of lignin. These are well below those commonly encountered in radical scission reactions, often postulated to represent the mechanistic features of lignin pyrolysis. Further, these activation energies are also lower than those for most single pericyclic reactions, a likely reaction possibility suggested by the lignin molecular topology. Thus, these DTA/DTG studies emphasize that overall lignin pyrolysis is likely a complex set of parallel and consecutive reactions of the type noted above. The superposition of these reactions evidently yields apparent overall activation energies lower than the fundamental values for most or all of the individual reactions.

#### 4.3 Effects of Additives on Lignin Pyrolysis

A major motivation for the elucidation of lignin and coal pyrolysis pathways is that these are often suggestive of reactions susceptible to catalysis, solvent effects and substituent effects, useful in the optimization of process conditions. Lignin has previously been subjected to thermolysis in the presence of various additives, and highlights of the research will be considered here. In preview, however, most of these investigations have been rather empirical in nature,

lacking in fundamental insights, and include dry distillation in the presence of metals, presumably to function as catalysts, distillation in an atmosphere of  $H_2$ , alkali addition and the more involved hydrogenation processes. Table 4.9 is a representative listing of some of the yields and products obtained by these various processes.

#### 4.3.1 Metals

As can be seen from Table 4.9, the addition of metals alone tends to increase the yields of tar only modestly. Phillips<sup>113</sup> has reported that the dry distillation of lignin in the presence of zinc dust yielded an oil in 16% quantity. Of this oil, 55% was phenolic in character, with guaiacol definitely identified. Likewise, Karrer and Bodding-Wiger<sup>114</sup> obtained a 17% yield of tar when pyrolysis of a lignin admixed with zinc dust.

Fuchs<sup>115</sup> distilled lignin in the presence of silver dust and obtained a 7% yield of tar. Melene and eugenol were notably identified among the pyrolysis products.

#### 4.3.2 Hydrogenations

As lignin is a carbon rich and hydrogen poor substrate, the more notable increases in yields of valuable tars and phenols occur in the presence of hydrogen. Inspired by the successes in the coal industry, many catalysts and operating conditions have been studied. While the yields of soluble products reported range from 10-100% of the lignin<sup>45</sup>, these hydrogenation processes are also expensive.

Table 4.9 Lignin Pyrolysis with Additives

REFERENCE	PROCESS	TAR	PHENOLS
116	Dist with H <sub>2</sub> and catalysts	17.8	6.9
117	Dist with H <sub>2</sub> and Zinc	16	9
54	Vacuum Dist <sup>2</sup> in CO <sub>2</sub>	28.3	9.8
139	Hydrogenation	44	
140	Hydrogenation	46.7	
118	Dist with H <sub>2</sub> and catalyst	62	35
141	Hydrogenation	55	15
142	"	70	26
	"	50	13.5
143	"	77	33
144	"	67	49
145	"	75	9
146	"	45	22.5
147	"		74.5
148	"	77	20
149	"		53
150	"		21
151	"		45
152	"	75	14
153	"	85	
121	"	65	21
154	"		29
155	"	73.5	47
156	"	65	45
46	"		46
157	"		50
159	"	48	9
158	"		32
160	"	86	40
161	"	80	35
162	"		46.2
114	Dist with Zinc dust	17	
163	Liquefaction	20-80	
64	Hydrogenation	20	to 80
113	Dist with Zinc	17	55
115	Dist with Silver	7	



Further, as in simple pyrolysis, the products are obtained as complex mixtures without a dominant compound.

An early lignin hydrogenation was performed by Fierz-David and Hannig<sup>116</sup>. In addition to the tar and phenols listed in Table 4.9, they also analysed the gases evolved during dry distillation. The gas consisted of CO, CO<sub>2</sub>, CH<sub>4</sub> and C<sub>2</sub>H<sub>6</sub> in proportions of 12.5%, 17.5%, 65% and 5.0% respectively. Comparison with the data of Heuser and Skioldebrand shows that the yield of CH<sub>4</sub> was increased considerably while that of CO dropped. Catechol is often reported as a significant phenolic hydrogenation product, indicating either the disruption of the guaiacyl methyl ether bond, or more facile hydrogenation of a diquinone type intermediate. The increase in CH<sub>4</sub> release paralleling the enhanced quantities of catechol may be indicative of mechanistic features for CH<sub>4</sub> formation.

Phillips<sup>117</sup> and Phillips and Goss<sup>54</sup> have examined the distillation of alkali lignin in the presence of zinc dust in an atmosphere of hydrogen. Phillips reported the detection of catechol, guaiacol and a considerable amount of CO<sub>2</sub>. He presumed the existence of a lactone, carboxyl or ester to account for the CO<sub>2</sub>. Phillips and Goss reported the detection of n-propylguaiacol as well as the products obtained by Phillips.

In 1941, Freudenberg and Adams<sup>118</sup> reported an increase in the yield of phenols by dry distillation in an atmosphere of hydrogen, but that a distinct advantage was gained in the use of a catalyst. They found nickel to be the best catalyst for this use.

Sergeeva, et al.<sup>64</sup>, have pyrolysed alkali lignin in a flow of hydrogen. From alkali lignins, a tar yield of 20% was obtained, with this tar comprised of 80 phenols and carbonyls.

Similarly, sulfuric acid lignins have been pyrolysed in a flow of hydrogen in the presence of catalysts<sup>119</sup>. A MoO catalyst with 5% ammonium molybdate was found to give the best results. A tar yield of 10% was realized.

The Japanese have studied the hydrogenolysis of lignin for some time. At the Noguchi Institute a catalyst was developed that produced a very high yield of liquid products. One yield reported was 36% phenols, of which 25% was p-cresol. A considerable amount of catechol was also reported<sup>120</sup>. A major advantage of this process is the relatively small number of phenols in the monophenol fraction, phenol, o-, p-cresol, ethyl- and propyl-phenol.

In 1961, the Crown Zellerbach Corporation obtained an option on this process, subject to laboratory evaluation of process conditions and economics. Although, many improvements were made, they were unable to make the process profitable for the U.S. market. However, Goheen<sup>121</sup> reported that the Noguchi process is the best liquefaction process available, with yields of distillable products approaching 65%. Monophenols are about 21% of the lignin charged, with 3% phenol, 4% o-cresol, and 6% m-, p-cresol. Goheen also discusses the major drawbacks and methods to increase profitability.

Hydrogenation effects higher yields of distillable products than does pyrolysis alone. Even the best process, however, is not

economically profitable, due to expensive hydrogen costs and complex product spectra.

#### 4.3.3 Alkali Addition

Less directly related to inert pyrolysis is the thermal treatment of lignin in the presence of alkali. Perhaps the first investigator to apply this technique was Erdmann<sup>122</sup>, who obtained catechol and protocatechuic acid as reaction products. It is noteworthy that catechol has been obtained as a dry distillation or pyrolysis product of lignin isolated by the alkali method.

Allan and Mattila<sup>36</sup> note that secondary oxidation of the catechol to oxalic acid may occur, and that this reaction is a strong function of the oxygen available to the fusion reactor. With the exclusion of oxygen, yields of 19% and 9% of protocatechuic acid and catechol, respectively, were obtained by Heuser and Winsvold<sup>123,214,125</sup>.

Early work also emphasized the significance of the reactor material. The use of iron greatly raised the yield of catechol, in part from the decarboxylation of the protocatechuic acid, which was not isolated. Experiments which added iron powder to the fusions increased the yields of both catechol and protocatechuic acid.

A review of this area including the chemical engineering advances is provided by Allan and Mattila<sup>30</sup>. Considered here will be the effect of alkali addition on pyrolysis.

Panasyuk and Panasyuk<sup>126</sup> have distilled hydrolysis lignin in various media, including 5%  $\text{Na}_2\text{CO}_3$  and NaOH. Yields of  $\text{CO}_2$ , phenols,

acids, and neutrals were 10.7%, 10.9%, 4.9%, and 8.5% for  $\text{Na}_2\text{CO}_3$  pyrolysis and 9.3%, 14.3%, 2.0% and 8.3% for pyrolysis with NaOH. These workers demonstrated that the  $\text{CO}_2$  evolution began at 260C, peaked at about 320C and then dropped off. Their data also showed that the yield of  $\text{CO}_2$  and phenols was sharply reduced when a high concentration of the impregnating catalyst was used. The authors concluded that the yield of degradation products was much higher in the presence of alkali than that in ordinary dry distillation.

Hydrolysis lignin was also pyrolysed in the presence of alkali by Chudakov and Sukhanovskii<sup>127</sup>. These workers mixed the lignin with the alkali to obtain a homogeneous plastic mass which was extruded in the form of filaments. The products obtained included protocatechuic acid and oxalic acid. At 200C, a yield of 34% oxalic acid could be realized.

Domburg, et al.<sup>128</sup>, have further studied the effect of alkali additions to lignin pyrolysis. They added to various lignin preparations 0.5-10.0% NaOH or  $\text{K}_2\text{CO}_3$ . They report that the main action of the NaOH additions above 300C was to facilitate rupture of aromatic-aliphatic bonds in the phenyl propane units, which lead to the formation of guaiacol and syringol. An optimal amount of 4% NaOH gave tars containing more than 40% guaiacol, syringol, and their derivatives.

In summary, it is notable that the yield of low molecular weight products can be affected by the presence of additives. The more telling changes occur with the use of hydrogenation catalysts, yet these processes are also more expensive and currently not economically

feasible. Alkali addition seems to change the nature of the products as well as the yields. As in the case of simple pyrolysis, the chemical pathways for pyrolysis in the presence of additives are obscure.

#### 4.4 Brief Comparison With Coal Pyrolyses

A comparison of the products of lignin and coal pyrolysis is provided in the data of Suuberg<sup>51</sup>, who has pyrolysed a Montana lignite and a bituminous coal in atmospheres of both helium and hydrogen. The lignite gave nominal ultimate yields of 5.4%, 1.4%, 8.4%, 7.1%, and 16.5% for tar, CH<sub>4</sub>, CO<sub>2</sub>, CO and H<sub>2</sub>O respectively, from pyrolysis in helium. The CH<sub>4</sub> proportion of the product gas was substantially lower from the lignite than from previous lignin pyrolysis, whereas the carbon oxides were higher. The rather significant lignite oxygen content is also reflected in the large yield of water, likewise characteristic of lignins. The same products were obtained in yields of 2.3%, 2.5%, 1.2%, 2.4% and 7.8% from the bituminous coal. These yields reflect the dehydration and deoxygenation reactions effected by the coalification process. Pyrolysis under 69 atm of hydrogen pressure resulted in significant increase in the CH<sub>4</sub> yield, reaching 9.5% for the lignite and 23.2% for the bituminous coal. The carbon-oxide and water yields were only modestly affected by lignite hydrolysis.

Thus, a significant difference in lignin and lignite pyrolysis is a reduced yield of CH<sub>4</sub> from the latter substrate, likely due in part

to the reduced methoxyl content of lignites. Both substrates yield carbon oxides in significant quantities, and water release seems facile for each. As might be suspected, coalification reduces the pyrolysis yields of water and oxygen containing species, reflected in the bituminous coal data of Suuberg. Not unexpectedly, pyrolysis under a high pressure of hydrogen can increase the yield of hydrogen containing volatiles significantly.

#### 4.5 Previous Model Compound Pyrolyses

To circumvent the uncertainties involved in the pyrolysis of the ill-defined lignin and coal substrates, compounds modelling the functionalities and chemical moieties of these have been employed for analysis. The investigations concerning the pyrolysis of model compounds have been related to a wide number of applications, and are thus rather diffuse in nature. With regard to lignin, these studies may be organized into four groups: the lignin interunit linkages, the methoxyphenols, the 3-carbon side chain units, and the CO<sub>2</sub> pathways. Table 4.10 is a list of the compounds and investigations referred to here, with model structure for clarification.

##### 4.5.1 Lignin Interunit Linkages

###### $\beta$ -ethers

The most prevalent lignin interunit linkage is the  $\beta$ -ether

Table 4.10 Previous Model Compound Pyrolyses

Compound	Structure	Reference
I. 1-(guaiacyl)-2-(2-methoxyphenoxy)propanol-1		Domburg <sup>75</sup>
II. 1-(3,4-dimethoxyphenyl)-2-(2-methoxyphenoxy)propanol-1		Domburg <sup>75</sup> , Savinykh <sup>76</sup>
III. 1-(guaiacyl)-2-(2-methoxyphenoxy)propanone-1		Domburg <sup>75</sup>
IV. monophenyglycol ether		Savinykh <sup>76</sup> , Kislitsyn <sup>77</sup>
V. 2-(2-methoxyphenoxy)ethanol		Savinykh <sup>76</sup>
VI. Phenetole(PHE)		Benjamin <sup>78</sup>
VII. Benzylphenyl ether (BPE)		Kayima <sup>79</sup> , Miller <sup>80</sup> , Savinykh <sup>81</sup>
VIII Guaiacyl benzyl ether		Savinykh <sup>81</sup>
IX. Phenylether(PE)		Kayima <sup>79</sup> , Ingold <sup>82</sup> , Starokadonskaya <sup>83</sup>

Table 4.10 Previous Model Compound Pyrolyses (cont'd)

Compound	Structure	Reference
X. Benzylether		Kayima <sup>79</sup> , Ingold <sup>82</sup>
XI. Benzylethyl ether		Collins <sup>84</sup> , Benjamin
XII. Pinoresinol		Domburg <sup>85</sup>
XIII. Bibenzyl		Miller <sup>80</sup> , Kayima <sup>79</sup> , Sato <sup>86</sup> Collins <sup>84</sup> , Benjamin <sup>78</sup> Brower <sup>87</sup> , Sweeting
XIV. o-hydroxydiphenylmethane		Benjamin <sup>78</sup>
p-hydroxydiphenylmethane		Benjamin <sup>78</sup>
diphenylmethane		Benjamin <sup>78</sup> , Sweeting <sup>88</sup> , Kayima
triphenylmethane		Benjamin <sup>78</sup>
tritoly methane		Benjamin <sup>78</sup>
ethyl diguaiacyl-methane		Domburg <sup>89</sup>
XV. Diphenyl		Ingold <sup>82</sup>



Table 4.10 Previous Model Compound Pyrolyses (cont'd)

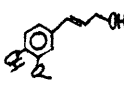
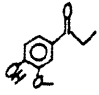
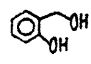

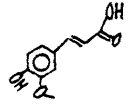
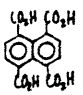
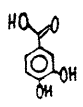
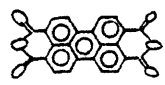
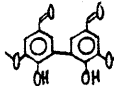
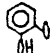

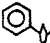
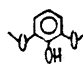

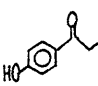
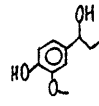
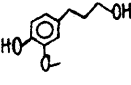
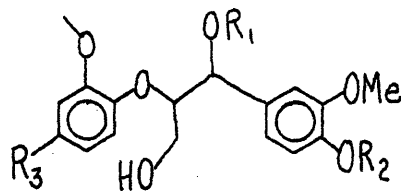
Compound	Structure	Reference
XXV. coniferylalcohol		Domburg <sup>99</sup>
XXVI. guaiacyl propanone-I		Kislitsyn <sup>100</sup>
XXVII. saligenol		Sprengling <sup>101</sup> , Gardner <sup>102</sup> , Cavitt <sup>103</sup> , Sliwa <sup>104</sup> , Brugidou <sup>105</sup> , Rapietrau <sup>106</sup> , Wakselman <sup>107</sup> , Cunneen <sup>108</sup>
XXVIII. acetone		Capelin <sup>109</sup> , Hinshelwood <sup>110</sup> , Wolf <sup>111</sup> , Froment <sup>115</sup>
XXIX. ferulic acid		Juntgen <sup>112</sup>
XXX. naphthalene tetracarboxylic acid		Juntgen <sup>112</sup>
XXXI. protocatechuic acid		Juntgen <sup>112</sup>
XXXII perylenetetracarboxylic acid anhydride		Juntgen <sup>112</sup>

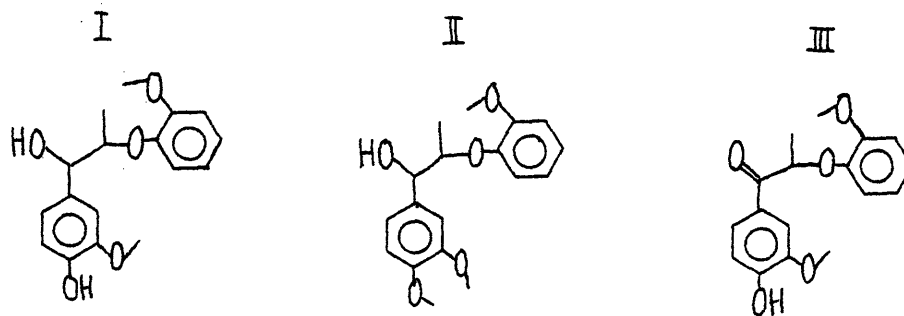
Table 4.10 Previous Model Compound Pyrolyses (cont'd)

Compound	Structure	Reference
XVI. dehydrodivanillin		Domburg <sup>90</sup>
XVII. guaiacol		Shaposhnikov <sup>91</sup> , Kravchenko <sup>92</sup> , Kiprianov <sup>93</sup> , Kislitsyn <sup>94</sup>
XVIII. veratrole		Shaposhnikov <sup>91</sup> , Kravchenko <sup>92</sup>
XIX. anisole		Shaposhnikov <sup>91</sup> , Friedli <sup>95</sup> , Obolentsev <sup>96</sup> , Kislitsyn <sup>97</sup> , Ingold <sup>82</sup>
XX. 2,6-dimethoxyphenol		Shaposhnikov <sup>91</sup>
XXI. benzaldehyde		Smith <sup>98</sup> , Ingold <sup>82</sup> , Brower <sup>87</sup>
XXII. p-hydroxyphenyl propanone-		Domburg <sup>99</sup>
XXIII. guaiacyl propanol-		Domburg <sup>99</sup> , Kislitsyn <sup>100</sup>
XXIV. guaiacyl propanol-3		Domburg <sup>99</sup>

linkage, which can be represented, in the lignin, as:



Relevant studies of the thermal behavior of these  $\beta$ -ether linkages have been reported by a small number of investigators, and among these, a study<sup>75</sup> of the thermal behavior of substituted  $\beta$ -ethers I, II and III is notable. The temperature of 50% weight loss for each of these was reported from DTA experiments conducted at 12C/min, the results aligning in the



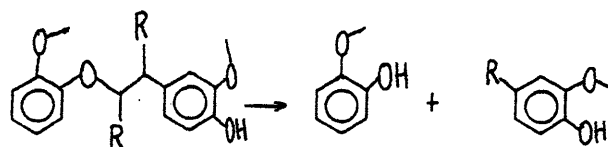
order I (280C) < II (310C) < III (365C). At temperatures lower than 340C, activation energies of 16, 15 and 82 kcal/mol were reported for I, II and III respectively. The thermal degradation products were analysed, and were as detailed in Table 4.11. The product spectra consisted of guaiacol, methyl-, ethyl- and propyl-guaiacols, cis- and trans-isoeugenol, vanillin, and acetovanillone, the latter two forming in much larger quantities from III than either I or II. The results were interpreted in terms of homolytic and heterolytic mechanisms. With regard to pathways, the large predominance of guaiacol and substituted guaiacols would appear indicative of a formal scission

Composition of thermal treatment products of  
 $\beta$ -ethers (%)

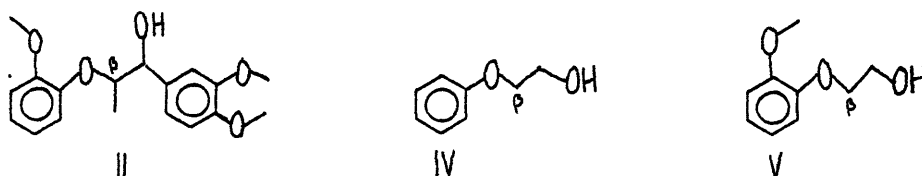
Compound	$\beta$ -ether I			$\beta$ -ether III	
	Thermal treatment temperature, °C				
	180	200	300	300	370
Guaiacol	1.2	6.2	11.2	8.4	23.5
Phenol	-	traces	traces	-	traces
Methylguaiacol	-	-	"	traces	"
Ethylguaiacol	-	-	"	3.6	6.4
Propylguaiacol	-	traces	"	-	-
Eugenol	-	"	"	-	-
cis-Isoeugenol	traces	0.5	0.4	-	-
trans-Isoeugenol	"	4.5	0.9	-	-
Vanillin	0.5	1.6	0.8	1.4	0.3
Acetovanillone	traces	0.3	2.9	10.4	14.2
X <sub>1</sub>	considerable amount	6.1	3.3	-	-
X <sub>2</sub>	"	5.5	2.9	-	-

Table 4.11 Products from  $\beta$ -ether pyrolysis (Domburg, et al.)

of the  $\beta$  carbon-oxygen linkage, of the type



Savinykh, et al.<sup>76</sup> probed the effect of methoxyl and phenyl substituents on the thermal behavior of lignin  $\beta$ -ethers. They heated compounds II, IV and V to 500C at a rate

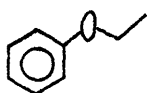


of 5C/min, and noted the temperature of 10% weight loss. The results aligned in the order IV (400C) > V(380C)  $\gg$  II(300C). While it is clear that the methoxyl group imparts modest pyrolysis activation (cf V,IV), the more pronounced effect is that of veratryl substitution (cf II,V). Compound II also differs from V in the existence of methyl substitution at the  $\beta$  carbon of II, but this is likely a smaller contribution to the increased reactivity of II than that imparted by the veratryl substituent. Overall, these experiments suggest that an appropriate  $\beta$ -ether model must incorporate the two benzene rings found in the 'true' lignin prototype.

An earlier study of the thermal behavior of  $\beta$ -ether IV was performed by Kislitsyn, et al.<sup>77</sup>, who report a heterolytic mechanism for ether degradation. These investigators pyrolysed IV in toluene at 400-500C, and neat at 400C, and determined the reaction products

by GLC. These products were phenol and ethylene oxide; notably absent was dibenzyl. The authors deduced the heterolytic mechanism on the basis of the clean pyrolysis to phenol and ethylene oxide, whereas radical pathways would have led to formation of other products, including dibenzyl.

The thermal behavior of phenetole (VI) in tetralin has been studied by Benjamin, et al.<sup>78</sup>, who



VI

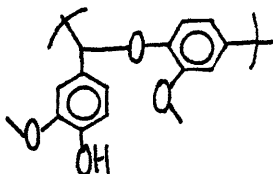
report a large number of compounds from pyrolysis at 400C. The major products were benzene, toluene, ethylbenzene, phenol, water, ethane and ethylene, while the minor products included propyl and butyl benzenes, p-ethyl phenol and a host of tetralin derived compounds. These workers report 5% substrate conversion at 500C and one hour reaction time, which corresponds to an apparent first order rate constant of  $10^{-4.85} \text{ s}^{-1}$ .

Overall, the experiments reported here for  $\beta$ -ethers suggest that an appropriate model must incorporate the two benzene rings found in the true lignin prototype; they further illuminate a lack of kinetic data and mechanistic insights.

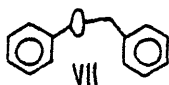
#### $\alpha$ -ethers

Another prevalent link in the lignin macromolecule arises from phenoxide attack of the intermediate quinonemethide yielding an  $\alpha$

alkyl aryl ether bond, as in:



This link has been studied in regard to both coal and lignin thermal behavior. A recent investigation was performed by Kayima, et al.<sup>79</sup>, who pyrolysed benzyl phenyl ether VII in tetralin at 320 and 400C.



At 400C, the ether was completely converted before 30 minutes of reaction time, and yielded 61% toluene, 66% phenol, and 27% benzyl phenol, on a product mole per reacted model compound basis. At 320C and 30 minutes, a conversion of 31.4% was attained, corresponding to an apparent first order rate constant of  $10^{-3.67} \text{ s}^{-1}$ . The product yields in this case were 55%, 50%, and 40% for toluene, phenol and benzylphenol, respectively.

An apparent first order rate constant of  $10^{-4.52} \text{ s}^{-1}$  was reported for BPE pyrolysis in tetralin at 300C by Miller and Stein<sup>80</sup>. These authors feel that free radical pathways are the predominant mechanistic feature of BPE pyrolysis, and extrapolate to coal chemistry as well. An estimate of the gas phase pyrolysis rate constant yielded a ratio  $k_{\text{liq}}/k_{\text{gas}} = 1.08$  at 300C, indicating a rather insensitive dependence of pyrolysis on phase differences.

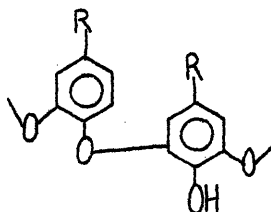
Savinykh, et al.<sup>81</sup>, have studied the thermal behavior of benzylphenyl ether VII and guaiacylbenzyl ether VIII in DTA experiments to

to 500C. Ether decomposition began at approximately 300C, reported to be cleavage of the alkyl C-O bond. The purported mechanism involved hydrogen abstraction by the generated phenoxy and benzyl radicals, which resulted in a phenoxbenzylidene ether radical. Further scissions and rearrangements of this radical resulted in a rather involved product spectrum, which included: benzene, benzaldehyde, dibenzyl, diphenylmethane, benzophenone, and o- and p- benzylphenols, as well as toluene and phenol.

The decomposition of lignin  $\alpha$ -aryl alkyl ether bonds thus appears to be a rather facile process resulting in predominantly phenol, toluene and benzylphenol derivatives in the presence of a hydrogen donor, and these and other secondary products without an external hydrogen donor. The constraints imposed by the macromolecular structure of lignin need be considered in any attempt to relate model  $\alpha$ -ether and lignin  $\alpha$ -ether pyrolyses, particularly with respect to secondary pathways.

#### Phenyl Ethers

The phenyl ether bond in lignin occurs in structures of the type,



and thus represents yet another interunit linkage. Diphenyl ether IX is thermally quite stable, as reflected in the pyrolysis studies reported in the literature. For example, at 450C, Kayima, et al.<sup>79</sup>, report essentially zero conversion of the substrate for 30 min. and



at 120 min. only 2%, implying an apparent  $\log_{10}k_{450}(s^{-1}) = -5.55$ . However, even at 120 minutes holding time, pyrolysis products were not reported.

As reported by Ingold and Lossing<sup>82</sup>, the ether will react at temperatures of 970-1175C. The products included hydrogen, carbon, acetylene, ethylene, CO, butadiene, benzene, diphenyl and trace amounts of phenol and radical species. These products are clearly indicative of aromatic ring opening reactions and secondary pyrolyses, demonstrating the refractory nature of the phenyl ether substrate.

In 1938, Starokadonskaya<sup>83</sup> determined an activation energy of 85 kcal/mol for the first order decomposition of phenyl ether. Even at 60 hr. reaction time, ether decomposition did not occur at temperatures lower than 440C. Thus, with regard to lignin pyrolysis, the phenyl ether linkage must be considered as a stable link at most temperatures of interest.

#### Pinoresinol Benzyl Ethers

Although the benzyl ether linkage does not exist as an isolable moiety in native lignin, the pinoresinol unit does contain elements likely to exhibit similar reactivity. Thus, it is reasonable to consider the literature of each simultaneously.

Kayima, et al.<sup>79</sup>, have pyrolysed benzyl ether X in tetralin and determined both product spectra and kinetics. The primary products, on a mole per reacted ether mole basis, were 106% toluene, 71% benzaldehyde, and 12% benzene. As CO was also detected, the benzene likely represents secondary decarbonylation of the benzaldehyde. The

authors note that the high yield of toluene was confirmed to result from hydrogenation of benzaldehyde by tetralin. At 400C and 30 minutes holding time, 65% ether conversion corresponds to an apparent first order rate constant  $k=10^{-3.23} s^{-1}$ , a rather facile cleavage.

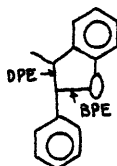
Benzyl ether thermal behavior has also been studied by Ingold and Lossing<sup>82</sup> who subjected the ether to temperatures of 860, 1050 and 1290C. The decomposition products included H<sub>2</sub>, CH<sub>4</sub>, ethylene, CO, formaldehyde, butadiene, benzene, benzaldehyde and trace amounts of benzyl alcohol and acetylene. They report little or no toluene present, and claim that this represents that the molecular rearrangement to toluene and benzaldehyde does not occur. However, the products are indicative of such severe primary and secondary pyrolysis that mechanistic insights must be considered tentative.

Benzyl ethyl ether XI has been examined in pyrolysis experiments by Collins, et al.<sup>84</sup> and Benjamin, et al.<sup>78</sup>. The former group report a product spectra consisting of ethane, ethylene, toluene and water, while the latter group report these and benzene. In both cases, water formation is considered significant and a likely source of water in coal solvent refining.

The actual pinoresinol structure XII was pyrolysed by Domburg, et al.<sup>85</sup>, in DTA and DTG experiments. The ether began to decompose at 240C, with maximal degradation at 320C. These workers report an apparent activation energy of 35 kcal/mol for ether degradation.

## Phenylcoumaran -- 1,2-Diphenylethane DPE

The lignin phenylcoumaran structure, depicted here, contains both benzyl phenyl ether and DPE (XII) elements, the former having been previously discussed.



Additionally, DPE units are present in small amounts in native lignins and further likely arise from lignin modification reactions in Kraft pulping. Thus a discussion of previous DPE pyrolysis is relevant here.

Miller and Stein<sup>80</sup> have studied both the gas and liquid phase pyrolysis of 1,2-diphenylethane (DPE). Their liquid phase rate data, obtained in tetralin over the temperature interval 325-425C can be represented by  $\log_{10} k_l = 16 - 64.8/\theta$ , where  $\theta = 0.004576 \cdot T$ , with T in Kelvins. A gas phase rate constant for 650C was established in low pressure experiments,  $k_g = 2 \cdot 9 s^{-1}$ , and assuming an activation energy of 61 kcal/gmol, these workers represent the gas phase data as  $\log_{10} k_g = 14.9 - 61/\theta$ . At 400C, these expressions yielded  $k_l/k_g = 0.54$ , in reasonable accord. At 375C, the product spectra consisted of toluene, trans-stilbene, 1,1 DPE, ethyl benzene, 1,2,3,4-tetraphenylbutane and phenanthrene. The products and kinetics were interpreted in terms of a free radical reaction scheme, and were extended to coal conversion processes as well.

Kayima, et al.<sup>79</sup>, have studied DPE pyrolysis in tetralin at 450C. They obtained toluene in 100% yield, with an apparent first order rate constant  $k_{450} = 10^{-3.67} s^{-1}$ . Sato, et al.<sup>86</sup>, studied the thermal

behavior of DPE in both the liquid and gas phases from 360 to 460C, in the presence of tetralin. The liquid phase reaction products were mainly toluene, naphthalene and hydrogen, in proportions suggesting the stoichiometry:  $\text{DPE} + \text{TET} \rightarrow 2\text{T} + \text{N} + \text{H}_2$ . The gas phase results were quite similar, with traces of benzene, ethylbenzene and styrene also detected. At higher conversions and lower proportions of the external hydrogen donor tetralin, transstilbene and phenanthrene were detected as well. Rate data were fit to the Arrhenius expression, yielding  $\log_{10} k_l s^{-1} = 14.4 - 61.5/\theta$  and  $\log_{10} k_g s^{-1} = 14.8 - 60.4/\theta$  for the liquid and gas phase data, respectively. A free radical scheme was proposed which accorded well with the observed pyrolysis behavior.

Collins, et al.<sup>84</sup> report 15% conversion to toluene from DPE pyrolysis at 400C and 18 hr., whereas at 300C and even 68 hr., the compound was inert. Similarly, Benjamin, et al.<sup>78</sup>, found less than 5% DPE conversion in tetralin at 400C for one hour. These workers have also pyrolysed a series of substituted 1,2 DPE moieties, and in general, substitution increased the reactivity.

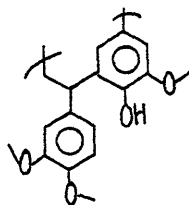
Other DPE pyrolyses include that of Brower<sup>87</sup>, who detected traces of toluene from DPE exposure at 400C in tetralin and that of Sweeting and Wilshire<sup>88</sup>. These latter workers provide neat pyrolysis data at 700C, where in addition to toluene, stilbene and phenanthrene, benzene, ethylbenzene, styrene, diphenyl, diphenylmethane and flourene were detected. The authors estimate the reaction time to be 24 seconds, which corresponds to an apparent first order rate constant

$k_{700} = 10^{-0.82} s^{-1}$  for the 2.56 pyrolysate weight percentage of DPE reported.

Overall, a wealth of quantitative and qualitative DPE pyrolysis data exist in the current literature. The major products are toluene, stilbene and phenanthrene, with many others reported at various conditions of tetralin dilution and reaction severity. Toluene has been reported to be generally the predominant major product, reported in yields even as high as 100%.

#### Diphenylmethane Units

The diphenylmethane linkage, existing in lignin as depicted here,

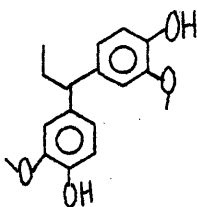


is best modelled as are ortho-hydroxy diphenylmethane (OHD) XIII unit. Benjamin, et al.<sup>78</sup>, have pyrolysed both the ortho- and para-isomers of this compound at 400C in tetralin. The ortho isomer yielded phenol and toluene exclusively as products, while the para isomer gave predominately these and also traces of benzene and paracresol. The ortho isomer was more reactive, being described by an apparent first order rate constant  $k_o = 10^{-4.21} s^{-1}$ , as compared to  $k_p = 10^{-4.53}$  for the para isomer at 400C. The similarity in product spectra for the two isomers is suggestive of common mechanistic features, perhaps involving isomerization of the para to the ortho compound. These investigators also found diphenylmethane, triphenylmethane, and tritolylmethane to be completely stable at 400C and 18 hr. reaction time, suggesting that the hydroxyl group may in fact participate in the decomposition

mechanism, rather than simply impart electronic activation. Similarly, Sweeting and Wilshire<sup>88</sup> found diphenylmethane essentially unreacted at 700C and an estimated 24 sec. contact time, with only very small amounts of toluene, benzene, and flourene reported. At 700C, an estimate of a first order rate constant implied by their data is  $k=10^{-2.54} s^{-1}$ , likely subject to considerable uncertainty due to the low conversions reported.

Kayima, et al.<sup>79</sup>, report a substrate conversion of 1.7% at 450C and 30 min. holding time in tetralin, yielding an apparent first order rate constant  $k_{DPM}=10^{-5.02} s^{-1}$  for diphenylmethane. The decomposed substrate gave benzene and toluene in 100 and 95% yields, respectively. As with the data of Sweeting and Wilshire, these data are likely subject ot the uncertainty inherent in very low conversion experiments.

A slightly more representative lignin model compound was studied by Domburg, et al.<sup>89</sup>, who pyrolysed ethyl diguaiacylmethane, XIV, shown here



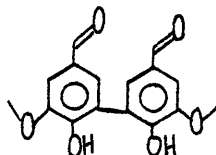
The compound was subjected to DTA study at a constant heat-up rate of 12C/min. The most vigorous decomposition occurred at 350-390C, with an apparent activation energy of 34 kcal/mol. The investigators attribute the decomposition to the cleavage of alkyl-aryl bonds, yet the guaiacyl methoxyls can hardly be expected to react only at higher

temperatures than the diphenylmethane moieties.

### Biphenyl Linkages

The biphenyl linkage as depicted by actual biphenyl XV is quite thermostable. For example, Ingold and Lossing<sup>82</sup> decomposed biphenyl from 1300 to 1500C, and detected a product spectra consisting of hydrogen, carbon, acetylene, ethylene, butadiene and benzene. However, the same authors have also pyrolysed benzene from 1350-1450C, and obtained a similar product spectrum. Thus, this high temperature biphenyl pyrolysis likely represents aromatic ring opening reactions either in addition to or to the exclusion of direct biphenyl cleavage to two phenyl radicals.

More representative lignin model compounds have been pyrolysed by Domburg, et al.<sup>90</sup>. These investigators studied the thermal behavior of dehydrodivanillin XVI when subjected to DTA experiments to 600C at 12C/min.



They report a maximal evolution of volatile products at 325C, and have identified a crystalline substance of m.p.83 C as vanillin. A yield of 12% vanillin was determined from methoxyl group loss, as Domburg, et al., parenthetically note that thermal treatment of vanillin to 350C does not result in methoxyl group loss. These authors report that vanillin formation is possible only by rupture of the carbon-carbon bond between guaiacyl units and that this, therefore, occurs at about 300C, with an activation energy of 61 kcal/mol, even in light of diphenyl bond energies of 93.7-103.0 kcal/mol. Assuming the cleavage

of this diphenyl bond to be a rate determining step in dehydrodivanillin pyrolysis, and an Arrhenius A factor as high as  $10^{16}$ ,  $\log_{10}k = 16 - 93.7/\theta_{300}$  as a maximal estimate, which at 300C yields  $k = 1.65 \times 10^{-20} \text{ s}^{-1}$ . Thus, at 300C, 12% conversion to vanillin could be realized in approximately  $t = -\ln X/k = 1.28 \times 10^{20} \text{ s} = 4.1 \times 10^{12}$  years. Even with an activation energy of 61 kcal/mol, this rupture would take approximately 1.33 years. Thus, while the addition of ortho hydroxyl groups might be expected to lower the thermostability of the diphenyl linkage, the direct rupture to vanillin at 300C is rather questionable. Of equal doubt is the stability of the carbonyl and guaiacyl methoxyl groups.

In summary, the literature depicts the reactivity of the various lignin interunit linkages as ranging from facile for the alkyl-aryl ethers to modest or negligible for aryl-aryl linkages. Thus, in a lignin pyrolysis at 400-600C, the  $\alpha$ - and  $\beta$ -ethers, pinoresinol, phenylcoumaran and orthohydroxy diphenylmethane units might be expected to be reactive, with the  $\alpha$ - and  $\beta$ -ethers dictating the essential lignin behavior by virtue of their predominant proportions.

#### 4.5.2 Methoxy Phenols

The aromatic methoxyl unit is a characteristic moiety of lignin. Pyrolysis of several simple related model compounds have been reported, many by Russian investigators. These will be discussed sequentially, by compound identity, as each models a unique aspect of lignin.

Guaiacol (XVII)

Coniferyl alcohol accounts for up to 80% of the monomer alcohols



which constitute lignin, and thus serves as the most important lignin methoxyphenol moiety for modelling. The phenolic hydroxyl of coniferyl alcohol exists in lignin as either a free or etherified hydroxyl, the former well depicted by guaiacol. The etherified hydroxyl can be modelled by veratrole, to be discussed below.

Shaposhnikov and Kosyukova<sup>91</sup> report both demethylation and demethoxylation from pyrolysis of guaiacol in an atmosphere of helium at 500-600C. Cresols and xylenols were obtained in yields of 40-50%, phenol in 20% yield, and catechol in 28% yield. The catechol yield could be increased to 45% with pyrolysis in a steam atmosphere, which also resulted in a decrease in cresol and xylene yield. These workers obtained similar results for p-methylguaiacol pyrolysis, indicating a relative insensitivity to para substitution.

Another study of guaiacol pyrolysis is that of Kravchenko, et al.<sup>92</sup>, who determined the variation of the product spectra with pyrolysis temperature. Pyrolysis at temperatures of 450-550C resulted in the formation of phenol, o-, m-, and p- cresol, xylene, catechol, and ethyl- and methyl-catechol. From 450-550C, the yields of cresols and phenols monotonically increased. Catechols, however, attained maximum proportions at about 530C, whereupon the yield dropped with further increases in temperature, suggesting secondary pyrolyses. In a similar vein, Kiprianov and Kravchenko<sup>93</sup> have pyrolysed guaiacol and determined a temperature of 530-550C and a holding time of 0.5 - 2 sec. as optimal for catechol production.

Pyrolysis at 500C and 2 seconds holding time in a flow reactor

effected a 30% guaiacol conversion as reported by Kislitsyn, et al.<sup>94</sup>. These workers determined a product spectrum consisting of: 4.2% phenol, 28.6% o-cresol, 13.5% 2,6-xyleneol, 10% 3,5 xyleneol, 4.8% salicaldehyde 40% catechol and 1.4% saligenol. The addition of benzoyl peroxide facilitated the reaction as evidenced by a 45% conversion at 430C.

The products of pyrolysis reported here provide insight into the reactions of guaiacol. The large proportions of catechol indicate that demethylation is an important reaction. The yields of phenol also suggest demethoxylation, however, the accompanying yields of cresols and xyleneols suggest that these pyrolyses were effected at rather high conversion, enhancing the likelihood of secondary pyrolyses. Finally, the reports of saligenol and methyl catechol indicate that isomerization and rearrangement reactions may be appreciable.

#### Veratrole (XVIII)

As earlier noted, etherified coniferyl alcohol monomers constitute a substantial portion of the lignin macromolecule. Assuming the methyl-ether to be a reasonable depiction of the general lignin alkyl-ether, veratrole has been pyrolysed in an effort to elucidate lignin thermal pathways. Shaposhnikov and Kosyukova<sup>91</sup> obtained phenol in 50% yield, cresols and xyleneols in 22-33% yield, and small amounts of catechol from veratrole pyrolysis. The high yield of phenol indicates both formal demethylation and demethoxylation. Similarly, Kravchenko, et al.<sup>92</sup>, report a veratrole product spectrum which consisted of phenols which were chiefly cresols and xyleneols. Thus, it is clear that veratrole degrades by both demethylation and demethoxylation

reactions, and is likely susceptible to secondary reactions at the temperatures required for primary pyrolysis. This should be expected, as the primary demethylation product would be guaiacol, already demonstrated susceptible to demethylation, demethoxylation and isomerization at temperatures in the range of 400-600C. The formal primary demethoxylation product is anisole, although an anisole isomer cresol may be equally likely.

#### Anisole (XIX)

Comparison of anisole pyrolyses with those of guaiacol and veratrole probes the effects of ortho hydroxy and methoxy substituents. As with the latter two models, anisole undergoes formal demethylation and demethoxylation reactions when subjected to pyrolytic conditions. For example, Shaposhnikov and Kosyukova<sup>91</sup> report a 66% yield of phenol from anisole pyrolysis accompanied by 6-7% cresols and xylenols. The 66% yield of phenols, indicative of predominant demethylation, contrasts with the 50% yield of phenol from veratrole, suggesting both demethylation and demethoxylation. In accord with these results, Freidlin, et al.<sup>95</sup>, report a phenol/benzene, ratio of 15/1 from anisole pyrolysis, again indicative of predominant demethylation. Other products included toluene, CO, CH<sub>4</sub>, and H<sub>2</sub>. The addition of steam did not affect the product spectrum but actually decreased the reaction rate.

A rather extensive analysis of the anisole pyrolysis product spectrum was provided by Obolentsev<sup>96</sup>, who studied the reactions of this substrate at 500C. At 40% conversion, product proportions, in weight percent of the total products included 1.3% H<sub>2</sub>O, 0.5% acetone,

10.6% benzene, 0.8% toluene, 24.4% phenol, 2% cresol, 6.1% benzaldehyde and 34.4% either unidentified or lost. The proposed reaction scheme involved primary isomerization to benzylalcohols and aromatic phenols, which condense to yield  $H_2O$  and dimers, the latter capable of degrading to toluene and benzaldehyde. The benzaldehyde produced is further capable of degradation to benzene and CO. Other products, notably  $CH_4$  and phenol, are interpreted in terms of free radical scission of the aromatic ether bonds.

Kislitsyn, et al.<sup>97</sup>, also suggest a free radical decomposition for anisole during pyrolysis. They suggest fission of the aromatic O-Me bond, yielding phenoxy and methyl radicals, which can participate in chain or rearrangement processes. The addition of benzoyl peroxide, presumably to function as a radical initiator, had no appreciable effect on the pyrolysis.

A higher temperature pyrolysis was effected by Ingold and Lossing<sup>82</sup>, who pyrolysed anisole to 800C. The products included  $H_2$  and CO in approximately equal yields, methane in about one-third of the quantity of CO, phenol and benzene in a ratio  $PhH/PhOH = 3/1$  and toluene, ethylene, ethane, formaldehyde and butadiene. Thus, at 800C, demethoxylation appears predominant over demethylation, as reflected in an approximate 3 fold ratio of both  $CO/CH_4$  and  $PhH/PhOH$ . As demethylation was predominant at lower temperatures, demethoxylation would like occur with a higher energy of activation.

#### 2,6-Dimethoxyphenol

A model of the sinapyl alcohol units incorporated into lignins,

2,6-dimethoxyphenol (XX) also probes the effect of methoxy substitution on the reactivity of guaiacol. The previous studies of the pyrolysis of this substrate are few, however, Shaposhnikov and Kosyukova<sup>91</sup> provide an exception. The authors describe the main reaction as demethylation of one methoxyl group, yet list the main pyrolysis products as o-cresol and guaiacol. Thus, any consistent reaction network must involve the secondary demethoxylation and other reactions of a methoxy catechol intermediate.

In comparison of guaiacol, veratrole, and anisole, it would appear that demethylation, demethoxylation and isomerization reactions occur for each. In the temperature range 400-600C, demethylation seems modestly predominant for guaiacol and veratrole, but overwhelmingly predominant for anisole. This is suggestive of demethoxylation pathways accessible to guaiacol and veratrole that are not accessible to anisole, which would obviously involve the ortho-hydroxy or methoxy substituent. In general, however, the literature pyrolyses appear to have been effected at rather high conversions, which would encourage the occurrence of significant secondary reactions and thus provide product spectra little indicative of reaction pathways. This is especially true for the reported pyrolysis of 2,6-dimethoxyphenol, which yields products suggestive of extensive secondary reactions.

#### 4.5.3 Side Chain Units

Previous experiments relating to lignin side chain unit pyrolyses arise from both lignin- and non-lignin-related experiments. As facile

ether cleavage likely renders many different potentially reactive substrate units, seemingly unrelated pyrolyses as well as more traditional lignin-related pyrolyses can be effectively blended to depict the essential elements of lignin side chain reactivity.

Rather direct lignin side chain model compounds have been studied by Domburg, et al.<sup>99</sup>, who have pyrolysed p-hydroxyphenylpropanone-1 (XXII), guaiacylpropanol-1 (XXIII), guaiacylpropanol-3 (XXIV), and coniferylalcohol (XXV), in a series of DTA experiments. They report a strong dependence of the mechanism of thermolysis on the structure of the side chain. Degradation occurred at temperatures of 320, 275, 320 and 380C for compounds (XXII)-(XXV), respectively.

For compound XXII, the start of volatile liberation occurred at about 210C, with the main process of destruction at 260C. This degradation peaked at 325C, corresponding to completion of carbon-carbon bond rupture. The energy of activation for this process was reported at 33.4 kcal/mol, a rather low value for carbon-carbon bond rupture. The authors estimate the value of the  $\alpha$  carbon-carbon bond to be 84-88 kcal/mol, while that of the  $\beta$  bond to be 62 kcal/mol. They thus propose cleavage of the  $\beta$  bond as most likely.

The degradation of compound (XXIII) began at 160C and reached a maximum at 250C. Domburg, et al., feel that due to the activating effect of the phenolic hydroxyl, the benzyl alcohol group is very reactive and participates in various intra- and intermolecular dehydration reactions. They point to a rather low activation energy for this stage of pyrolysis, 15.1 kcal/mol, as evidence for these, as well as other possible condensation reactions. After the

dehydrations, a second stage comprised of carbon-carbon bond rupture in the propane side-chain occurred at 275C. The activation energy in this stage was 37.0 kcal/mol, reported to reflect rupture between the  $\alpha$  carbon and the benzene nucleus as well as  $\alpha$ ,  $\beta$  carbon cleavage.

The behavior of compound (XXIV) was similar to that of compound (XXII). The maximum rate of destruction was at 330C, with an activation energy of 33-36 kcal/mol. Again, carbon-carbon bond rupture was presumed.

The thermal breakdown of compound (XXV) was the most complex observed. The investigators proposed three stages for this breakdown.

In the first, it was suggested that intermolecular condensation-polymerization reactions occur, at temperatures from 240-300C. The activation energy was low, about 5.3-9.1 kcal/mol, with little heat absorption. Domburg, et al., proposed a mechanism of thermal polymerization similar to the enzymatic polymerization of coniferyl alcohol reported by Freudenberg<sup>4</sup>.

The second stage was one of carbon-carbon bond rupture proceeding at a maximum rate near 420C. Even with a double bond in the side chain, the reported activation energy was only 27.5 kcal/mol. A significant exotherm on the DTA trace at 444C was reported, presumably due to condensation and recombination processes. Additionally a large amount of volatile emission was reported in this stage.

The third stage consisted of rearrangement without volatile emission, yielding a coke by 600C.

From these studies, it was concluded that the structure of the side chain had a significant effect on the nature of phenylpropane

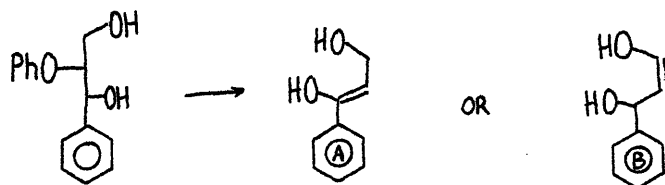
degradation. From the DTA traces they concluded that carbon-carbon bond rupture occurred by a free radical mechanism at temperatures as low as 275C and with activation energies from 27-37 kcal/mol.

Phenylpropane derivatives with variations in the side chain have also been pyrolysed by Kislitsyn, et al.<sup>100</sup> These workers compared the thermal behavior of guaiacylpropanol-1 (XXIII) and guaiacylpropanone-1 (XXVI). The pyrolyses were at 400-500C, and the reaction products were analysed by GLC.

Guaiacylpropanol-1 decomposed in two manners. The first was dehydration with the formation of isoeugenol. The isoeugenol both isomerized to eugenol as well as dealkylated with the formation of guaiacol. The second pyrolysis pathway was considered to be intramolecular rupture of the aryl-alkyl carbon bond leading to the formation of guaiacol and propionic aldehyde.

The guaiacylpropanone-1 degraded in a different manner. At 500C, scission between the carbonyl and methylene carbon as well as conversions of the guaiacyl nucleus were important.

A different type of side chain moiety could arise from reversion of the prevalent  $\beta$ -ether link as in,



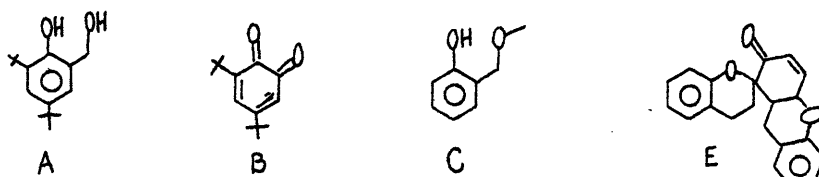
These dihydroxyl ene-ol moieties are likely very unstable and are thus difficult to model. However, saligenol (XXVII) provides an isolable model with the same essential ene-ol characteristics, stabilized by



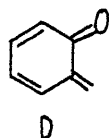
the benzene ring. The relevance of saligenol to the true lignin dihydroxyl is illustrated here.



Saligenol pyrolysis has been rather well studied with regard to Diels-Alder additions involving the saligenol dehydration product. For example, Sprengling<sup>101</sup> heated an olefin and the methylolphenol (A) to 180C and determined a nearly exact molar equivalence of H<sub>2</sub>O evolution and substrate (A) disappearance. The product residue was divided into three fractions, two of which were self-condensation products of the methylolphenol, and one which was an olefin adduct containing only about 1% hydroxylic groups. All three fractions were considered to arise via the quinonemethide.

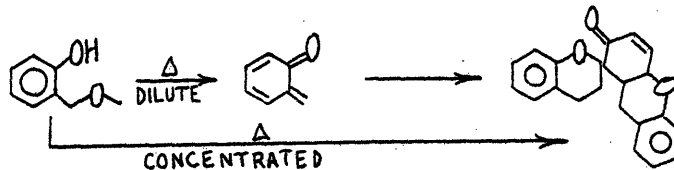


Gardner, et al.<sup>102</sup>, have isolated the quinonemethide (D) and its

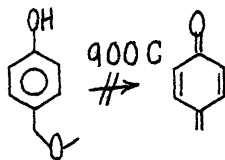


self condensation product from pyrolysis of o-methoxymethylphenol (C). In dilute gas-phase experiments, (D) was trapped at liquid nitrogen temperature. The substance was solid up to -50C, and a stable liquid

from here to 0C. From 0-25C a solid slush was formed and identified as the trimer of D. This trimer, E, could also be formed on the reactor walls at conditions of high substrate concentrations. Subsequent experiments (103) identified the trimer as the product of two successive Diels-Alder reactions via the scheme:



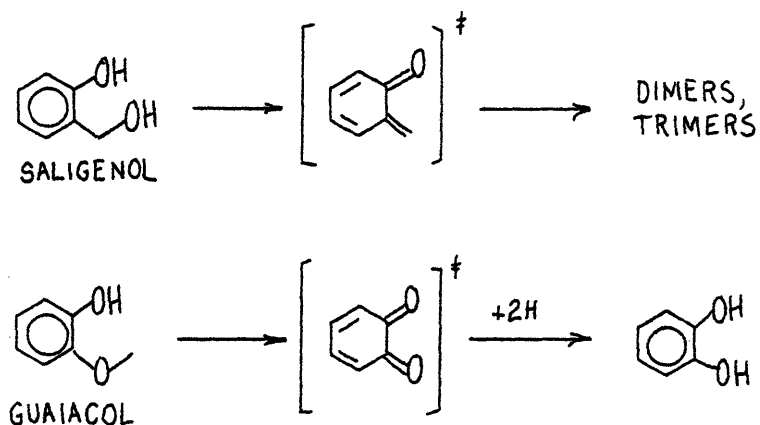
These workers also report the para-methoxymethylphenol stable to 900C, and therefore unable to form the paraquinonemethide in a similar manner, i.e.,



Numerous other investigations have been reported which have varied either the phenolic substrate or the dienophile used to trap the intermediate quinonemethide<sup>104-108</sup>. In each case, the condensation reaction is reported to occur through the highly reactive quinonemethide, which establishes that the principal reaction of saligenin must be considered to be a stoichiometric dehydration to water and the ortho-quinonemethide (D). The kinetics of this reaction have not been reported, and are required for applications to lignin pyrolysis. However, it should be noted that these reactions have been performed

at temperatures near 200C, at least 150C below the reaction temperatures of other lignin model compounds. Thus, even with the stabilization provided by the aromaticity of the benzene ring, the dehydration of saligenol is quite facile. The analogous lignin reaction must then be rapid indeed, as aromatic stabilization of the ene-ol moiety is absent.

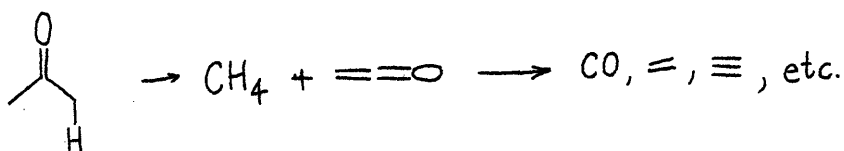
Distinction between the literature of saligenol and the literature of guaiacol is manifest in consideration of the fate of the quinonemethide. Dehydration of saligenol might be formally compared to demethanation of the isomeric guaiacol, which would result in an analogous diquinone intermediate. Catechol is reported as a major product of guaiacol pyrolysis, whereas o-cresol is not reported for saligenol. Thus reactions of the quinonemethide and the hypothetical diquinone are not similar. The former readily participates in a condensation reaction, while the latter would seem to more readily abstract hydrogen, as in:



Of course, it is quite likely that many of the unidentified products

reported from guaiacol pyrolysis arise from an intermediate of the type formally described here.

With regard to the Freudenberg structure, units 2 and 18 depict 1-guaiacyl-3-hydroxyl substituted acetone moieties. Thus an understanding of acetone (XXVIII) pyrolysis would have applications in the thermal behavior of lignin side chains. A high temperature acetone pyrolysis has been performed by Capelin, et al.<sup>109</sup>, who obtained CO, CH<sub>4</sub>, H<sub>2</sub>, acetylene, ethylene, ethane and benzene in yields of 1.14, 0.85, 0.54, 6.23, 0.1, 0.07 and 0.04 mols from 1.36 original acetone mols. Thus, most of the carbonyl group of acetone leads to CO production, and about half of the methyl groups yield methane, the other half leading to hydrogen, ethane, ethylene, acetylene, and benzene. The reaction has been envisioned<sup>110</sup> to occur through a unimolecular decomposition to ketene, which suffers further secondary pyrolysis to CO, ethylene and polyketenes, as in:



However, more recent studies propose free radical mechanisms for temperatures as low as 510C. Finally, studies over a wider temperature range<sup>111</sup> demonstrated that acetone pyrolysis occurs as low as 500C.

The hydroxylic and guaiacyl substituents will not only change the nature of the product spectrum, but should likely affect the reactivity of the whole lignin acetone moiety. In analogy to the effect of phenyl and electron donating substituents on the reactions

of  $\beta$ -ethers, both should serve to increase the acetone unit degradation rate.

Of the compounds similar to other carbonyl moieties initially present or formed as reaction intermediates in lignin pyrolysis, benzaldehyde (XXI) has been the most extensively studied. An early study of benzaldehyde pyrolysis behavior is provided by Smith and Hinshelwood<sup>98</sup>, who determined the major reaction pathway at 500C to be decomposition to benzene and CO, with a side reaction yielding diphenyl. The reaction rate was lowered a finite amount by the addition of nitric oxide, a free radical chain inhibitor. Thus, the reaction was postulated to be composed of two parts, a first order uninhibited component and a variable order inhibited component. The kinetic results were thus explained in terms of a superposition of a first order molecular rearrangement reaction to yield stable products and a free radical chain reaction.

A higher temperature benzaldehyde pyrolysis was performed by Ingold and Lossing<sup>82</sup> who studied the decomposition reactions at 1100 and 1400C. The major products were hydrogen, CO, and benzene, accompanied by carbon, methane, acetylene, ethylene, formaldehyde, butadiene and diphenyl, and possibly acrolein and 1,5-hexadiene-3-ene. These workers also detected phenyl and a trace of benzoyl radicals. Again, these authors conclude that it is quite probable that the direct molecular rearrangement to benzene and carbon monoxide is substantial.

Brower<sup>87</sup> has studied the reactions of benzaldehyde in tetralin at 400C. Benzaldehyde was not hydrogenated, but rather it was decarbonylated to carbon monoxide and benzene in 17% yield. As the reaction was

conducted in a glass tube, catalysis analagous to that of transition metals was considered unlikely. Thus, these results are also consistent with a molecular elimination of CO to yield benzene from benzaldehyde.

From the reported studies of benzaldehyde pyrolysis, it would appear that decarbonylation reactions may be a significant source of the high CO porportion of the lignin pyrolysis gas fraction. Clearly, vanillin, cinnamaldehyde, and acetophenone pyrolyses are needed to probe the effects of substitutions more typical of lignin carbonyl moieties, such as the guaiacyl hydroxyl activation, the effects of styrene conjugation, and carbonyl substitution, respectively. However the results of previous benzaldehyde pyrolyses suggest this to be a fruitful area of investigation for the elucidation of CO producing lignin pyrolysis pathways.

#### 4.5.4 CO<sub>2</sub> Precursors

The major lignin pyrolysis product gases, CO and CH<sub>4</sub>, are accompanied by much smaller amounts of CO<sub>2</sub>. The origin of this gas is not clear, either arising from the lactonic and carboxylic groups arising from lignification free radical exchange reactions, or from modifications of the lignin induced by isolation methods.

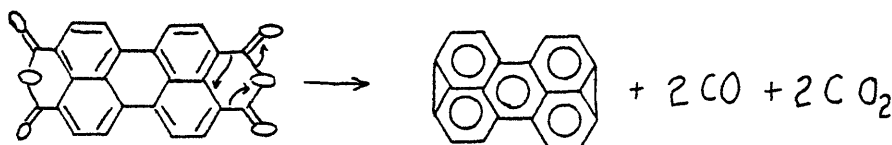
A series of carboxylic acids was pyrolysed by Juntgen and van Heek<sup>112</sup> while studying gas release from coal as a function of heating rate. These investigators pyrolysed ferulic acid XI, naphthalene tetracarboxylic acid XXX, protocatechuic acid XXXI, and perylenetetracarboxylic acid anhydride XXXII.

Ferulic acid XXIX, a lignin precursor with the guaiacyl moiety, decarboxylated at a maximum rate near 225C. The activation energy for this process was 27.7 kcal/mol. At these temperatures no other products were reported.

Compound XXX dehydrated in a range of temperature from 150 to 250C, with a maximum rate at 200C. The release of water resulted in anhydride formation. An activation energy of 33.5 kcal/mol was reported for this process.

Protocatechuic acid XXXI released water in two stages and CO<sub>2</sub> in one. The first stage of water release occurred near 100C, and had a low energy of activation, 18.8 kcal/mol. This led the researchers to conclude that this was a physical release of water. In the second stage, both water and CO<sub>2</sub> were eliminated, with a maximum rate near 250C. The activation energy for this stage was 40.4 kcal/mol.

The maximum rate of CO and CO<sub>2</sub> release for compound XXXII was at 500C. Activation energies were reported at 65 and 72 kcal/mol for CO and CO<sub>2</sub> release, respectively. It is interesting that the release of CO and CO<sub>2</sub> paralleled one another, suggesting a concerted reaction, of the type,



The previous model compound pyrolyses reported here provide a reasonable framework for an analysis of further model compound pyrolysis

studies. Kinetic results are notably few, and detailed characterization of product spectra are infrequent. Further, many studies are of the non-isothermal DTA variety employed frequently by many Russian investigators. The accompanying DTG studies are particularly difficult to interpret, as a chemical transformation, an isomerization for example, need not be attended by weight loss. Other studies, particularly those of saligenol dehydration, provide overwhelming pathway evidence and thus require only kinetic analysis. In short, the literature provides a reasonable basis for more fruitful extensions of lignin model compound pyrolysis.



## 5.0 Present Approach

The previous chapters have examined the background material related to lignin and lignin pyrolyses which motivated the present investigation. The present approach involves two parts, both experimental and theoretical. The latter approach involves an analysis of lignin structure and reactions in an effort to achieve a more fundamental description of lignin pyrolysis. The experimental approach includes the pyrolyses and kinetic analysis of compounds modelling the essential moieties and functional groups likely involved in whole lignin thermolysis. This chapter will first motivate these approaches by considering the limitations of the previous lignin investigations. An analysis of the lignin structure will then follow, which will suggest formal reaction pathways for lignin thermolysis. A direct result of this reaction will be the development of a list of experimental model compounds. The chapter will conclude with a discussion of the present simulation approach, which is based on the integration of the chapter material.

### 5.1 Limitations of Previous Lignin Investigations

#### Lignin structure

The classic work pioneered by Freudenberg has elucidated most of the important chemical characteristics of lignin. For example, the Freudenberg structure Figure 3.5 is a rather accurate description of the types of interunit bonds, methoxyphenols, and 3-carbon side chains constituting the lignin macromolecule. As developed in Chapter 3, this model accords very well with experimental determinations of

elemental composition, oxygen types, and oxygen distribution.

However, while the aromatic units comprising Figure 3.5 are rather well established, based on synthesis isolation of actual lignols as well as other experimental evidence, the exact juxtaposition of these is unknown. Hence, the Freudenberg structure must be considered as a depiction of the important features of lignin, as opposed to an unequivocal chemical formula or structure. Thus, only the features of this high molecular weight polymer are depicted 18 aromatic units. This results in the likely overrepresentation of any one discrete aromatic unit, best considered by example. The aromatic unit 2 is comprised of an hydroxyacetone side chain and a coumaryl alcohol methoxyphenol. However, it is clear that every hydroxyacetone side chain in the lignin macromolecule need not be associated with a free coumaryl alcohol methoxyphenol. This side chain could associate with the phenylcoumaran methoxyphenol, as in unit 18, or a host of other possible methoxyphenol substituents. In short, while the Freudenberg model depicts the global atomic and functional group distributions of lignin rather well, the details of each aromatic unit must be considered as schematic. It is quite unlikely that actual lignin is simply the superposition of many Freudenberg formulae.

Even if the Freudenberg structure could be interpreted as a well defined repeating molecule, the pyrolytic description of this molecule would be complicated. That is, the rigorous delineation of the many possible consecutive and parallel reaction

paths likely involved in the pyrolysis of this 'molecule' would involve a sem-infinite number of possibilities ,

Thus, literal interpretation of the Freudenberg structure is cumbersome in two ways. First, the exact types of lignin aromatic units are likely ill-proportioned in a structure of only 18 units. Secondly, the complexity of even these 18 units renders pyrolytic description obscure.

This interpretation of the Freudenberg structure motivated the use of a statistical description of both lignin and lignin pyrolysis, to be developed below.

#### Previous pyrolyses

The previous lignin pyrolyses provide little fundamental insight into the mechanisms and pathways of degradation. Even in those investigations reporting detailed product spectra, evidence of reaction paths is obscure. That is, pyrolyses of complex substrates to yield complex product spectra have thus far failed to unequivocally elucidate the origins, pathways, and mechanisms of formation of each product. This is likely due in part to the wide range of lignin types, lignin isolation methods, and lignin pyrolysis reactors employed. Lignins can vary with and within plant type, and the material of Chapter 3 has already described the often substantial chemical modification induced by lignin isolation procedures. Further, certain pyrolysis reactors were designed to emphasize primary reactions, while still others were of the destructive distillation or DTA/DTG type.

Model compound pyrolyses have provided some fundamental insights. The literature suggests that the reactivity of lignin interunit linkages be ranked in the order:

$\alpha$ -ether >  $\beta$ -ether  $\gg$  diphenylmethane > phenylether > biphenyl, yet detailed product spectra and rigorous kinetic analyses of these are few. Previous methoxyphenol pyrolyses have provided insight into the nature of the products obtained from thermal degradation. Products indicative of formal demethylation, demethoxylation and isomerizations have been reported. Interestingly, methanol yields appear low or zero. However, rigorous kinetic analyses delineating reaction order and Arrhenius parameters are lacking for the methoxyphenols. Model compound studies utilizing DTA and DTG techniques generally provide some form of kinetic analysis, but the implications of these non-isothermal experiments are difficult to discern. Further, these studies have generally provided little product spectra information. In short, the previous model compound pyrolyses provide insights into likely classes of lignin pyrolysis reactions, but often fail to provide detailed product spectra or rigorous kinetic parameters.

Of equal significance and importance is that these model compound studies have not been applied to describe whole-lignin pyrolysis. The results of isolated model compound studies need be assembled and integrated before the more profound implications of each to whole lignin thermolysis can be realized. For example, it is quite unlikely that the reversion of a whole-lignin  $\alpha$ -or  $\beta$ -ether bond would not have some effect on a corresponding 3-carbon side chain and/or

methoxyphenol unit. Thus, the interrelationships of seemingly isolated bond and moiety types may be crucial in whole lignin pyrolysis. These interrelationships arise only by assimilation of the details of both lignin structure and lignin moiety pyrolysis behavior. Hence, the present investigation will attempt to examine and integrate lignin structural details with the pyrolysis behavior of important functional groups. The latter behavior will be discerned by experiment.

## 5.2 Analysis of Lignin Structure

Lignin is a complex macropolymer comprised of the phenylpropanoid monomer units coniferyl, sinapyl and coumaryl alcohol. Although the principles of lignification are well known, the monomer units are bonded in apparently random fashion. Synthesis and degradation studies have revealed the essential functional groups and bonding patterns of the substrate, and further analytical data have delineated the types and distributions of lignin oxygen, carbon and hydrogen atoms. The best pictorial description of lignin is that due to Freudenberg, Figure 3.5.

Closer examination of the Freudenberg structure reveals simplifying features. The macropolymer is comprised of only single ring aromatic units, each of these containing a 3-carbon side chain and methoxyphenol substituent para to each other on the aromatic ring. The aromatic units are connected by relatively few types of inter-unit linkages, these being, in descending prevalence,  $\beta$ -ether,  $\alpha$ -ether, diphenylmethane, diarylether, diaryl, pinoresinol, and phenylcoumaran

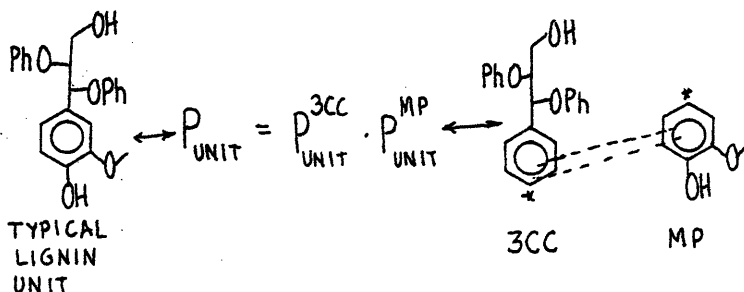
types. Thus, lignin is simply an ensemble of single ring aromatic units, linked by only seven possible types of inter-unit bonds. Each aromatic unit, in turn, is comprised of an aromatic ring with para 3-carbon side chain and methoxyphenol substituents.

An essential feature of lignin constitution thus arises. While the methoxyphenol of a given aromatic unit is involved in bonding with the 3-carbon chain or methoxyphenol of an adjacent unit, it is never involved in bonding with the 3-carbon chain of the same aromatic unit. This observation suggests that the nature of methoxyphenol substitution of a given aromatic unit be independent of the nature of 3-carbon side chain substitution of the same unit. As an example, consider aromatic unit number 2 in the Freudenberg structure. As depicted, the unit consists of an hydroxy-acetone type side chain in conjunction with a coumaryl, or simple free phenol, methoxyphenol substituent. Equally well, the methoxyphenol unit could have been of the coniferyl alcohol type, and further be etherified, as in unit 18.

However, this example illustrates a shortfall in the Freudenberg structure. Unit 18 depicts a phenylcoumaran structure, which are in fact quite few in lignin. Hence, as shown in the Freudenberg structure, the 3-carbon chain of units 2 and 18 are arbitrarily depicted in conjunction with a free phenolic coumaryl unit and a phenylcoumaran unit, respectively. However, the principles of lignification dictate that this type of side chain could be associated with any of the types of methoxyphenols. In fact, coumaryl alcohol accounts for only 11% of the lignin monomer alcohols, and the phenylcoumaran linkage is less than 1 of 18. Thus, that unit 2 or 18 should depict 1 of every 18

lignin aromatic units is a certain overrepresentation of each. Further, since only 2 of 18 of the side chain units are of the hydroxyacetone type, finding 1 of every 18 lignin aromatic units as the type depicted by units 2 or 18 would be highly unlikely. Rather, the 2 in 18 proportions of the hydroxyacetone side chain should be weighed against each type of possible methoxyphenol unit to more accurately depict lignin. In short, while the overall bond types, functional groups, and analytical data of lignin are well reflected by the Freudenberg structure, the exact details of each aromatic unit must be overstated since the structure is limited to only 18 units. A more accurate description of lignin would be a statistical match of all possible 3-carbon chain substituents against all possible methoxyphenol substituents. In this way, the proportion of a given aromatic unit in the lignin macromolecule would more accurately reflect the distributions of side chain and methoxyphenol substituents.

These arguments suggest that lignin be described in terms of probability. Each lignin aromatic unit is comprised of both a 3-carbon chain and methoxyphenol substituent. The occurrence of a particular aromatic unit necessitates an exact match between complimenting 3-carbon chain and methoxyphenol substituents. Thus, as illustrated here, the probability of the occurrence in lignin of an overall aromatic



unit, must be equal to the probability of the proper side chain multiplied by the probability of the proper methoxyphenol. That is, the probability of the simultaneous occurrence of two independent events is the product of the individual probabilities, i.e.,

$$P_{A \text{ and } B} = P_A \times P_B$$

This probabilistic matching applied to the rather well established distributions of 3-carbon side chains and methoxyphenols should yield the most accurate depiction of lignin available. Of course, this depiction is not amenable to a pictorial description such as that of Freudenberg. However, the overall distribution of 3-carbon side chains and methoxyphenols is well represented by the Freudenberg structure, only each given aromatic unit cannot be literally interpreted in the depicted proportions. That is, in the terminology described above,  $P_{\text{unit}}^{3CC}$  and  $P_{\text{unit}}^{MP}$  are well represented by the Freudenberg structure; the true lignin distribution of aromatic unit  $P_{\text{unit}}$  cannot possibly be described in an 18 unit molecular formula. Thus, this analysis will use the completed Freudenberg model, Figure 3.6, as the basis for determining the distribution of methoxyphenols and 3-carbon chains. These distributions are detailed in Figures 3.7 and 3.8 and can be easily altered to more accurately depict lignins with different distributions than those depicted by the Freudenberg model.

With reference to Figure 3.7, the methoxyphenol substituents arise from only three monomeric units, coniferyl, sinapyl and coumaryl alcohols. The former of these is predominant. The methoxyphenols can be further subdivided as free phenolic or etherified phenolic, the



latter group involving only PPE, BPE, PE and phenylcoumaran types. Of these the PPE linkage is predominant. Thus, the largest proportion of the methoxyphenol units will emanate from coniferyl alcohol units, and be either free hydroxyls or involved in PPE bonding. Turning to the 3-carbon side chains, only eight different types are depicted in the Freudenberg structure. The most prevalent of these is the guaiacyl-glycerol- $\beta$ -ether moiety, followed by guaiacyl-glycerol- $\beta$ -ether- $\alpha$ -ether or alkanes, hydroxyacetones, cinnamaldehyde, pinoresinol, lactone and phenylcoumaran. The latter three are likely overrepresented to some degree, but this is easily altered and presents little difficulty. In short, that only eight different side chains are involved in the Freudenberg structure is a surprising simplification.

Further significant are the types of interunit linkages which bond the various methoxyphenols and 3-carbon chains, forming the higher molecular weight oligomers of the Freudenberg structure. The aromatic units are linked by rather few bond types, these being  $\alpha$ - and  $\beta$ -aryl-alkyl ethers, diphenylmethanes, diphenylethers, biphenyl, pinoresinol and phenylcoumaran moieties.

The differences between a literal and the present interpretation of the Freudenberg structure are cogently summarized here. Figure 5.1 is a numerical summary of true types of aromatic units present in the Freudenberg structure. These units result from the formal superposition of a methoxyphenol and 3-carbon side chain substituent, the whole lignin distributions of which are depicted in Figures 3.7 and 3.8. The methoxyphenol types are listed as the left-most column

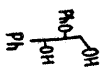
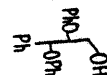
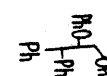
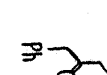
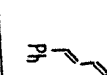
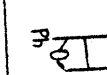
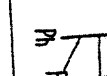
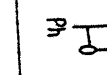
		3CC / MP								
CENTRIFUGAL ALCOHOL	FREE									$\Sigma$ MP
		1	1	0	0	0	1	1	1	5
CORIMARYL ALCOHOL	ETHER	3	1	2	1	1	1	0	10	
	FREE	0	0	0	1	0	0	0	1	
SINAPYL ALCOHOL	ETHER	1	0	0	0	0	0	0	0	
	FREE	0	0	0	0	0	0	0	1	
$\Sigma$ 3CC	ETHER	1	0	0	0	0	0	0	1	
		6	2	2	2	1	2	1	18	

Figure 5.1 Aromatic unit grid : Freudenberg structure

of Figure 5.1. For simplicity of illustration, the methoxyphenols are categorized only as free or etherified derivatives of coniferyl, coumaryl, and sinapyl alcohol; the etherified methoxyphenols are not further subdivided by ether type. The 3-carbon side chain types are detailed as the uppermost reference row. The grid points in Figure 5.1 show the 18 aromatic unit types, depicted in the Freudenberg structure, and are positioned in the grid so as to represent the appropriate match of methoxyphenol and 3-carbon side chain substituents.

As evidenced by the grid, the most common lignin aromatic unit in the Freudenberg model is the etherified guaiacyl-glycerol- $\beta$ -ether unit. This reflects the prevalence of the glycerol- $\beta$ -ether side chain and the coniferyl alcohol starting monomer. However, the Freudenberg model accounts for no matching of these side chains with a free coumaryl or sinapyl alcohol methoxyphenol unit. Further, the coumaryl or sinapyl alcohol monomer units are not depicted in conjunction with any glycerol- $\alpha$ ,  $\beta$ -ether or glycerol- $\beta$ -ethers- $\alpha$ -phenyl groups. All cinnamaldehyde, pinoresinol, lactone and phenyl-coumaran side chains are also shown with coniferyl alcohol-related methoxyphenols. These in fact, could have been associated with coumaryl or sinapyl type methoxyphenols as well. Thus, while the Freudenberg structure may well represent the relative proportions of the 3-carbon chains and methoxyphenol lignin substituents, the 18 rather arbitrary grid points of Figure 5.1 do not likely depict the actual distributions of aromatic units.

The present interpretation of the Freudenberg structure is schematized in Figure 5.2. Using the distributions of 3-carbon side chains and methoxyphenols detailed in Figures 3.7 and 3.8, a grid of 18 total aromatic units has been generated which should more realistically account for the wide range of aromatic unit types likely present in whole lignin. Only 18 aromatic units have been selected to facilitate comparison with the Freudenberg structure and Figure 5.1. Thus, fractional numbers of aromatic units will arise in the grid of Figure 5.2. Of course 18, 1, or  $18 \times 10^{18}$  total aromatic units could have been selected with equal generality. This aromatic unit grid was generated by multiplying all possible methoxyphenol types against all possible 3-carbon side chain substituent types. Thus, many of the grid points with zero entries in Figure 5.1 now have non-zero entries in Figure 5.2; correspondingly, the proportions of certain overemphasized aromatic units in Figure 5.1 have been reduced. For example, whereas the Freudenberg model depicts 1 in 18 proportions for aromatic unit number 2, which arises from the match of an hydroxyacetone side chain and a free coumarylalcohol methoxyphenol, the present redistribution of aromatic unit types would predict this particular unit in .11/18 proportions.

Further refinement of this type should account for free hydroxyl sinapyl alcohol as well as all possible types of etherified methoxyphenol units. This is the type of distribution used to describe the lignin substrate in the present simulation model, which further redistributed proportions of etherified coumaryl and sinapyl


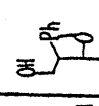
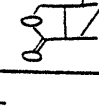
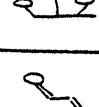
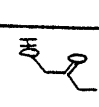
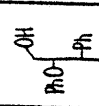
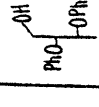
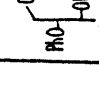
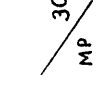
MP / 3CC										$\sum$ MP
NORMALIZED DISTRIBUTION	(.33)	(.11)	(.11)	(.11)	(.11)	(.11)	(.11)	(.11)	(.11)	(.1)
FREE (.28)	1.66	.55	.55	.30	.55	.55	.30	.55	.30	5
ETHERIFIED (.56)	3.33	1.11	1.11	.60	1.11	1.11	.60	1.11	.60	10
FREE (.055)	.327	.11	.11	.060	.11	.11	.060	.11	.060	1
ETHERIFIED (.055)	.327	.11	.11	.060	.11	.11	.060	.11	.060	1
FREE (0)	0	0	0	0	0	0	0	0	0	0
ETHERIFIED (.055)	.327	.11	.11	.060	.11	.11	.060	.11	.060	1
$\sum$ 3CC (1)	6	2	2	1	2	2	1	2	1	18

Figure 5.2 Aromatic unit grid : Present approach

methoxyphenols based on the analagous distribution of etherified coniferyl alcohol moieties; the possibility of a phenylcoumaran-sinapyl alcohol methoxyphenol unit was excluded due to steric hindrance effects.

Thus, to more accurately, and indeed more easily, describe the whole lignin pyrolysis substrate, this investigation will utilize a statistical matching approach. Lignin will be described as an ensemble aromatic units, each with a methoxyphenol and a 3-carbon side chain substituent. These are connected by well defined types of interunit linkages. Each aromatic unit will be described by the probabilistic matching of the distributions of methoxyphenols against the distribution of 3-carbon side chains.

At the temperatures of interest in most lignin thermal applications, lignin aromatic nuclei will persist. Thus, the essential reactivity of whole lignin will be that of the methoxyphenols, 3-carbon side chains, and interunit linkages. Hence, the integrity of each aromatic ring will remain intact during pyrolysis, and the transformations of the aromatic substituents should describe lignin conversion. The experimental model compounds will therefore mimic the reactive methoxyphenols, side chains, and interunit linkages, as well as compounds likely generated in reaction of these. It is therefore reasonable to consider some of the possible reactions constituting lignin pyrolysis, as these motivate the selection of model compounds.

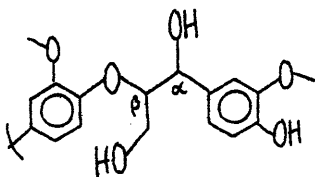
### 5.3 Formal Pathways in Lignin Thermolysis: Selection of Model Compounds.

As previously discussed, the seat of lignin reactivity will likely lie in the reactive interunit linkages, methoxyphenols, and 3-carbon side chain units. Consideration of those units present in the Freudenberg structure, as well as possible reactions of these, generates a set of compounds capable of describing the essential features of lignin pyrolysis. The types of reactive units are conveniently divided into five groups, representing: 1) Lignin interunit linkages, 2) Methoxyphenol units, 3) hydroxylic side chains, 4) carbonyl side chains, and 5) carboxylic side chains. Table 5.1 represents the list of model compounds generated from consideration of these units.

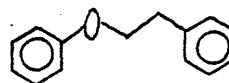
#### 5.3.1. Lignin Interunit Linkages

##### $\beta$ -ether

The prevalent guaiacyl  $\beta$ -ether link, schematized as structure I, will be modelled as phenethylphenyl ether, compound 1.



(I)



(1) phenethyl-phenylether, PPE.

Phenethylphenylether clearly depicts the essence of the  $\beta$ -ether carbon-oxygen chain. Absent from the true lignin moiety are the  $\alpha$ -hydroxy

Table 5.1 Model Compounds to be Pyrolysed

## Interunit linkages

1.	Phenethylphenylether	PPE
2.	o-hydroxydiphenylmethane	OHD
3.	phenylether	PE
4.	biphenol	BPhOH
5.	biphenyl	BP

## Methoxy phenols

6.	guaiacol	G
7.	veratrole	VE
8.	anisole	AN
9.	2,6-dimethoxyphenol	DMP
10.	isoeugenol	I
11.	vanillin	VA

## Carbonyl Units

11.	vanillin	VA
12.	benzaldehyde	BA
13.	acetophenone	AP
14.	cinnamaldehyde	CAD

## Propanoid side chains

14.	cinnamaldehyde	CAD
15.	cinnamylalcohol	CAL
16.	saligenol	SAL

CO<sub>2</sub> precursors

17.	ferulic acid	FA
18.	cinnamic acid	CA
19.	1-napthoic acid	1NA
20.	2-napthoic acid	2NA

SEE ACCOMPANYING ILLUSTRATION FOR CHEMICAL STRUCTURES



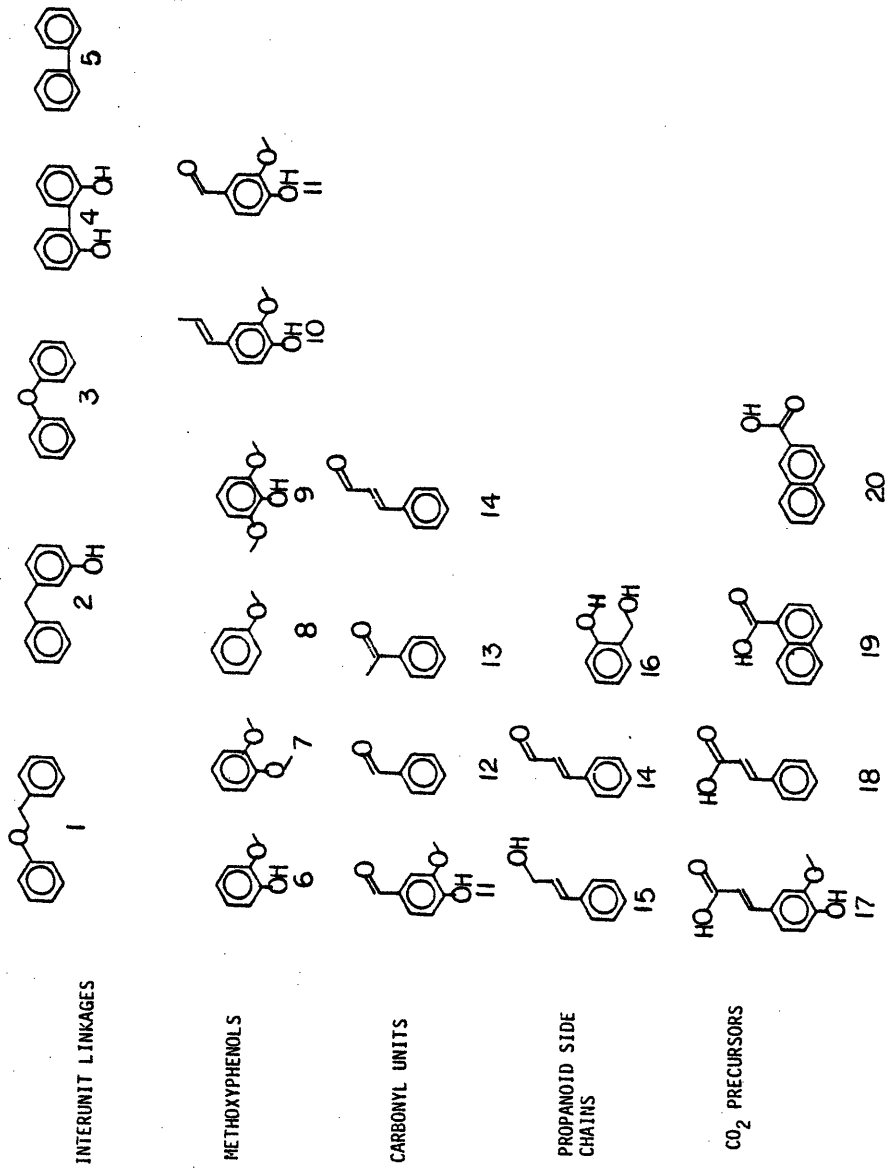
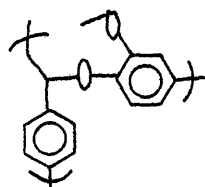


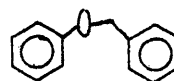
Table 5.1 (cont.) Chemical structure key

and  $\beta$ -methyloxy substituents, as well as the guaiacyl substituents. Effects of these substituents can be accounted theoretically or experimentally, yet should be of second order importance as compared to the base reactivity of the PPE link. That is, PPE is the simplest, complete depiction of the lignin  $\beta$ -ether link.

The  $\alpha$ -ether link, may be similarly modelled by benzylphenylether, as illustrated by structures II and 2. The literature contains many studies of the thermal behavior of BPE, and these experiments will



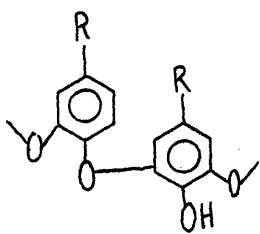
II lignin  $\alpha$ -ether link



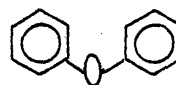
2 benzylphenylether(BPE)

not be duplicated in this study. For purposes of modelling and comparison, reference to these investigations will be made.

The phenylether lignin link, III, will be studied by pyrolysis of



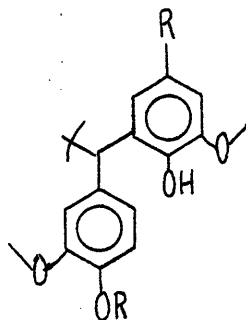
III



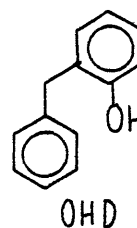
3 phenylether

phenylether (3). The orthohydroxy and methoxy substituents of structure III are not accounted for by phenylether, again the simplest account of the true lignin link possible. It is expected that the electron donating tendencies of these substituents might effect an increase in pyrolysis rate.

Orthohydroxydiphenylmethane (4) was chosen to model the diphenylmethane unit of Figure 5 (IV).



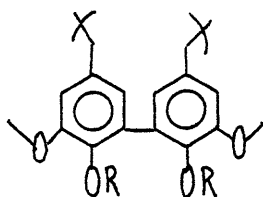
IV



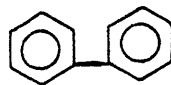
4

This model includes not only the essential diphenylmethane bond, but also the orthohydroxy substituent. The latter feature is considered important in light of the mechanism of formation of this lignin link, namely rearrangement of a benzylphenylether unit.

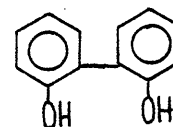
The remaining lignin interunit link to be studied, the biphenyl unit (V), has been modelled by both biphenyl (5) and biphenol (6), the latter more realistically depicting the true lignin linkage.



V



5



6

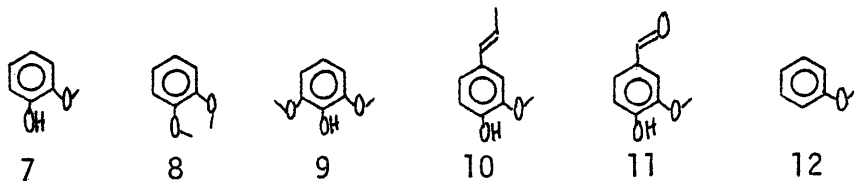
Comparison of 5 and 6 also probes the influence of the orthohydroxy-substituent.

The degradation of these interunit linkages will produce single ring aromatic units during lignin pyrolysis. Equally important, the

reactions of these linkages will likely exert profound influence on the reactivities of other lignin groups. This point will become more fully clear in consideration of the models of the remaining reactive moieties.

### 5.3.2 Methoxyphenol Units.

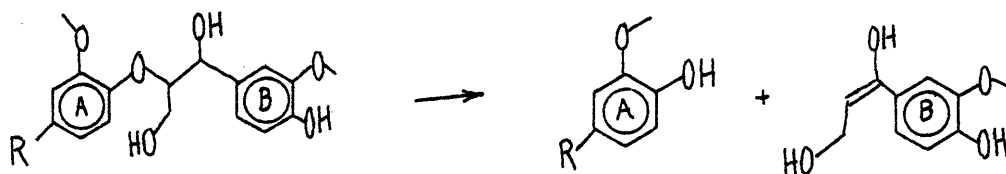
As present in the unperturbed lignin substrate, the methoxyphenol units exist as two types, namely, free hydroxylic and etherified hydroxylic moieties. Figure 3.8 describes the distributions of these as presented in the Freudenberg structure. The prototype model of the free hydroxylic methoxyphenol is guaiacol (7), whereas the etherified methoxyphenol will be depicted as veratrole (8). Note that this depiction approximates the true lignin alkyl ether as a methyl ether. The prototype sinapyl moiety will be modelled by 2,6-dimethoxyphenol (9), which also probes the effect of methoxy substitution on guaiacol reactivity. Other guaiacol substituent effects are studied in the pyrolysis of isoeugenol (10) and vanillin (11), which depict para-conjugative and electron withdrawing substitution, respectively. The pyrolysis of these is especially cogent, as all lignin methoxyphenols contain substitution in the para position, namely, the 3-carbon side chain. Finally, anisole (12) probes the effect of the ortho-hydroxy unit on the methoxyl group reactivity.



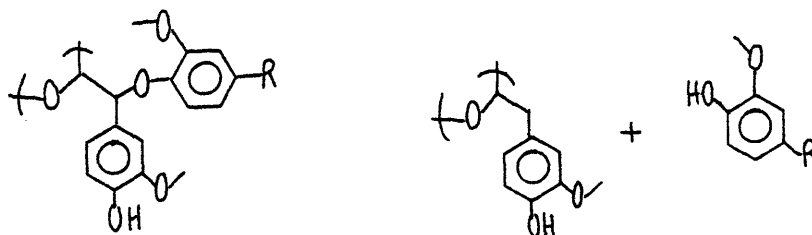
In total, this set of model compounds represents the forms of

methoxyphenols likely present in the lignin substrate.

Of particular significance is the relationship of interunit linkage reactivity to the distribution of the type of lignin methoxyphenols. For example, formal reversion of the guaiacyl-glycerol- $\beta$ -ether may in fact generate a guaiacol-type methoxyphenol from a veratrole-type unit, as in:



Thus, unit A, initially a veratrole-type methoxyphenol, could be transformed into a different type of methoxyphenol, by ether cleavage. Hence, if the reactivities of veratrole and guaiacol are not identical, the reactions of the lignin interunit linkages could have an accelerating or decelerating effect on overall methoxyphenol reactivity. Similarly, reversion of an  $\alpha$ -ether could also effect transformation of veratrole units into guaiacols, as in:



This reaction is based on the literature reports of BPE pyrolysis to toluene and phenol, the latter corresponding to guaiacol in the present reaction.

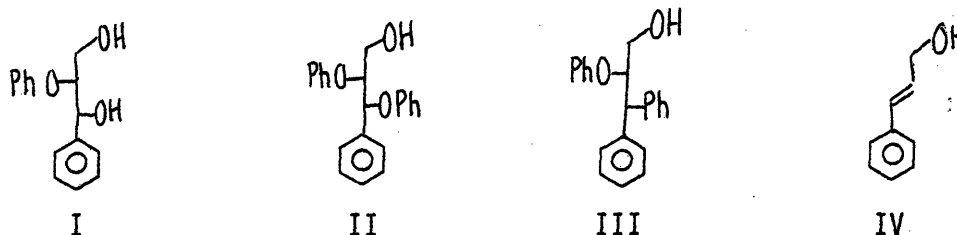
Similarly, reversion of other interunit linkages can be envisioned to alter the nature of the methoxyphenol units, either directly at the

methoxyphenol or through the 3-carbon side chain para substituent.

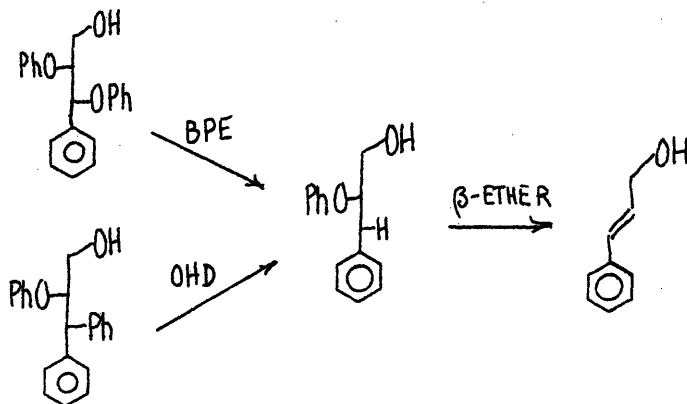
These latter reactions are to be considered next.

### 5.3.3 Hydroxylic Side Chain Units

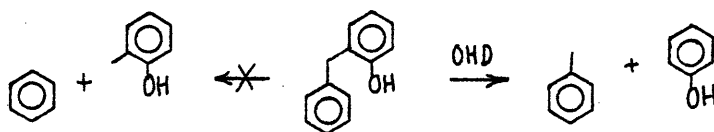
As existing in the unperturbed native lignin, the major hydroxylic 3-carbon side chain units are guaiacyl-glycerol- $\beta$ -ether (I), guaiacyl-glycerol- $\beta$ - $\alpha$ -ether (II), guaiacyl glycerol- $\beta$ -ether  $\alpha$ -phenyl unit (III), and the cinnamyl alcohol moiety (IV). The



latter of these, cinnamyl alcohol, mimics the side chain of the monomeric lignification alcohols and occurs in the Freudenberg structure in small amounts. However, reversion of units (II) and (III) might also serve to generate these moieties, as in:

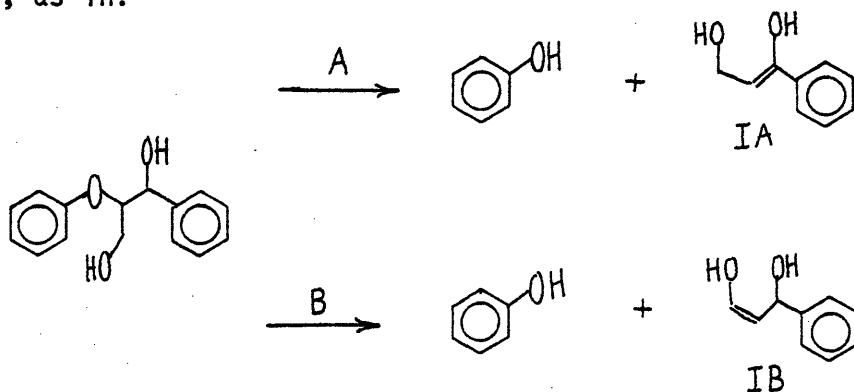


The OHD pathway is based on the literature report of OHD pyrolysis to toluene and phenol, rather than to cresol and benzene, as in,

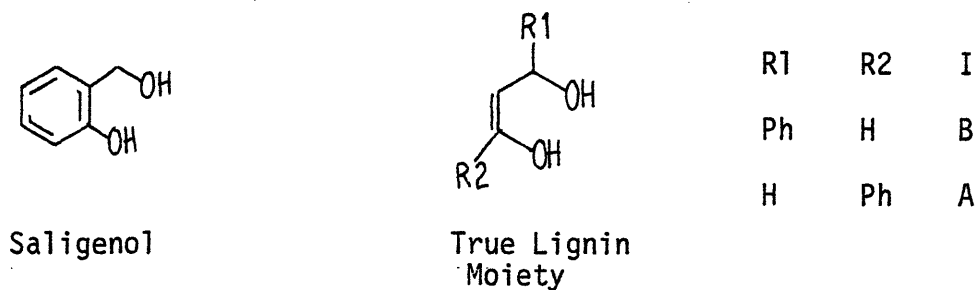


Thus, the thermal behavior of these cinnamylalcohol moieties will likely exert considerable influence on whole lignin thermolysis.

Similarly, reversion of the prevalent guaiacyl-glycerol- $\beta$ -ether unit might result in the formation of a saligenol-type side chain, as in:



Reversion of the  $\beta$ -ether link by either pathway A or B could yield a dihydroxy saligenol-type moiety, IA or IB, as emphasized here:



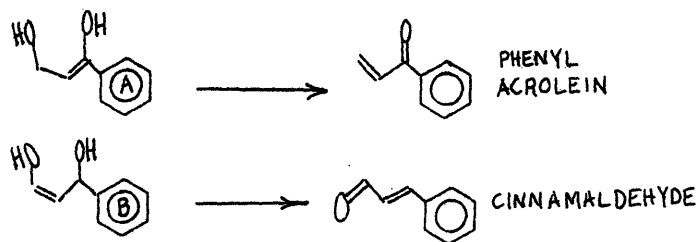
The true lignin dihydroxy unit would be a chemical ene-ol, susceptible to tautomeric conversions, and is thus not suitable for use as a

model compound. The aromatic stability provided by the benzene ring allows saligenol to exist in the ene-ol form, and thus saligenol was selected for pyrolysis. The aromatic ring would be expected to impart thermal stability to saligenol relative to IA or IB, a factor which must be considered in application of saligenol pyrolyses to lignin.

Thus, the importance of the lignin interunit linkages, as well as the likely parallel and consecutive nature of lignin pyrolysis, becomes evident. Reversion of these interunit linkages is likely capable of modifying the initial methoxyphenols and 3-carbon side chain units. The former change is one of veratrole type transformations to guaiacols, whereas reactive ene-ols are generated from saturated propylglycols or propanols in the latter. Further possible reactions of the ene-ols are considered next, as these may generate additional reactive moieties.

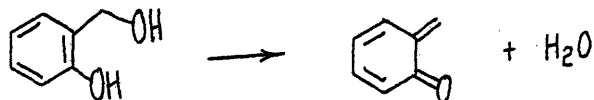
#### 5.3.4 Carbonyl Moieties

Carbon monoxide is a major component of lignin pyrolysis product gas, likely derived in part from the degradation of lignin carbonyl units. These may be initially present in the unperturbed lignin or generated in the early stages of pyrolysis. For example, dehydration of the saligenol moieties might produce acrolein and cinnamaldehyde carbonyls, as in

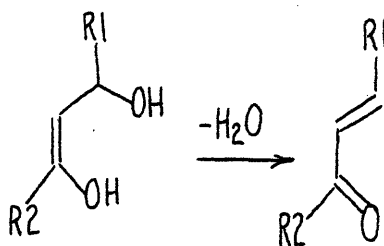




As was noted in section 4.5, saligenol thermolysis readily produces water and a quinonemethide, as in:

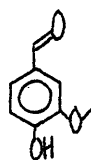


Thus, as related to the true lignin intermediates, the type of dehydration would produce the phenyl acrolein and cinnamaldehyde carbonyls. This relationship is further illustrated here, where:

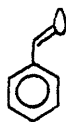


R1	R2	I	Carbonyl
Ph	H	B	Cinnamaldehyde
H	Ph	A	Phenylacrolein

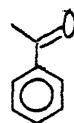
The compounds chosen to model the lignin carbonyl functionalities were vanillin (11), benzaldehyde (13), acetophenone (14), and cinnamaldehyde (15).



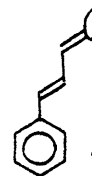
11



13



14



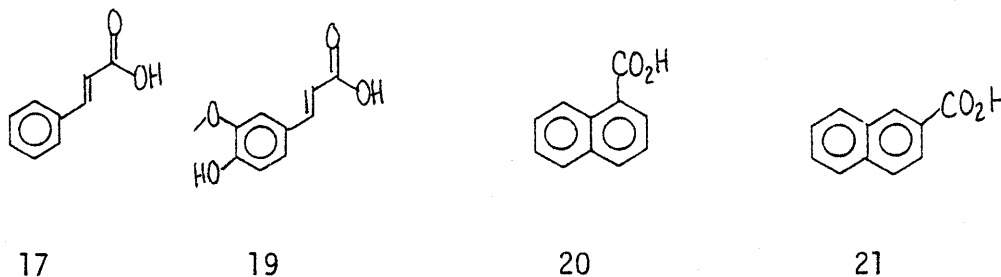
15

Vanillin, benzaldehyde, and acetophenone depict those  $\alpha$ -carbonyls, initially present in the lignin in rather modest proportions, but more importantly those  $\alpha$ -carbonyls likely produced in the early stages of pyrolysis. Comparison of vanillin and benzaldehyde should

reveal the effect of guaiacyl substitution on carbonyl reactivity, while comparison of benzaldehyde and acetophenone should probe the effect of direct alkyl substitution on the carbonyl. Cinnamaldehyde should reveal the likely effects of vinyl conjugation on carbonyl reactivity, and is further significant since present in modest amounts in the unreacted substrate. In short, this set of carbonyl compounds should clarify many of the essential features concerning CO release in lignin.

### 5.3.5 CO<sub>2</sub> Precursors

A small portion of the lignin pyrolysis product gas is comprised of CO<sub>2</sub>, which may arise in part from decarboxylation of lignin carboxylic acids. The model CO<sub>2</sub> precursors selected for investigation were cinnamic (17), ferulic (19), 1 - (20) and 2 - (21) naphthoic acid.



The former two acids are likely present in the unreacted lignin in very small amounts, arising from radical exchange reactions of the type listed in Section 3.1. The naphthoic acids are models of 'humic acids', thought to be important intermediates in the metamorphosis of lignin to coal. These acids may also arise from the room temperature air oxidation of exposed coal and biomass substrates.

In summary, the selection of model compounds based on the Freudenberg structure has been effected in two ways. The first of these has been to select compounds which mimic the functionalities and moieties known to exist in the unreacted lignin substrate. These include the interunit linkages, the methoxyphenols and several of the side chain moieties. The second method of selection was to choose compounds reflecting likely pyrolysis intermediates. These included saligenol, many of the carbonyl substituents, and in fact, guaiacol and 2,6-dimethoxyphenol as well. Thus, an integration of many interrelated consecutive and parallel reaction pathways is likely involved in the simulation of lignin pyrolysis.

#### 5.4 Simulation of Lignin Thermolysis

As described in sections 5.2 and 5.3, the essential reactivity of the lignin substrate should be well represented by the reactivities of the component aromatic units. In turn, the reactivity of the aromatic units should be described by the reactivities of the interunit linkages, methoxyphenols, and 3-carbon side chains. In the previous section a set of model compounds was selected on the basis of the likely reaction paths of these interunit linkages, methoxyphenols and side chains.

The following describes the present approach toward simulation of whole lignin thermolysis. In particular, whole lignin pyrolysis will be modelled as a superposition and integration of the experimental results obtained from the model compounds. Thus, the task involves describing the rather complex substrate in terms of the model

moieties followed by delineation of the consecutive and parallel reactions of this substrate in terms of the model pathways. Finally, the products implied by the model pyrolyses must be related to those of whole lignin.

Aside from the obvious need for such a model to accurately depict true lignin thermolysis, other features considered desirable are flexibility and fundamental rigor. With regard to the former, the ideal lignin simulation model must be applicable to a wide range of lignin substrates. Specifically, lignin isolated from various biomass sources will vary in constitution, notably in the proportions of the three cinnamyl alcohols incorporated during lignification. Of more consequence, however, are those lignin structural modifications arising due to isolation methods. A host of lignin isolation methods exist, each with its own effect on the lignin structure. Many of these retain significant cellulosic or other carbohydrate components as well. Lignins recovered from pulping operations are also significantly modified, which must be accounted if the pyrolysis of these is to be simulated. The ability to describe pyrolysis over a wide temperature range, with or without catalysts, solvents, or other additives, is another desirable flexibility feature.

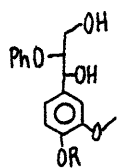
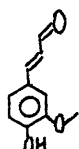
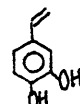
Turning next to fundamental rigor, it is useful to incorporate only those rate constants or catalyst effects which are either experimentally or theoretically determinable. That is, fundamental parameters which can at least in principle be measured or predicted are desired, as discriminated from empirical parameters obtained by regression of the very phenomenon to be modelled. The empirical

parameters would be limited in application to small perturbations about the conditions used to obtain them, whereas the fundamental parameters, as such, should be exploitable over a wider range of conditions. Thus, for example, the effect of a given catalyst on guaiacol demethanation or saligenol dehydration could be independently measured and then incorporated into the whole-lignin model. As a corollary, the model could be used to judge the likely gains expected from a catalyst as yet undeveloped, and thus be used as a decision making tool.

#### 5.4.1 Definition of Aromatic Ring Unit

Since the extent of whole lignin conversion will be dictated by the conversions of the 3-carbon side chains and methoxyphenols, it is clear that the nature of these substituents will vary during pyrolysis. Thus, a precise simulation definition of each is in order.

Each aromatic unit is conceptualized as containing a 3-carbon side chain and methoxyphenol unit in position para to each other on the aromatic ring. The units have the backbone of the original cinnamyl alcohol monomers, and may also contain substituent groups arising during lignification. Thus, the exact nature of the 3-carbon chains and methoxyphenols will change during pyrolysis, and exist only as conceptual aromatic substituents. This is best illustrated by example. Consider the structures shown here.

I ( $t=0$ )II ( $t=t_1$ )III ( $t=t_2$ )

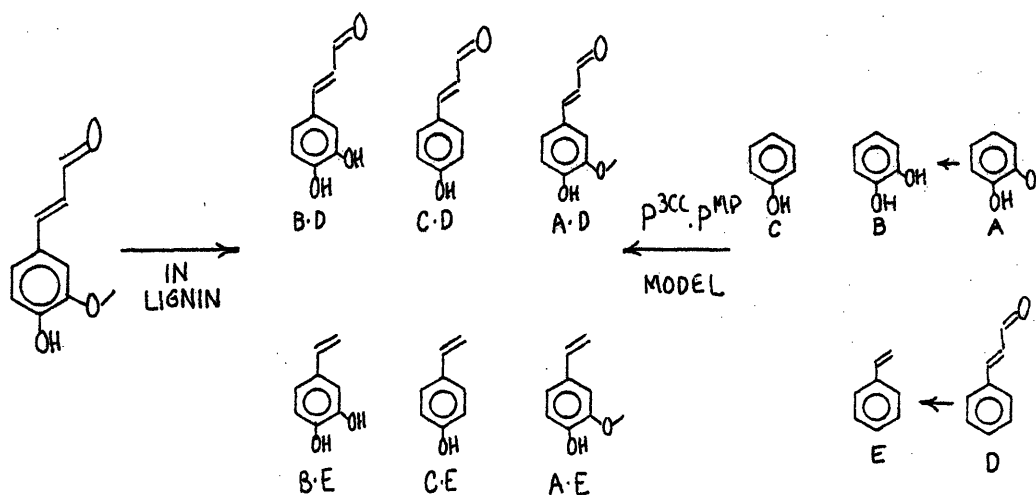
Unit I depicts a typical aromatic unit as found in lignin, the 3-carbon chain contains an  $\alpha$  and  $\gamma$  -hydroxyl substituent and a  $\beta$ -ether group. The methoxyphenol is etherified, of unspecified type. Reversion of the  $\beta$ -ether on the side chain followed by subsequent side chain dehydration, coupled with methoxyphenol ether cleavage, may alter the aromatic unit to II. In this case, the 3-carbon side chain is of the cinnamaldehyde type, and the methoxyphenol is a guaiacol. The original hydroxyl and ether substituents are no longer considered as part of the 3-carbon chain or methoxyphenol, but rather are either stable products or associated with the 3-carbon chains or methoxyphenol of another aromatic unit. Similarly, further reaction, such as side chain decarbonylation and methoxyphenol demethanation can alter the aromatic unit to that as described by structure III. Here the side chain is now of the type depicted by styrene and the methoxyphenol a catechol unit. Thus, the methoxyphenol and 3-carbon chain comprising each aromatic unit will change with the extent of pyrolysis, and are defined only as para substituents on the aromatic ring. The limiting 3-carbon side chain substituent is in fact a hydrogen atom, whereas the limiting methoxy phenol is simple phenol since cleavages of the phenolic hydroxyl are unlikely. The aromatic unit remains intact, and the changes of the 3-carbon side chains and methoxyphenols describe the lignin pyrolysis.

#### 5.4.2 Description of Aromatic Unit Pyrolyses

Just as whole lignin can be represented as an ensemble of aromatic units generated by the superposition of 3-carbon side chain

and methoxyphenol substituents, the pyrolysis of whole lignin is to be modelled as the integration or summation of the pyrolysis of each individual aromatic unit. Each aromatic unit is comprised of a given methoxyphenol and 3-carbon chain substituent, which are in turn characterized by the types of reactive groups and interunit linkages associated with each. Lignification generated independent 3-carbon side chains and methoxyphenols in the sense that these are not involved in intra-unit bonding. That is, the methoxyphenol of a given aromatic unit is never involved in bonding with the 3-carbon chain of the same unit. Similarly, the pyrolyses of the aromatic units will be modelled as the independent degradation of the 3-carbon chain and methoxyphenol of a given unit. That is, while the degradation of the methoxyphenol of one unit may be intimately involved in the pyrolysis of the 3-carbon chain of another, the methoxyphenol and 3-carbon side chain of the same unit will degrade independently. For example, with reference to the Freudenberg structure, the PPE linkage coupling units 12 and 15 may degrade to yield a saligenol side chain on unit 12 and a free guaiacol methoxyphenol on unit 15, but the methoxyphenol of 12 and 3-carbon chain of 15 are unchanged. This assumption involving the independent pyrolysis of the 3-carbon chain and methoxyphenol of a given aromatic unit simplifies overall pyrolysis description greatly. By accounting for the interunit linkage reactions, the results of each aromatic unit can be integrated to describe whole lignin pyrolysis. Thus, the pyrolysis of a given aromatic unit in the lignin macromolecule is to be represented by superposition of methoxyphenol and 3-carbon side chain reactions. The pyrolysis

products then will be found as the statistical match of the corresponding product from methoxyphenol and 3-carbon side chain pyrolyses, dictated by the kinetic reactions of each. That is, the probability of a given product from the pyrolysis of a particular aromatic unit will equal the probability of the methoxyphenol product multiplied by the complimenting 3-carbon chain product. For example, guaiacol pyrolysis might yield phenol and catechol, whereas cinnamaldehyde might yield styrene. Thus, a coniferaldehyde lignin aromatic unit might be expected to yield all of the products delineated here.



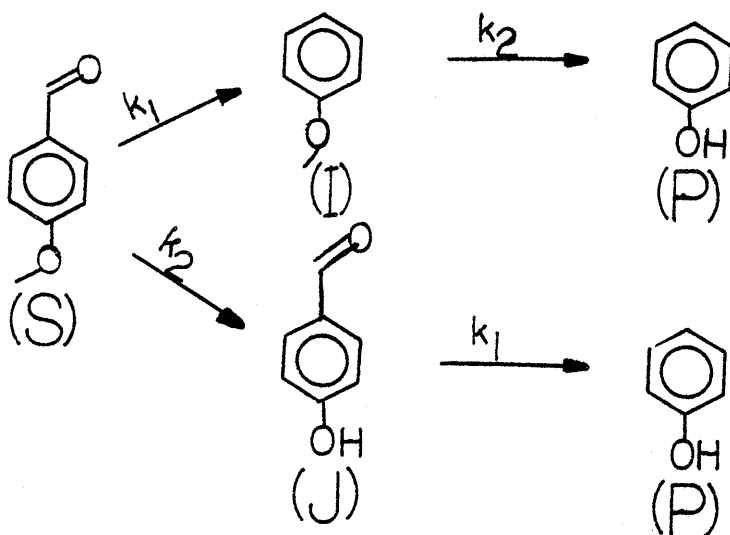
The proportions B·D, C·D, A·D, B·E, C·E, and A·E are dictated by the individual yields of A-E obtained by experimental pyrolysis of the models guaiacol and cinnamaldehyde. Integration (summation) over the entire distribution of aromatic units should then describe the products from whole lignin pyrolysis.



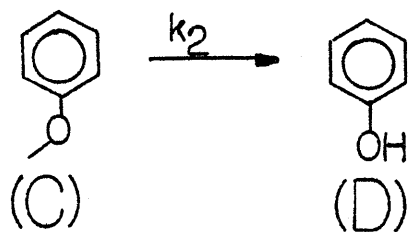
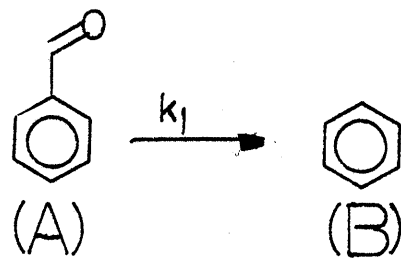
The possible products from the degradation of a given aromatic unit have been described as the probabilistic match of complimenting methoxyphenol and 3-carbon chain product spectra. The probability of a given product from methoxyphenol degradation at any time is dictated by the overall reaction kinetics. That is, the probability of any product will be equal to its molar yield at any time of interest. At low conversions, the probability that substrate dominates the product spectrum approaches unity, whereas at intermediate conversions substrate and other products are probable in proportion to their molar yield.

Similar arguments hold for 3-carbon side chain product probabilities, and the final lignin product spectrum is thus the match of these methoxyphenol and 3-carbon side chain product probabilities.

That this probabilistic argument can describe rigorous reaction kinetics is demonstrated in Figure 5.3, where the possible pyrolysis reactions of the hypothetical substrate p-methoxybenzaldehyde are delineated by both rigorous and probabilistic kinetic analysis. The example is for illustrative purposes only, intended to describe the mathematical, not the chemical reaction features of the lignin pyrolysis model. With regard to Figure 5.3, the substrate (S) will be assumed to degrade by only two pathways, decarbonylation and demethylation. Such a simplification is made for illustrative purposes, to facilitate mathematical description of the model. With regard to the rigorous analysis, decarbonylation results in the anisole moiety (I), which can further demethylate to phenol (P). Similarly, primary demethylation of (S) results in the hydroxybenzaldehyde (J), which can further



TRUE KINETICS  $P/S_0 = 1 + \exp(-(k_1+k_2)t) - \exp(-k_1t) - \exp(-k_2t)$



MODEL KINETICS  $B/A_0 = 1 - \exp(-k_1t)$  ;  $D/C_0 = 1 - \exp(-k_2t)$

$$P/S_0 = (B/A_0)(D/C_0) \quad \text{or} \quad P_P = P_B \cdot P_D$$

Figure 5.3 Simulation kinetic approach

decarbonylate to phenol (P). In both primary and secondary reactions, decarbonylation and demethylation are represented by rate constants  $k_1$  and  $k_2$  respectively. This reflects the assumption of independent pyrolyses of the 3-carbon side chains and methoxyphenols. Rigorous kinetic analysis of the parallel and consecutive network for the pyrolysis of the hypothetical substrate (S) reveals an expression for phenol yields as:

$$P/S_0 = 1 + \exp(-(k_1+k_2)t) - \exp(-k_1t) - \exp(-k_2t).$$

Turning next to the probabilistic model kinetics, degradation of hypothetical (S) has been conceptualized as the superposition of benzaldehyde decarbonylation and anisole demethylation. The rate constants for these reactions,  $k_1$  and  $k_2$ , are identical to those used in the rigorous kinetic analysis. In the model kinetics, the yields of benzene (B) and phenol (D) represent decarbonylation and demethylation of benzaldehyde (A) and anisole (C), respectively. In order for phenol (P) to be produced from substrate (S), both decarbonylation and demethylation are necessary. That is, in terms of the probabilistic model, both of products (B) and (D) must be generated. The probability of simultaneous generation of (B) and (D) is equal to the probability of generation of (B) multiplied by the probability of (D). These individual probabilities of (B) and (D) are equal to the yields of (B) from (A) and (D) from (C), where routine integration yields:

$$P_B \equiv B/A_0 = 1 - \exp(-k_1t); \quad P_D \equiv D/C_0 = 1 - \exp(-k_2t).$$

Thus, in order for (P) to form from (S), formation of both (B) from (A) and (D) from (C) must occur, or

$$P_p = P_{(B \text{ and } D)} = P_B \cdot P_D \equiv (B/A_0)(D/C_0) = (1 - \exp(-k_1 t))(1 - \exp(-k_2 t)),$$

or, by multiplying

$$P_p = 1 + \exp(-(k_1 + k_2)t) - \exp(-k_1 t) - \exp(-k_2 t).$$

This expression for the probability of the formation of (P), derived solely from the model kinetics, is exactly that expression obtained previously for phenol (P) yield from hypothetical substrate (S) as derived from rigorous analysis. Similarly, the yields of the intermediate products (I) and (J) as well as unconverted substrate are also described exactly by the probabilistic model. As applied to lignin, the probabilistic kinetic approach will deal with many more parallel and consecutive reactions, but the general logic and approach will be that as exemplified here. The lignin pyrolysis product spectrum will then be deduced from a probabilistic matching of complimentary 3-carbon side chain and methoxyphenol products.

Certain volatile products do not require this matching technique. These are the permanent gases, water, and methanol evolved in the degradation of side chains and methoxyphenols. These arise as 'complete' products from both methoxyphenols and 3-carbon side chains, and are described in total by the kinetic simulation.

In summary, the simulation model will depict lignin pyrolysis as the integration of the thermal reactions of individual aromatic units. The aromatic units will be described as a superposition of reactive 3-carbon side chains and methoxyphenols, which in turn

undergo independent pyrolysis reactions. Aspects of the reactivity of the 3-carbon side chains and methoxyphenols, as well as the bonds linking the aromatic units, were the focus of the experimental part of this investigation, and will be incorporated into the model. The product spectra from whole lignin pyrolysis will then be described as the probabilistic matching of complimentary 3-carbon side chains and methoxyphenol pyrolyses products. This is similar to the description of the original unperturbed lignin substrate, depicted as the probabilistic matching of 3-carbon side chains and methoxyphenols, the distributions of each delineated in the literature and reflected in the Freudenberg structure. The essence of the model is the conceptualization of lignin as discrete aromatic units, each comprised of independent 3-carbon side chains and methoxyphenols, and linked by a rather small number of interunit bonds.

#### 5.4.3 Mathematics of the Simulation

The chemical reaction networks resulting from methoxyphenol and 3-carbon side chain pyrolyses will serve as the basis for modeling whole lignin thermolyses. Previous discussion has delineated the motivation and strategy for the probabilistic matching of methoxyphenol and complimentary 3-carbon side chain pyrolysis products to describe the whole-lignin products. This section discusses the mathematical approach to generating the products implied by the methoxyphenol and 3-carbon side chain reaction networks.

Ordinary differential equations describing the variation with time of each methoxyphenol and 3-carbon side chain moiety will be

generated. As such, the simulation will describe either a constant volume batch pyrolysis, or the equivalent plug flow pyrolysis in the absence of volumetric expansion. Both of these are limiting cases, likely not met exactly by many previous experimental pyrolyses. However, the kinetic equations may be further applied to well stirred reactors, and qualitative generalization to other reactor situations is possible. Of special interest may be a reactor designed to emphasize only primary reactions, where volatile species may leave the zone of reactions.

A linear ordinary differential equation will describe the molar generation and disappearance of each pyrolysis product. Thus, the rate of change of each product will in general be proportional to the number of mols of each other product, or in vector form

$$\frac{d\vec{X}}{dt} = \underline{K}\vec{X} ; \quad \frac{d\vec{Y}}{dt} = \underline{L}\vec{Y} \quad \begin{array}{l} \vec{X}(t=0) = \vec{X}_0 \\ \vec{Y}(t=0) = \vec{Y}_0 \end{array}$$

where the vector X represents all methoxyphenol products, and Y is the 3-carbon side chain product vector. The equations will be numerically integrated forward in time via a fourth order Runge-Kutta technique. Although the set of first order equations are in principle solved by analytical methods, the numerical technique allows for extreme flexibility. Thus, the addition of the effects of a pulping operation might simply involve one or two additional numerical steps, compared to the need for a completely new analytical solution. The initial conditions required for the solution of these equations were obtained from the distribution of methoxyphenols and 3-carbon chains depicted in the Freudenberg structure. These conditions vary as lignin type is

varied, and those conditions used here are only one possible set.

The initial conditions reflect the molar, or moiety, fraction of each methoxyphenol or 3-carbon chain moiety as represented in the initial lignin structure. As light gases, water, and MeOH are evolved in pyrolysis, total simulation moles are not conserved. However, the total number of methoxyphenol and 3-carbon side chain moieties is conserved, these being chemically altered in pyrolysis. For example, a cinnamaldehyde side chain may degrade to only a hydrogen substituent, the remainder of the side chain released as gas or other volatiles. Thus, while total mass of the pyrolysis system is conserved, only the number and not the mass of the side chains and methoxyphenols need be constant.

With regard to the 18 units of the Freudenberg structure, the number of each type of side chain has been divided by 18 to yield the normalized side chain distribution. Similarly the number of each type of methoxyphenol have been normalized to one total mole. The total weight of the 18 Freudenberg units is 3299 gm, thus the normalized weight per aromatic unit is  $3299/18 = 183$  gm/unit. On the basis of one total aromatic unit of weight 183 gm, the distribution of side chains will sum to one total side chain. Similarly, the methoxyphenols sum to one total methoxyphenol moiety. Product yields are thus based on this one total aromatic moiety, of weight 183 gms. Hence, the molar evolution of volatiles and single ring aromatic ring products are easily transformed to mass yields based on original lignin mass.

The permanent gases, water and MeOH evolve as integral molecules

and are thus easily conceptualized. However, the generation of single ring aromatics necessitates that all interunit linkages of the side chain and the methoxyphenols be cleaved. That is, the cleavage of a methoxyphenol interunit linkage alone does not guarantee single ring aromatic formation, rather this must have occurred in addition to the cleavage of all interunit linkages of the side chain. Two types of side chains thus arise, those entirely free of interunit linkages, designated as S, and those involved in interunit bonding, designated M. Similarly, S and M types of methoxyphenols arise as well. Since a single ring aromatic will form only when an S-type 3-carbon chain and an S-type methoxyphenol are formed, the probability of single ring aromatic formation from lignin,  $P_S^{LIG}$ , is:

$$P_S^{LIG} = P_S^{MP} \cdot P_S^{3CC}$$

Any other combination, such as  $P_S^{MP} \cdot P_M^{3CC}$ ,  $P_M^{MP} \cdot P_S^{3CC}$  or  $P_M^{MP} \cdot P_M^{3CC}$ , represents the formation of a multiple aromatic ring product. Thus, total single ring aromatics yield will be obtained by multiplying the sum of S type methoxyphenols by the sum of S type 3-carbon side chains. All other combinations yield products of interconnected aromatic units, and will be designated as the carbonaceous residue. Of course, the procedure used for matching the 3-carbon side chain products with the methoxyphenol products will automatically discriminate between S- and M-type individual products.

With regard to the matching procedure, the simulation will use appropriate looping techniques to match all possible methoxyphenol products against all possible 3-carbon side chain products, save the permanent gases, water, and MeOH which arise 'intact'. Thus a large



number of different possible whole lignin pyrolysis products will be generated. Many of these will arise in small proportions, however, which serves to reduce the practical complexity of the product spectra. Further, many products will be M-type, which can be collectively lumped as residue. In short, those products of interest, notably those reported from previous pyrolyses, are limited to about 30-40 in number, and the yields of these will be individually detailed.

In summary, the simulation numerically solves a set of first order differential equations which describes the variation with time of the number of each type of 3-carbon side chain and methoxy phenol moiety per unit weight of lignin substrate. The initial conditions for each moiety number concentration were obtained from the distributions depicted in the Freudenberg structural model for lignin. A statistical matching of methoxyphenol and 3-carbon side chain products then describes the products expected from whole lignin thermolysis.

## 6.0 Experimental Methods

Table 6.1 is a summary detailing the range of operating conditions for the experimental pyrolyses. Listed are the model compound, structure, purity and the temperature, time and concentration range studied. The experimental details are conveniently grouped into three categories, namely, the source of the chemicals used for pyrolysis, the actual apparatus used to effect the pyrolysis, and the chemical analysis system used for product characterization.

### 6.1 Chemicals used

Excepting phenethylphenyl ether, all model compounds were available commercially and were used as received as listed in Table 6.1. Phenethylphenylether was not commercially available and required synthesis. The substrate was obtained via a Williamson ether synthesis as described by Mademov and Khydyrov<sup>164</sup>. Phenolate anion was prepared by adding 36gm of powdered NaOH to 94gm of phenol in 200gm of benzene. This mixture was heated to about 95C, whereupon 93gm of 1-bromo-2phenyl ethane were added. Stirring was continued at this temperature for about 12 hours. The reaction product was washed and extracted by volumes of water and benzene, respectively, and the product recovered by rotary evaporation. The structural details of the synthesis product were confirmed by NMR, and a quantitative account of impurities was ascertained by GC. Figure 6.1 is the NMR trace of the synthesis product used for pyrolysis. Analysis by GC on OV-17 showed the ether to be 95% in purity, with phenol accounting for 20% of this. Other impurities were higher in

Table 6.1 Experimental Grid for Model Compound Pyrolyses

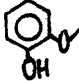
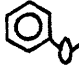
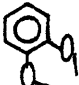
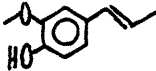
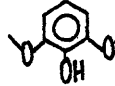
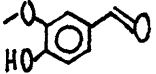
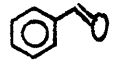
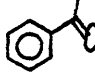
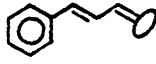
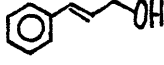
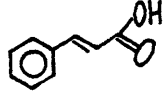
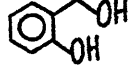

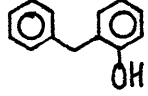

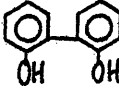
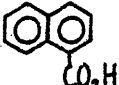
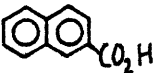
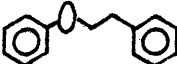
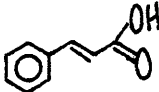
COMPOUND	STRUCTURE	PURITY Wt%	TEMPERATURE RANGE C	HOLDING TIMES s	CONCENTRATION mol/l
GUAIACOL		99	250-535	110-6000	0.46-3.07
ANISOLE		98	344-550	180-1500	0.46-3.07
VERATROLE		98	350-550	60-1500	0.33
ISOEUGENOL		99	300-500	60-1560	0.33
2,6-DIMETHOXY-PHENOL		99	300-500	120-1800	0.32
VANILLIN		99	300-500	120-1500	0.85
BENZALDEHYDE		99	300-500	120-3600	0.16-3.3
ACETOPHENONE		98	350-550	120-4980	0.14-1.4
CINNAMALDEHYDE		99	250-400	120-1500	0.38-1.3
CINNAMYL ALCOHOL		98	300-500	60-1500	0.37-1.1
CINNAMIC ACID		98	300-400	120-1800	.20
SALIGENOL		97	175-350	60-1500	.37
PHENYL ETHER		99	500-587	240-9000	.3
O-HYDROXY-DIPHENYL METHANE		99	400-550	120-6000	.27

Table 61 Experimental Grid for Model Compound Pyrolyses (cont'd)

COMPOUND	STRUCTURE	PURITY Wt%	TEMPERATURE RANGE C	HOLDING TIMES s	CONCENTRATION mol/l
BIPHENYL		95	400-587	360-1380	0.40
BIPHENOL		99	400-587	600-1500	.34
1-NAPTHOIC ACID		98	350-450	60-1500	.3±.2
2-NAPTHOIC ACID		99	350-450	60-1500	.3±.2
PHENETHYL PHENYL ETHER		97	300-550	30-14400	0.083-1.68
FERULIC ACID		99	200-350	120-1500	.5

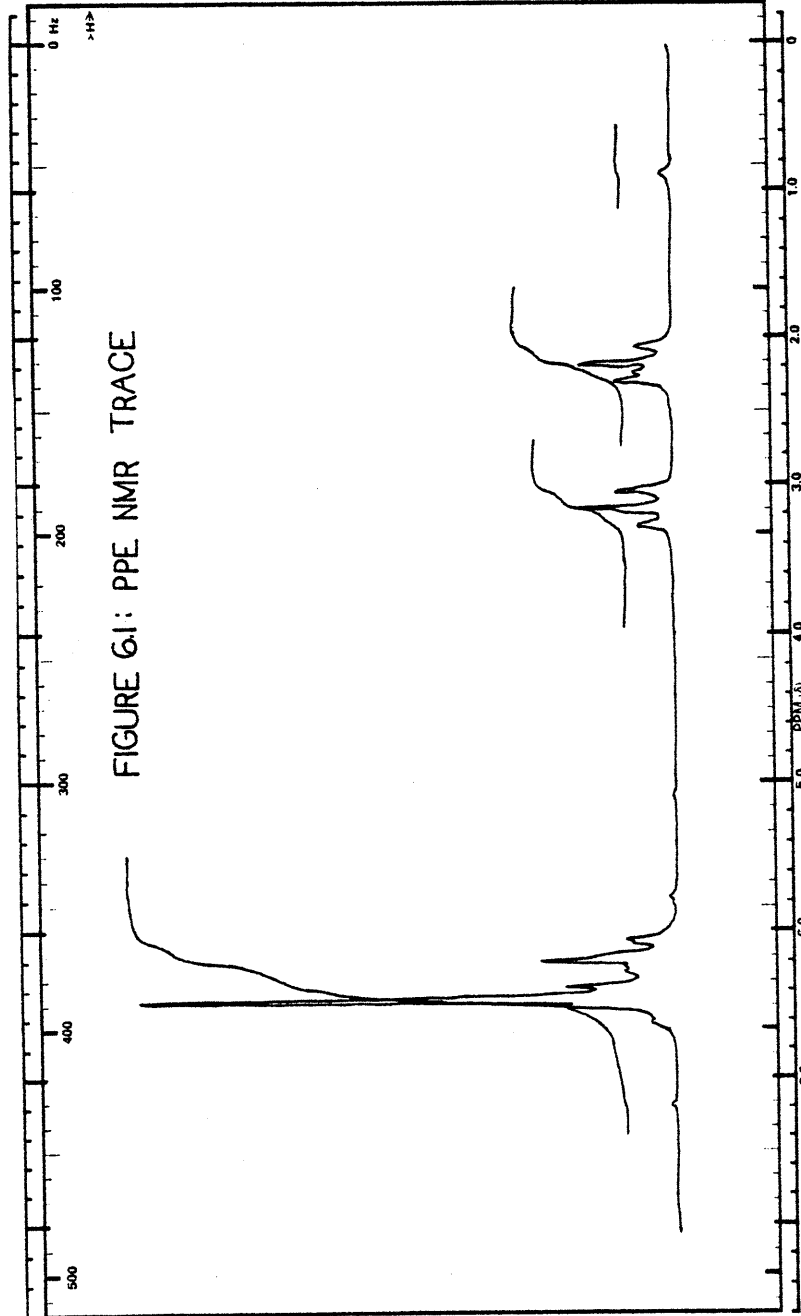


FIGURE 61: PPE NMR TRACE

SWEEP OFFSET (HZ): 0  
 SPECTRUM AMPLITUDE: 2  
 INTEGRAL AMPLITUDE: 1  
 SPINNING RATE (RPS): 40

MANUAL  AUTO  SAMPLE: \_\_\_\_\_  
 SWEEP TIME (SEC): (250)  
 SWEEP WIDTH (HZ): (500)  
 FILTER: ( 2)  
 RF POWER LEVEL: (.05) SOLVENT: \_\_\_\_\_

REMARKS: \_\_\_\_\_

WILMAD GLASS CO., INC.  
 U.S. Route 40 and S.A. Hwy. 111  
 BUENA, N.J. 08310 U.S.A.  
 Printed in U.S.A. 1-79-300 WP

DATE: 2/27/80 OPERATOR: \_\_\_\_\_  
 CHART NO. WCV-60T 60 MHz NMR SPECTRUM NO. \_\_\_\_\_

molecular weight, and were not a factor in the pyrolysis experiments.

## 6.2 Apparatus

Because of the wide range of physical properties of the model compounds used, and in an effort to minimize consumption of scarce and costly chemicals, a batch reactor system was employed for all pyrolyses. Two major problems associated with flow reactors, reactant injection and product recovery were thus entirely avoided. The major limitation of the batch system used was the exclusion of very small residence time pyrolyses due to human reflex and reactor heat-up time, principally, the latter.

The time for each reactor to attain 90% of the final pyrolysis temperature was noted experimentally as a shift in the conversion intercept at time  $t = 0$  and calculated theoretically for each size reactor used. The heat-up time was on the order of one to two minutes for reactors used in kinetic studies, small in relation to the holding times for most pyrolyses.

The batch reactors employed were stainless steel "tubing bombs" fashioned from Swagelok components. Four different size reactors were used, having volumes of 0.2, 0.6, 3.5, and 10.6 cm<sup>3</sup>. Kinetic studies were confined to the reactors of 0.2 and 0.6 cm<sup>3</sup> in volume in an effort to minimize the effect of heat-up time. The latter two reactors were used for quantitative gas and liquid stoichiometry studies, and were often equipped with valves for sampling. The use of valves was shown to be unnecessary when the reactors were opened in an atmosphere of helium, the GC carrier gas. This gas sampling procedure enabled the acquisition of gas phase data from the 0.6cm<sup>3</sup>

reactor as well. In total, 85% of the experimental pyrolyses were effected in the  $0.6 \text{ cm}^3$  reactors since these were amenable to both gas phase and liquid phase kinetic analysis. Figure 6.2 is a schematic of the reactors used.

A Tecam model SBS-4 fluidized sand bath equipped with a temperature controller was used as the heating medium into which the batch reactors were immersed. The sand bath temperature capabilities ranged from ambient to  $600^\circ\text{C}$  and thus provided a wide range of temperatures for pyrolysis. An ice-water bath served to quench the reactor and its contents in experiments where analysis for water was not critical; water accumulation on the Swagelok threads was unavoidable when the ice-water quench was employed. In other selected experiments, saligenol dehydration, for example, ethanol was carefully used for quench. A small number of pyrolyses were allowed to air-cool in order to characterize the pyrolysis product spectra, but these were not included in kinetic analyses.

The experimental pyrolysis procedure can be summarized as follows: the batch reactors were either loaded and sealed in a glove box maintained with a nitrogen or argon inert atmosphere, or were externally loaded and slowly purged with an inert flow before closure. The former technique was amenable to pyrolyses of model compounds which were liquid at or near room temperature, the latter technique more applicable to solids which necessitated weighing. In any event, at these temperatures, no effect of air could be discerned from duplicate experiments without the inert purge. The inert also served as an internal standard for later gas

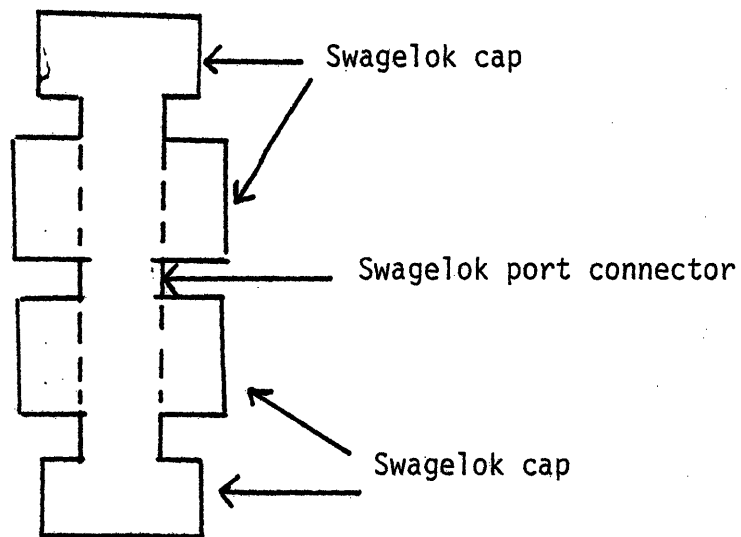


Figure 6.2 Schematic of experimental tubing bomb reactor



analyses. The loaded reactors were then immersed in the fluidized sand bath for the duration of reaction, and finally quenched in the ice-water bath. In experiments where comparisons at a given temperature were of prime interest, such as neat and in-tetralin phenethyl-phenyl ether pyrolysis and pyrolyses at varying initial substrate concentrations, reactors were co-immersed to insure identical temperature-time histories. After quenching, the reactors were dried, opened, and septum capped in a helium environment for GC gas analysis. As helium was the carrier gas for the GC, this technique eliminated the risk of introducing detectable contaminants which would invalidate the GC gas analysis. Since a known amount of inert was in each reactor, only relative amounts of products and inerts were required. The remaining liquid and solid products were then solvent-collected for later GLC/GC gas analysis. Figure 6.3 is a schematic representation of the experimental pyrolysis and sampling procedure.

### 6.3 Chemical Analysis

As illustrated in Figure 6.3, the pyrolysis products were identified and analysed by Gas-Chromatography. An HP5720A thermal conductivity detector interfaced with an HP3380 reporting integrator was used for both gas and liquid analyses. Early studies on anisole, guaiacol, vanillin, 2,6 - dimethoxyphenol and isoeugenol were performed with graphical area measurements. Selected analyses were performed on the same GC system equipped with an FID detector, these being few in number and occurring primarily during repair of the TCD/GC. An account of the GC details for each model compound is given in Appendix 6.1. Several generalizations are possible. Gases

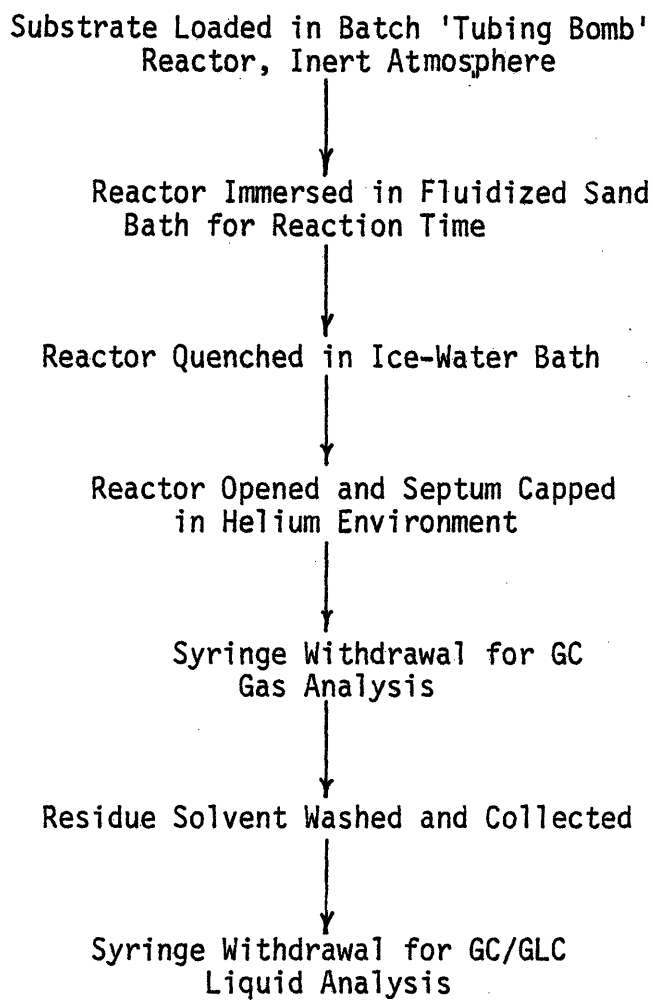


Figure 6.3 Schematic of experimental procedures

were separated by either molecular sieve (10'), silica gel (6') or porapak Q (6') columns. The latter of these was used for CO<sub>2</sub> and higher molecular weight gases while the silica gel was extensively used for its resolving power of N<sub>2</sub>, CO and CH<sub>4</sub>. The molecular sieve was also used for CO and CH<sub>4</sub> separations and it additionally separated O<sub>2</sub> and N<sub>2</sub> at room temperatures, a measure of the efficiency of attaining an inert atmosphere. The GC carrier gas was helium, and therefore hydrogen was detectable but not quantifiable. Analysis for light liquids, such as H<sub>2</sub>O, MeOH, EtOH and up to about toluene and phenol were effected on porapak Q and principally porapak P (6') columns. The heavier compounds, including alkyl benzenes, phenols and the model compounds were separated primarily by an OV-17 (6') column. Saligenol was an exception being analysed on 20" of 10% UCW-98% column. Product identification was primarily by GC with standard coinjection although a single GC-MS analysis was performed for phenethylphenyl ether for more unequivocal determination of individual peaks. Quantitative product mol fractions were determined utilizing calibration factors previously obtained from standard samples of known composition. These calibration factors were monitored routinely during the course of the analysis of a given model compound. The factors were constant about a statistical mean for nearly all pyrolyses, only changing when a given peak size or shape was changed drastically. This was the case for PPE pyrolysis, for example, where the dilution by tetralin effected a change in the peak shape and size for substrate. This caused the calibration factor for the PPE

peak to be a function of S, the mol ratio tetralin/PPE. These calibration factors were monitored as a function of S and were used as such in all quantitative product spectra calculations.

Overall, the experimental apparatus and procedure provided for rapid, meaningful data acquisition with the flexibility to study a wide spectrum of model compounds over a large range of conditions.

## 7.0 Experimental Results

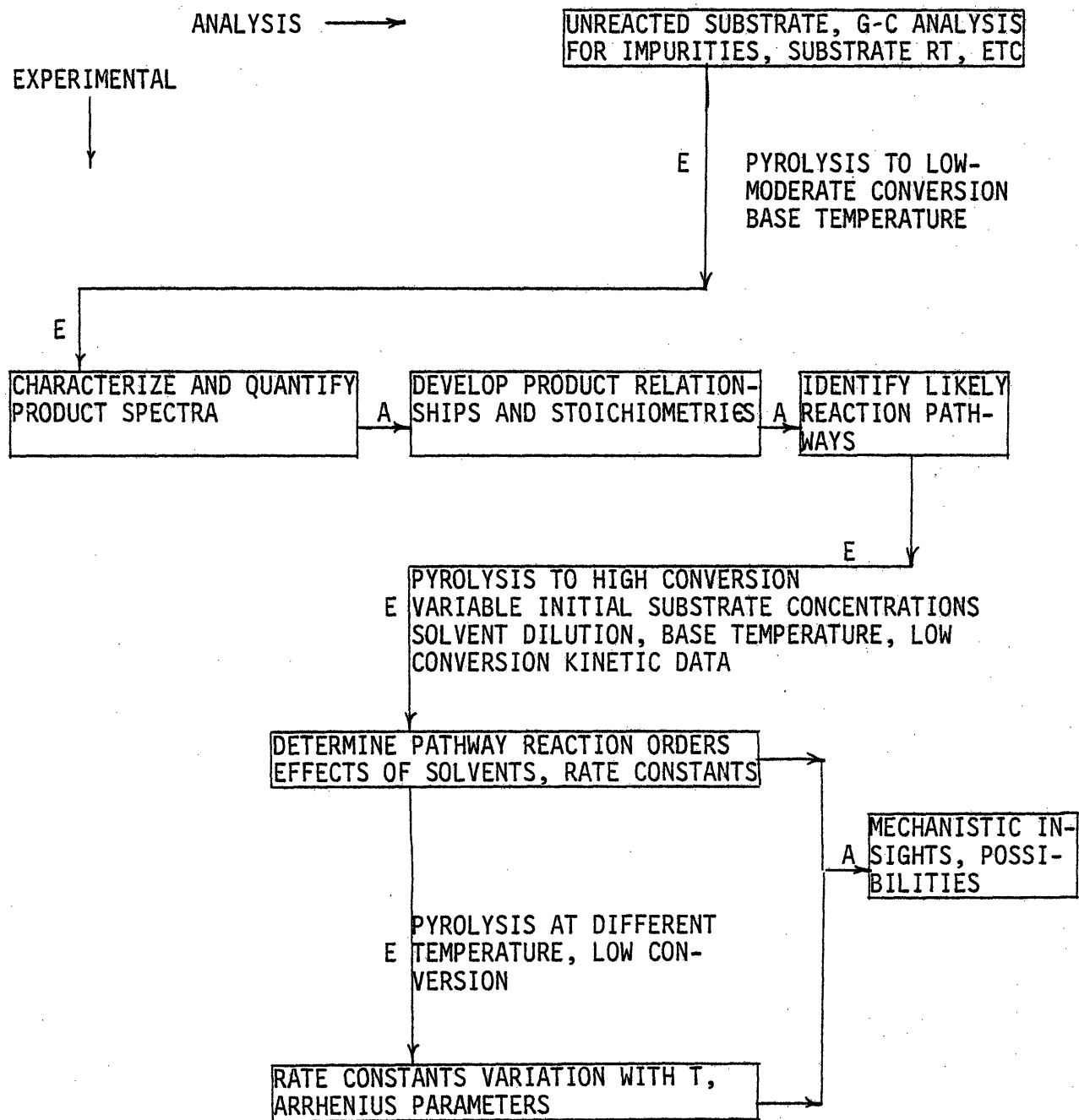
The model compounds were pyrolysed over the range of conditions detailed in Table 6.1, a summary of the present experimental grid. The overall experimental strategy is depicted in Figure 7.1. For each compound, it was desired to:

1. Characterize and quantify pyrolysis product spectra
2. Develop product relationships and stoichiometries
3. Identify likely reaction pathways
4. Determine reaction orders
5. Estimate reaction kinetics and Arrhenius parameters

The results for each model compound are discussed in this manner.

Tables listing the details of the pyrolysis product spectra for each model compound are given in Appendix 7.1. In many instances, tables and graphs depicting the important features of these spectra are included in the main text. A comprehensive summary of the kinetic parameters obtained from each pyrolysis is given as Appendix 7.2. Appendix 7.2 includes values of  $-\log_{10}k(s^{-1})$  of each temperature, substrate concentration, and solvent dilution studied; inferred Arrhenius parameters are listed as well.

The results are described with reference to each compound listed in order of descending importance. The discussion thus begins with PPE, followed by a consideration of methoxyphenol and 3-carbon side chains. Less important pyrolyses were those of the remaining inter-unit linkage and  $CO_2$  precursor models.

Figure 7.1 Experimental Strategy for Model Compound Pyrolyses

### 7.1 Phenethyl Phenyl Ether

Phenethyl Phenyl Ether (PPE) was obtained via a Williamson ether synthesis as described by Mademov and Khrydrov<sup>164</sup>. Phenolate anion was prepared by adding 36 gm of powdered NaOH to 94 gm of phenol in 200 gm of benzene. This mixture was heated to about 95 C, where upon 93 gm of 1-bromo-2phenyl-ethane were added. Stirring was continued at this temperature for about 12 hours. The reaction product was washed and extracted by volumes of water and benzene, respectively, and the product recovered by rotary evaporation. The structural details of the synthesis product were confirmed by NMR, and a quantitative account of impurities was ascertained by GC. Analysis on OV-17 showed the ether to be 95% in purity, with phenol accounting for 20% of this. Other impurities were higher in molecular weight and were not a factor in the pyrolysis experiments.

The pyrolyses were effected over the range of operating conditions detailed in Table 6.1. The experiments were conducted at temperatures from 300 to 550C, with holding times of 1 to 240 minutes. Substrate conversions were generally held to less than 30% in an effort to emphasize primary reactions; however, kinetic data were obtained at conversions as high as 90%. Initial substrate concentrations ranged from 0.083 to 1.66 mol/l in the gas phase.

The ether was pyrolysed in the presence of tetralin at temperatures of 350, 400 and 450 C. at substrate concentrations of 0.25 mol/l. The effect of tetralin was examined in detail at 400C, where the mol ratio of tetralin to ether S (molT/molPPE), was varied

from 0.245 to 9.8.

Liquid and solid reactor contents were dissolved in either acetone or methylene chloride solvent in preparation for GC analysis. The products were separated over an OV-17 column and analysed by a thermal conductivity detector HP 5720 gas chromatograph. Analyses for gases and light liquid products were performed on silica gel and porapak P columns, respectively. Gaseous products were sampled by syringe, in an atmosphere of helium, the GC carrier gas. Product identification was principally by GC with standard coinjection, although a single GC-MS analysis was performed for more unequivocal determination of individual peaks. Quantitative product mol fractions were determined utilizing calibration factors previously obtained from standard sample blends of known composition.

Care was taken to monitor material balance closure, quantified by the determination of the parameter  $\langle M \rangle$ , physically the average molecular weight of the pyrolysis products, where

$$\langle M \rangle \equiv \frac{\sum_{i=2}^n X_i M_i}{\sum_{i=2}^n X_i} \quad \begin{array}{l} n = \text{total number of products,} \\ \text{including unreacted ether} \\ i = 1 \equiv \text{ether} \end{array}$$

In this expression  $X_i$  is the mol fraction and  $M_i$  the formula weight of product  $i$ ,  $i=1$  designates unreacted ether. Thus only true products are considered in the  $\langle M \rangle$  calculation, with unreacted ether excluded. An ideal production of two product mols from each ether substrate mol would thus yield an  $\langle M \rangle$  value of  $\sim 198/2=99$ .



Reaction kinetics could be discerned using a similar approach.

Material balance constraints dictate that

$$(1a) W_{EO} = W_{PRODUCTS} = W_{UNREACTED\ ETHER} + W_{OTHER\ PRODUCTS}$$

where  $W$  designates the weight of material under consideration. Since the weight of a given material is equal to the number of mols times its molecular weight,  $W_i = N_i M_i$ , then

$$(1b) N_{EO} M_E = N_E M_E + \sum_{i=2}^n N_i M_i, \quad i = 1 \Rightarrow i = E$$

Thus on the basis of one product mol,  $N_T = N_E + \sum_{i=2}^n N_i = \sum_{i=1}^n N_i = 1$ ,

$$(1c) N_{EO} M_E = X_1 M_E + \sum_{i=2}^n X_i M_i = N_E M_E + \sum_{i=2}^n X_i M_i$$

and hence

$$(2) N_{EO} - N_E = \sum_{i=2}^n X_i M_i / M_E$$

$$(3) \frac{N_i}{N_{EO} - N_E} = \frac{X_i M_E}{\sum_{i=2}^n X_i M_i}$$

$$(4) N_E / N_{EO} = \frac{X_1}{X_1 + \sum_{i=2}^n X_i M_i / M_E}$$

The GC product mol fractions are thus readily transformed into conversion parameters.

The 157 experimental PPE pyrolyses yielded a mean value  $\langle M \rangle = 100.5 \pm 3.98$  as a quantitative measure of pathway closure to two product mols. Carbon, hydrogen and oxygen atom balances were effected and the ratios H/C and O/C were within  $\pm 3.2\%$  and  $\pm 11.7\%$  of those for the unreacted substrate; the latter provide a measure of overall

material balance. The results will be described in two parts, neat pyrolyses and pyrolyses in tetralin.

### Neat Pyrolysis

A. Primary Products Neat ether decomposition was detected at a temperature as low as 300C with a reaction time of one hour. The products from representative pyrolyses at various temperatures and times are listed in Table 7.1.1. Two major observations emerge from inspection of Table 7.1.1. While 13 various pyrolysis products were detected and quantified, it is clear that the major products were limited to phenol and the hydrocarbons styrene, ethylbenzene, toluene and benzene. The remaining products, in sum total, amounted to at most about 6% of the phenol and hydrocarbons. Of the hydrocarbons, styrene was predominant at low conversions, with increasing amounts of toluene as conversion increased. Secondly, the details of the product spectra were relatively insensitive to temperature, although a slight dependence on initial substrate concentration and a strong dependence on conversion were observed. These latter two observations are reflected most strongly in the relative proportions of major hydrocarbon product.

The time dependencies of the substrate and major products proportions for pyrolysis at 400C and initial ether concentration of 0.25 mol/l are depicted in Figure 7.1.1. The slopes of the phenol appearance and ether disappearance lines in Figure 7.1.1 are suggestive of a stoichiometric production of phenol from substrate.

E <sub>0</sub>	.25	.25	0.083	0.25	1.66	0.083	0.25	1.66	0.25	0.24	0.25
T, C	325	240	400	400	400	400	400	400	400	550	550
t, s	115	40	5	15	15	15	25	25	25	1	2
E, s	.9821	.894	.8270	.8863	.869	.5230	.6520	.442	.417	.6723	.0207
PhOH	.0603	.064	.0960	.0601	.057	.2420	.1880	.284	.3040	.1520	.4000
ST	.0151	.036	.0640	.0375	.044	.1010	.0833	.037	.0885	.0876	.1380
T	.0031		.0052	.0102	.0161	.6350	.0373	.0033	.0813	.0434	.206
EB	.0077		.0077	.0042	.0057	.0710	.0200	.0584	.0550	.0128	.112
S	0		0	.0000	0	0	.0021	.0078	.0118	.0050	.0640
BPE	.0037		0	.0011	.0072	.0054	.0096	.0542	.0195	.0072	.022
BB	.0004		0	.0006	.0015	.0035	.0060	.0156	.0164	.0070	.031
PhTol	0		0	0	0	.0005	0	.0014	.0005	.0001	.0024
PhPhOH	.0008		0	0	0	.0007	0	0	0	.0003	.0083
PhOPh	0		0	0	0	0	0	0	.0003	.0002	.0020
PH <sub>2</sub>	0		0	0	0	0	0	0	0	0	.0002
DPM	.0002		0	0	0	0	.0003	.0009	.0009	.0003	.0020
Hvys	0		0	0	0	0	0	0	0	0	0

Table 7.1.1 Representative product spectra from PPE pyrolysis.

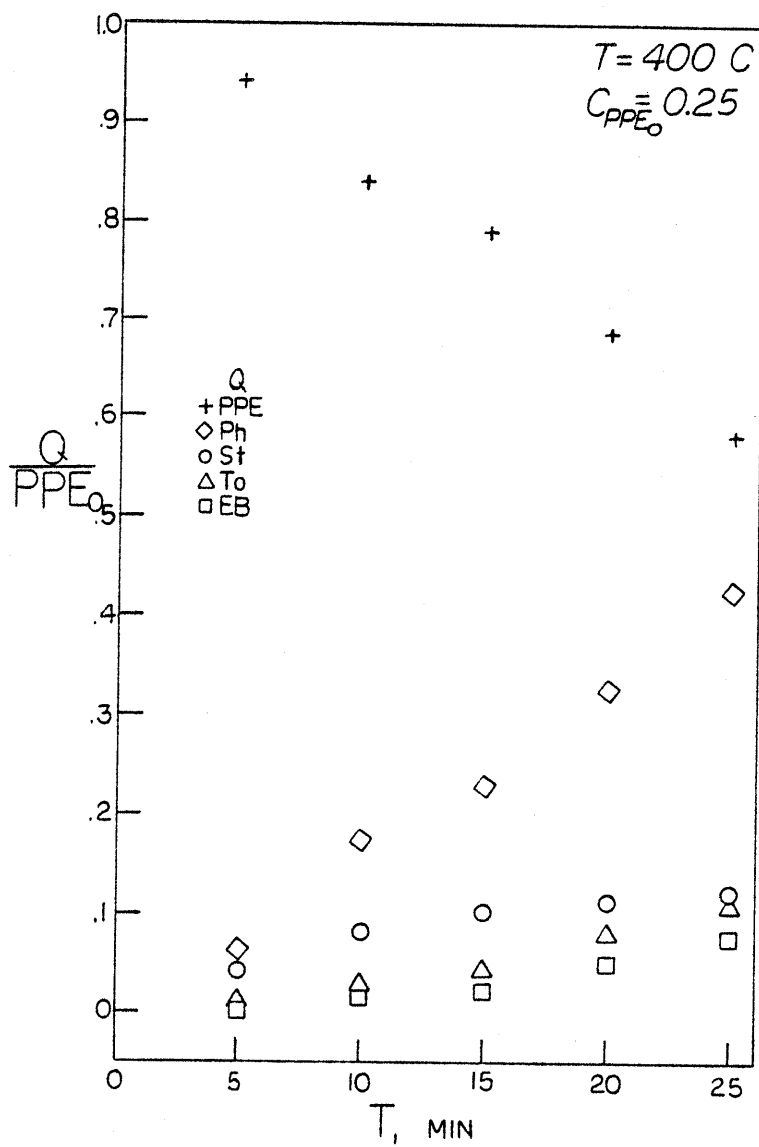


Figure 7.1.1 Major products from neat PPE pyrolysis.

Figure 7.1.1 further depicts the behavior of the styrene product, seemingly produced stoichiometrically with phenol at  $t=5$  min. and reaching maximal proportions by 25 minutes. The maximum yield attained by styrene, coupled with apparent initial slopes of zero for toluene and ethylbenzene production, is suggestive of secondary reactions of the styrene to other products, including toluene, ethylbenzene and benzene.

The stoichiometric implications of Figure 7.1.1 are further developed in Figure 7.1.2 where the yield of phenol, styrene, and the sum (styrene + ethylbenzene + toluene + benzene=(HC)) per mol of decomposed substrate are plotted as a function of substrate conversion. Evidenced by the constant value of unity for phenol in Figure 7.1.2, it is clear that for each mol of ether decomposed a mol of phenol was produced. At conversions of about 80%, the ratio  $Ph/E_0 - E$  may in fact approach  $\sim 0.9$ , indicative of experimental uncertainties at very high conversion. Overall, however, it is quite reasonable to conclude that degradation of phenethyl phenylether resulted in essentially stoichiometric production of phenol. The behavior of styrene is also depicted in Figure 7.1.2. At conversions of about 80%, the styrene selectivity was only about 0.2, whereas this ratio approached at least 0.8 and possibly 1.0 at low conversion. The latter assessment is tentative, since data at very low (i.e.  $\sim 1\%$ ) conversion are lacking. However, it is evident that styrene was initially produced in stoichiometric proportions with phenol; at higher conversions, styrene proportions were considerably less than those of phenol. A secondary styrene degradation was thus suggested by the data of

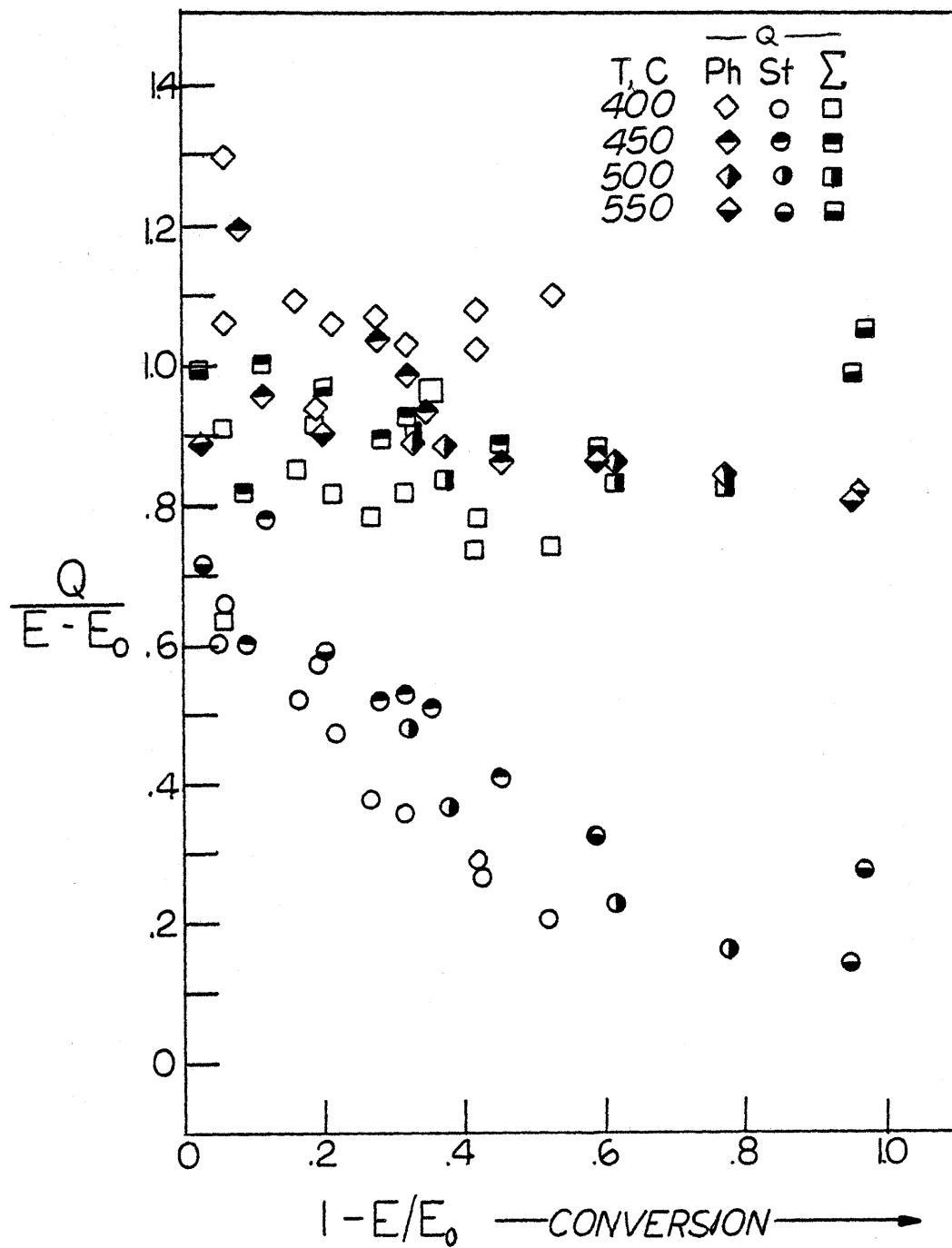
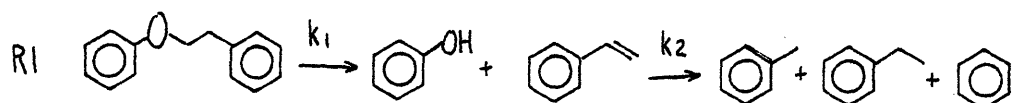


Figure 7.1.2 Product relationships in neat PPE pyrolysis.

Figure 7.1.1 and is further implied by Figure 7.1.2. This plot also depicts the conversion dependence of the instantaneous yield  $(St + EB + TOL + B)/(E_0 - E) \equiv HC/(E_0 - E)$ .

It was experimentally observed that while the styrene proportion dropped rapidly, the sum HC was nearly stoichiometric with ether decomposition for all conversion. This behavior is followed in Figure 7.1.2 for conversions as high as 98%. In sum, the product relationships of Figure 7.1.2 are suggestive of a pathway for ether decomposition of the type R1, with the production



of phenol and hydrocarbons very nearly stoichiometric and equal to substrate conversion.

The order of reaction (R1) was examined in a series of experiments at 400C and at initial substrate concentrations ranging from 0.083 to 1.16 mol/l. Figure 7.1.3 plots the variation with time of  $\ln E/E_0$  for each initial concentration studied. A reaction with rate expression  $r = kC_E^\alpha$ , i.e., rate constant  $k$  and order  $\alpha$ , would yield an initial slope  $|d \ln (E/E_0)/dt|_{t \rightarrow 0} = kC_{E_0}^{\alpha-1}$ . The data of Figure 7.1.3 show no systematic dependence on  $C_{E_0}$  and are described by a single average slope, implying  $\alpha = 1$  and first order ether pyrolysis. The linearity of  $\ln E/E_0$  vs  $t$  for conversion to at least 70% is further indicative of first order kinetics. The rate constants implied in Figure 7.1.3 for each initial substrate concentration were separately determined and are plotted in Figure 7.1.4, where  $k(s^{-1})$  is presented versus  $C_{E_0}$  (mol/l). Here the rate constant

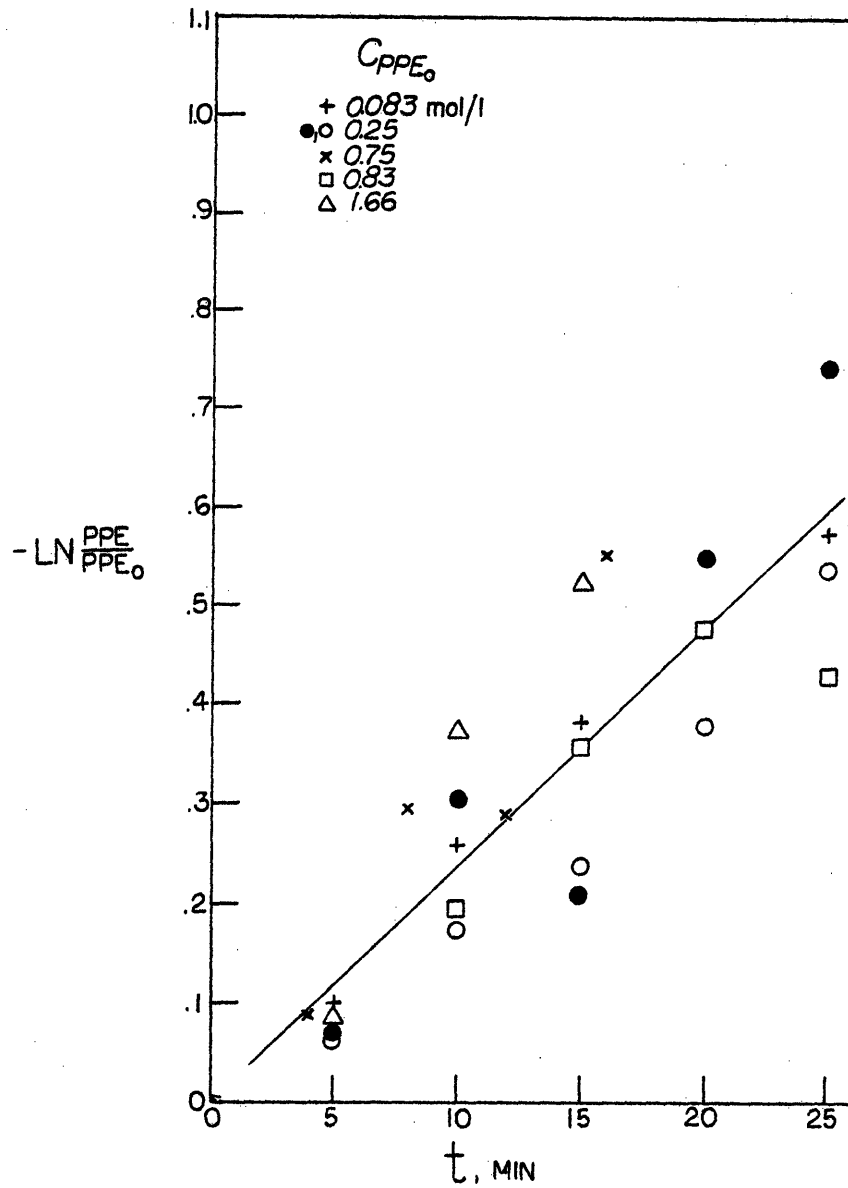


Figure 7.1.3 PPE pyrolysis kinetics at 400 C.



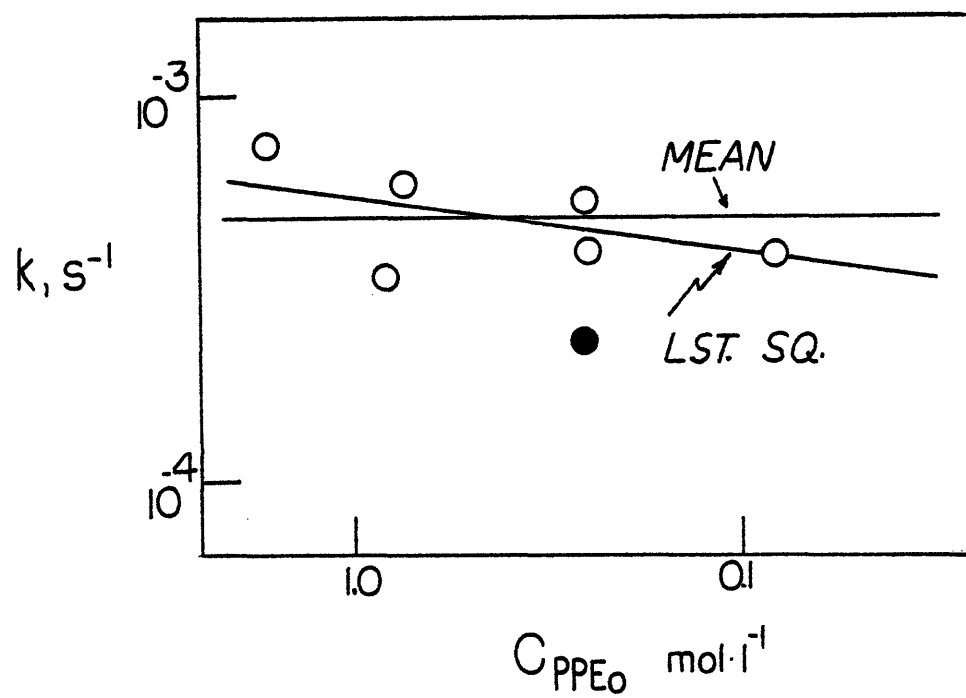


Figure 7.1.4 Variation of  $k_1^{\text{PPE}}$  with initial PPE concentration

was found to be substantially invariant with  $C_{E_0}$ , although a least squares analysis revealed a slight dependence which could be represented as  $k \propto C_{E_0}^{0.16}$ , implying in order of  $\alpha = 1.16$ . However, the variance of the 0.16 slope of  $\log k$  vs  $\log C_{E_0}$  was 0.12, implying that within any reasonable confidence limit the order can be considered unity. That is, the data did not allow discrimination beyond the assessment of first order kinetics.

Further pyrolyses at temperatures from 300-500C revealed the temperature dependence of the first order rate constant  $k_1$ . These data are shown in Figure 7.1.5 an Arrhenius diagram with coordinates of  $\log_{10} k (\text{s}^{-1})$  vs  $\theta^{-1}$ , where  $\theta = 4.573 \times 10^{-3}$  in Kelvins. The usual Arrhenius relationship is thus described as the straight line  $\log_{10} k = \log_{10} A - E^* \theta^{-1}$ , where the pre-exponential factor A has units of the rate constant and the activation energy  $E^*$  is expressed in kcal/mol. It is evident from Figure 7.1.5 that  $\log_{10} k_1$  follows the Arrhenius relationship over a range of five orders of magnitude in  $k_1$ . The best fit of these data yields Arrhenius parameters  $(\log_{10} A (\text{s}^{-1}), E^* (\text{kcal/mol})) = (11.1 \pm 0.9, 45.0 \pm 2.7)$

B. Secondary Products Table 7.1.1 and Figures 7.1.1 and 7.1.2 suggest that ethylbenzene, toluene and benzene appeared as secondary products of styrene degradation. As evidenced in Table 7.1.1 and Figure 7.1.1 and 7.1.2 the mol ratio  $St/(T+EB+B)$  decreased as a function of conversion for all temperatures and initial substrate concentrations. That toluene, ethylbenzene and benzene were derived from styrene is indicated by the initial zero slope of the T,EB,B

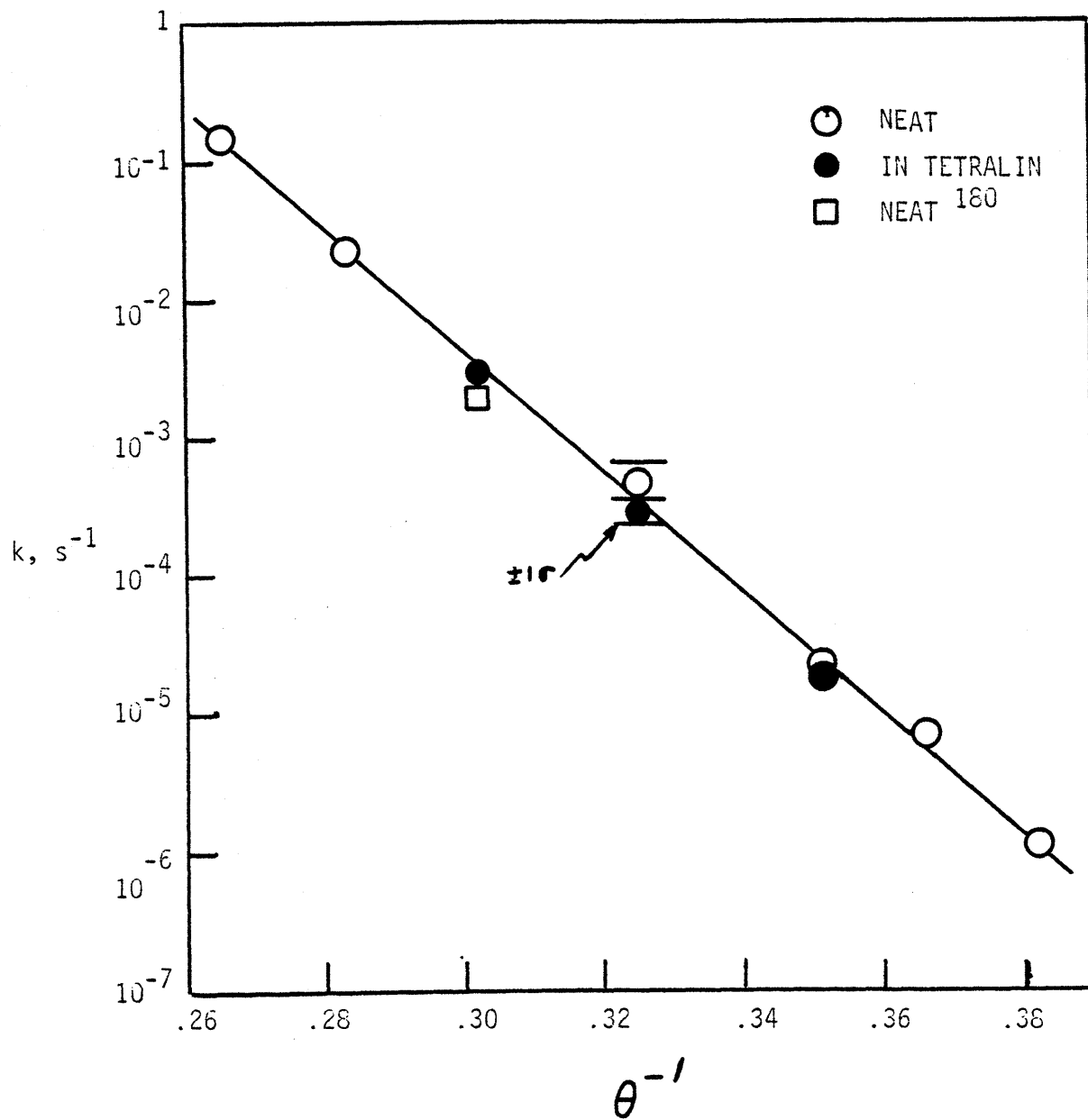
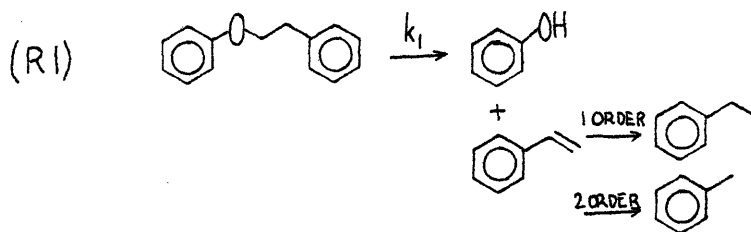
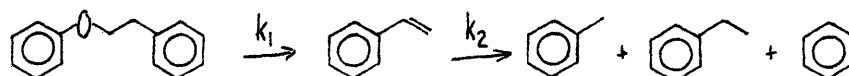


Figure 7.1.5 Arrhenius diagram for PPE pyrolysis.

appearance rates as well as the observed stoichiometric production of the sum HC with phenol. The secondary reaction of styrene was found to be concentration dependent, as depicted in Figure 7.1.6, a plot of product appearance vs substrate conversion at 400 C for  $E_0$  ranging from 0.083 to 1.66 mol/l. While the ratios  $Ph/(E_0-E)$  and  $HC/(E_0-E)$  were substantially unity independent of  $E_0$ , a definite trend in the decrease of  $St/(E_0-E)$  could be discerned with  $E_0$ . That styrene decreased more rapidly with increasing substrate concentration is indicative of reaction order in excess of unity for overall secondary styrene reaction. As can be seen in Table 7.1.1, this higher order reaction path can be linked with toluene production, which was dependent upon  $E_0$ . In contrast, the EB product appearance was relatively insensitive to  $E_0$ , suggesting a first order appearance reaction. Thus, the pathways to secondary products appear to be of the type:



Assessment of the magnitude of the rate for secondary styrene degradation was effected by modelling the reaction network as a consecutive reaction series, namely:



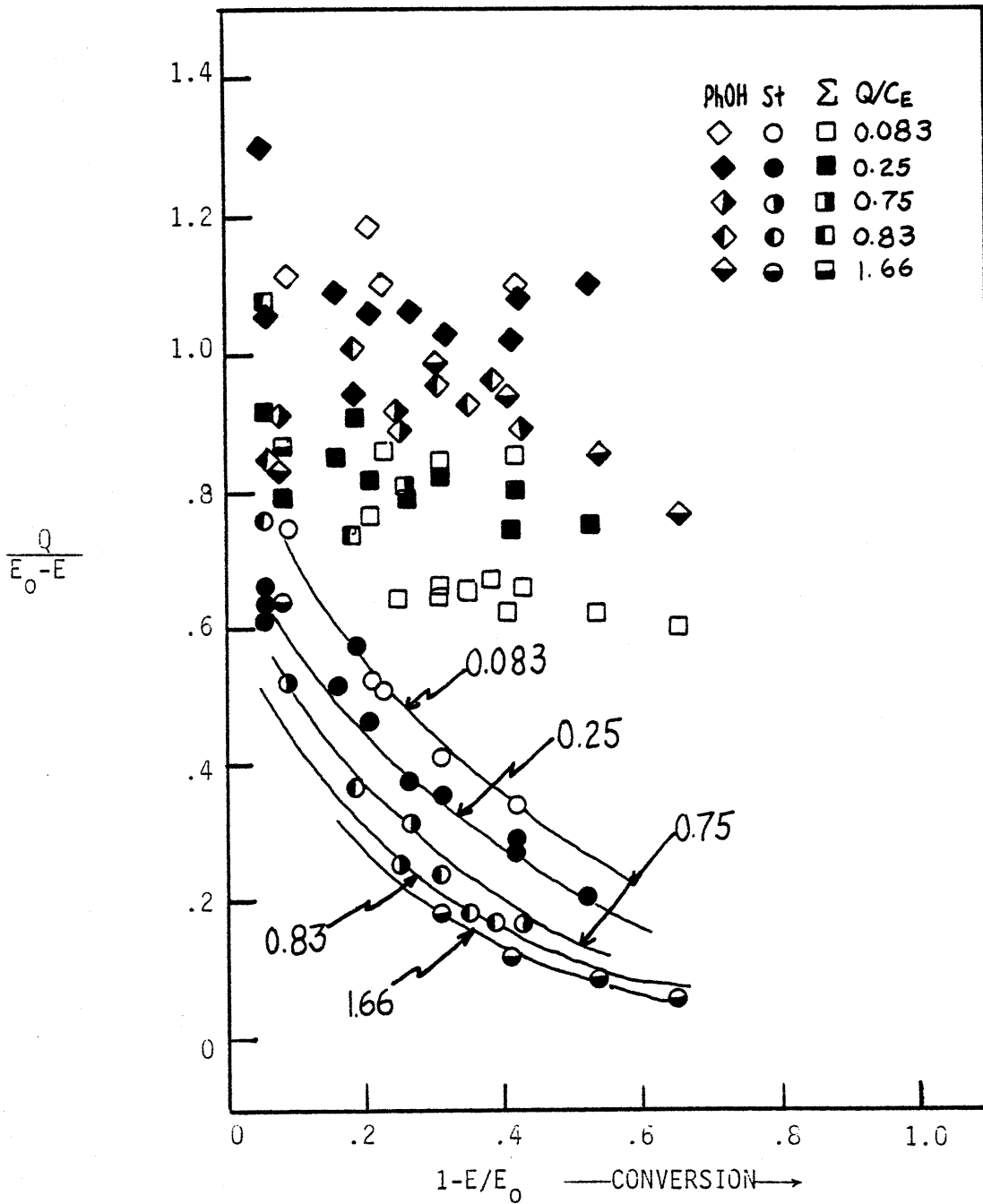


Figure 7.1.6 Product relationships in PPE pyrolysis,  $T=400^\circ\text{C}$ .

An overall pseudo-first order rate constant for secondary styrene degradation can be obtained from either the maximum concentration or the time for maximum concentration of styrene where:

$$t_{\text{MAX}}^{\text{St}} = \frac{\ln(k_2/k_1)}{k_2 - k_1} \quad ; \quad \frac{\text{STY}_{\text{MAX}}}{\text{PPE}_0} = \left( \frac{k_1}{k_2} \right)^{(k_2/(k_2 - k_1))}$$

As evidenced by Figure 7.1.1, styrene only gradually approached maximal proportions, which suggests the use of maximum concentration rather than time for maximum concentration data. That is, the former datum is well defined, whereas the exact time of maximal styrene yield is subject to considerably more uncertainty. The resulting value of  $K(K=k_1/k_2)$  at 400 C and  $\text{PPE}_0=0.25$  was  $K=0.173$ , yielding  $k_2=0.0031 \text{ s}^{-1}$ . These calculations were repeated for the other PPE pyrolyses where a styrene maximum was apparent. The resulting temperature and concentration dependencies of  $k_2$  arose as listed here.

T(C)	PPE <sub>0</sub> (mol/l)	K(k <sub>1</sub> /k <sub>2</sub> )	k <sub>2</sub> (s <sup>-1</sup> )
400	.083	.226	.00172
400	.25	.173	.00310
400	.25	.173	.00225
400	.75	.10	.00585
400	.83	.091	.00370
400	1.66	.074	.01
450	.25	.317	.006
500	.25	.495	.0180
500	.75	.248	.0655

These dependencies are best described with reference to the parameter K, since uncertainty in the absolute determination of  $k_1$  will

propagate uncertainty to the value  $k_2$ . At a given temperature, in this case 400C, the value of K was found to decrease with increasing initial ether concentrations; this reflects the higher order character of styrene degradation relative to ether reversion. That is, for a given reduced ether conversion to styrene,  $St/E_0$ , a higher initial ether concentration will yield a higher number of absolute styrene mols. Thus, a pseudo-first order rate constant  $k_2$  should increase with increasing ether concentration as shown algebraically here:

RATE styrene degradation =  $k_{TRUE}St^2 = k_2St$ ;  $k_2 = k_{TRUE}St$ .  
 The increase in  $k_2$  (decrease in K) with an increase in  $PPE_0$  is also apparent at 500C.

It is also evident that  $k_2$  increased with increasing pyrolysis temperature, as illustrated in comparison of the data for 400, 450 and 500C. The pseudo-first order rate constant  $k_2$  was fit with apparent Arrhenius parameters ( $\log_{10}A, E^*$ ) = (4,20) and (6,25) for  $PPE_0=0.25$  and  $0.75$  mol/l, respectively. Thus, secondary styrene degradation would seem to be considerably less activated than the primary reversion of PPE.

#### Pyrolysis in Tetralin:

The ether was pyrolysed in tetralin at temperatures of 350, 400 and 450C. The primary product spectra were substantially unchanged from those for neat ether pyrolysis, as illustrated in Figure 7.1.7, a plot of product yields as a function of reaction time at 400C,  $S=1.48$  and  $C_{E0} = 0.25$ . The only significant change was in the secondary reaction of styrene, where the presence of tetralin shifted the secondary selectivity toward ethylbenzene.

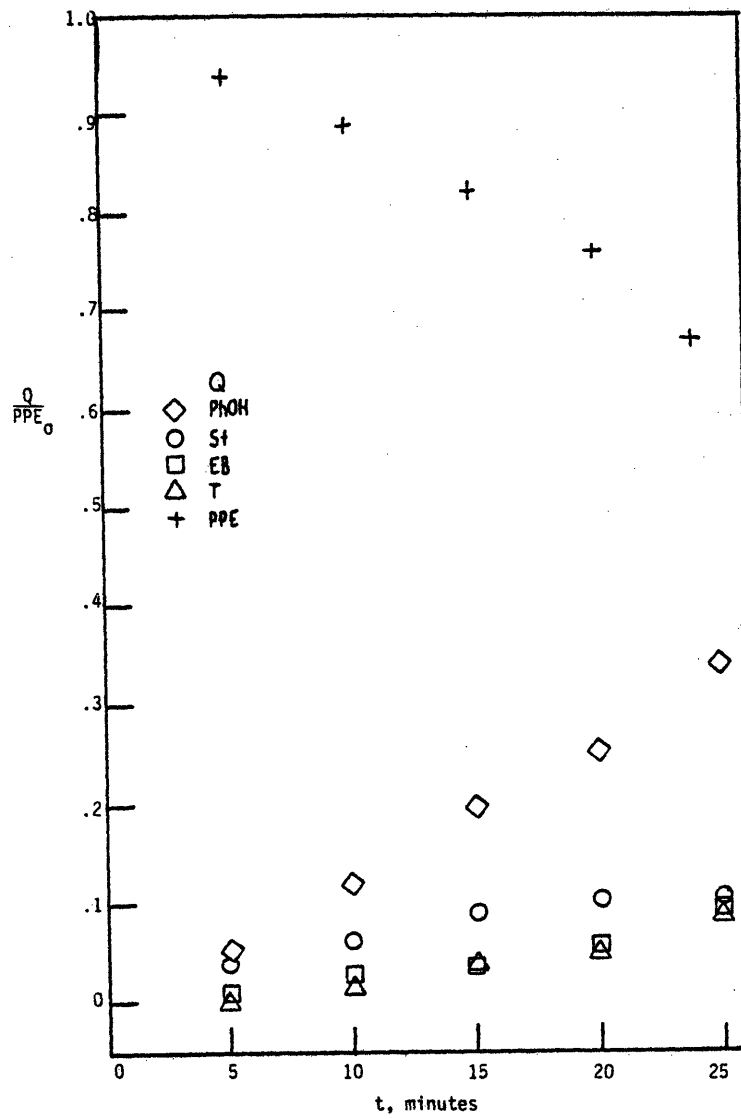


Figure 7.1.7 Major products from PPE pyrolysis in tetralin at 400 C;  $C_E=0.25$ ,  $S=1.46$



The product relationships were further examined in Figure 7.1.8, where the mol ratios  $\text{Ph}/(E_0 - E)$ ,  $\text{St}/(E_0 - E)$  and  $\text{HC}/(E_0 - E)$  ( $\text{HC} = \text{St} + \text{T} + \text{EB} + \text{B}$ ) are plotted as a function of ether conversion. As was the case with neat pyrolysis, both the ratio  $\text{Ph}/(E_0 - E)$  and  $\text{HC}/(E_0 - E)$  were near unity for all conversions attained, while the ratio  $\text{St}/(E_0 - E)$  dropped rapidly with conversion. Hence, the primary pathway for ether decomposition to phenol and styrene was unchanged. The rate of styrene decrease was increased by the presence of tetralin, as evidenced in Figure 7.1.8. Here it is seen that the open circles depicting neat pyrolysis represent a higher styrene concentration at each conversion than do the closed circles indicative of  $S \neq 0$ . This is characteristic of a higher order reaction of styrene and tetralin to ethylbenzene, earlier noted as the major secondary pathway for  $S \neq 0$ .

The kinetics of ether pyrolysis in tetralin were examined for varying values of  $S$  at 350, 400 and 450. These data are presented in Figure 7.1.9, a plot of the first order rate constant versus the mol ratio  $S$  for each temperature studied. A scale change in Figure 7.1.9 allows the inclusion of the rate constant from neat pyrolysis for comparison. The rate data obtained at 350 and 450C were over 2 orders of magnitude change in  $S$ . It is evident the rate constants were virtually independent of the presence and amount of tetralin. More comprehensive study at 400C revealed a slight diminution of the rate constant with increasing tetralin proportions, of the order of  $0.2 \log_{10} k$  units for the range  $S=0$  to  $S=9.8$ . Statistical analyses of the neat and tetralin pyrolysis for all  $S$  revealed that the difference

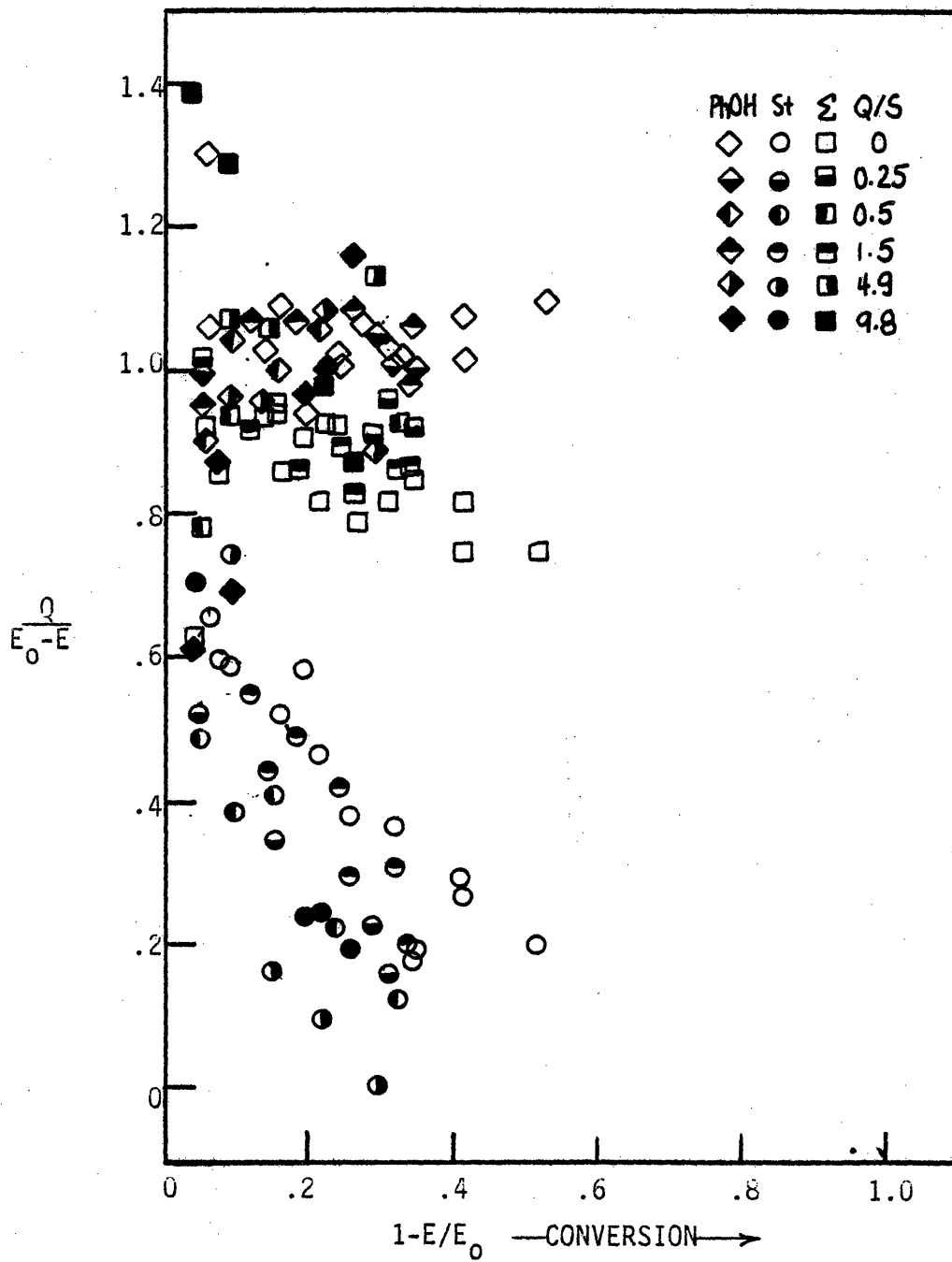


Figure 7.1.8 Product relationships as function of substrate conversion for PPE pyrolysis in tetralin at 400 C.

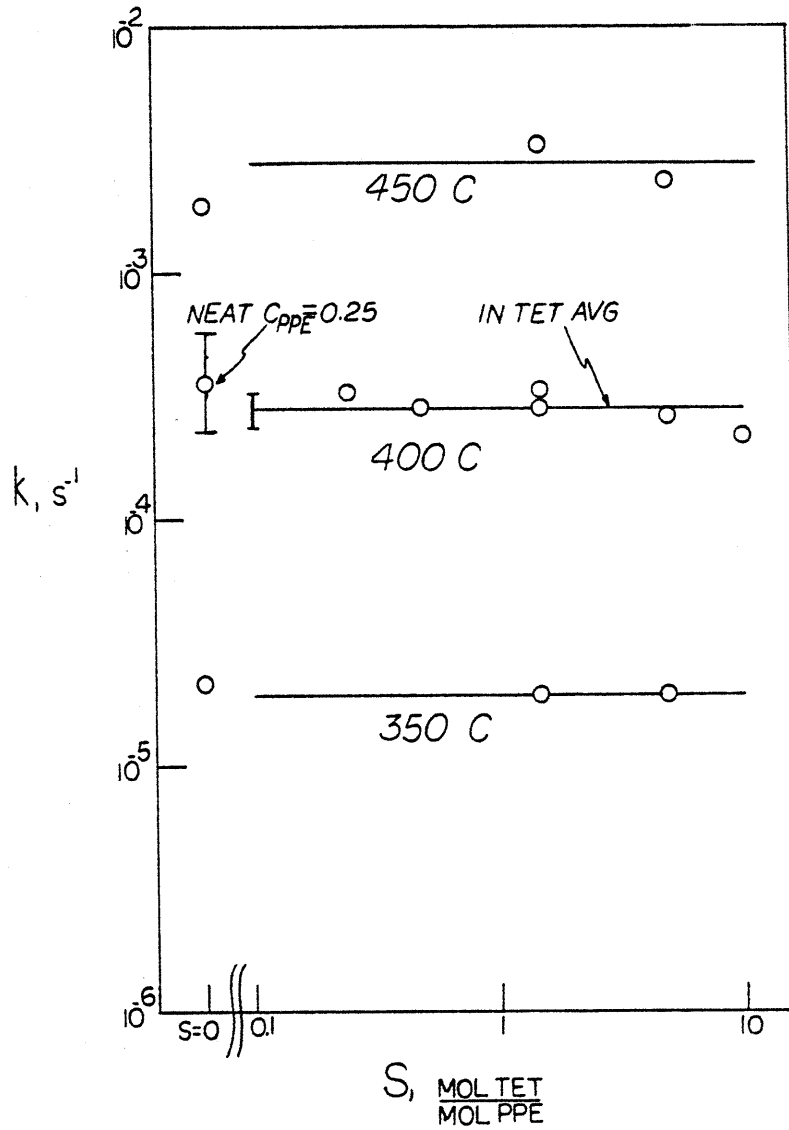


Figure 7.1.9 PPE pyrolysis kinetics, in tetralin

in the means of each were less than the standard deviation of this difference. Further comparison of the neat and in-tetralin pyrolyses is presented in Figure 7.1.5, an Arrhenius diagram. The dark circles representing  $k$  for pyrolysis in tetralin differ only slightly from the neat values.

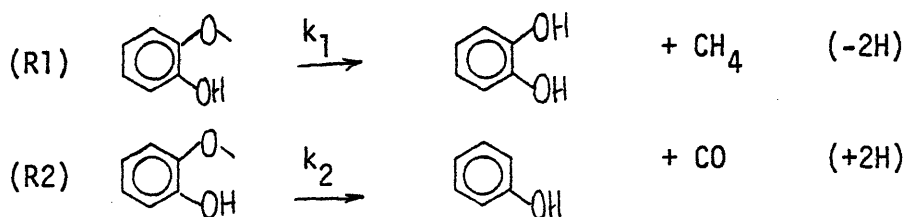
In summary, PPE was pyrolysed both neat and in the presence of tetralin. Neat ether pyrolysis resulted in the primary stoichiometric production of phenol and styrene, with extensive secondary degradation of the latter. Overall ether pyrolysis was substantially first order, and was fit by Arrhenius parameters ( $\log_{10}A(s^{-1})$ ,  $E^*$  (kcal/mol) = (11.1±0.9, 45.0±2.7). Secondary pyrolyses of styrene were of reaction order greater than unity, and proceeded with apparent pseudo first order Arrhenius parameters of ( $\log_{10}A$ ,  $E^*$ ) = (5±2, 22±3). Pyrolysis in tetralin was similar to neat ether pyrolysis, the only significant difference arising as an increased selectivity of secondary styrene pyrolysis to ethylbenzene. As evidenced in Figure 7.1.5, rate data for neat and in-tetralin pyrolyses were similar.

## 7.2 Guaiacol

For substrate conversions of less than 10%, the products identified from the pyrolysis of guaiacol were methane, carbon monoxide, catechol and phenol; at high conversions a solid 'coke' also formed, being accompanied by reduced yields of catechol relative to the other products.

Although catechol was identified in the solvent-washed product liquor by GC and GC with catechol coinjection, its assignment as a direct pyrolysis product is as yet tentative. Catechol may in fact arise from interactions with acetone during the solvent-collection-analysis step; this point is more cogently discussed below. In any event, catechol was an experimentally determined pyrolyzate liquor product, and the results of guaiacol pyrolysis will be described as such.

The time evolution of these pyrolysis products at 350C is illustrated in Figure 7.2.1, where each product yield is plotted for each reaction holding time examined. These data suggest a synchronous formation of the product pairs catechol-methane and phenol-carbon monoxide for each mol of decomposed guaiacol. The relationships among these products are further illustrated in Figure 7.2.2. The mol ratios of (methane/catechol), Figure 7.2.2a and (carbon monoxide/phenol), Figure 7.2.2b, were each separately close to unity in essentially all cases, covering fractional substrate conversions  $0.5 \times 10^{-3} < X < 0.10$  at all temperatures from 250 to 450 C. Also, the mol ratios of (CO/CH<sub>4</sub>) and (phenol/catechol) were each substantially independent of substrate conversion at any given temperature, as shown in Figure 7.2.2c. These observations suggest two parallel pathways for guaiacol decomposition, respectively termed (R1) and (R2):



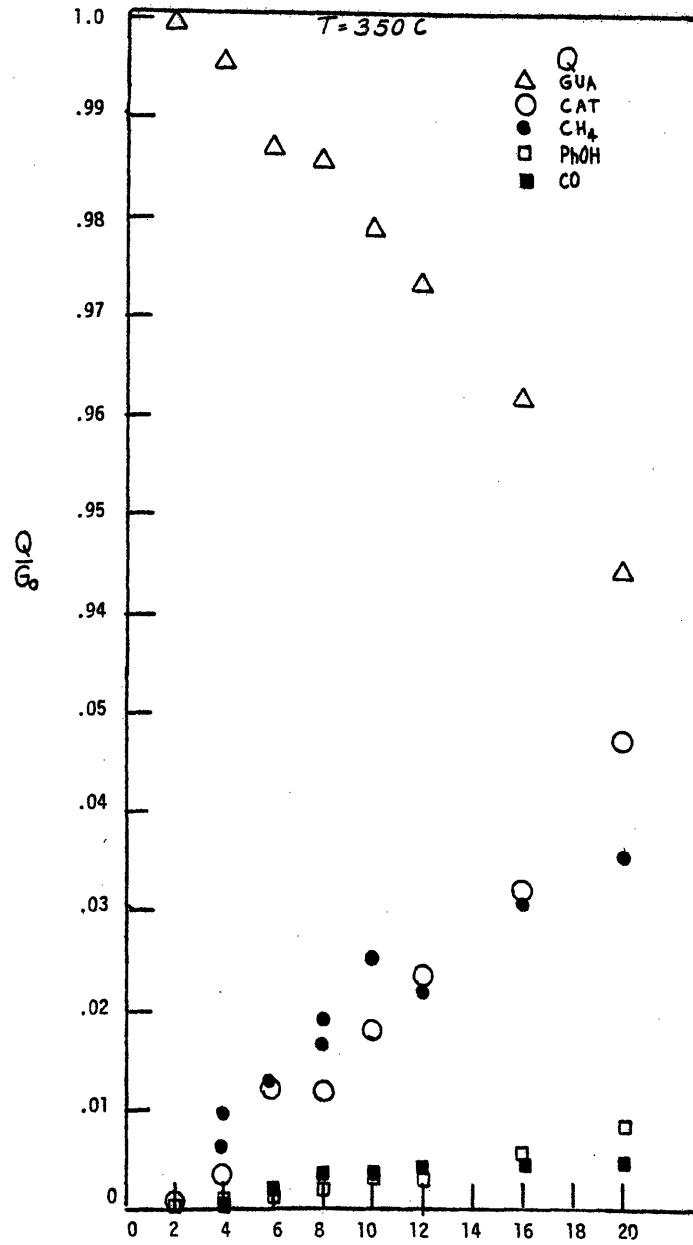


Figure 7.2.1 Guaiacol pyrolysis product evolution.

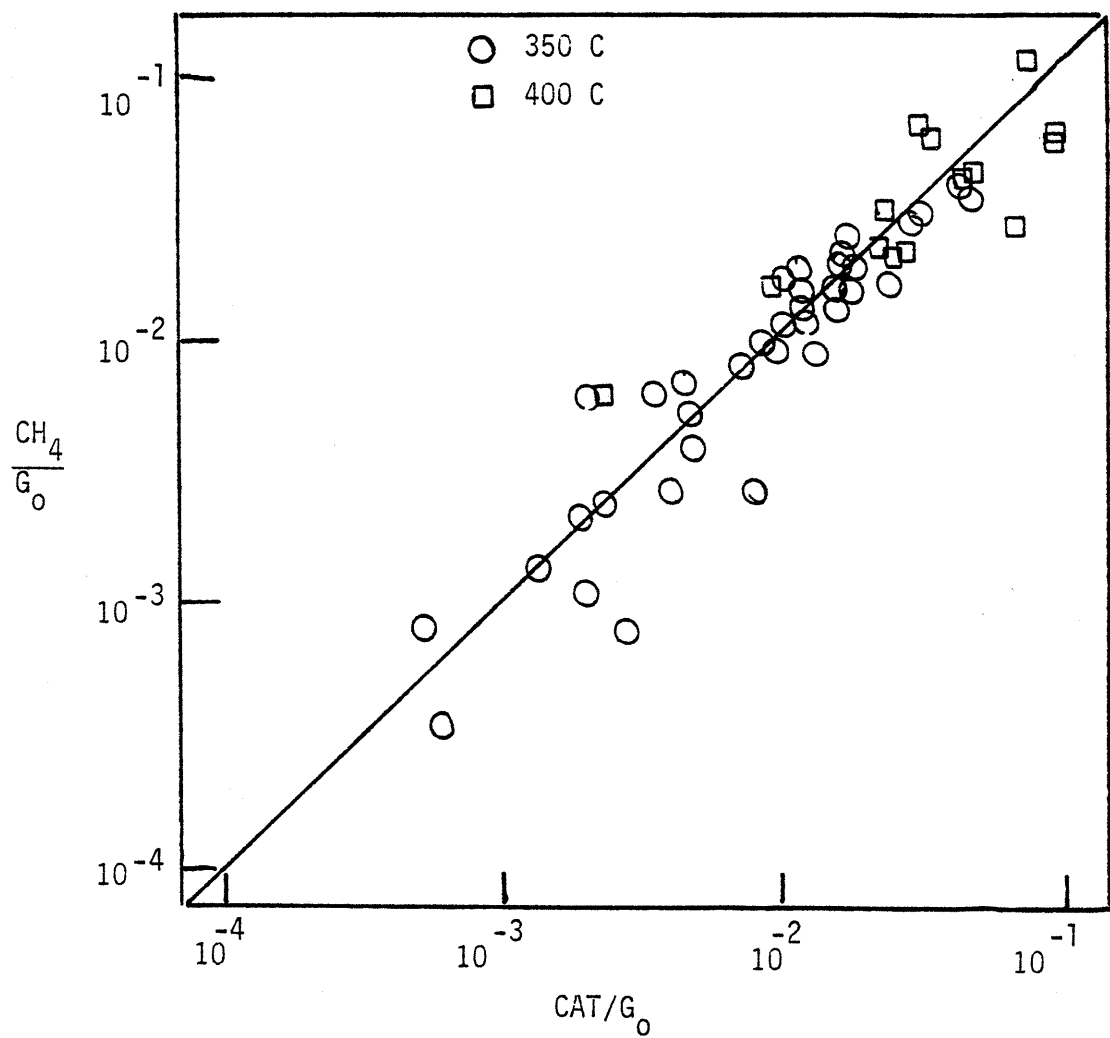


Figure 7.2.2 Product relationships in guaiacol pyrolysis  
a) methane vs. catechol

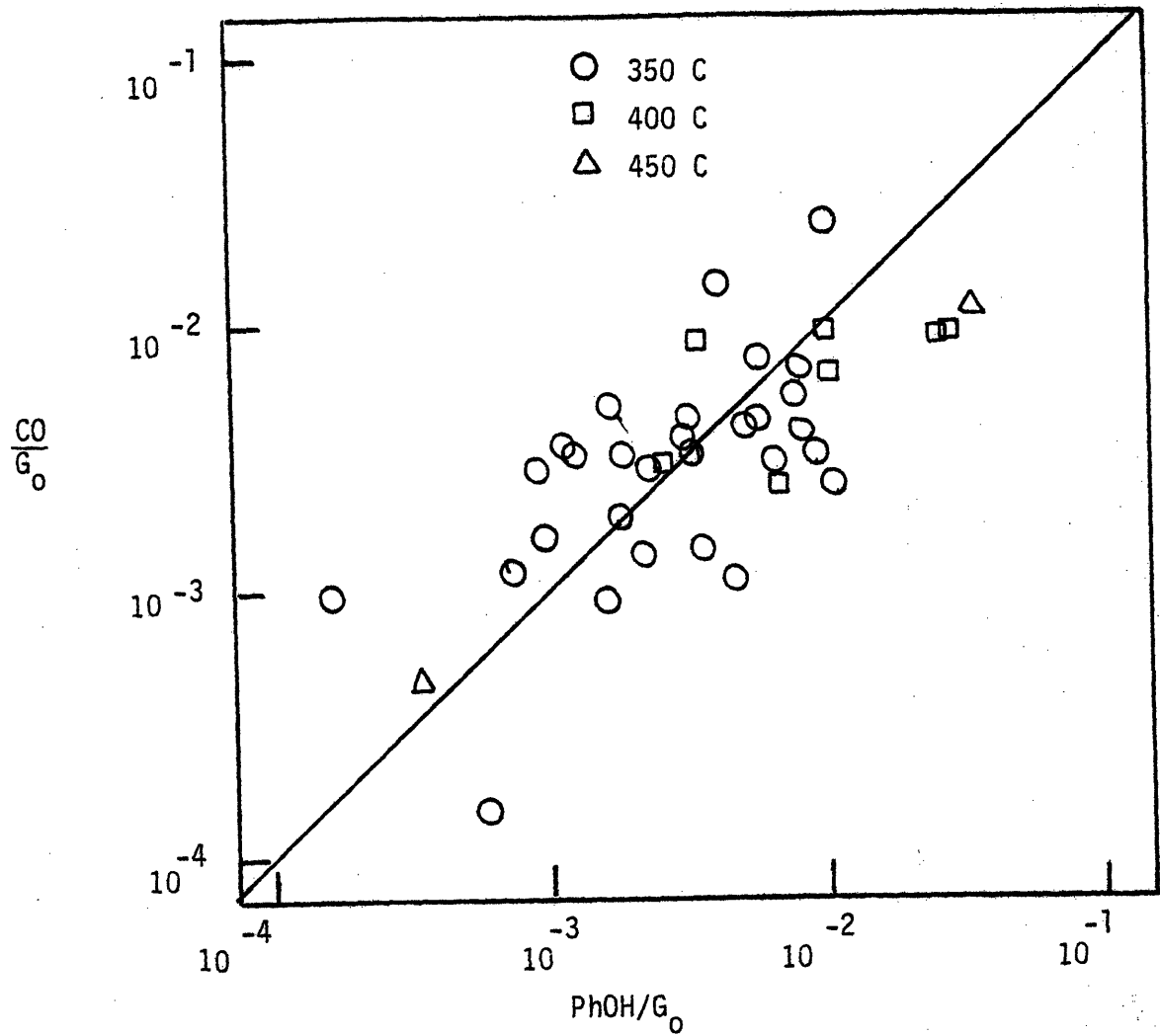


Figure 7.2.2b CO vs PhOH



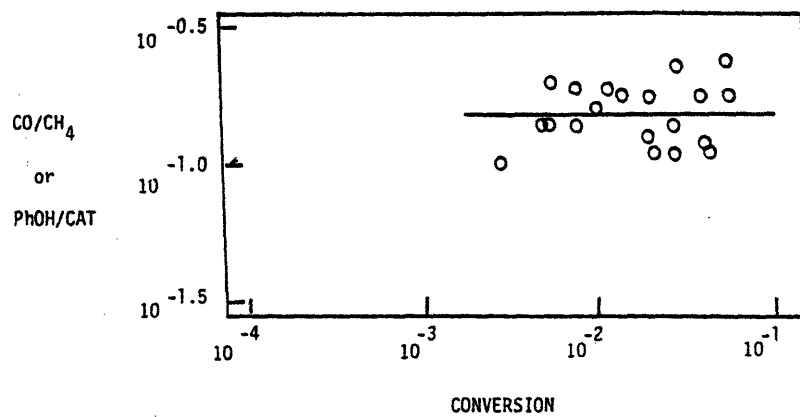
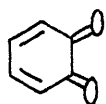


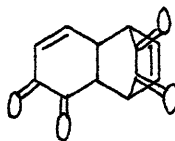
Figure 7.2.2c Phenol/Catechol or CO/CH<sub>4</sub> vs substrate conversion

The parentheses to the right of each expression indicate the difference in hydrogen atoms between the substrate and the observed pair of stable products.

It is the formal negative hydrogen balance for pathway R1 that forces the identification of catechol as a direct pyrolysis product to be uncertain. As noted above,  $\text{CH}_4$  and catechol appeared in stoichiometric proportions for conversion of  $0.5 \times 10^{-3} < X < 0.10$ . However, as written, pathway R1 depicts the formal uptake of two hydrogen atoms. Although pathway R2 evolves net hydrogen, the mol ratio phenol/catechol =  $R2/R1 \sim 0.1$ ; thus, R2 cannot account for the net hydrogen uptake of R1. As will be developed more fully in the discussion section, two possible explanations for this behavior arise. The first of these involves the carbonaceous coke detected at higher conversions. The coke species is likely hydrogen deficient, and could thus formally account for quantities of hydrogen uptake by R1. The second possibility involves hydrogen transfer by the acetone during the solvent wash period. The catechol identified in the product liquor was recovered by acetone wash. The acetone was added in large excess, and it or other hydrogen-containing solvent impurities could be capable of hydrogen transfer to hydrogen deficient pyrolyzate species. With regard to both possible hydrogen sources, it is cogent to note that differential IR analyses of pure guaiacol and unwashed, air cooled guaiacol pyrolyzates showed an increase in the relative intensities of carbonyl peaks for the pyrolyzate. These carbonyl peaks might suggest the presence of quinone species of the type:



(A)



(B)

from guaiacol pyrolysis. Further, it is not inconceivable that diquinone (A) could exist as a stable product and elute near or with catechol on OV 17 silicone oil columns. These assignments are tentative, unequivocal determination of which awaiting further IR, NMR, and other spectroscopic studies. These possibilities are considered in further detail in the discussion section, chapter 10. With regard to the present investigation, since catechol was identified as the GC and GC-coinjection product, the results will be considered as such. Thus, pathway R1 represents the decomposition of guaiacol to catechol and  $\text{CH}_4$ , with a net uptake of two hydrogen atoms.

The order of reactions (R1) and (R2) with respect to guaiacol was examined by varying the initial substrate concentration from 0.45 to 3.0 mol/l in a series of experiments at  $T = 350\text{C}$ . These data are displayed in Figure 7.2.3., parts a, b, and c of which respectively plot the variation with time of guaiacol, catechol, and phenol concentrations, each normalized by the initial guaiacol concentration. On the co-ordinates of Figure 7.2.3, a reaction with rate expression  $r = kC^\alpha$ , i.e., rate constant  $k$  and order  $\alpha$ , would yield an initial slope  $[\text{dln}(C/C_0)/\text{dt}]_{t \rightarrow 0} = kC_0^{\alpha-1}$ . In each of Figures 7.2.3a, b and c, a single average slope sufficed to describe all of the data. No systematic variation of initial slope with initial substrate concentration could be discerned and the absolute

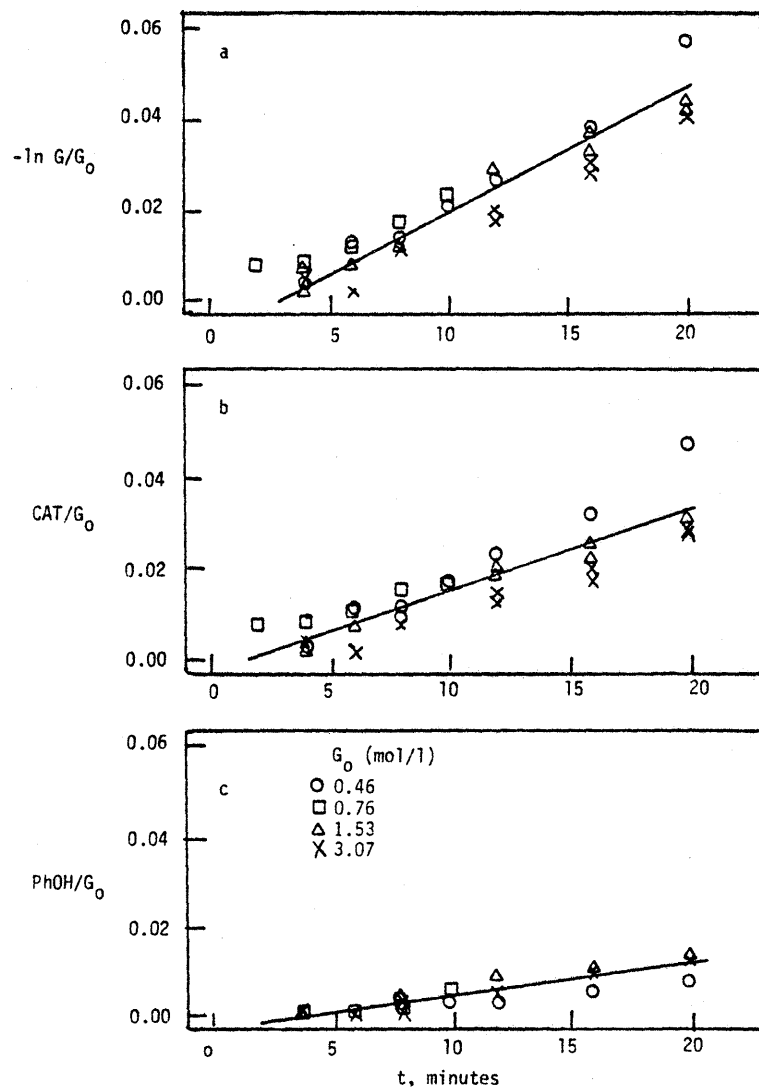


Figure 7.2.3 Guaiacol pyrolysis kinetics at 350 C.

uncertainties in the slope, respectively  $\pm 20\%$  in Figures 7.2.2a and b and  $\pm 50\%$  in Figure 7.2.2c, were small relative to the seven-fold range of initial concentrations used. This is further developed with reference to Figure 7.2.4, where the data of Figure 7.2.2b are replotted along with the catechol yield predicted for reaction orders of  $3/2$  and  $1/2$ . Relative to an arbitrary reference concentration of  $0.46 \text{ mol/l}$ , the catechol yields predicted for the other initial concentrations studied are parametrically represented by the uppermost dashed lines for  $3/2$  order, the lowermost lines for  $1/2$  order. The foregoing show that  $\alpha = 1$  for each of reactions (R1) and (R2); that is, the kinetics of guaiacol disappearance, catechol appearance, and phenol appearance were all essentially first order in guaiacol.

Further study of guaiacol pyrolyses at temperatures from 300 to 525 C with fixed initial concentration  $0.45 \text{ mol/l}$  revealed the temperature-dependence of the first order rate constants  $k_1$  and  $k_2$  respectively associated with reactions (R1) and (R2). These results are shown in Figure 7.2.5, an Arrhenius diagram with co-ordinates of  $\log_{10} k \text{ (s}^{-1}\text{)}$  vs. reciprocal temperature  $\theta^{-1}$  where  $\theta = 4.573 \times 10^{-3} T$  in Kelvins; on these co-ordinates, the usual Arrhenius relationship describes a straight line,  $\log_{10} k = \log_{10} A - E^*/\theta$ , where the pre-exponential factor A has units of the rate constant k and the activation energy  $E^*$  is expressed in kcal/mol. In Figure 7.2.5 is evident that  $\log_{10} k_1$  (shown by circles) increases linearly with decreasing reciprocal temperature  $\theta^{-1}$ , obeying an Arrhenius relation-

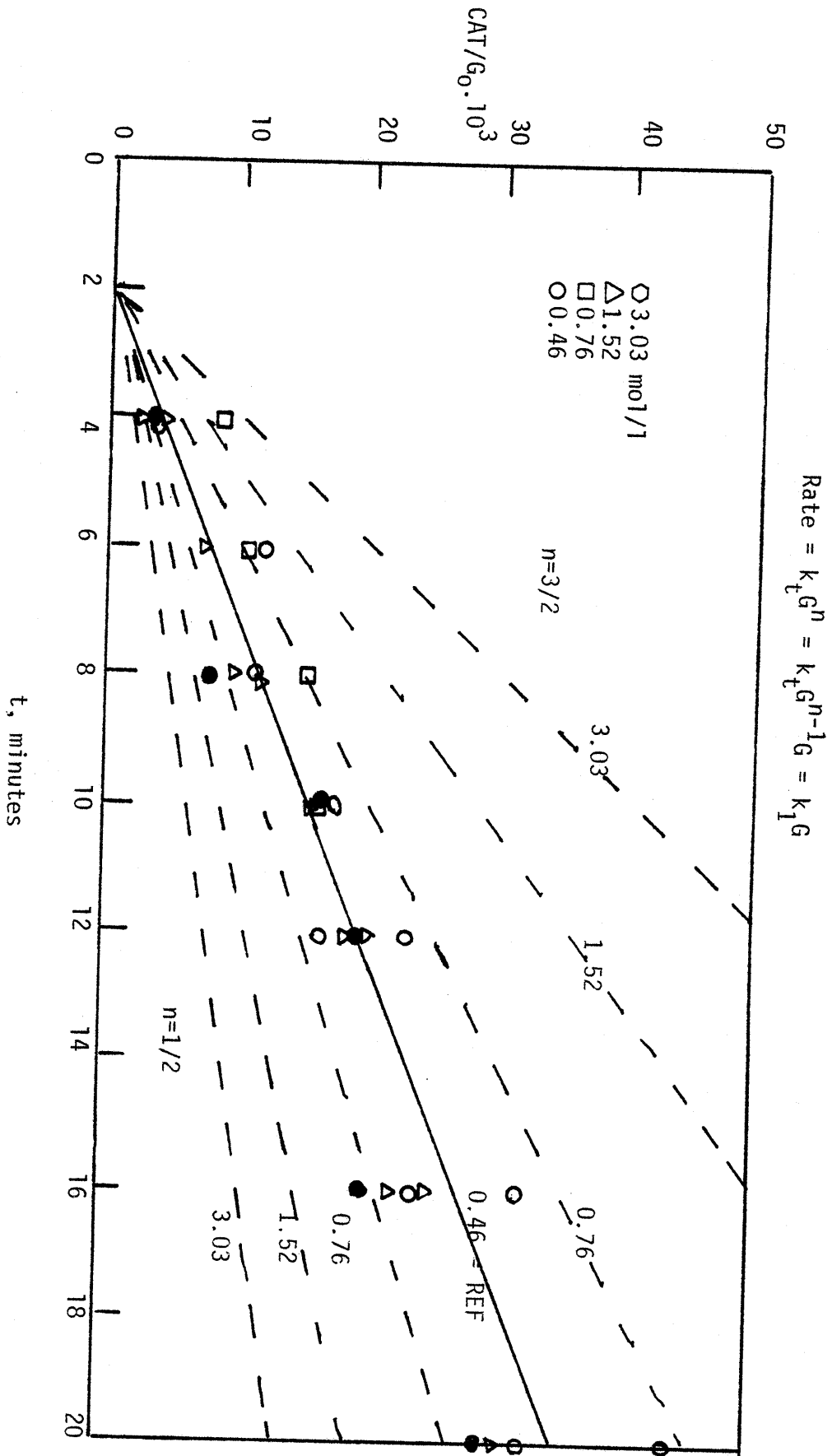


Figure 7.2.4 Catechol appearance at 350 C.

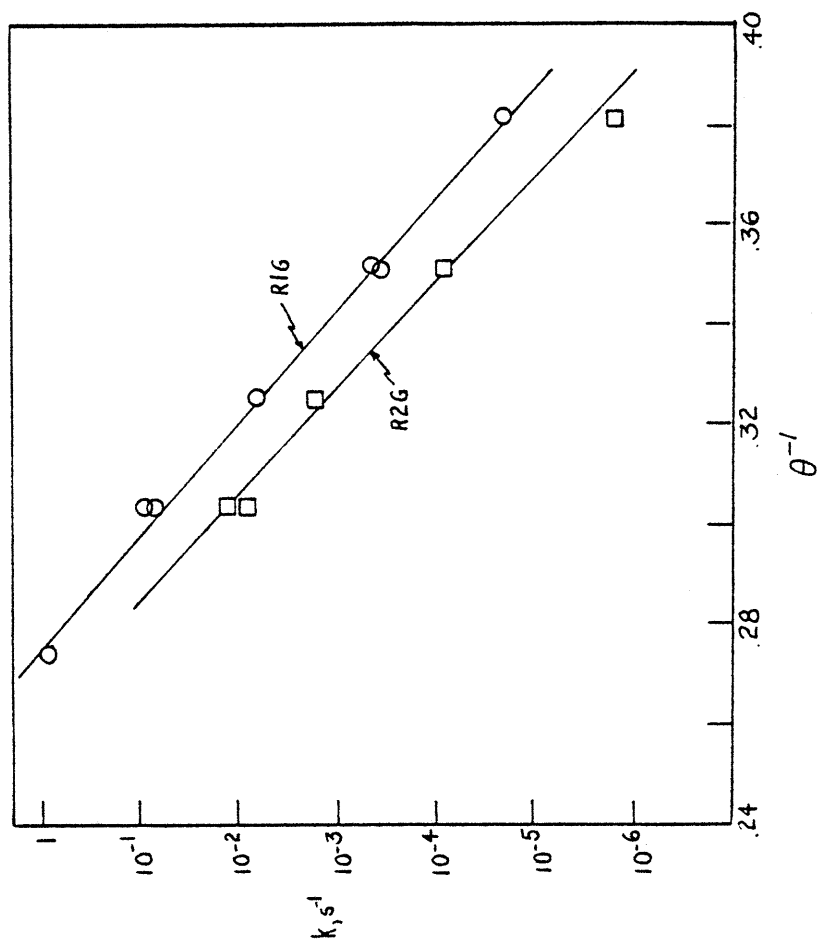


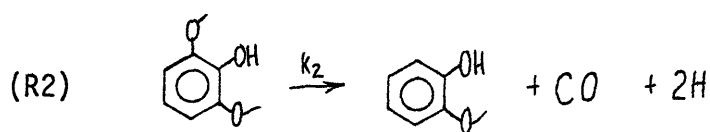
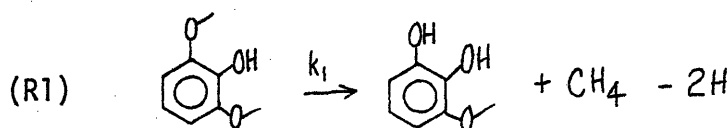
Figure 7.2.5 Arrhenius diagram for guaiacol pyrolysis

ship over a range of five orders of magnitude in  $k_1$ . The best fit of these data yields Arrhenius parameters of  $(\log_{10}A \text{ (s}^{-1}\text{)}, E^* \text{ (kcal/mol)}) = (10.9 \pm 0.5, 43.7 \pm 1.4)$  for the reaction (R1). Also in Figure 7.2.5  $\log_{10}k_2$  (squares) is seen to decrease linearly with  $\theta^{-1}$  over a range of four orders of magnitude in  $k_2$  and this provides the Arrhenius parameters  $(\log_{10}A \text{ (s}^{-1}\text{)}, E^* \text{ (kcal/mol)}) = (11.5 \pm 0.5, 47.4 \pm 1.6)$  for reaction (R2). These results also reveal that the selectivity of  $(\text{CO}/\text{CH}_4)$  formation from guaiacol, given directly by the ratio  $(k_2/k_1)$ , was typically on the order of  $10^{-1}$  but increased with increasing temperature, from 0.05 at 300C to 0.25 at 450C.

### 7.3 Substituted Guaiacols: 2,6-Dimethoxyphenol (DMP), Isoeugenol, Vanillin

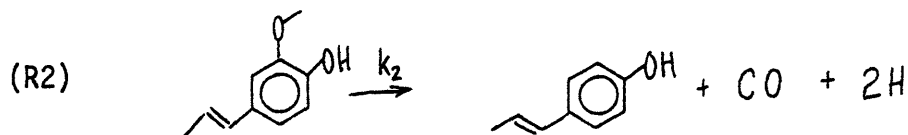
Pyrolysis of 2,6-dimethoxyphenol, isoeugenol and vanillin probed the effect of substituents on the guaiacol pathways described above.

Both of the 2,6- dimethoxyphenol and isoeugenol substrates decomposed by pathways R1 and R2 analagous to guaiacol to yield methane, carbon monoxide and the corresponding liquid products. The catechol derivatives are subject to the same uncertainty previously noted for catechol from guaiacol. The pathways were of the form, for 2,6-dimethoxyphenol:

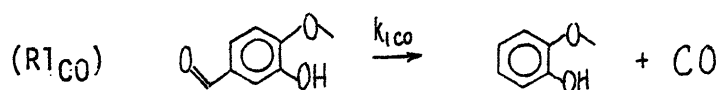
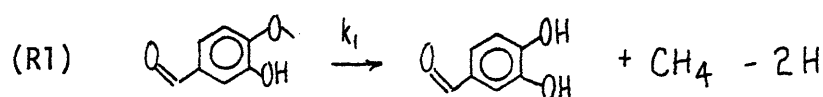




and for isoeugenol,



Vanillin pyrolysis yielded CO and methane as the principal gaseous products, the former predominantly. Among liquids, at low conversions, guaiacol and dihydroxybenzaldehyde were major products, the former predominant, while at higher conversions catechol also arose, along with lesser amounts of phenol; at the highest conversions solid coke formed. At conversions of  $0.02 < X < 0.20$ , the mol ratios of (CO/guaiacol) and ( $\text{CH}_4$ /dihydroxybenzaldehyde) were each approximately unity; the latter pair of products were always less than the former at low conversions, with the ratio  $(\text{CH}_4/\text{CO})_{x \rightarrow 0} = 0.1$  at  $T=400\text{C}$ . These data suggest that vanillin decomposed by pathways of the type (R1), analogous to guaiacol demethanation, and (R1<sub>CO</sub>), a decarbonylation pathway to be more fully discussed in a later section dealing with CO release. The rapidity of pathways R1<sub>CH<sub>4</sub></sub> and R1<sub>CO</sub> for vanillin pyrolysis precluded the determination of a CO releasing pathway analogous to R2 for guaiacol. The pathways are of the form:



At high substrate conversions, the guaiacol and dihydroxybenzaldehyde products could further decompose by the same kinds of pathways to yield the catechol and phenol products observed.

Pyrolyses of 2,6-dimethoxyphenol, isoeugenol and vanillin at temperatures from 300-500C revealed the kinetic data tabulated in Appendix 7.2 and presented in Figure 7.3.1, an Arrhenius diagram. As illustrated in Figure 7.3.1, the demethanation kinetics of guaiacol, 2,6-dimethoxyphenol, isoeugenol and vanillin are all similar, whereas the same is true for CO release from 2,6-dimethoxyphenol and isoeugenol. The decarbonylation of vanillin was significantly faster than both of pathways R1 and R2 for the guaiacols.

#### 7.4 Anisole

Anisole pyrolysis produced methane and carbon monoxide as the major gaseous products with hydrogen also present in appreciable amounts. The major liquid products were o-cresol, phenol and benzene, with smaller amounts of toluene, xylenes, and xylenols also detected. At low substrate conversions, the product proportions were strongly influenced by reaction temperature. Thus at 400C it was found that  $\text{CH}_4:\text{CO} :: 10:0.4$  and  $\text{o-cresol}:\text{phenol}:\text{benzene}::0.1:1.0:0.1$ , whereas at 550C these ratios were  $\text{CH}_4:\text{CO}::1:1$  and  $\text{o-cresol}:\text{phenol}:\text{benzene}::0.6:1.0:1.0$ . The time evolution of the major pyrolysis products at 450C is described in Figure 7.4.1. The predominant liquid products were phenol and benzene, the ratio of these approximately 1.9/1. Methane and carbon monoxide were prevalent at 450C, the former by a ratio  $\text{CH}_4/\text{CO} \sim 1.3$ . No unequivocal relationship between gas phase and

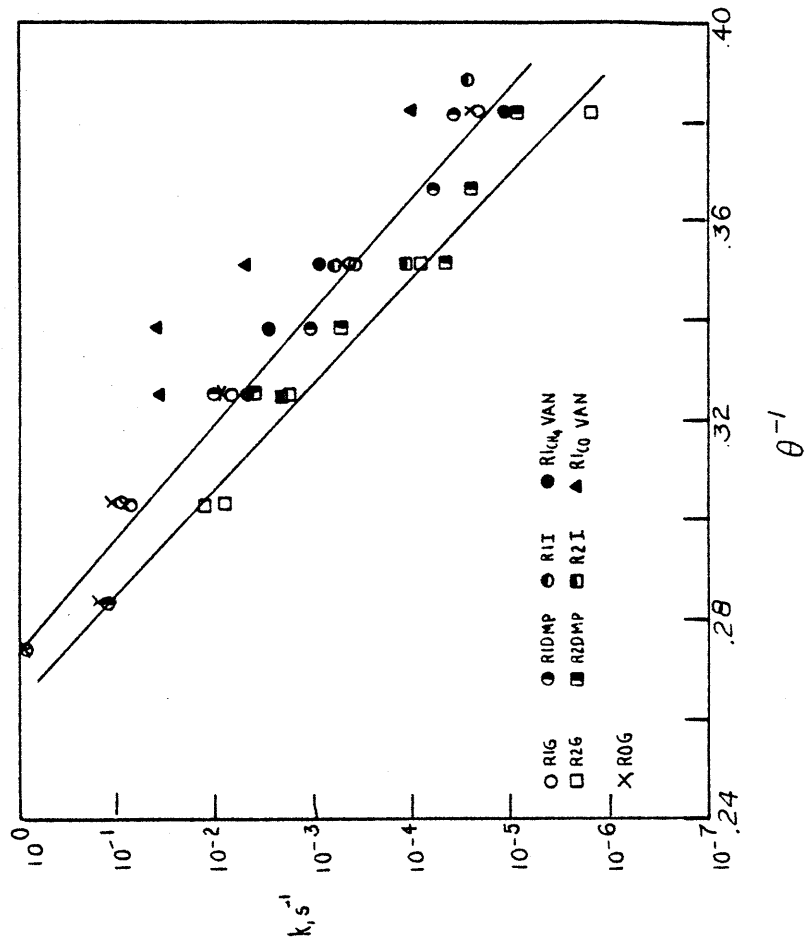


Figure 7.3.1 Arrhenius diagram for methoxyphenol pyrolysis.

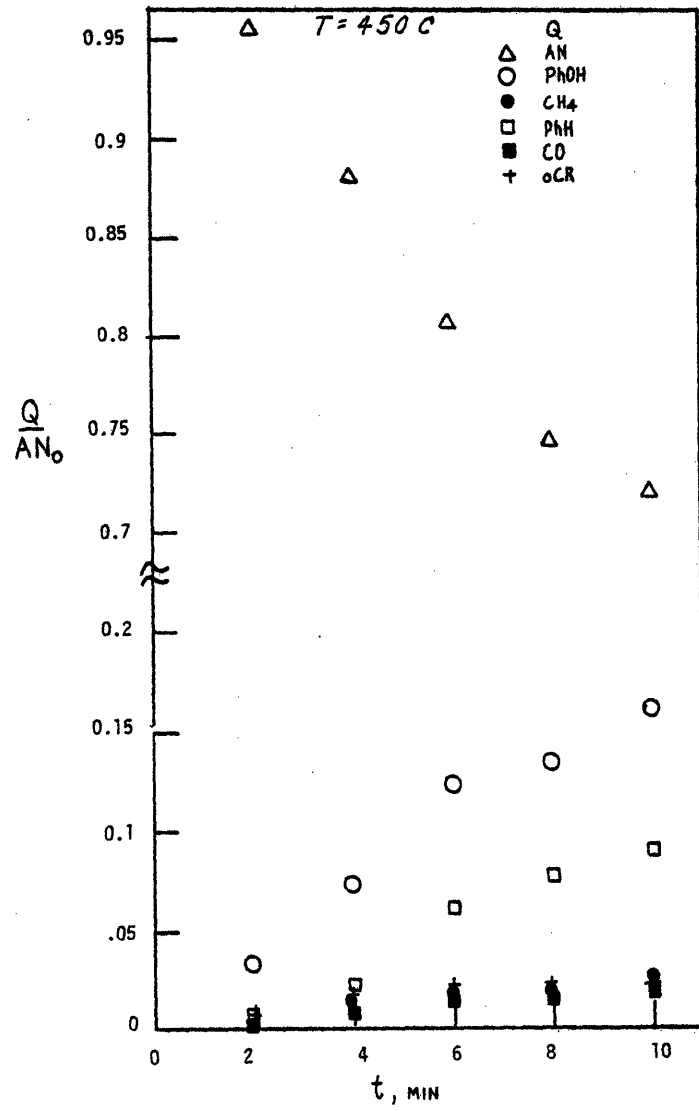


Figure 7.4.1 Anisole pyrolysis product evolution.

liquid phase products could be discerned. This is further evidenced in Figure 7.4.2 which plots the methane yield versus the demethylated liquid product phenol yield as well as the carbon monoxide yield against the demethoxylated liquid product benzene yield. The ratios ( $\text{CH}_4/\text{phenol}$ ) and ( $\text{CO}/\text{benzene}$ ) each differed significantly from unity, averaging  $0.2 \pm 0.1$  and  $0.6 \pm 0.2$ , respectively. The presence of toluene, xylenes and xylenols as methylated side products is cogently noted here. These products are as yet not decisively quantified, but may account for part of the deviation between  $\text{CH}_4$  and phenol yield.

The product relationships in anisole pyrolysis are further developed in Figure 7.4.2c, where the ratios  $\text{CO}/\text{CH}_4$  and  $\text{B}/\text{Ph}$  are plotted as a function of conversion, thus, the selectivity of formal demethoxylation to demethylation is plotted versus conversion. Since each pathway is likely differently thermally activated, Figure 7.4.2c discriminates among pyrolysis temperatures. The lowest ratios of  $\text{B}/\text{Ph}$  occur at low conversions, where the pyrolysis temperatures were also generally low. No benzene at all was detected at 344C. As the conversion approached unity, the ratio  $\text{B}/\text{Ph}$  also approached 1; these conditions were attained at 550C. Inspection of the data at 434 and 450C, which span conversions from  $\sim 0.1 - 0.4$ , suggests that the  $\text{B}/\text{Ph}$  ratio may increase due to conversion alone. However, this behavior is not evidenced in the relatively few 490C data, which span conversions from  $\sim 0.45 - 0.9$ . In general, anisole pyrolysis appears to be rather complex, with product selectivities dependent upon both temperature and conversion. The former would appear to exert the more substantial effect, as evidenced by the

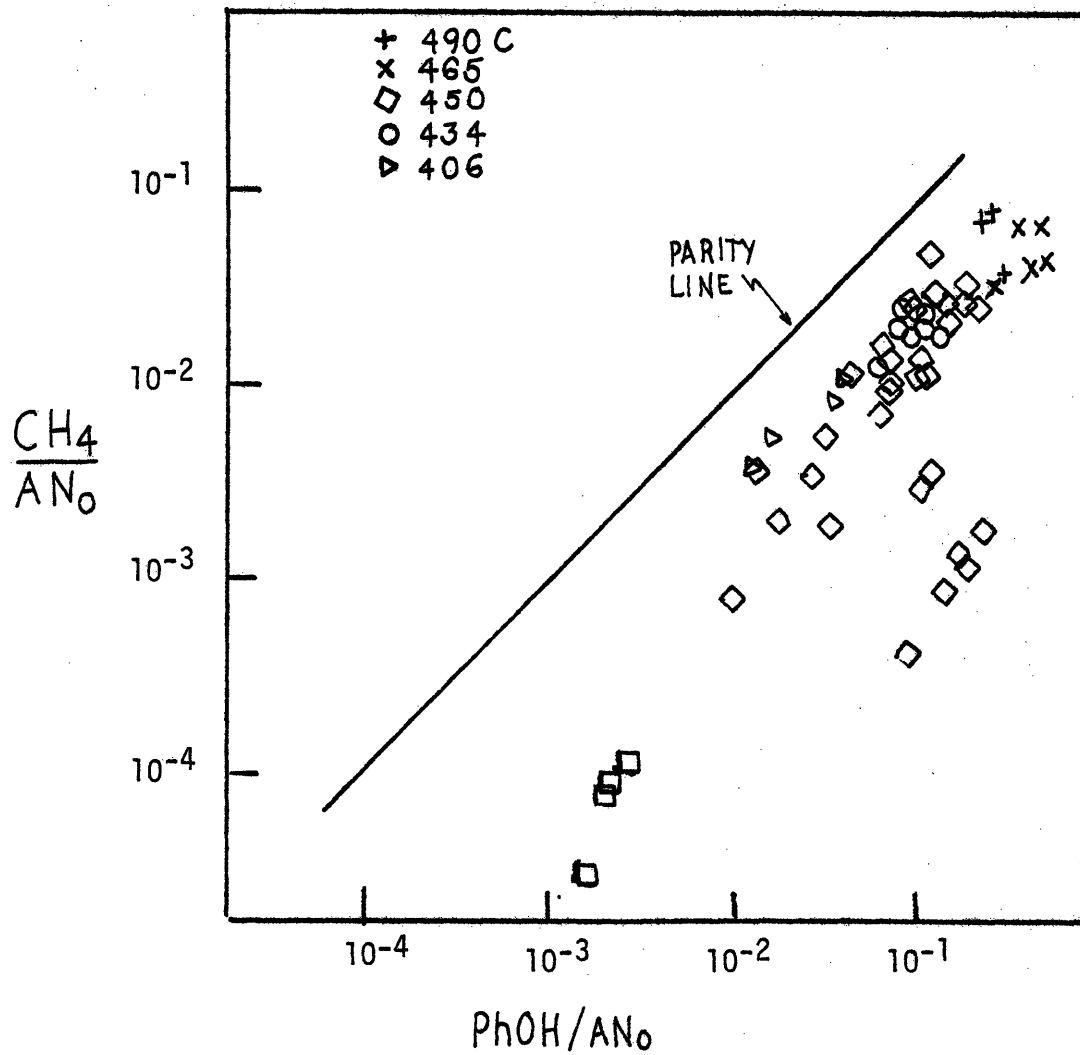


Figure 7.4.2 Product relationships in Anisole pyrolysis.  
a)  $\text{CH}_4$  vs. phenol

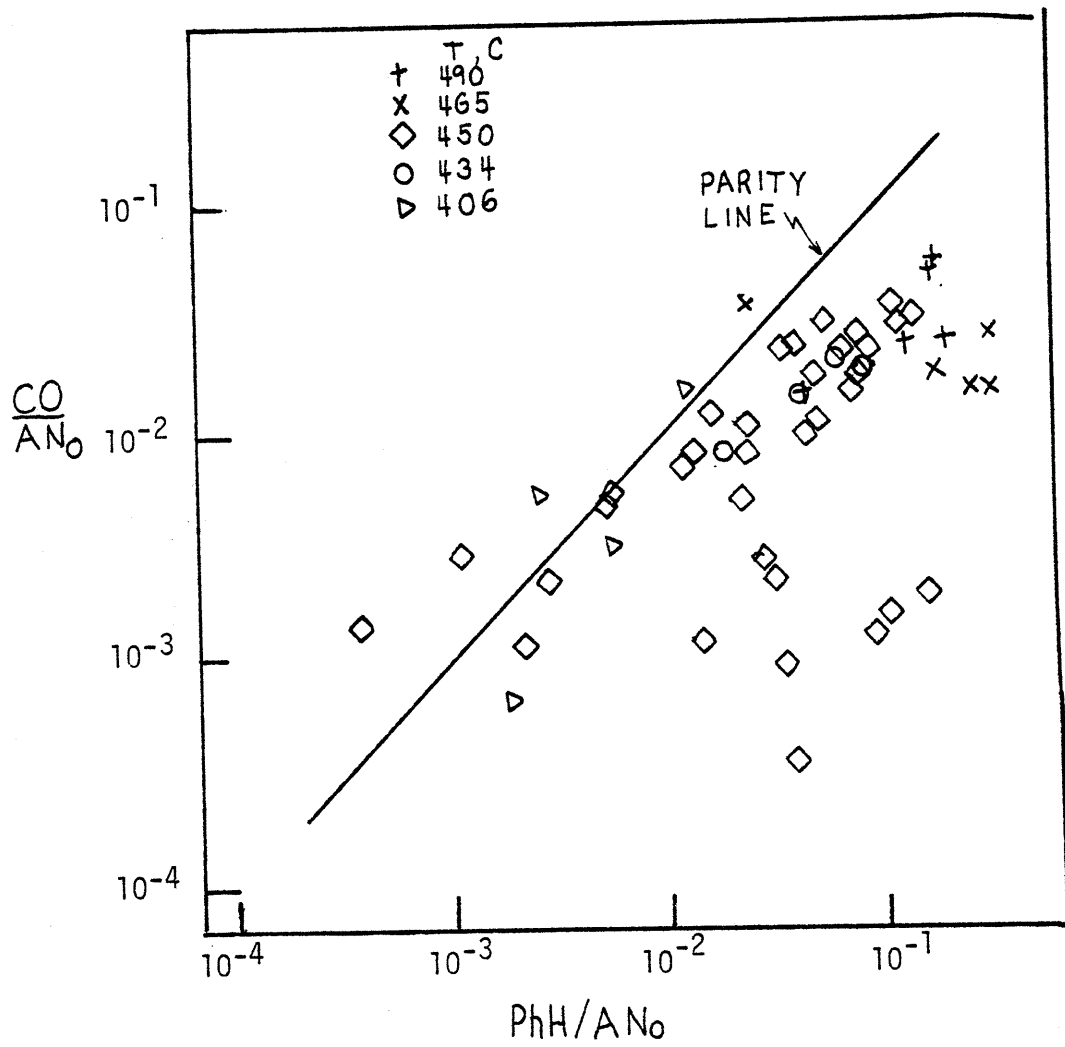


Figure 7.4.2b CO vs. benzene.

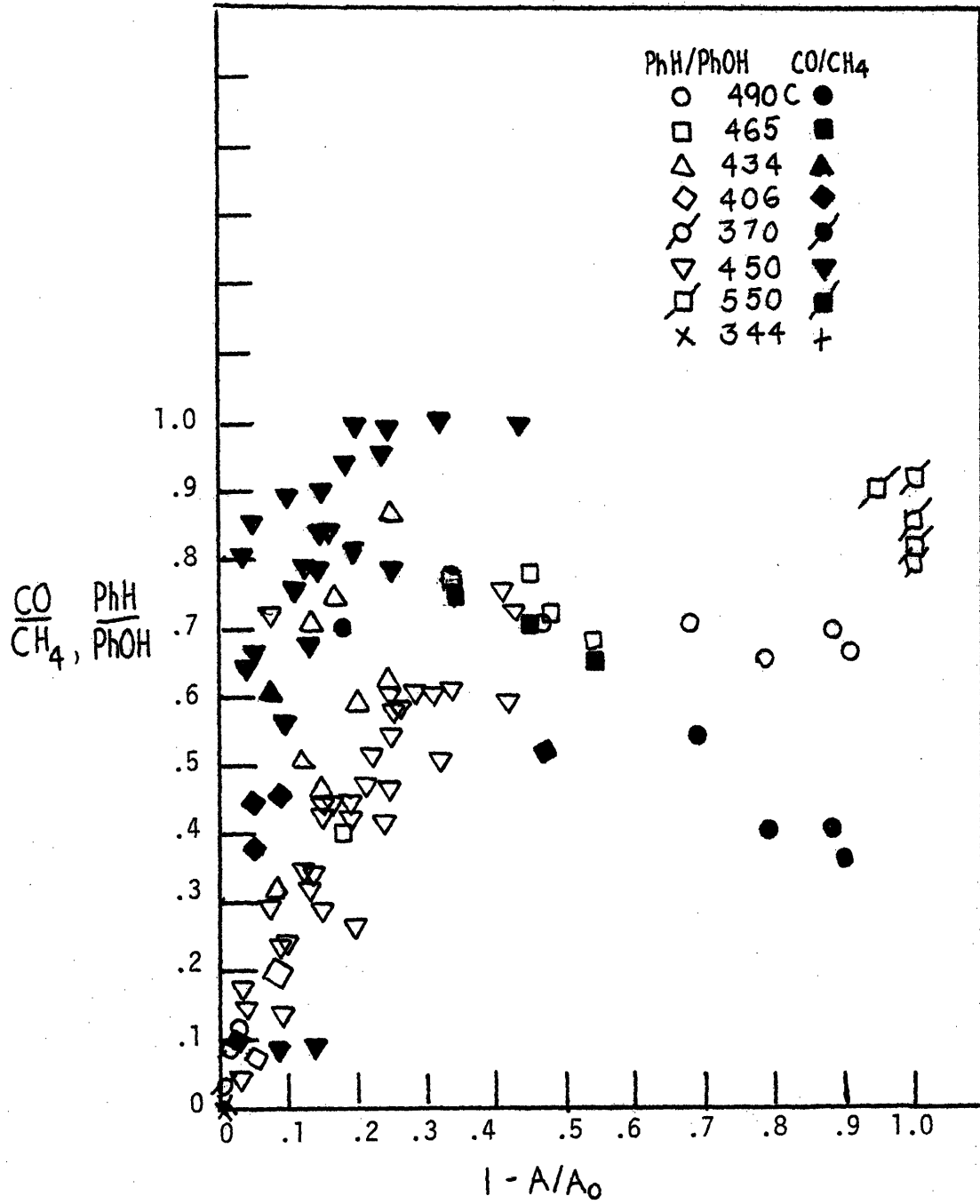
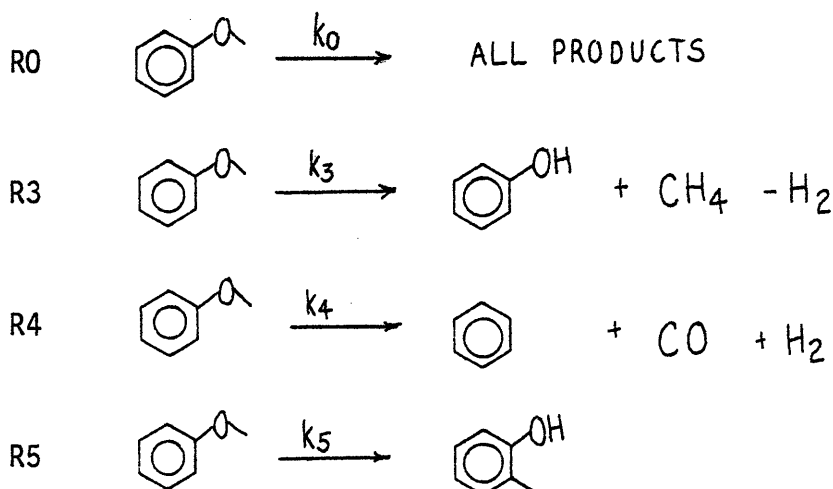


Figure 7.4.2c Product ratios vs. conversion.



ratio of B/Ph  $\sim 0$  at 344C and  $\sim 0.9$  at 550C. However, the data at 434 and 450C suggest that benzene selectivity also increased with increasing conversion. With regard to gaseous products, Figure 7.4.2 also suggests that the ratio CO/CH<sub>4</sub> increases with both conversion and pyrolysis temperature; the ratio CO/CH<sub>4</sub> was also generally higher than the ratio B/Ph.

The predominant liquid products suggested three major pathways for anisole pyrolysis, namely:



These pathways were based on the appearance of the liquid products; those gas phase products suggested by stoichiometric balance are included for completeness. Further experiments at 450C and spanning initial substrate concentrations from 0.45 to 3.1 mol/l showed that the overall substrate disappearance as well as the normalized phenol and benzene product appearances were all essentially first order in anisole. These data are presented in Figure 7.4.3, where parts a, b, and c depict these respective determinations. That a single average slope described the pyrolysis pathways is indicative of first

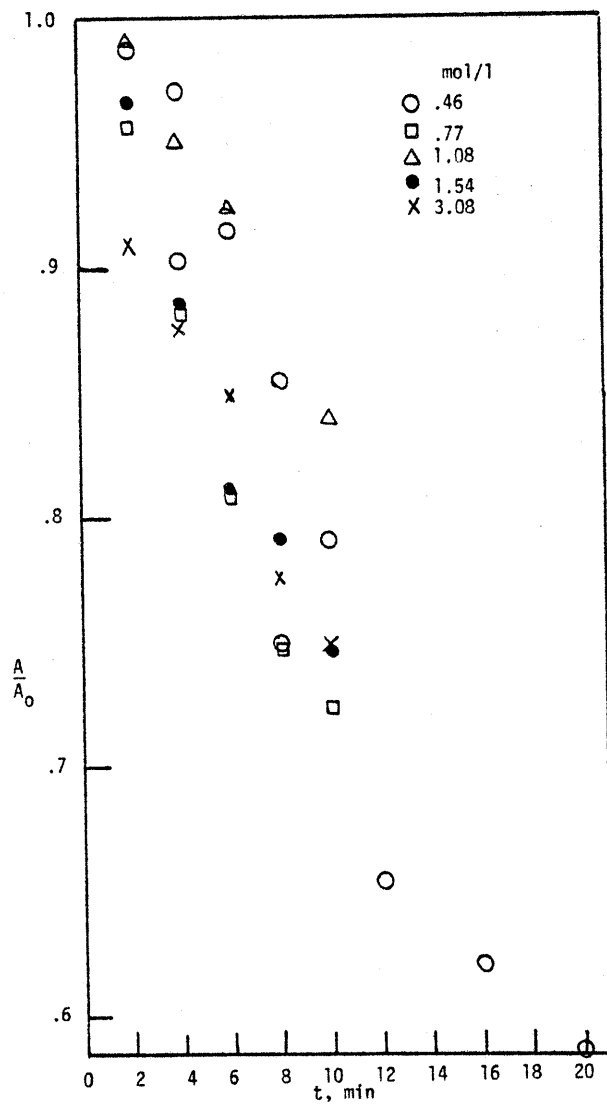


Figure 7.4.3 Anisole pyrolysis kinetics at 450 C.  
a) anisole disappearance

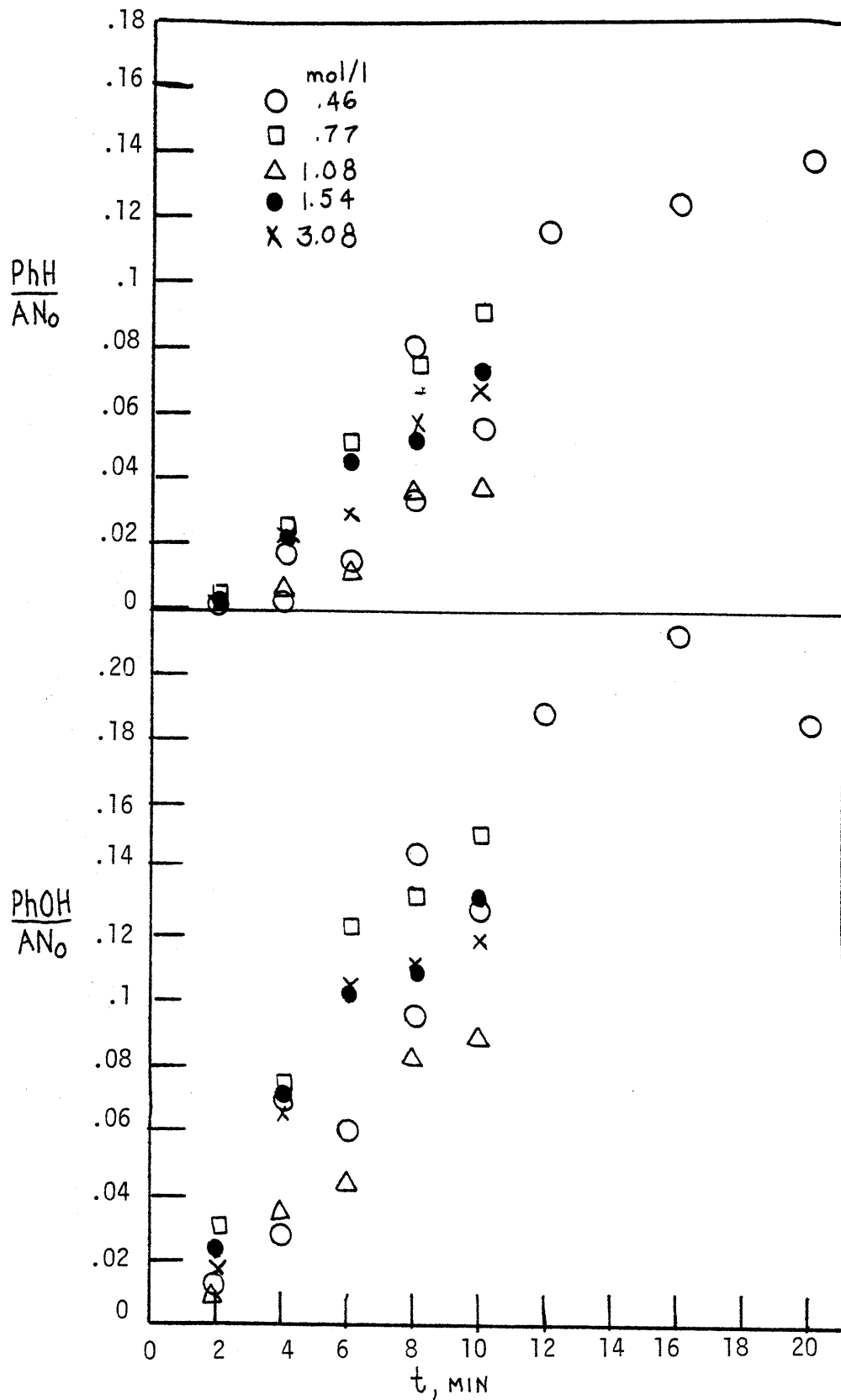


Figure 7.4.3b phenol appearance and 7.4.3c benzene appearance

order degradation. Thus, in spite of the complexity suggested by the anisole pyrolysis product relationships, anisole apparently degraded via first order pathways.

Study of anisole pyrolysis at various temperatures provided the kinetic data depicted in Figure 7.4.4, an Arrhenius diagram; these rate data were based on the time evolution of the appropriate liquid phase product. In the temperature range studied, production of phenol was most facile, while benzene appearance was less rapid but more thermally activated. Ortho-cresol appearance was intermediate in rate, but occurred with the least energy of activation. As listed in Figure 7.4.4, apparent first order Arrhenius parameters for pathways R0, R3, R4 and R5 were  $(\log_{10}A(s^{-1}), E^*(kcal/mol)) = (12.9 \pm 0.5, 53.2 \pm 1.6)$ ,  $(13.0 \pm 1.0, 54.7 \pm 3.1)$ ,  $(14.5 \pm 1.2, 61.0 \pm 4.0)$ , and  $(7.9 \pm 1.5, 40.5 \pm 4.9)$ , respectively.

As evidenced in reference to Figures 7.2.5 and 7.4.4, each individual pathway as well as overall anisole disappearance was significantly slower than pathways R1 and R2 for guaiacol. Anisole decomposition by R0 was typically at least an order of magnitude slower than guaiacol decomposition by R1 in the present experiments. Comparisons between the release of  $CH_4$  and CO from guaiacol and from anisole suggest that both gases form roughly a hundred times faster from the former substrate.

### 7.5 Veratrole

Pyrolysis of veratrole yielded methane and carbon monoxide as the major gaseous products with  $(CH_4/CO) \sim 2$  at 400C; at 550C a trace

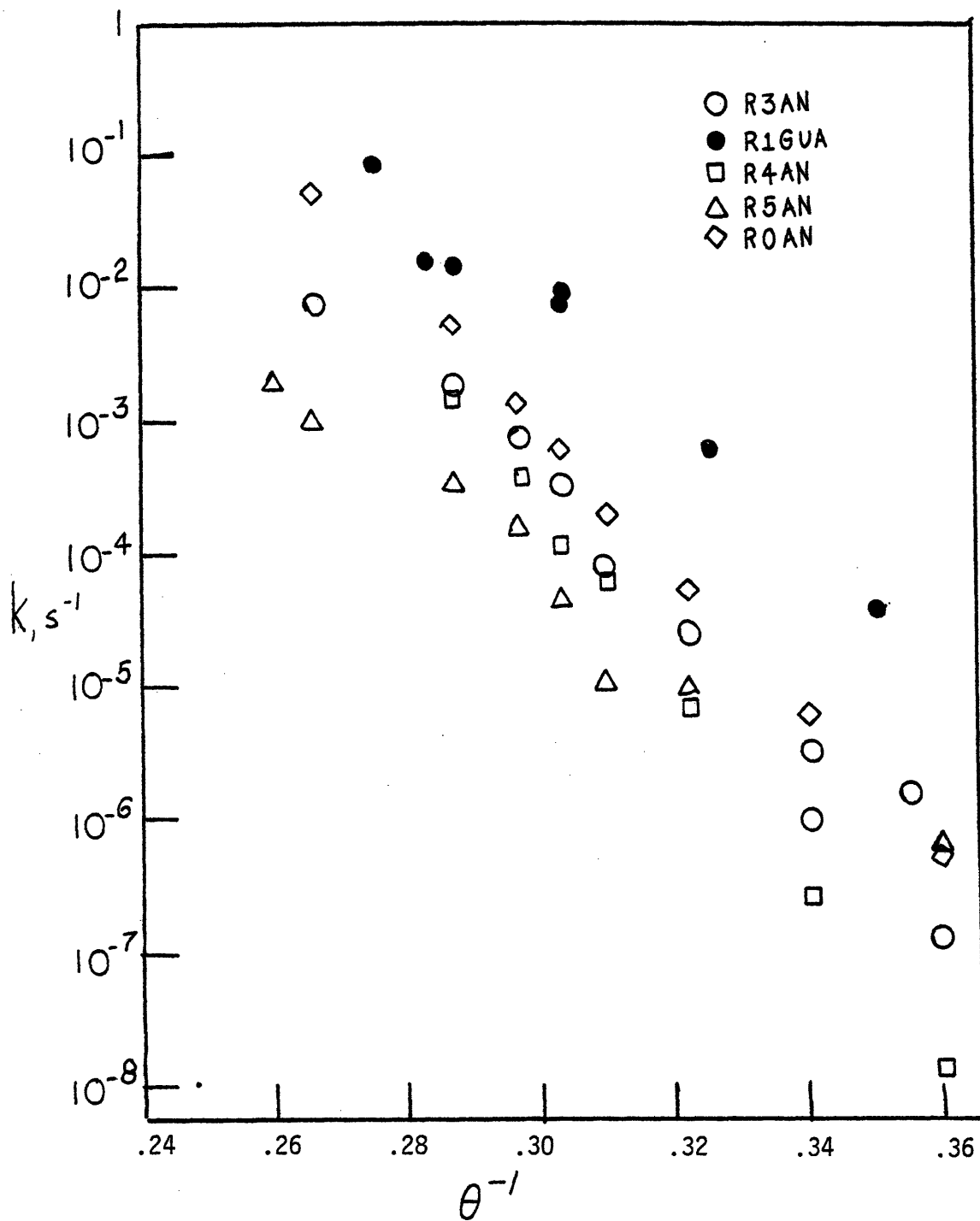


Figure 7.4.4 Arrhenius diagram for Anisole pyrolysis.

amount of ethane was also detected. The liquid product spectra were mixtures of phenols and alkylbenzenes, the composition of which strongly temperature dependent. The time evolution of the major pyrolysis products is presented in Figure 7.5.1a, b, and c, for reaction temperatures of 350, 400 and 450C, respectively. With reference to Figure 7.5.1a, pyrolysis at 350C yielded predominantly guaiacol, accompanied by smaller amounts of anisole and phenol. At 400C, Figure 7.5.1b, guaiacol was again predominant, with o-cresol, anisole and phenol each significant; small amounts of catechol were also detected. At 450C guaiacol proportions were less prevalent, and the amounts of catechol, o-cresol, and phenol increased substantially. At 15 minutes holding time the product spectrum was dominated by o-cresol and phenol. Pyrolysis at 500 and 550C yielded complicated product spectra consisting of chiefly o-cresol, phenol and catechol.

A simple relationship between one gas and one liquid phase product could not be discerned. However, an overall relationship between gas and liquid phase product spectra was determined, as evidenced in Figure 7.5.2. Here the molar yields of  $\text{CH}_4$  and  $\text{CO}$  are plotted versus the parameter  $Q_{\text{CH}_4}$  and  $Q_{\text{CO}}$ , respectively. Defined as:

$$Q_{\text{CH}_4} \equiv 1 - \frac{V}{V_0} - \frac{A}{V_0} - \frac{oCr}{V_0} - \frac{B}{V_0} + \frac{C}{V_0} ,$$

$$Q_{\text{CO}} \equiv 1 - \frac{V}{V_0} - \frac{G}{V_0} - \frac{C}{V_0} + \frac{B}{V_0} ,$$

these quantities represent an ideal stoichiometric conversion to liquid products which are attended by  $\text{CH}_4$  and  $\text{CO}$  release, respectively.

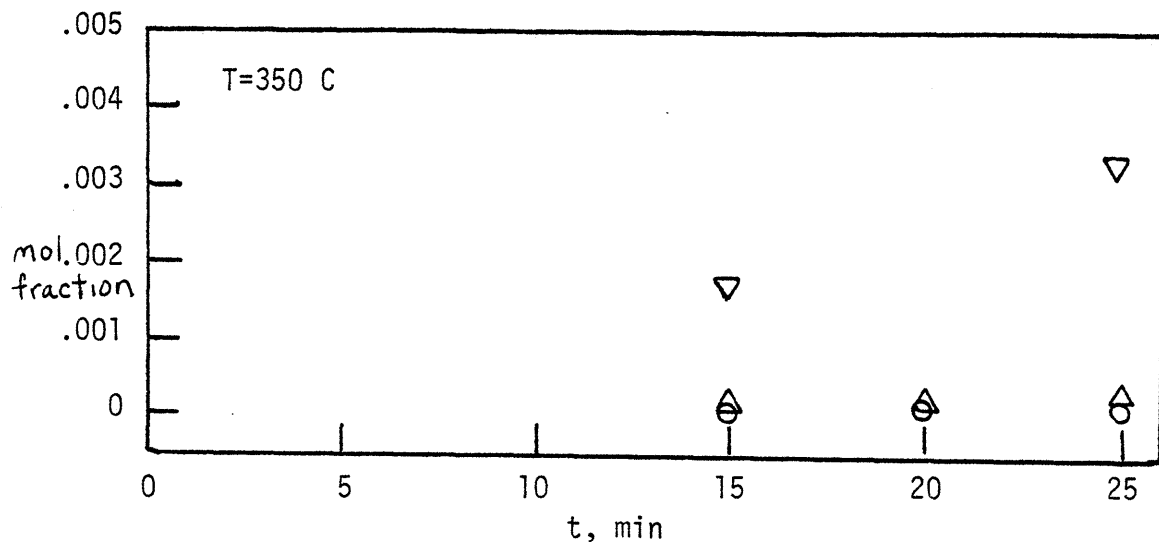


Figure 7.5.1 Veratrole pyrolysis product spectra.  
a) T=350 C

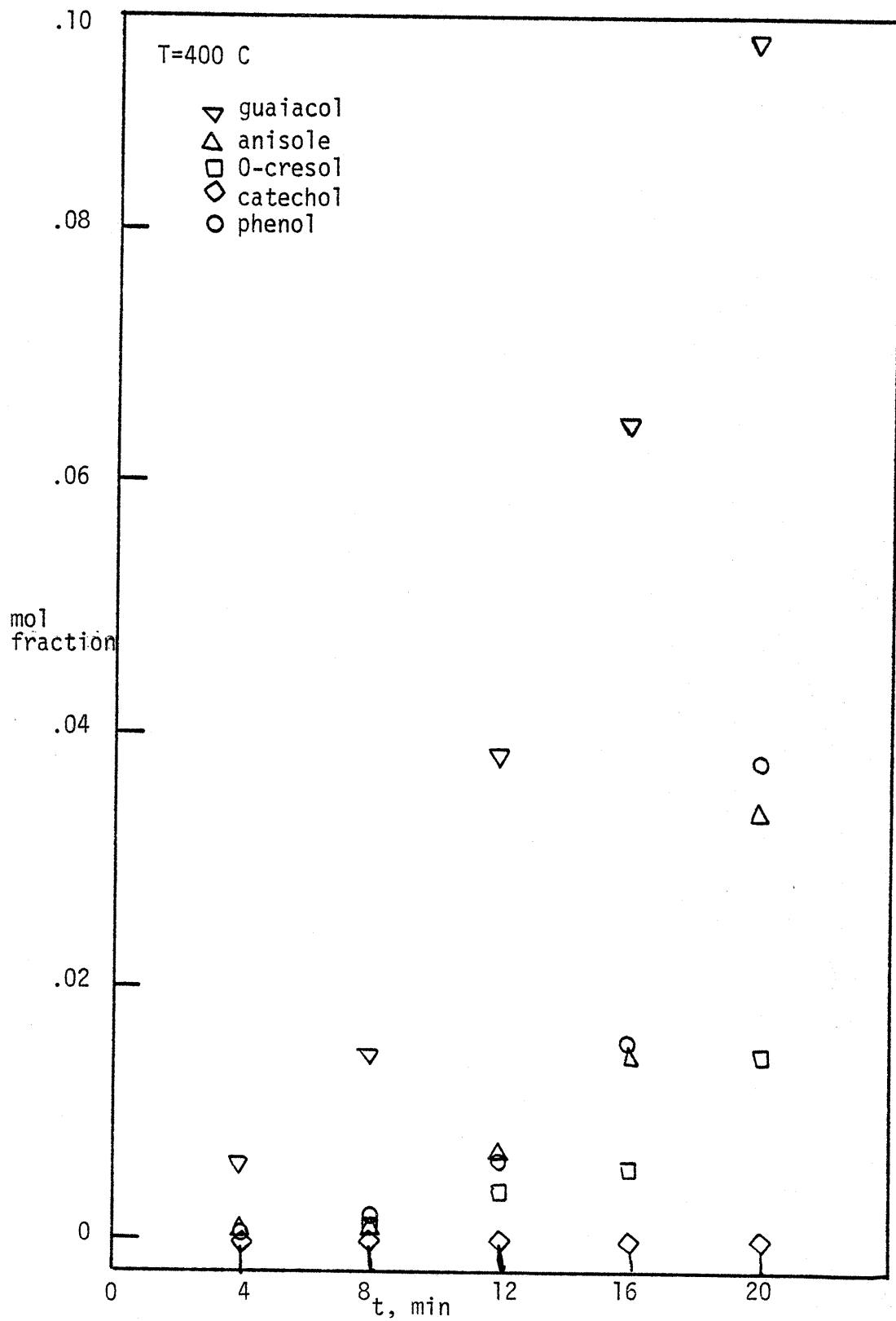


Figure 7.5.1b T=400C



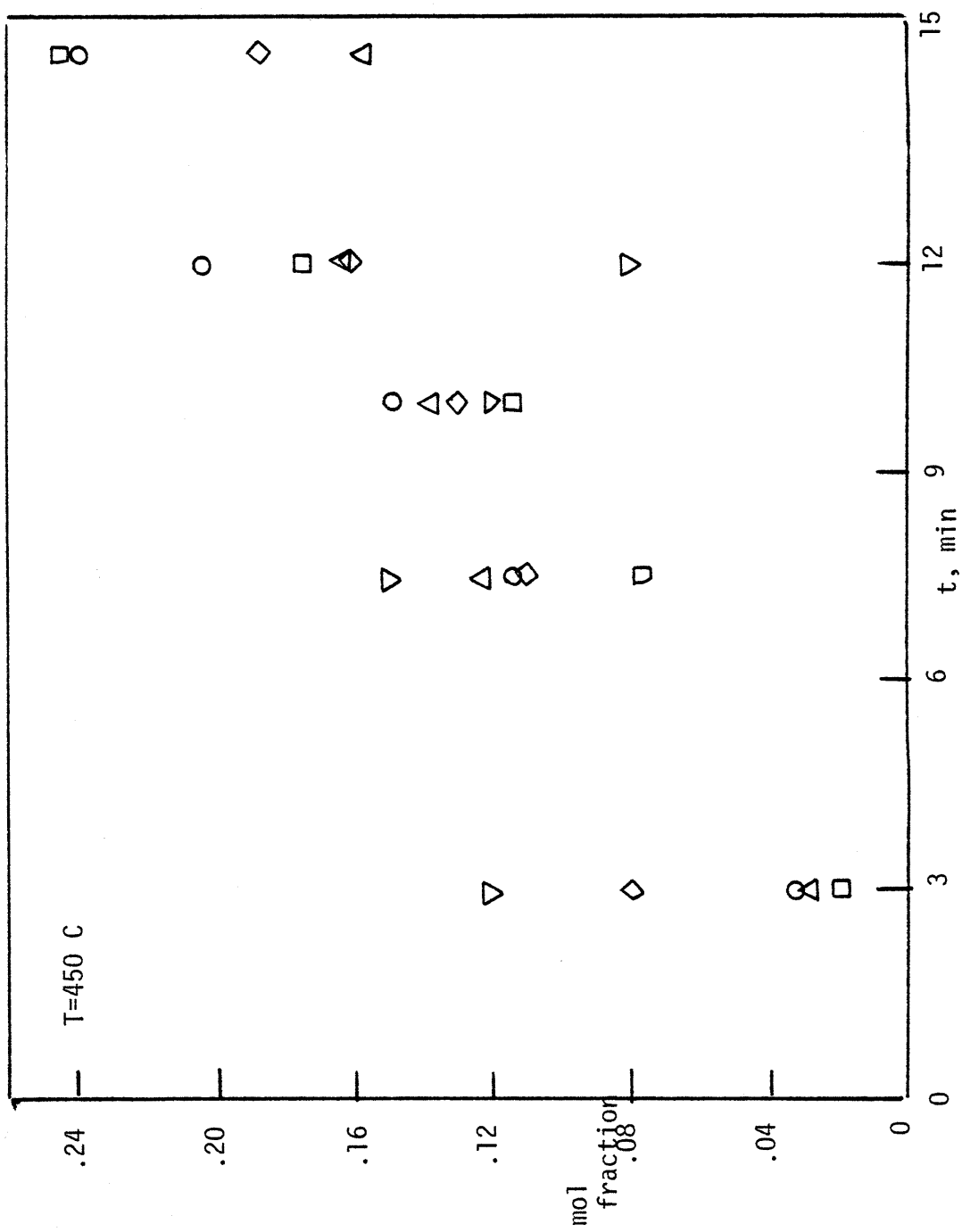


Figure 7.5.1c T=450 C

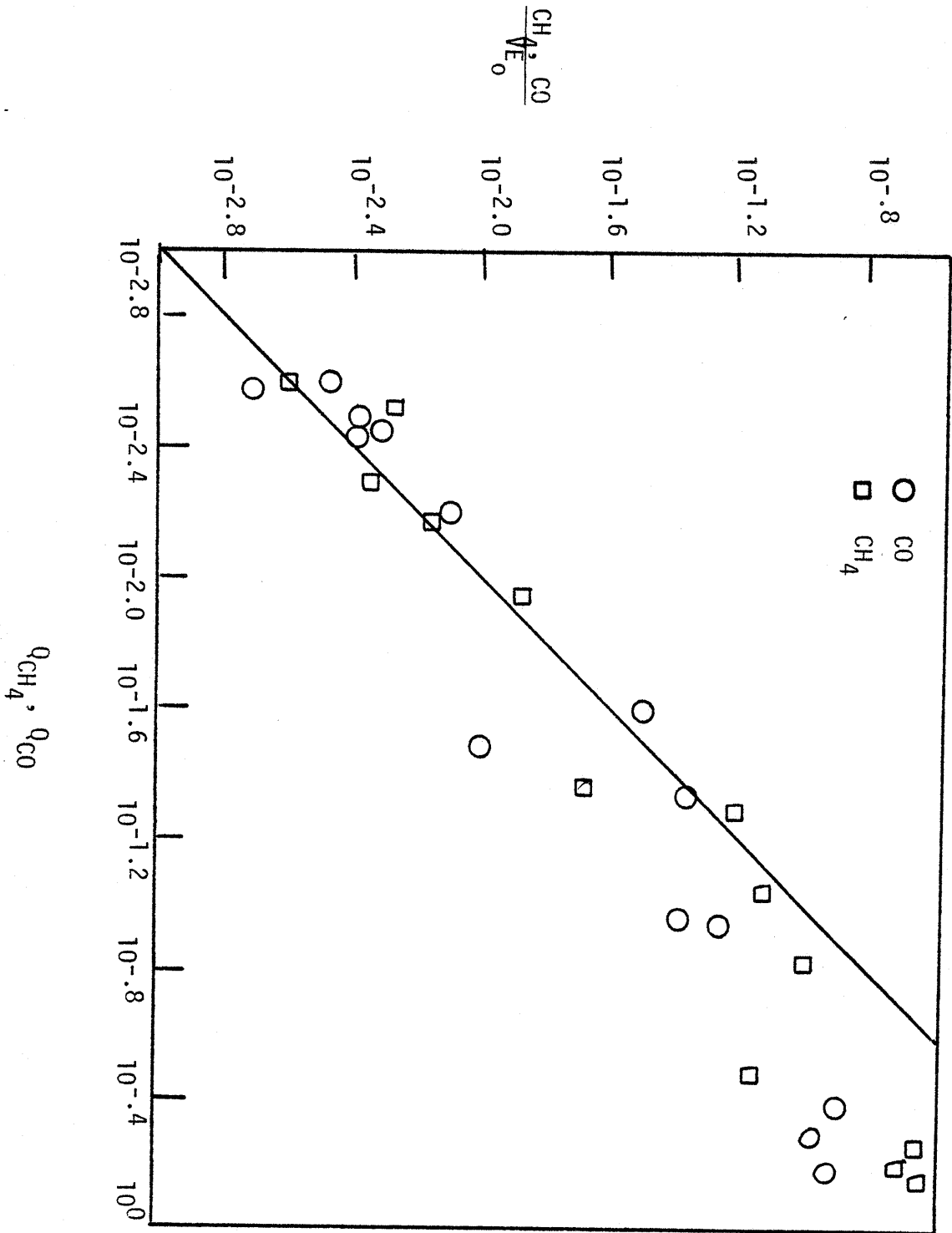
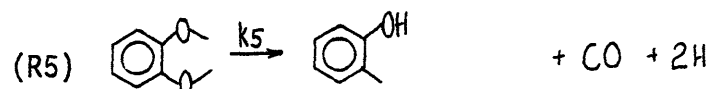
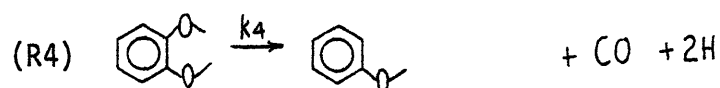
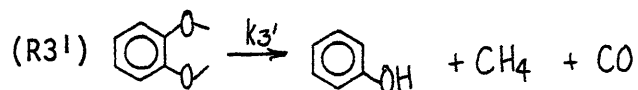
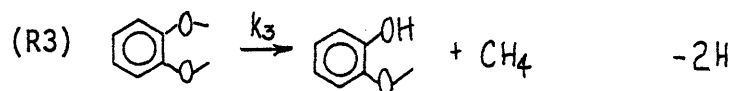
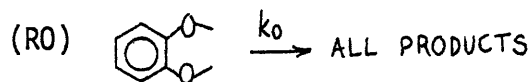


Figure 7.5.2 Product relationships in veratrole pyrolysis.

In this formalism, substrate demethylation represented methane release, and demethoxylation depicted CO release. Because each mol of benzene depicts the formal evolution of two CO mols, the quantity  $+B/V_0$  appears in  $Q_{CO}$ ; a similar argument accounts for  $+C/V_0$  in  $Q_{CH_4}$ . With regard to Figure 7.5.2, this gas-liquid product balance is evident for pyrolysis at 350 and 400C, yet deviates significantly, in the direction of gas/liquid  $< 1$ , for the higher conversions attained at 450C.

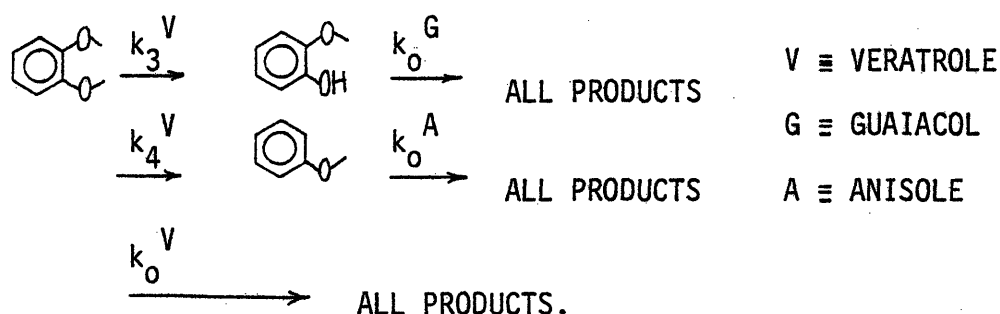
The observations from Figures 7.5.1 and 7.5.2 suggest that four primary veratrole pyrolyses pathways were important, these leading to the formation of guaiacol, phenol, anisole and o-cresol. These pathways are of the form previously delineated for anisole, namely:



The guaiacol and anisole products are susceptible to reactions of the type previously described for these substrate; this accounts for the decreased yields of guaiacol and anisole and the increased yields of catechol, phenol and o-cresol with increasing substrate conversion.

Kinetic data for each of these pathways are presented in Figure 7.5.3, an Arrhenius diagram. The reactivity of each pathway aligned in the order  $R3 > R4 > R3' > R5$  for the temperature range studied here. First order Arrhenius parameters ( $\log_{10} A(s^{-1})$ ,  $E^*(kcal/mol)$ ) =  $(13.9 \pm 1.3, 55.5 \pm 4.0)$ ,  $(14.1 \pm 1.0, 58.4 \pm 2.8)$ ,  $(14.8 \pm 1.8, 60.1 \pm 5.7)$ , and  $(11.2 \pm 2.2, 49.2 \pm 7.1)$  were determined for pathways R3, R3', R4 and R5, respectively. Veratrole pyrolysis was thus similar to that of anisole. Accounting for reaction path degeneracy ( $\log_{10} 2 \sim 0.3$ ), the rate of both demethylation to guaiacol and isomerization to o-cresol were similar to the corresponding R3 and R5 anisole pathways.

The products evolved from veratrole pyrolysis suggest comparison of overall methoxyphenol results. Since guaiacol and anisole were primary products from veratrole pyrolyses, the secondary degradations of these should accord with the kinetic data previously determined for these as methoxyphenol substrates. This comparison is best effected at 450C, where the secondary degradations of guaiacol and anisole were significant. Thus, the important kinetic reactions are:



These reactions are sufficient to predict the time evolution of guaiacol and anisole yields, kinetic analysis of which revealing:

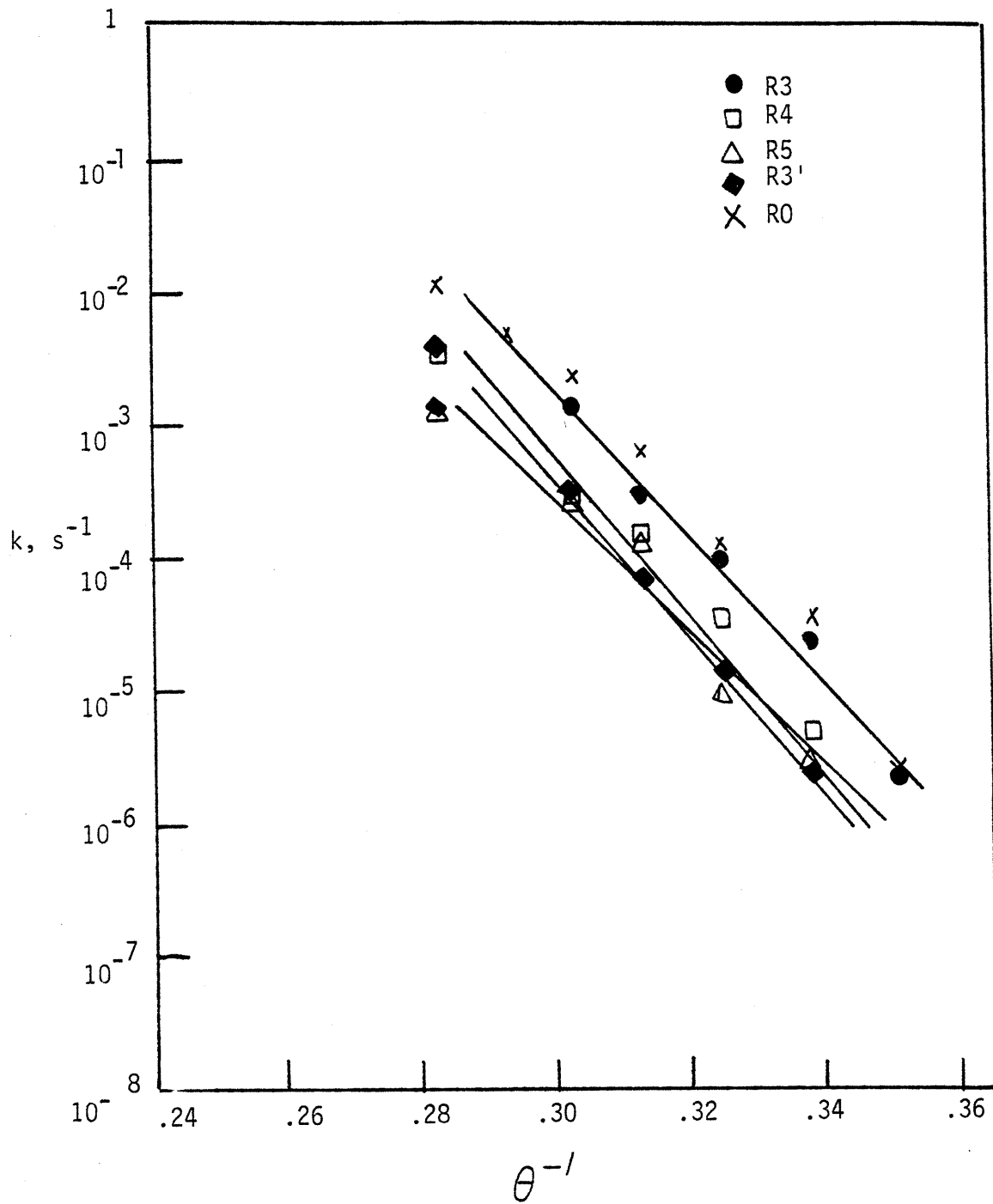


Figure 7.5.3 Arrhenius diagram for veratrole pyrolysis.

$$\frac{G}{V_0} = \frac{k_3^V}{k_0^V - k_0^G} \left( e^{-k_0^G t} - e^{-k_0^V t} \right) ; \quad \frac{A}{V_0} = \frac{k_4^V}{k_0^V - k_0^A} \left( e^{-k_0^A t} - e^{-k_0^V t} \right)$$

The parameters  $k_0^G$  and  $k_0^V$  were obtained from the previous kinetic data determined for pyrolysis of pure guaiacol and anisole. The constants  $k_3^V$ ,  $k_4^V$ , and  $k_0^V$  were obtained from Arrhenius interpolation of the data determined for veratrole pyrolysis at other temperatures. As such, these represent the most unbiased sources of kinetic constants available for incorporation into the above kinetic model. The predictions of the above equations are compared with the true experimental data in Figure 7.5.4, where hollow points depict the model predictions and the solid points represent the experimental data. The predictions are in excellent qualitative agreement with experiment whereas quantitative agreement deviates up to about 30%. This is considered quite reasonable in light of the experimental complexity involved in the veratrole pyrolysis product spectra, as well as the limits of uncertainty inherent in the anisole, guaiacol and veratrole kinetic parameters. Thus, overall methoxyphenol pyrolyses accord quite well.

## 7.6 Saligenol

Saligenol was pyrolysed over a temperature range of 175-350C, with holding times of 0.5 - 25 minutes. The pyrolysis was rapid at all temperatures and yielded water as the principal identifiable product. The only major co-product was an obscure higher molecular weight polymer which could be assessed only qualitatively. The

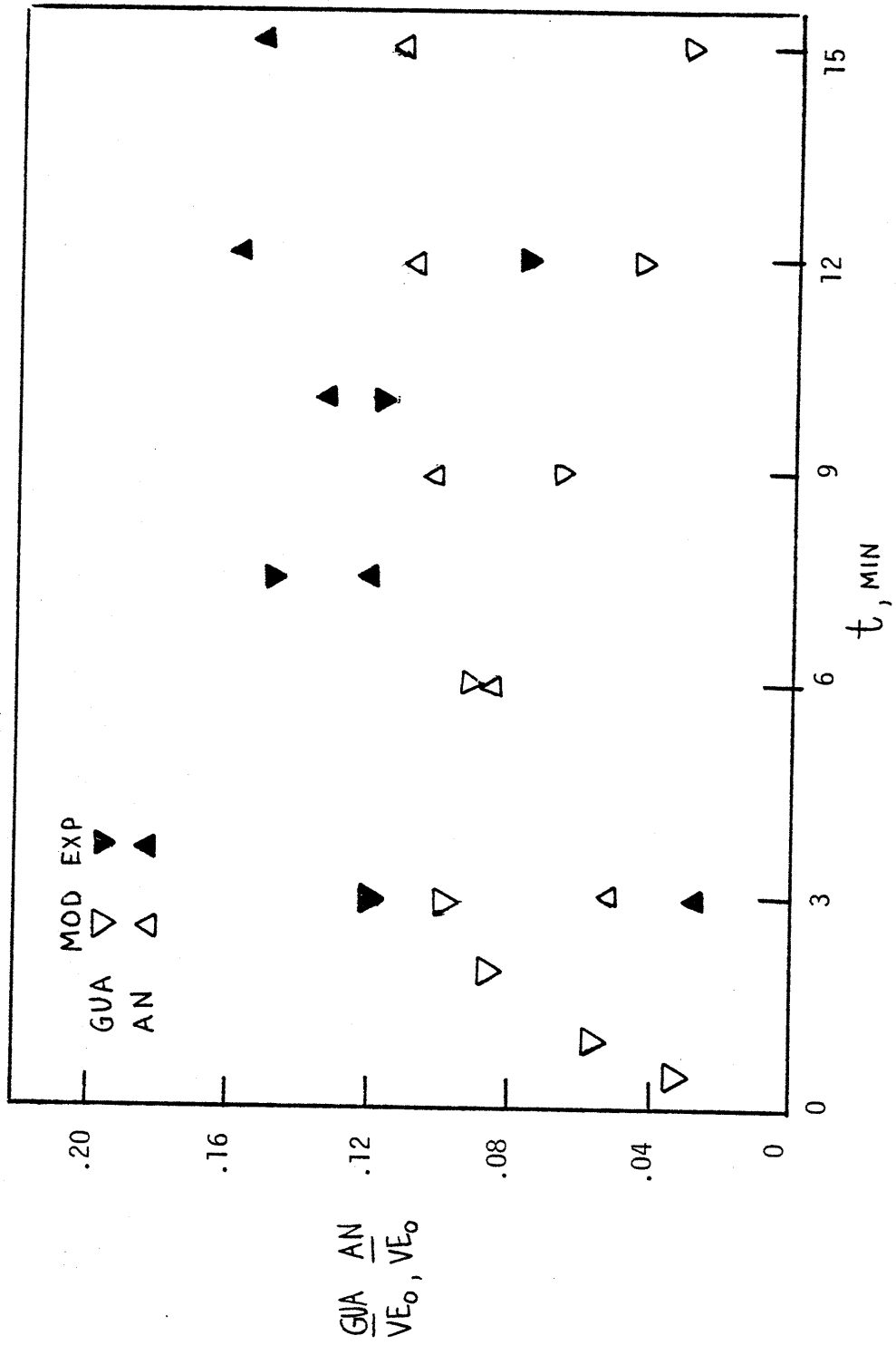
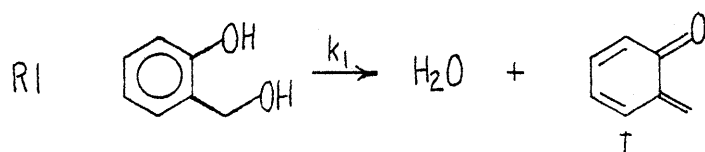


Figure 7.5.4 Comparison of 'model' and experimental veratrole pyrolysis.

polymers were rapidly formed at every temperature and accounted for the facile disappearance of substrate. Only trace amounts of o-cresol were detected, even with the addition of tetralin in a molar ratio (tetralin/saligenol)=(10/1).

Since the polymeric materials could not be quantified by the present GLC techniques, toluene was added to the reaction vessel as an inert internal standard to monitor water and cresol appearance and substrate disappearance. As the coking reactions were quite rapid, these studies were limited to temperatures of 175, 200 and 225C. Figure 7.6.1 depicts the yield of water and substrate conversion as a function of holding time for pyrolysis at 225C. The data for water production and saligenol disappearance do not differ significantly, indicating that the overwhelming pyrolysis reaction is one of stoichiometric saligenol dehydration, as in,



the stoichiometry of pathway R1 is further illustrated in Figure 7.6.2 where the water yield is plotted versus saligenol conversion for all temperatures and conversions studied. As evidenced in Figure 7.6.2 for conversions ranging from essentially 0.0-1.0, each mol of converted saligenol yielded one mol of water. The coproduct of saligenol dehydration, the quinonemethide (I), would be expected to either add hydrogen to form o-cresol or dimerize to polymers. Under the conditions of this study, the selectivity



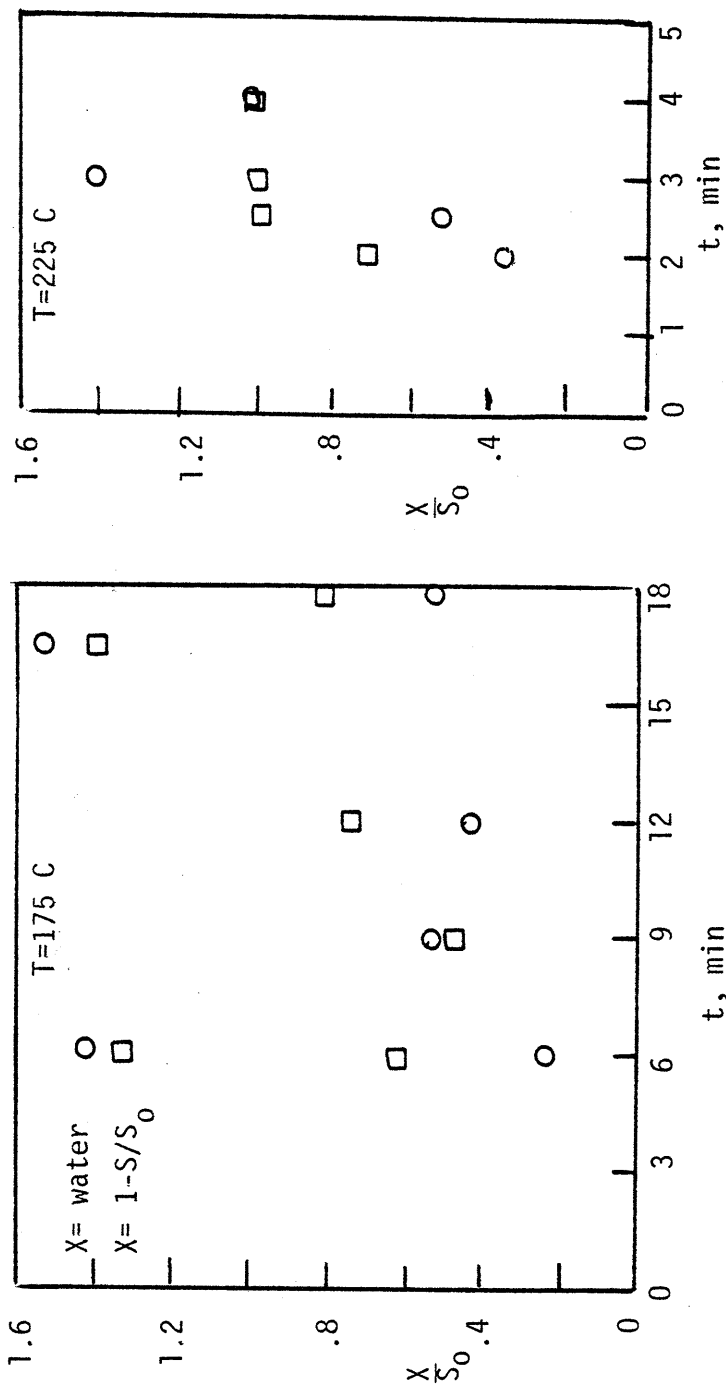


Figure 7.6.1 Saligenol pyrolysis kinetics.

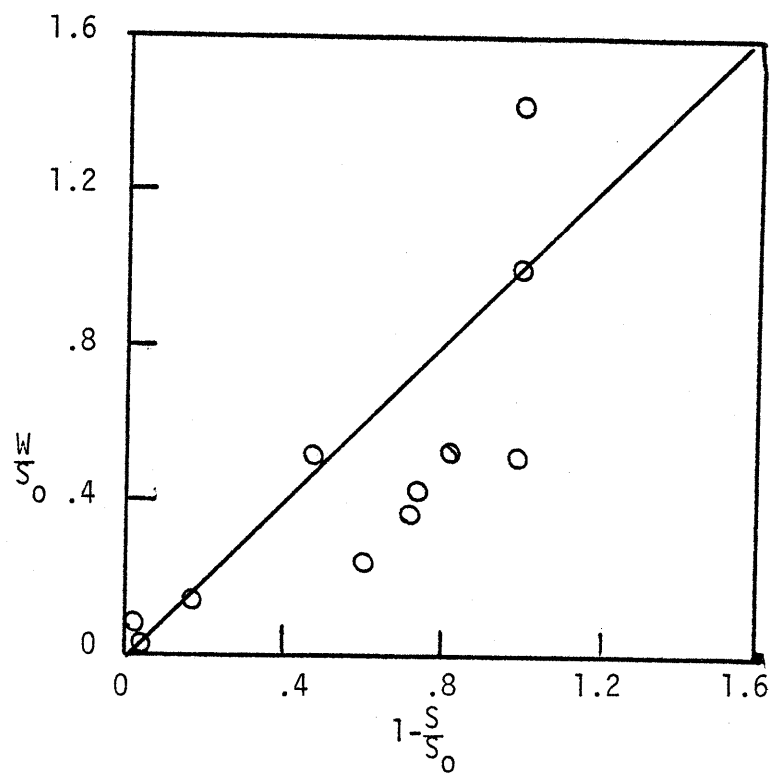


Figure 7.6.2 Product relationships in saligenol pyrolysis.

to polymers was evidently favored, as evidenced by the product spectra noted above.

Study of reaction R1 at 175, 200, and 225 C allowed the determination of first order rate constants and thus Arrhenius parameters. At 175, 200, and 225 C,  $-\log_{10} k_1 (s^{-1})$  was 2.79, 2.22 and 1.2, respectively; these correspond to Arrhenius parameters ( $\log_{10} A (s^{-1})$ ,  $E^* (kcal/mol)$ ) = (13.4±2.9, 33.4±6.3). Thus, saligenol dehydration is quite facile.

### 7.7 Benzaldehyde

Benzaldehyde pyrolysis yielded carbon monoxide and benzene as the major products; traces of biphenyl and phenolic products were also detected, their concentrations being from one to two orders of magnitude less than that of benzene. The time evolution of benzaldehyde pyrolysis products at 400C is depicted in Figure 7.7.1, where the yields of CO and benzene, as well as benzaldehyde decomposition, are plotted as a function of reaction holding time. Inspection of Figure 7.7.1 reveals that benzene and CO were produced in near stoichiometric proportions, each closely equalling the mols of benzaldehyde that disappeared. The relationship between CO and benzene production was further examined at temperatures of 300-500C covering fractional conversions of 0.01-0.30. These data are presented in Figure 7.7.2 where the yield of CO is plotted as the ordinate versus an abscissa of benzene yield. The data fall closely about the line  $y=x$ , indicative of a stoichiometric appearance of CO and benzene for all conditions examined. The mol ratio of

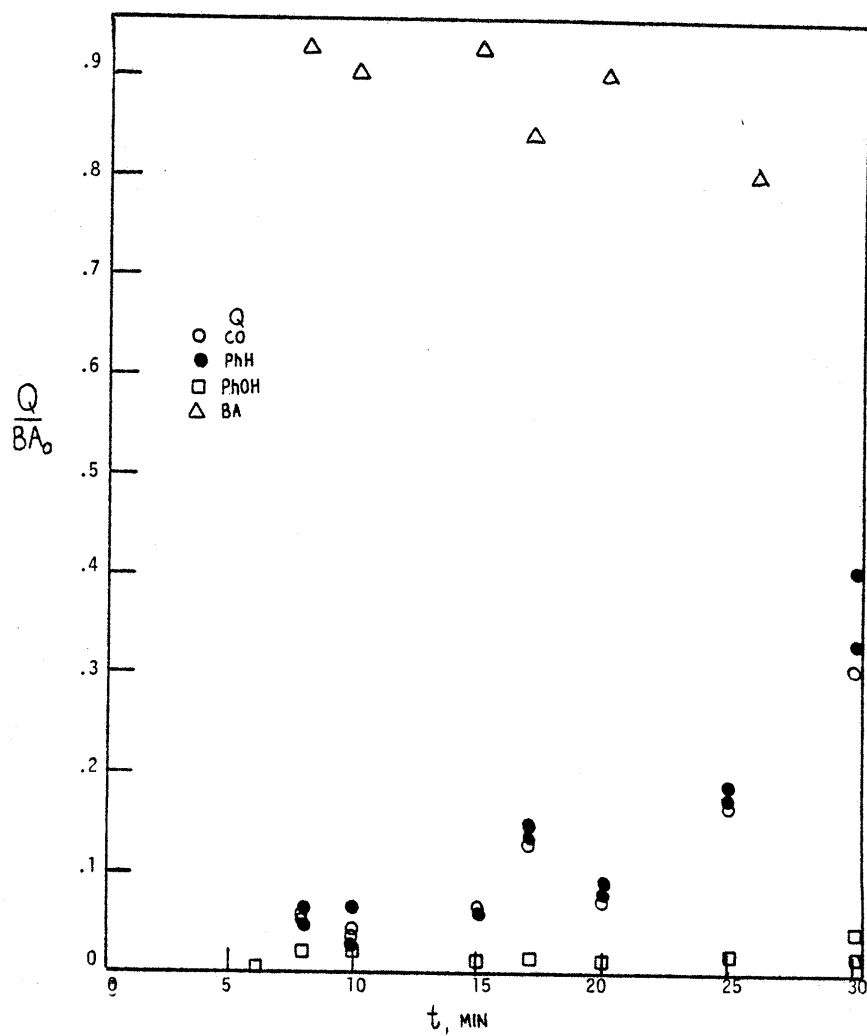


Figure 7.7.1 Benzaldehyde pyrolysis product evolution, T=400 C.

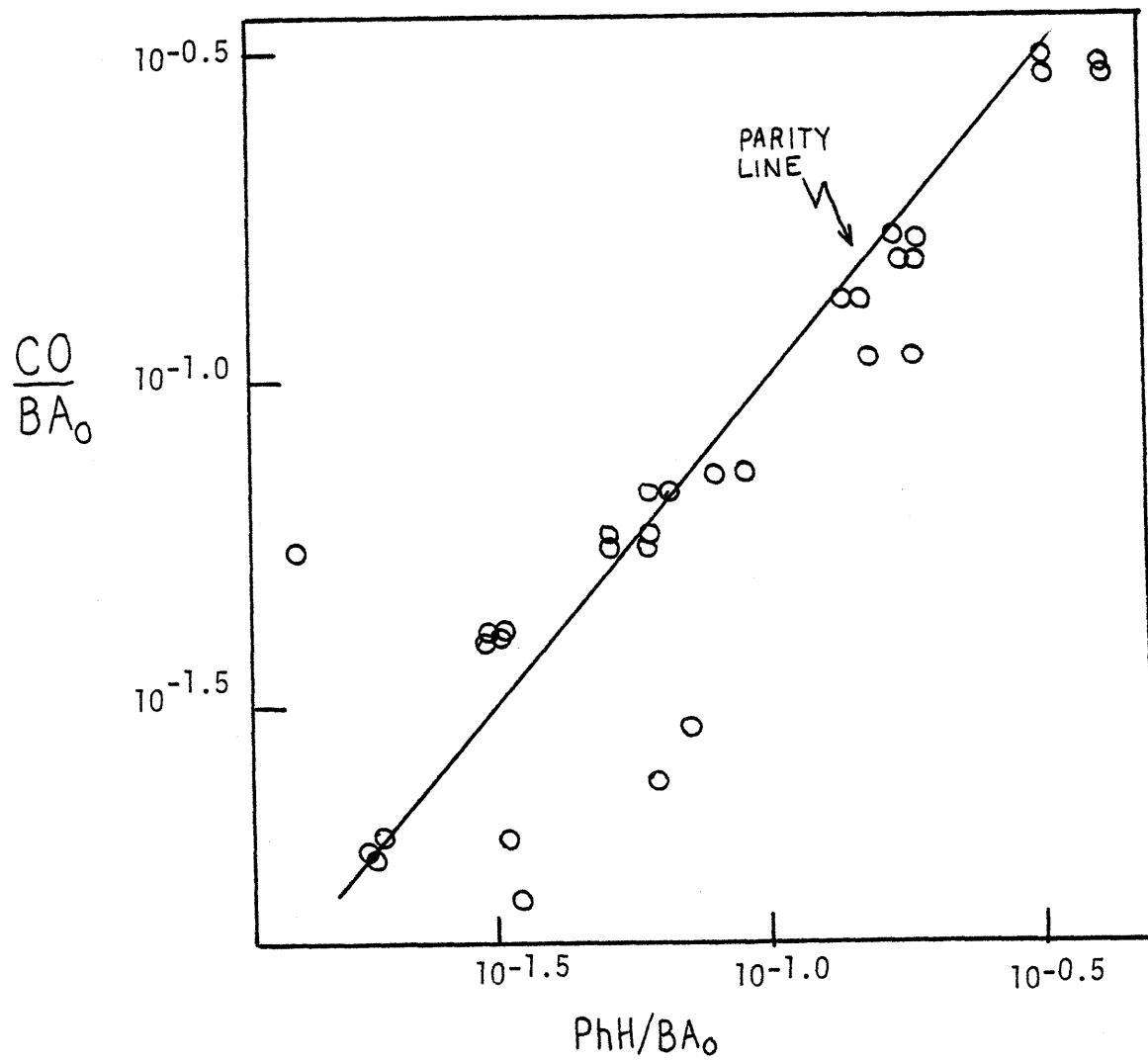
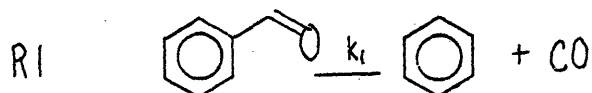


Figure 7.7.2 Product relationships in benzaldehyde pyrolysis.

(CO/benzene) products was thus unity,  $1.0 \pm 0.1$ , suggesting a benzaldehyde decomposition pathway of the form.



Variation of the initial substrate concentration from 0.16 to 3.28 mol/l at 400C showed reaction R1 to be first order in benzaldehyde concentration, with first order rate constant  $k_1 = (1.3 \pm 0.3) \times 10^{-4} \text{ s}^{-1}$  essentially independent of concentration. These data are depicted in Figure 7.7.3 where  $-\ln(\text{BA}/\text{BA}_0)$  is plotted versus holding time at 400C for each initial concentration studied. Such a plot predicts a family of lines with slope of  $k_1 \text{BA}_0^{\alpha-1}$ , where  $\alpha$  is the benzaldehyde reaction order. That a single, average slope described the data was indicative of a reaction order of unity.

Measurement of the kinetics of R1 at temperatures from 300-500C provided the data shown in Figure 7.7.4, an Arrhenius diagram. It is evident that  $\log_{10} k$  increased linearly with decreasing  $\theta^{-1}$ , the best fit Arrhenius parameters equalling  $(\log_{10} A(\text{s}^{-1}), E^*(\text{kcal/mol})) = (9.5 \pm 0.8, 41.5 \pm 2.7)$ . These parameters were obtained from kinetic constants spanning nearly five orders of magnitude in value, determined in the previously noted temperature interval of 200C.

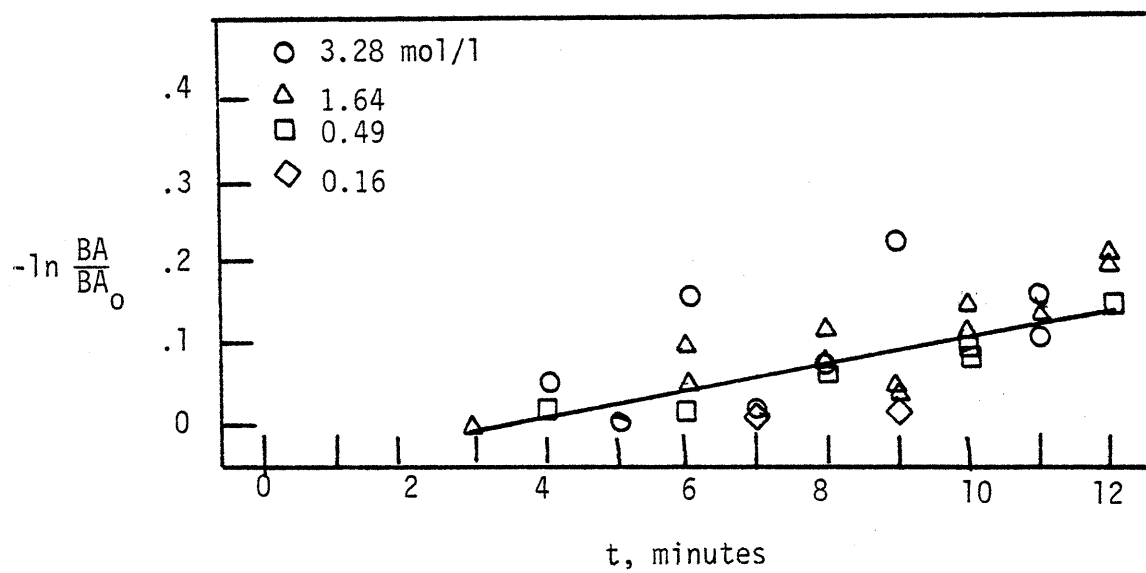


Figure 7.7.3 Benzaldehyde pyrolysis kinetics at 400 C.

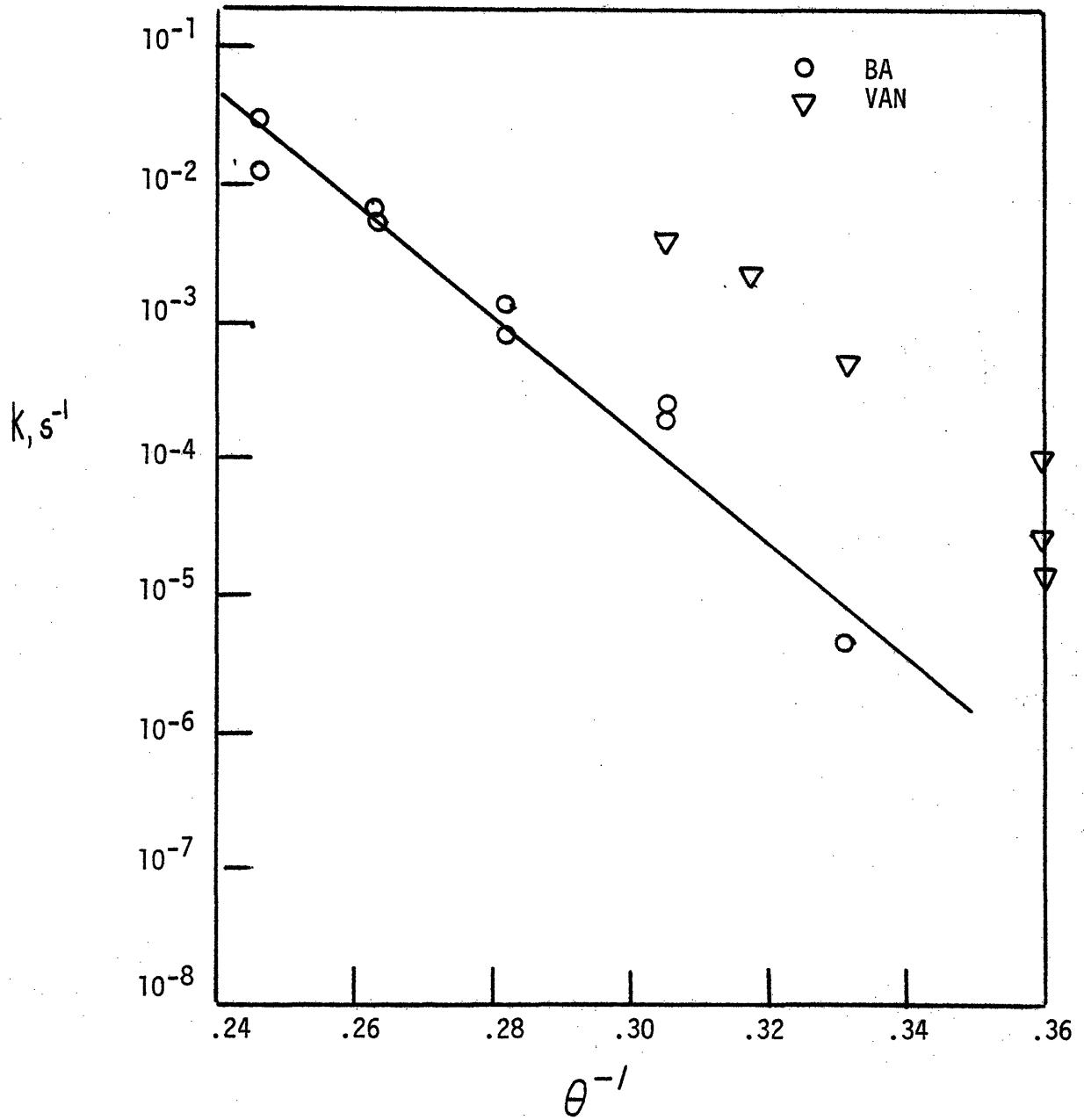
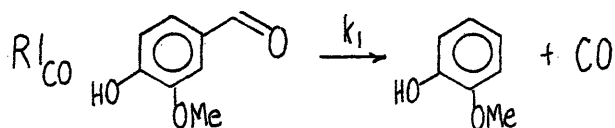


Figure 7.7.4 Arrhenius diagram for benzaldehyde pyrolysis.



## 7.8 Vanillin

Vanillin pyrolysis resulted in carbon monoxide and methane as the principle gaseous products, the former predominant. As aspects of methane release have been discussed in a previous section, this discussion will focus upon the CO producing reactions. Among liquid products at low conversions, guaiacol and dihydroxybenzaldehyde were major, the former predominant, while at higher conversions, catéchol also arose, along with lesser amounts of phenol; at highest conversions, polymers and a solid coke also formed. Figure 7.8.1 represents a rather high conversion vanillin product spectrum, where for pyrolysis at 400C the yield of substrate and each product is plotted as a function of reaction holding time. The facile appearance of guaiacol suggested a coincident release of CO, the relationships of these further examined in Figure 7.8.2; here the yield of CO is plotted as a function of guaiacol yield at 350C for rather low conversions; these low conversions emphasize primary reaction. The mol ratio (CO/guaiacol) was substantially unity at conversions ranging from  $0.02 < X < 0.20$ , suggesting a stoichiometric decarbonylation of vanillin to CO and guaiacol as a major degradation pathway; this pathway operates in addition to guaiacol-type reactions of the guaiacyl moiety. Thus, the pathways of vanillin pyrolyses are likely of the type:



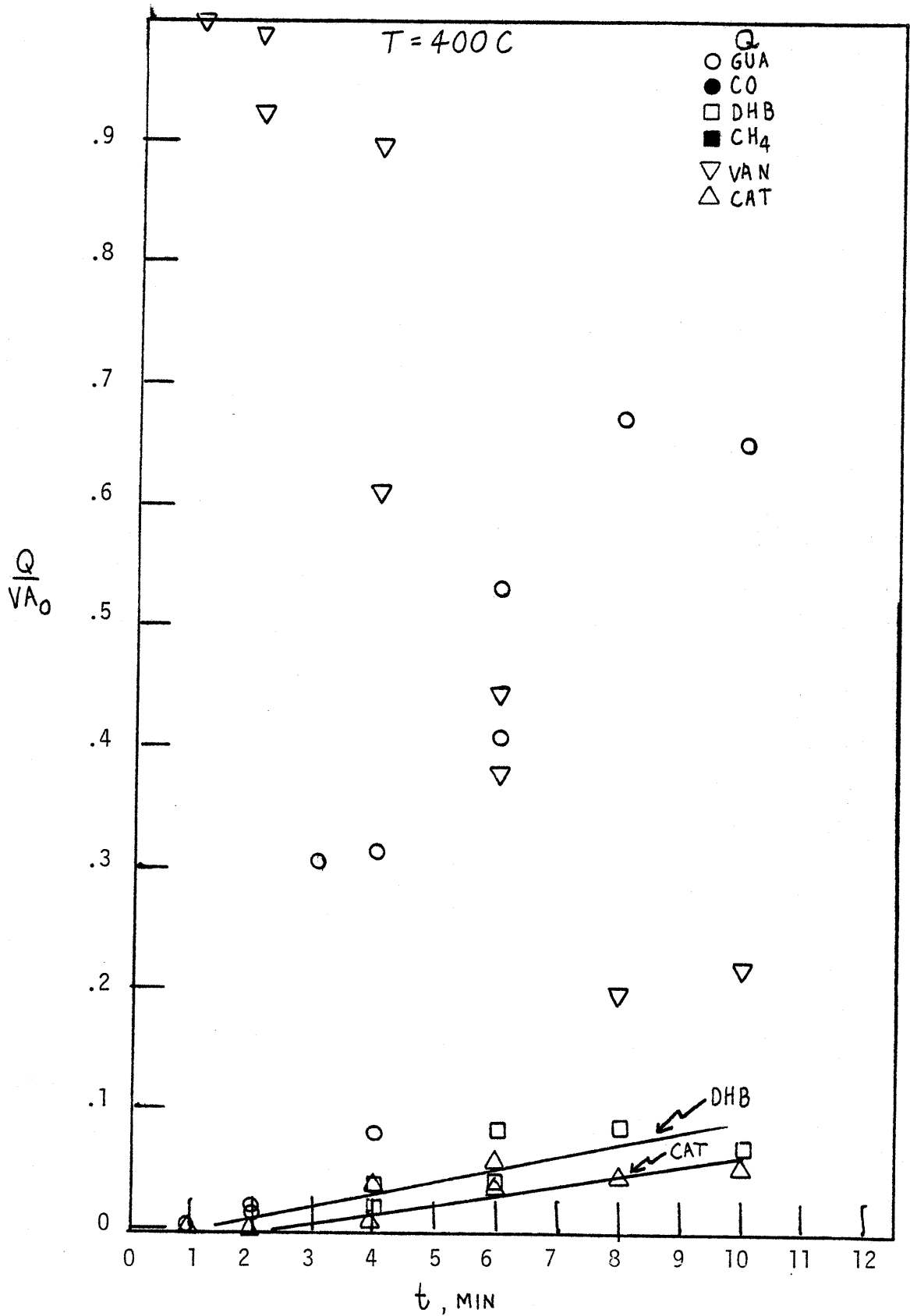


Figure 7.8.1 Vanillin pyrolysis product evolution.

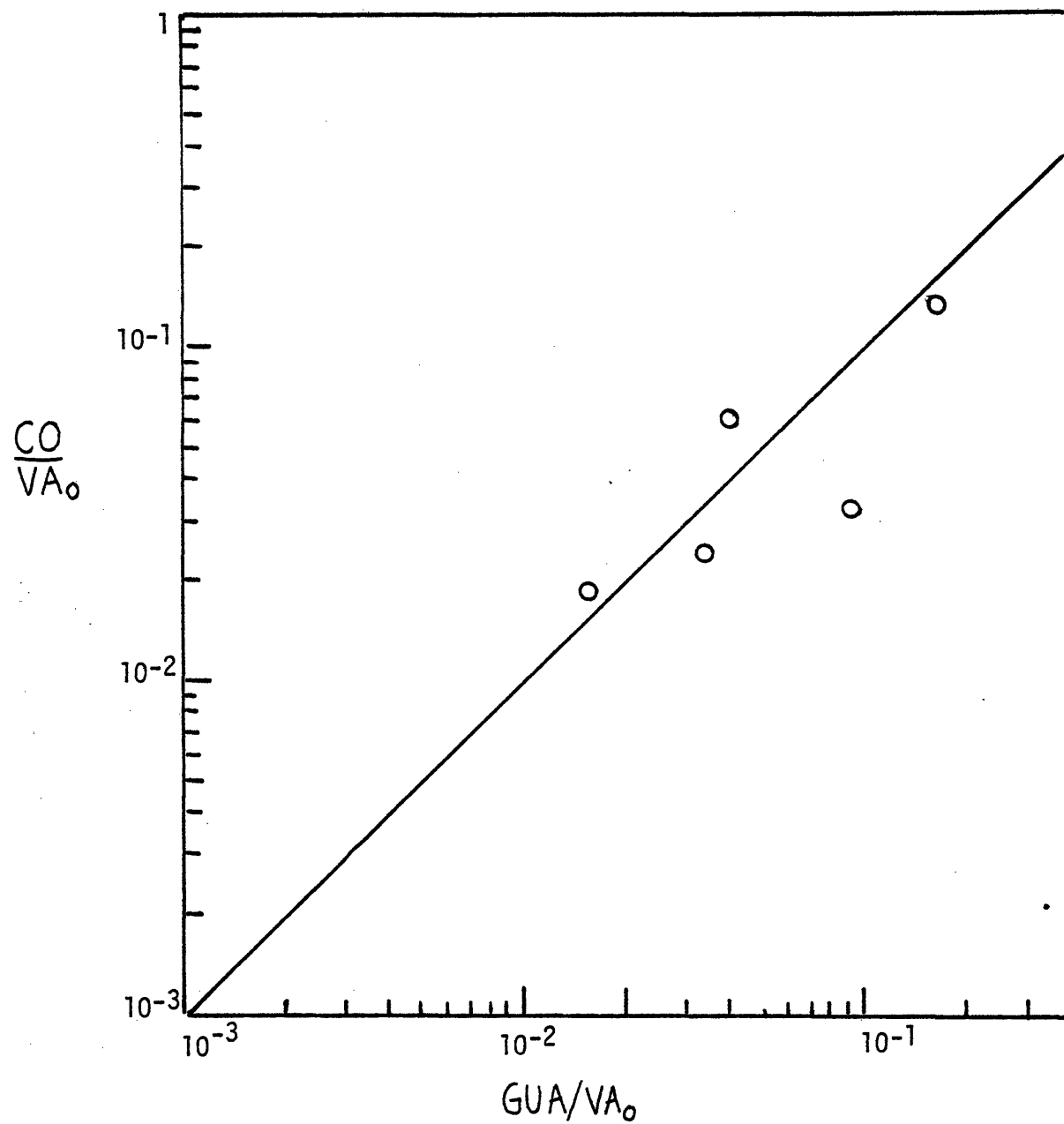
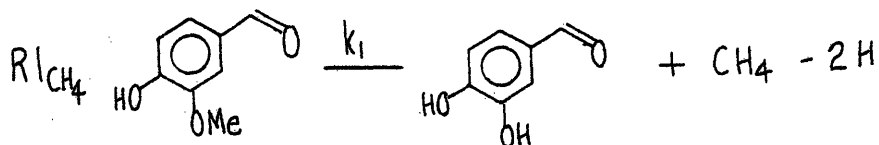


Figure 7.8.2 Product relationships in vanillin pyrolysis.



Pathway  $(R1)_{CO}$  was always predominant over  $(R1)_{CH_4}$ , the ratio (dihydroxybenzaldehyde/guaiacol)<sub>x→0</sub> ~ 0.1 at 400 C. At higher substrate conversions, the guaiacol and dihydroxybenzaldehyde products could further decompose by the same kinds of pathways to yield the catechol and phenol products observed.

Kinetic data for vanillin pyrolysis are summarized in Figure 7.8.3, an Arrhenius diagram. It is notable that the rate constant  $k_1$  for vanillin decarbonylation far exceeded that for benzaldehyde, while the rate of demethanation was essentially equal to that of guaiacol. Thus, the rate of arylaldehyde decarbonylation was markedly enhanced by guaiacyl substituents while the rate of guaiacyl demethanation was virtually unaffected by the carbonyl substituent.

### 7.9 Acetophenone

Acetophenone pyrolysis yielded carbon monoxide and methane as the major gaseous products with  $CO/CH_4 \sim 2-3$  from 400-500C. Liquid product spectra were complex, with benzene, toluene, xylenes and other alkylbenzenes being the major components, along with apparent dimers; additionally present were benzaldehyde, biphenyl, cresols and aromatic ethers. The product spectrum resulting from pyrolysis at 550C is depicted in Figure 7.9.1, where each product yield is

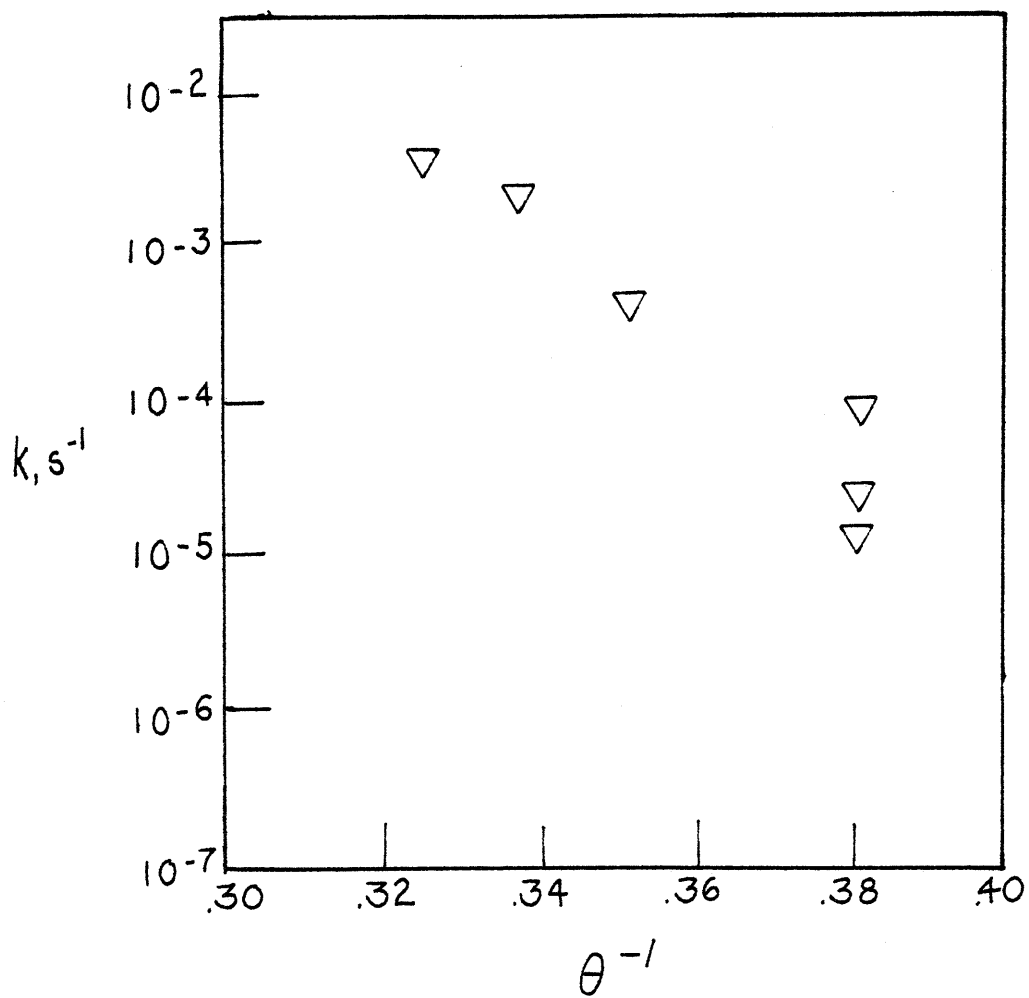


Figure 7.8.3 Arrhenius diagram for vanillin pyrolysis.

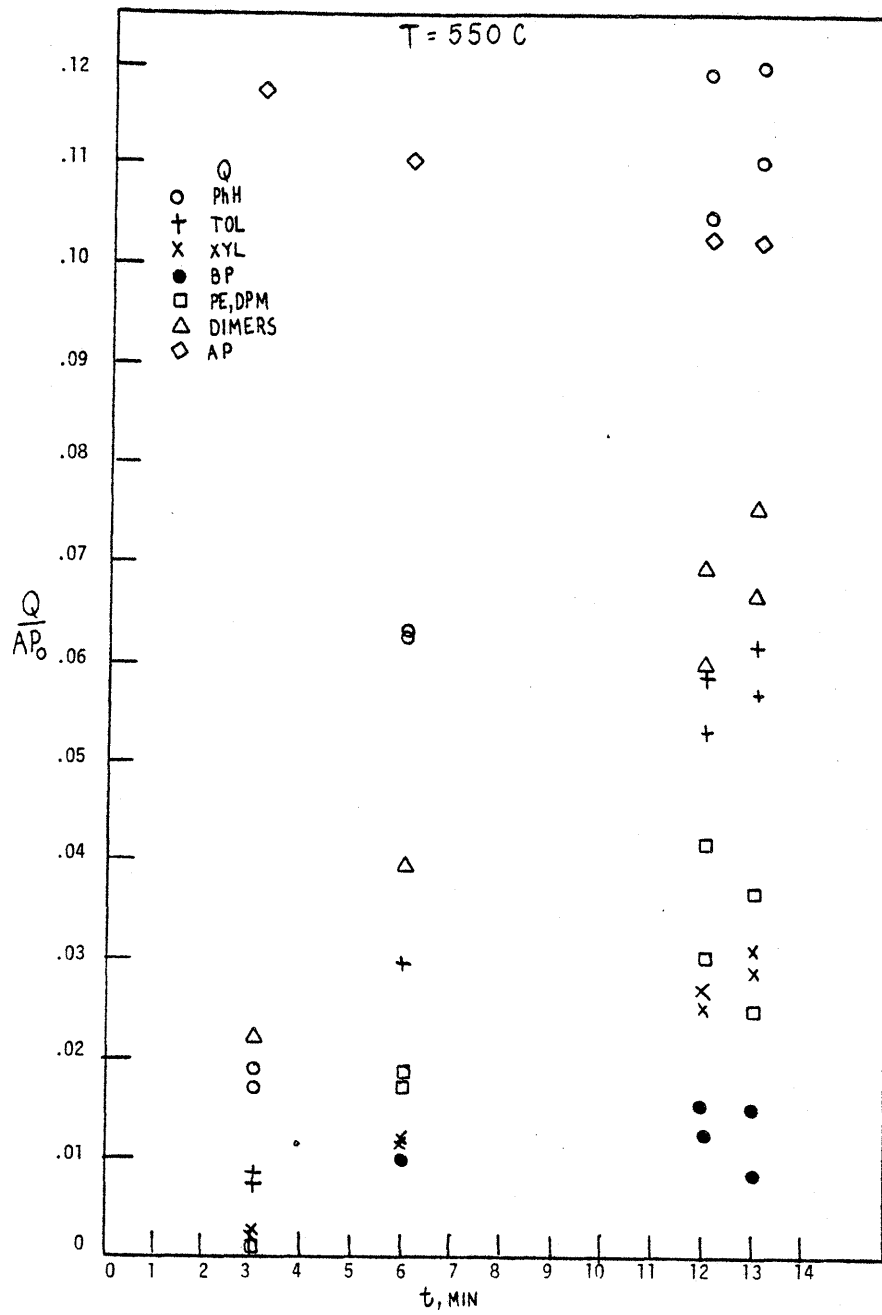


Figure 7.9.1 Acetophenone pyrolysis product evolution.

plotted versus reaction holding time. Inspection of Figure 7.9.1 reveals that the favored light products, in descending order of prevalence, were benzene, toluene and xylene, whereas dimers, biphenyl, diphenylmethane and phenyl ether were favored heavy products.

Because of the refractory nature of the substrate and the complexity of the liquid product spectra, no clear link could be established between gaseous and condensed phase products. This is illustrated in Figure 7.9.2, where CO, CH<sub>4</sub> and the major liquid products are plotted versus time for a pyrolysis effected at 550C in a reactor especially equipped to facilitate gas and liquid product analyses. As evidenced in Figure 7.9.2, the yield of CO far exceeded the yield of any one liquid product, whereas benzene and methane yields were comparable. For all temperatures studied, the ratio CO/(B+T+X) exceeded unity; this is indicative of likely condensation reactions leading to the formation of the biphenyl, diphenylmethane, and other dimeric products observed.

The complexity of the product spectra precluded elucidation of unequivocal individual reaction pathways, yet the appearances of CH<sub>4</sub>, CO, benzene and toluene, as well as overall substrate disappearances, were monitored. With regard to the liquid products, acetophenone decomposition and benzene and toluene formation were studied at 550C for substrate concentrations ranging from 0.14 to 1.4 mol/l. These data are presented in Figure 7.9.3. The data exhibit considerable uncertainty, reflecting the severe conditions required for rather modest acetophenone conversion. For substrate decomposition, the least squares rate constant obtained for each

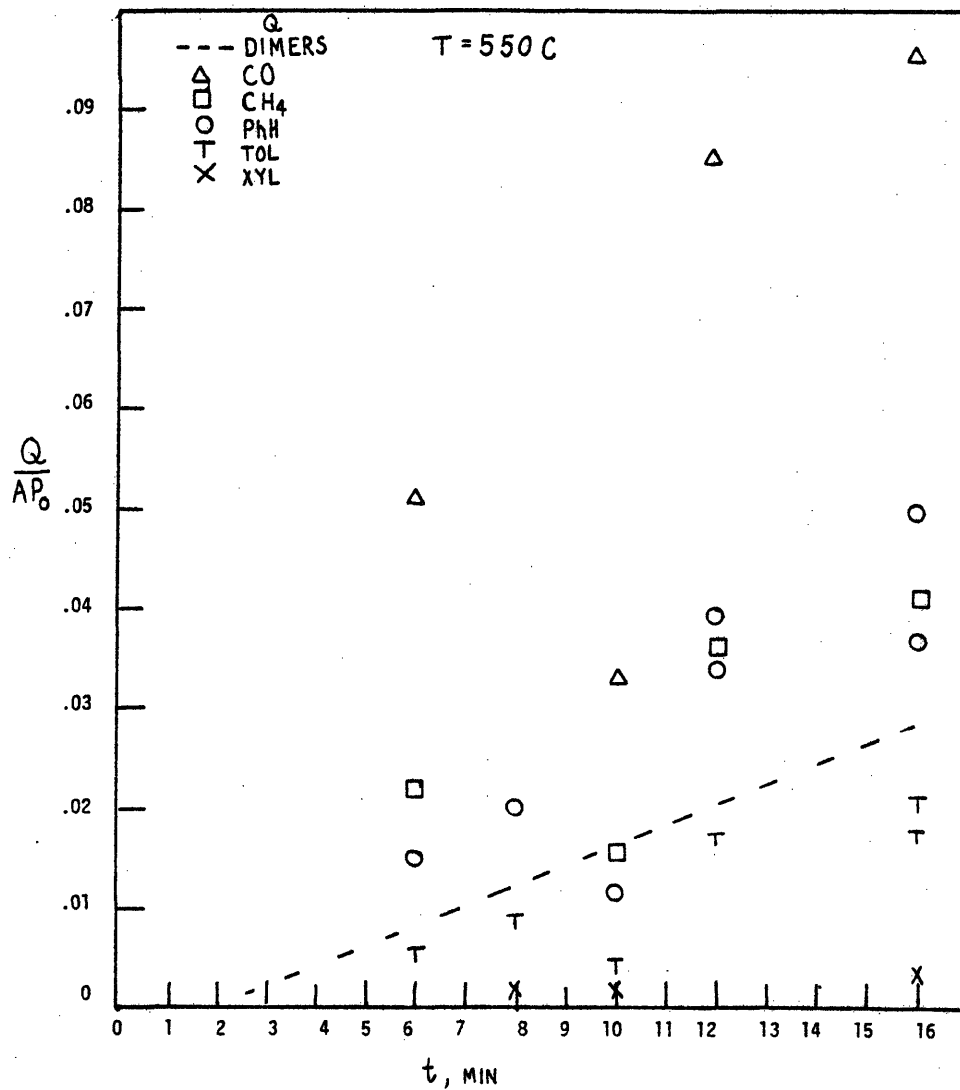


Figure 7.9.2 Product relationships in acetophenone pyrolysis, t=550 C.



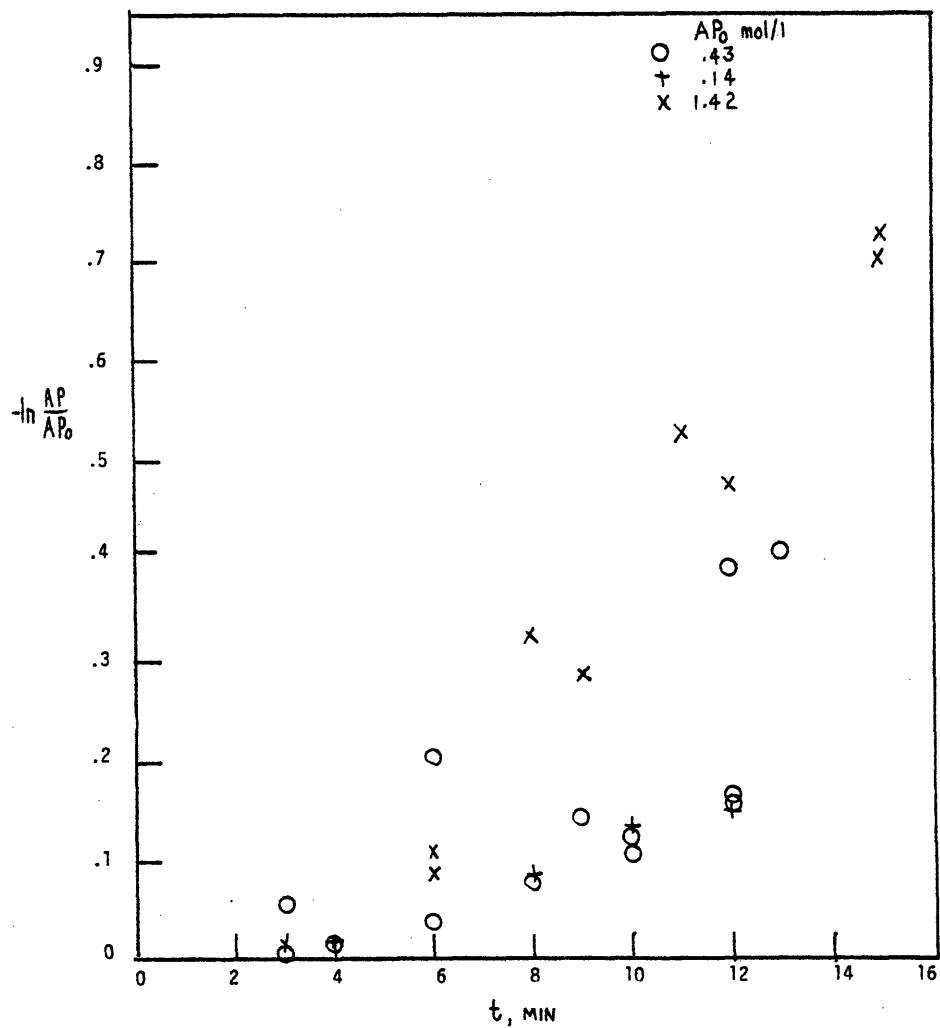


Figure 7.9.3 Acetophenone kinetics at T=550 C.  
a) acetophenone disappearance

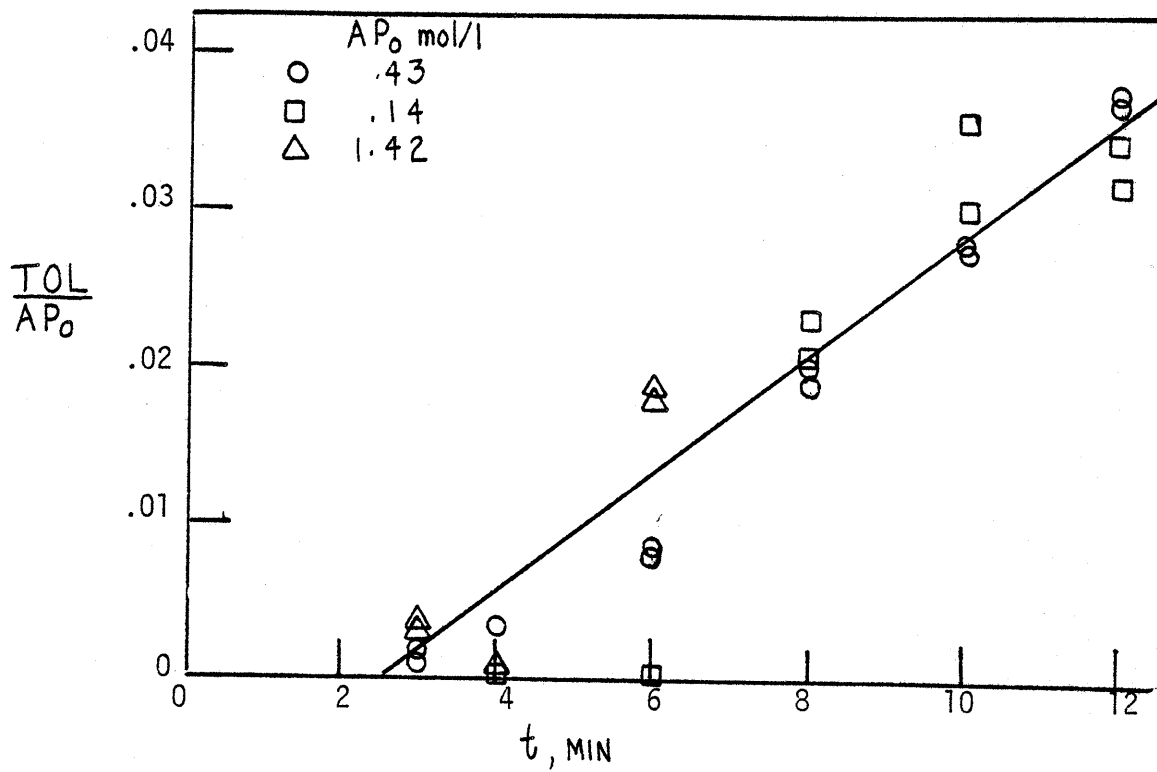


Figure 7.9.3b Toluene appearance.

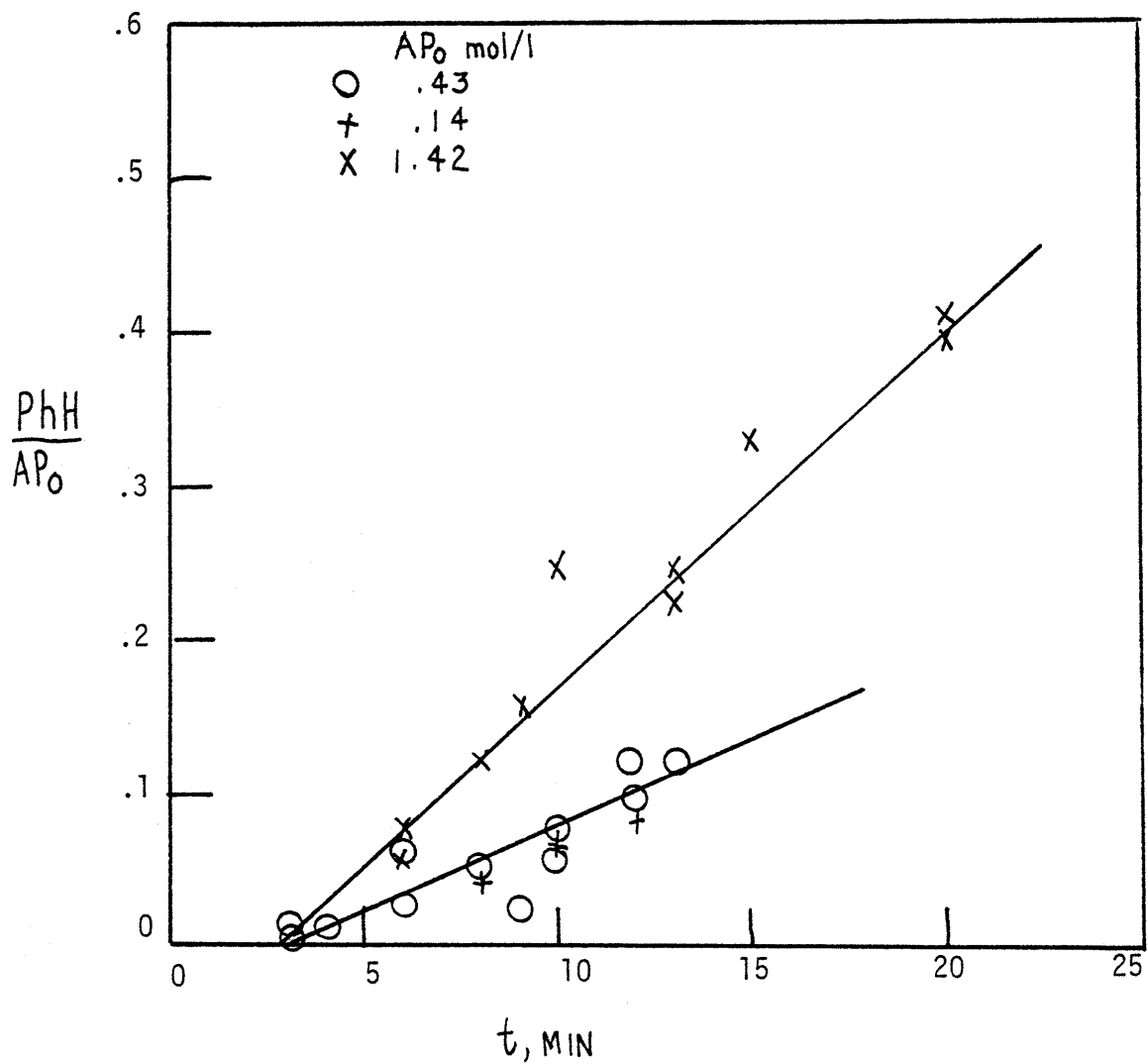


Figure 7.9.3c Benzene appearance.

initial substrate concentration was found to increase slightly with increasing substrate concentration. An apparent reaction order of 1.2-1.3 was thus determined. As illustrated in Figure 7.9.3b, the rate constant for toluene appearance was substantially independent of initial substrate concentration, as in 1 order reaction kinetics. A rate constant for benzene appearance increased with increasing substrate concentration, indicative of a reaction order in excess of unity. In fact, the concentration dependence of this pseudo-first order rate constant revealed an apparent order of 1.6 for benzene appearance.

Experiments at temperatures from 400-500C yielded apparent first order rate constants for the formation of CO, CH<sub>4</sub>, benzene and toluene, as well as for the overall disappearance of substrate. These data are presented in Figure 7.9.4, an Arrhenius diagram. Inspection of Figure 7.9.4 reveals that CO and benzene were formed in comparable rates, while the same is true for the product pair CH<sub>4</sub>-toluene. The former pair evolved about 2-3 times faster than did the latter. Thus, even though an exact stoichiometric relationship between products could not be discerned, kinetic data suggest that the light liquid products benzene and toluene and the gas products CO and CH<sub>4</sub> are formed in similar rates. Arrhenius parameters for overall acetophenone decomposition, benzene appearance, and toluene appearance were ( $\log_{10} A(s^{-1})$ ,  $E^*(kcal/mol)$ ) = (10.9±1.2, 52.1±4.1), (9.57±1.9, 50.5±6.7), and (10.9±2.2, 56.4±7.6) respectively. The previously described kinetic results for benzaldehyde decomposition are also included in Figure 7.9.4; these demonstrate that overall

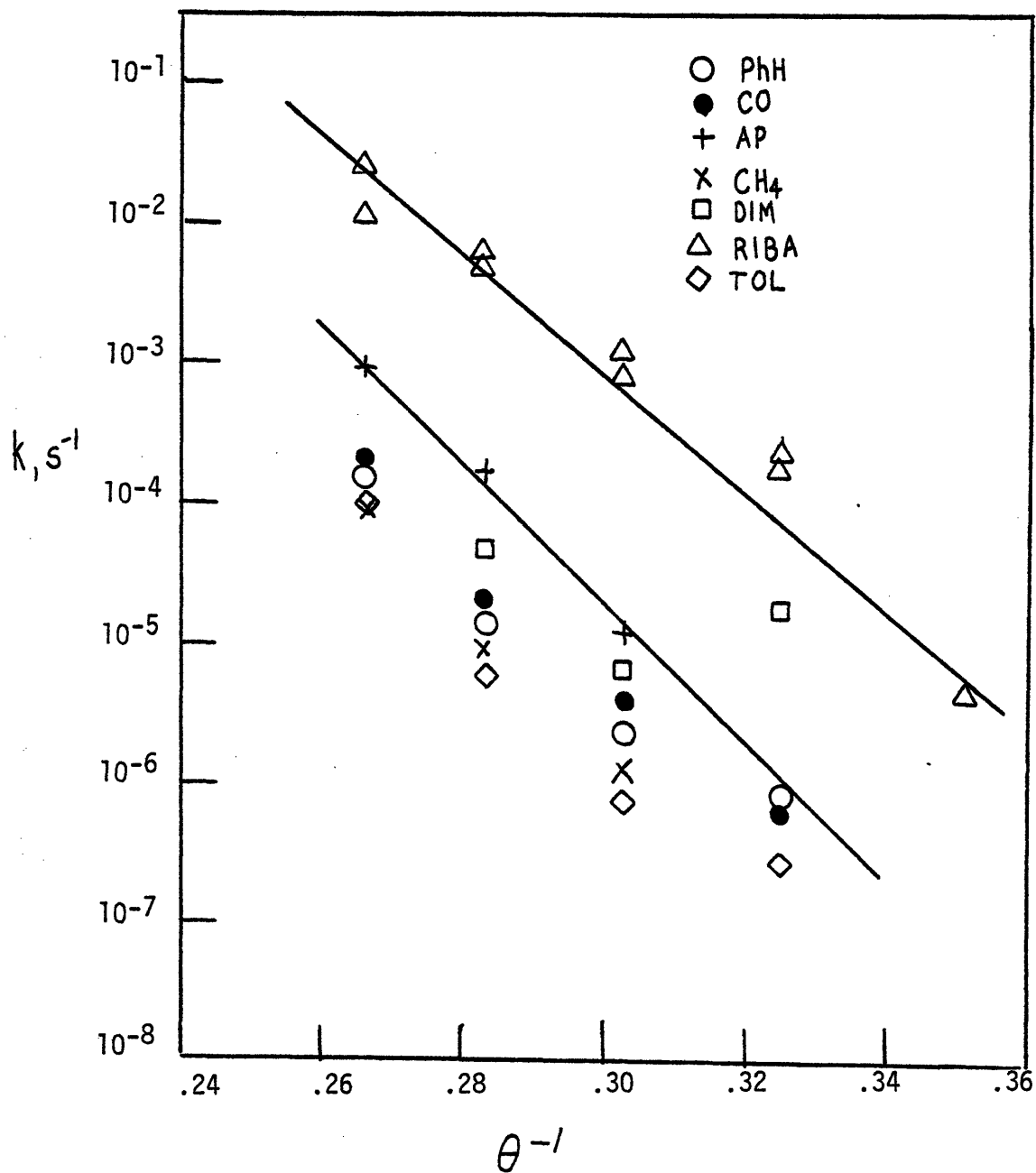


Figure 7.9.4 Arrhenius diagram for acetophenone pyrolysis.

acetophenone pyrolysis was typically two orders of magnitude slower than benzaldehyde pyrolysis for the temperature range studied here.

### 7.10 Cinnamaldehyde

Pyrolysis of t-cinnamaldehyde yielded CO as the major gaseous product, with much smaller amounts of hydrogen, methane and acetylene detected. A large number of liquid products arose, among which a dimeric condensation product, phenols, cresols, styrene, toluene and ethylbenzene were each appreciable, along with lesser amounts of benzene, other alkyl-benzenes and phenols and biphenyl. Figure 7.10.1 demonstrates the relative yields of these obtained from pyrolysis at 400C. As evidenced by Figure 7.10.1, product relationships and stoichiometrics were obscure. However, at low conversions the CO and styrene yields coincided, suggesting a primary stoichiometric production of these.

The relationship between CO and styrene is further explored in Figure 7.10.2, where the yield of each is plotted versus reaction time at 350 and 400C. At low conversions, the two products are formed synchronously, whereas styrene attained maximal proportions at intermediate conversions. This behavior suggests that styrene is subject to further secondary degradation.

Thus, styrene, phenols, CO, and dimers were clearly primary products, whereas toluene and ethylbenzene, while both appreciable, appeared with zero initial slope in Figure 7.10.1, and were thus likely secondary products. That toluene and ethylbenzene eventually exceeded the CO yield indicated that these are formed by pathways

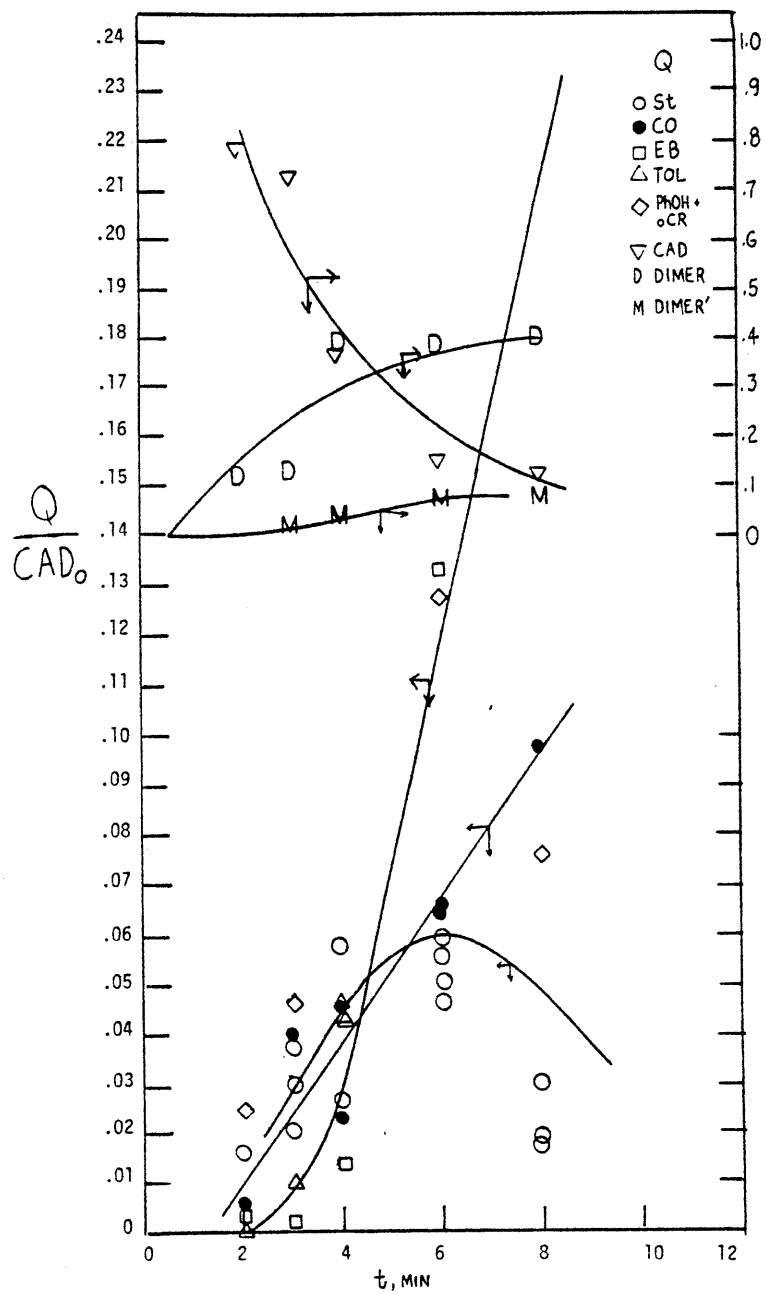


Figure 7.10.1 Cinnamaldehyde pyrolysis product evolution.

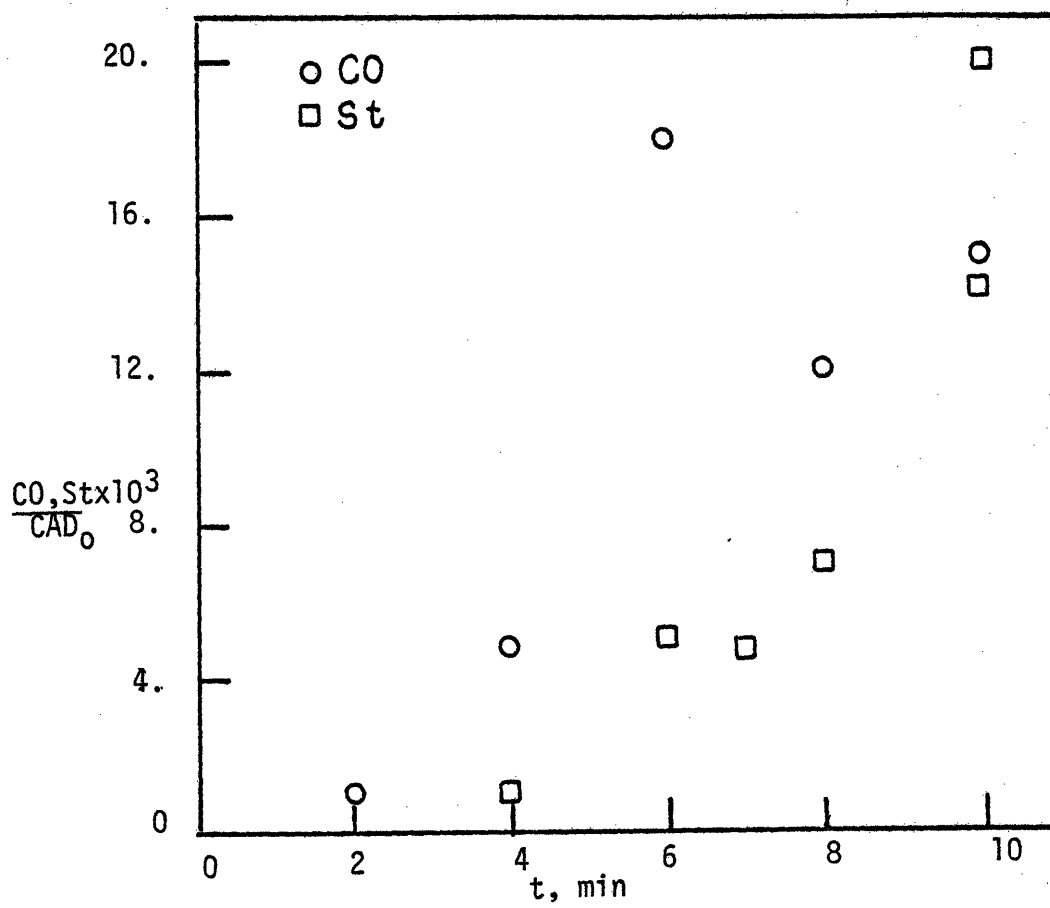


Figure 7.10.2 Product relationships in cinnamaldehyde pyrolysis. a)  $T=350$  C



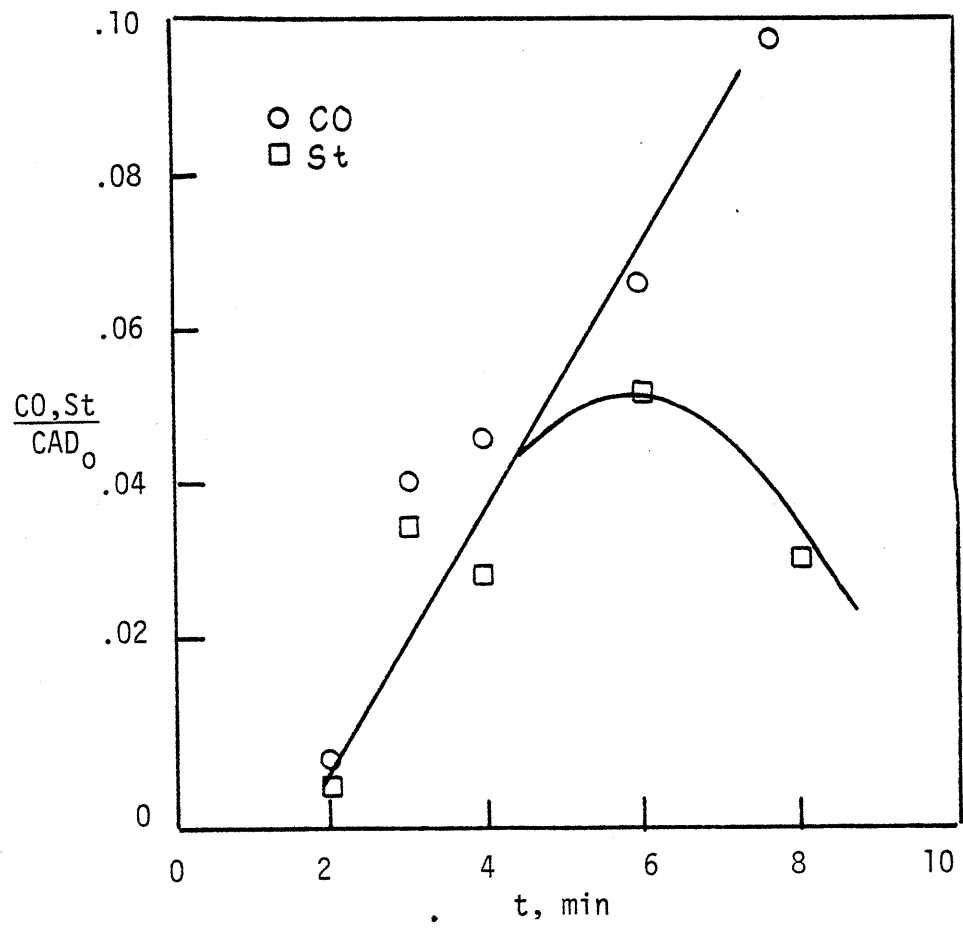


Figure 7.10.2b T=400 C.

additional to secondary styrene degradation; styrene has previously been demonstrated to degrade to alkylbenzenes, both here in relation to PPE pyrolysis, and in the literature<sup>78</sup>. Likely additional sources of toluene and ethylbenzene include the rapidly formed dimeric condensation products, which may be envisioned to degrade to light aromatic hydrocarbons without CO release. However, the complexity of the pyrolysis product spectra precluded unequivocal assignment of product origins and pathways.

The appearance of both dimeric condensation products and low molecular weight single ring aromatics was suggestive of a complex set of parallel and sequential reaction pathways. Pyrolysis over a twenty-fold initial cinnamaldehyde concentration range at 400C enabled the determination of a global reaction description. The decomposition of cinnamaldehyde was described in two parts, a set of first and a set of second order reactions. Thus arose a global kinetic rate expression of the form:

$$(I) \quad -d(\text{CAD})/dt = k_1(\text{CAD}) + k_2(\text{CAD})^2; \quad (\text{CAD}) [=] \text{mol/l}$$

Expression (I) can be transformed to an absolute mol basis by introducing the reactor volume,  $V [=] \text{l}$ , and thus

$$(Ia) \quad -d\text{CAD}/dt = k_1\text{CAD} + k_2V^{-1}\text{CAD}^2; \quad \text{CAD} [=] \text{mol}$$

Dividing by CAD yields,

$$(Ib) \quad -d\ln\text{CAD}/dt = k_1 + k_2V^{-1}\text{CAD}$$

Thus a plot of  $-d\ln\text{CAD}/dt$  versus CAD had slope  $V^{-1}k_2$ , a parameter accounting for second order reactions and intercept  $k_1$ , describing first order reactions. These data are described in Figure 7.10.3.

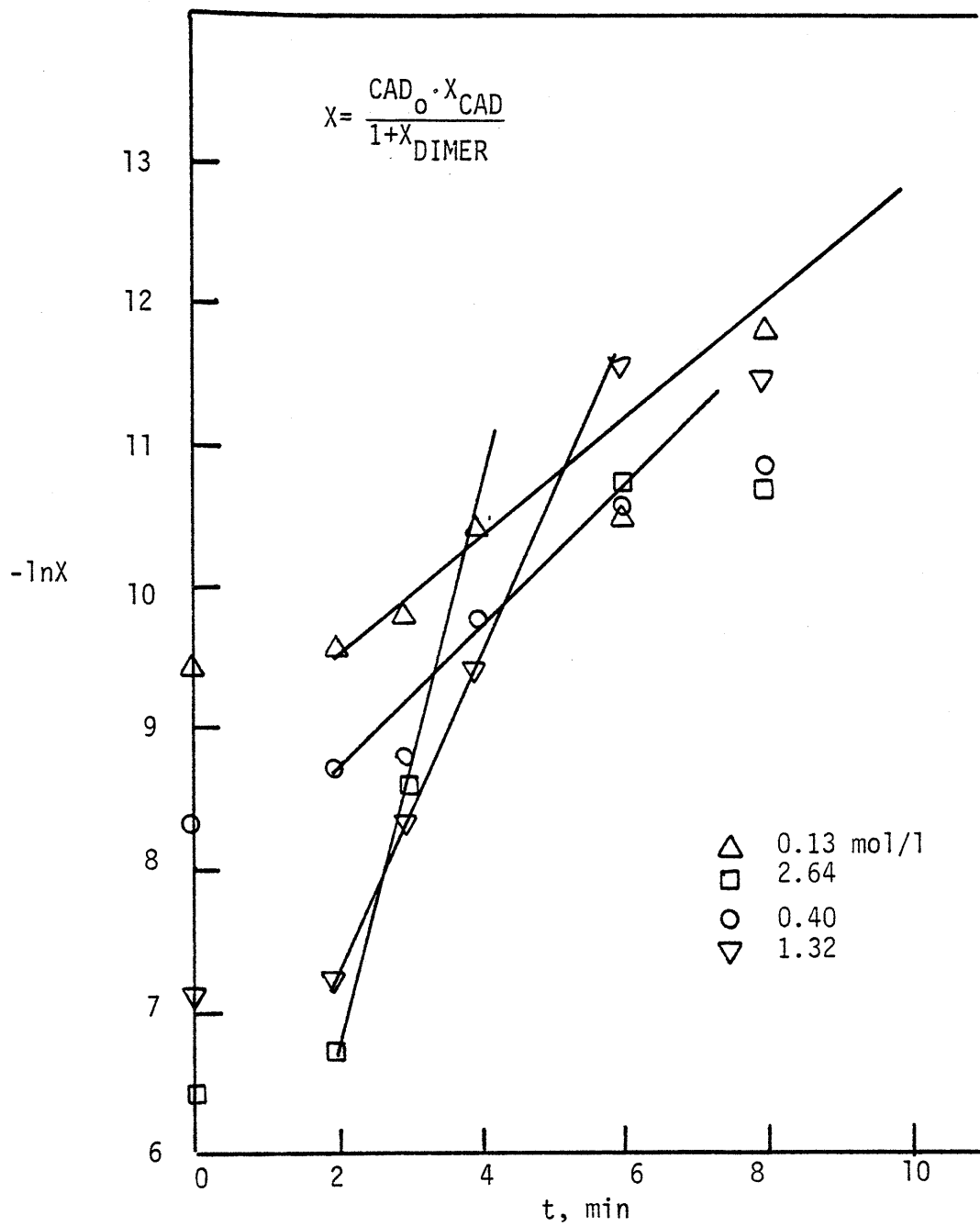


Figure 7.10.3 Global cinnamaldehyde pyrolysis kinetics. a) initial rates

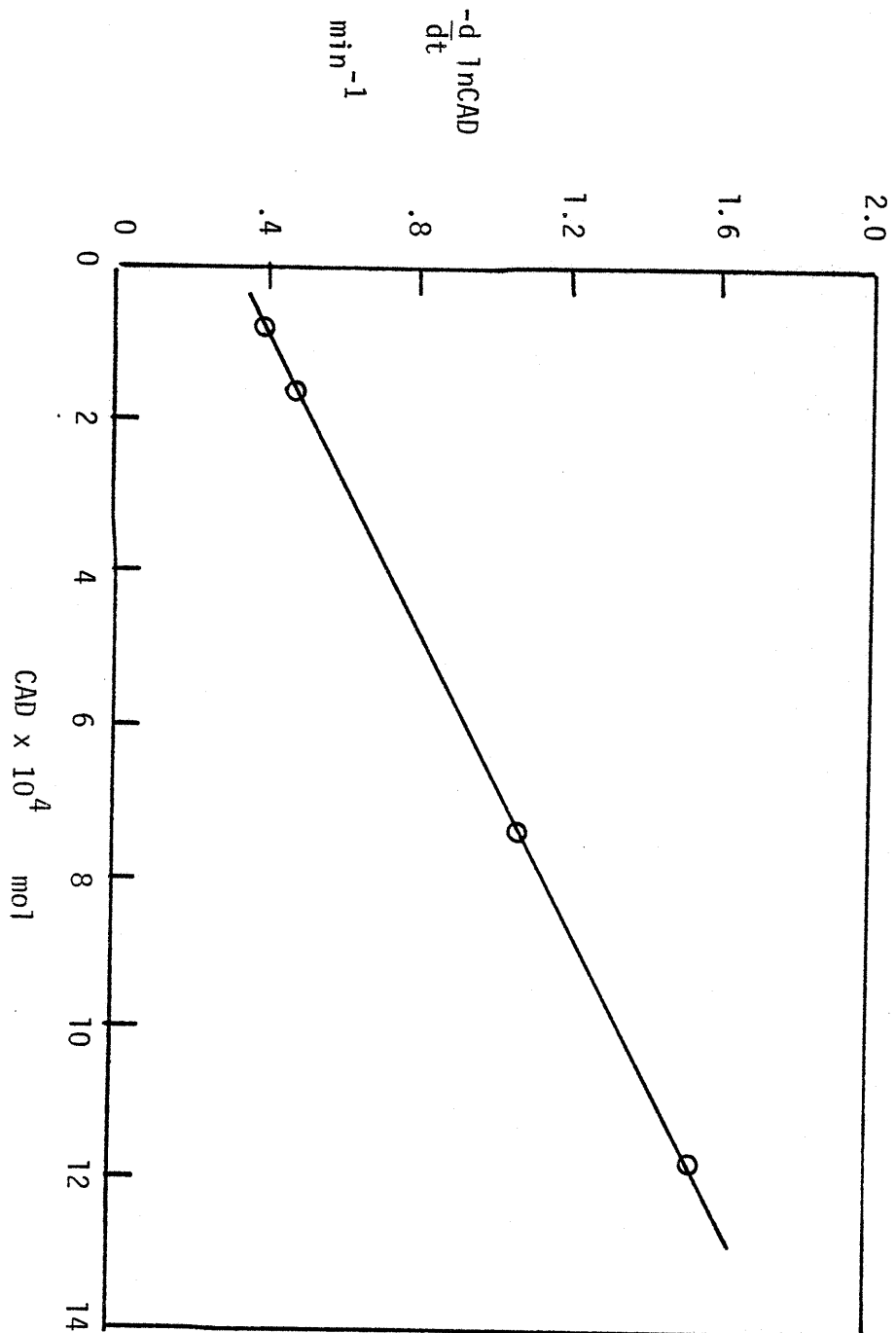


Figure 7.10.3 b Variation of cinnamaldehyde pyrolysis rate with substrate concentration.

Figure 7.10.3a plots the time variation of CAD, which takes the form

$$\text{CAD} = \frac{\text{CAD}_0 X_{\text{CAD}}}{1 + X_{\text{DIMER}}} \quad X = \text{product mol fraction}$$

due to molar decrease caused by the formation of dimers. The instantaneous slope of this plot was estimated at two minutes holding time, due to uncertainty introduced by reactor heat up effects. Thus, with reference to expression (Ib), both  $d\ln\text{CAD}/dt$  and CAD were estimated at two minutes holding time for each initial cinnamaldehyde concentration studied. This is nearly equivalent to using initial rate data for expression (Ib), save the time transposition due to reactor heatup. Figure 7.10.3b depicts the resulting dependency of  $d\ln\text{CAD}/dt$  on CAD. The linearity of this plot establishes the validity of the assumed rate form (I). Least squares analysis revealed parameter values  $k_1 = 5.08 \times 10^{-3} \text{ s}^{-1}$ ,  $k_2 = 5.20 \times 10^{-3} \text{ mol}^{-1} \text{ s}^{-1}$ .

As might be expected from an overall kinetic expression of the type (I), the product spectra were also dependent upon absolute substrate concentration. Thus, the dimeric product was most favored at high concentrations, while the selectivity turned toward styrene at low concentrations. These data are displayed in Figure 7.10.4, a plot of major product mol fraction as a function of reaction holding time with initial concentration as a parameter. As evidenced by Figure 7.10.4, the dimer selectivity increased with increasing initial concentration at the expense of phenol and styrene products. For example, at 400C and six minutes holding time, the mol fractions dimer:phenol:styrene=0.16:0.16:0.07 for  $(\text{CAD}_0)=0.13 \text{ mol/l}$ , while

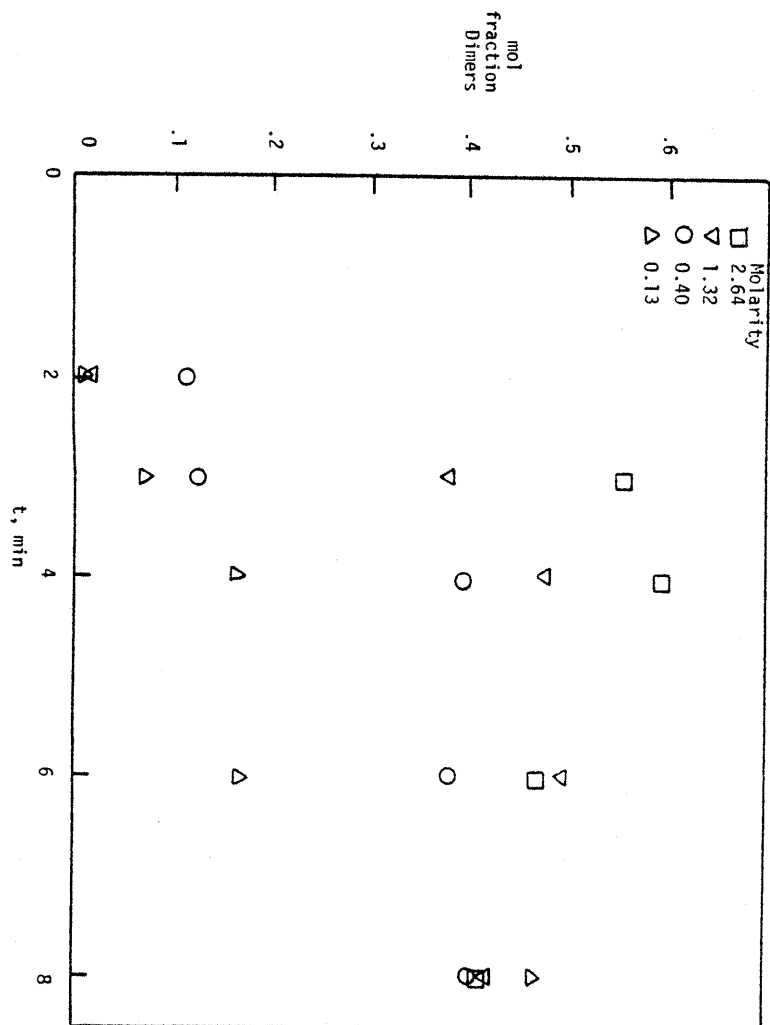


Figure 7.10.4 Variation of product mol fraction with initial cinnamaldehyde concentration. a) Dimers

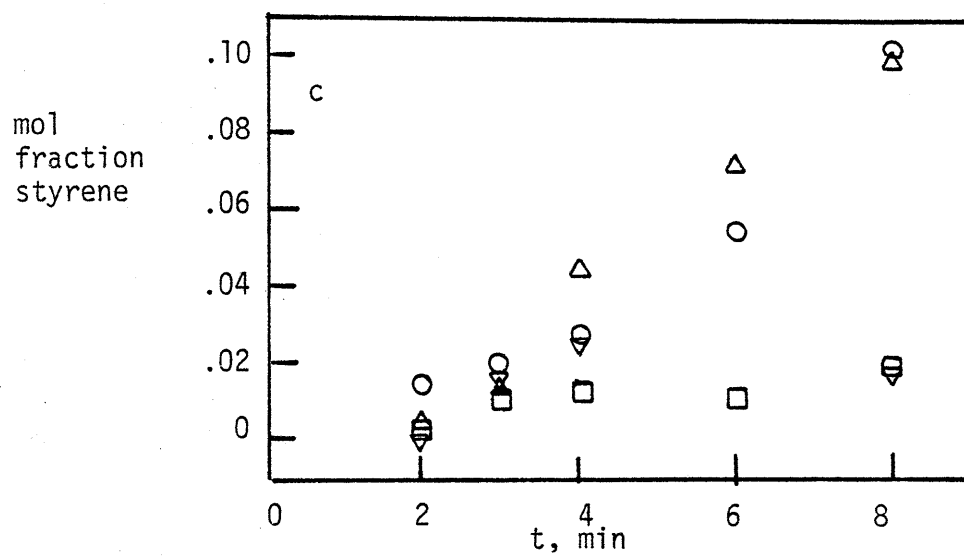
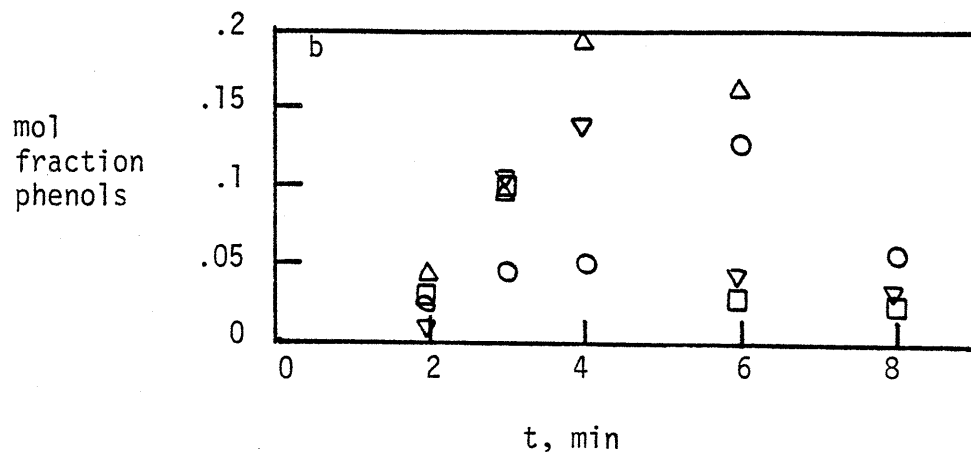
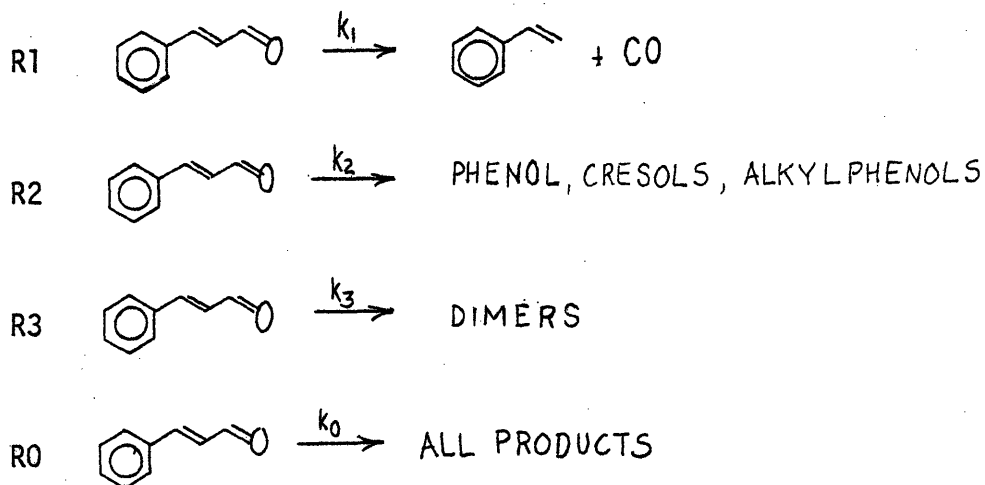


Figure 7.10.4 b) phenols and c) styrene

for  $(CAD_0)=2.64$  mol/l these were 0.47:0.025:0.011. These variations suggest that dimers may account for the second order component of (I), whereas styrene and phenol arise via a first order pathway.

Thus, the composition, low conversion product relationships, and initial concentration dependence of the cinnamaldehyde product spectra suggest the following major pyrolysis pathways:



where R0 is the sum R1-R3 plus all other minor primary degradation pathways. Further study of cinnamaldehyde pyrolysis at temperatures from 250-450C allowed the determination of the rate constants illustrated in Figure 7.10.5, an Arrhenius diagram. These rate constants are likely first order for R1 and R2, pseudo-first order for R3 and R0; the latter may be corrected to any true reaction order by noting the initial concentrations listed in Table 6.1. With regard to activation by temperature, Figure 7.10.5 reveals that dimers and phenols were favored by low-temperature pyrolysis, whereas styrene selectivity increased with temperature. These observations are reflected in the Arrhenius parameters for R1-R0, where styrene



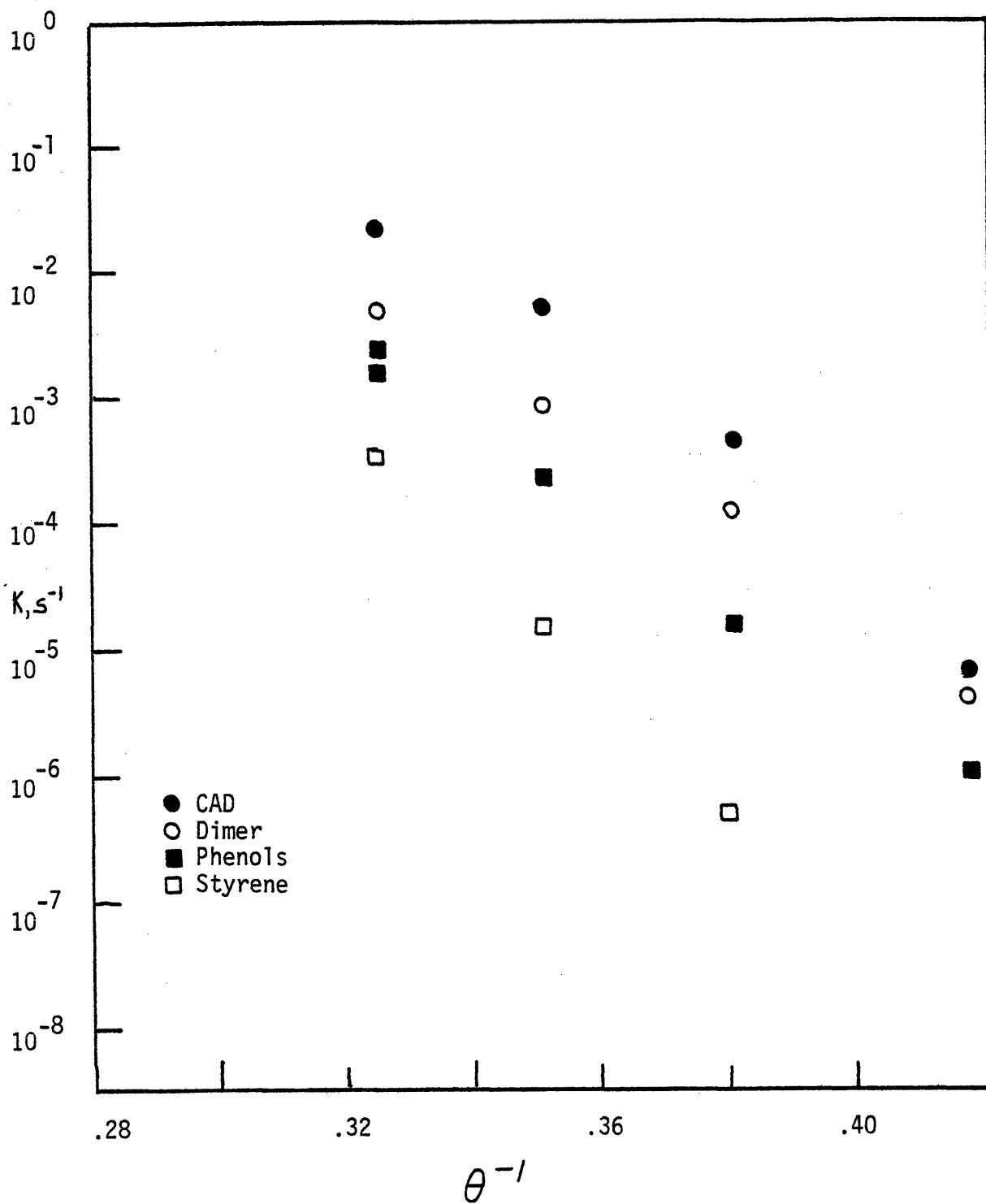
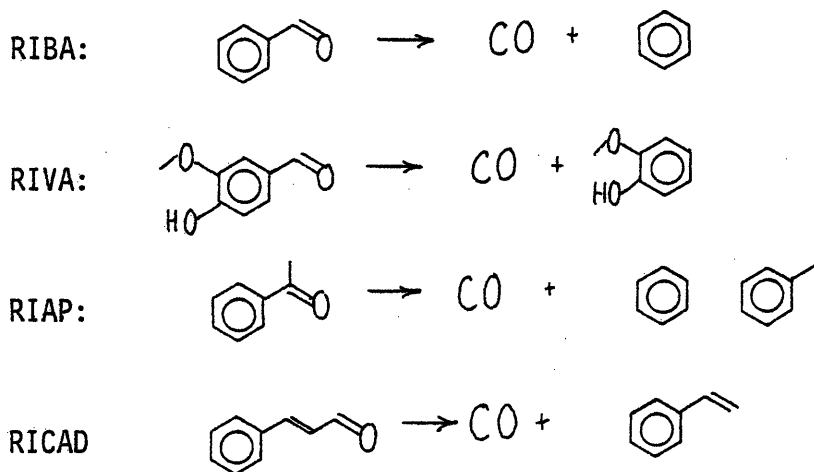


Figure 7.10.5 Arrhenius diagram for cinnamaldehyde pyrolysis.

formation was more activated than that of phenol and dimers by about 15 kcal/mol. Apparent first order Arrhenius parameters for R1, R2, R3 and R0 were  $(\log_{10}A(s^{-1}), E^*(kcal/mol)) = (12.1 \pm 0.4, 48.2 \pm 1.1)$ ,  $(8.5 \pm 0.4, 34.5 \pm 1.0)$ ,  $(8.6 \pm 1.4, 33.7 \pm 3.07)$ , and  $(9.7 \pm 1.7, 35.4 \pm 4.6)$ , respectively.

In summary, each carbonyl compound was found to release CO through pathways formally similar yet vastly different in rate. These were of type R1, namely,



No clear product relationships were established in acetophenone pyrolysis, yet the kinetic results suggest that CO and benzene are the most closely parallel products. Styrene and CO were generated from cinnamaldehyde pyrolysis in stoichiometric proportions at low conversions, the former apparently suffering secondary degradation at higher substrate conversions. The relative rates of these R1 decarbonylation pathways are illustrated in Figure 7.10.6, a comparative Arrhenius diagram. The most striking conclusion is that the rate of decarbonylation was significantly enhanced by

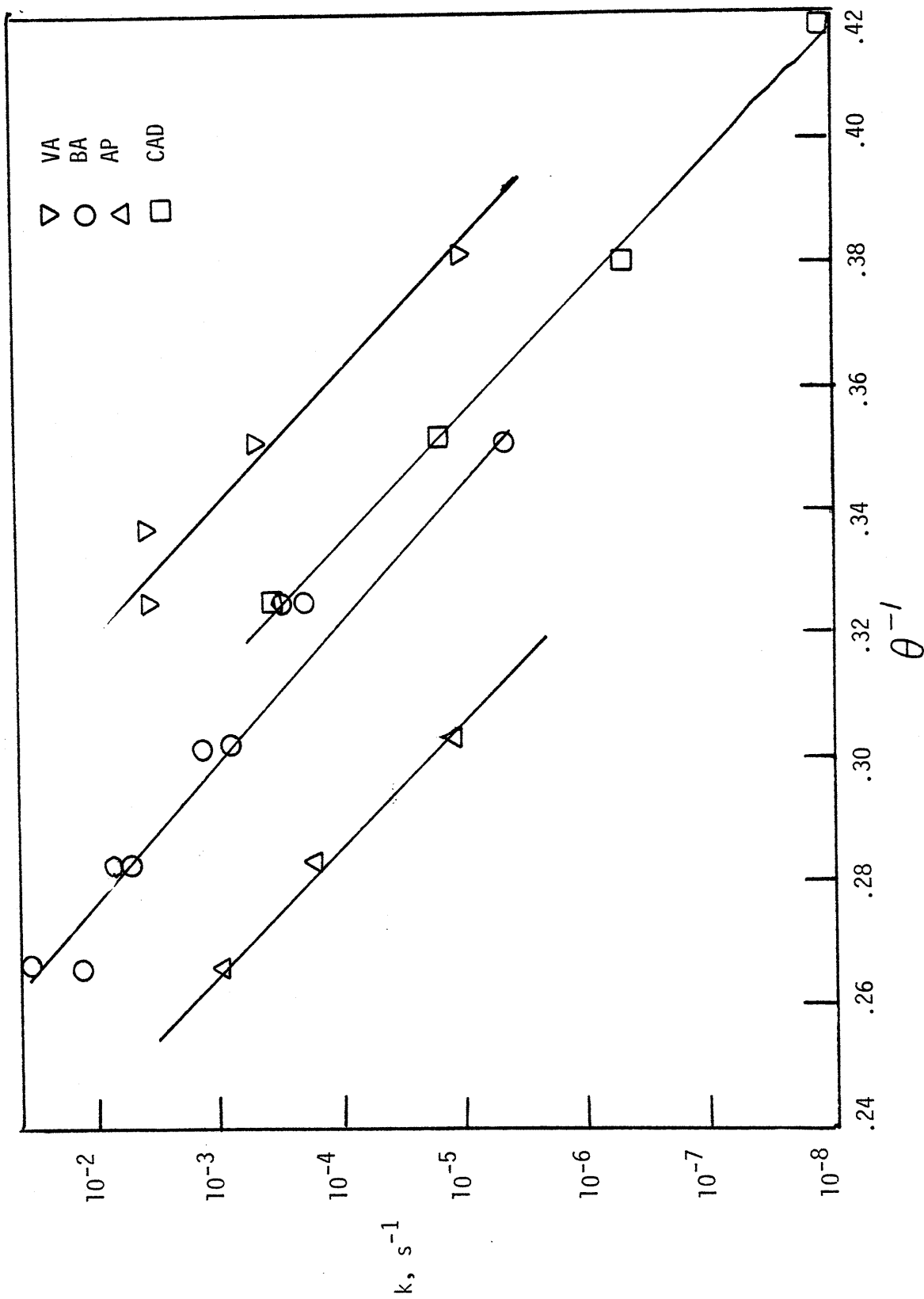


Figure 7.10.6 Arrhenius diagram for carbonyl R1 pathways, all carbonyls.

guaiacyl substitution (cf.BAVsVA), whereas the reaction was hindered by carbonyl methyl substitution (cf.BAVsAP). The more modest influence of cinnamaldehyde vinyl conjugation was to effect a slight rate increase as compared to benzaldehyde pyrolysis.

### 7.11 Cinnamyl Alcohol

The products from cinnamyl alcohol pyrolysis fall into one of four categories: a gas fraction, water soluble light liquids, monoaromatics, and a polymeric fraction. The gas phase products were dominated by CO, accompanied by lesser amounts of H<sub>2</sub>, CH<sub>4</sub>, and C<sub>2</sub>H<sub>4</sub>. Among the light liquids, water and methanol were prevalent, with smaller amounts of acetaldehyde, ethanol and formaldehyde. Cinnamaldehyde, styrene, allylbenzene, phenols and unreacted cinnamyl alcohol were the chief components of the monoaromatic fraction. Of these, cinnamaldehyde predominated, especially at low temperatures and conversions. Other compounds in this fraction were toluene, ethylbenzene and cresols. The final polymeric fraction included compounds of higher molecular weight which appeared to be at least dimers of cinnamyl alcohol or aldehyde.

The time evolution of the significant products is illustrated in Figure 7.11.1, where the product mol fraction is plotted as a function of reaction time for each temperature studied. Pyrolysis at 300C yielded chiefly dimers, cinnamaldehyde, water and phenols, with smaller amounts of CO and allylbenzene. Methanol and acetaldehyde mol fractions were small, of order 10<sup>-4</sup>-10<sup>-3</sup>. Styrene and lighter hydrocarbons were not detected at 300C. At 350C, the

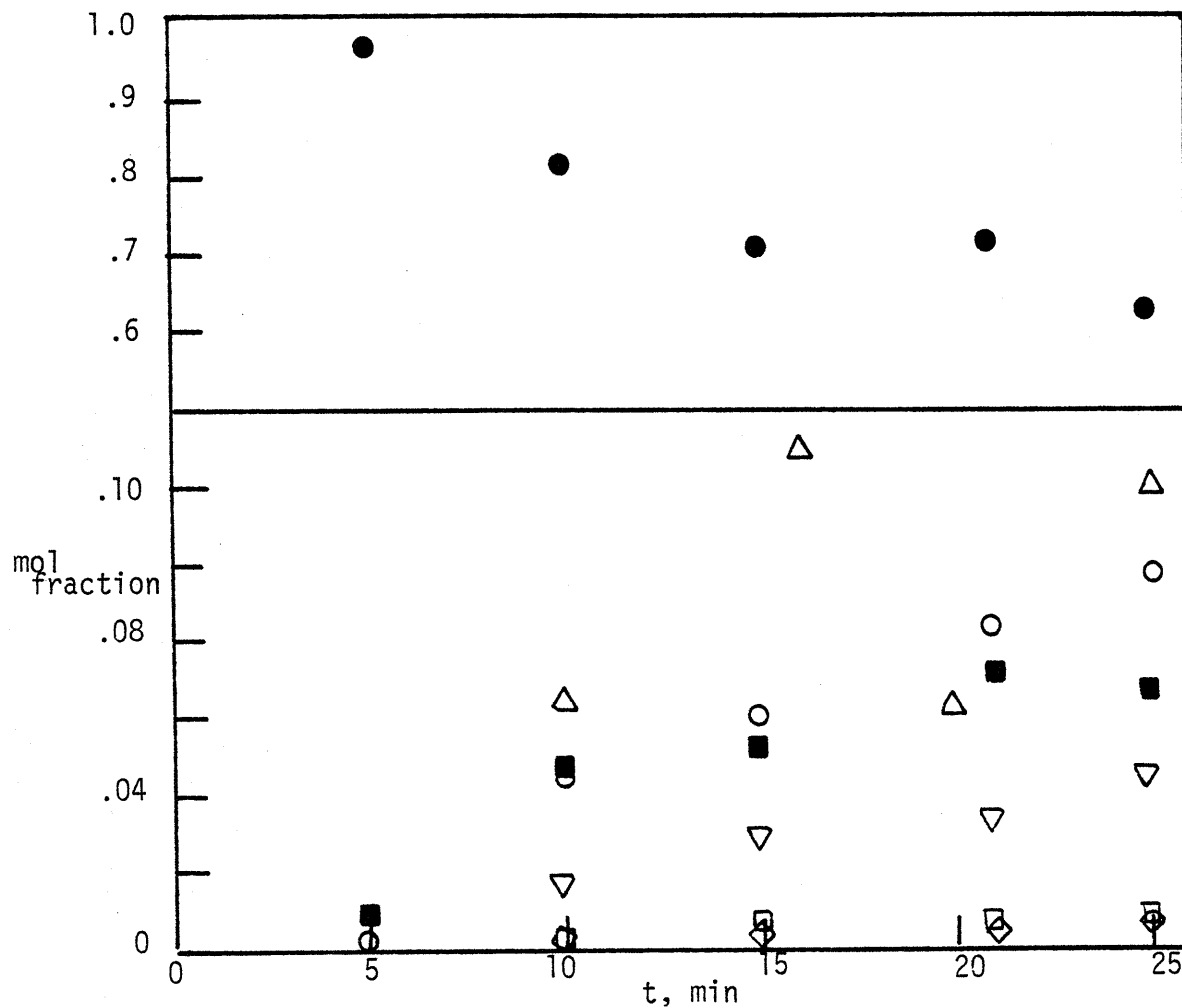


Figure 7.11.1 Cinnamyl alcohol pyrolysis product spectra  
a) 300 C.

- Cinnamyl alcohol
- Cinnamaldehyde
- △ Dimers
- ▽ Phenols
- Allylbenzene
- × Styrene
- Water
- ◇ Carbon Monoxide
- E Ethylbenzene
- T Toluene
- + MeOH

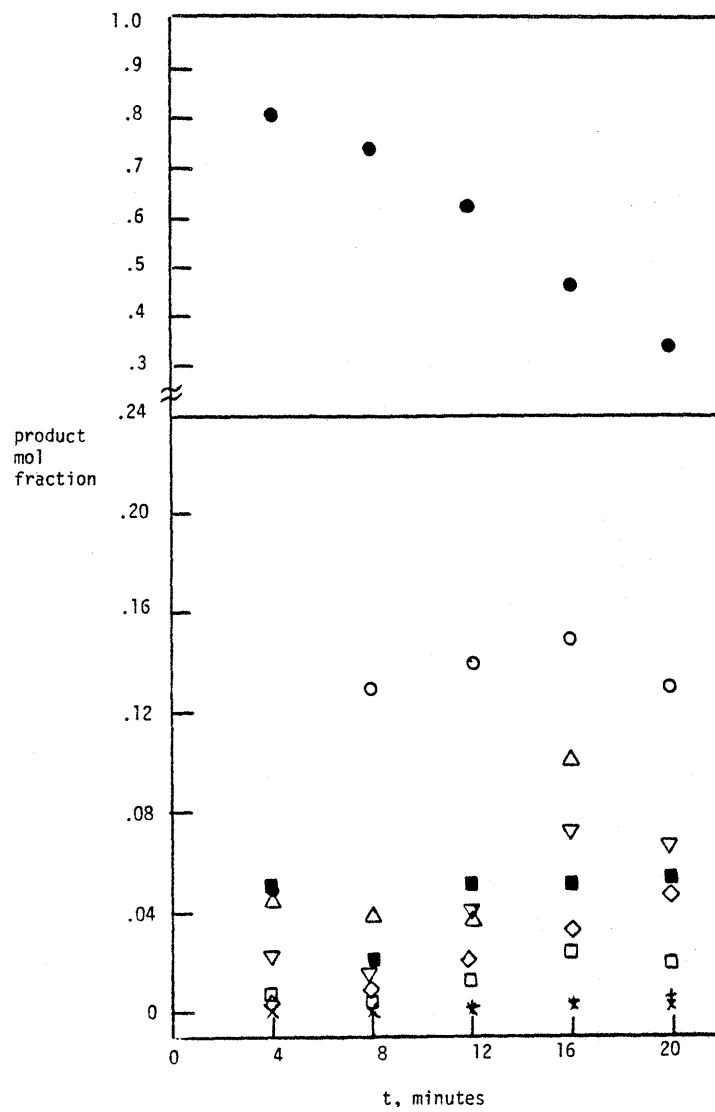


Figure 7.11.1b 350 C.

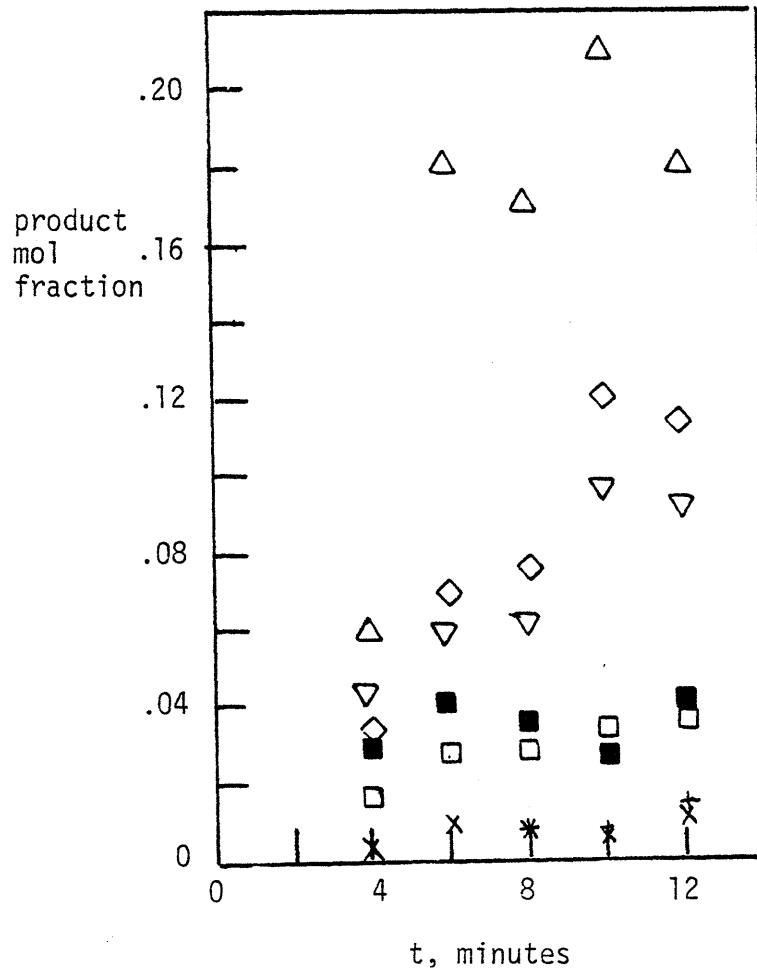
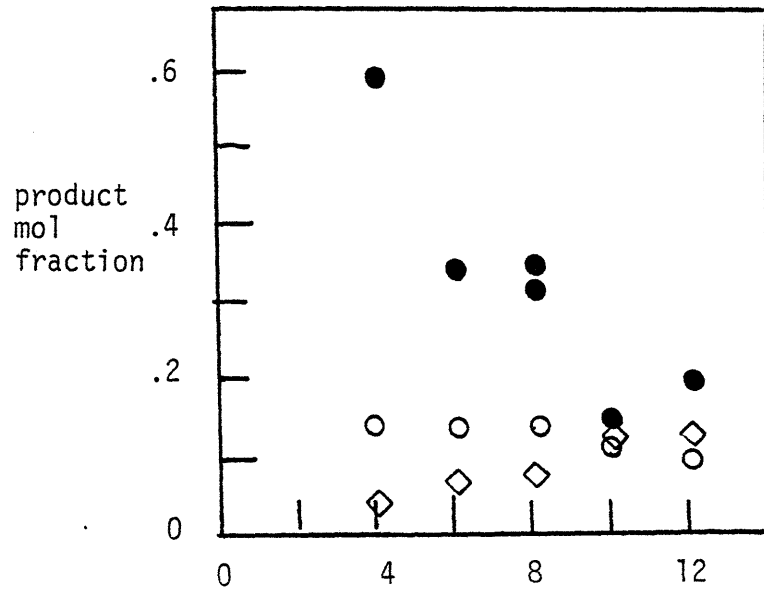


figure 7.11.1c T=400 C

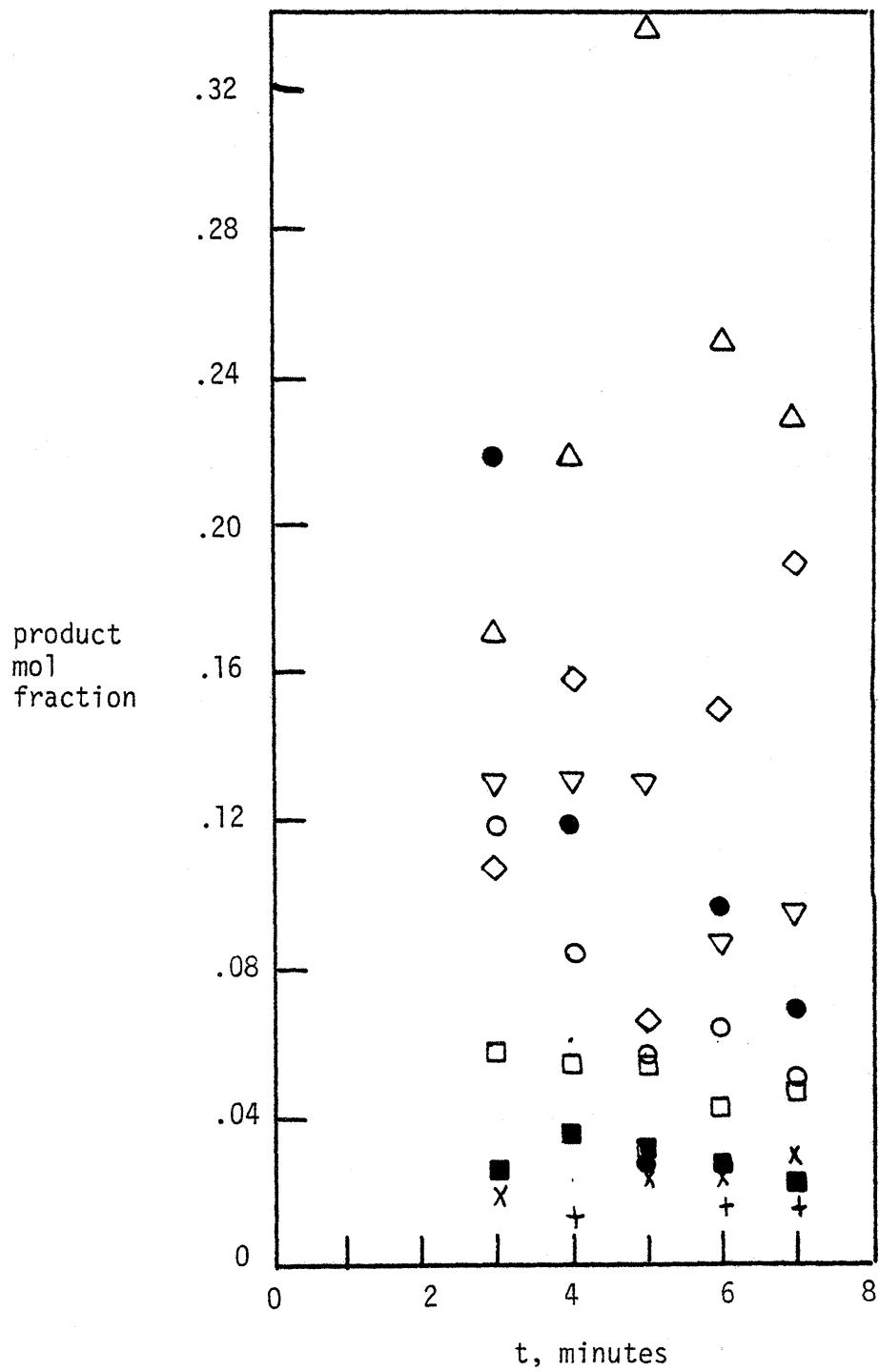


Figure 7.11.1d T=450 C.



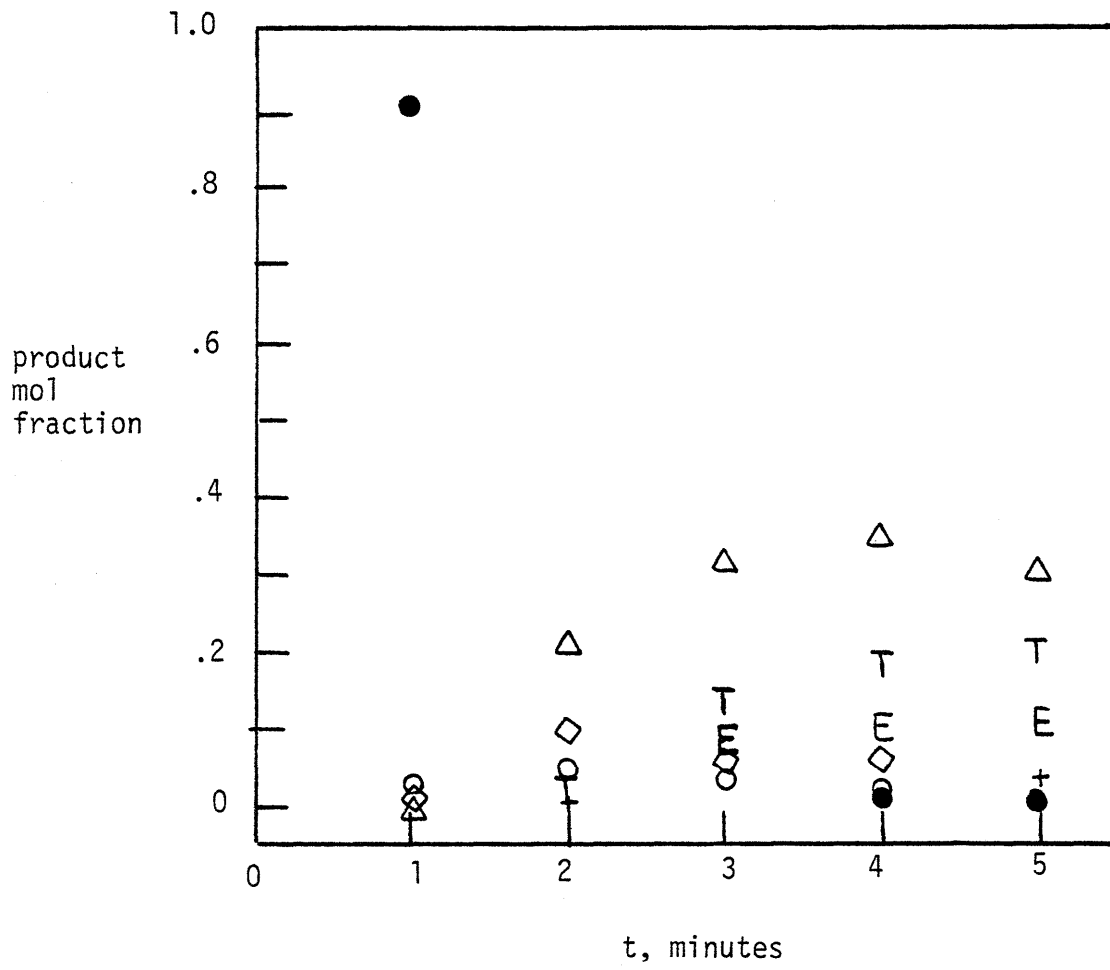


Figure 7.11.1e T=500 C

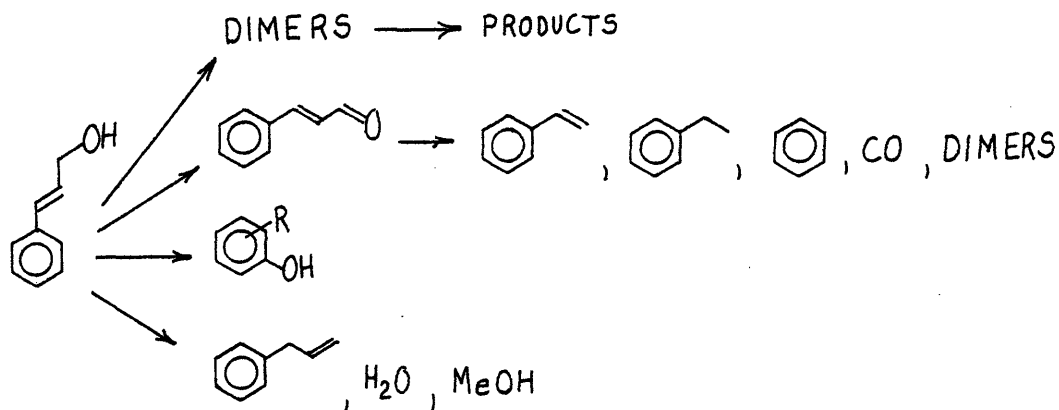
aforementioned products, styrene and larger amounts of CO were detected. A maximum in cinnamaldehyde concentration was observed at about 15 minutes holding time. The proportions of phenols, cresols, methanol and acetaldehyde were increased, however toluene and ethylbenzene remained undetected. By 400C, substantially larger amounts of CO, styrene, and phenols were produced, in addition to more modest yields of allylbenzene and methanol. Toluene and ethylbenzene were detected in small proportions at 400C; the yield of cinnamaldehyde was substantially reduced at this temperature.

Pyrolysis at 450C resulted in a complex product spectrum where each product was appreciable at low reaction times, with cinnamaldehyde and styrene proportions decreasing with increasing reaction times. Larger amounts of CO were produced, and the concentrations of toluene and ethylbenzene became pronounced. Cinnamyl alcohol pyrolysis at 500C was very rapid and yielded a product spectrum dominated by dimers, toluene and ethylbenzene, with smaller amounts of the additional products reported above.

In spite of the complexity of the product spectra, several generalizations regarding cinnamyl alcohol pyrolysis are possible. The lower temperature data suggest that dimers, cinnamaldehyde, phenols, allylbenzene, water and methanol were primary reaction products, whereas styrene, toluene, ethylbenzene and likely CO arose from secondary pyrolyses. The maximum in cinnamaldehyde proportions suggests that this compound serves as a precursor for CO, styrene, toluene, ethylbenzene, additional dimers and phenols; as previously

detailed in section 7.10, all of these products were observed from pyrolysis of cinnamaldehyde alone. It is further significant that water formation was modest at all temperatures and was not strongly activated with temperature. Thus, cinnamyl alcohol dehydrogenation appears far more significant than the competing dehydration. Methanol was in small but significant proportions at each temperature studied, realized in a maximal mol fraction approaching 0.04 at 500C. Finally, although detectable, acetaldehyde, formaldehyde, and ethanol were not substantial stable pyrolysis products.

Thus, the important cinnamyl alcohol pathways appear to be primary reactions to dimers, cinnamaldehyde, phenols, water and methanol, attended by secondary reactions of the dimers and cinnamaldehyde. The reaction network is likely of the type:



The complexity of the cinnamyl alcohol product spectra has thus far precluded the unequivocal delineation of product relationships and pathway stoichiometries. Thus, apparent pseudo-first order rate constants for the initial rates of formation of dimers, cinnamaldehyde, phenols, water and methanols, as well as overall substrate disappearance,

were estimated for conditions of low substrate conversion from 300-400C. Above 400C, rapid secondary pyrolyses precluded estimation of these save overall substrate, water and methanol. These results are depicted in Appendix 7.2 and Figure 7.11.2, the latter an Arrhenius diagram. Referring to Figure 7.11.2, it is clear that dimer and aldehyde formation were the favored alcohol degradation pathways. Phenol production was intermediate in overall rate, with water and methanol formation least rapid. Methanol formation was generally at least two orders of magnitude slower in rate than overall alcohol decomposition. Water formation was very uncertain, as a low temperature curvature was observed in the Arrhenius diagram. The magnitude of water formation was experimentally reproducible subject to considerable variations in analytical methods, and is considered real. The low temperature curvature is likely due to equilibrium or other more complex kinetic effects, but as yet is obviously not unequivocally explained.

#### 7.12 Orthohydroxydiphenylmethane (OHD)

Pyrolysis of OHD resulted in relatively simple yet highly temperature and conversion dependent product spectra. Phenol, toluene, and apparent triaromatic sesquimers were the major products, with smaller amounts of benzene, diphenylmethane, phenylphenol and other diphenyl-ethers and alkanes detected. These latter products were generally at least an order of magnitude smaller than the former three. The apparent sesquimer was not unequivocally identified but eluted in the vicinity of other triphenylalkanes on the GC trace. The GC peak was thus treated as an unidentified compound with response factor equal to that of

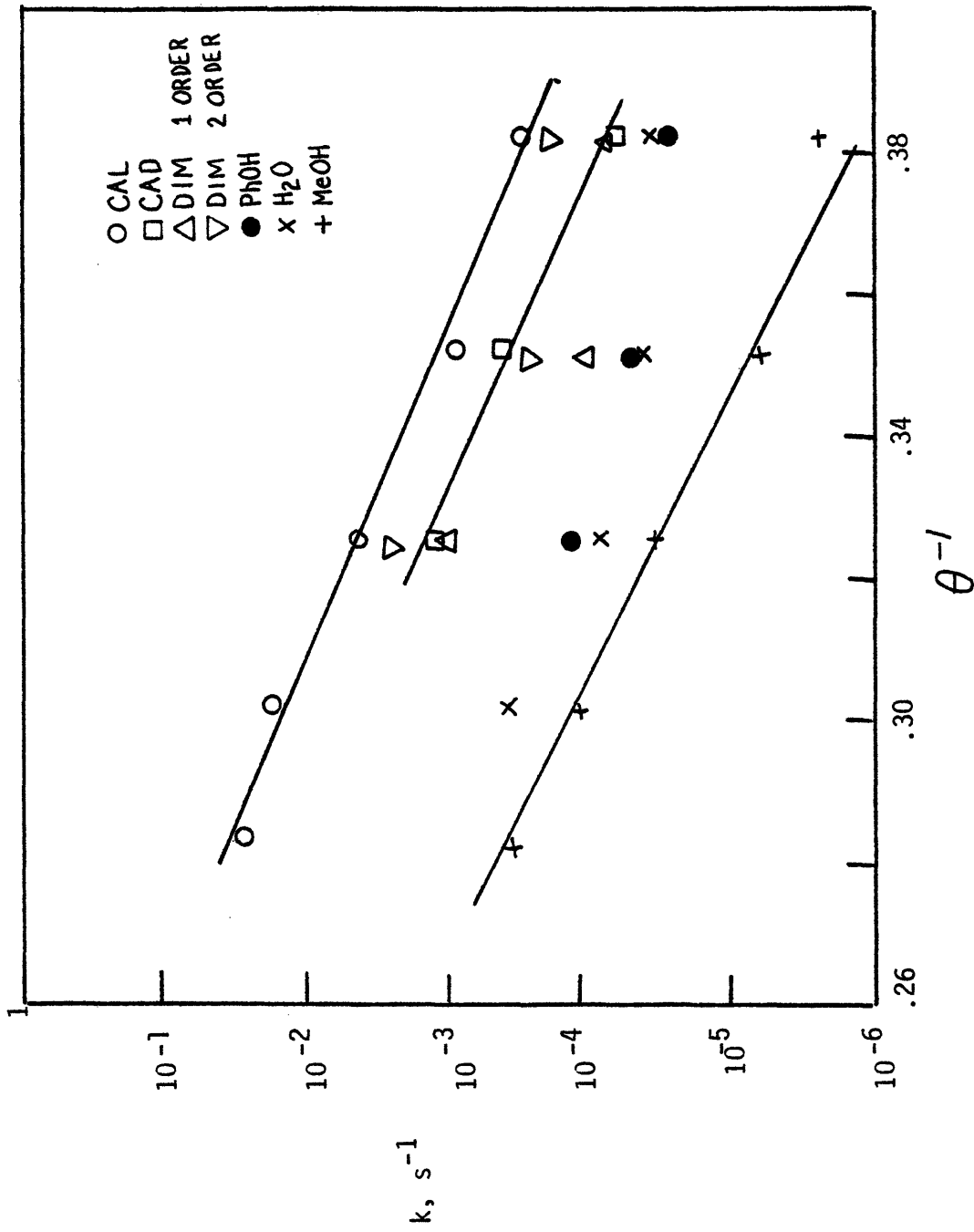


Figure 7.11.2 Arrhenius diagram for cinnamyl alcohol pyrolysis.

other calibrated phenyl alkanes.

The time evolution of the major products from pyrolysis at 400, 450, 500 and 550C is depicted in Figure 7.12.1. At 400C, the primary products were phenol and sesquimer, with smaller amounts of toluene and diphenylmethane detected. The latter products arose with zero initial rate. At 450C, phenol and sesquimers were again predominant, with toluene formation appreciable by five minutes holding time. Toluene again appeared with zero initial rate, and the sesquimer mol fraction approached a maximum value of about 0.075. By 500C, OHD pyrolysis resulted in virtual stoichiometric appearance of toluene and phenol, with small amounts of sesquimer, diphenylmethane and other products observed. In fact, the proportion of sesquimer steadily decreased with increasing pyrolysis holding time. Pyrolysis at 550C resulted in comparable formation of toluene and phenol as major products, the former slightly larger in proportion than the latter. A complex spectrum of diphenylmethane, sesquimers, benzene and other aromatic arose in proportions far less than the toluene and phenol.

The uncertainty of the chemical structures of the sesquimer and other smaller aromatic and larger polymeric products precluded the unequivocal determination of product relationships, stoichiometry, and atom material balances, notably hydrogen. However, rather firm generalizations and observations were apparent. Assimilation of the low temperature and high temperature product spectra suggests that phenol and sesquimers were primary OHD pyrolysis products, the latter degrading by secondary pathways to toluene. Thus, an OHD degradation pathway of the

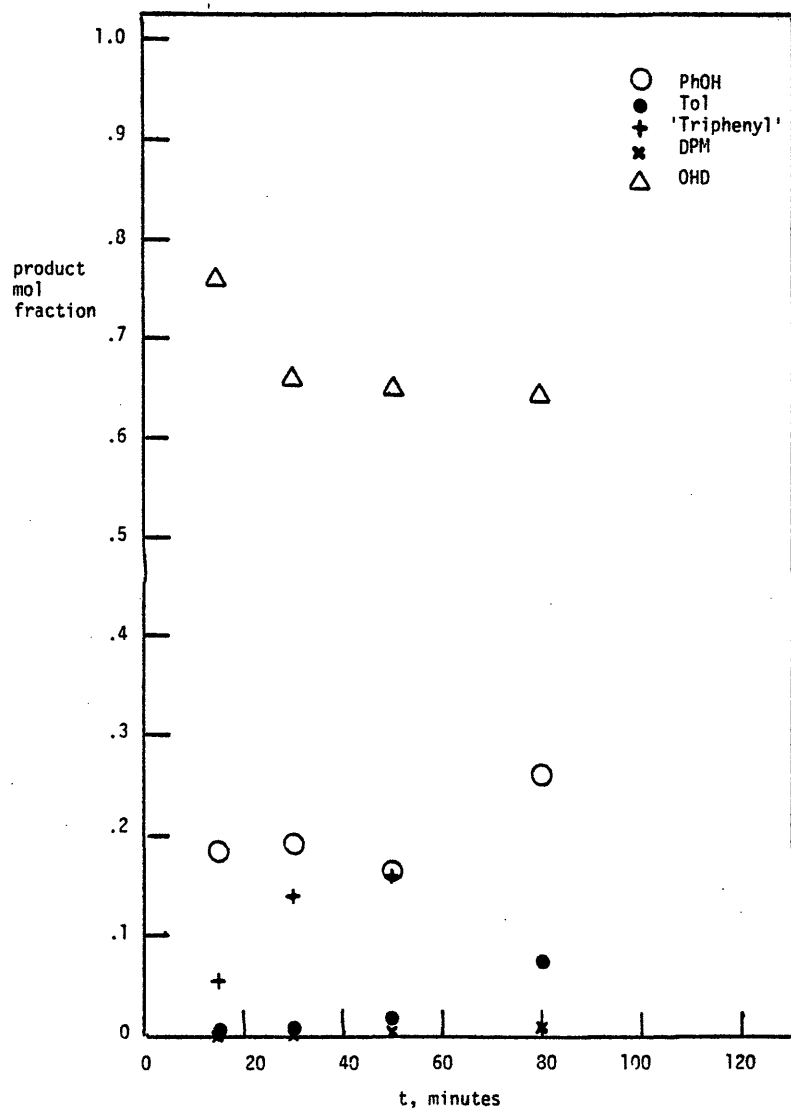


Figure 7.12.1 OHD pyrolysis product evolution a)T=400 C

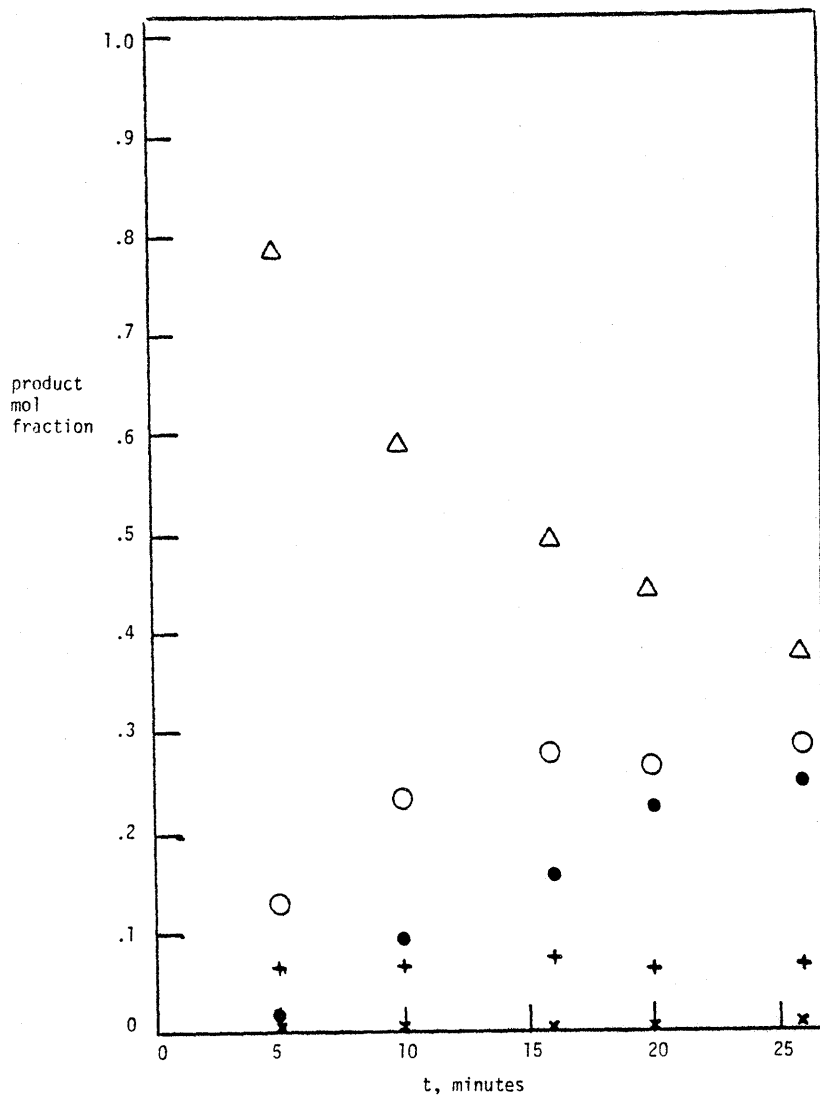


Figure 7.12.1b T=450 C



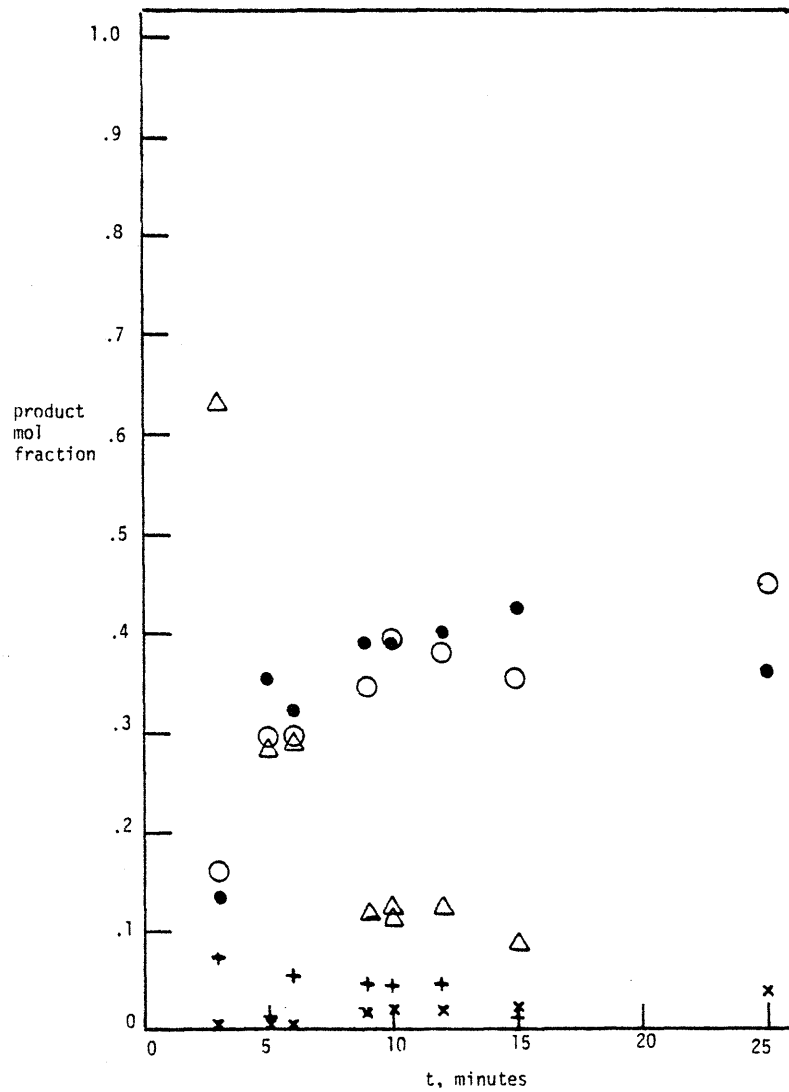


Figure 7.12.1c T=500 C

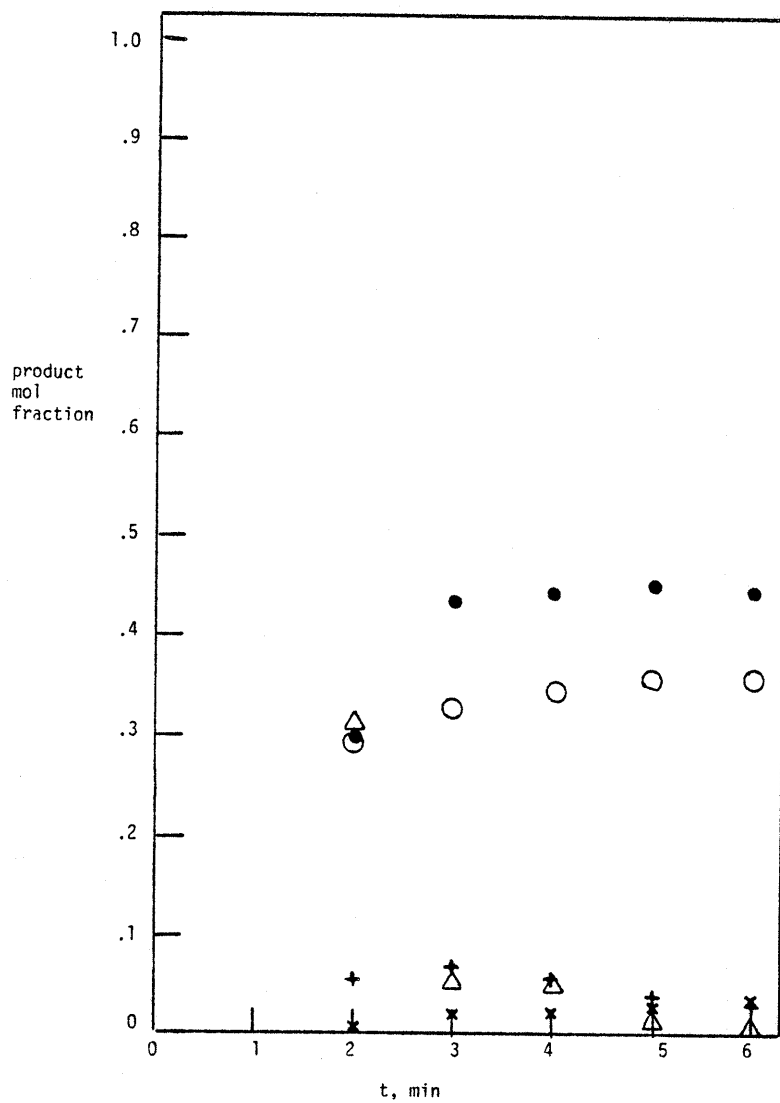
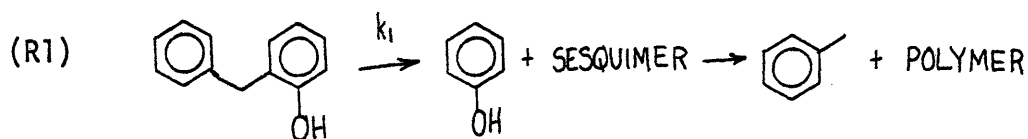


Figure 7.12.1d T=550 C

type R1 is suggested, namely:



The initial hydrogen balance was likely satisfied in the appearance of the hydrogen deficient sesquimer. As reflected in the product spectrum at 450C, the triphenyl sesquimer species was likely capable of further degradation to toluene and obscure polymeric species. Thus, while phenol was generated in a primary step, toluene was likely a secondary product; this explains the low ratio T/PhOH at low OHD conversion. That this ratio was strongly conversion dependent is demonstrated in Figure 7.12.2, where T/PhOH is plotted versus conversion for each temperature studied. Rather independent of temperature, this ratio increased as conversion decreased. Similar behavior has been observed in the pyrolysis of other diphenyl ethers<sup>165</sup>, where phenol was produced in greater quantities than the corresponding benzylic coproduct in neat pyrolysis.

Degradation of OHD was thus formally described by pathway R1, the kinetics of which obtained by monitoring the time dependence of the appearance of phenol and the disappearance of OHD. That is, since the OHD pyrolysis product spectra were dominated by compounds emanating from R1, overall OHD pyrolysis should be well described by phenol appearance. Hence, a plot of  $\ln(1+\text{PhOH}/\text{OHD})$  versus time should have slope  $k_1$ . Analysis in this manner at each pyrolysis temperature yielded the rate data shown in Figure 7.12.3, an Arrhenius diagram.

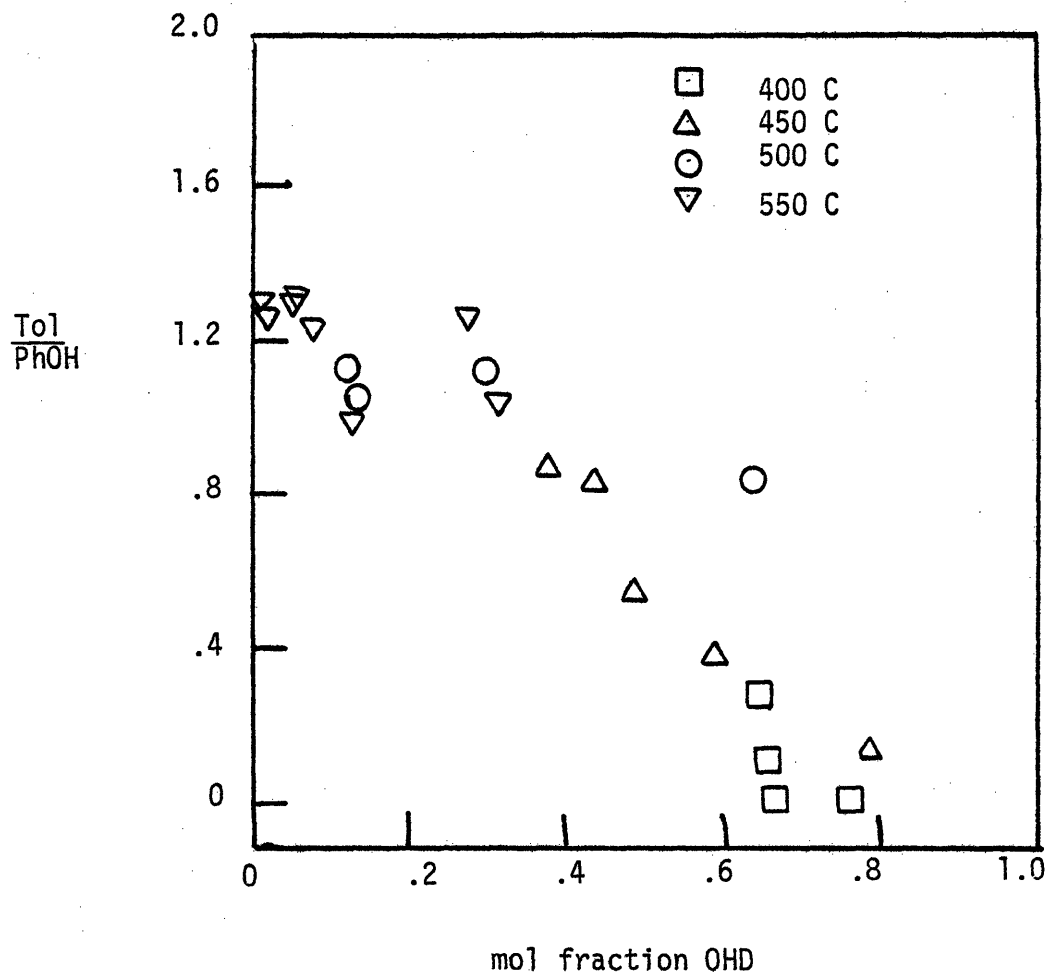


Figure 7.12.2 Product relationships in OHD pyrolysis

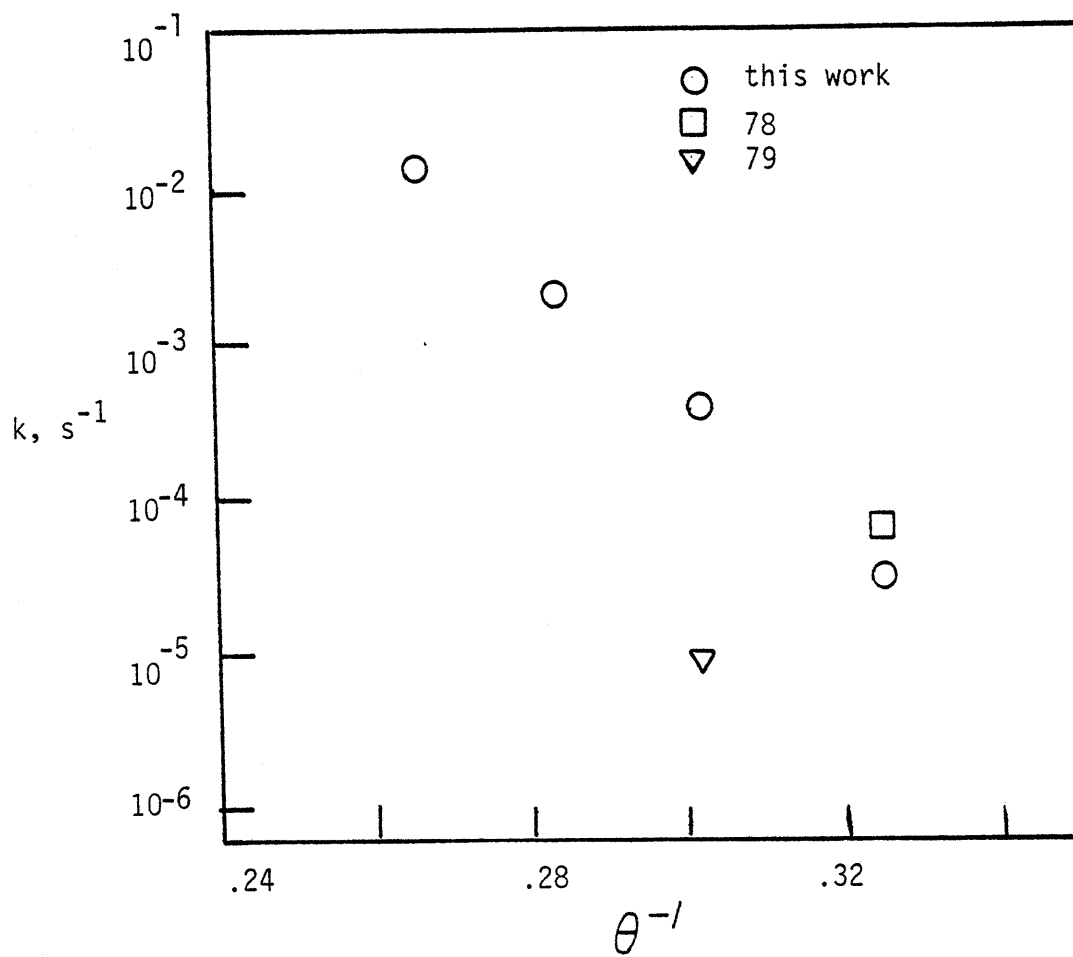


Figure 7.12.3 Arrhenius diagram for OHD pyrolysis

It is evident that  $\log_{10}k_1$  decreased linearly with increasing  $\theta^{-1}$ , the best fit Arrhenius parameters equalling  $(\log_{10}A(s^{-1}), E^*(kcal/mol)) = (9.6 \pm 0.4, 43.4 \pm 1.4)$ . For comparison, the conversion data of Benjamin, et al.<sup>78</sup>, for pyrolysis of OHD in tetralin at 400C are reported in Figure 7.12.3 as well. This apparent first order rate constant is in substantial agreement with the present results. In contrast, a diphenylmethane pyrolysis at 450C<sup>79</sup> yielded an apparent first order rate constant almost two orders of magnitude slower than that for OHD at the same temperature.

### 7.13 Phenyl Ether

The pyrolysis of phenyl ether from 500-587C yielded phenol, benzene and apparent triphenyl sesquimers as major products; pyrolysis at 400 and 450C effected no substrate conversion. The time evolution of the major pyrolysis products is depicted in Figure 7.13.1, where the mol fraction of each product is plotted as a function of holding time for each temperature studied. At 500C, only phenol and sesquimers were detected, with the ratio PhOH/TRIPHENYL  $\sim 3$  for pyrolysis to 150 minutes; benzene was notably absent. However, by 550C, the products arose in the proportions PhOH:PhH:TRI::5.3:3.0:1 at 100 minutes, although benzene was detected only in excess of 40 minutes. Pyrolysis at 570 and 587C were similar, with PhOH:PhH:TRI  $\sim 4:2:1$  at each temperature. The ratio PhH/PhOH was a strong function of phenyl ether conversion, as depicted in Figure 7.13.2, a plot of PhH/PhOH versus ether mol fraction. For each temperature studied, PhH/PhOH was essentially zero at low conversions

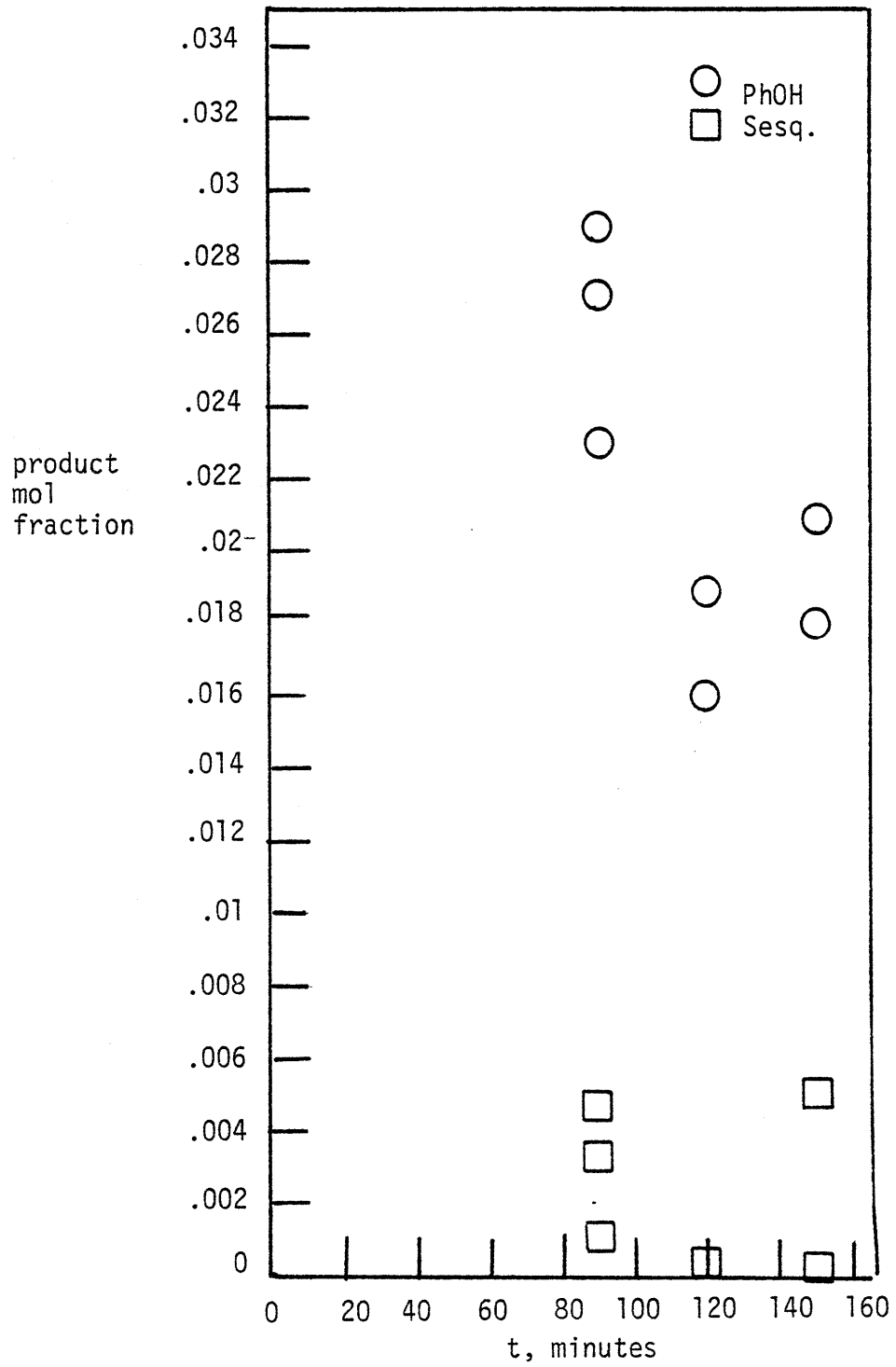


Figure 7.13.1 Phenyl ether pyrolysis  
product spectra  
a) T=500 C

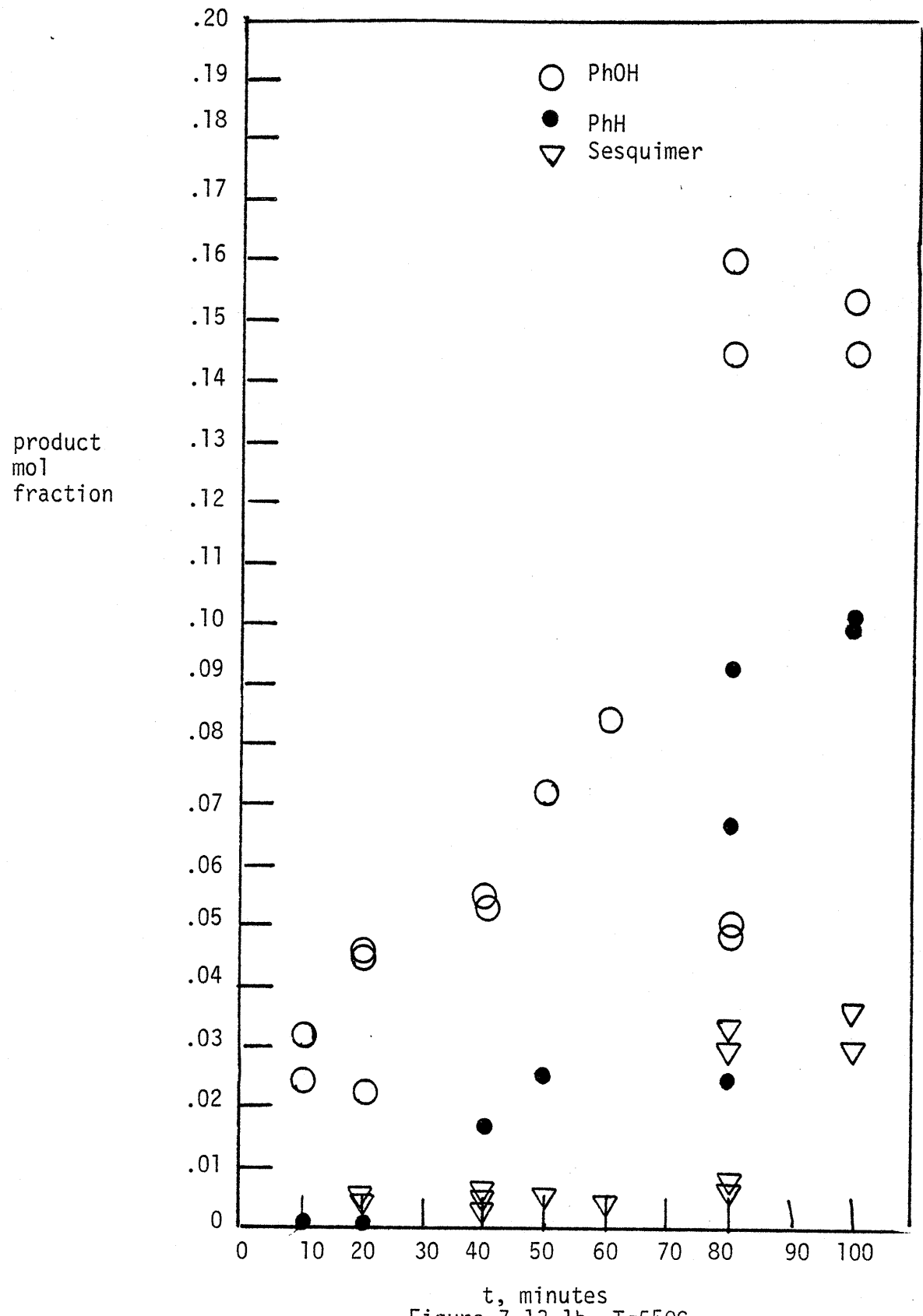


Figure 7.13.1b T=550C



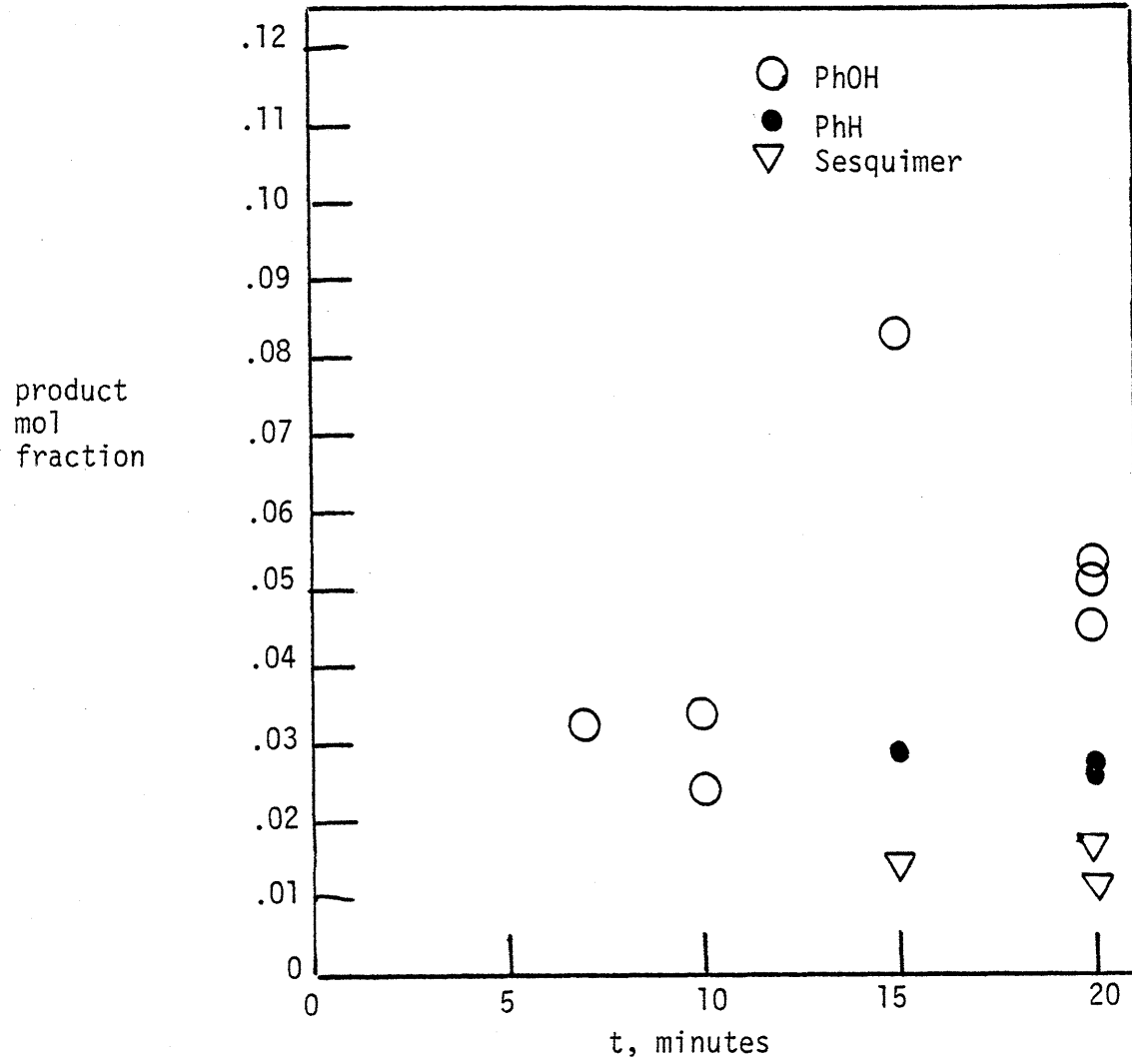


Figure 7.13.1c T=570 C

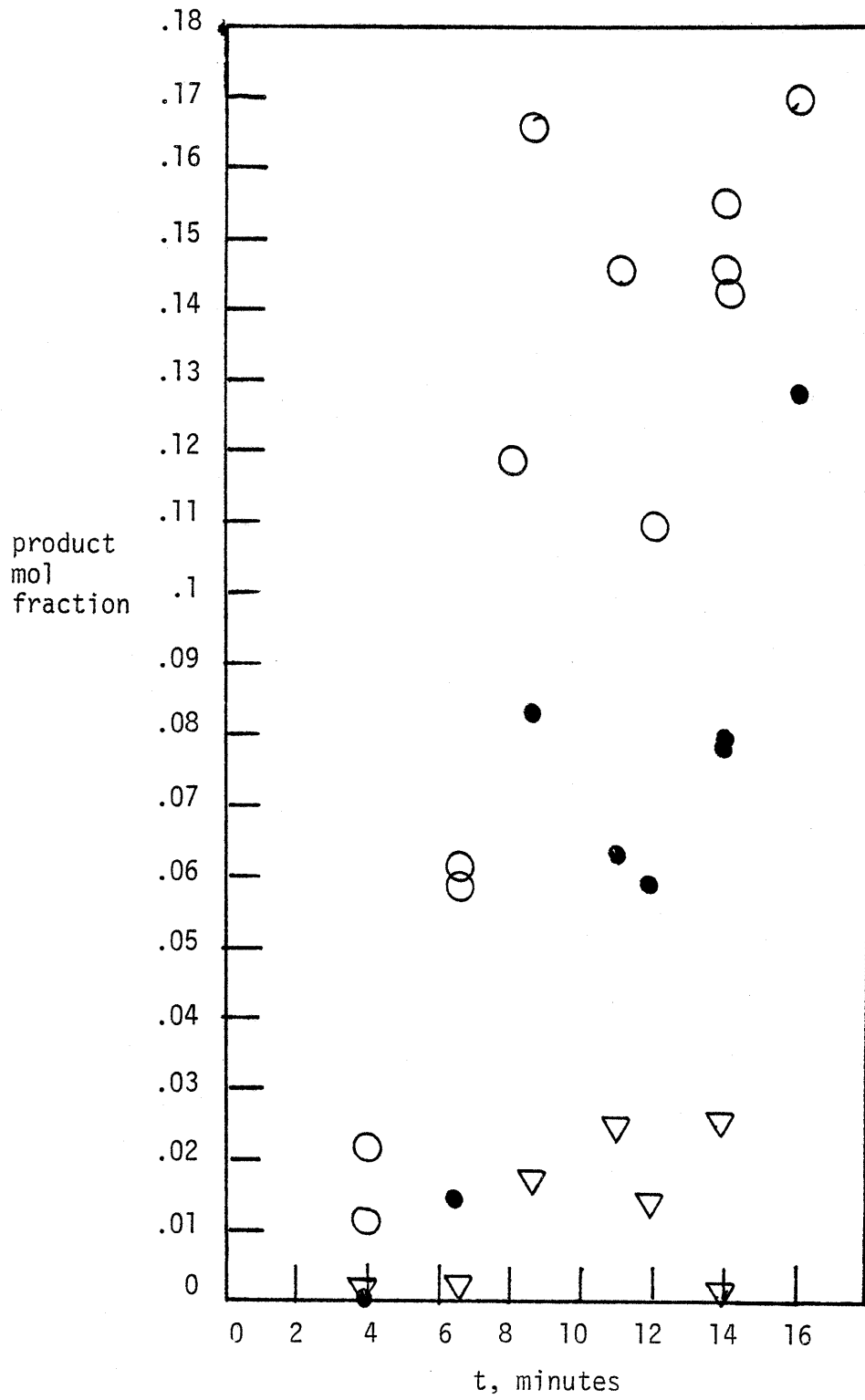


Figure 7.13.1d T=587 C

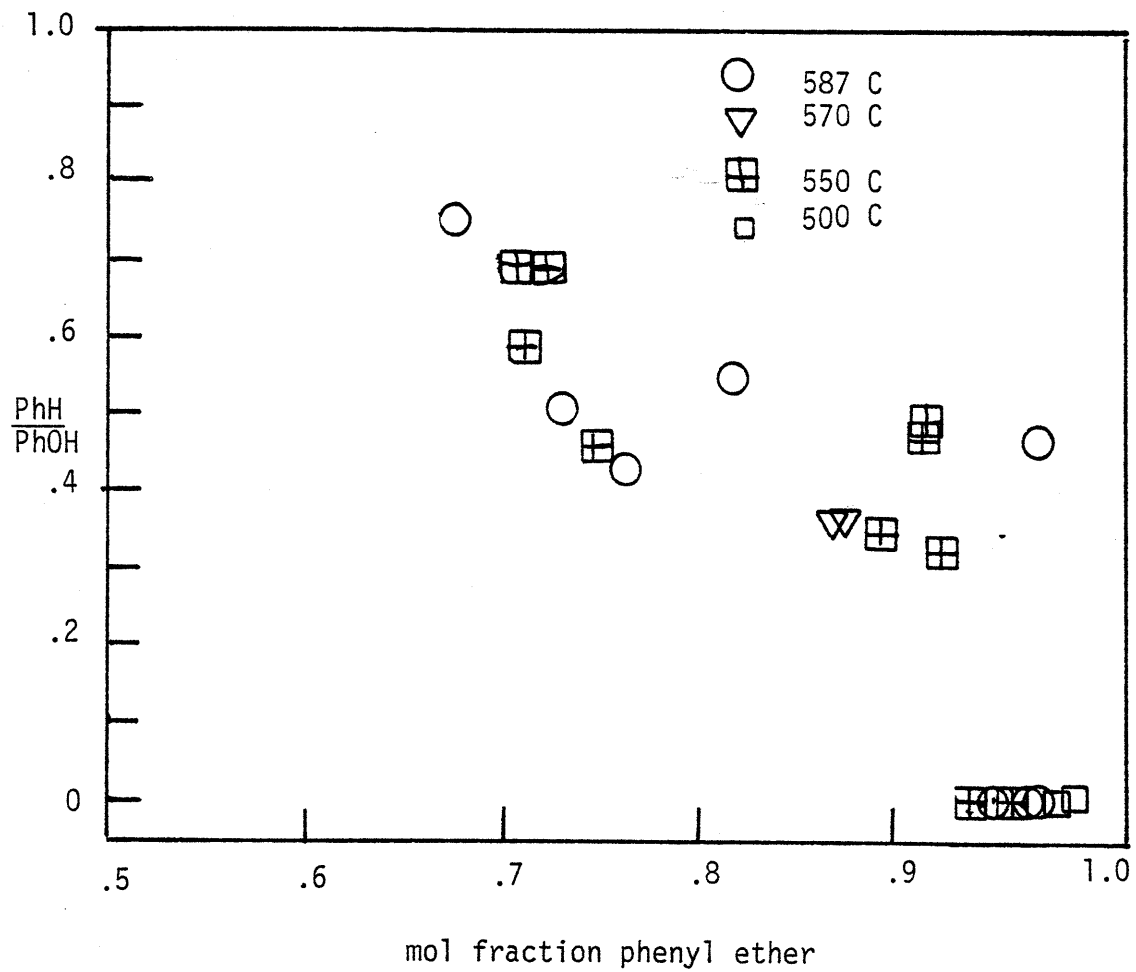
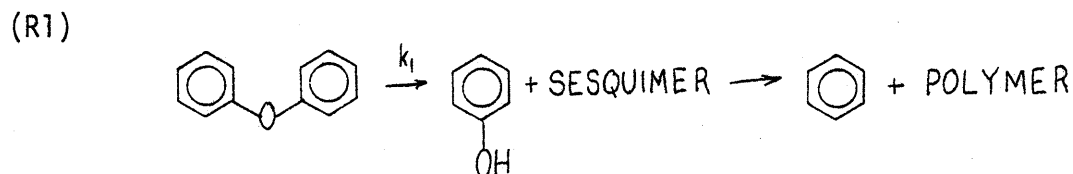


Figure 7.13.2 Product relationships in phenyl ether pyrolysis.

and approached unity at higher conversions. Experimental conversions of 0.3-0.6 were achieved, and the ratio PhH/PhOH reached 0.7.

Thus, phenylether pyrolysis would appear to proceed via primary degradation to phenol and sesquimers, the latter capable of secondary degradation to benzene and polymers. Thus, a pathway of the type R1 is suggested, where:



Pathway (R1) for phenyl ether pyrolysis is thus very similar to that previously proposed for OHD decomposition.

The kinetics of pathway (R1) were estimated by noting the time dependence of phenol appearance and ether disappearance. Thus, a plot of  $\ln(1+\text{PhOH/PE})$  versus time had slope  $k_1$  at each temperature studied. These data are depicted in Figure 7.13.3, an Arrhenius diagram. Figure 7.13.3 reflects the refractory nature of this ether. The best fit Arrhenius parameters were  $(\log_{10}A(\text{S}^{-1}), E^*(\text{kcal/mol})) = (14.8 \pm 1.3, 72.1 \pm 4.8)$ ; these compare favorably with those reported in the literature, notable  $E^* \sim 85 \text{kcal/mol}$ <sup>83</sup>.

#### 7.14 Biphenyl

Biphenyl was pyrolysed at temperatures from 400-587C, with only modest decomposition to benzene occurring at 587C. At this one temperature where degradation occurred, the time variation of benzene was used as a measure of the rate of biphenyl pyrolysis. Higher molecular weight materials, which were presumably formed to maintain hydrogen balance,

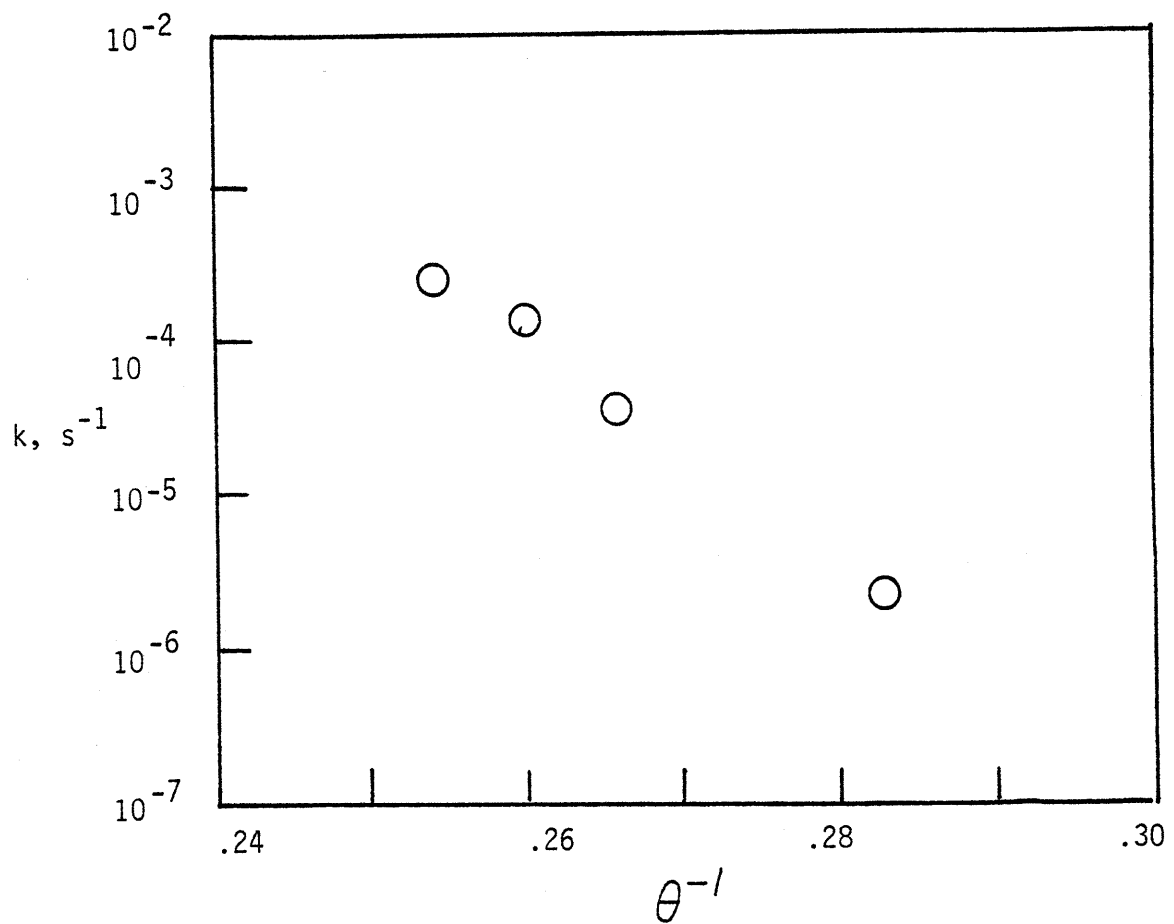


Figure 7.13.3 Arrhenius diagram for phenyl ether pyrolysis.

went undetected in the present analysis. The rate data are shown in Figure 7.14.1, and correspond to an apparent first order rate constant  $k=10^{-3.82} \text{ s}^{-1}$ .

### 7.15 Biphenol

Biphenol (o,o-dihydroxybiphenyl) was pyrolysed at 500C to a holding of 30 minutes. The compound was very stable, and no degradation to any light products could be discerned. Thus, pyrolysis to phenol, anticipated by analogy to biphenyl decomposition to benzene, did not occur for severity to 500C and 30 minutes holding time.

### 7.16 Cinnamic Acid

Pyrolysis of cinnamic acid over a temperature range of 300-400C resulted in production of  $\text{CO}_2$  and styrene as major products, with smaller amounts of toluene, ethylbenzene and dimers, which were generally two orders of magnitude smaller in concentration. For example, at 300C and 20 minutes holding time, T:EB:ST:CA:DIM = 0:0.00321:0.36:0.62:0, while at 400C and 4 minutes the proportions were 0.00892:0.049:0.457:0.453:0.027. The time evolution of cinnamic acid pyrolysis products is depicted in Figure 7.16.1, where each product yield is plotted versus reaction time for each temperature studied. As reflected in Figure 7.16.1a, styrene and  $\text{CO}_2$  were produced in stoichiometric proportions at 300C, where little toluene or ethylbenzene was detected. Higher temperature pyrolyses resulted in the production of  $\text{CO}_2$ , less than stoichiometric amounts of styrene, and toluene and ethylbenzene. The

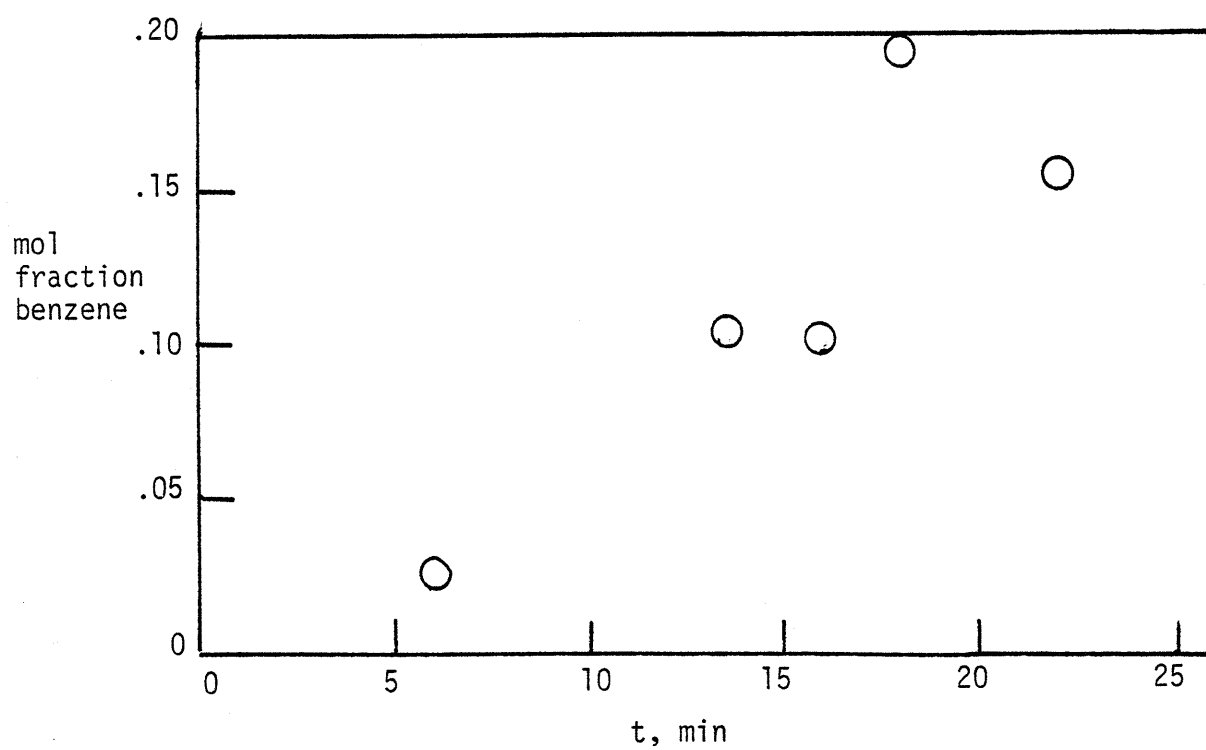


Figure 7.14.1 Benzene appearance from biphenyl pyrolysis at T=587 C.

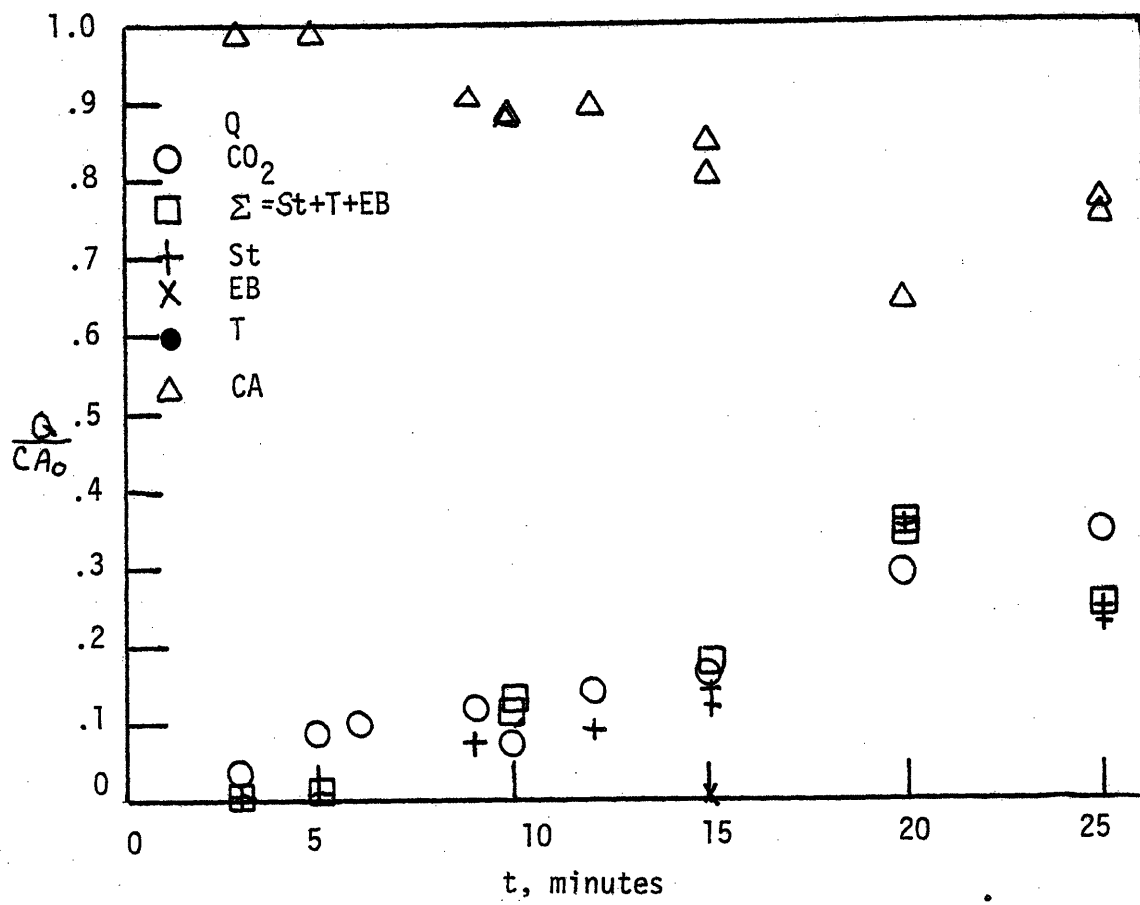
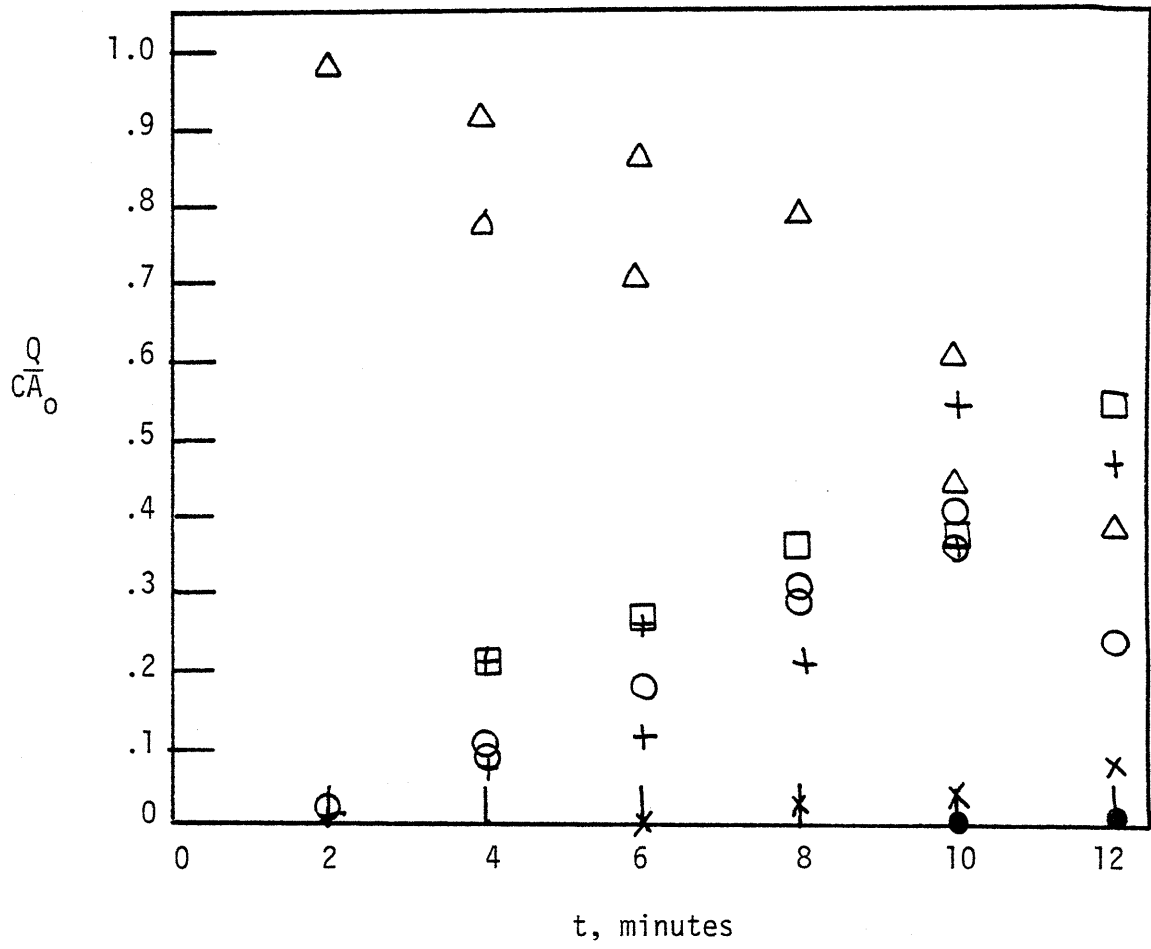


Figure 7.16.1 Product evolution from cinnamic acid pyrolysis.  
a)  $T = 300$  C.



Figure 7.16.1b  $T=350\text{ C}$

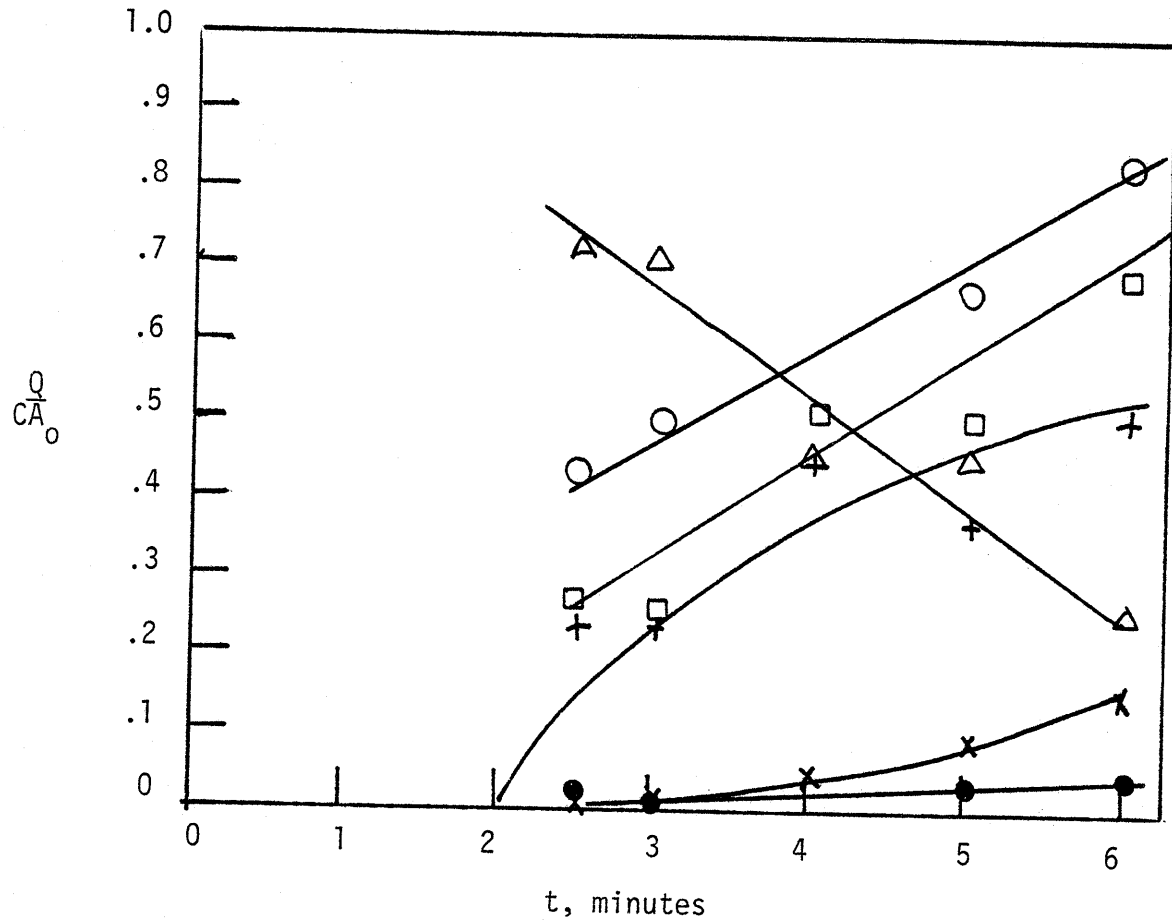
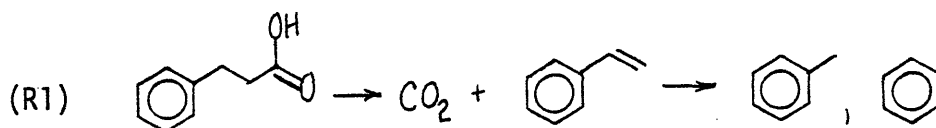


Figure 7.16.1c T=400 C

ratio  $\text{CO}_2/\text{styrene}$  increased with conversion. However, as illustrated in Figure 7.16.2a, the ratio  $\text{CO}_2/(\text{St}+\text{Tol}+\text{EB})$  was approximately unity at all conversions. Figure 7.16.2a depicts the  $\text{CO}_2$  yield as a function of the yield of light aromatics,  $\Sigma = \text{St}+\text{Tol}+\text{EB}$ . Thus, with regard to Figure 7.16.2a, the ratio  $\text{CO}_2/\Sigma$  was essentially unity for conversions from 0-70%. Further, each mol of decomposed acid yielded essentially one mol of  $\text{CO}_2$ , as evidenced in Figure 7.16.2b; the ratio  $\text{CO}_2/(\text{CA}_0 - \text{CA}) = 1.047 \pm 0.4$  for conversions from 0-70%. Also depicted in Figure 7.16.2b, the ratio  $\Sigma/(\text{CA}_0 - \text{CA})$  was substantially unity for the same range of conversions.

Thus, the major cinnamic acid pyrolysis pathway was evidently of the type R1, namely:



As was delineated for the pyrolysis of PPE and cinnamaldehyde, the styrene thus generated is evidently capable of secondary degradation to toluene and ethylbenzene.

The kinetics of reaction R1 were examined at 300, 350, and 400°C. An apparent first order rate constant for each temperature was estimated, based on the initial rates of styrene and  $\text{CO}_2$  appearance. The resulting rate constants,  $-\log_{10} k_1(300, 350, 400^\circ\text{C}) = (3.78, 3.06, 2.00)$  are plotted in Figure 7.16.3, an Arrhenius diagram; these correspond to Arrhenius parameters of  $(\log_{10} A(\text{s}^{-1}), E^*(\text{kcal/mol})) = (8.0 \pm 1.8, 31.0 \pm 5.0)$ .

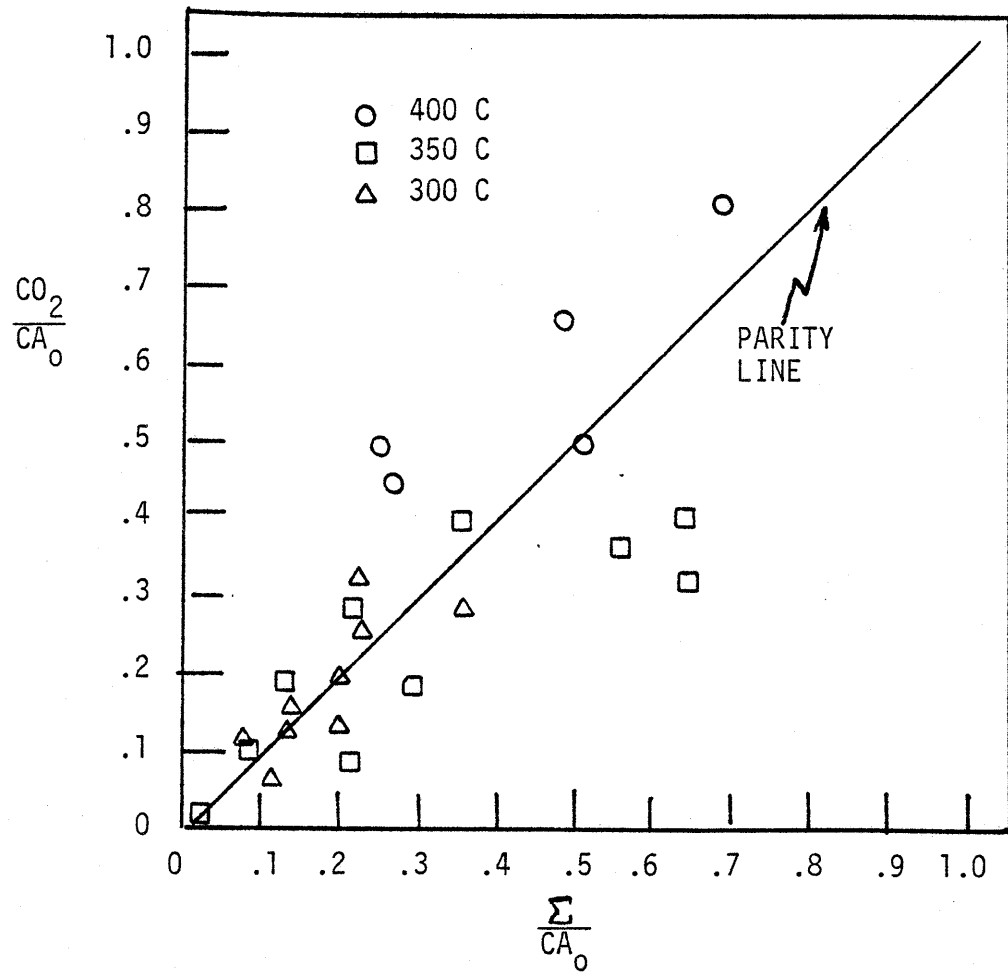


Figure 7.16.2 Product relationships in cinnamic acid pyrolysis.  
a)  $CO_2$  vs. St+T+EB

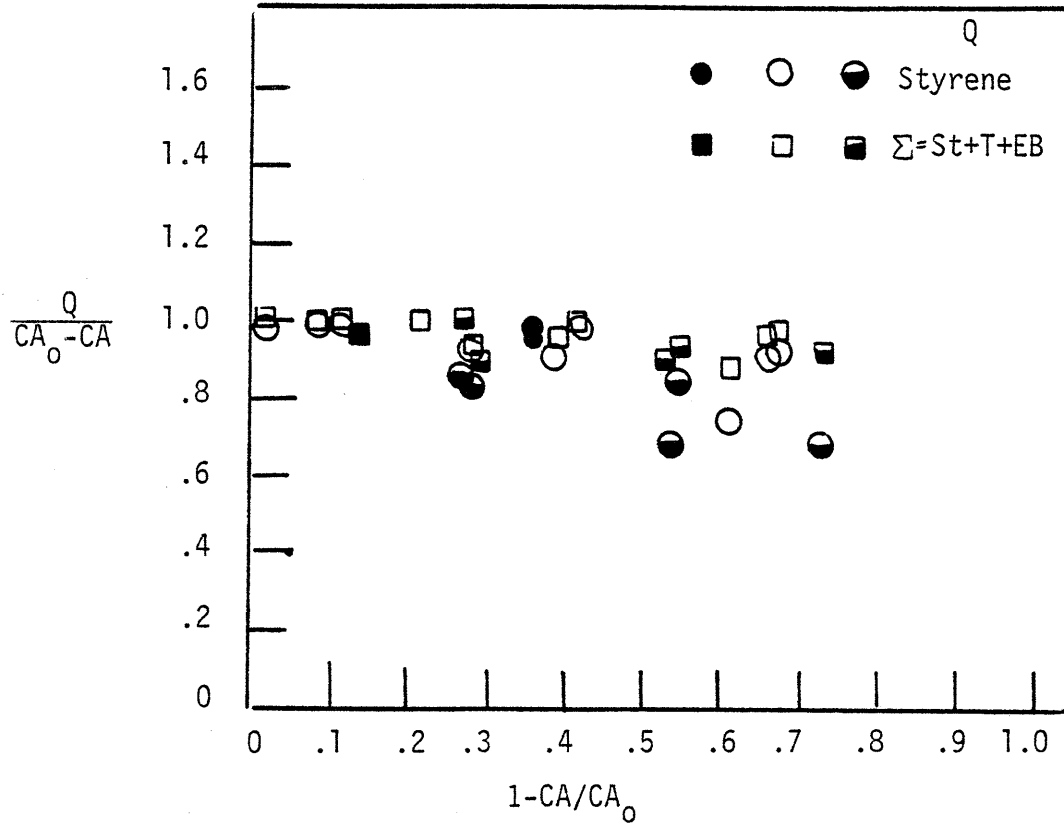


Figure 7.16.2 b) Product yields vs. conversion.

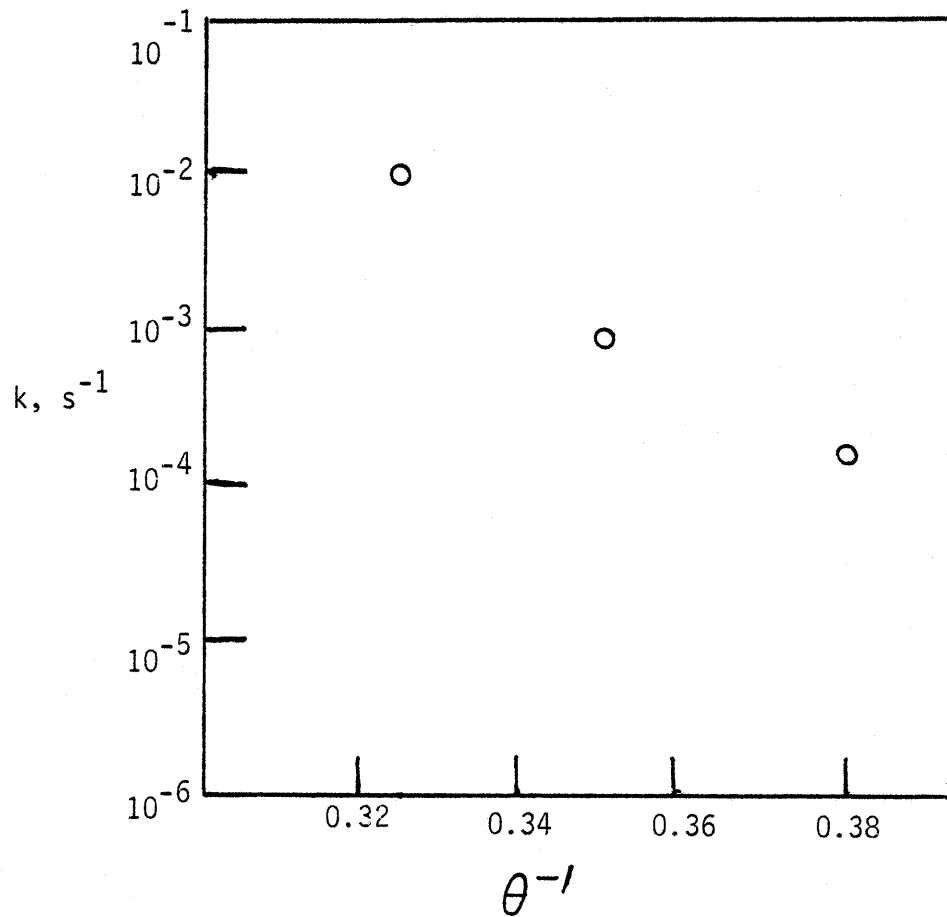


Figure 7.16.3 Arrhenius diagram for cinnamic acid pyrolysis.

### 7.17 Ferulic Acid

Pyrolyses of ferulic acid were effected from 200-350C. These experiments were aimed toward the further elucidation of the effect of guaiacyl substitution on 3-carbon side chain reactivity; the specific goal was to measure the effect of guaiacyl substitution on cinnamic acid decarboxylation propensity. As such, only gas phase analyses of CO<sub>2</sub> yield were performed. Figure 7.17.1 presents the CO<sub>2</sub> yield from ferulic acid pyrolysis as a function of reaction holding time at each temperature studied. For comparison, corresponding CO<sub>2</sub> yields from cinnamic acid pyrolysis are presented as well. As evidenced in Figure 7.17.1, initial rates of CO<sub>2</sub> release were much higher for ferulic acid than for cinnamic acid. This is most dramatic at 250C, where the CO<sub>2</sub> yield at five minutes holding time was about 30-40 times larger for ferulic acid. In fact, ferulic acid readily decarboxylated at 200C, where no reaction was observed for cinnamic acid; at 200C, ferulic acid pyrolysis was ~ 10 times as fast as that for cinnamic acid at 250C.

Apparent first order rate constants were estimated for ferulic acid decarboxylation by noting the initial rates of CO<sub>2</sub> formation. The resulting rate constants were  $\log_{10} k(250,300,350C) = (3.02, 2.60, 1.68)$ , and are presented in Figure 7.17.2, an Arrhenius diagram; the implied Arrhenius parameters arose as  $(\log_{10} A, E^*) = (5.2 \pm 2.0, 19.8 \pm 5.2)$ . Hence, as was true in comparison of vanillin and benzaldehyde decarbonylation, guaiacyl substitution evidently enhanced cinnamic acid decarboxylation.

### 7.18 Napthoic Acids

Further study of CO<sub>2</sub> evolution from lignin and lignite model precursors

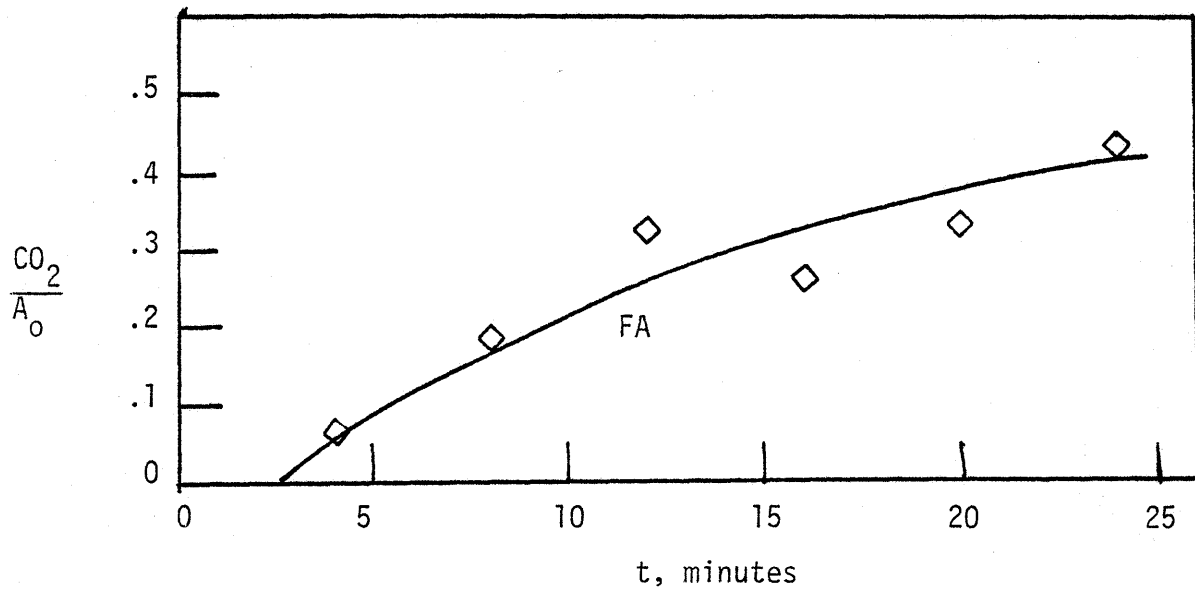


Figure 7.17.1 CO<sub>2</sub> evolution in ferulic acid pyrolysis  
a) T=200 C



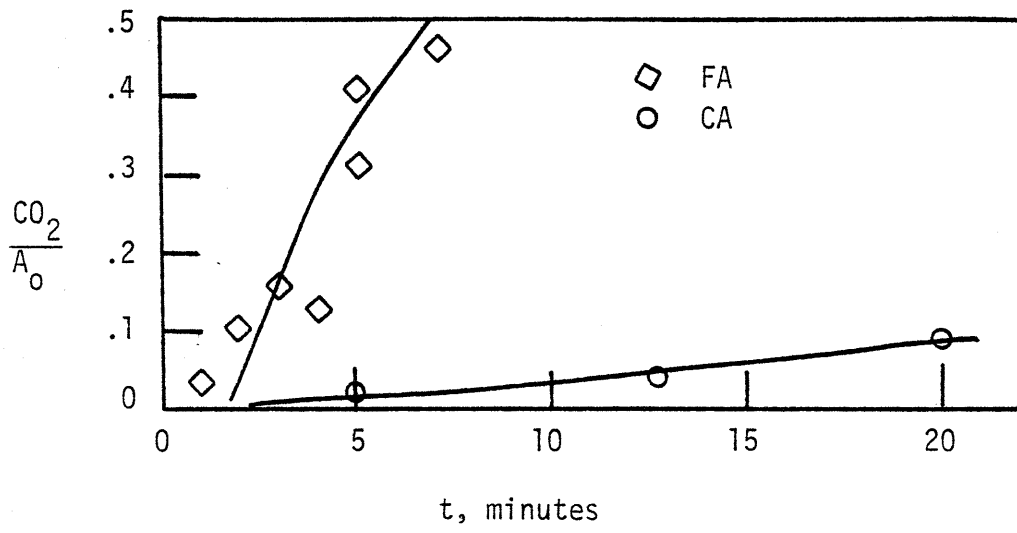


Figure 7.17.1b T=250 C

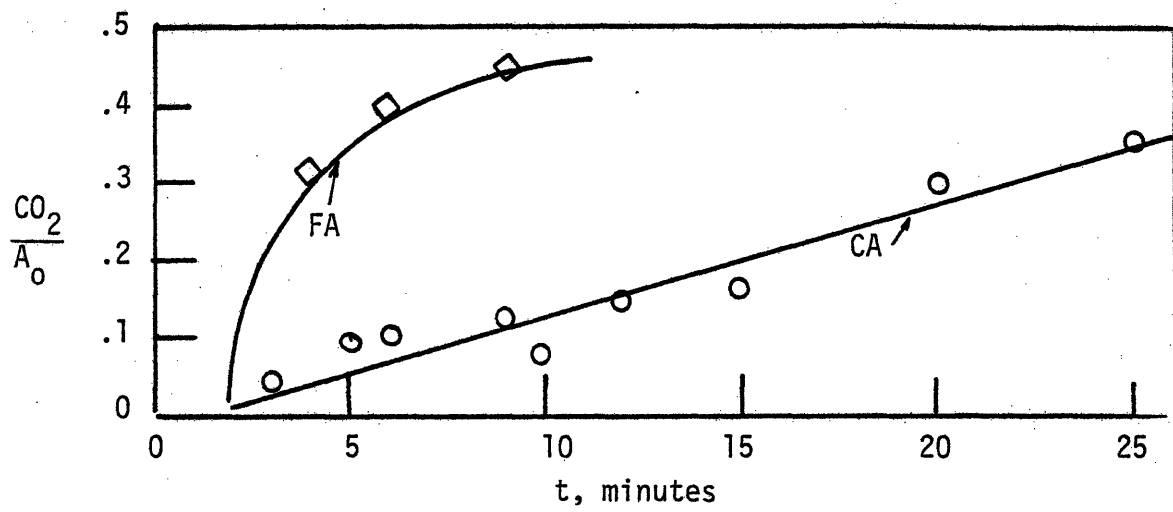


Figure 7.17.1c T=300 C

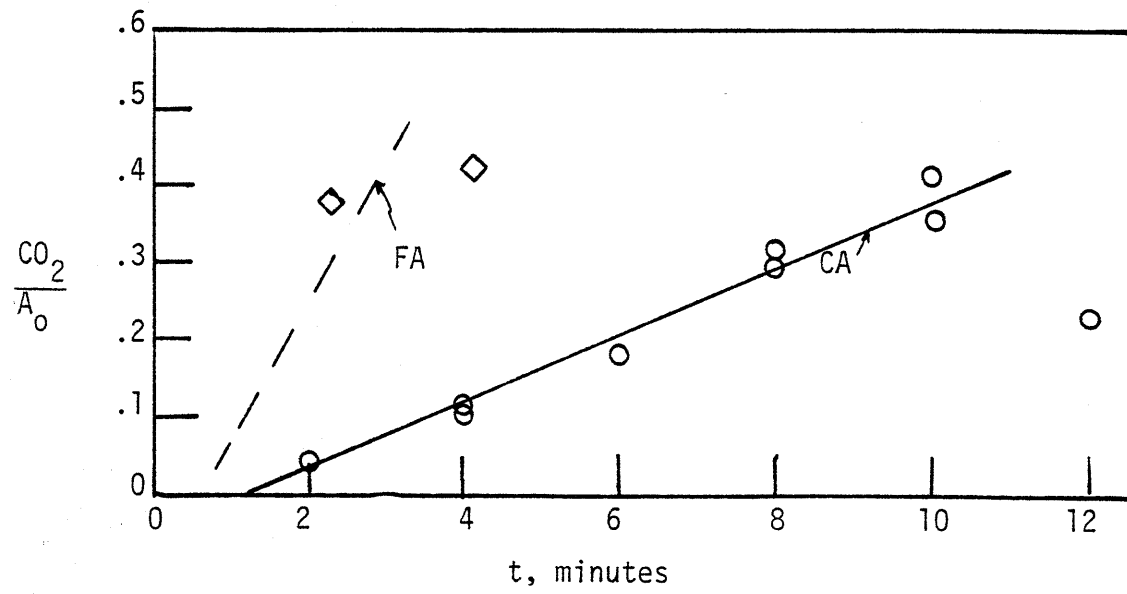


Figure 7.17.1d T=350 C

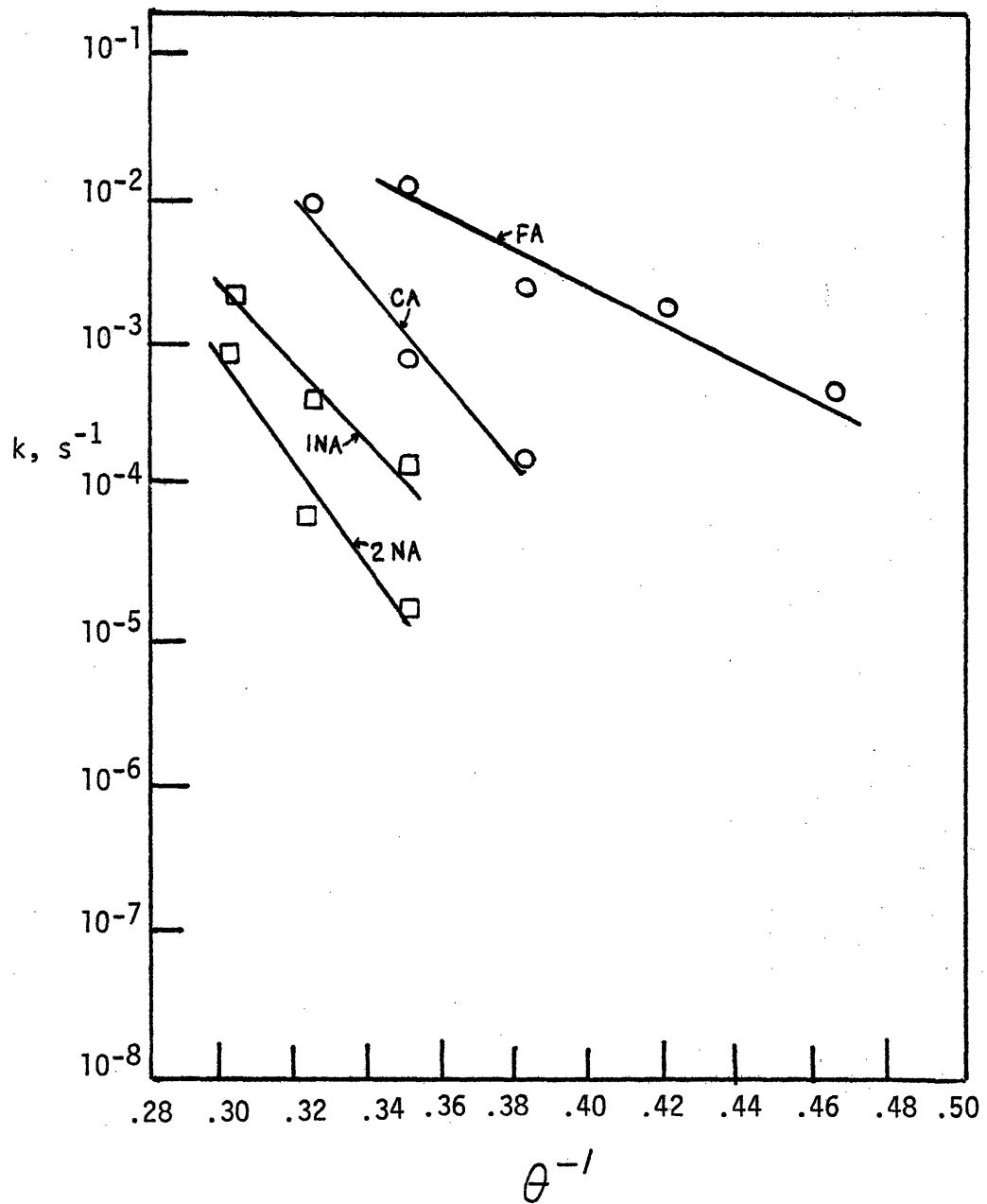
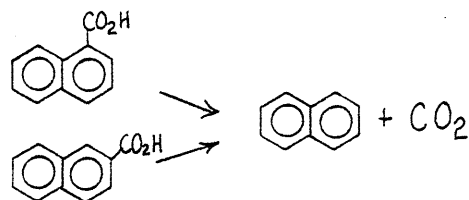


Figure 7.17.2 Arrhenius diagram for carboxylic acid pyrolyses.

involved pyrolyses of 1- and 2- naphthoic acids. The pyrolyses were effected such that each isomer experienced an identical temperature-time history for a given overall holding time. The evolution of  $\text{CO}_2$  from each was monitored by GC analysis and normalized by original substrate mols. These data are presented in Figure 7.18.1, where conversion based on  $\text{CO}_2$  yield from each isomer is plotted as a function of holding time at each temperature studied. Inspection of Figure 7.18.1 reveals that  $\text{CO}_2$  evolution from 1-naphthoic acid was considerably larger than that from 2-naphthoic acid, for each temperature and time studied. This effect was greatest at lower temperatures, suggesting a greater temperature activation for 2-naphthoic acid decarboxylation.

The pyrolyses were thus modelled as the stoichiometric evolution of  $\text{CO}_2$  and naphthalene from naphthoic acid, as in:



The kinetics of naphthoic acid pyrolyses were thus determined from the time dependence of  $-\ln(1-\text{CO}_2/\text{NA}_0)$  at each temperature. The least squares rate constants were  $-\log_{10}k(350,400,450) = (3.81,3.36,2.65)$  for 1-naphthoic acid and  $(4.82,4.20,3.05)$  for 2-naphthoic acid, where  $k$  has units of inverse seconds. These data indicate that  $\text{CO}_2$  release from 1-naphthoic acid is more facile than that from 2-naphthoic acid by about 1 order of magnitude at 350 and about 0.4 orders of magnitude at 450, implying  $E^*_2 > E^*_1$ . Apparent first order Arrhenius parameters of  $(\log_{10}A(\text{s}^{-1}), E^*(\text{kcal/mol})) = (4.5 \pm 1.4, 24.0 \pm 1.3)$  and  $(7.9 \pm 2.7, 36.5 \pm 8.1)$  were determined for 1- and 2- naphthoic acids, respectively.

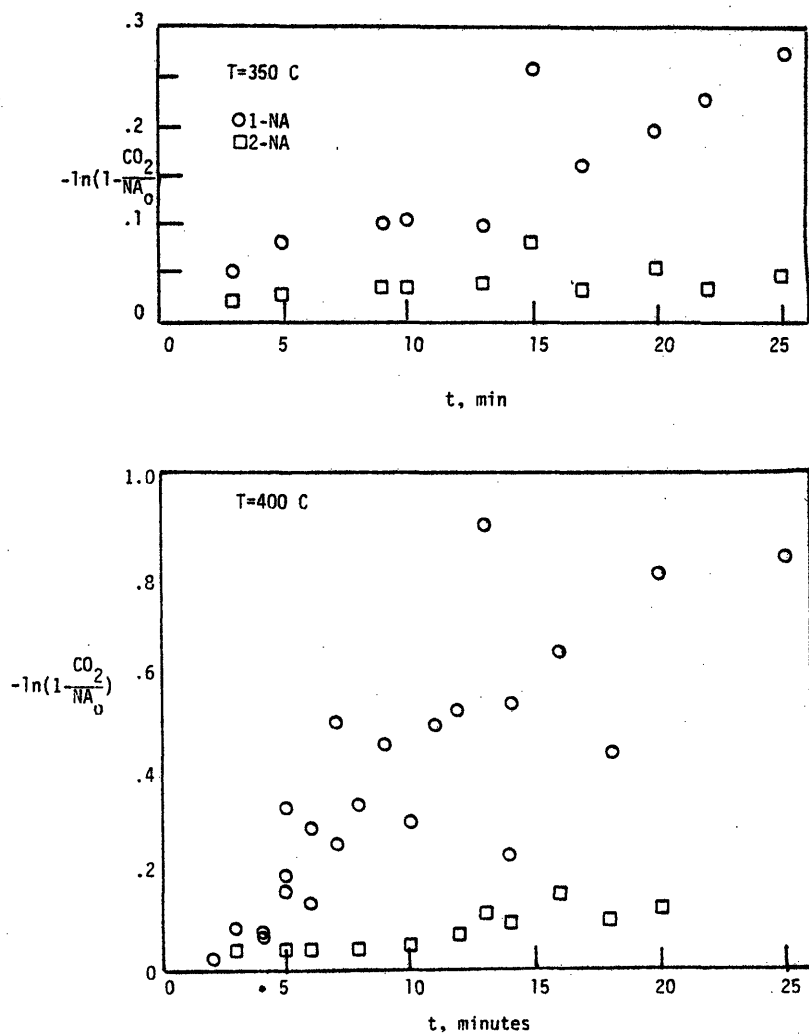


Figure 7.18.1 CO<sub>2</sub> evolution from 1- and 2- naphthoic acids.  
a) T=350 C b) T=400 C.

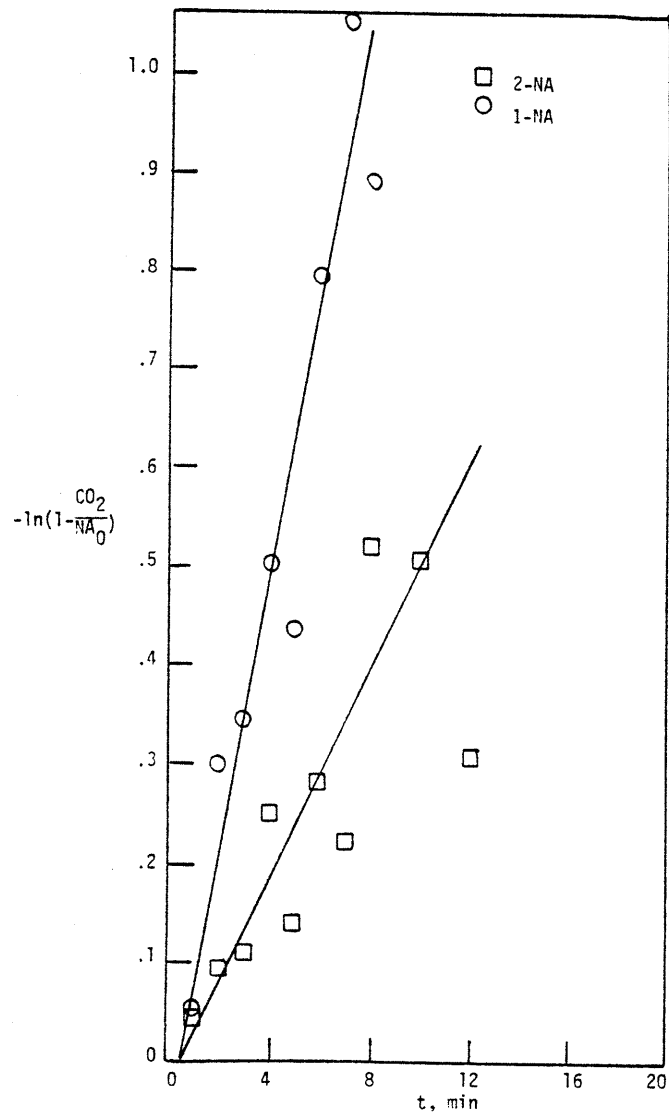


Figure 7.18.1c T=450 C

### 7.19 Summary of Experimental Results

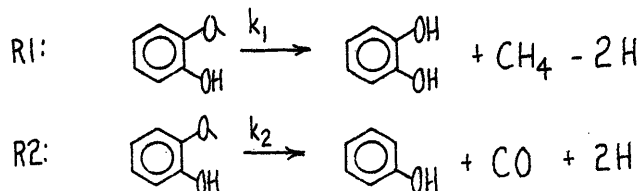
A series of 20 different model compounds has been pyrolysed in the experimental part of the present investigation. Thus, a rather terse summary of the salient experimental results is cogent here.

#### Phenethyl phenyl ether(PPE)

Phenethyl phenyl ether was pyrolysed both neat and in the presence of tetralin. Neat ether pyrolysis resulted in the primary stoichiometric production of phenol and styrene, with extensive degradation of the latter to toluene, ethylbenzene and benzene. Overall ether pyrolysis was first order, occurring with Arrhenius parameters ( $\log_{10}A(s^{-1}), E^*(kcal/mol) = (11.1 \pm 0.9, 45.0 \pm 2.7)$ ). Secondary pyrolyses of styrene were via reactions yielding an overall degradation order in excess of unity, and proceeded with pseudo-first order Arrhenius parameters of ( $\log_{10}A, E^*$ ) =  $(5 \pm 1, 11 \pm 3)$ . Pyrolysis in tetralin was similar to neat ether pyrolysis, the only significant difference arising as an increased selectivity of secondary styrene pyrolysis to ethylbenzene.

#### Guaiacol

Two parallel pathways were developed to describe guaiacol pyrolysis, these being demethanation to catechol and methane and demethoxylation to phenol and CO, namely,



The former pathway was prevalent by about a factor of 10. The assignment



of catechol as a direct pyrolysis product is as yet tentative, for reasons detailed in Section 7.2 and Chapter 10. In short, catechol was identified by GC and GC with catechol coinjection to be part of the solvent washed pyrolyzate liquor, and results are thus interpreted as such.

Both of the demethanation and demethoxylation pathways were first order in substrate, and proceeded with respective Arrhenius parameters of  $(\log_{10} A, E^*) = (10.9 \pm 0.5, 43.7 \pm 1.4)$  and  $(11.5 \pm 0.5, 47.4 \pm 1.6)$ .

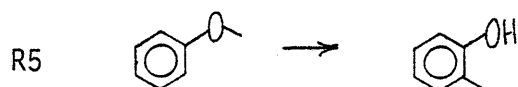
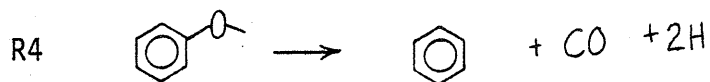
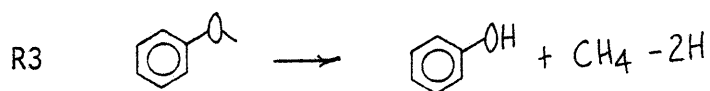
#### Substituted Guaiacols: 2,6-Dimethoxyphenol (DMP), Isoeugenol, Vanillin

Pyrolyses of DMP, isoeugenol and vanillin probed the respective effects of electron donating, conjugative, and electron withdrawing substitution on guaiacol reactivity. The substrates decomposed by demethanation (R1) and demethoxylation (R2) pathways similar to those for guaiacol; vanillin underwent extensive decarbonylation reactions, to be summarized below. As evidenced in the rate data of Appendix 7.2 the kinetics of guaiacol demethanation and demethoxylation were virtually unaffected by substitution.

#### Anisole

Anisole pyrolysis probed the effect of ortho-hydroxy substitution on the reactions of the guaiacol methoxyl group. The effect is marked, as overall anisole pyrolysis was typically at least an order of magnitude slower in rate than that of guaiacol. Three pathways were developed for anisole pyrolysis, these leading to the formation of phenol, benzene,

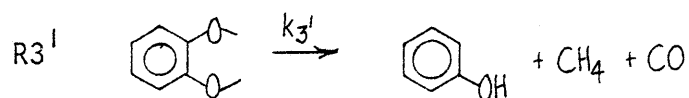
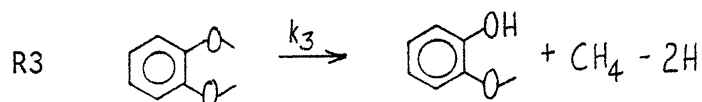
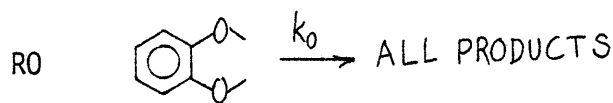
and o-cresol products. These pathways were of the form:

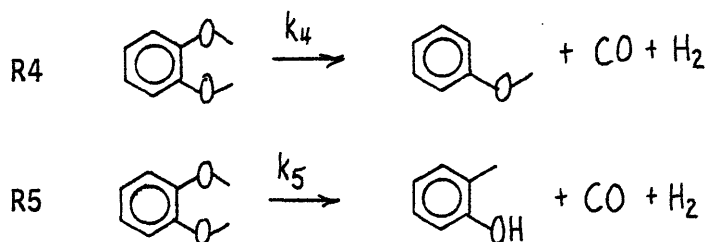


Gas phase products suggested by stoichiometry are included in pathways R3-R5, although an unequivocal relationship between gas and liquid phase products could not be discerned. First order Arrhenius parameters for R3, R4 and R5 were  $(\log_{10} A, E^*) = (13.0 \pm 1.0, 54.7 \pm 3.1), (14.5 \pm 1.2, 61.0 \pm 4.0)$  and  $(7.9 \pm 1.5, 40.5 \pm 4.9)$ , respectively.

### Veratrole

Four primary reaction pathways were important in veratrole pyrolysis. These were similar to those previously described for anisole, and took the form:



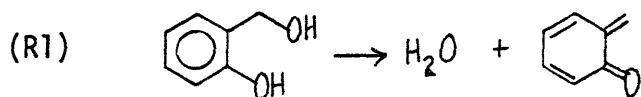


The kinetics of pathways R3 and R5 were comparable to those for analogous R3 and R5 anisole pathways, and apparent first order Arrhenius parameters ( $\log_{10} A, E^*$ ) = (13.9±1.3, 55.9±4.0), (14.1±1.0, 58.4±2.8), (14.8±1.8, 66.1±5.7) and (11.2±2.2, 49.2±7.1) were determined for pathways R3, R4 and R5, respectively.

The products evolved from veratrole pyrolysis allowed comparison of overall methoxyphenol results. Thus, the secondary degradations of the primary guaiacol and anisole products were in substantial agreement with that predicted by a kinetic model using rate constants obtained from pyrolyses of pure guaiacol and anisole. Thus, overall methoxyphenol results accorded quite well.

### Saligenol

Saligenol underwent facile dehydration at temperatures as low as 175-225°C. Each mol of decomposed substrate yielded one product mol of water. Thus, a pathway of the type R1 was postulated, where,

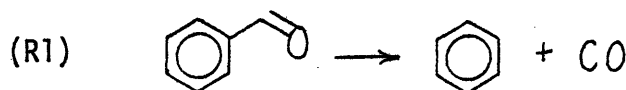


The quinonemethide was not isolated, as this was evidently a labile precursor to the only major pyrolysis co-product, an obscure higher

molecular weight polymer. Apparent first order Arrhenius parameters of  $(\log_{10} A, E^*) = (13.4 \pm 2.9, 33.4 \pm 6.3)$  were determined for R1.

### Benzaldehyde

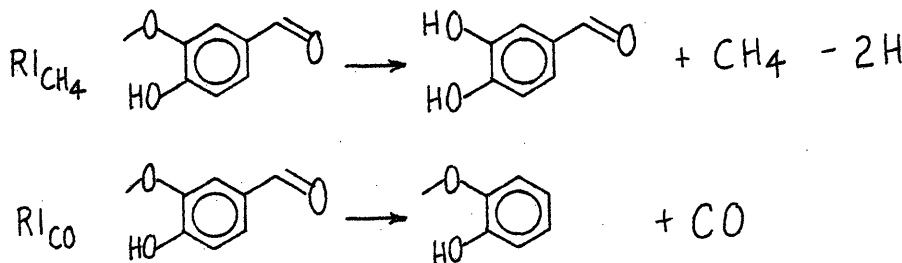
The major pyrolysis route of benzaldehyde was one of first order degradation to stoichiometric amounts of CO and benzene. This pathway was thus of the form R1, where,



Kinetic description of R1 at temperatures from 300-500C provided first order Arrhenius parameters  $(\log_{10} A, E^*) = (9.5 \pm 0.8, 41.5 \pm 2.7)$ .

### Vanillin

As previously described, vanillin pyrolysis involved to major pyrolysis pathways, demethanation to dihydroxybenzaldehyde and decarbonylation to guaiacol; the latter pathway was predominant by a factor of about 10. Thus, vanillin pyrolysis pathways were of the form R1 previously delineated for guaiacol and benzaldehyde, where,



Kinetic analysis of vanillin pyrolysis yielded demethanation Arrhenius parameters of  $(\log_{10} A, E^*) = (12.2 \pm 3.0, 47.3 \pm 8.6)$  and decarbonylation

parameters of  $(10.2 \pm 2.1, 38.5 \pm 5.9)$ . Thus, guaiacol demethanation was essentially unaffected by carbonyl substitution, whereas benzaldehyde decarbonylation was markedly enhanced by guaiacyl substitution.

### Acetophenone

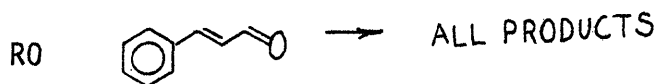
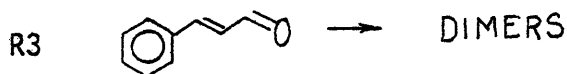
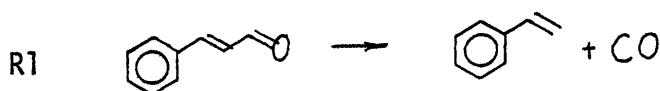
Acetophenone pyrolysis yielded CO, CH<sub>4</sub>, benzene and toluene as the major light products, along with appreciable amounts of alkylbenzenes, phenols and apparent dimers. Because of the refractory nature of the substrate and the complexity of the liquid product spectra, no clear link could be established between gaseous and condensed phase products. An apparent overall acetophenone decomposition reaction order of 1.2-1.3 was determined, with a reaction order of unity for toluene appearance and 1.5 for benzene appearance. Pseudo-first order Arrhenius parameters for overall acetophenone decomposition, benzene appearance, and toluene appearance were  $(\log_{10} A, E^*) = (10.9 \pm 1.2, 52.1 \pm 4.1)$ ,  $(9.57 \pm 1.9, 50.5 \pm 6.7)$  and  $(10.9 \pm 2.2, 56.4 \pm 7.6)$ , respectively. Overall acetophenone pyrolysis was thus typically two orders of magnitude slower than benzaldehyde pyrolysis for the temperature range studied here.

### Cinnamaldehyde

Pyrolysis of cinnamaldehyde yielded styrene, phenols, apparent dimers, and CO as primary products, as well as toluene and ethylbenzene as secondary products. Styrene and CO were formed stoichiometrically at low substrate conversions. Overall cinnamaldehyde pyrolysis was described in two parts, a set of first and a set of second order reactions. Thus arose a global kinetic rate expression of the form,

$$(I) = d(\text{CAD})/dt = k_1(\text{CAD}) + k_2(\text{CAD})^2$$

where  $k_1$  accounts for first order reactions and  $k_2$  the second order reactions. Styrene and phenol appearance were best described as first order, and dimer formation by a reaction order in excess of unity, likely two. Thus, the major cinnamaldehyde pyrolysis pathways were of the form R1, R2, R3 and R0, where:

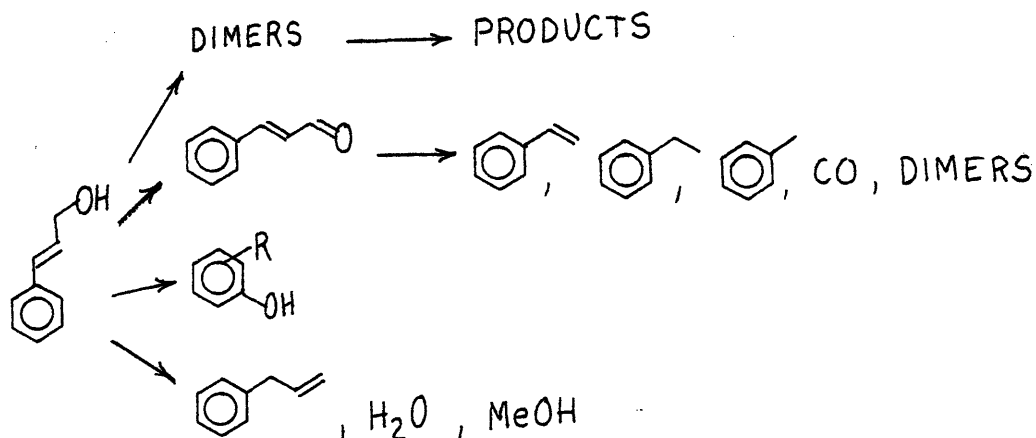


Pseudo-first order Arrhenius parameters for R1, R2, R3 and R0 were  $(\log_{10} A, E^*) = (12.1 \pm 0.4, 48.2 \pm 1.1), (8.5 \pm 0.4, 34.5 \pm 1.0), (8.6 \pm 1.4, 33.7 \pm 3.07)$  and  $(9.7 \pm 1.7, 35.4 \pm 4.6)$ , respectively.

### Cinnamyl Alcohol

The products from cinnamyl alcohol pyrolysis fell into one of four categories: a gas fraction, water soluble light liquids, monoaromatics and a polymeric fraction. Significant among these were

CO, H<sub>2</sub>O, MeOH, cinnamaldehyde, styrene, phenols, allylbenzene and apparent dimers. In spite of complex product spectra, several generalizations regarding cinnamyl alcohol pyrolysis were possible. Lower temperature pyrolysis data suggested that dimers, cinnamaldehyde, phenols, allylbenzene, water and methanol were primary reaction products, whereas styrene, toluene, ethylbenzene and likely CO arose from secondary pyrolyses. An overall reaction network was developed, of the type:

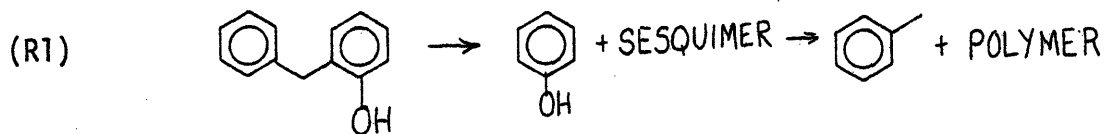


Of the primary reactions, cinnamaldehyde, dimer, and alkylphenol formation were the most facile, whereas methanol formation was typically two orders of magnitude slower in rate than overall alcohol decomposition. Water formation was intermediate, and is as yet not decisively delineated.

#### Orthohydroxydiphenyl methane (OHD)

Pyrolysis of OHD resulted in relatively simple yet highly conversion dependent product spectra. Phenol, toluene, and apparent triphenyl sesquimers were the major products. Of these, phenol and

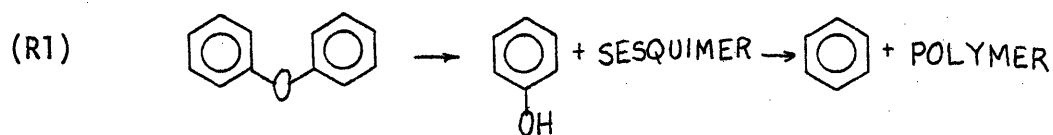
sesquimers appeared as primary products, the latter degrading by secondary pathways to toluene. Thus, an OHD degradation pathway of the type R1 was suggested, where:



Apparent first order Arrhenius parameters ( $\log_{10} A, E^*$ ) = (9.6±0.4, 43.4±1.4) were determined.

### Phenyl Ether

The pyrolysis of phenyl ether could be effected only at temperatures in excess of 500C. The major pyrolysis products were phenol, benzene and apparent sesquimers. Ether pyrolysis appeared to proceed via primary degradation to benzene and sesquimers, the latter capable of secondary degradation to benzene and polymers. Thus, a pathway of the type R1 was suggested where:



Apparent first order Arrhenius parameters of ( $\log_{10} A, E^*$ ) = (14.8±1.3, 72.1±4.8) compared favorably with those found in the literature.

### Biphenyl

Pyrolysis of biphenyl to benzene occurred only at 587C. Higher molecular weight materials, which were presumably formed to maintain hydrogen balance, went undetected in the present analysis. An apparent first order rate constant  $-\log_{10} k_{587C} = 3.82$  was determined.

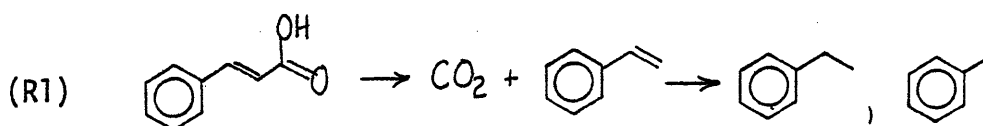


Biphenol

Biphenol was pyrolysed to 500C and 30 minutes holding time. The compound was quite stable, and no degradation to any light products could be discerned.

Cinnamic Acid

Pyrolysis of cinnamic acid over a temperature range of 300-400C produced CO<sub>2</sub> and styrene as major primary products, the latter capable of secondary degradation to toluene and ethylbenzene. The major cinnamic acid pathway was thus of the type R1, namely:



Apparent first order Arrhenius parameters of  $(\log_{10}A, E^*) = (8.0 \pm 1.8, 31.0 \pm 5.0)$  were determined.

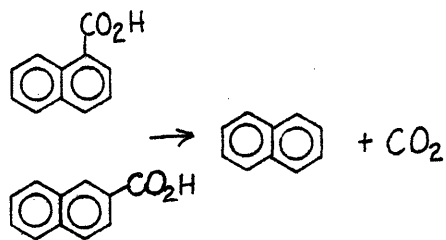
Ferulic Acid

Pyrolysis of ferulic acid from 200-350C elucidated the effect of guaiacyl substitution on cinnamic acid decarboxylation propensity. Initial rates of CO<sub>2</sub> release were much higher for ferulic acid than for cinnamic acid. Apparent first order rate data were estimated by noting the initial rates of CO<sub>2</sub> formation. Arrhenius parameters arose as  $(\log_{10}A, E^*) = (5.2 \pm 2.0, 19.8 \pm 5.2)$ , indicative of substantial guaiacyl enhancement of cinnamic acid decarboxylation propensity.

Napthoic Acids

The time evolution of CO<sub>2</sub> from 1- and 2- napthoic acids was monitored from pyrolysis at 300, 400 and 500C. The pyrolyses were modelled as a

stoichiometric evolution of  $\text{CO}_2$  and naphthalene, as in:



The data indicated that  $\text{CO}_2$  release from 1-naphthoic acid was more facile than that from 2-naphthoic acid, although pyrolysis of the latter substrate was more thermally activated. Apparent first order Arrhenius parameters of  $(\log_{10}A, E^*) = (4.5 \pm 1.4, 24.0 \pm 1.3)$  and  $(7.9 \pm 2.7, 36.5 \pm 8.1)$  were determined for 1- and 2- naphthoic acids, respectively.

## 8.0 Implications and Applications of Experimental Results to Lignin Thermolyses

The experimental results considered in the previous chapter allowed the formulation of formal reaction pathways for each substrate. The present investigation will describe whole-lignin pyrolysis in terms of these model pathways. Thus, this chapter will consider the likely implications of the experimental results to whole lignin. Discussion will begin with a consideration of the significance of the experimental results to isolated lignin moieties, where whole-lignin pathway interrelationships will be developed. This discussion will then allow the development of a formal whole-lignin reaction network, obtained by superposition of the moiety results. Application of these results to the mathematical simulation of lignin will then be developed, where simulation pathways, rate constants, and differential equations will be delineated.

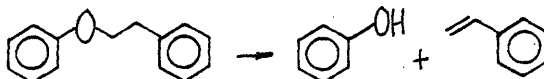
### 8.1 Implications to Lignin Moieties and Functional Groups: Pathway Interrelationships

The goal of the present section is to consider the experimental model compound results in light of their implications to whole-lignin structural features. Initial discussion commences with those compounds depicting the linkages of lignin aromatic units, as these interunit linkages likely exert crucial influence on overall pyrolysis behavior. In addition to those initially present in the unperturbed lignin, disruption of the interunit linkages produces further reactive methoxyphenols and 3-carbon side chains. Hence a discussion of

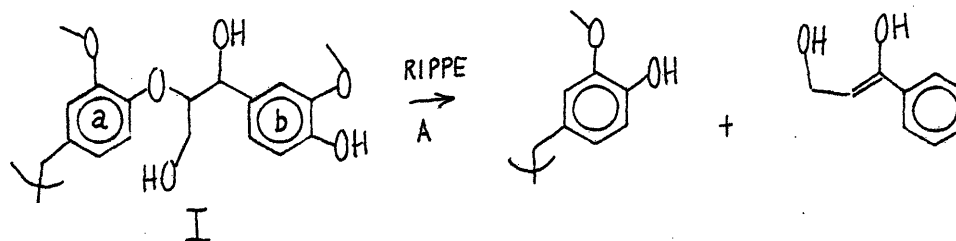
these latter models logically follows interunit linkage consideration. Similarly, the reactions of the 3-carbon side chains generate additional lignin carbonyl moieties, to be considered next. Finally, the significance of the carboxylic acid pyrolyses is discussed in light of potential CO<sub>2</sub> producing pathways.

#### Interunit linkages:

With regard to lignin interunit linkages, inspection of the lignin structure, Figure 3.6, reveals that the  $\beta$ -ether of the type phenethyl-phenylether (PPE) is overwhelmingly predominant. As has been delineated, the major reaction of PPE is the stoichiometric production of phenol and styrene, as in:

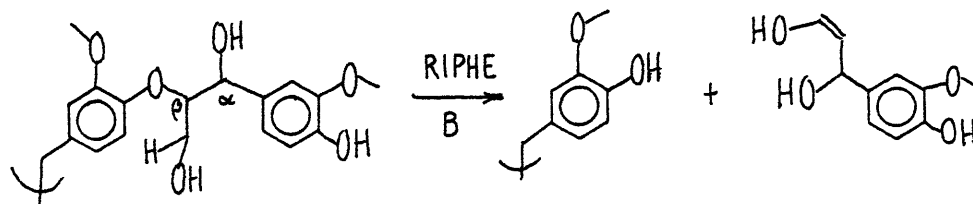


As found in lignin, the  $\beta$ -ether link is in fact a substituted PPE backbone, typically a guaiacylglycerol  $\beta$ -ether, (I). Thus, as applied to whole lignin, pathway R1 generates a guaiacol and saligenol-type moiety, as in:



As will be developed in greater detail later, the methoxyl and hydroxyl units of structure Ia are best modeled as veratrole and saturated hydroxyls, respectively, which are considerably less reactive than the guaiacol and unsaturated hydroxyls generated by ether reversion. Hence, reversion of the  $\beta$ -ether bond accelerates

lignin pyrolysis by generating further reactive substrates. An additional, although kinetically less favorable, pathway for guaiacyl-glycerol  $\beta$ -ether reversion is that analogous to phenetole decomposition, depicted as:



This pathway involves the  $\beta$ -substituent on the  $\beta$ -ether backbone and was not available to PPE, through lack of  $\beta$ -methylol substitution.

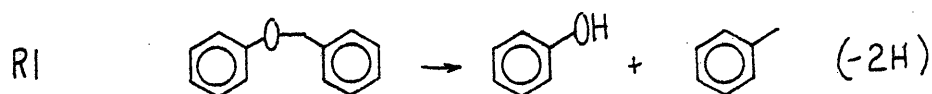
Phenetole decomposition has been studied elsewhere<sup>78</sup>, and it is significantly less reactive than PPE. The guaiacol generated by RIB and RIA are identical, however the saligenol moieties from RIA and RIB are isomers. Thus, while this PHE pathway likely operates on whole lignin pyrolysis, it is kinetically subordinate to  $\beta$ -ether reversion by RIA. In either case, however  $\beta$ -ether reversion effects an increase in lignin methoxy and hydroxy reactivities.

The reaction of PPE is in hydrogen balance, and thus requires no external hydrogen donor. In fact, the present investigation has determined little effect of added tetralin to PPE pyrolysis behavior. In comparison with other model pathways, PPE reversion is quite facile, and should require little catalysis. Further, as the saligenol-type moieties generated by RIA and RIB are susceptible to almost instantaneous dehydration, as detailed later, catalysis of PPE reversion may not be desirable. Instead, initial modification of lignin reactivity should be aimed at preventing hydrogen loss as

water, which may be realized by action toward saturated hydroxyls prior to PPE reversion.

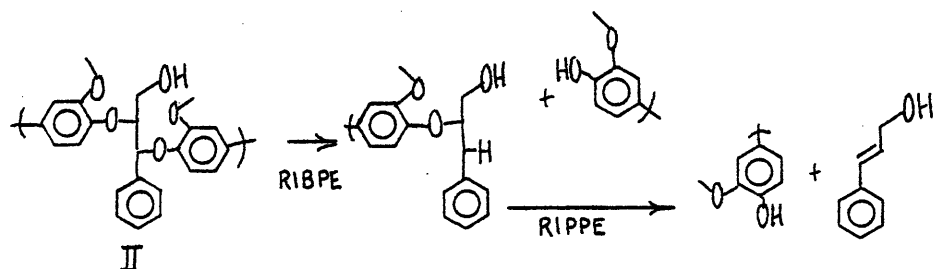
Only one example of the PPE reactivity in whole lignin pyrolysis has been presented thus far, that of guaiacyl-glycerol  $\beta$ -ether reversions. However, the PPE link occurs in other lignin arrangements as well, in conjunction with other linkages to the  $\alpha$  carbon of the 3-carbon side chain. Consideration of these further emphasizes the prevalence of the PPE type linkage.

For example, another prevalent lignin interunit is that of an  $\alpha$ -arylether, of the type benzylphenyl ether BPE. This compound has not been studied here, as it has been exhaustively investigated in the literature<sup>79,80</sup>. The major reaction of BPE involves degradation to phenol and toluene as in:



where the net hydrogen balance of R1 for BPE is depicted in the parenthesis to the right. Other reactions to higher molecular weight materials, presumably through bimolecular interactions, are likely less favorable in lignin pyrolysis due to the steric rigidity of the lignin macromolecule. This is akin to noting that whereas pure model compound pyrolyses are effected at concentrations where bimolecular reactions can be appreciable, one limiting conceptualization of lignin thermolysis is that each model moiety pyrolyses at low concentration, where bimolecular reactions are less favored than unimolecular paths. Thus, the major lignin  $\alpha$ -arylether reaction will likely be degradation to phenol and toluene analogues.

As found in lignin, the BPE linkage is generally in conjunction with a PPE linkage, as in structure (II). Hence, formal application of pathways R1 for PPE and BPE yields reactive guaiacol and alcohol moieties, as in

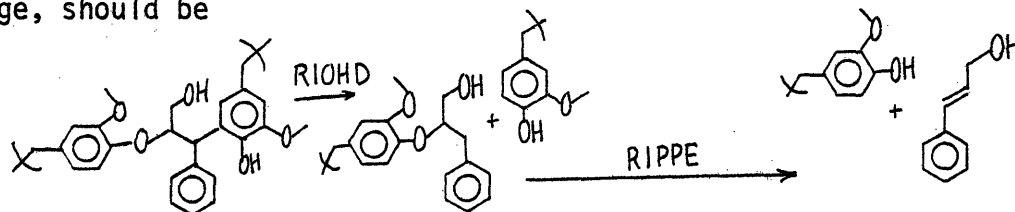


Of course, PPE reversion and BPE degradations can occur both in parallel and in series in whole lignin, and are formally separated here for illustrative purposes only. Hence, the net result of interunit disruption of moiety II is the production of two guaiacol methoxyphenols from what were previously veratrole type methoxyphenols, as well as the generation of a cinnamyl alcohol-type 3-carbon side chain. These units are more reactive than their precursors in structure II, and thus overall lignin pyrolysis is facilitated in their production.

The cleavage of BPE units is more facile than that of PPE in the temperature range of interest, and thus would require minimal catalysis. However, the net reaction is hydrogen deficient, and thus requires hydrogen donor, either external or from within the lignin structure itself. The latter possibility would therefore enhance the tendency toward char formation from overall lignin pyrolysis.

Orthohydroxydiphenylmethane (OHD) modelled another interunit linkage likely important in lignin pyrolysis. As with BPE, the major

reaction significant to whole lignin pyrolysis was degradation to toluene and phenol, as distinguished from reaction to benzene and o-cresol. As with the  $\alpha$ -arylether linkage, the low concentration description of lignin has been assumed, which lowers the selectivity and importance of bimolecular reactions. OHD occurs in lignin in conjunction with a PPE linkage, as did BPE. This is not surprising, actually, as lignin diphenylmethane linkages arise through  $\alpha$ -arylether isomerization during lignification. Thus, the major pathway for degradation of the prototype lignin diphenylmethane linkage, should be



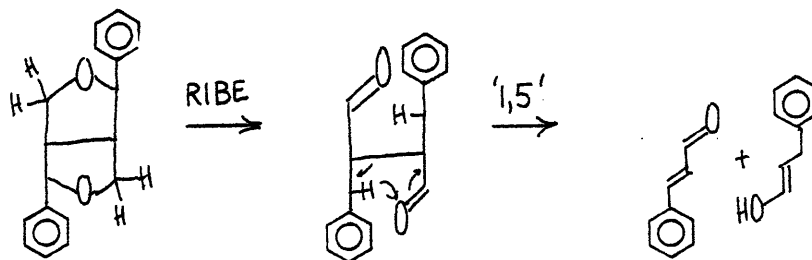
As with BPE degradation, OHD pyrolysis produces two free guaiacol groups and one cinnamyl alcohol group, each prone to rather facile secondary pyrolyses.

Based on laboratory pyrolyses of OHD, the lignin diphenylmethane linkage would be expected to exhibit only modest reactivity. Thus, such a linkage might be a prime candidate for catalytic conversion, perhaps as in hydrocracking. The latter hypothesis arises because the net degradation of OHD is hydrogen deficient, again requiring internal or external hydrogen transfer.

Although predominant, not all lignin interunit linkages are of the type PPE. For example, the pinoresinol structure contains elements of the isomeric dibenzylether (DBE) moiety. Dibenzylether



pyrolysis was not investigated here, as the literature<sup>79</sup> provides degradation to benzaldehyde and toluene as a major reaction. Thus, as applied to the pinoresinol structure, this reaction might yield a cinnamyl alcohol isomer and aldehyde moiety via



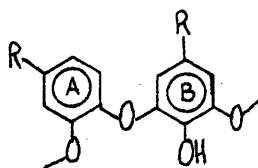
The aldehyde and ene-ol generated would be subject to facile secondary pyrolysis. The pathway outlined above has not been studied and is thus as yet conjecture, but is based on analogous reactions of dibenzylether. Pinoresinol is not a true dibenzyl ether, however, lacking the second phenyl substituent. Thus, the reaction of pinoresinol might be slower than that of benzylether, based on the analogous phenetole-PPE kinetic differences. This clearly illuminates a need for further study. The postulated pathway is in hydrogen balance, and may be a candidate for catalytic study. However, pinoresinol is not a dominant lignin unit, and thus is of secondary importance to overall lignin pyrolysis behavior.

Another less prevalent lignin interunit linkage is that of the phenylcoumaran structure. The ring compound formally combines aspects of BPE and diphenylethane DPE units, both extensively studied as coal model structure<sup>79,80,86</sup>. The unit has not been investigated

in the present study, as it accounts for relatively few of the total interunit linkages.

The final lignin interunit linkage models studied were the thermostable diphenyl(DP) and phenylether(PE) substrates. These were essentially inert to pyrolysis to 600C. As a consequence, these moieties should be less reactive in whole lignin thermolysis. Both linkages are therefore candidates for catalytic studies, preferentially hydrocracking as formal rupture of each requires net hydrogen gain.

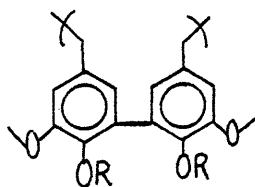
The phenylether (PE) linkage occurs in lignin in structural moieties of the type,



reversion of which would generate a reactive free guaiacol unit on aromatic unit A. Since the diaryl ether link should be relatively stable in lignin pyrolysis, it is clear that the methoxyl group on unit A will exhibit reactivity more closely akin to veratrole and anisole. Thus, the frequency of diaryl ether linkages in the whole lignin should closely depict those less reactive methoxyls which are less activated by ether reversion. Of course, aromatic unit B, here depicted with free phenolic hydroxyl, could also be etherified through the types of linkages outlined above (PPE, BPE, or PE), and will thus exhibit the corresponding reactivity.

With regard to the diphenyl linkage, lignin diaryl bonds occur

as,



and should exert only modest influence on overall lignin pyrolysis behavior, save the preclusion of single ring aromatic formation. That is, pyrolysis to 600C will not likely generate single ring aromatics from diaryl precursors, but the essential reactivities of the 3-carbon side chains and methoxyl units should be only marginally affected.

In summary, it is clear that disruption of lignin interunit linkages should not only formally degrade the macromolecule to smaller and single ring aromatic units, but also exert significant influence on other aspects of lignin reactivity, namely the reactions of the 3-carbon side chains and methoxyphenol units. The single most important interunit linkage, that having an ether backbone of the type PPE, undergoes facile reversion to generate reactive guaiacols and hydroxyl units. The other interunit linkages, occurring in lignin with considerably less frequency, exhibit a wide range of reactivity and influence, varying from the readily cleaved BPE to the thermostable diaryl units.

#### Methoxyphenols.

The previous discussion has suggested that the nature of lignin methoxyphenol units is dependent upon whole lignin conversion. That is, the percentage of lignin methoxyphenol that exists as free guaiacol, 2,6-dimethoxyphenol, phenol, and etherified versions of

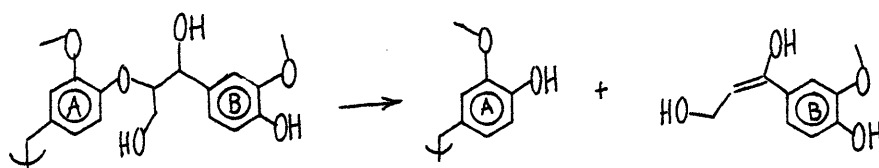
these, as depicted by veratrole, need not be constant as found in the original, unperturbed native lignin. The significance of this variable methoxyphenol distribution is considered here.

As described by the model compound studies, the primary reactions of the methoxyphenols resulted in the formation of  $\text{CH}_4$ ,  $\text{CO}$ , catechols, phenols, cresols, pyrogallol, methoxycatechol, and further guaiacols. As detailed in a consideration of previous pyrolyses,  $\text{CH}_4$  and  $\text{CO}$  are in fact the predominant lignin pyrolysis gases. Further, the phenolic product spectra include catechol, phenol, guaiacol, cresols, pyrogallol and methoxycatechol and their para substituted derivatives. Thus, the reactions of the lignin model compounds describe many essential features of the lignin pyrolysis product spectra.

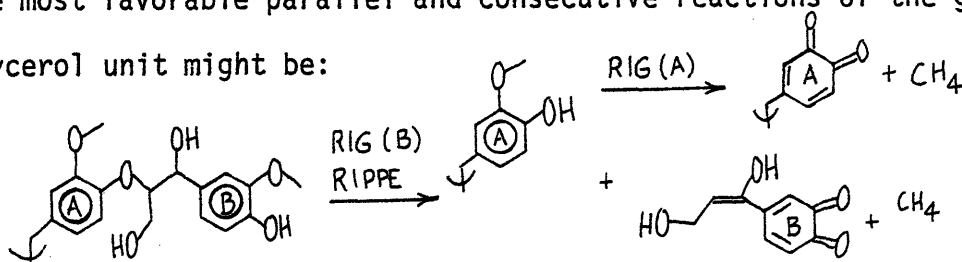
Comparison of the model compounds demonstrates that both demethanation and demethoxylation reactions were faster from guaiacol than from both of anisole and veratrole. As applied to lignin, this suggests that guaiacol units with a free phenolic hydroxyl unit should react with greater ease than those with an etherified hydroxyl. Further, the studies of isoeugenol, 2,6-dimethoxyphenol, and vanillin, which exhibited essentially identical reactivity to that of guaiacol, suggest substitution other than the phenolic hydroxy group exerts no detectable influence on pyrolysis behavior. Thus, guaiacol reactivity was unaffected by para substitution, and therefore should apply directly to lignin, unaltered by the nature of the three carbon side chain. In short, the only essential influence on methoxyphenol reactivity is the nature of the phenolic oxygen, be it a

free or etherified hydroxyl.

Thus, the primary methoxyl reactivity of lignin will be as dictated by the original distributions of guaiacol and veratrole type methoxyphenols. However, facile ether reversion can transform more sluggish veratrole units into reactive guaiacols, thus accelerating lignin pyrolyses. As an example, consider the guaiacyl glycerol  $\beta$ - ether reversion described earlier,



The methoxyl of aromatic unit A is of the type depicted by veratrole, whereas that of B is a free guaiacol. Thus, a primary methoxyphenol reaction of the guaiacyl glycerol  $\beta$ - ether would be demethanation of unit B, whereas methoxyphenol reactivity of unit A would be slower. However, ether reversion generates a free guaiacol at unit A, capable of further demethanation. Thus, a formal reaction network depicting the most favorable parallel and consecutive reactions of the guaiacyl glycerol unit might be:



Of course, the true lignin reactions will be the combination of all possible consecutive and parallel guaiacol, veratrole, anisole, and PPE reactions, a confusing array for even the guaiacyl glycerol  $\beta$ - ether. This network has been used to illustrate the essential

features of methoxyphenol reactivity, where guaiacol and PPE reactivity are comparable with veratrole reactivity at least an order of magnitude slower in rate.

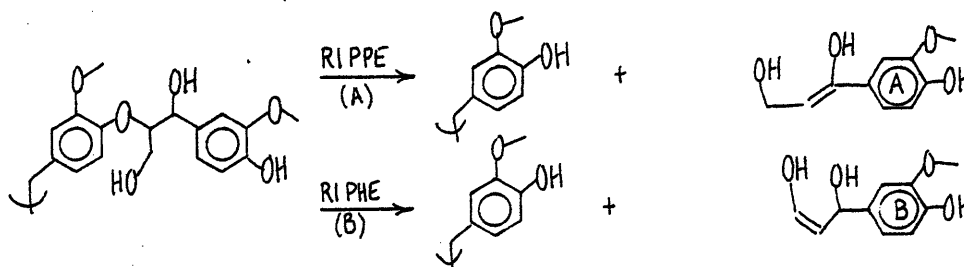
As with the diquinone in guaiacol pyrolysis, the diquinone generated in guaiacyl-glycerol demethanation can undergo further reaction to abstract hydrogen or polymerize to coke. The latter pathway has been postulated as consecutive Diels-Alder additions, likely occurring via pathways similar to those well documented for o-quinonemethide polymerization. As such, these bimolecular reactions should be less favored in the lignin macromolecule, where structural rigidity and steric hindrance likely impose conditions of 'low concentration'. Hydrogen abstractions by the diquinone may in fact yield hydrogen deficient species which may act as further coke precursors. The mechanisms of coke formation have not been addressed in the present investigation, and remain a rather obscure area in need of further study.

The relative insensitivity of guaiacol reactions to substituent effects might suggest little promise for methoxyphenol catalysis. However, while this may be true for demethanation, where the energy levels of the methane frontier orbitals are quite low, other possibilities arise. For example, catalysis to promote methoxyphenol rearrangement to cresols, or rearrangement leading to CO and H<sub>2</sub> evolution, might be a fruitful area of research. In fact, depending on the overall lignin process goal, demethanation might be an undesirable loss of hydrogen. Altogether new reactions, such as hydrocracking to effect methanol formation, might be studied. In any event, the model pathways have elucidated the likely pathways that do and do not occur in whole lignin pyrolyses, and thus suggest

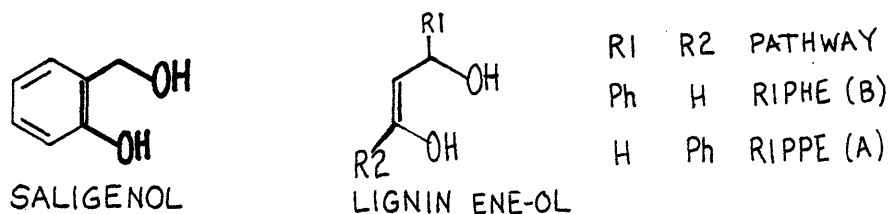
possible routes subject to catalytic modification. Even in the absence of catalysis, the kinetic parameters alone allow for optimization to a specific product.

#### Hydroxylic Side Chain Units:

Just as  $\beta$ -ether revision resulted in the formation of reactive guaiacols from veratrole type units, so too do reactive ene-ol hydroxyls arise. Thus, the pathways previously described for guaiacyl-glycerol  $\beta$ -ether degradation are relevant here, these being:



In either case, the essential reactive features of the generated ene-ol are well depicted by saligenol, as emphasized here:

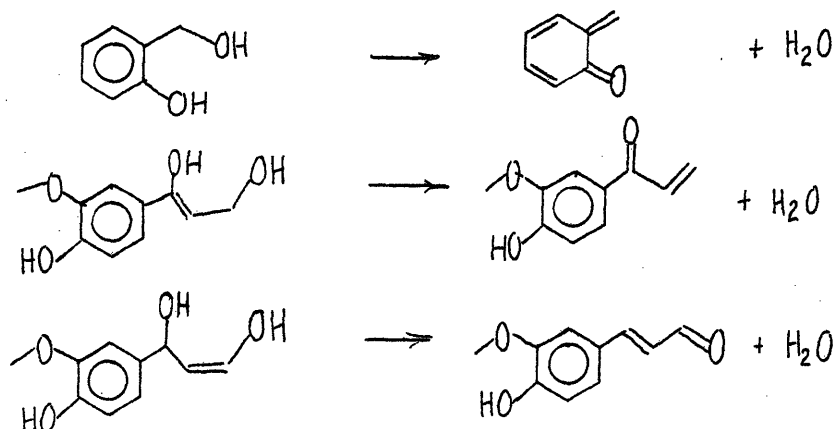


In fact, as the ene component of saligenol is part of an aromatic ring, saligenol likely is a rather conservative model of lignin ene-ol reactivity. However, the rapidity of even saligenol dehydration as compared with other lignin reactions renders this point moot.

Saligenol rapidly dehydrated to water and the o-quinonemethide in the temperature range 175-225 C. Thus, large yields of water from lignin pyrolyses likely arise from this chemical source, as

discriminated from physically associated water evaporation.

The reaction can be applied to the lignin ene-ols as in:



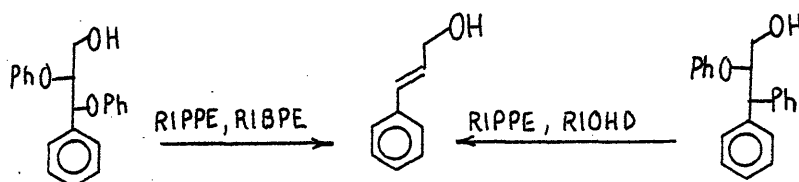
which generates further reactive carbonyl units, to be discussed below. Thus, similar to its effect on lignin methoxyphenol pyrolysis, PPE reversion generates reactive propene-diols from less reactive propylglycols.

In any liquefaction or gasification of an H-poor and C-rich substrate, the rejection of oxygen as water is undesirable since 2 atoms of hydrogen accompany each atom of oxygen. Thus, modifications aimed at preventing water formation are desirable. For example, thermodynamic considerations might suggest pyrolysis in an atmosphere of steam. As the reaction is likely enhanced by considerable hydrogen bonding, kinetic considerations suggest a disruption of this feature, perhaps via solvent effects. Alternatively, if the notions concerning the importance of prior ether reversion are correct, catalyses of other desired reactions relative to PPE activity may reduce water release selectivity. Further, hydrocracking the PPE

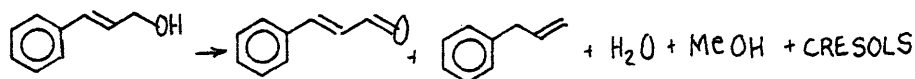


backbone to phenol and ethylbenzene rather than phenol and styrene would still yield the reactive guaiacols but render the propylglycols unchanged.

Whereas reversion of lignin moieties of the type guaiacylglycerol- $\beta$ -ether generated saligenol type hydroxyls, reversion of guaiacylglycerol  $\beta$ - $\alpha$ -ethers and guaiacylglycerol  $\beta$ -ether- $\alpha$ -aryl units generates cinnamyl alcohol moieties, as has been previously discussed. These reactions can be summarized as:



Cinnamyl alcohol pyrolysis resulted in the production of CO, small amounts of water and methanol, cinnamaldehyde, allylbenzene, phenols and dimers. The latter product was disfavored at low concentrations, and may not be significant in the 'low concentration' description of lignin. The other products are in good accord with observed lignin pyrolysis product spectra, which include CO, H<sub>2</sub>O, MeOH, cinnamaldehyde-type 3-carbon side chain phenols, and eugenols, which feature the allylbenzene 3-carbon side chain. Further, cinnamaldehyde pyrolysis yielded styrene, toluene and other alkylbenzenes, each corresponding to para substituted guaiacyl derivatives found as lignin pyrolysis products. Of the products relevant to whole lignin pyrolyses, those generated by primary cinnamyl alcohol reactions were H<sub>2</sub>O, MeOH, allylbenzene, phenols, and cinnamaldehyde, i.e.



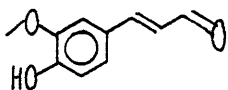
The ultimate yields of  $H_2O$  from cinnamyl alcohol were small, especially in light of the overwhelming dehydration propensity of saligenol. Thus, while water formation from cinnamyl alcohol side chains is likely real and significant, it must be considered second order to saligenol dehydration. Of course, an overwhelming prevalence of cinnamyl alcohol moieties and a scarcity of saligenol units could alter this conclusion. On the other hand, while methanol yields from cinnamyl alcohol were of the same order as the water yields, these are of prime significance. No other experimental methanol-producing pathway could be unequivocally delineated. An ultimate molar yield of 4% obtained here for cinnamyl alcohol pyrolysis extrapolates to approximately 1% by weight of lignin, if applied to each 3-carbon side chain. The phenols generated by cinnamyl alcohol rearrangement were not decisively examined, yet the production of these accords with the complex set of phenols produced in whole lignin pyrolyses. Similarly, as previously noted, the detection of allylbenzene is significant in light of the eugenols obtained from lignin pyrolysis. Eugenol itself is the result of a formal matching of an allylbenzene side chain para to a guaiacol methoxyphenol unit. Finally, whereas the cinnamyl alcohol products  $H_2O$ , MeOH, phenols, and allylbenzene reflect lignin pyrolysis products and can be expected to be stable, a major product, cinnamaldehyde, is capable of further pyrolytic degradation.

In summary, the hydroxylic side chain units generated by ether and alkane reversions pyrolysed to yield products that accord well with those obtained in whole lignin pyrolyses. Certain reactions

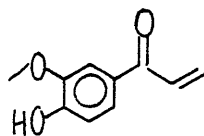
of these generate potentially reactive carbonyl units further capable of continuing lignin reactivity.

#### Carbonyl side chain units:

Whereas methane and carbon monoxide arose from methoxyphenol pyrolysis in proportions of  $\text{CH}_4/\text{CO} > 1$ , CO has often been reported as the more prevalent from whole-lignin pyrolysis. The likely resolution of this apparent discrepancy rests in the facile release of CO observed from the model carbonyl moieties. These are present in the unperturbed lignin in rather small proportions, arising primarily from the dehydration or dehydrogenation of those hydroxylic side chains generated from interunit linkage disruption. As detailed above, the major carbonyl units formed are coniferylaldehyde and guaiacylacrolein, shown here.



CONIFERYLALDEHYDE



GUAIACYL ACROLEIN

The model compounds cinnamaldehyde, benzaldehyde, vanillin and acetophenone probed aspects of the reactivity of these. With regard to CO release, cinnamaldehyde, a direct model of the coniferylaldehyde side chain, underwent decarbonylation to CO and styrene. Benzaldehyde probed the effect of vinyl conjugation, and decarbonylated to CO and benzene with essentially the same kinetics as did cinnamaldehyde. Vanillin displayed the effect of para guaiacyl substitution on aldehyde decarbonylation propensity, and demonstrated an increased reactivity on the order of one decade in rate. Vanillin

and benzaldehyde also served as aldehydic models of the  $\alpha$ -carbonyl guaiacyl acrolein, whereas acetophenone served as the ketonic model. As reflected in comparison of acetophenone and benzaldehyde kinetics, methyl substitution on the carbonyl moiety itself resulted in a suppression of decarbonylation rate.

The foremost implication of these comparisons is that guaiacyl substitution can be expected to exert marked influence on the reactivity of the 3-carbon side chain carbonyls. Hence, whereas cinnamaldehyde depicts the essence of the 3-carbon side chain of coniferylaldehyde, comparison of vanillin and benzaldehyde suggests that the rate constants for cinnamaldehyde decarbonylation should be modified by the factor  $(k^{VAN}/k^{BA})$  when applied to lignin pyrolysis. This is further validated by comparison of benzaldehyde and cinnamaldehyde kinetics, which were quite similar. It is cogent to note here that the guaiacyl activation demonstrated by the comparison  $(k^{VAN}/k^{BA})$  was also observed in comparison of ferulic and cinnamic acid decarboxylation rates; the relative insensitivity to vinyl conjugation is seen in comparison of ferulic and protocatechuic acid decarboxylation.<sup>112</sup> Thus, the conclusions drawn by the comparison vanillin-benzaldehyde and benzaldehyde-cinnamaldehyde are reasonably well supported.

Turning next to the guaiacyl acrolein moiety, the acetophenone results suggest that methyl substitution suppresses decarbonylation propensity. However, it is not clear that this behavior can be extrapolated to the guaiacyl acrolein moiety, as methyl and vinyl substituents are well known to exert potentially different influences

on the frontier orbitals controlling chemical kinetics.<sup>176</sup> The vinyl substituent enhances the possibility of a wide variety of pericyclic rearrangements to labile compounds. The guaiacyl acrolein is isomeric, in fact, with coniferylaldehyde. Thus, yet another area in need of further investigation arises.

The products obtained from the pyrolyses of these model carbonyl moieties accord well with those products known to result from lignin thermolysis. For example, one cinnamaldehyde decomposition pathway is decarbonylation to CO and styrene, the latter which suffers further degradations to toluene, ethylbenzene, and benzene. The high proportion of CO in the pyrolysis off-gas has been previously noted. The production of styrene, toluene, ethylbenzene, and benzene from cinnamaldehyde rationalizes the detection of para-substituted guaiacols, catechols and phenols. The phenolics obtained from lignin pyrolysis contain large amounts of these, particularly the methyl-guaiacols and catechols. This is as in the secondary styrene degradation in PPE pyrolysis, where toluene predominated over benzene and ethylbenzene in the absence of external hydrogen donor. Cinnamaldehyde rearrangement to alkylphenols also accords with the other substituted catechols and pyrogallols detected in the phenolic fraction of lignin pyrolysis. As with other bimolecular reactions, dimer formation from lignin cinnamaldehyde moieties is likely less favored than that from the model compound alone, as the steric constraints and structural rigidity likely impose conditions of low concentration. The pyrolysis products of aceto-

phenone, notably CO, CH<sub>4</sub>, toluene and benzene, suggest that not only CO but also light hydrocarbon gases might arise in small proportions from 3-carbon side chain reactions.

Effective catalysis of decarbonylation of lignin carbonyls should focus on either ether cleavage or alcohol dehydrogenation, since CO elimination from vanillin, and thus likely coniferaldehyde, is quite facile. The former action would more rapidly generate the reactive carbonyls, through dehydration of saligenol type intermediates. However, if prior dehydrogenation of propylglycol moieties can be effected, resulting in a different pathway to carbonyl formation, hydrogen loss as water can be prevented. In the latter scenario, ether reversion could generate reactive carbonyls without proceeding through saligenol-type intermediates.

#### Carboxylic side chains

The final group of pyrolysis substrates to be discussed are those depicting likely carboxylic acids either present or generated in lignins and lignites. Cinnamic acid side chains can arise from lignification radical exchange reactions, whereas naphthoic acids are idealizations of those 'humic acids' related to peat and lignites. Carboxylic acids might also be envisioned to arise from the air oxidation of lignin and lignites. Even so, these are present in lignins in very small proportions, and will thus not exert extreme implications to overall lignin pyrolysis behavior. They do, however, represent facile precursors for CO<sub>2</sub>, itself only a small percentage of lignin pyrolysis gas, and thus merit consideration.

It must be recognized, however, that the  $\text{CO}_2$  content of lignin pyrolysis gas may arise from carbohydrate impurities not removed in the isolation procedure, or even from modifications to the lignin structure effected by the isolation method. For example, Kraft pulping is known to introduce carboxylic acid moieties into the lignin macromolecule. (cf Figure 3.11).

Cinnamic acid underwent facile pyrolysis to  $\text{CO}_2$  and styrene, the latter capable of further degradation. Similarly, ferulic, 1-naphthoic and 2-naphthoic acid each also readily decarboxylated. Of decisive interest is the relative rate of decarboxylation of ferulic and cinnamic acid, where  $k_{\text{CO}_2}^{\text{FA}} / k_{\text{CO}_2}^{\text{CA}} \sim 20$ , in the same range as  $k_{\text{CO}}^{\text{VAN}} / k_{\text{CO}}^{\text{BA}}$ . Thus, guaiacyl activation is significant for decarboxylation and decarbonylation of 3-carbon side chains, and likely extends to other reactions as well. As reflected in the data of Juntgen and VanHeek<sup>112</sup>, ferulic and protocatechuic acids decarboxylated in similar temperature intervals, indicating again the relative insensitivity of side chain reactions to vinyl conjugation.

## 8.2 Whole Lignin Considerations

The preceding discussion has delineated the implications of the model compound pyrolyses to whole-lignin functional groups, and has further implied a relationship among the various moiety types. These allow depiction of an overall lignin pyrolysis scheme. Of course, the actual lignin pyrolysis will be comprised of a complex set of consecutive and parallel reactions, major and minor. However,

this primary reaction network should describe the essential features of lignin pyrolysis; the network should provide insight into the expected gains and ramifications of actions intended to modify the lignin pyrolysis product spectrum. Hence, from such a formal reaction network an overall modification strategy can be developed which delineates the best choices of catalysts, solvents and reaction conditions.

The network is presented as Figure 8.1. For illustrative purposes, lignin has been depicted as the oligomeric unit I. The primary reactions depicted in Figure 8.1 are PPE reversion, BPE cleavage, guaiacol demethanation, and cinnamaldehyde decarbonylation. Of only modest reactivity are those veratrole methoxyls of aromatic units 1,2,3 and 4, and are thus not depicted as reactive. Among the interunit linkages, the diphenylether linkage of units 4 and 5 is inert. Application of the facile guaiacol, cinnamaldehyde, PPE and BPE R1 pathways to structure I generates the structures shown as set II. The cinnamaldehyde reaction of unit I released CO and generated a styrene side chain. Reversion of PPE and BPE links resulted in guaiacol formation at units 1,2 and 3, as well as a saligenol moiety on unit 2 and a cinnamyl alcohol on unit 4. Demethanation resulted in the formation of a diquinone at unit 5. The net release of gases and water is tabulated as well in Figure 8.1. For lignin depicted as structure I, one mol each of CO and CH<sub>4</sub> were formed in transition to set II. The aromatics generated in



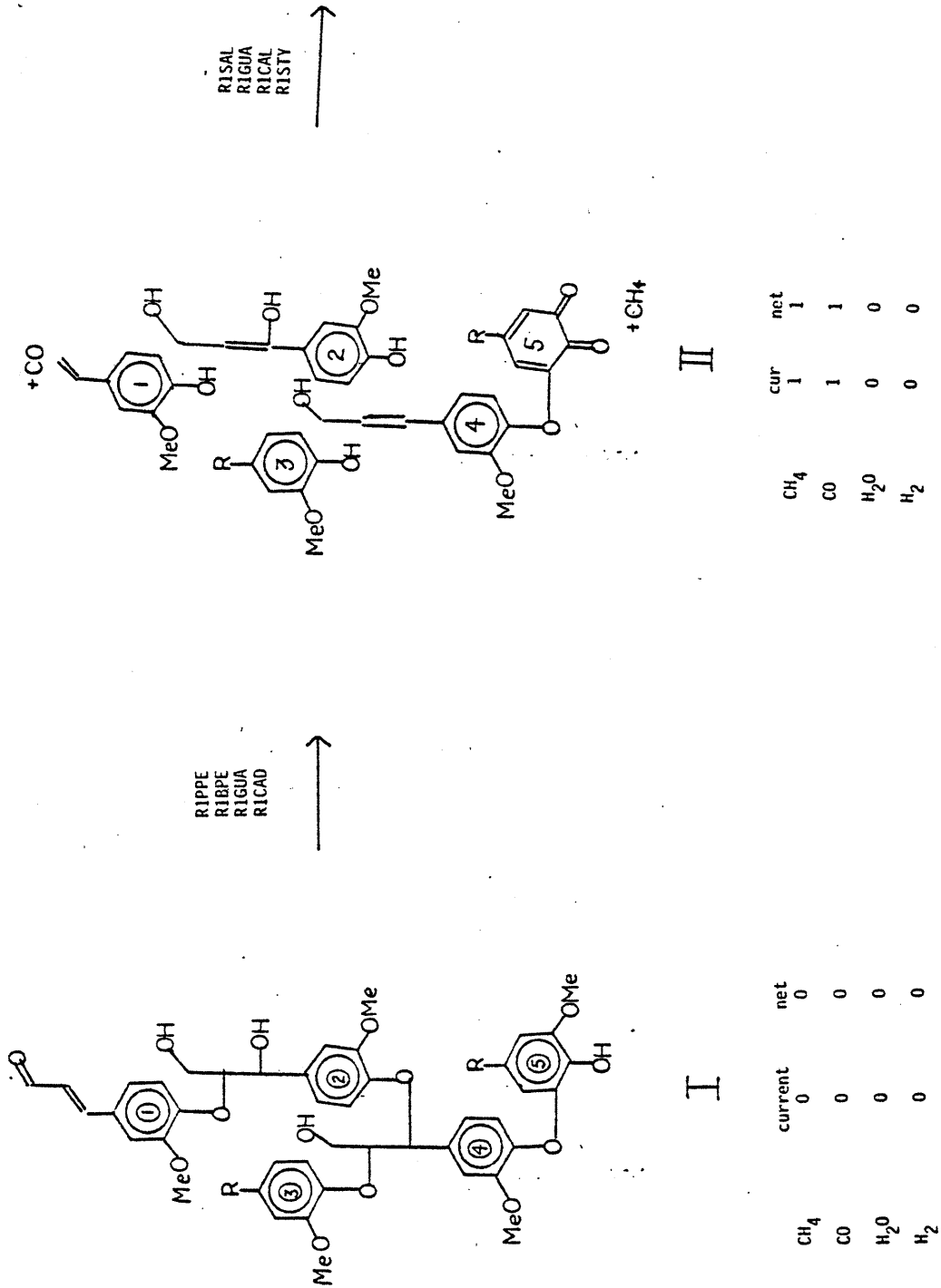


Figure 8.1 Model pathway for lignin pyrolysis.

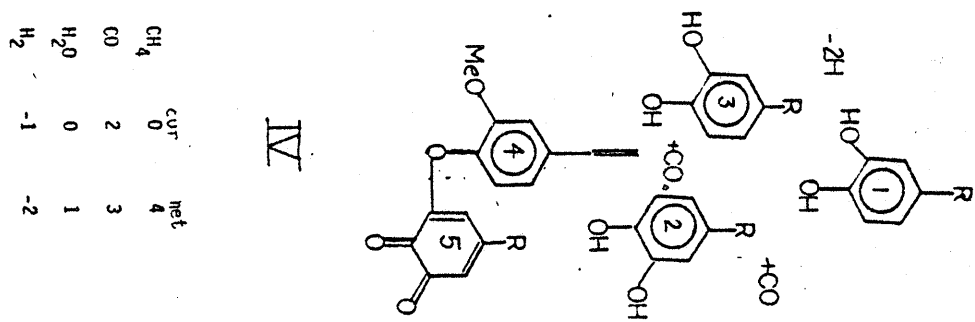
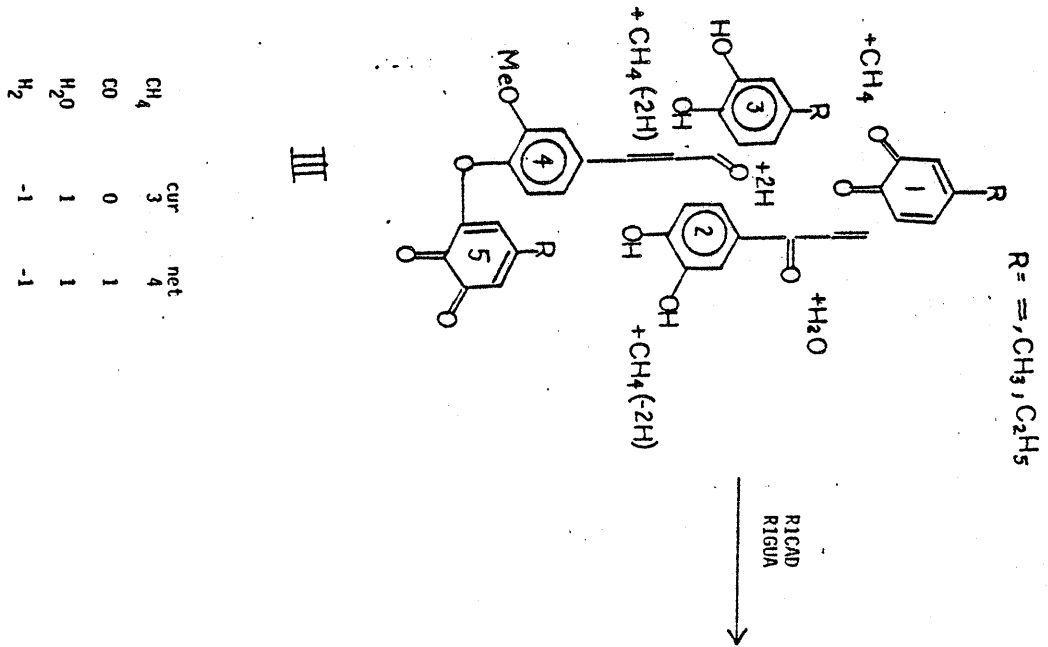


Figure 8.1 (cont)

in set II are subject to further reaction of the same and different types, and result in the products shown as set III. With regard to set III, unit I depicts guaiacyl demethanation as well as the degradation of styrene to toluene, ethylbenzene and benzene. The products from whole lignin pyrolysis, then, would be catechol, methylcatechol and ethylcatechol precursors. Units 2 and 3 similarly depict guaiacyl demethanation, greatly facilitated by ether reversion. Water arose from dehydration of the saligenol moiety of unit 2, which generated the guaiacyl acrolein as well. Unit 4 depicts cinnamyl alcohol dehydrogenation to cinnamaldehyde, as well as the stability of the phenylether link and thus the associated veratrole methoxyl. Application of the same kinds of reactions to the aromatics of set III generates the compounds of set IV, of which some may further degrade. However, the veratrole methoxyl of unit 4 will react, on average, only at higher temperatures and/or holding times, and the diphenylether will remain essentially inert, thus concentrating in the carbonaceous deposit.

The structural moieties and possible reactions of Figure 8.1 depict only a small number of the pathways involved in whole lignin pyrolysis. A more accurate description of lignin pyrolysis must incorporate more of the structural details of the Freudenberg model, Figure 3.5, as well as account for the complex set of parallel and consecutive reactions. The logic of Figure 8.1, however, should reveal the essential features of whole lignin pyrolysis, effected by an integration of pathways suggested by the model compounds.

### 8.3 Simulation

The pyrolysis pathways of the model compounds illustrate essential features of lignin thermolysis. However, the complexity of both the substrate and the pyrolysis reaction network of this substrate render quantitative and qualitative description of lignin thermolysis difficult. Thus, the need for a quantitative model to simulate lignin pyrolysis was motivated.

A formal lignin thermolysis network, Figure 8.1, was generated in the preceding section. This network included the major reactions likely for each lignin moiety. However, actual lignin thermolysis will, in fact, likely involve many parallel and consecutive reaction paths. Thus, an accurate simulation of lignin thermolysis must incorporate all of these reactions.

Since whole lignin thermolysis is to be conceptualized as the integration of discrete aromatic ring unit pyrolyses, the complexity of lignin pyrolysis will be reduced to the summation of the parallel and consecutive paths of these units. The units are in turn described by the juxtaposition of a 3-carbon side chain substituent and a para-methoxyphenol group. Hence, it is relevant to consider the pyrolysis reactions of these. As the aromatic ring will remain intact for the temperatures of interest in lignin thermolysis, the decomposition reactions of the 3-carbon side chains and methoxyphenols will simulate whole lignin thermolysis. The former are considered first.

#### 8.3.1 3-Carbon Side Chain Reactions

The pyrolysis reactions of the 3-carbon side chains are divided

into two types, designated as primary and secondary. These reactions, as incorporated into the simulation model, are presented as Figure 8.2. The primary reactions are of those 3-carbon chains initially present in the unperturbed lignin, while the secondary reactions are of those side chains arising in pyrolysis. Certain side chains present in the original lignin are also generated from the pyrolysis of others.

With regard to the primary reactions, the eight primary substrate moieties are those previously depicted in Figure 3.8. The most important of these is the guaiacyl-glycerol- $\beta$ -ether side chain, labeled moiety 1 in Figure 8.2. This unit is modelled as pyrolysing by two primary pathways, ether reversion by PPE and phenetole (PHE) routes. The former of these is based on the experimental PPE pyrolysis of the present investigation, whereas the latter is based on literature thermolyses of phenetole and phenetole analogues. Rate constants for these pathways, as well as for all other pathways delineated in this section, are motivated separately in the next section.

The guaiacyl-glycerol- $\alpha, \beta$ -ether, 2, can also degrade by these PPE and PHE routes, but may additionally suffer  $\alpha$ -ether reversion as a primary reaction. This additional pathway is also based on the previous literature, namely previous BPE pyrolysis yielding phenol and toluene as the major light products. The 'low concentration' assumption of the present simulation renders condensations to higher molecular weight materials negligible. The reversion of the  $\alpha$ -ether requires the addition of two external or internal hydrogen atoms, which will be considered instantaneous in the present version of the simulation model. The result of this simplification will be a likely overprediction

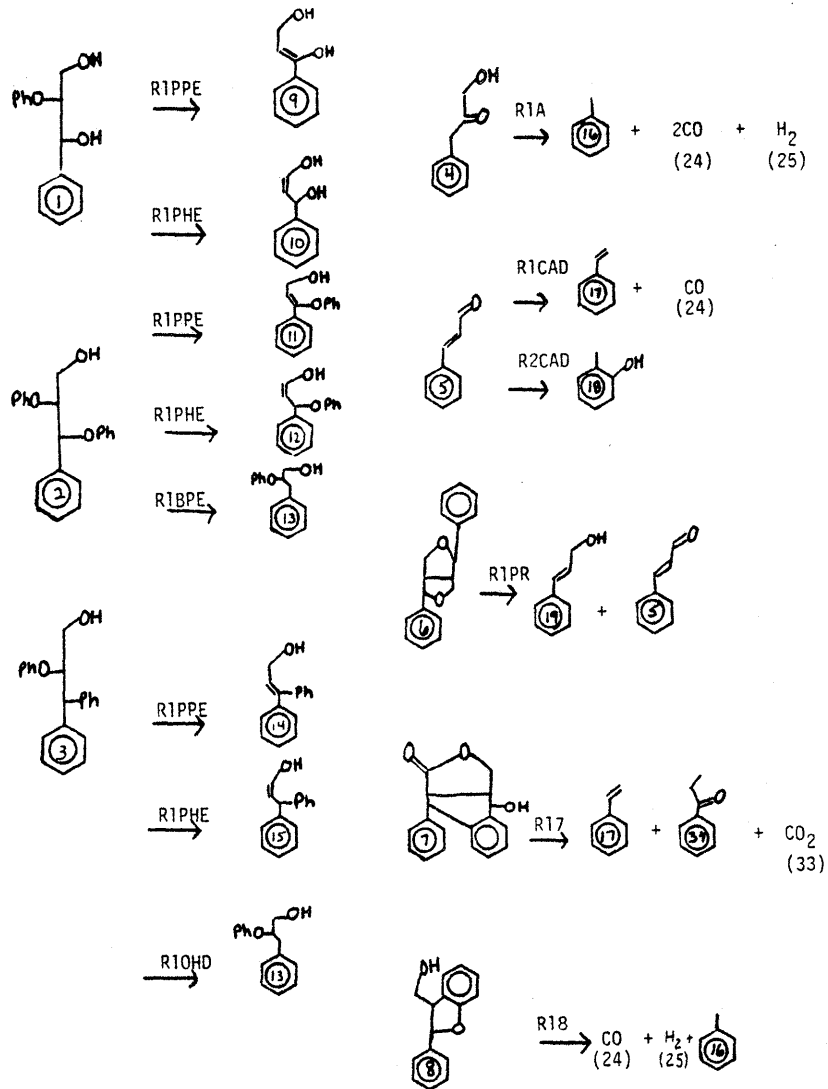
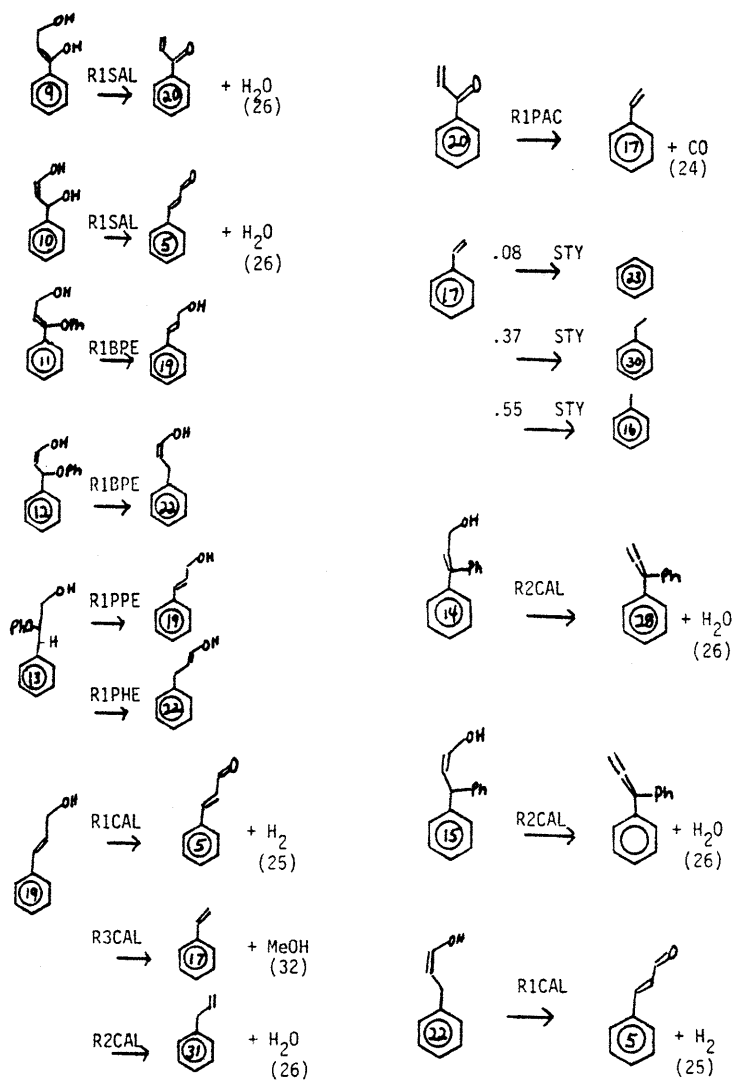


Figure 8.2 3-carbon side chain reactions as in simulation

Figure 8.2(cont.)



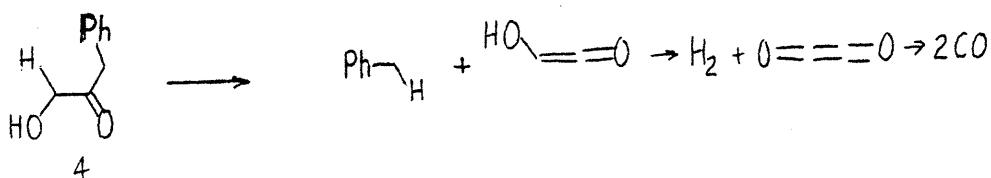
of light products and an underprediction of carbonaceous residue. The present simulation will calculate the carbonaceous residue as 'remaining' multiple ring aromatic units, and coke formation from condensations and dimerizations has been neglected. Thus, the simulation will account for net hydrogen uptake and production stoichiometrically. This will be used as a measure of the likely error introduced by the assumption of instantaneous hydrogen addition to net hydrogen-deficient model reactions. Further sophistication of the simulation model must include more realistic treatment of the coking reactions and net hydrogen deficient reactions.

The guaiacyl-glycerol- $\beta$ -ether- $\alpha$ -phenyl unit 3 has been modelled to degrade by PPE, PHE and OHD routes. As with the previous unit involving an  $\alpha$ -ether unit, degradation of moiety 3 is net hydrogen deficient, and is further modelled as selective to light products. Thus, the 'instantaneous hydrogen' and 'low concentration' assumptions have been invoked. A more subtle point regarding the products of pyrolysis of unit 3 arises. The OHD pathway, based on the present experimental results, but also well supported in the literature, produces phenol and toluene as the exclusive major products. This is to be contrasted to the stoichiometrically equivalent degradation to benzene and o-cresol, which is evidently disfavored for at least the temperatures of interest here. As related to lignin, this selectivity implies that the  $\alpha$ -carbon of unit 3 will remain with the 3-carbon side chain when R1OHD is applied.

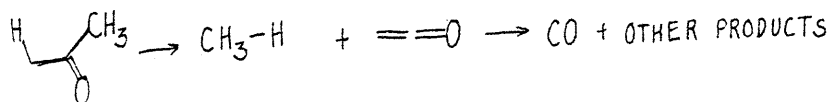
Pyrolysis of the hydroxy acetone unit 4 has been based upon the previous literature pyrolyses of acetone. The unit was not modelled



in the experimental part of the present investigation, since it occurs in lignin in relatively modest amounts. Thus, uncertainty introduced by simulating 4 pyrolysis by analogous acetone pyrolyses should affect whole-lignin simulation less drastically. This clearly emphasizes an experimental point for future study. The simulation pathway for degradation of 4 produces toluene, hydrogen, and CO, as in:



This pathway is speculative, of course, and other pathways might be equally acceptable or likely. However, the pathway is loosely based on analogous acetone pyrolysis, emphasized formally via:

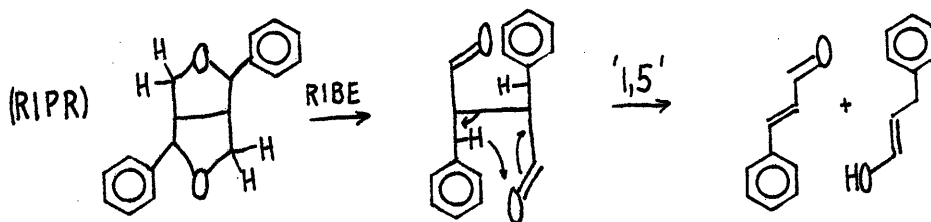


The pyrolysis reactions of acetone have been considered in greater detail in Section 4. To reiterate, the simulation pathway for 4 degradation is rather speculative, based on analogous pathways of acetone. The substrate moiety occurs in lignin in relatively modest proportions, and should thus propagate relatively little uncertainty to whole-lignin pyrolysis. The simulation is quite flexible, and further experimental insights into the nature of degradation of 4 are readily incorporable.

Simulation moiety 5 is the cinnamaldehyde side chain unit, pyrolysis of which was extensively studied in the experimental phase

of this investigation. The pathways for degradation of 5 are thus based on the experimental results previously delineated for CAD. Consistent with other simulation reactions, dimerization of CAD has been suppressed by the 'low concentration' assumption.

Unit 6 is a pinoresinol moiety, pyrolysis of which has been modelled by analogous literature benzyl ether reactions, namely benzyl ether degradation to toluene and benzaldehyde. Thus, the simulation degradation of unit 6 produces two single ring aromatic units, as in:



As with the pyrolysis of unit 4, degradation of 6 is rather speculative, based on one possible interpretation of analogous benzylether pyrolyses. However, the pinoresinol unit is regarded as more of an interesting oddity of lignification in the present analysis and thus much less relevant to the whole lignin pyrolysis than other lignin moieties, namely 1, 2, 3 and 5. Thus, the relatively small proportions of the pinoresinol units in whole lignin should suggest modest simulation uncertainty due to the assumed pathway RIPR. A more detailed simulation of whole lignin reactivity should of course contain experimental pinoresinol details.

Possible pathways for degradation of the lactone unit 7 and the phenylcoumaran unit 8 are presented in Figure 8.2, although these have

not been incorporated into the simulation model. These moieties should occur in whole lignin in quantities even less than the small proportions depicted in the Freudenberg model, and should thus affect whole lignin pyrolysis behavior little. Further, no clear analogous pyrolyses were discerned, and thus inclusion of pathways for degradation of 7 and 8 could not be justified. Naturally, further refinement of the simulation should include the experimental details of lactone and phenylcoumaran pyrolyses. The initial concentrations of the moieties were proportionately redistributed to the other substrate 3-carbon side chain moieties, in order that the normalized initial simulation concentration vector sum to unity.

Turning next to the secondary pathways, the dihydroxy units generated by guaiacyl-glycerol- $\beta$ -ether reversion are simulated to dehydrate via saligenol-type pathways. This dehydration generates the carbonyls 20 and 5, the latter cinnamaldehyde. The appearance of cinnamaldehyde from secondary pyrolysis illustrates the complex nature of the consecutive and parallel lignin reactions. Pathways for degradation of units 11, 12, 13 and 19 are all based on either previously described literature pyrolysis routes or the experimental results of the present investigation. The cinnamyl alcohol unit 19 is notable, simulation paths for this compound arising for the first time here. This reflects a simplification of the Freudenberg structure, since unit 14C in fact depicts a cinnamyl alcohol moiety. It is rather curious that cinnamyl alcohol units are not depicted to a greater extent in the Freudenberg structure, as less than 100% modification of the monomer alcohol side chains during lignification would seem reasonable. With regard to simulation, incorporation of

non-zero initial proportions of cinnamyl alcohol simply requires re-evaluation of the initial concentration vector, and poses no mathematical complication.

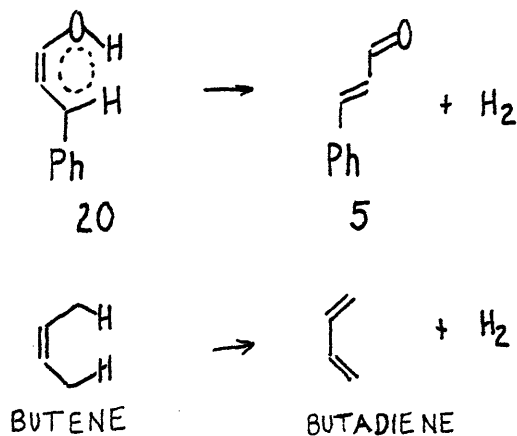
Pyrolysis of the phenylacrolein unit 20 was not part of the experimental strategy of the present investigation, although similar compounds, acetophenone, benzaldehyde, vanillin and cinnamaldehyde, were studied. A major route common to the compounds was decarbonylation, although the latter three pyrolysed in rates much faster than did acetophenone. Thus, as a first approximation, the pyrolysis of the phenylacrolein 20 has been modelled as degradation to CO and styrene, occurring with the kinetics determined for acetophenone pyrolysis. Thus the products of phenylacrolein pyrolysis have been based on those from pyrolysis of the isomeric cinnamaldehyde, whereas the kinetics are based on the structurally more similar acetophenone. This would seem to be the most reasonable assumption, since the methyl substituent on the acetophenone carbonyl evidently decreased the decarbonylation rate substantially. Of course, this approximation is subject to further theoretical and experimental refinement, but should serve the present version of the simulation quite well.

Unit 17 depicts a styrene-type side chain. The simulation pathways for this moiety are the pseudo-first order pyrolyses to benzene, ethylbenzene, and toluene. These pathways were observed as secondary pyrolyses in PPE, cinnamaldehyde, cinnamic acid, and cinnamyl alcohol thermolyses, but were best quantified in the experiments with PPE. Thus, the products, product distributions, and kinetics incorporated into the simulation model are those determined from these latter

experiments. Because of the complexity of the secondary styrene degradations, individual rate constants for the formation of each product (T,B,EB) could not be discerned. Thus, simulation product distributions of T, B and EB from styrene are based on average proportions of T, B and EB obtained in the PPE experiments. These arise as a weighting factor on the overall styrene degradation constant.

The secondary pyrolyses of Units 14 and 15 are based on the water forming routes of cinnamyl alcohol. In fact, the units are phenyl substituted cinnamyl alcohol units and isomers, respectively, and may thus exhibit different reactivities. The water pathway is likely the least affected by this substitution, and was thus selected for simulation purposes. Further experimental and theoretical work might provide additional refinement.

Finally, the degradation pathway for 20 has been modelled to proceed via a concerted  $6_e$  group transfer reaction, analagous to the isoskeletal butene  $\rightarrow$  butadiene reactions. Thus, the pyrolysis of 20 is of the form:



As a first approximation, the reaction has been modelled to proceed with the experimental kinetics determined for the isomeric reaction of cinnamyl alcohol to cinnamaldehyde.

Whereas Figure 8.2 emphasizes that some aspects of 3-carbon side chain pyrolyses remain unclear, the experimental study has provided sufficient framework on which to build a lignin pyrolysis simulation model. The majority of the moieties involved have been experimentally studied, such as the interunit linkages, cinnamaldehyde, cinnamyl alcohol, saligenol and other carbonyls. Other minor moieties, such as the pinoresinol and phenylcoumaran structures remain to be examined. The pyrolysis results have also suggested other 3-carbon side chains for study, notably the acrolein moiety. Study of these coupled with further experimental refinement of the previous models, such as study of coniferaldehyde in addition to cinnamaldehyde, should yield greater predictive capability to the simulation model by further reduction of estimated in favor of experimentally observed pathways. However, the present set of 3-carbon side chain reactions should reveal many of the essential features of lignin pyrolysis.

### 8.3.2 Methoxyphenol Reactions

As with the 3-carbon side chains, methoxyphenol pyrolysis reactions can be classified as primary or secondary. The distribution of the primary methoxyphenol substrates is as depicted in Figure 3.7. Pyrolyses of these may either regenerate other primary methoxyphenol substrates, or result in the appearance of different methoxyphenols capable of secondary pyrolyses. A rather comprehensive methoxyphenol

reaction network is presented as Figure 8.3, where the experimental results of guaiacol, anisole, veratrole and 2,6-dimethoxyphenol pyrolyses have been used to predict virtually all possible parallel and consecutive reactions. Thus, the possible veratrole- and anisole- type pyrolysis reactions have been included as competitive with the more facile ether reversion. Relative to phenylether, these slower veratrole type reactions will be significant, whereas BPE and PPE pyrolyse at least 1.5 orders of magnitude faster in rate, rendering the veratrole type reactions near irrelevant. It is the formal inclusion of these less important veratrole and anisole reactions that accounts for the size and complexity of Figure 8.3. Preliminary computer simulations had in fact demonstrated that many of these slower reactions were insignificant, suggesting that Figure 8.3 be amenable to simplification.

The simplified methoxyphenol reaction network is presented as Figure 8.4. Figure 8.4 contains all of the primary substrates depicted in Figure 8.3, but kinetically less important pathways have been omitted. Thus, while the free phenolics pyrolyse as did guaiacol and 2,6-dimethoxyphenol, only select veratrole reactions have been included as competitive with ether reversion. For methoxyphenols of the PPE type, as in unit 7, only veratrole demethanation, over 1 order of magnitude slower than PPE reversion, has been included. All other veratrole reactions were omitted for PPE type methoxyphenols, as these were in turn slower than demethanation. For methoxy phenols involved in BPE bonding, as in Unit 13, no competing veratrole reactions have been included, as these are all over two orders of magnitude slower in

## I. Primary

$$1 \xrightarrow{1G} 2 + 54 - 56$$

$$1 \xrightarrow{2G} 3 + 55 + 56$$

$$4 \xrightarrow{PPE} 1$$

$$\xrightarrow{PHE} 1$$

$$\xrightarrow{5VE} 5$$

$$\xrightarrow{3VE} 6 + 54 - 56$$

$$\xrightarrow{4VE} 7 + 55 - 56$$

$$\xrightarrow{5AN} 8$$

$$9 \xrightarrow{BPE} 1$$

$$\xrightarrow{3VE} 10 + 54 - 56$$

$$\xrightarrow{4VE} 11 + 55 + 56$$

$$\xrightarrow{5AN} 12$$

$$\xrightarrow{5VE} 5$$

$$13 \xrightarrow{PE} 1$$

$$\xrightarrow{3VE} 14 + 54 - 56$$

$$\xrightarrow{4VE} 15 + 55 + 56$$

$$\xrightarrow{5AN} 16$$

$$17 \xrightarrow{3VE} 18 + 54 - 56$$

$$\xrightarrow{4VE} 19 + 55 + 56$$

$$\xrightarrow{5AN} 20$$

$$21 \xrightarrow{1G} 22 + 54 + 56$$

$$\xrightarrow{2G} 1 + 55 + 56$$

$$23 \xrightarrow{PPE} 21$$

$$\xrightarrow{PHE} 21$$

$$\xrightarrow{5VE} 24$$

$$\xrightarrow{3VE} 25 + 54 - 56$$

$$\xrightarrow{4VE} 4 + 55 + 56$$

$$\xrightarrow{5AN} 26$$

$$27 \xrightarrow{BPE} 21$$

$$\xrightarrow{3VE} 28 + 54 - 56$$

$$\xrightarrow{4VE} 9 + 55 + 56$$

$$\xrightarrow{5VE} 24$$

$$\xrightarrow{5AN} 30$$

$$31 \xrightarrow{PE} 21$$

$$\xrightarrow{3VE} 32 + 54 - 56$$

$$\xrightarrow{4VE} 13 + 55 + 56$$

$$\xrightarrow{5AN} 33$$

$$7 \xrightarrow{PPE} 3$$

$$\xrightarrow{PHE} 3$$

$$11 \xrightarrow{BPE} 3$$

$$15 \xrightarrow{PE} 3$$

Figure 8.3 Comprehensive methoxyphenol reaction network. See accompanying illustration for chemical formulae.



## II Secondary

6	$\underline{\text{PPE}} \rightarrow 2$	$\underline{\text{4VE}} \rightarrow 8 + 55 + 56$
	$\underline{\text{PHE}} \rightarrow 2$	$\underline{\text{5VE}} \rightarrow 42$
	$\underline{\text{2G}} \rightarrow 58$	28 $\underline{\text{BPE}} \rightarrow 22$
8	$\underline{\text{PPE}} \rightarrow 34$	$\underline{\text{2G}} \rightarrow 36$
	$\underline{\text{PHE}} \rightarrow 34$	$\underline{\text{3VE}} \rightarrow 43 + 54 - 56$
	$\underline{\text{2G}} \rightarrow 58$	$\underline{\text{4VE}} \rightarrow 10 + 55 + 56$
10	$\underline{\text{BPE}} \rightarrow 2$	$\underline{\text{5VE}} \rightarrow 29$
	$\underline{\text{2G}} \rightarrow 59$	$\underline{\text{5AN}} \rightarrow 44$
12	$\underline{\text{BPE}} \rightarrow 34$	24 $\underline{\text{3AN}} \rightarrow 29 + 54 - 56$
	$\underline{\text{2G}} \rightarrow 59$	$\underline{\text{4AN}} \rightarrow 5 + 55 + 56$
14	$\underline{\text{PE}} \rightarrow 2$	$\underline{\text{5AN}} \rightarrow 42$
16	$\underline{\text{PE}} \rightarrow 34$	30 $\underline{\text{BPE}} \rightarrow 39$
22	$\underline{\text{1G}} \rightarrow 35 + 54 - 56$	$\underline{\text{2G}} \rightarrow 40$
	$\underline{\text{2G}} \rightarrow 2 + 55 + 56$	$\underline{\text{3VE}} \rightarrow 44 + 54 - 56$
25	$\underline{\text{PPE+PHE}} \rightarrow 22$	$\underline{\text{4VE}} \rightarrow 12 + 55 + 56$
	$\underline{\text{2G}} \rightarrow 36$	$\underline{\text{5VE}} \rightarrow 42$
	$\underline{\text{5VE}} \rightarrow 29$	$\underline{\text{5AN}} \rightarrow 45$
	$\underline{\text{5AN}} \rightarrow 37$	32 $\underline{\text{PE}} \rightarrow 22$
	$\underline{\text{3VE}} \rightarrow 38 + 54 - 56$	$\underline{\text{3VE}} \rightarrow 46 + 54 - 56$
	$\underline{\text{4VE}} \rightarrow 6 + 55 + 56$	$\underline{\text{4VE}} \rightarrow 14 + 55 + 56$
26	$\underline{\text{PPE+PHE}} \rightarrow 39$	$\underline{\text{5AN}} \rightarrow 47$
	$\underline{\text{4G}} \rightarrow 46$	33 $\underline{\text{PE}} \rightarrow 39$
	$\underline{\text{3VE}} \rightarrow 41 + 54 - 56$	$\underline{\text{3VE}} \rightarrow 47 + 54 - 56$

Figure 8.3 (cont)

$$\xrightarrow{4VE} 16 + 55 + 56$$

$$\xrightarrow{5AN} 48$$

### III Tertiary

$$36 \xrightarrow{3A} 49 + 54 - 56$$

$$\xrightarrow{4A} 59 + 55 + 56$$

$$\xrightarrow{5A} 29$$

$$\xrightarrow{5A} 50$$

$$37 \xrightarrow{PPE+PHE} 51$$

$$\xrightarrow{2G} 50$$

$$38 \xrightarrow{PPE+PHE} 35$$

$$\xrightarrow{2G} 49$$

$$39 \xrightarrow{1G} 51 + 54 - 56$$

$$\xrightarrow{2G} 34 + 55 + 56$$

$$\xrightarrow{5AN} 52$$

$$40 \xrightarrow{3AN} 56 + 54 + 56$$

$$\xrightarrow{4AN} 58 + 55 + 56$$

$$\xrightarrow{5AN} 53$$

$$\xrightarrow{5AN} 42$$

$$43 \xrightarrow{BPE} 35$$

$$\xrightarrow{2G} 49$$

$$44 \xrightarrow{BPE} 51$$

$$\xrightarrow{2G} 50$$

$$45 \xrightarrow{BPE} 52$$

$$\xrightarrow{2G} 53$$

$$46 \xrightarrow{PE} 35$$

$$47 \xrightarrow{PE} 51$$

$$41 \xrightarrow{PPE+PHE} 51$$

$$\xrightarrow{5VE} 50$$

$$48 \xrightarrow{PE} 52$$

Figure 8.3 (cont)

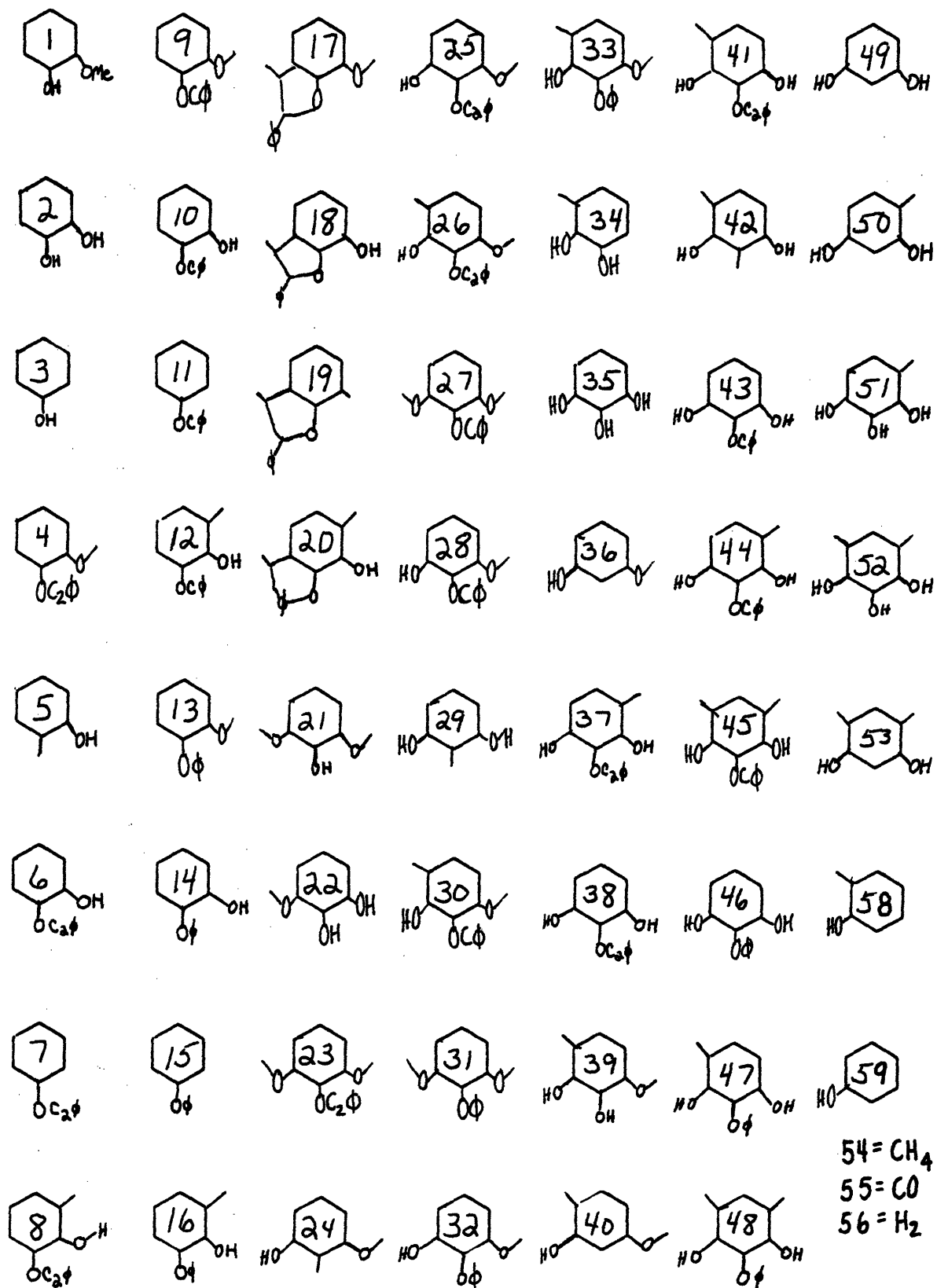
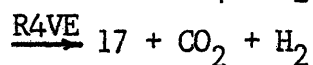
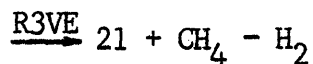
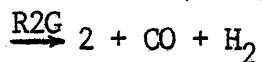
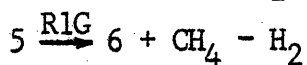
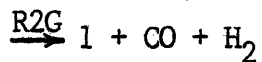
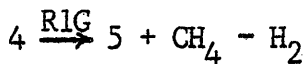
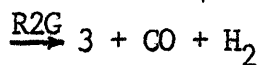
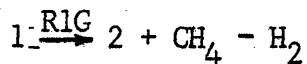
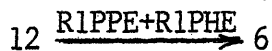
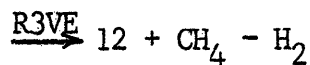
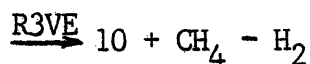
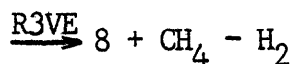
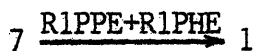


Figure 8.3 (cont) Chemical formula key for comprehensive methoxy-phenol reaction network.

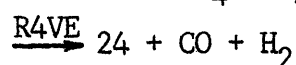
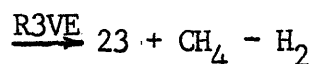
## FREE PHENOLS



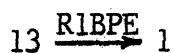
## PPE ETHERIFIED



## PHENYL COUMARAN



## BPE ETHERIFIED



## PE ETHERIFIED

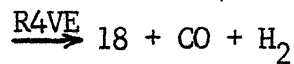
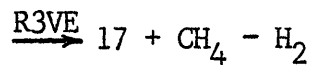


Figure 8.4 Simplified methoxyphenol reaction network. See accompanying illustration for chemical formulae.



MOIETY NUMBER	R1	R2	R3	R4	R5
1	H	OMe	OH	H	H
2	H	OH	OH	H	H
3	H	H	OH	H	H
4	H	OMe	OH	OMe	H
5	H	OH	OH	OMe	H
6	H	OH	OH	OH	H
7	H	OMe	OC <sub>2</sub> φ	H	H
8	H	OH	OC <sub>2</sub> φ	H	H
9	H	OMe	OC <sub>2</sub> φ	OMe	H
10	H	OMe	OC <sub>2</sub> φ	OH	H
11	H	H	OC <sub>2</sub> φ	H	H
12	H	OH	OC <sub>2</sub> φ	OH	H
13	H	OMe	OCφ	H	H
14	H	OMe	OCφ	OMe	H
15	H	H	OCφ	H	H
16	H	OMe	Oφ	H	H
17	H	OH	Oφ	H	H
18	H	H	Oφ	H	H
19	H	OMe	Oφ	OMe	H
20	H	OH	Oφ	OMe	H
21	H	OH	Oφ	OH	H
22	H	OMe	PC	PC	H
23	H	OH	PC	PC	H
24	H	H	PC	PC	H
25	—	CH <sub>4</sub>			
26	—	CO			
27	—	H <sub>2</sub>			
PC	≡	Phenylcoumaran link			

Figure 8.4 (cont) Chemical formula key for simplified methoxy-phenol reaction network.

rate. In contrast, both veratrole-type demethanation and demethoxylation reactions have been included for methoxyphenols involved in phenylether bonding, due to the extreme thermostability of this interunit linkage. Note, however, that veratrole pathways R3<sup>1</sup> and R5 are not possible for phenylethers, due to lack of aliphatic hydrogen  $\alpha$  to the ether oxygen. The veratrole reactions have also been included for phenylcoumaran methoxyphenols, since the pathways for phenylcoumaran degradation are as yet not decisively delineated. The structure is rather minor in proportion, and thus has not been included in the experimental section of the present investigation. However, analogous reactions of  $\alpha$ -ethers suggest that the coumaran ring structure may yield a phenolic hydroxyl. This moiety emphasizes a need for further model study. Overall, the simulation reactions of the methoxyphenol units are firmly based on the experimental part of this investigation, with reference to the literature BPE pathway.

The reaction network for methoxyphenol pyrolyses is rather more complete than the corresponding network for 3-carbon side chain pyrolyses. Only the phenylcoumaran pathways have been estimated, the remaining based upon the experimental pyrolyses of the various interunit links and methoxyphenols. The methoxyphenol network can accommodate various changes in lignin constitution by changing the initial proportions of the cinnamyl alcohols incorporated. Changes in cinnamyl alcohol proportions should effect the 3-carbon side chain model little, if any. However, it is this latter model which would most likely be effected by the structural modifications induced by lignin isolation or pulping operation methods, and this would require introduction of additional

pyrolysis pathways and substrates.

#### 8.4 Simulation Rate Constants

The reaction networks used in the simulation of whole lignin thermolysis are presented as Figures 8.2 and 8.4. Each individual reaction path is associated with a reaction rate constant, based on either the experimental part of the present investigation or analogous reactions as found in the literature. The section will describe the application of these to whole lignin thermolysis.

The rate constants are presented in Table 8.1. The rate constants are phrased in terms of the Arrhenius temperature relationship, which provides for simulation at temperatures other than a base case of 400C. The reactions of the 3-carbon side chain moieties are modified to include acceleration due to lignin guaiacyl substitution, reflected in the parameter AF. This parameter, which is a multiplicative factor on 3-carbon side chain rate constants, assumes a temperature independent value of 10. This value is based on the relative rates of vanillin and benzaldehyde decarbonylation, averaged over temperature. Further refinement of the vanillin-benzaldehyde kinetic data, or the generation of new guaiacyl substituted 3-carbon side chain data, could depict a temperature sensitivity of this parameter. Additional detailed experiments involving guaiacyl substituted side chain moieties should eventually render this parameter unnecessary.

With reference to Table 8.1, a prevalent simulation rate constant is that for PPE reversion to phenol and styrene. This has been selected to describe the actual lignin  $\beta$ -ether unit after consideration of the

```

TH=(TEMP+273.)#0.004576
AF=10.
B1PPE=10**((11.1-45.0/TH)
B1PHE=10**((11.1-49.1/TH)
B1XPE=10**((11.1-40.3/TH)
B1OHD=10**((9.6-43.4/TH)
BA=AF*10**((9.9-52.9/TH)
B1CAD=AF*10**((12.1-48.2/TH)
B2CAD=AF*10**((8.5-34.4/TH)
B1PR=AF*10**((11.1-44.1/TH)
B1B=0.0
B1GAL=10**((13.4-53.4/TH)
B1CAL=AF*10**((4.22-31.6/TH)
B2CAL=AF*10**((1.4-16.7/TH)
B3CAL=AF*10**((1.1-24.7/TH)
B1PAC=AF*10**((10.7-52.1/TH)
B2TY=AF*10**((12.0-29.0/TH)
B17=0.0
B10=10**((10.9-43.7/TH)
B2C=10**((11.8-47.4/TH)
B3UR=10**((13.6-55.4/TH)
B4VE=10**((14.0-60.1/TH)
B1PE=10**((14.0-70.1/TH)
B1PC=0.0

```

Table 8.1 Simulation rate constants.

B= rate constant [=]  $s^{-1}$

AF= guaiacyl activation factor

TEMP [=] Celcius

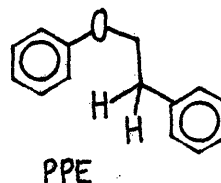
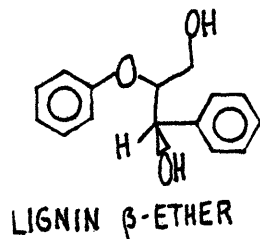
### 8.1a Simulation Arrhenius expressions



Table 8.1b Rate constant values at 300-600 C, listed as in Table 8.1a

0.8646460721354400D -6	0.4070674081311771D -5
0.236689R163105373D -7	0.1434232164239743D -4
0.5374459087667831D -4	0.11032977722761331D -3
0.1116999091927097D -6	0.2211216800811701D -4
0.5307997895191192D -9	0.5299961800804193D -7
0.0217022088835049D -5	0.1819998727500086D -2
0.2401509214970778D -3	0.0137431216647630D -1
0.1910231180709798D -4	0.602R11A419048543D -2
0.0000000000000000D 0	0.0000000000000000D 0
0.45905585335119361D 1	0.2085958774839797D -3
0.80517129751408954D -3	0.1283403372544618D -1
0.1073823161779130D -3	0.9493789498541200D -3
0.95473445428466572D -5	0.13948403726157001 -7
0.1071507034073481D -7	0.5604683457742094D -5
0.7029388976151021D -3	0.16100725774102D -1
0.0000000000000000D 0	0.0000000000000000D 0
0.171203094698487D -5	0.0115409470470099D -3
0.2645621638740134D -11	0.1084193840137112D -4
0.2961066721011594D -7	0.4080596336082115D -3
0.3793073946850489D -8	0.7688475807147830D -5
0.000634470088544D -12	0.2144744800147880D -7
0.0000000000000000D 0	0.0010000000000000D 0
300 C	400 C
0.2087162186086498D -1	0.6846857871897380D 0
0.1656351541815996D -2	0.64442059229812164D -1
0.5092846999037240D 0	0.102803073910981D -2
0.2140793242109137D -2	0.0445116514850689D -1
0.7807872539924135D -4	0.4549296308071710D -2
0.2975689431620568D 0	0.1087578961116897D 0
0.5953600978035831D 0	0.274099006389917D 1
0.409298144684970D 0	0.1100210114201412D 7
0.0000000000000000D 0	0.0000000000000000D 0
0.2070500396028689D 4	0.10948192240598348D 6
0.1140294978875497D 0	0.5793906624180642D 6
0.4774280831267150D -2	0.1638118892201171D -1
0.0613188027265738D -2	0.1440390319499758D -1
0.1482639485787527D -2	0.7214432338640478D -3
0.1670817941856072D 0	0.9823304637018321D 0
0.0000000000000000D 0	0.0000000000000000D 0
0.4513686692766431D -1	0.9139247790881820D 0
0.1258207077190369D 1	0.4312384894945280D 0
0.0671783244665205D -2	0.5396873239603883D 0
0.3231397249071540D -2	0.2855109980764269D 0
0.2611698460129377D -5	0.5846168911731081D 3
0.0000000000000000D 0	0.0000000000000000D 0
500 C	600 C

likely effects of whole-lignin substituent groups. As appearing in whole lignin, the  $\beta$ -ether is of the type shown here:

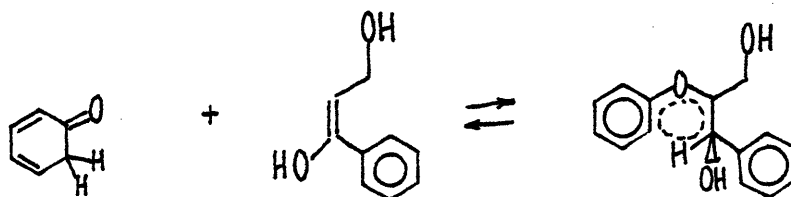


Thus, PPE differs from the true lignin  $\beta$ -ether due to  $\alpha$ -hydroxyl and  $\beta$ -methylol substitution of the latter. Both substituents are of the electron donating type, yet hydroxyl substitution is generally more significant. Thus, this group will likely exert the most profound effect on the base PPE reactivity.

As will be substantiated in a later section, the PPE reaction to phenol and styrene has been interpreted in terms of a pericyclic retro-ene reversion. In any case, consideration of substituent effects in light of this mechanism should be applicable to competing and even predominant alternative mechanisms. Substituent effects on retro-ene reactions are not well detailed in the literature, but the microscopic reverse, ene addition (and equivalent cycloaddition) is well detailed. Assuming a negligible substituent effect on thermodynamic equilibrium, microscopic reversibility dictates that effects on the cycloaddition should be mirrored by the retro-ene.

The literature provides at least two relevant examples for comparison. Sauer<sup>177</sup> provides kinetic comparison of the cycloaddition of hexachlorocyclopentadiene with the dienophiles styrene and methoxystyrene. The relative rate constants  $k_{\text{MeOSt}}/k_{\text{St}} \sim 2$ ,

indicative of kinetic acceleration due to the electron donating methoxyl substituent. With regard to the PPE reversion example, the true lignin hydroxy substituted styrene unit will function as the dienophile, the phenolic unit the diene, as in:

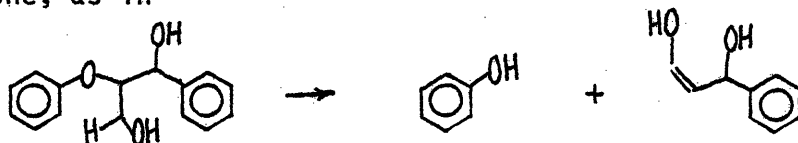


Similarly, Sauer presents another case where the relative rates of cycloadditions of methoxystyrene and styrene dienophiles were  $k_{\text{MeO-st}}/k_{\text{st}} \sim 4$ . Thus by analogy, the true lignin  $\beta$ -ether might be expected to degrade about two to four times as fast as does PPE. However, a more subtle point regarding the differences in PPE and the true lignin  $\beta$ -ether arises. Whereas PPE contains two  $\alpha$ -hydrogen atoms, the true  $\beta$ -ether contains only one, due to the hydroxyl  $\alpha$  substituent. Thus, if the notions of  $\beta$ -ether reversion by a retro-ene mechanism are correct, PPE enjoys a reaction path degeneracy of two, whereas the true lignin  $\beta$ -ether backbone contains only one shiftable  $\alpha$ -hydrogen. The overall effects would thus seem to compensate, and result in similar reactivities for the true lignin  $\beta$ -ethers and PPE. That is, the  $\alpha$ -hydroxyl substituent in the lignin  $\beta$ -ether exerts electronic activation that is likely balanced by the loss in reaction path degeneracy caused by its presence.

Thus, the simulation  $\beta$ -ether kinetics were based on those experimental parameters determined here for PPE, namely

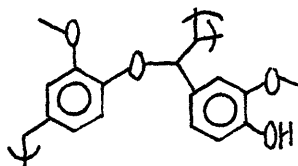
$$(\log_{10}A(s^{-1}), E^*(kcal/mol)) = (11.1, 45.0).$$

The rate constant for the phenetole pathway has been based on the literature conversions of phenetole reported by Benjamin, et al.<sup>78</sup>. The reaction involves the  $\gamma$ -carbon hydrogens of the PPE backbone, as in



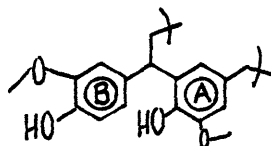
Thus, as with the case in  $\rho$ -ether reversion by PPE routes, the likely electronic and RPD effects have been considered to balance. The literature does not provide activation parameters for phenetole pyrolysis; the Arrhenius parameters listed in Table 8.1 were obtained by assuming that  $\log_{10}A$  for PPE and PHE pyrolysis were identical, and calculating  $E^*$  from the literature conversion data at 400 C. This seems the most reasonable approach, as the relative activation of PPE is likely due to the second phenyl group, and should thus be reflected in a lower  $E^*$ . It is also quite reasonable that PPE and PHE should have similar activation entropies, which would yield similar  $\log_{10}A$  values.

The rate constant for lignin  $\alpha$ -ether cleavage has been based on literature pyrolyses of BPE. Occurring in true lignin, the  $\alpha$ -ether enjoys alkyl substitution, as in



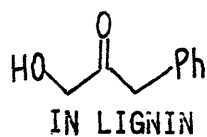
The alkyl group should offer only modest kinetic activation, and thus BPE reactivity has been incorporated directly. As with PHE, Arrhenius parameters were obtained by forcing the literature conversions at 400 C to fit an Arrhenius  $\log_{10}A$  factor of 11.1. However the simulated predictions can be sharpened as more detailed pyrolyses of BPE are reported in the literature.

The pyrolysis pathways of lignin diphenylmethane units have been represented by OHD kinetics. As occurring in true lignin, this linkage is of the type:



As OHD pyrolysis is at least an order of magnitude faster than that of simple diphenylmethane<sup>79</sup>, OHD is clearly the more relevant lignin model. The effect of the orthohydroxyl substituent has been described in terms of a mechanistic degradation through a BPE intermediate, a point to be more cogent when considering diaryl-ether reactivity. Thus, assuming negligible additional activation by the  $\alpha$ -carbon alkyl substitution and the guaiacyl substituent of unit B, the experimental kinetics determined here for OHD pyrolysis have been incorporated into the model directly.

The kinetics of the lignin hydroxyacetone unit have been based on previous literature acetone pyrolyses<sup>175</sup>, where Arrhenius parameters of  $(\log_{10}A, E^*) = (9.9, 52.9)$  were reported. However, the true lignin hydroxyacetone unit is considerably substituted, emphasized by:



Thus, the likely effects of a phenyl and hydroxyl substituent were considered.

The actual pyrolysis of acetone is not well enough understood to allow a fundamental assessment of these substituent effects. Rather, reference was made to the differences in PPE and PHE reactivity, where phenyl substitution lowered the equivalent PPE  $E^*$  by about 4 kcal/mol. This difference corresponds to roughly one order of magnitude in rate at 600 C. Anticipating similar activation due to the hydroxyl substituent, the true lignin acetone moiety was simulated to react about two orders of magnitude faster than simple acetone. This activation was distributed equally in the  $\log_{10}A$  and  $E^*$  parameters, and thus final simulation values of  $(\log_{10}A, E^*) = (10.9, 48.9)$  were determined. Although these parameters were obtained in a rather arbitrary fashion, they represent a reasonable estimation for simulation purposes. Experimental pyrolyses of more typical hydroxyacetone units should sharpen simulation predictions.

The hydroxyacetone rate constant is the first encountered thus far to include the guaiacyl activation AF multiplicative multiplier. This activation is distinct from that of the acetone phenyl substituent. The effect can be considered as emanating from the guaiacyl hydroxyl and methoxyl, transmitted through the aromatic ring. It is thus properly considered as a separate, extra acceleration in addition to those just described from the true lignin

phenyl and hydroxyl substituents. However, unlike these latter effects which relate specifically to the hydroxylacetone moiety, the guaiacyl activation factor will apply to all 3-carbon side chain moieties.

The rate constants for 3-carbon side chain degradation by cinnamaldehyde pathways R1 and R2 include this guaiacyl activation factor. Cinnamaldehyde pyrolysis was an important part of the experimental portion of this investigation and experimental kinetic parameters were thus incorporated into the simulation model otherwise unaltered.

The simulation pathway for pinoresinol degradation was based on the analogous reactions of dibenzyl ether. Literature results for dibenzyl ether were directly incorporated, with no modification for possible pinoresinol structural subtleties. Conversion data at 400 C<sup>79</sup>, were interpreted in terms of a first order rate constant, which was forced to fit an Arrhenius  $\log_{10} A$  of 11.1. The resulting  $E^*$  was 44.1, of the same order of that for PPE. It is quite reasonable that the isomeric PPE and BE ethers should pyrolyse with similar activation entropies and energies. Of course, more detailed analyses of pinoresinol reactivity is suggested.

The true lignin saligenol moieties should be considerably more reactive than actual saligenol. Degradation of the model compound proceeded with aromatic ring disruption, whereas the true lignin unit contains no such aromatic stability. Thus, the true lignin unit should pyrolyse more readily by a reduction in activation

energy requirements of the order of the resonance stability of benzene. With regard to whole lignin pyrolysis, saligenol itself degrades about four orders of magnitude faster than any other lignin moiety, and thus further acceleration of the true lignin moiety is unnecessary. In fact, in order to avoid instabilities in the numerical solution of the simulation differential equations, the model depicts saligenol dehydration as instantaneous.

Simulation rate constants for each of R1, R2 and R3 in cinnamyl alcohol pyrolysis were abstracted directly from the experimental portion of the present investigation. Although pyrolysis of the substrate was complex, definite real pathways for formation of cinnamyldehyde, water and methanol could be discerned. Each of these simulation pathways is accelerated by the guaiacyl activation factor.

The phenyl-acrolein moiety 20 was not directly studied in the experimental part of the present investigation. A hybrid simulation pathway was thus developed, based on analogous decomposition pathways of cinnamaldehyde, acetophenone, benzaldehyde and vanillin. Basically, the simulation pathway assumes stoichiometric degradation of the phenylacrolein to styrene and CO, a rather simplifying assumption. This pathway is thus based on the isomeric pathway of cinnamaldehyde decarbonylation. However, since the styrene thus produced is subject to further degradation to benzene, toluene and ethylbenzene, net phenyl acrolein decomposition does produce a wide range of products. The simulation kinetics for this pathway are based on a combination of acetophenone, cinnamaldehyde, and benzaldehyde kinetics. Acetophenone



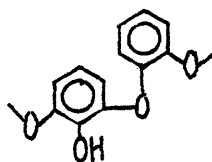
pyrolysis was much slower than that of benzaldehyde and cinnamaldehyde, whereas the latter two were nearly identical. Thus, whereas vinyl conjugation affected the benzaldehyde decarbonylation propensity little, direct methyl substitution suppressed this reaction markedly. Hence, it was necessary to assess the likely effect of direct vinyl substitution on decarbonylation. The net result was to use the acetophenone  $\log_{10}A$  factor and the cinnamaldehyde  $E^*$ , which reflects an intermediate compromise. Thus, the entropic term was modelled similar to that for acetophenone, whereas the energetic term more closely to that for cinnamaldehyde. This assumes that the energetics of vinyl conjugation and direct vinyl substitution are similar, which might be a rather crude approximation. Because of its relative prevalence, the phenyl acrolein moiety arises as the single most important compound for further experimental research. This further work should more decisively delineate both kinetics and product spectra.

The experimental studies of PPE served as the basis for the simulation kinetics for styrene pyrolysis. Styrene decomposition to benzene, ethylbenzene, and toluene was observed in cinnamic acid, alcohol and aldehyde experiments as well, but was most completely quantified in the PPE experiments. The overall pathway for PPE degradation was modelled as a classical  $A \rightarrow B \rightarrow C$  reaction path, where A represents PPE, B represents styrene, and C represents benzene, toluene and ethylbenzene. Thus, the time for or magnitude of the maximal concentration of styrene was used to define an overall pseudo-first order decomposition rate constant to benzene, toluene,

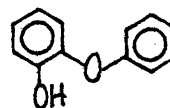
and ethylbenzene. The distribution of these latter products is based on that obtained at 400C and  $PPE_0=0.25$ , and arises through multiplicative factors on the overall rate constant. Repeating the analysis at 450 and 500C yielded the global Arrhenius parameters listed in Table 8.1.

The experimental results for guaiacol and veratrole pyrolyses were incorporated directly into the simulation model. The substituted guaiacols vanillin, isoeugenol, and 2,6-dimethoxyphenol pyrolysed essentially as did guaiacol, indicating that para propanoid substitution should have little influence on guaiacyl reactivity. The same behavior was assumed for veratrole.

The remaining simulation rate constant is that for phenyl ether cleavage. As appearing in whole lignin, the unit is more properly an orthohydroxyphenylether, as in

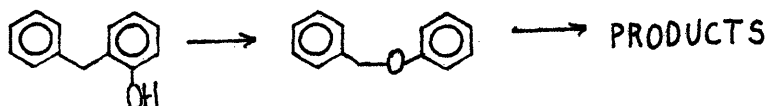


TRUE LIGNIN PHENYL ETHER MOIETY



OHPE

Thus, by analogy to the relative reactivities of orthohydroxydiphenylmethane and diphenylmethane, the true lignin moiety might be expected to react at least an order of magnitude faster than actual phenyl ether. However, this was not incorporated into the model, for reasons regarding the likely mechanism of hydroxylic activation in OHD pyrolysis. As motivated in a later section, the orthohydroxyl unit may facilitate OHD pyrolysis by providing the opportunity for rearrangement to BPE, as in:



However, the same logic applied to phenylether would yield an unlikely peroxide intermediate, as in:



Since this step is considered highly unfavorable, actual phenyl ether parameters were incorporated. In any event, increasing the reactivity of phenylether would have little real effect in the simulation model. For example, the Arrhenus parameters obtained for PE pyrolysis were  $(\log_{10}A, E^*) = (14.8, 72.1)$ , which predict  $\log_{10}k(600C) = -3.25$ . By contrast,  $\log_{10}k(600C) = .032$  for veratrole demethylation. Thus, increasing phenyl-ether reactivity by one order of magnitude would effect little real change in overall lignin selectivity. The rate increase would have even less effect at lower temperatures, due to the high  $E^*$  for PE cleavage. In short the true lignin phenylether unit was modelled as simple phenylether.

### 8.5 Differential Equations

The reaction networks of Figures 8.2 and 8.4 and the rate constants of Table 8.1 form the basis for the mathematical simulation of lignin thermolysis. From these, a set of differential equations were generated which describe the time variation of each molecular simulation component. The equations were obtained from species material balances in a constant volume batch reactor, and are listed in Figure 8.5.

The equations were numerically integrated forward in time utilizing a fourth order Runge-Kutta technique. For the cases considered in this investigation, convergence was excellent; certain equations are

```

DY(1)=- (BIPPE+BIPHE)*Y(1)
DY(2)=- (BIPPE+BIPHE+BIPPE)*Y(2)
DY(3)=- (BIPPE+BIPHE+BIPHE)*Y(3)
DY(4)=-BASY(4)
DY(5)=- (BICAD+B2CAD)*Y(5)+BIPHE*Y(1)+BIPHE*Y(6)+BICAL*Y(19)+BICAL*Y(20)
DY(6)=-2*BIPHE*Y(6)
DY(7)=-2*BIPHE*Y(7)
DY(8)=-BIPHE*Y(8)
DY(9)=0.0
DY(10)=0.0
DY(11)=BIPPE*Y(2)-BIPHE*Y(11)
DY(12)=BIPHE*Y(2)-BIPHE*Y(12)
DY(13)=BIPHE*Y(2)+BIPHE*Y(3)-(BIPPE+BIPHE)*Y(13)
DY(14)=BIPPE*Y(3)-B2CAL*Y(14)
DY(15)=BIPHE*Y(3)-B2CAL*Y(15)
DY(16)=BASY(4)+BIPHE*Y(8)+0.5*BIPHE*Y(17)
DY(17)=BICAD*Y(5)+BIPHE*Y(7)+BICAL*Y(19)+BIPHE*Y(20)-BIPHE*Y(17)
DY(18)=B2CAD*Y(5)
DY(19)=BIPHE*Y(6)+BIPHE*Y(11)+BIPHE*Y(13)-(BICAL+B2CAL+B3CAL)*Y(19)
DY(20)=BIPPE*Y(1)-BIPHE*Y(20)
DY(21)=0.0
DY(22)=BIPHE*Y(12)+BIPHE*Y(13)-BICAL*Y(22)
DY(23)=0.0*BIPHE*Y(17)
DY(24)=2*BIPHE*Y(4)+BIPHE*Y(5)+BIPHE*Y(8)+BIPHE*Y(20)
DY(25)=BIPHE*Y(4)+BIPHE*Y(8)+BICAL*Y(19)+BICAL*Y(22)
DY(26)=(BIPPE+BIPHE)*Y(1)+B2CAL*Y(19)+B2CAL*Y(14)+Y(15)
DY(27)=0.0
DY(28)=B2CAL*Y(14)+Y(15)
DY(29)=0.0
DY(30)=0.5*BIPHE*Y(17)
DY(31)=B2CAL*Y(19)
DY(32)=B3CAL*Y(19)
DY(33)=BIPHE*Y(7)
DY(34)=BIPHE*Y(7)
DX(1)=- (BIPPE+BIPHE)*X(1)+BIPHE*X(4)+(BIPPE+BIPHE)*X(7)+BIPHE*X(13)+BIPHE*X(16)
1+BIPHE*X(22)
DX(2)=BIPHE*X(1)+BIPHE*X(1)+(BIPPE+BIPHE)*X(5)+BIPHE*X(17)+BIPHE*X(23)
DX(3)=BIPHE*X(1)+(BIPPE+BIPHE)*X(11)+BIPHE*X(15)+BIPHE*X(18)+BIPHE*X(24)
DX(4)=- (BIPPE+BIPHE)*X(4)+(BIPPE+BIPHE)*X(9)+BIPHE*X(14)+BIPHE*X(19)
DX(5)=BIPHE*X(4)-(BIPPE+BIPHE)*X(5)+(BIPPE+BIPHE)*X(10)+BIPHE*X(20)
DX(6)=BIPHE*X(5)+(BIPPE+BIPHE)*X(12)+BIPHE*X(21)
DX(7)=- (BIPPE+BIPHE+BIPHE)*X(7)
DX(8)=BIPHE*X(7)-(BIPPE+BIPHE)*X(8)
DX(9)=- (BIPPE+BIPHE+BIPHE)*X(9)
DX(10)=BIPHE*X(9)-(BIPPE+BIPHE+BIPHE)*X(10)
DX(11)=- (BIPPE+BIPHE)*X(11)
DX(12)=BIPHE*X(10)-(BIPPE+BIPHE)*X(12)
DX(13)=-BIPHE*X(13)
DX(14)=-BIPHE*X(14)
DX(15)=-BIPHE*X(15)
DX(16)=BIPHE*X(19)-(BIPPE+BIPHE+BIPHE)*X(16)
DX(17)=BIPHE*X(16)-BIPHE*X(17)+BIPHE*X(20)
DX(18)=BIPHE*X(16)-BIPHE*X(18)
DX(19)=- (BIPPE+BIPHE+BIPHE)*X(19)
DX(20)=BIPHE*X(19)-(BIPPE+BIPHE+BIPHE)*X(20)
DX(21)=BIPHE*X(20)-BIPHE*X(21)
DX(22)=- (BIPPE+BIPHE+BIPHE)*X(22)
DX(23)=BIPHE*X(22)-BIPHE*X(23)
DX(24)=BIPHE*X(22)-BIPHE*X(24)
DX(25)=BIPHE*X(1)+X(4)+X(5)+BIPHE*X(7)+X(9)+X(10)+X(16)+
1X(19)+X(20)+X(22)
DX(26)=BIPHE*X(1)+X(4)+X(5)+BIPHE*X(16)+X(19)+X(20)+X(22)
DX(27)=DX(26)-DX(25)

```

Figure 8.5 Simulation differential equations

$Y = 3CC$   
 $X = MP$   
 $D = \frac{d}{dt}$

easily solved by analytical methods, and thus provide a basis for exact-numerical solution comparison. The convergence was well beyond any reasonable limit of numerical significance.

In summary, this section has considered the experimental results in light of their significance toward the description and simulation of whole lignin thermolysis. These results have been discussed in terms of the likely interrelated reactions of lignin functional groups, and have allowed the development of a mathematical description of whole lignin thermolysis. Thus, a discrete set of substrate reaction pathways were developed based on the model reactions. The rationalization for the selection of individual pathways and rate constants was also presented, and finally, the actual list of simulation equations was delineated. Thus, a consideration of the simulation results is now cogent.

## 9.0 Simulation Results

Spruce lignin pyrolysis was simulated at temperatures of 300, 400, 500 and 600 C, and to holding times of  $10^4$ ,  $10^4$ ,  $10^2$  and seven seconds, respectively. For each case studied, tabulated results are presented in Appendix 9.1. Figure 9.1 is a graphical presentation of the more interesting pyrolysis product yields at each temperature studied. The present discussion will consider the more important aspects of this simulation, which will be described in terms of the gas, light liquid, phenolic, and carbonaceous coke product fractions. Thus, this discussion will parallel that of the previous lignin experimental pyrolyses, considered in Chapter 4.

### 9.1 Gas Evolution

The model presently accounts for methane, carbon monoxide, and hydrogen release. Formal hydrogen uptake in selected reactions, such as guaiacol demethanation and rupture of certain interunit linkages, often resulted in a negative net hydrogen yield. This provided a measure of hydrogen balance and implied that alternative stable products and additional coke likely arise from thermolysis in the absence of external hydrogen donor.



Pyrolysis to  $10^4$  seconds produced methane in yields of 0.05% and 6.2% at 300 and 400C, respectively. The greater yield at 400C reflects not only guaiacol and veratole activation, but also activation of the prevalent PPE linkage. Reversion of this bond

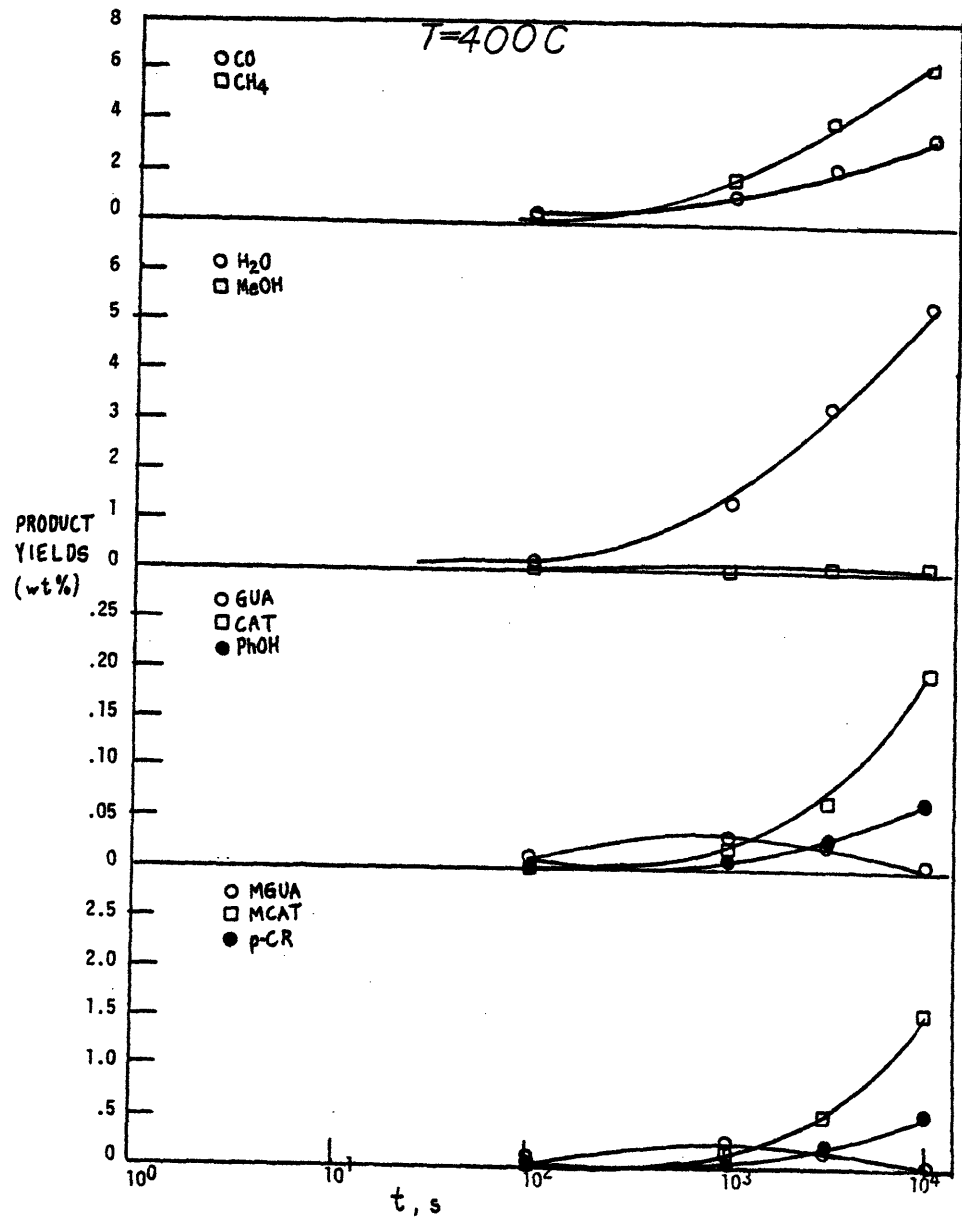


Figure 9.1a Model predictions at 400 C.

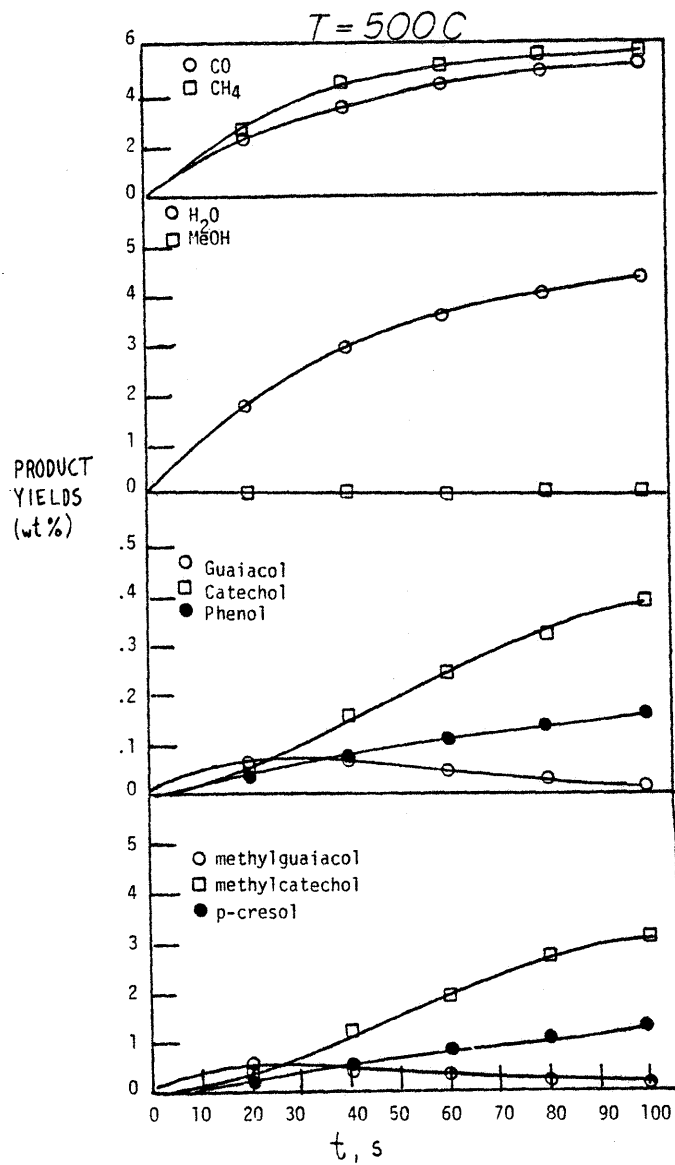


Figure 9.1b Model predictions at 500 C.



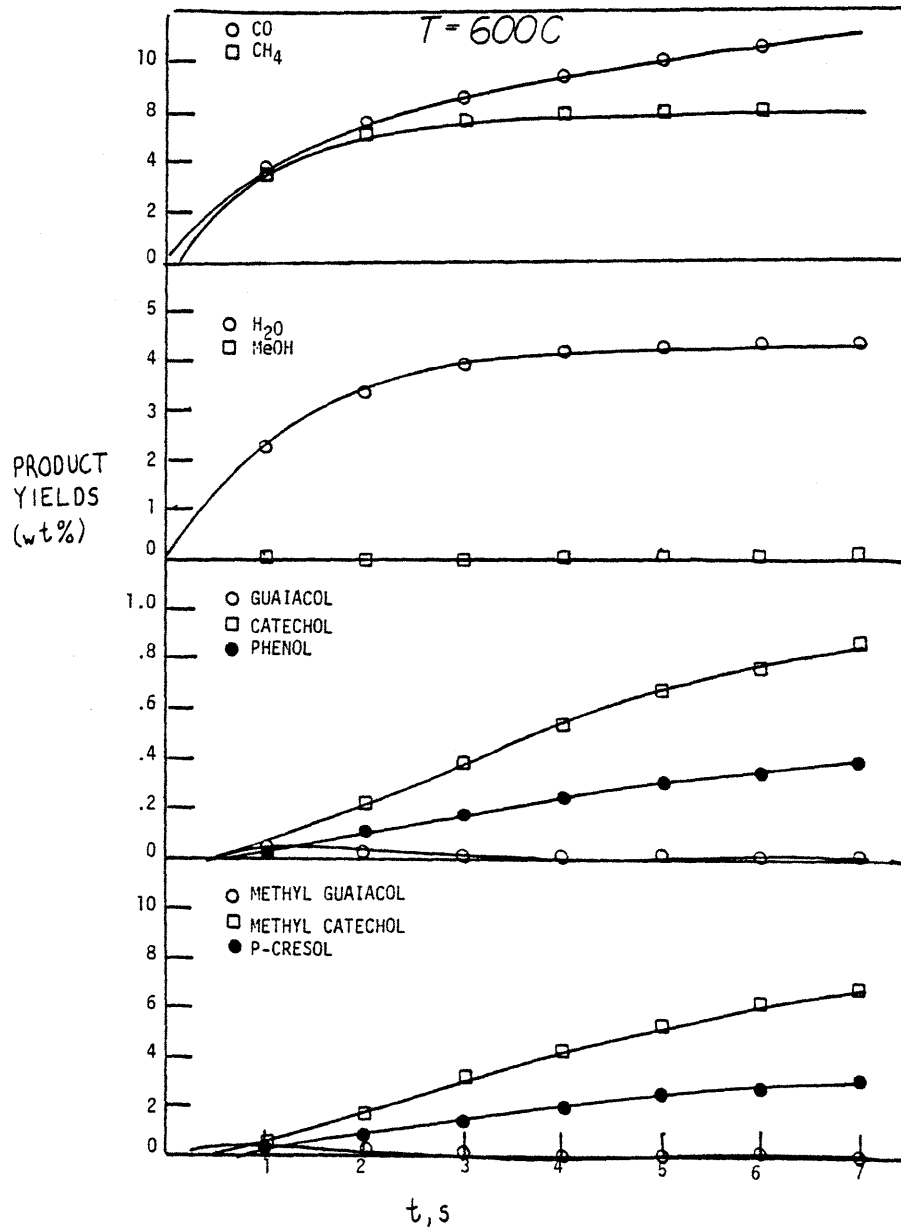


Figure 9.1c Model predictions at 600 C.

generated guaiacols from veratrole type intermediates. At 500C and 100s, the simulation predicted a methane yield of 5.9%, whereas at 600C and 7s, a yield of 6.1% was predicted. Thus, these increases in the pyrolysis temperature resulted in a sharp decrease in the time required to reach a nominal yield of 6%. These yields compare with a theoretical maximum of about 9%, obtained by assuming each aromatic unit could contribute one methane mol.

#### CO

Simulation to  $10^4$ s at 300 and 400C produced CO in yields of 0.037% and 3.5%, respectively. In both cases, these were less than the corresponding methane yield, yet initial rates of formation of CO at 300 and 400C were faster than that for methane. This is evidenced by the short time data of Figure 9.1a. This early CO arises due to the initial concentrations of lignin cinnamaldehyde side chains, which decarbonylate rather easily. Since saligenol dehydration is extremely rapid, ether reversions generate further carbonyl and guaiacol units. However, a large fraction of the carbonyls are of the acrolein type, which decarbonylate much slower than cinnamaldehydes. Hence, CO precursor activities fall short of those for methane release as pyrolysis proceeds, and  $\text{CH}_4/\text{CO}$  thus exceeds unity for modest conversions at 300 and 400C.

On the other hand, CO again predominates at 600C. This behavior is shown in Figure 9.1c, where the yield of CO amounted to 9% at 600C

and 7s. CO predominates at 600C due to both greater acrolein activation as well as greater demethoxylation selectivity of methoxyphenols. The methoxyphenol Arrhenius parameters suggest that CO should be the kinetically favored product at higher temperatures. In short, the ratio CO/CH<sub>4</sub> varies from greater than unity at low temperatures and low conversions, to less than one at low modest temperatures and modest-long holding times, and back to greater than unity at high temperatures. This behavior is well explained in terms of dual sites for CO release and the comparative kinetics of carbonyl and guaiacyl pyrolyses.

#### Hydrogen

Hydrogen yields predicted by the simulation model were generally less than zero, of the order -0.25% at 600C and 7s. Hydrogen arises stoichiometrically with CO from demethoxylation, as well as in the reaction of cinnamyl alcohol to cinnamaldehyde. Hydrogen is consumed in guaiacyl demethanation to catechols, and in certain interunit cleavages. Additional hydrogen is likely formally generated (or rather not consumed) through lignin condensation reactions, which remain unaccounted in this version of the simulation model. Hydrogen yields are not generally reported in the experimental lignin pyrolyses, and thus comparisons of the model results are difficult. Rather, the negative hydrogen yields imply that the yields of light products might be reduced to some extent in favor of condensation products. A likely need for external hydrogen is also suggested, since intra-lignin hydrogen transfer will result in high yields of

carbonaceous residue.



The present version of the simulation model does not provide for  $\text{CO}_2$  release, although ferulic acid, humic acid, and lactone groups present in the lignin in modest amounts should serve as facile  $\text{CO}_2$  precursors. As the experimental section of the present investigation included the pyrolyses of ferulic, cinnamic, and naphthoic acids, inclusion of these into the reaction model requires only an accurate assessment of the proportions of these acid sites in the substrate lignin.

## 9.2 Liquid Products

The present version of the model accounts for only two components of the aqueous distillate, water and methanol. The former is considered first.



The simulation provides for water formation predominantly through saligenol-type unit dehydrations. Cinnamyl alcohol side chains provide less important precursors. Ultimate water yields were rather modest, amounting to 0.05%, 5.3%, 4.4% and 4.4% at  $(300\text{C}, 10^4\text{s})$ ,  $(400\text{C}, 10^4\text{s})$ ,  $(500\text{C}, 10^2\text{s})$  and  $(600\text{C}, 7\text{s})$ , respectively. The low yields at 300C reflect the stability of saturated propylglycol moieties, whereas PPE reversion generates the reactive saligenol units readily at temperatures in excess of about 350C. As evidenced in Figure 9.1, the simulation model seems to predict ultimate water yields of about 6%. Absolute experimental determinations of water production have not often been reported, yet Table 4.1 presents total aqueous distillate

yields of 8.7-30%, averaging about 15%. Thus, the water yields predicted by the simulation are from about 1/3 to 1/2 that reported from experimental investigations, occasionally as close as 3/4. These discrepancies are considered significant, and are considered in greater detail in a later section.

#### MeOH

An ultimate methanol yield of only about 0.1% is predicted by the simulation model. The yields are low at each temperature, increasing rather monotonically with pyrolysis holding time and temperature. The single simulation methanol formation pathway is through degradation of cinnamyl alcohol side chain units. These units are rather few in overall lignin; the methanol pathway of this unit is in turn relatively minor. Thus, it is not totally surprising that the simulation model generally underpredicted those methanol yields reported in the literature, which are of the order 0.28-1.5%. The reasons for the smaller methanol predictions are not clear, and could be due to kinetic limitations or the presence of additional precursors.

### 9.3 Phenolic Products

As evidenced in Appendix 9.1, the simulation model faithfully predicts most of the 30+ phenols reported in previous experimental pyrolyses. The model also predicts other products not hitherto delineated in the literature. The latter compounds likely eluded experimental detection because of their small relative proportions and/or molecular complexity. Overall, the product yields are close to, or within, the rather generous band of yields reported in the

literature. The simulation predictions of phenols will be reported by phenol types.

### Guaiacols

Guaiacols arise in lignin pyrolysis through the degradations of both the 3-carbon side chain and etherified methoxyphenol substituents. Thus, the products coniferaldehyde, guaiacylacrolein, eugenol, propylguaiacol, vinylguaiacol, ethylguaiacol, methylguaiacol and guaiacol represent various stages of 3-carbon chain degradation. Of these, coniferaldehyde and guaiacylacrolein are the most primary, degradation of these yielding vinyl guaiacols. These, in turn, yield methylguaiacols, ethylguaiacol, and guaiacol with further pyrolysis. These trends are reflected in the simulation predictions. At 400C and 100s, the ratios (coniferaldehyde: vinylguaiacol: methylguaiacol: guaiacol) were (0.68: 0.13: 0.088: 0.011), whereas at 500s the proportions were (0.096: 0.02: 0.26: 0.034) and at  $10^4$ s (0.000128: 0.000218: 0.03: 0.0039). By  $10^4$  s, the data reflect not only 3-carbon side chain degradation of the aldehyde, but also secondary pyrolysis of guaiacols to catechols. Thus, each guaiacol product is both formed and degraded during pyrolysis, and therefore attains maximal proportions at some point. As evidenced in the tables of Appendix 9.1, the behavior at higher temperatures was similar, the relative proportions of each guaiacol varying due to unequal reaction energetics.

Notable among other guaiacols predicted by the model are guaiacylacrolein, coniferaldehyde, and the eugenols. Only the more exhaustive investigations have reported the latter two,<sup>38, 39, 41, 34</sup> whereas the

acrolein is not generally reported. The ultimate acrolein precursors are guaiacyl-glycerol- $\beta$ ethers which undergo PPE type ether reversion, and this guaiacol is thus produced in rather significant proportions.

#### Syringols (2,6-dimethoxyphenols)

With two exceptions, the reactions of syringol compounds directly mimic those of guaiacol compounds. The more important difference is the reaction path degeneracy inherent in syringols, provided by the multiple methoxyl substitution. The second exception involves lignification steric effects, which prevent the formation of biphenyl and phenyl coumaran links in aromatic units arising from sinapyl alcohol monomers. However, the consecutive and parallel nature of the reaction paths generating syringol products is substantially as described above for guaiacols.

The initial conditions imposed on the present simulation reflect those of a spruce lignin, which incorporates relatively few sinapyl alcohol units. Thus, the present simulation will not align with those experimental pyrolyses involving aspen-wood lignins. Further application of the model might be directed toward aspen-wood lignins, and this would involve only major change in the initial concentration vector of the methoxyphenols. In fact, this change might have slight implications toward the 3-carbon side chain vector because of the reduced likelihood of phenylcoumaran units.

#### Catechols

Rather substantial amounts of catechols are predicted by the simulation model, due to the relatively facile demethanation kinetics of guaiacol and substituted guaiacols. Thus, the catechols are

clearly secondary products, most selectively favored at lower temperatures and longer holding times. These conditions are optimal for catechol production because demethoxylation is the more activated guaiacol reaction pathway. Thus, phenols would be favored at higher temperatures. These generalizations are reflected in the data. At 300C and  $10^4$ s, the proportions (catechol: methylcatechol: vinylcatechol) aligned as  $(4 \times 10^{-5}: 3 \times 10^{-4}: 6 \times 10^{-5})$ . These low yields depict the rather slow reactions of PPE linkages, cinnamaldehyde side chains, and methoxyphenols at 300C. At 400C and 100s, the proportions arose as  $(5 \times 10^{-4}: 4 \times 10^{-3}: 6 \times 10^{-3})$ , whereas for pyrolysis to  $10^4$ s, the yields were (0.2: 1.6: 0.012). At 500C and 10s holding time the ratios were (0.02: 0.15: 0.16), changing to (0.38: 3.03: 0.19) at 100s. Finally at 600C and 1s, the proportions were (0.069: 0.54: 1.2), aligning as (0.86: 6.8: 1.2) at 7s. Thus, the yields of catechol and methylcatechol increased dramatically with increasing holding time and temperature, whereas the vinyl catechols increased more slowly. The vinyl catechols would thus attain maximal proportions due to secondary 3-carbon chain degradation.

As was the case with guaiacols and syringols, the simulation predicts the formation of complex single ring catechols, such as 3,4-dihydroxycinnamaldehyde and 3,4-dihydroxyphenylacrolein. These would quite likely remain undetected in the experimental CO analyses. Further, the multiple ring aromatic products likely also contain significant quantities of catechol units, which might be extrapolated to describe the carbonaceous residue.

#### Phenols

The simulation model predicts rather modest proportions of phenols



from lignin pyrolysis. Phenols arise from two sources, these being aromatic units initially derived from incorporation of coumaryl alcohols during lignification, and from the demethoxylation reactions of guaiacol and syringol units. The statistical matching procedure demands that the phenol types be analogous to the guaiacols and syringols, thus simple phenol, cresol, ethylphenol, propylphenol, vinylphenol, allylphenol, coumaraldehyde and hydroxyphenylacrolein all arise as products. The simulation yields for phenol and cresols (overwhelmingly para) aligned as (PhOH,pCR) @ ((300C,10<sup>4</sup>s), (400C, 10<sup>4</sup>s), (500C,10<sup>2</sup>s), (600C,7s)) = ((0.00031, 0.0024), (0.067,0.55), (0.16,1.3), (0.39,3.1)). Thus, not unexpectedly, the absolute yields of phenols increased with increasing pyrolysis severity. Comparison with catechol yields provides insights into guaiacol reaction selectivity. This is complicated by the initial concentrations of coumaryl alcohol units, but these are relatively modest in lignin, and should not alter the selectivity conclusions greatly. At 400C and 10<sup>4</sup>s, the ratio (Phenol/Catechol) = (0.34), whereas at 600C and 7s, the ratio equalled (0.45). Thus, the greater energy of activation for guaiacol demethoxylation relative to demethylation shifts the higher temperature selectively to phenols.

#### 9.4 Carbonaceous Residue - Kinetics

Although the simulation model has been primarily concerned with the evolution of gases, liquids, and light phenolics, several generalizations regarding the carbonaceous deposit are possible. As depicted by the present model, the carbonaceous deposit is comprised of all aromatic units involved in any possible interunit bonding. Thus, the

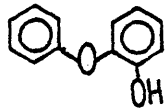
deposit should be characterized by a much higher concentration of phenylether and diphenylmethane linkages than in the initial lignin, as these units are quite thermostable. Further, the methoxyl content should be markedly reduced, due to demethanation and demethoxylation reactions of guaiacyl and veratryl units. Hence, catechol and diquinone moieties should concentrate in the carbonaceous coke as well.

The latter moieties introduce an area where the simulation model should presently fail to depict true lignin pyrolysis. This area concerns condensation, or other coking reactions, which have not been modelled in the present simulation version. Here a 'low concentration' assumption reducing the selectivity of bimolecular reactions, which likely describe coking reactions, has been invoked. Thus the demonstrated formation of coke from guaiacol and saligenol, dimers from cinnamylalcohol and aldehyde, and oligimers from certain interunit linkages have been neglected. One result of this is the negative hydrogen balance, obtained by a stoichiometric accounting of hydrogen consumption and formation.

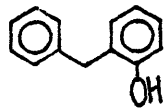
A further aspect regarding the carbonaceous coke involves the more complex single ring aromatics. The present analysis includes the guaiacyl acrolein and coniferaldehyde products as single ring phenols, although these are not often reported as such in experimental pyrolyses. These compounds may simply escape GC detection, but may also preferentially remain with the 'carbonaceous' deposit. Condensation adducts of these would likely be classified as coke.

Thus, the carbonaceous deposit from lignin pyrolysis should

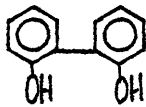
concentrate in the less reactive protolignin aromatic units, as well as be comprised of condensation adducts from precursors to other products. Hence, the coke should include structures of the type listed here:



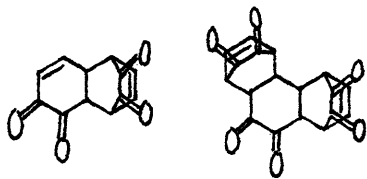
Phenyl Ether



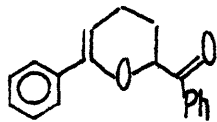
Diphenylmethanes



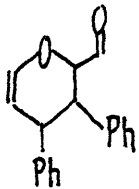
biphenyls



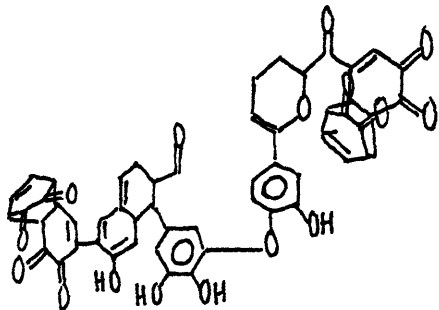
guaiacol adducts



guaiacyl acrolein adducts



cinnamaldehyde adducts



combination of these

The carbonaceous deposit can also be interpreted kinetic terms. Most kinetic analyses of lignin pyrolysis focus upon substrate weight loss, labeling the remaining materials as unreacted lignin. This is clearly a global description, subject to considerable uncertainty. For example, isomerization or rearrangement reactions would effect no weight loss, but would certainly alter the character of the substrate. In any event, weight loss is a reasonable operational definition of global lignin reactivity. With regard to the simulation, single ring aromatic units and light liquids and gases can rather arbitrarily be designated as volatile, and hence, by difference, the multiple ring aromatics as non-volatile. If the latter group is conceptualized as 'unreacted lignin', the model then provides a measure of lignin 'conversion'.

As a consequence of the statistical matching of the methoxyphenol and 3-carbon chain distributions in unreacted lignin used to describe the substrate, the initial mol fraction of multiple ring aromatics is not 1.0, rather 0.9276. This arises because a fraction of the initial side chains are of the cinnamaldehyde and hydroxyacetone type, not involved in interunit bonding, and because a fraction of the methoxyphenols are not etherified, rather free phenols. The statistical matching then predicts that about 7% of the aromatic units in the unreacted lignin are already single ring aromatics. Although somewhat surprising, this prediction is reasonable, as single ring aromatics were the starting monomers in lignification. It is quite likely that lignification need not occur at 100% conversion of each monomer. Further, exchange reactions should generate aldehydes

and acids equally well for multiple and single ring aromatic units. The 'initial' single ring aromatics may in fact account for the seemingly low temperature 'reactivities' (vaporization) determined in DTA/DTG studies. In any event, the model predictions will more closely represent experimental pyrolyses if the initial mol fraction of multiple ring aromatics is considered to be unity, and long time data at each temperature are used to describe lignin conversion.

Under these conditions, volatilization and pyrolysis should be rendered indistinguishable, as is likely the case in experimental pyrolysis.

The fraction of multiple ring aromatics remaining at  $(300\text{C}, 10^4\text{s})$ ,  $(400\text{C}, 10^4\text{s})$ ,  $(500\text{C}, 10^2\text{s})$ ,  $(600\text{C}, 7\text{s})$  = (0.914, 0.314, 0.420, 0.385), which correspond to global first order rate constants of  $\log_{10}k(\text{s}^{-1})$  (300, 400, 500, 600C) = (-5.05, -3.94, -2.06, -0.98). The rate constants correspond to Arrhenius parameters of  $(\log_{10}A(\text{s}^{-1}), E^* (\text{kcal/mol}))$  = (7.06 $\pm$ 1.3, 32.4 $\pm$ 4.10). Thus, the complex set of parallel and consecutive reactions incorporated into lignin pyrolysis yield a rather low set of global first order Arrhenius parameters, on the order of those reported from the Russian DTA/DTG experiments. It should be emphasized that these calculations were effected at the longest holding times studied for each temperature, in an effort to better coincide with DTA/DTG and destructive distillations experimental studies. Shorter time pyrolysis results will be considered below. DTA studies have been performed on a wide range of lignin types by Domburg, et al.<sup>39</sup>, who heated the various preparations at 12C/min to 600C. These workers determined pyrolysis activation energies generally in the range 26-30 kcal/mol, with extremes of 17.4 and 31.1. One additional determination

yielded an activation energy of 54.8 kcal/mol. Similarly Domburg and Sergeeva<sup>129</sup> report activation energies ranging from 17.8-38.3 kcal/mol from DTG studies on birch, aspen and oak woods. The values were similar from experiments in the presence of the pyrolysis vapours and gases and from those in which these volatiles were removed. Thus, the DTA/DTG studies conducted at rather slow heating rates yield Arrhenius parameters of the same order as those determined from the model predictions at long times. However, the predictions are of little kinetic interest, since the true lignin kinetics are likely not first order, and thus an arbitrary selection of long time data is inadequate. Further the experimental DTA/DTG studies were not isothermal, adding further complication to kinetic analysis. Of more direct interest for comparison with the simulation model would be an isothermal pyrolysis executed at well defined time intervals.

The experiments of Iatridis and Gavalas<sup>26</sup>, performed at very high heating rates and well defined holding times, approach this ideal quite well. These workers present weight loss data for a precipitated Kraft lignin as a function of reaction holding time. They report values for weight loss of about 27%, 45% and 57% for (400C, 120s), (500C, 60s) and (600C, 40s), respectively. These correspond to pseudo first order rate constants  $-\log_{10}k(s^{-1})$  (400, 500, 600C) = (2.58, 2.00, 1.67). Thus, these data align with the simulation predictions only where similar times are compared at each temperature. For example, the simulation predicts  $-\log_{10}k(400C, 100s) = 2.94$ , in much closer agreement with the experimental data at 400C and 120s. Further, Iatridis and Gavalas report about 50% weight loss at 600C and

7s, corresponding to  $-\log_{10}k=1.00$ . Thus, the simulation data accord quite well with the experimental data when the kinetic constants at a given temperature are compared at near equal holding times. The table below emphasizes the agreement of the weight loss data of Iatridis and Gavalas and the simulation results presented here

PRESENT SIMULATION		IATRIDIS AND GAVALAS		
$-\log_{10}k(s^{-1})$	t (s)	T(°C)	t(s)	$-\log_{10}k(s^{-1})$
2.94	100	400	120	2.58
1.92	60	500	60	2.00
0.87	7	600	7	1.00

The above discussion has compared the data of Iatridis and Gavalas with the simulation model in terms of implied first order rate constants. Alternatively, the simulation weight loss prediction can be compared to the actual experimental weight loss curves. Thus, Figure 9.2 is a superposition of the present simulation curves and the experimental weight loss curves of Iatridis and Gavalas. As evidenced by Figure 9.2, the experimental and simulation curves align best at 500C, with a slight simulation over-prediction at 600C and under-prediction at 400C. Overall, however, the simulation and experiments agree quite well, with maximal weight loss differences of about 10%.

In summary, the simulation can describe the essential features of whole lignin pyrolysis. The model predicts most of the major lignin pyrolysis products, including  $CH_4$ , CO,  $H_2O$ , MeOH and a wide variety of phenols. Further pathways to describe  $CO_2$  evolution can be easily incorporated. More detailed quantitative comparison of simulation and experimental product yields is presented in Chapter 10. The

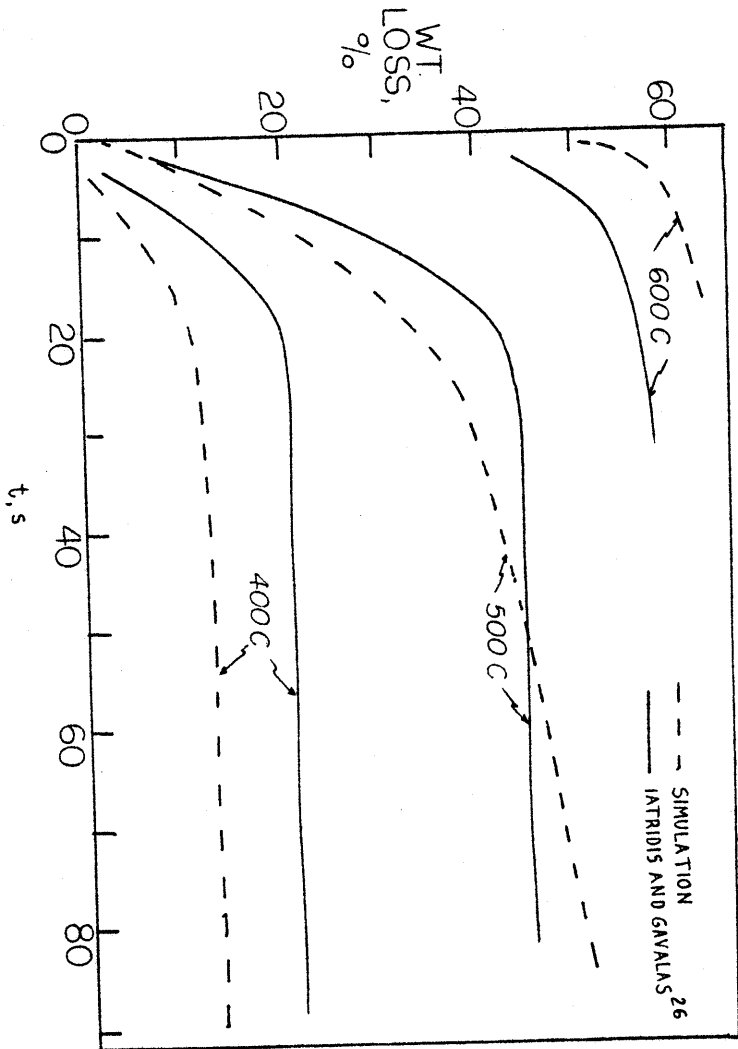


Figure 9.2 Comparison of simulation weight loss predictions with the experimental data of Iatridis and Gavalas<sup>26</sup>



carbonaceous residue has been described in terms of likely structural moieties, and has been used as a measure of overall lignin conversion. The kinetic data implied by the time variation of this conversion agree reasonably well with literature pyrolysis weight loss data. The implications of these kinetics are also further discussed in Chapter 10.

## 10.0 Discussion

Discussion of the model pathways used to describe lignin pyrolysis will be divided into three parts. The first of these will be concerned primarily with the experimental pyrolyses as related to the model compound results per se. That is, the individual model compound results will be compared with relevant literature citations in an attempt to develop mechanistic insights and interpretations. This first part will also consider some of the thermochemical dictates and limitations to each reaction pathway developed in Chapter 7. The second part of this chapter will consider the application of the model pathways, namely the simulation model predictions. These predictions will be compared with both previous experimental whole-lignin pyrolyses as well as with theoretical estimates of the upper limits for individual product and product fraction yields. The limitations and strengths of the simulation model will thus arise. The final part will consider possible strategies for modification of lignin thermolyses aimed toward the optimal production of useful products. These strategies will be developed from both the experimental and simulation results.

### 10.1 Model Compound Pyrolyses

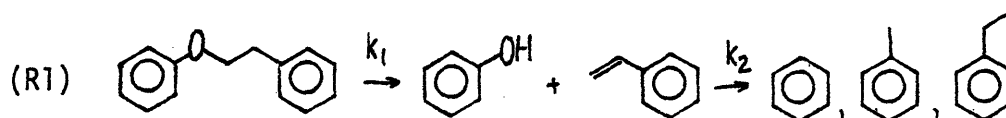
This section will consider the present model compound results and relevant literature studies in an attempt to formulate plausible mechanistic insights for the reaction pathways developed in Chapter 7. Interpretation of likely elementary or molecular reactions in light of the limitations imposed by thermodynamics should provide additional relevant mechanistic insight.

### 10.1.1 Pathways Mechanisms - Relevant Literature Comparisons

#### Phenethyl Phenyl Ether (PPE)

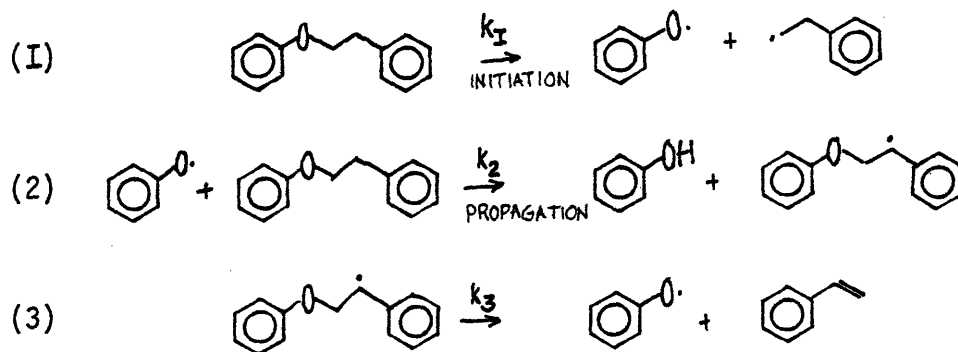
As described in section 7.1, neat and in-tetralin pyrolyses of PPE resulted in the stoichiometric primary production of phenol and styrene, the latter product capable of secondary degradations to toluene, ethylbenzene, and benzene. This secondary reaction selectivity favored toluene for neat ether pyrolysis, whereas ethylbenzene was favored in tetralin. As evidenced in Figure 7.1.5, the kinetics for neat and in-tetralin degradation were indistinguishable. These results invite mechanistic interpretation.

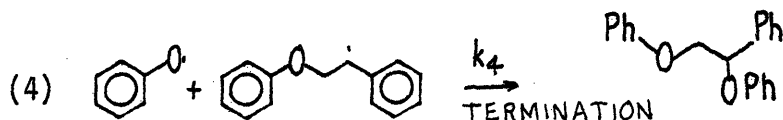
The relatively clean pyrolysis of the ether to phenol and styrene suggested an overall pathway of the type R1, namely



These results can be rationalized in terms of both a free radical chain or a pericyclic retroene mechanism.

The former mechanism can be formally represented as:





where only the likely important reactions have been included. Termination to peroxide has been excluded, as has termination by the initial ethylbenzene or a subsequent hydrogen radical. Coupling of PPE radicals is a possible candidate, but has been considered less probable than cross coupling; this assessment has not been unequivocally established.

Invoking the steady state hypothesis for the radical species <sup>175</sup>, an overall PPE decomposition expression can be derived for long chains, namely

$$-\frac{dE}{dt} \cong k_2 [\text{C}_6\text{H}_5\text{O}^\bullet] [E] = \sqrt{\frac{2 k_2 k_3 k_I}{k_4}} \cdot E$$

A signal feature of the mechanism is the prediction of first order kinetics. Other termination steps would have yielded orders different from unity; specifically, 3/2 order would be the result of a combination of two phenoxy radicals, thermodynamically unlikely. The major products predicted by this mechanism would be phenol and styrene, in accord with the observed experimental results.

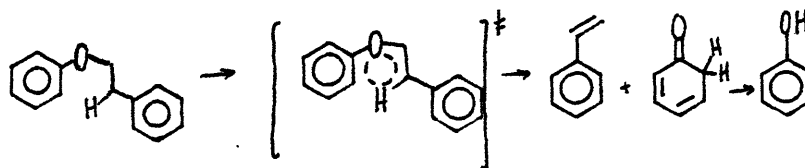
However, a free radical chain might be expected to be affected by large amounts of tetralin. The tetralin could cap the chain carrier to phenol, hindering chain propagation and thus overall reactivity. In the limit of infinite dilution by tetralin, the 'chain' could essentially be reduced to one of initiation only, i.e., the unimolecular fission of PPE to phenoxy and ethylbenzene radicals as a rate determining

step. These radicals could be quenched to phenol and ethylbenzene, although the latter radical could still undergo  $\beta$ -scission to styrene. However, the primary degradation product was styrene, whereas ethylbenzene was clearly secondary. Further such a unimolecular fission should proceed with an activation energy at least as great as the bond strength, of order  $61 \pm 5 \text{ kcal/mol}$ ; the estimation of this bond strength based on the techniques due to Benson<sup>169</sup>. The accompanying transition state would be 'loose', resulting in a  $\log_{10} A(\text{s}^{-1})$  factor in excess of 13.5. The experimental Arrhenius parameters of  $(\log_{10} A, E^*) = (11.1, 45.0)$  accord with neither of these predictions.

The long chain length kinetic expression can be compared to the experimental Arrhenius parameters as well. Estimating thermochemical parameters<sup>169</sup> for the elementary reactions 1, 2, 3 and 4 as  $(\log_{10} A, E^*) = (17.0, 70.0), (8.6, 25.0), (12.8, 20.0)$  and  $(9.0, 0.0)$ , respectively, the long chain expression yields overall first order parameters of  $(14.9, 57.5)$ . These parameters differ significantly from the present experimental parameters, yet at 400C yield a rate constant  $\log_{10} k_1 = -3.78$ , in reasonable accord with the present results.

Overall, the long chain free radical mechanism represented a plausible possibility, but the observed experimental effects of tetralin and Arrhenius parameters were in disaccord. Thus arose the pericyclic alternative.

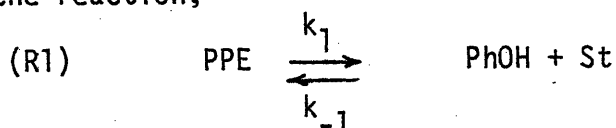
The concerted pathway depicting the mechanistic features of R1 can be represented as:



where the intermediate carbonyl undergoes rapid hydrogen tautomerism to regenerate the aromatic phenol. Thus, PPE is depicted to suffer direct unimolecular retro-ene reversion to phenol and styrene, and should clearly decompose by first order kinetics. The transition state of this pericyclic pathway should be highly ordered, representing the decrease in entropy attended by the loss of molecular degrees of freedom; this would imply a value of less than 13.5 for the Arrhenius  $\log_{10} A$  factor. Further, such a unimolecular decomposition should be relatively insensitive to solvent effects, as is generally the case for pericyclic reactions.<sup>170</sup> Hence, tetralin would exert little overall effect on PPE pyrolysis. In short, the experimental details of the present investigation accord quite well with the postulated retroene elimination.

If PPE reversion in fact proceeds by the pericyclic mechanism postulated above, then the reverse reaction should occur with Arrhenius parameters characteristic of an ene cycloaddition. That is, the principle of microscopic reversibility dictates that the forward and reverse reactions should share a common transition state. Estimation of thermochemical parameters for PPE<sup>169</sup>, coupled with those for phenol and styrene, yields overall reaction thermochemical parameters of  $(\Delta H_R^\circ$  (kcal/mol),  $\Delta S_R^\circ$  (e.u.)) = (11.3, 33.8). These may be combined with the forward activation parameters to yield the cycloaddition parameters in the following manner:

For the reaction,



equilibrium is achieved where the net reaction rate vanishes, or

$$0 = k_1(\text{PPE}) - k_{-1}(\text{St})(\text{PhOH}) \rightarrow \frac{(\text{St})(\text{PhOH})}{(\text{PPE})} = \frac{k_1}{k_{-1}} = K_1(\text{atm})$$

where

$$\log_{10} K_1(\text{atm}) = -\Delta G_R^0 / \theta = -\frac{\Delta H_R^0}{\theta} + \frac{\Delta S_R^0}{2.303R}$$

Thus,

$$\log_{10} K_1(\text{atm}) = \log_{10} k_1 - \log_{10} k_{-1}$$

and

$$(1) \log_{10} A_{-1} = \log_{10} A_1 - \Delta S_R^0 / (2.303R)$$

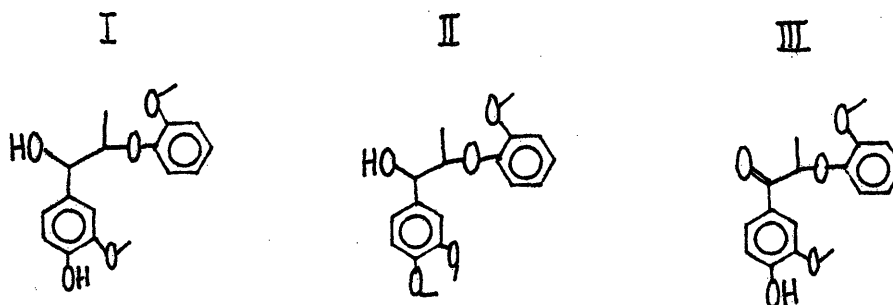
$$(2) E_{-1}^* = E_1^* - \Delta H_R^0$$

The experimentally determined forward Arrhenius parameters coupled with the estimated thermochemical constants yield reverse activation parameters ( $\log_{10} A(1/\text{mol}\cdot\text{s})$ ,  $E^*(\text{kcal/mol})$ ) = (5.9, 35.9); these values reflect conversion from pressure to concentration units at 400C. The reverse Arrhenius parameters agree quite well with those for typical bimolecular cycloaddition reactions<sup>167,171</sup>.

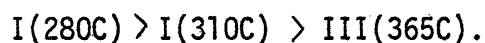
Of the two mechanistic rationalizations of R1, the pericyclic pathway accords better with the present experimental results. The product spectra, kinetics and effect of tetralin were as predicted by the concerted mechanism. The experimentally determined forward and the inferred reverse Arrhenius parameters are in excellent agreement with those typically found for similar concerted pathways. Further, the pericyclic mechanism well rationalizes the results of previous experimental pyrolyses of  $\beta$ -ethers of the type PPE.

Relevant pyrolyses of  $\beta$ -ethers have been reported by a small number

investigators. Among these, an investigation<sup>75</sup> of the thermal behavior of substituted  $\beta$ -ethers I, II and III is notable. The temperature

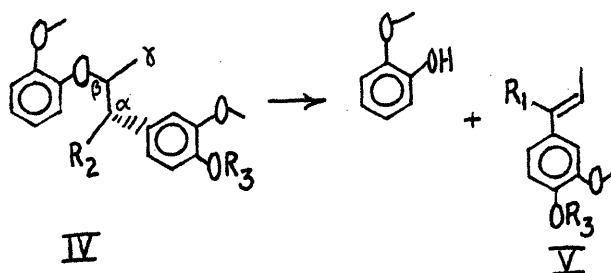


of 50% weight loss for each of these was reported from DTA studies conducted at 12 C/minute. The ethers were reactive in the order



At temperatures lower than 340 C, activation energies of 16, 15 and 82 kcal/mol were reported for I, II and III respectively. The product spectra consisted of guaiacol, methyl-, ethyl- and propyl-guaiacols, cis- and trans-isoeugenol, traces of eugenol, vanillin and acetovanillone; the latter two formed in much larger quantities from III than from I. A detailed account of these product spectra is presented as Table 4.11. These results were interpreted in terms of homolytic and heterolytic mechanisms, yet they accord well with the results, pathways and mechanisms reported here.

With regard to product spectra, the large predominance of guaiacol is completely analogous to the large yields of phenol determined here. In the present formalism for PPE, their reactions may be viewed as



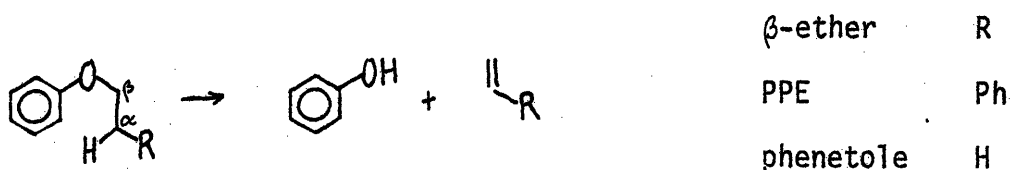
Ether	R <sub>1</sub>	R <sub>2</sub>	R <sub>3</sub>
I	OH	H	H
II	OH	H	Me
III	O=	-	H



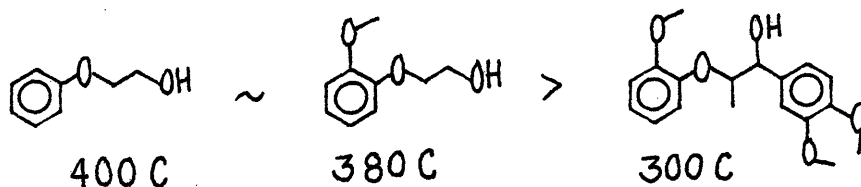
with appropriate modifications of structure V when emanating from ether III. Thus it is quite reasonable that guaiacol should predominate from pyrolysis of I-III, just as phenol was found from PPE. For pyrolysis of I and II, the co-product V can be visualized to suffer dehydration to yield the isoeugenols. For pyrolysis of III, co-product V can be envisioned as a facile precursor to vanillin and acetovanillone. Hence formation of co-product V is rather analogous to the production of styrene from PPE. Further, the methyl-, ethyl- and propylguaiacols likely arose from V in much the same way that benzene, toluene and ethylbenzene arose from secondary pyrolyses of styrene. In short, the product spectra of Domburg, et al., is completely analogous to that reported here for PPE.

The pericyclic mechanism also rationalizes the kinetics implied by the order of 50% weight loss temperature. The pericyclic mechanism is available to both I and II, but unavailable to III. This arises as a consequence of the lack of H substituent R<sub>2</sub> in III; the corresponding  $\alpha$ -hydrogen in PPE was shifted as an integral part of the pericyclic mechanism. Thus, I and II may easily participate in a concerted retroene reaction of the type postulated for PPE, whereas an alternate pathway is required for III. This alternate pathway is evidently a high energy process, emphasized by the respective temperatures for 50% weight loss of I, II and III. This higher energy pathway could be direct scission of the  $\beta$ -carbon and oxygen atoms of structure IV, or a phenetole-type pathway involving the  $\gamma$ -carbon of structure IV. Phenetole degradation in tetralin has been studied by Benjamin, et al.<sup>78</sup>, who report 5% substrate decomposition after one hour at 400C. The major

pyrolysis products were phenol, ethane and ethylene. This conversion corresponds to an apparent first order rate constant of  $\log_{10}k(s^{-1}) = -4.85$ , which is over one order of magnitude lower than that for PPE at the same temperature. Phenetole is structurally similar to PPE, differing in phenyl substitution at the  $\alpha$  carbon. The similarity is emphasized here, both with regard to structure and reactions.



The  $\alpha$ -phenyl substituent evidently enhances ether reversion considerably. Similarly, Savinykh, et al.<sup>76</sup>, found that phenyl substitution reduced the temperature of 10% weight loss in certain  $\beta$ -ethers, as they determined the series:



in DTA and DTG experiments at 5 c/min.

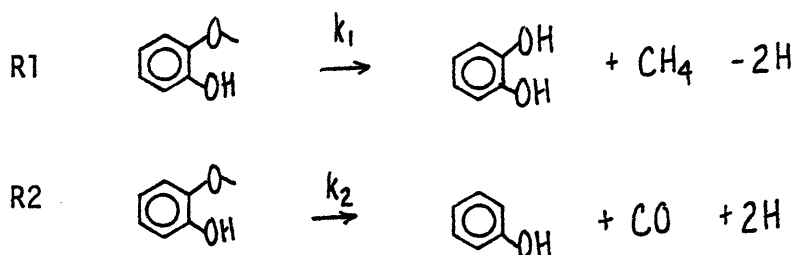
In short, the DTA data of Domburg, et al., are in substantial agreement with the present results. A phenetole-type pathway may operate for pyrolysis of III, and could further explain the traces of eugenol detected in higher temperature pyrolyses of I. However, this pathway is kinetically less significant than that for PPE, also available to I and II, by at least one  $\log_{10}k$  unit. These observations are

reflected in the observed temperature for 50% weight loss of each ether. The product spectra obtained from pyrolysis of I and III are further analagous to those reported here for PPE.

In summary, two competing mechanistic interpretations of the present PPE results have been examined. Of a free radical chain and concerted retroene elimination possibilities, the latter accorded more favorably with the experimental product spectra, kinetics, and effect of tetralin solvent. The pericyclic mechanism also accords with and further explains the result of previous  $\beta$ -ether pyrolyses.

#### Guaiacol

Catechol and phenol were the chief liquid products identified in guaiacol pyrolyses, with evolution of  $\text{CH}_4$  and  $\text{CO}$  in amounts stoichiometric with the former and latter, respectively. First order pathways of the type R1 and R2 were determined, namely:



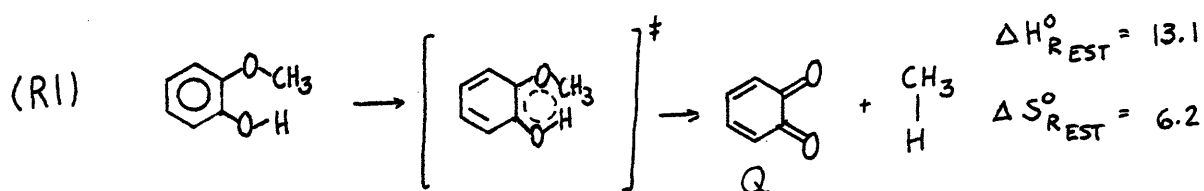
Arrhenius parameters of  $(\log_{10} A(\text{s}^{-1}), E^* (\text{kcal/mol})) = (10.9 \pm 0.5, 43.7 \pm 1.4)$  and  $(11.5 \pm 0.5, 47.7 \pm 1.6)$  were determined for R1 and R2 respectively; these were determined over a range of five orders of magnitude in  $k_1$  and four orders of magnitude in  $k_2$ .

Quantitative comparison of the present results with previous literature is possible only in a few instances. Prior studies of guaiacol pyrolyses<sup>91,92,95,96</sup> provide no activation parameters but do give overall substrate conversions corresponding to apparent first order rate constants  $\log_{10}k_1(s^{-1}) = -1.0$  at 500 C and  $\sim 0$  at 540C. These are of the order of magnitude of those found in the present study in that temperature range. With regard to product spectra, both demethylation and demethoxylation have been reported in guaiacol pyrolysis from 500-600C<sup>91</sup>. In this range, cresols and xylenols were obtained in yields of 40-50%, and phenol and catechol in 20% and 28%, respectively. Another investigation<sup>92</sup> determined the sensitivity of the product spectra to pyrolysis temperature. Reaction at 450-550C resulted in the formation of catechol, phenol, cresols, xylenols, and alkylcatechols. Whereas phenol and cresol yields monotonically increased with temperature, catechol attained maximal proportions at 530C. This is suggestive of secondary reactions of catechol or catechol precursors. Similarly, a temperature of 530-550C and reaction time of 0.5-2s have been determined as optimal for catechol yield from guaiacol pyrolysis<sup>93</sup>. An additional pyrolysis<sup>94</sup> at 500C and 2 s holding time produced a product spectrum consisting chiefly of catechol and phenols, with xylenols, salicaldehyde and saligenol also reported.

The pyrolysis products reported in the literature are in overall agreement with the results reported here. In both cases, catechol and phenol predominate, whereas the literature reports more substantial

amounts of cresols and xylenols; the literature also reports maximal yields of catechol. Thus, the literature pyrolyses, conducted principally from 500-600C, were effected at conditions generally more severe than those of the present study, which would enhance the likelihood of secondary and more activated primary degradation routes. In order to emphasize primary reactions, the present studies were conducted at low conversion levels. Thus, the product spectra of the literature and present investigation accord well; a notable point of agreement is the routine detection of catechol, to be further developed below.

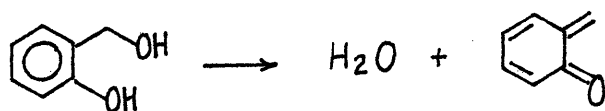
The experimental results invite mechanistic interpretation. Consistent with the product spectra and kinetics is a concerted group transfer mechanism for pathway R1 and an isomerization followed by retroene reversion for R2. Specifically, for R1, the first order stoichiometric demethanation of guaiacol to catechol and  $\text{CH}_4$  can be represented by,



where the diquinone is subject to hydrogen abstraction, yielding catechol, and condensation reactions, which yield the coke detected at higher conversions. The experimental activation parameters obtained for R1,  $(\log_{10} A, E^*) = (10.9, 43.7)$  are relevant here. The value of  $\log_{10} A$  implies a tight transition state, with activation entropy  $S^\ddagger = -12 \text{ cal/molK}$ ;

this is close to the magnitude expected for the loss of two bond rotations that must accompany guaiacyl moiety alignment for the concerted methane elimination. Further, the observed activation energy for R1 is close to the values of  $45 \pm 3$  kcal/mol that have been reported for isoelectronic group transfer eliminations of hydrogen and methane for various 1,4-cyclohexadienes<sup>167</sup>. If R1 is indeed pericyclic, then its kinetics should be dominated by frontier orbital interactions between the methane and o-diquinone products. Methane has a relatively large HOMO-LUMO energy gap, while the diquinone, which is further conjugated, must have a small HOMO-LUMO separation. Thus, the dominant frontier orbital differences of the form HOMO(methane) - LUMO (diquinone) and v.v., should be relatively large and only little influenced by substituents on the diquinone. The experiments were consistent, to be discussed in further detail with regard to vanillin, isoeugenol and 2,6-dimethoxyphenol pyrolyses.

Precedent for the postulated mechanism of R1 exists in the literature. Saligenol, an isomer of guaiacol, has been well documented<sup>102-106</sup> to pyrolyze via a pathway of the type:

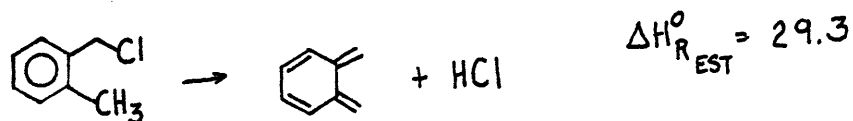


$$\Delta H_{R_{EST}}^{\circ} = 16.7 \text{ kcal/mol}$$

$$\Delta S_{R_{EST}}^{\circ} = 16.7 \text{ e.u.}$$

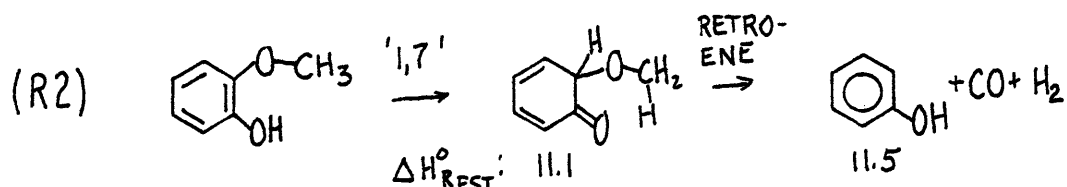
One product mol of water was generated for each mol of decomposed substrate; the quinonemethide has been identified. The experimental Arrhenius parameters obtained in the present investigation for saligenol pyrolysis are also consistent with a negative entropy of activation.

Another analogous pyrolysis<sup>169</sup> yielded a dimethide by a pathway of the type:



with Arrhenius parameters  $(\log_{10}A, E^*) = (11.5, 47.0)$ , in substantial agreement with those reported here for guaiacol. Thus, precedent for the postulated but unidentified diquinone of pathway R1 exists in the literature, found in an examination of analogous isoelectronic reactions.

With regard to phenol and CO formation, a pathway of the type:



is consistent with the product spectra, order, and kinetics determined here. A primary formaldehyde product has been demonstrated<sup>168</sup> to undergo facile pyrolyses to  $H_2$  and CO, the products observed. The Arrhenius parameters  $(\log_{10}A, E^*) = (19.5, 47.4)$  are indicative of a tight transition state, of the type implied by both of the 1,7-sigmatropic hydrogen shift and the retroene elimination steps. As with demethanation, the energy of activation is of the order of other reported pericyclic reactions.

Thus, an overall reaction network for guaiacol pyrolysis is likely of the type represented in Figure 10.1.1, where both R1 and R2 are depicted as occurring through the cyclic transition states discussed

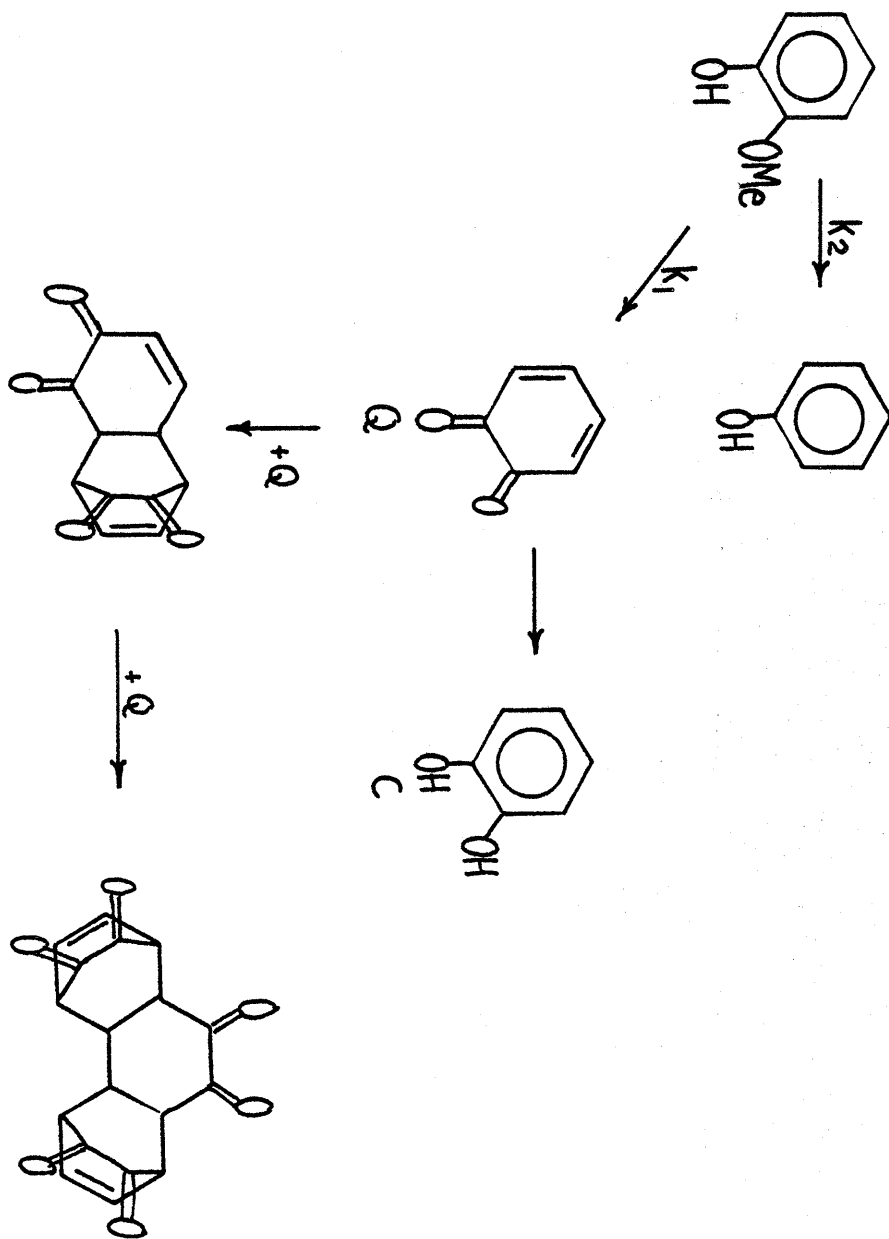


Figure 10.1.1.1 Guaiacol pyrolysis pathways.



above. The secondary reactions of the diquinone as depicted as an hydrogen abstraction to yield catechol in competition with Diels-Alder additions to yield dimeric and trimeric products. The latter pathway is speculative, but is consistent with well documented reactions of the isoelectronic quinonemethide. The former pathway is necessary for hydrogen balance closure of pathway R1, which is discussed next.

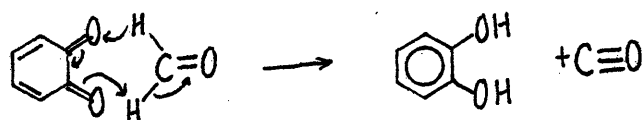
As noted in section 7.2, the net hydrogen evolution of pathway R2 cannot account for the hydrogen uptake of pathway R1, since the ratio  $R1/R2 \sim 10$  for the temperature range studied here. However, catechol was identified by GC and GC with catechol injection as a definite product in the solvent washed pyrolyzate. Further, the yields of catechol and  $CH_4$  were stoichiometric. Thus, it is apparent that pathway R1 is formally hydrogen deficient. Three possible explanations arise to rationalize these apparently anomalous experimental observations.

The first of these deals with the nature of the guaiacol pyrolyzate GC trace. Although catechol was identified by GC with catechol coinjection, it is conceivable that the actual product eluting was the diquinone. Although different from catechol by two hydrogens, the two compounds might elute with similar retention times on an OV-17 silicone oil column.

Preliminary studies comparing the IR spectra obtained from pure guaiacol and an air-cooled, non solvent-washed guaiacol pyrolyzate show an increased proportion of carbonyl peaks for the latter.

These studies are as yet preliminary, and further IR as well as NMR and GC-MS studies would be useful. The actual diquinone could not be obtained for coinjection. This possibility is considered marginally likely, perhaps best illustrated by the unavailability of the pure diquinone. More importantly, the literature pyrolyses of guaiacol have all reported substantial quantities of product catechol. Nevertheless, this possibility cannot be unequivocally dismissed.

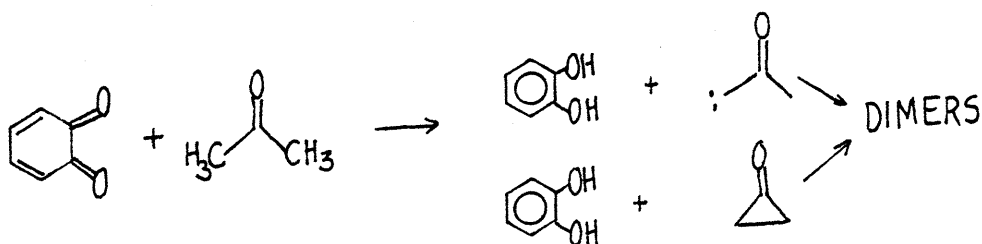
A second possibility is that the quinone abstracted hydrogen from an internal pyrolysis source. Likely internal hydrogen donors include the formaldehyde or molecular hydrogen gas products, or the guaiacol substrate itself. The former pathway might yield catechol and CO by a reaction of the type:



However, the ratio (catechol/phenol) was generally at least 10, and thus only a portion of the apparent hydrogen uptake could be accountable by a reaction of this type. Hydrogen abstraction from guaiacol would yield a hydrogen deficient low molecular weight material, which might be further capable of polymerization reactions to coke. No such low molecular weight species could be detected, although coke yields increased with increasing substrate conversion.

A third possibility for hydrogen uptake by pathway R1 arises in a consideration of the experimental technique. An excess of acetone was used to recover all guaiacol pyrolysis products into one liquor.

Thus, even if the diquinone Q was in fact the direct pyrolysis product, hydrogen transfer by acetone or solvent impurities could account for the presence of catechol in the solvent washed pyrolyzate. Again relevant are the preliminary IR studies of guaiacol and non solvent-washed guaiacol pyrolyzates. This external hydrogen transfer reaction would thus yield a somewhat hydrogen deficient solvent (acetone was used in large excess), perhaps resulting in the formation of acetone dimers. These speculative reactions could take the form:



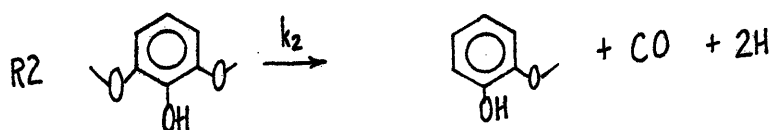
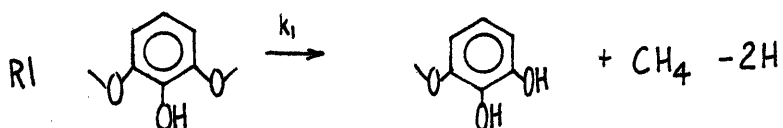
In short, the exact mechanism of hydrogen uptake by pathway R1 has not been decisively delineated. Of the three possibilities presented here, the latter two involving internal and solvent hydrogen transfer, respectively, are considered the most likely. The details of this hydrogen transfer are not clear, and present a significant need for further research which could benefit enormously from use of IR and NMR spectroscopy and mass spectrometry capabilities. With regard to the present investigation, catechol was an identified GC product formed in amounts stoichiometric with methane.

Overall, the present pyrolysis results are consistent with and suggestive of pericyclic pathways for guaiacol degradation, of the type R1 and R2 in Figure 10.1.1. The product spectra and kinetics determined here are in substantial agreement with those found in the literature. The literature also provides isoelectronic precedent and agreement for the postulated mechanistic features of R1.

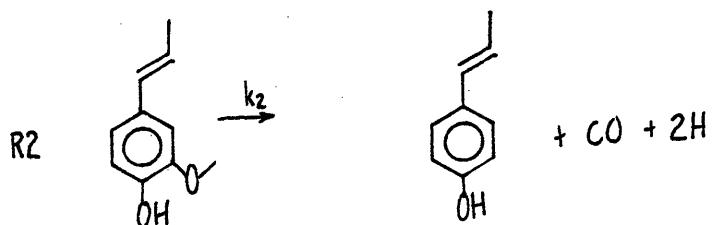
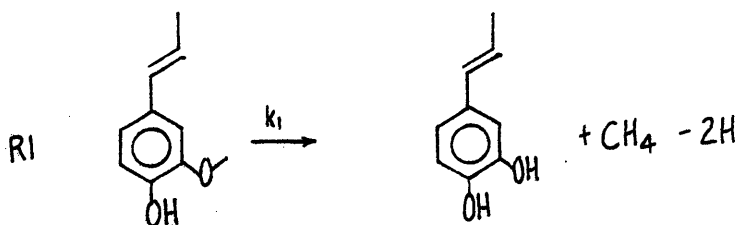
Substituted Guaiacols: 2,6-dimethoxyphenol,  
isoeugenol and vanillin

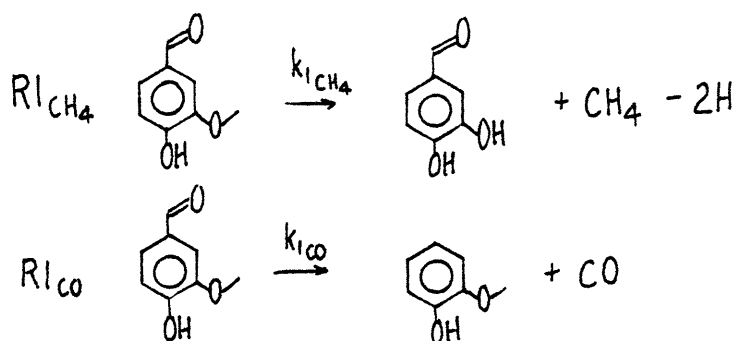
Isoeugenol, 2,6-dimethoxyphenol (DMP) and vanillin served dual functions as lignin prototype moiety models and substituted guaiacols. The latter function is considered here. The compounds underwent pyrolysis reactions of the type R1 and R2 for guaiacol, with the exception of vanillin, which decarbonylated to CO and guaiacol; a pathway analogous to R2 for guaiacol was not identified for vanillin. The primary pathways for these substrates were thus of the form:

DMP



ISOEUGENOL





The last of these pathways is to be more fully discussed in a later section.

As evidenced in Figure 7.3.1, the kinetics of pathway  $R1_{CH_4}$  for guaiacol, DMP, isoeugenol and vanillin are virtually indistinguishable; likewise the kinetics of  $R2$  for guaiacol, DMP and isoeugenol are near identical. Thus, it is evident that para conjugative or electron withdrawing and ortho electron donating substitution had little effect on guaiacol reactivity. These results are well rationalized in terms of the postulated mechanism for guaiacol demethanation, namely group transfer elimination of methane to yield a diquinone.

Perturbation theory<sup>176</sup> yields an expression for kinetic reactivity comprised of three terms, namely:

$$(I) \quad \Delta E = \underbrace{-\sum_{ab} (q_a + q_b) \beta_{ab} S_{ab}}_{(A)} + \underbrace{\sum_{k < l \in R_{kl}} \frac{Q_k Q_l}{\epsilon R_{kl}}}_{(B)} + \underbrace{\sum_r \sum_s^{occ} \sum_s^{un} - \sum_s^{un} \sum_r^{occ} \frac{2 (\sum_{ab} C_{ra} C_{sb} \beta_{ab})^2}{E_r - E_s}}_{(C)}$$

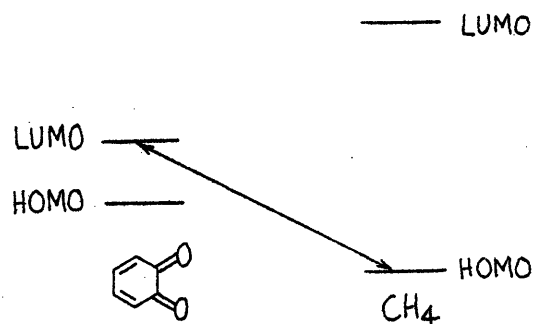
Molecular interactions which have important energy lowering (reactivity increasing) effects are the combination of filled with unfilled orbitals, separated by energy gap  $E_r - E_s$ . The important feature of this equation is that reactivity will increase as the denominator of term (IC) decreases. The major molecular orbitals

affecting this energy gap are those termed Frontier Molecular Orbitals (FMO), which are the highest occupied and lowest unoccupied molecular orbitals, the HOMO and LUMO respectively. Phrased in terms of the back addition of methane to the diquinone, the important interactions will be between the HOMO(CH<sub>4</sub>)-LUMO(diquinone) and vice versa.

Because the diquinone is a heteroatom  $\pi$ -electron system, its FMO levels will be lowered relative to the all-carbon dimethide analogue.

The methane molecule represents a sigma ( $\sigma$ ) bond system, and should have widely separated HOMO-LUMO energy level orbitals. In both cases, the LUMO level will be more antibonding than the HOMO is bonding, because of electron repulsion in the latter. Thus, as seen in the energy level diagram here, the dominant FMO interaction should be between the HOMO(CH<sub>4</sub>)-LUMO(diquinone). These are the important

FMO interaction for Diels-Alder reactions



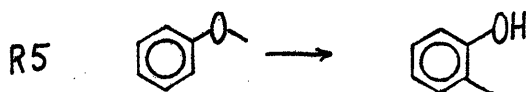
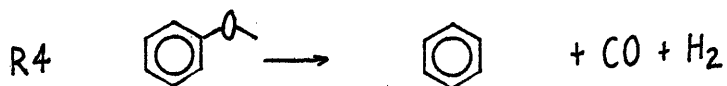
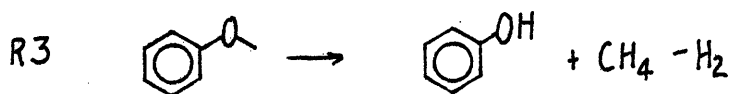
with reverse electron demand. Conjugative substitution on the diquinone will raise its HOMO and lower the LUMO, whereas electron donating and electron withdrawing substituents will raise and lower both, respectively. Thus, with reference to equation (I), isoeugenol and vanillin might be expected to be more reactive than guaiacol, whereas DMP reactivity would be expected to be suppressed. However, in the present case,

the substituents evidently effect a rather insignificant change to an already large energy gap. That is, LUMO (diquinone)-HOMO(CH<sub>4</sub>) is so large that small changes in the energy levels of the diquinone will exert little influence on overall reactivity. Hence, guaiacol, DMP, isoeugenol and vanillin all exhibited essentially the same guaiacyl-type reactivity. It must be noted that substitution will likely affect the coefficients of the relevant frontier orbitals, and that this effect can be comparable to and even in excess of that due to energy level changes.

With regard to whole lignin, the experimental effect of substitution suggests that all lignoid guaiacyl groups can be expected to exhibit pyrolysis behavior exactly analogous to guaiacol itself.

## Anisole

Anisole pyrolysis yielded a more complex product spectrum than that for guaiacol, with  $\text{CH}_4$ ,  $\text{CO}$ , phenol, benzene, cresol and toluene as the major products. No clear link between gas and liquid phase products could be established, although the ratio  $\text{CO}/\text{PhH}$  was only slightly less than unity. Three major pathways were established, namely,



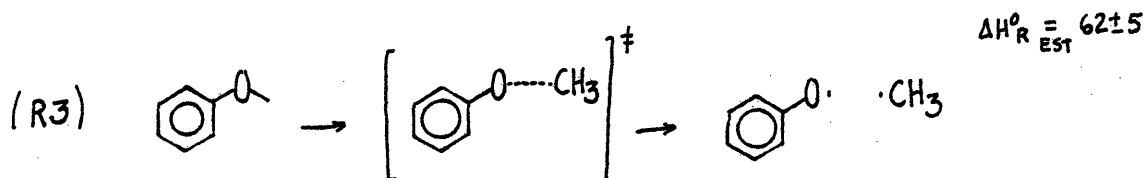
Previous anisole pyrolyses are in good accord with the results presented here. Shaposhnikov and Kosyukova<sup>91</sup>, reported a 66% yield of phenol and 6-7% yield of cresols and xylenols from anisole pyrolysis, indicative of predominant demethylation. Likewise, Friedlen, et al.,<sup>95</sup> report a phenol/benzene ratio of 15/1 from anisole, again indicative of a large selectivity toward demethylation. A rather extensive analysis of anisole pyrolyses product spectra was provided at 500C<sup>96</sup>. At 40% conversion, product proportions, in weight percent of the total products, included: 1.3%  $\text{H}_2\text{O}$ , 0.5% acetone, 10.6% benzene, 0.8% toluene, 24.4% phenol, 2% cresol, 6.1% benzaldehyde, and 34.4% either unidentified or lost. The proposed reaction scheme



involved primary isomerization to benzyl alcohols and phenols, which condensed to yield  $H_2O$  and dimers, the latter degrading to toluene and benzaldehyde. The benzaldehyde was further capable of degradation to CO and benzene. Other products, notably  $CH_4$  and phenol, were interpreted in terms of free radical fission of the ether bonds. Kislitsyn, et al.<sup>97</sup>, have also interpreted anisole pyrolysis in terms of free radical mechanisms. They suggest fission of the aromatic O-Me bond, yielding phenoxy and methyl radicals, which participate in chain rearrangement processes. At 800 C, anisole pyrolysis<sup>82</sup> produced  $H_2$  and CO in approximately equal yields, both of these about three times the quantity of methane. Benzene was produced in yields similar to  $H_2$ , and was further about three times the quantity of phenol. This is in excellent agreement with the results reported here, where benzene formation occurred with greater activation than did phenol formation. The ratio PhOH/PhH, approached unity at about 550 C, and thus the 3/1 predominance of PhH/PhOH at 800 C accords with the present findings. With regard to kinetics, two prior anisole pyrolyses<sup>95,96</sup> at 500 C yield apparent decomposition rate constants  $\log_{10} k(s^{-1}) = -1.8$  and  $-1.9$  which compare reasonably well with the present value of  $-2.5$  at 490C. Overall, the product spectra and kinetics reported in the literature for anisole pyrolyses are in good agreement with those results reported here.

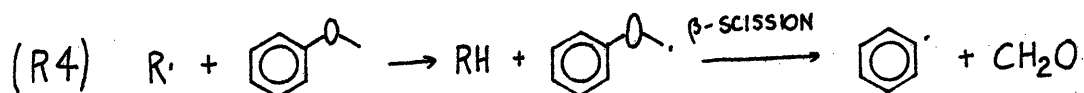
The results determined here and in the literature are consistent with free radical mechanisms for anisole pyrolysis. Anisole was a relatively refractory substrate, degrading as much as two orders of

magnitude slower than guaiacol. Further, whereas the guaiacol primary product spectra were simple, anisole yielded a complex set of phenols, benzene and their derivatives. Thus, for pathway R3, phenol formation likely involves the direct scission of the aromatic ether bond, as in

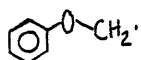


The radicals thus generated can abstract hydrogen to yield phenol and  $\text{CH}_4$ , or can participate in a variety of recombination, disproportionation, and metathesis reactions leading to toluene, cresols, xylenols and xylenes. Mechanistically, a pathway analogous to  $R_1$  for the guaiacols is unavailable to anisole, due to the absence of ortho-hydroxy substitution. Thus, the higher temperature pathway R3 is necessitated, with  $E^* = 50$  kcal/mol, which is about 7 kcal/mol greater than that for guaiacol demethanation. Such a pathway should formally exist for guaiacol pyrolysis also, but is kinetically disfavored in the temperature range studied here. This pathway, R3, for anisole demethanation is in substantial agreement with that proposed and noted earlier in the Russian literature.

The radicals generated in pathway R3 can serve as initiators for another radical pathway leading to the formation of benzene and  $\text{CO}$ . Such a pathway can be visualized as:

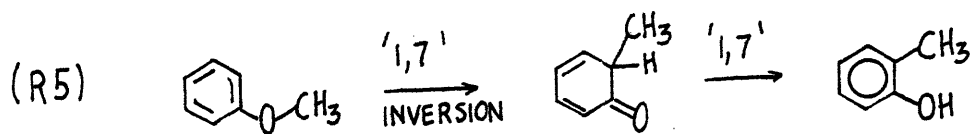


As in guaiacol pyrolysis the primary formaldehyde can undergo facile pyrolyses to CO and H<sub>2</sub>, the products observed. The generated phenyl radical can abstract hydrogen to form benzene, which would serve to propagate the  $\beta$ -scission reaction, or recombine leading to the eventual formation of the alkyl benzenes and phenols observed. For example, the recombination of a benzene radical with the anisole



radical generates benzylphenylether, which is well known to pyrolyse to phenol, toluene and other products.

Formation of o-cresol can be visualized as methyl radical substitution attack on phenoxy radicals or phenol, and as such would be a secondary product. However, the low temperature appearance of o-cresol as a primary product suggests an alternate mechanism, namely a sigmatropic shift similar to that previously postulated in guaiacol pyrolysis. Such a pathway can be visualized as:



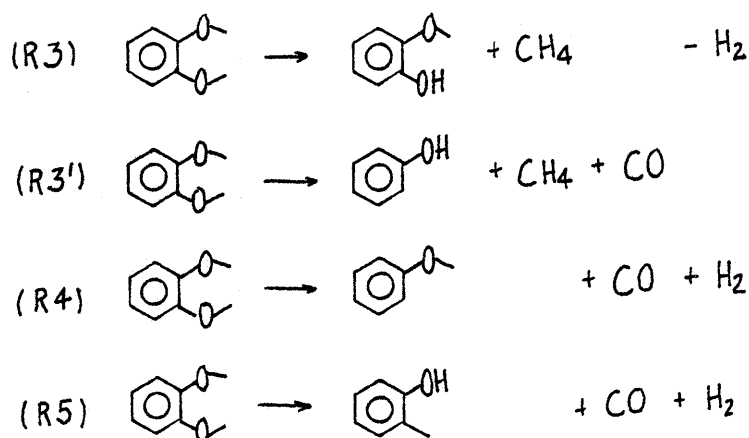
where the cresol is formed by a similar hydrogen shift regenerating aromaticity. The Arrhenius parameters for R5 are consistent with other pericyclic reactions, and reflect a negative entropy of activation. Pathway R5 was considerably slower in anisole pyrolysis than was R2 in guaiacol pyrolysis, which reflects the greater mobility and ease of hydrogen shift relative to methyl shift. The complexity of anisole pyrolysis precludes unequivocal present determination of the mechanism for R5, yet the results reported here are consistent

with and well explained by such a pathway.

In summary, the complex product spectra and relatively high energy kinetics of anisole pyrolysis reported here and in the literature are suggestive of free radical degradation pathways. Hydrogen abstraction, recombination, disproportionation and substitution reactions of the primary radicals can account for the formation of the observed products, chiefly phenol, benzene, toluene, cresols, H<sub>2</sub>, CO and CH<sub>4</sub>. Further, the kinetics of o-cresol formation are consistent with a concerted sigmatropic shift mechanism for pathway R5.

#### Veratrole:

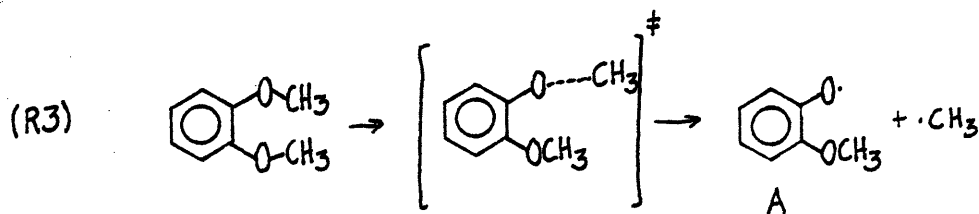
Veratrole pyrolysis resulted in the appearance of CH<sub>4</sub>, CO, guaiacol, anisole, o-cresol and phenol as primary products. Although the liquid product spectra were complex, an overall balance between gas and liquid products was achieved at modest conversion. The pathways of veratrole degradation were determined to be of the type:



The literature provides few pyrolyses for comparison. A Russian investigation<sup>91</sup> of veratrole pyrolysis reported phenol in 50% yield,

cresols and xylenols in 22-33% yield, and only small amounts of catechol. Similarly, another reported product spectrum consisted of phenol, cresols and xylenols as chief products<sup>92</sup>. In contrast to the literature, guaiacol and anisole were detected as primary products in the present work. However, at high conversions guaiacol and anisole experienced severe secondary pyrolysis and in fact, guaiacol was absent at 500C and 6 minutes. Thus, the literature is in agreement with the present study at conditions favoring secondary pyrolysis. However, the high proportions of phenol relative to catechol indicates that the former product did not evolve solely from secondary pyrolysis, but was rather a primary product.

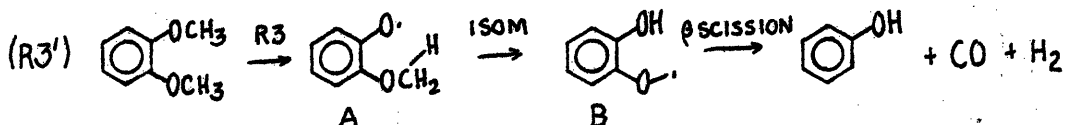
Guaiacol formation from veratrole likely proceeds through a mechanism similar to that for formation of phenol from anisole, namely,



The pathway is designated R3 because of the similarity of the transition state with that in R3 for anisole pyrolysis. Pathway R3 for veratrole pyrolysis was approximately twice as fast as R3 for anisole, which is in exact agreement with predictions due to reaction path degeneracy. That is, pathway R3 can operate on either veratrole methoxyl group, which accounts for a two-fold rate increase. Comparison of R3 Arrhenius parameters for anisole and veratrole pyrolysis also suggests mechanistic similarities, as these are in good agreement. The guaiacol formed in R3

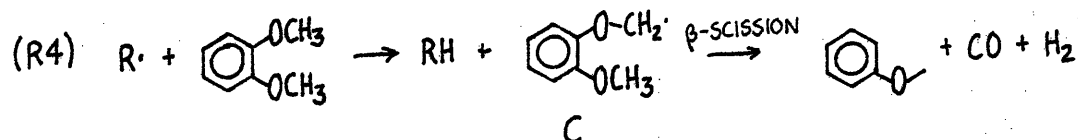
is subject to reactions already delineated for guaiacol, which result in further phenol and the observed secondary catechol product.

Isomerization of the radical generated in R3 can account for the primary appearance of phenol. Such a pathway, designated R3':



thus has elements of pathways R3 and R4 of anisole pyrolysis. Therefore, the radical A generated by pathway R3 can add hydrogen to form guaiacol or isomerize to yield the hydroxy anisole radical B which can further decompose to phenol and CO via  $\beta$ -scission. Significantly, the activation energies for phenol and guaiacol are quite similar, suggesting that initial formation of the radical A may be rate determining.

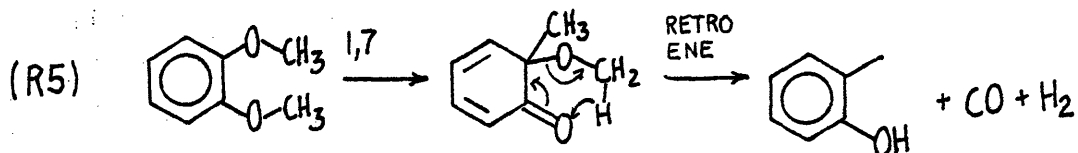
Radical attack on the veratrole substrate can also account for the formation of anisole, by a  $\beta$ -scission pathway of the type:



Thus, radical C can degrade by a pathway similar to that for radical B, for former methoxy- and the latter hydroxy- substituted. Anisole formation from veratrole is formally akin to benzene appearance from anisole, and thus this pathway is designated R4. Both pathways had common Arrhenius parameters of  $(\log_{10} A, E^*) = (14.7 \pm 0.1, 60.5 \pm 0.5)$ , indeed suggestive of common mechanistic features. Pathway R4 for veratrole

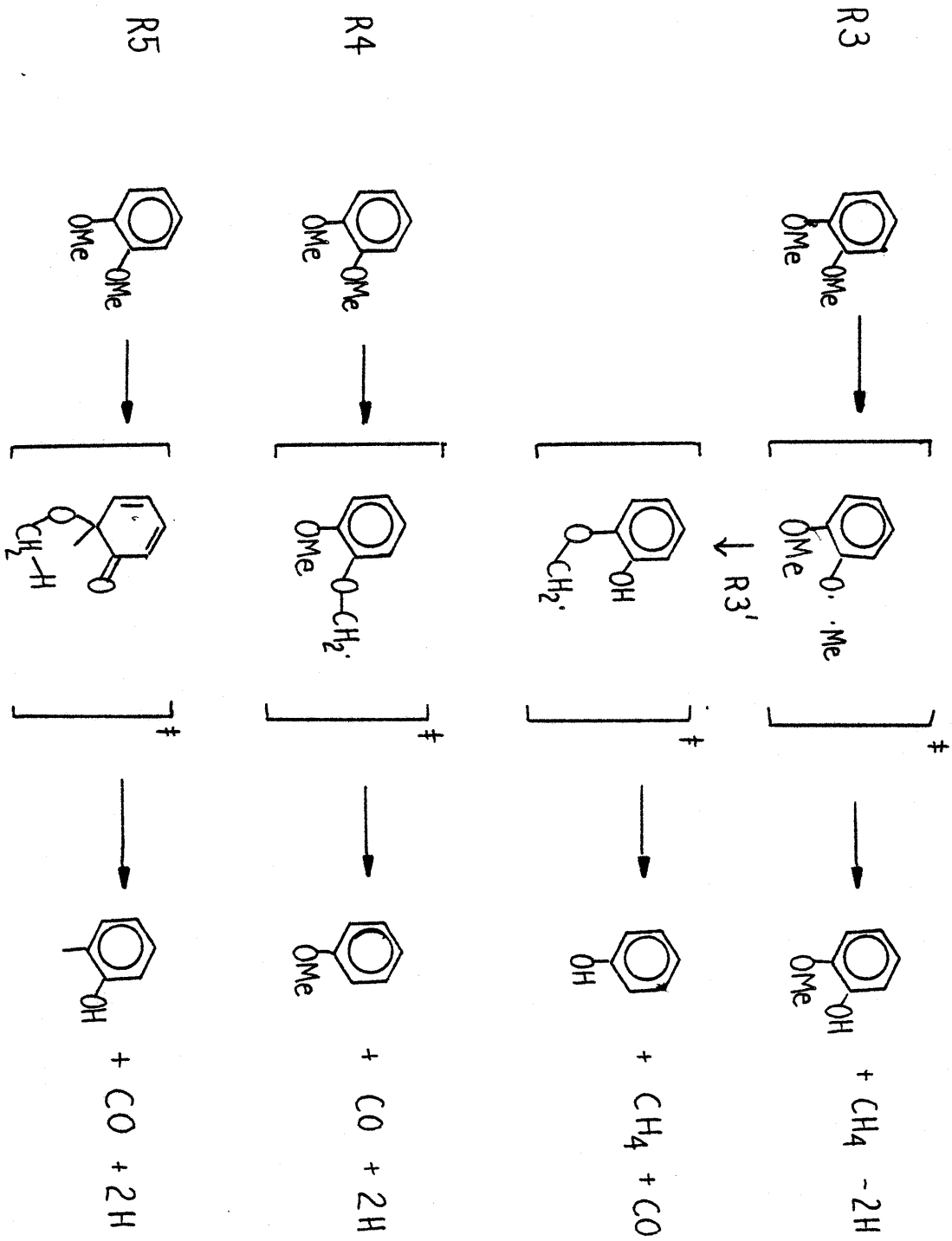
exceeds that for anisole by at least a factor of two in rate, consistent with reaction path degeneracy expected.

The formation of o-cresol from veratrole is formally similar to the concerted pathway R5 for o-cresol appearance from anisole. Thus designated R5:



o-cresol formation likely involves initial 1,7 methyl migration followed by a thermally allowed retroene elimination yielding the observable o-cresol, CO and H<sub>2</sub>. The retroene is exactly analogous to the retroene of pathway R2 in guaiacol pyrolysis, yet initial methyl migration is required and likely rate determining; this pathway is designated R5 in analogy with the 1,7 methyl shift in anisole pyrolysis. The activation parameters ( $\log_{10} A, E^*$ ) = (11.2, 49.2) are consistent with the negative entropy of activation implied by the postulated mechanism for R5; the activation energy further reflects the greater ease of hydrogen shift relative to methyl shift, evident in kinetic comparison with guaiacol. Finally, o-cresol formation from veratrole and anisole are comparable in rate, further evidence of a common mechanistic feature.

An overall network for veratrole pyrolysis is presented as Figure 10.1.2. The primary reaction pathways are interpreted in terms of reactions analogous to anisole, namely ether bond rupture R3, anisole-type radical  $\beta$ -scission R4, and sigmatropic methyl shift R5.



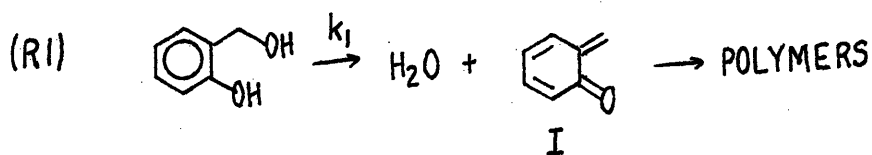


One further primary pathway, R3', involves both R3 and R4 through an isomerization of the radical generated by R3. The phenolic and o-cresol products are stable end products, whereas secondary degradations of guaiacol and anisole account for the catechol, benzene, alkylbenzenes and increased amounts of phenol and o-cresol observed. These assertions are consistent with the results reported in the literature for pyrolyses presumably effected at high conversion levels, where phenol and cresols dominated.

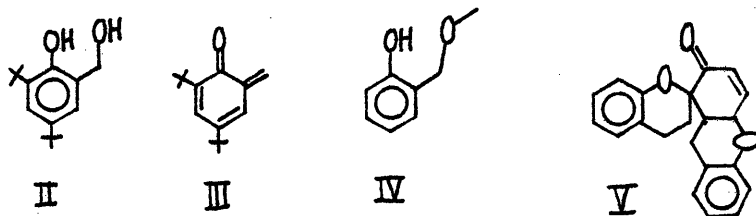
The overall methoxyphenol experimental results are well summarized with reference to Figure 7.5.4. Here, the experimental guaiacol and anisole yields obtained from pyrolysis of veratrole are compared against those yields predicted by a kinetic model using independent kinetic parameters obtained from pyrolyses of pure guaiacol and anisole; an overall veratrole decomposition rate constant was obtained by Arrhenius-type interpolation of data at other temperatures. The agreement demonstrated in Figure 7.5.4 lends credence to the present experimental methods. Every experimental detail regarding the pyrolysis of each individual model compound has not been decisively delineated, and certain areas arise as notable for future research. Yet overall products, pathways, and kinetics and some mechanistic insights have been discerned. The agreement in Figure 7.5.4 shows that the guaiacol pathways R1 and R2, the anisole pathways R3, R4, and R5, and the veratrole pathways R3, R3', R4 and R5 and their associated kinetics describe overall methoxyphenol pyrolysis quite well.

### Saligenol

Saligenol pyrolysis resulted in the formation of one mol of water for each mol of decomposed substrate. No other light products were detected, with o-cresol notably absent. The only major co-product was a high molecular weight material, not identified. This pyrolysis was the most facile studied, and proceeded with first order Arrhenius parameters  $(\log_{10} A, E^*) = (13.4, 33.4)$ . The only pyrolysis pathway was thus designated:

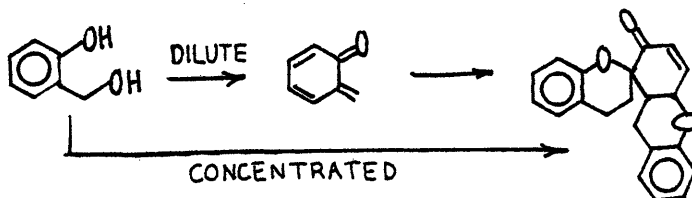


The results reported here are in excellent agreement with those from the literature. For example, Sprengling<sup>101</sup> heated an olefin and the methylolphenol II to 180C and determined a nearly

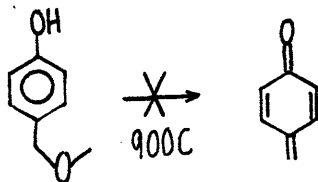


exact molar equivalence of H<sub>2</sub>O evolution and substrate II disappearance. The product residue was divided into 3 fractions, two of which were self condensation products of the methylolphenol and one which was an olefin adduct containing only ~1% hydroxylic groups. All three fractions were thought to arise via the quinonemethide III. Gardner, et al.<sup>102</sup>, have isolated the quinonemethide I and its self condensation products from pyrolysis of o-methoxymethyl phenol IV. In dilute gas phase experiments, I was trapped at liquid nitrogen temperatures. At 0-25C

a solid slush was formed and identified as the trimer of I. This trimer, V, could also be formed on the reactor walls at conditions of high substrate concentrations. Subsequent experiments<sup>103</sup> identified the trimer as the product of two successive Diels-Alder reactions via the scheme:

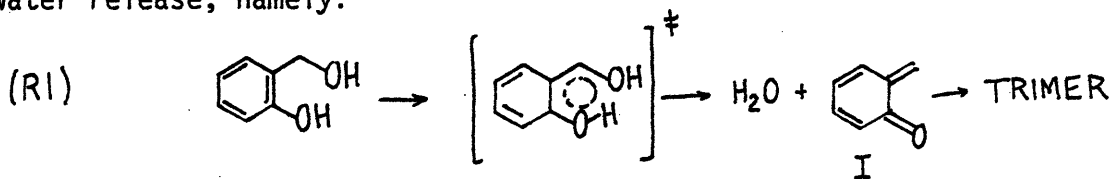


These workers also report the para-methoxymethyl phenol stable to 900C and therefore unable to form the paraquinonemethide in a similar manner, i.e.,

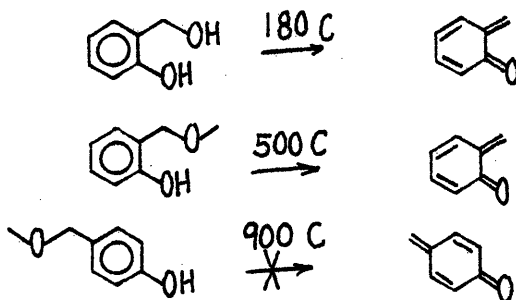


Numerous other investigations have been reported which vary either the phenolic substrate or the dienophile used to trap the intermediate quinonemethide (I or III, eg.), and in each case the condensation reaction is reported to occur through this intermediate<sup>104-108</sup>. Thus, these previous studies and the present results offer strong evidence in support of pathway R1 for saligenol pyrolysis.

These references and the results reported here for the first time are consistent with and suggestive of a group transfer mechanism for water release, namely:



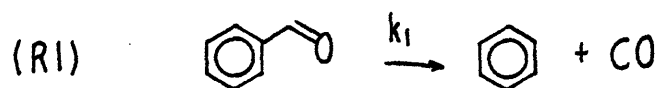
where the generated quinonemethide rapidly formed the trimer. At the temperatures studied here. Such a pathway should produce one mol of water for each mol of substrate decomposed and be characterized by a tight transition state. These were experimentally observed, here or in the literature. The factor  $\log_{10} A = 13.4$  is suggestive of an entropy of activation  $\Delta S^\ddagger \sim 0$ , probably because saligenol is strongly H-bonded, even at room temperature; the actual change in entropy to the transition state,  $\Delta S^\ddagger$ , would not be expected to be as large in absolute magnitude as that for non-hydrogen bonded substrates, the isomer guaiacol for example ( $\log_{10} A_G = 10.9$ ). It is clear that the phenolic group is an integral mechanistic part of this reaction, reflected in the stability of the para-methoxymethyl phenol. Pathway R1 does not exist for the para-isomers, whereas ortho isomers form the quinonemethides readily, as in the series



The phenolic group clearly functions as more than an electronically activating substituent, as the differences between ortho- and para-substitution can scarcely be expected to explain a minimal 400C gap between the temperature needed for reaction of each isomer. Hence, the intramolecular group transfer postulated for saligenol pyrolysis appears to be quite consistent with the results reported here and in the literature.

Benzaldehyde

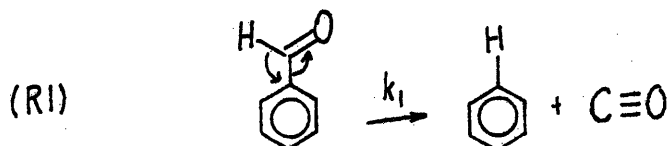
Pyrolysis of benzaldehyde resulted in the first-order stoichiometric appearance of benzene and CO by a pathway of the type R1, namely:



Rate constants spanning nearly five orders of magnitude yielded Arrhenius parameters  $(\log_{10} A, E^*) = (9.5 \pm 0.8, 41.5 \pm 2.7)$ , indicative of rather facile pyrolysis through an ordered transition state.

Previous pyrolyses are in good accord with the results presented here. An early investigation<sup>98</sup> determined the major reaction pathway at 550C to also be decomposition to CO and benzene, with a side reaction yielding biphenyl. The overall mechanism was postulated to be of two parts, a first order decomposition in parallel with a variable order nitric oxide inhibited reaction. The results were thus explained in terms of a superposition of a first order molecular rearrangement to yield stable products and a free radical chain reaction. A benzaldehyde pyrolysis at 1100 and 1400C<sup>82</sup> produced CO, benzene and a host of products indicative of benzene ring-opening reactions. These authors concluded that the direct molecular rearrangement to benzene and CO was likely substantial. Brower<sup>87</sup> has studied the reactions of benzaldehyde in tetralin at 400C. The benzaldehyde was not hydrogenated, but rather decarbonylated to CO and benzene. Thus, the literature confirms the primary reaction of benzaldehyde as one of decarbonylation to CO and benzene, and suggests that a molecular rearrangement is a likely mechanistic pathway.

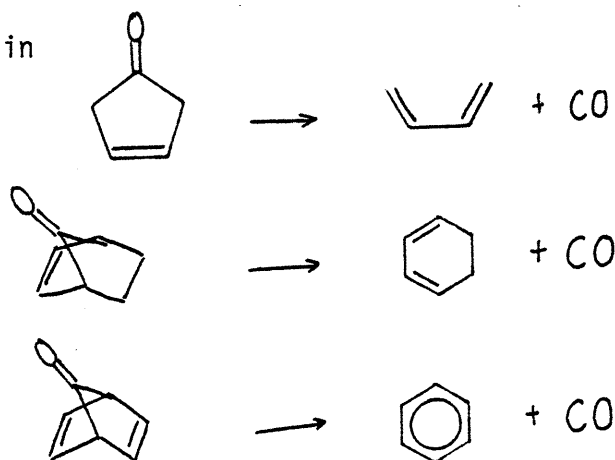
The results obtained here are also in accord with the notion of a molecular pathway for benzaldehyde decarbonylation. More specifically, the reaction is likely of the type termed cheletropic extrusion by Woodward and Hoffmann<sup>170</sup>. A geminal group transfer for benzaldehyde pyrolysis may be visualized as,



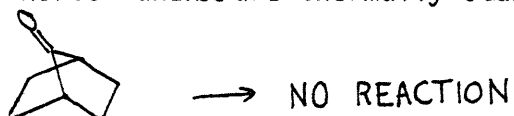
Pericyclic cheletropic extrusions are rather ambiguous in that the stereo-chemical constraints imposed by the Woodward-Hoffmann rules for concerted reactions are not reflected in the products. However, such a reaction must be consistent with the thermochemical constraints and dictates of the reaction transition state. The Arrhenius parameters  $(\log_{10}A, E^*) = (9.5, 41.5)$  are consistent with an ordered transition state of the type likely encountered for this decarbonylation. Further, these forward parameters can be combined with thermochemical data of  $(\Delta H_R(\text{kcal/mol}), \Delta S_R(\text{cal/molK})) = (2.3, 25.5)$  to provide activation parameters for the bimolecular reverse reaction, namely  $(\log_{10}A (1/\text{mol s}), E^*) = (6.7, 40.5)$ . The reverse of cheletropic extrusion is, of course, cheletropic addition, which is well known<sup>170,171</sup> to possess tight transition states akin to cycloaddition. It is therefore consistent that the parameters inferred for the reverse of reaction R1 yield an activation entropy  $\Delta S^\ddagger = -36\text{cal/molK}$ , of the magnitude typically encountered in cycloadditions.

The literature does provide precedent for the cheletropic extrusion of carbonyl moieties. For example, cyclopent-3-en-1-ones, norbornen-7-ones,

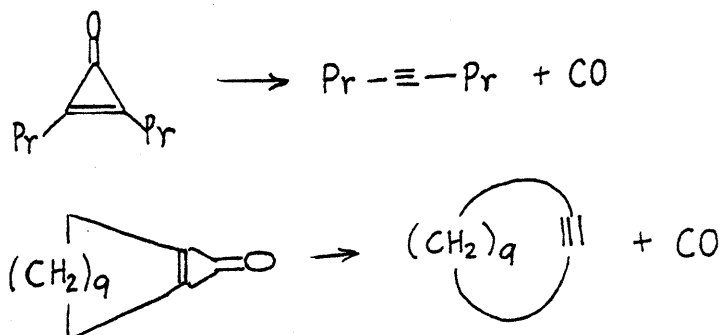
and norbornadien-7-ones readily undergo thermal decarbonylation<sup>170,172</sup>,  
as in



whereas norbornanones are thermally stable<sup>172</sup>,

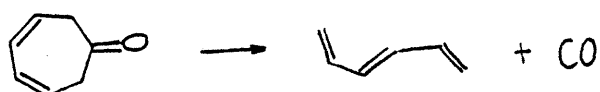


Cyclopropanones also decarbonylate readily when heated<sup>173</sup>, as in



Decarbonylation also occurs readily for cyclopropanones, where the three membered ring assumes features of a carbon-carbon double bond.

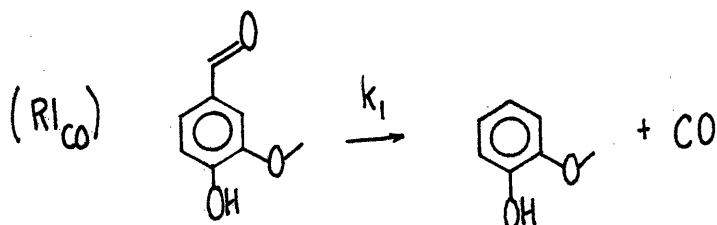
Finally, in accord with the Woodward-Hoffmann rules, 3,5-cycloheptadienone undergoes photolysis to CO and hexatriene, as in



Thus, cheletropic extrusion or geminal group transfer constitutes a plausible reaction mechanism for the first order decarbonylation of benzaldehyde reported here and in the literature. The kinetic parameters for both forward and reverse reactions are consistent with similar reactions reported in the literature ; the literature also provides ample precedent for analagous thermal decarbonylations.

### Vanillin

Vanillin pyrolysis reflected aspects of the guaiacol and benzaldehyde pyrolyses discussed previously. The guaiacol type reactions have already been delineated, and thus only the benzaldehyde-type pathway will be considered here. This reaction was one of vanillin decarbonylation to stoichiometric amounts of CO and guaiacol via a pathway of the type  $R1_{CO}$ , namely



Arrhenius parameters of  $(\log_{10} A, E^*) = (10.2, 38.5)$  were determined for  $R1$ , and reflect an enhancement of vanillin decarbonylation relative to that for benzaldehyde, where  $k_1^{VA}/k_1^{BA} \sim 10-20$  for the temperature range studied here.

This rate enhancement due to guaiacyl substitution is likely the most important feature elucidated by the vanillin pyrolyses. That is, since vanillin is a guaiacyl substituted benzaldehyde moiety, the ratio



$k_1^{VA}/k_1^{BA}$  provides a direct measure of the effect of guaiacyl substitution. Since vanillin likely decarbonylates with mechanistic features similar to those for benzaldehyde, the effect of guaiacyl substitution is plausibly one of electron donation or electronic induction. Since thermally-allowed geminal group transfers are non-linear, or antarafacial in nature, the synchronous rearrangement of two  $\sigma$  bonds attending extrusion likely disrupts the vanillin  $\pi$  system conjugation. Hence, electrostatic induction effects are most likely.

In short, vanillin was experimentally determined to pyrolyse at rates about 10-20 times faster than did benzaldehyde, indicative of a substantial kinetic enhancement due to guaiacyl substitution.

#### Acetophenone

Acetophenone pyrolyses produced complex product spectra consisting chiefly of CO, CH<sub>4</sub>, benzene, toluene and apparent dimers; other products included xylenes, benzaldehyde, biphenyl, cresols and aromatic ethers. No unequivocal gas-liquid product relationship could be established, however, the products of the pairs CO-benzene and CH<sub>4</sub>-toluene were formed in comparable rates, evidenced in Figure 7.9.4. The substrate was quite stable, characterized by overall rate parameters approximately two orders of magnitude slower than those for benzaldehyde in the temperature range studied here. Overall substrate degradation was of reaction order of approximately 1.2-1.3, whereas toluene appeared with 1 and benzene with 1.5 order kinetics. Pseudo-first order Arrhenius parameters for these reactions were  $(\log_{10} A, E^*) = (10.9 \pm 1.2, 52.1 \pm 4.11)$ ,

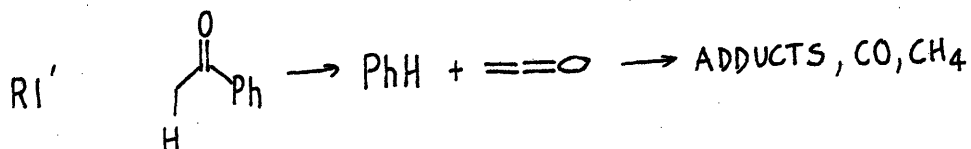
( $10.9 \pm 2.2, 56.4 \pm 7.6$ ) and ( $9.6 \pm 1.9, 50.5 \pm 6.7$ ), respectively.

Since toluene was produced neither stoichiometrically with CO nor in overwhelming predominance indicates that a direct molecular rearrangement to toluene and CO was not the major pathway for acetophenone decomposition. However, the apparent first order appearance of toluene suggests that this may be a contributing reaction at the temperatures studied here. This pathway is similar to that previously described for benzaldehyde and vanillin, except that the extrusion involves methyl shift rather than hydrogen shift. For comparison, both of pathway R1 for benzaldehyde and R1 for acetophenone are listed here, where



Kinetic comparison with benzaldehyde reveals that  $R1_{AP}$  is significantly slower than  $R1_{BA}$ , where  $k_{1BA} / k_{1AP} \sim 10^3$  at 500C. This analysis reveals that the propensity for hydrogen shift is far greater than that for methyl shifts.

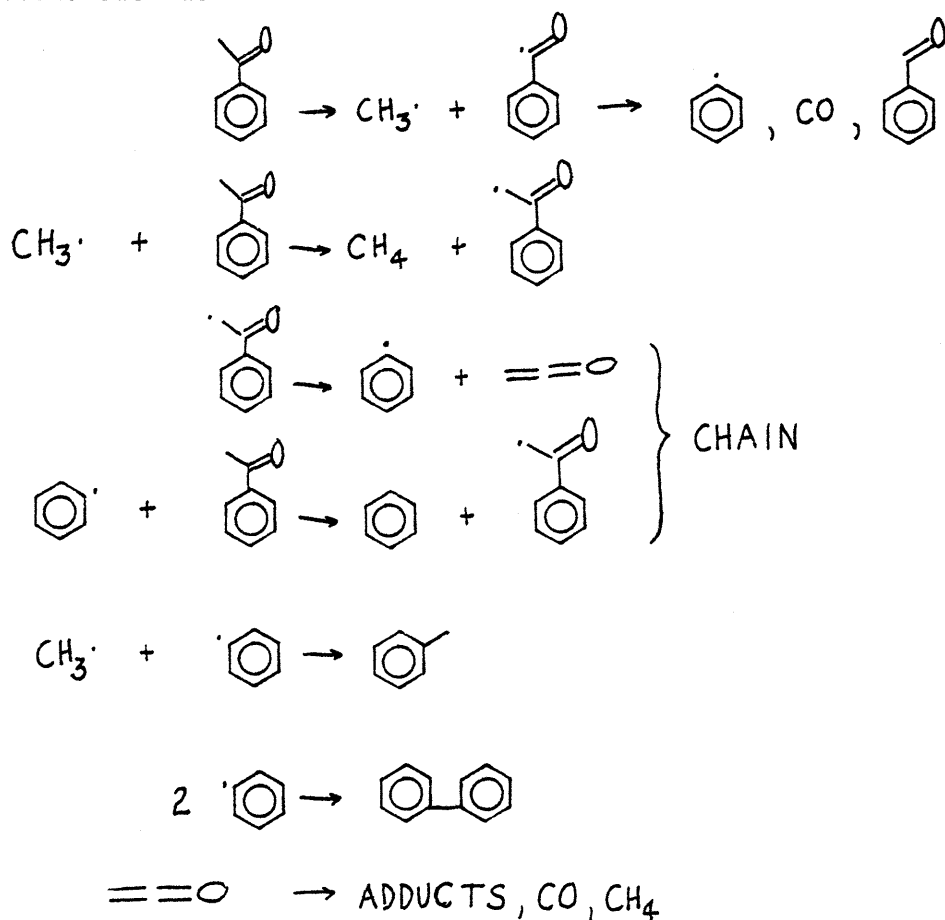
A similar molecular reaction involving hydrogen shift might be envisioned for decomposition to benzene and ketene, as in:



This pathway would rationalize the near equivalent rates of benzene and

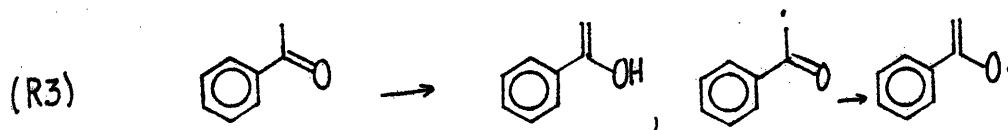
CO production, presuming each mol of ketene decomposed to nearly one mol of CO.

While these molecular pathways are plausible, the thermal stability of the substrate, relatively high experimental Arrhenius parameters, and complex pyrolysis product spectra are indicative of free radical decomposition pathways. Overall acetophenone pyrolysis could involve reactions such as:



and thus account for the observed products equally well.

The initiation and chain steps each produce benzene or phenyl radicals, as well as CO and CH<sub>4</sub> and CO precursors. Ketenes are well known to dimerize, and secondary pyrolyses of these can account for the CO and CH<sub>4</sub> products observed, as well as predict ethylene and other products not accounted for in this study. Radical recombination, hydrogen abstraction, and other termination reactions can account for additional quantities of CH<sub>4</sub>, benzene, toluene, diphenyl and other alkylbenzenes observed. Isomerization of the ketone to aromatic ene-ols can further account for ether and phenolic precursors, as in:



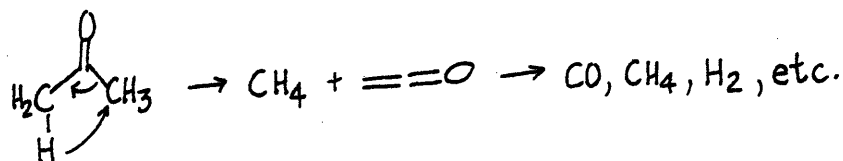
Acetophenone is formally very similar in chemical structure to acetone, as depicted here; literature references to acetone pyrolysis



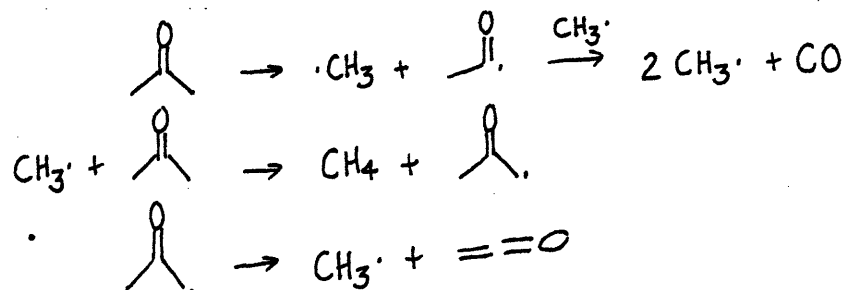
may thus be relevant. High temperature acetone pyrolyses have been effected by Capelin, et al.<sup>109</sup>, who obtained CO, CH<sub>4</sub>, H<sub>2</sub>, acetylene, ethylene, ethane, and benzene at 850C. Thus, most of the acetone carbonyl group led to CO production, whereas about half of the methyl groups yielded methane, the other half leading to hydrogen, ethane, ethylene, acetylene and benzene. Thus, it is consistent that acetophenone should yield a CO/CH<sub>4</sub> ratio of the order 2-3, as found in the present

study, since the multiplicity of methyl groups in acetone is not present for acetophenone. Early mechanistic interpretations of pyrolysis were of unimolecular homogenous decomposition<sup>110</sup>, however more recent studies propose free radical mechanisms for temperatures as low as 510C.

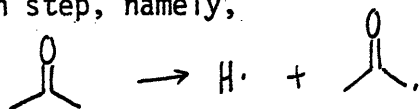
In fact, studies over a wider temperature range<sup>111</sup> have demonstrated that acetone pyrolysis occurs as low as 500C, at which temperature acetophenone was modestly reactive as well. Although acetone is well known to yield ketene, this product was not detected in the laboratory studies noted here, presumably due to facile secondary degradation. Ketene was not detected in the present study of acetophenone pyrolysis, as well. However, most acetone degradation mechanisms involve the intermediate production of ketene. Specifically, for unimolecular degradation:



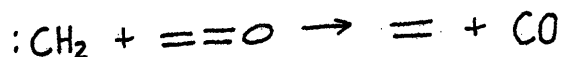
or for the radical mechanisms of Rice and Walters<sup>174</sup>,



the mechanism proposed by Caplelin, et al.<sup>109</sup>, involves a different initiation step, namely,



as well as similar propagation reactions. These workers also propose carbene and carbon monoxide formation from ketene, leading to a variety of observed acetone pyrolysis products, as in:



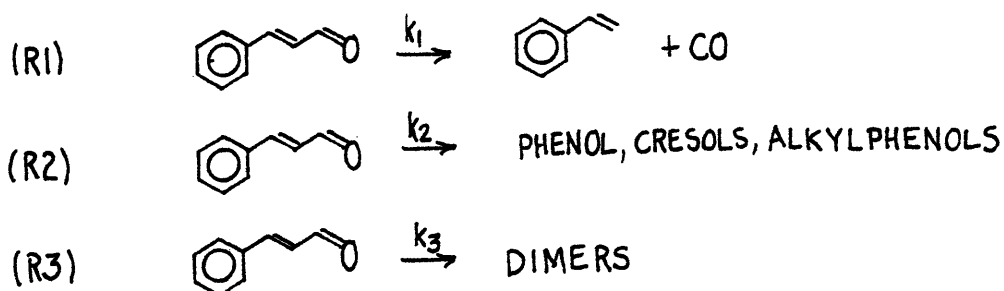
Froment, et al.<sup>175</sup>, have determined a reaction order of 3/2 for acetone pyrolysis in the temperature range 700-750C, which is quite plausible given the nature of the likely radical reactions involved. This agrees quite well with the observed acetophenone behavior, where overall order was determined to be intermediate between 1 and 3/2 order, and benzene appearance 3/2 order. The overall acetone Arrhenius parameters ( $\log_{10} A, E^*$ ) = (9.9, 52.9) reported by Froment, et al., also agree well with those pseudo first order parameters found here for overall acetophenone, (10.9, 52.1).

In summary, although acetophenone pyrolysis produced carbon monoxide as the major gaseous product, a pathway mechanistically similar to R1 for benzaldehyde and vanillin was neither dominant nor unequivocally apparent. Rather, radical pathways closely akin to those previously postulated in the literature for acetone are likely also involved. Similar aspects in pyrolysis of these two substrates include the complex product spectra with  $CO/CH_4 > 1$ , an apparent reaction order of 3/2 for acetone disappearance and benzene appearance from acetophenone, rather large energies of activation, and Arrhenius A factors indicative of complex reactions. It is apparent, therefore, that while guaiacyl

substitutions enhanced benzaldehyde pathway R1 markedly, methyl substitution on the benzaldehyde carbonyl suppressed group transfer decarbonylation to such a degree that high temperature radical reactions were likely kinetically favorable. The geminal group transfer R1 to CO and toluene in a unimolecular step may thus account for a minor portion of overall acetophenone reactivity, but is much slower than analogous decarbonylation paths for benzaldehyde and vanillin.

### Cinnamaldehyde

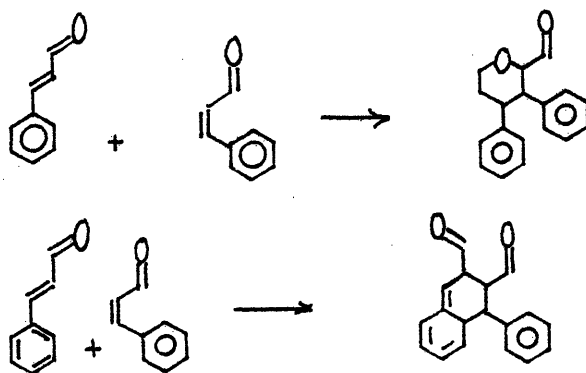
Overall cinnamaldehyde decomposition was described by a sum of first and second order reaction components. The pyrolysis product spectra included CO and styrene, stoichiometric at low conversions, as well as dimeric condensation products, phenols, cresols, toluene, ethylbenzene, benzene, biphenyl and many other products present in very small proportions. The production of styrene and phenol were described as first order, whereas dimers arose via an apparent second order process. Three major pathways were suggested, namely,



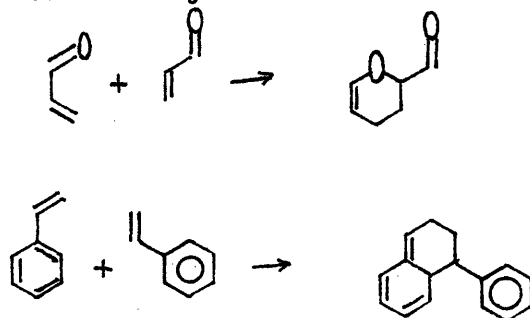
Pathway R1 for cinnamaldehyde pyrolysis is formally quite similar to pathway R1 for benzaldehyde and vanillin. Decarbonylation from cinnamaldehyde was kinetically more akin to benzaldehyde than vanillin.

As was the case with these latter two substrates, the Arrhenius parameters ( $\log_{10} A, E^*$ ) = (12.1, 48.2) are consistent with both the forward geminal extrusion and reverse bimolecular cycloaddition of pathway R1. Thus, internal conjugation affected the benzaldehyde decarbonylation propensity only modestly, as reflected by cinnamaldehyde, whereas guaiacyl substitution, reflected by vanillin, accelerated decarbonylation greatly.

Dimer formation from cinnamaldehyde occurred with relative ease and was favored at high concentrations. The second order process was not well delineated, but likely occurred by Diels-Alder additions of the type:



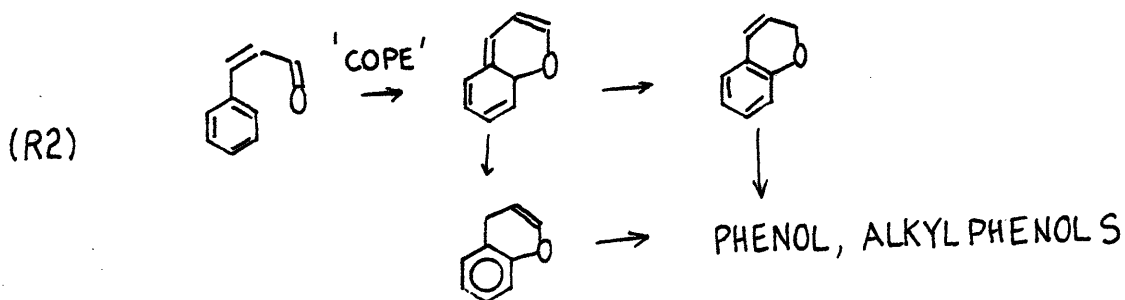
where cinnamaldehyde provides ample multiplicity for both ene and diene sites. Diels-Alder cycloadditions are well known thermally allowed reactions, and these postulated for cinnamaldehyde are closely analogous to those for acrolein and styrene<sup>178,176</sup>. These latter reactions are of the type:





Thus, just as styrene pyrolysis results in the formation of polymers, toluene, ethylbenzene and benzene<sup>78</sup>, isomerization and reversion of cinnamaldehyde adducts can account for additional quantities of alkylbenzenes and phenols observed.

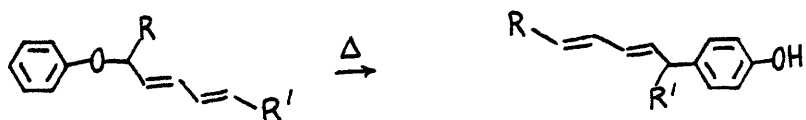
First order formation of phenols and cresols from cinnamaldehyde likely occurs via intramolecular rearrangements in addition to the dimer reversions outlined above. Such a rearrangement can be visualized as a Cope reaction, namely



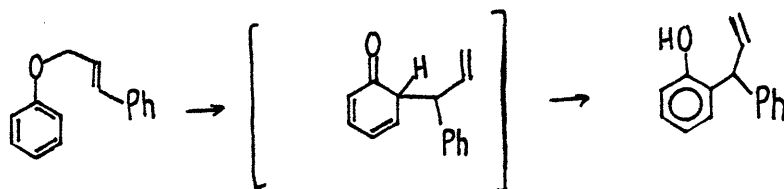
which can yield ethers further capable of pyrolysis to phenol and cresols.

The literature provides examples of analogous isomerization reactions.

For example, a facile stereospecific concerted shift of the type



has been reported<sup>170</sup>. Another reaction is of the type<sup>176</sup>,



which generated a substituted phenol from the phenyl substituted ether.

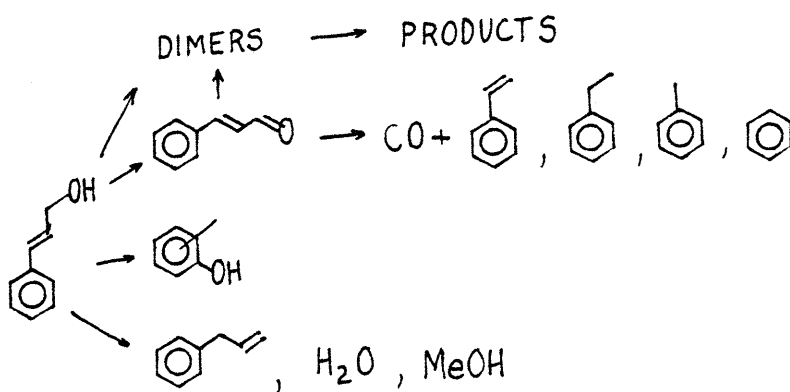
Thus, rearrangements of the type R2 have ample precedence in the literature and, although not decisively delineated here, are likely pathways

in cinnamaldehyde pyrolysis.

The complexity of the cinnamaldehyde product spectra has thus far prevented unequivocal delineation of each reaction pathway. However, three major reactions have been observed, these leading to styrene, dimers and phenols. The production of styrene appears to occur through a geminal extrusion of the type previously described for benzaldehyde and vanillin, whereas pathways to dimers and phenols are less clear. More comprehensive examination of the pyrolysis product spectra is necessary to clarify these latter reaction paths.

#### Cinnamyl Alcohol

The products of cinnamyl alcohol pyrolysis were divided into four categories, a gas fraction, water soluble light liquids, monomeric aromatics, and a polymeric fraction. Particularly significant products were CO, H<sub>2</sub>O, MeOH, cinnamaldehyde, allylbenzene, and phenols. Kinetic analysis revealed that likely primary pyrolysis products included cinnamaldehyde, allylbenzene, phenols, water and methanol, whereas styrene, toluene, ethylbenzene and further phenols and dimers arose from secondary pyrolyses. As has been previously described, styrene is a primary cinnamaldehyde pyrolysis product, as well as dimers and phenols. Further, styrene is well known to polymerize and degrade to toluene, benzene, ethyl- and isopropyl-benzene. Thus, the complexity of the cinnamyl alcohol product spectra is due to not only a multiplicity of primary pathways, but also to secondary, tertiary and further pyrolyses as well. An overall reaction network was developed, namely,

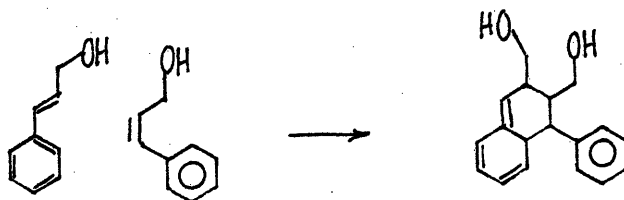


This reaction network shows primary pathways to dimers, cinnamaldehyde, alkylphenols, allylbenzene,  $H_2O$  and methanol. With regard to dimer formation, a secondary pathway from cinnamaldehyde must be included in the reaction network, as previous pyrolyses of this substrate also revealed dimer formation. Cinnamaldehyde pyrolysis to CO and styrene was stoichiometric at low conversions, whereas styrene underwent further pyrolysis to toluene and alkylbenzenes. With cinnamyl alcohol, the proportion of these light alkylbenzenes eventually significantly exceeded CO yield, indicative of a pathway to the alkylbenzenes in addition to styrene degradation. Secondary pyrolysis of dimers likely accounted for this excess of light aromatics. Alkylphenols arose as primary products of both cinnamyl alcohol and aldehyde pyrolyses, which is also accounted for in the postulated reaction network. Finally, allylbenzene, water, and methanol were detected solely from cinnamyl alcohol pyrolysis.

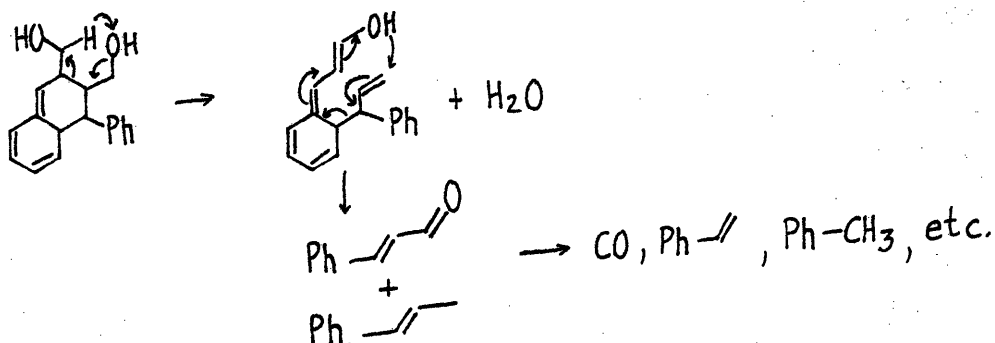
The complexity of the cinnamyl alcohol pyrolysis product spectra has thus far precluded the identification of definitive reaction paths or mechanisms. Products relationships were obscure, and the likely multiplicity of pathways has prevented even overall stoichiometric analysis. Even the case of cinnamaldehyde, where dimer and alkylphenol

formation were obscure, a relationship between CO and styrene could be determined. Thus, without the identification of unequivocal pathways, mechanistic interpretation of the pyrolysis results is rather speculative.

Dimer formation from cinnamyl alcohol was likely very similar to that from cinnamaldehyde, save the additional ene and diene moieties of the latter substrate. Thus, the predominant Diels-Alder condensation was likely of the type:



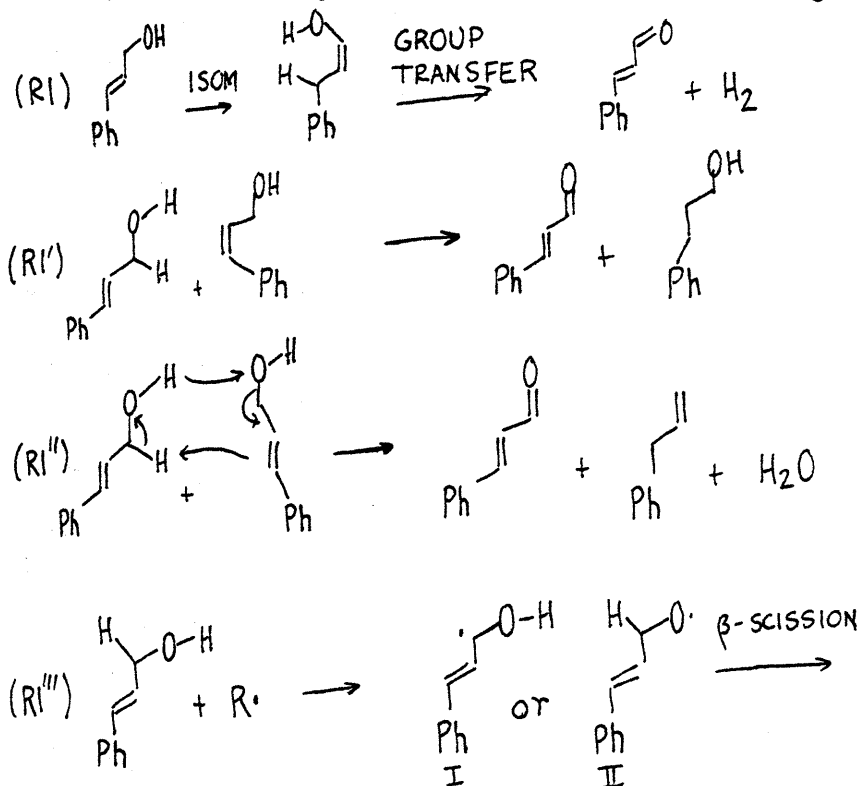
Secondary isomerization and degradation of the adduct could produce light products by pathways of the type:



These pathways set forth above are speculative, but based on analogous reactions detailed in the literature. Further, they reflect the features of the cinnamyl alcohol product spectra, where dimer formation was prevalent, and degradation to lighter aromatics suggested.

Cinnamaldehyde was also produced via a primary cinnamyl alcohol pyrolysis pathway. As noted above, degradation of dimers may account

for some part of the aldehyde production, but likely would not occur with such rapidity as to appear primary. Rather, primary cinnamaldehyde production may be envisioned to occur through pathways such as:

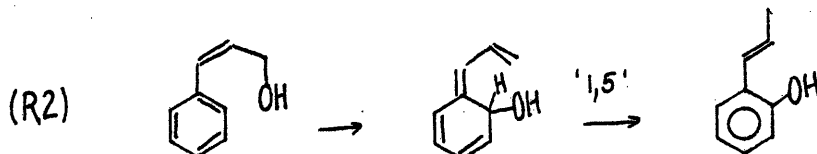


Thus, pathways R1' and R1'' would be second order in substrate, whereas pathway R1, if operative, would likely be first order. Although not clearly determined, each of pathways R1 incorporate reactions well documented in the literature, such as pericyclic hydrogen group transfer elimination in R1 and ethane-ethylene type group transfer in R1'. Further, pathway R1'' also provides for facile formation of water and allylbenzene, both detected as primary products. Although formed in comparable quantities, these latter products were not stoichiometric, suggesting R1'' was not operating exclusively. This accords with the pathways noted earlier for dimer degradation yielding water and cinnamaldehyde products, as well as the overall multiplicity and complexity of the postulated reaction network. Pathway R1''' denotes the possibility of a free-

radical mechanism for cinnamaldehyde production. Radical abstraction or bond fission reactions could yield cinnamyl alcohol radicals capable of  $\beta$ -scission reaction to cinnamaldehyde, or in the case of radical II, styrene as well. However, reaction path degeneracy favors the formation of radical I; styrene was also not detected as a primary or major product.

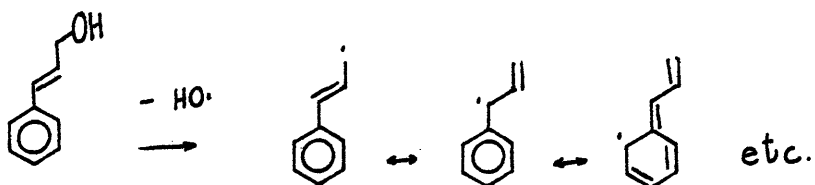
In any event, cinnamaldehyde was experimentally observed to be a primary and major cinnamyl alcohol pyrolysis product. The mechanistic features of the aldehyde formation are as yet unclear, but likely involve reactions of the type listed as R1.

The production of phenols from cinnamyl alcohol was also likely mechanistically similar to pathway R2 postulated for cinnamaldehyde. Thus, a likely rearrangement pathway is of the type:

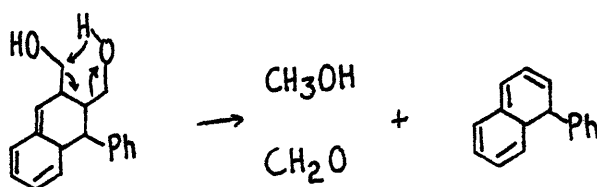


The alkylphenol produced in R2 could undergo various rearrangement and condensation reactions to yield the complex set of phenols which have been lumped as alkylphenols in this analysis.

The remaining primary pyrolysis products are allylbenzene, water, and methanol. The former two products have been previously discussed in terms of pathway R1''' for cinnamaldehyde appearance, where a bimolecular rearrangement led to the aldehyde, water, and allylbenzene in one concerted reaction. Radical formation of these cannot be ignored and may occur as in



Reversion of the dimeric products may also account for the formation of methanol, as in



which could account for the small amounts of formaldehyde and further CO detected as well. Such a path would indicate that methanol was in fact a secondary product, which is possible considering the low proportions of methanol and the high proportions of dimers detected. In short, however, the pathways to methanol formation are at best unconvincing, and signal need for future study. Methanol formation from cinnamyl alcohol is quite significant, however, even though formed in low yields. A molar yield of about 4%, for example, achieved here readily at 450C corresponds to approximately 1 weight percent methanol from lignin, if extrapolated to each lignin aromatic unit. This is of the order commonly reported in lignin pyrolysis, and thus demonstrates the need for further research. On the other hand, water formation from cinnamyl alcohol is meager compared to that from saligenol. Water formation from cinnamyl alcohol at 450C is about an order of magnitude

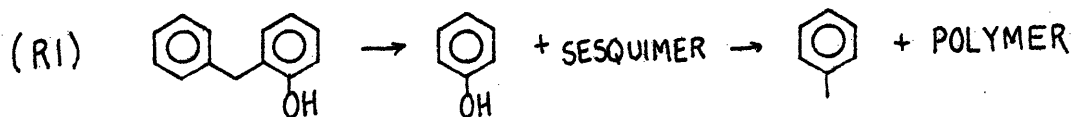
slower than that from saligenol at 175°C. Thus, even though produced in comparable yields, water formation is clearly less significant than methanol release in cinnamyl alcohol pyrolysis.

The details of cinnamyl alcohol pyrolyses remain rather obscure. Information about the product spectra and kinetics has been gained, and will be quite useful in a description of lignin pyrolysis.

### Orthohydroxydiphenylmethane (OHD)

Phenol, toluene, and higher molecular weight materials, collectively lumped as sesquimers were the major products of OHD pyrolysis. Other products, of at least an order of magnitude smaller in proportion, were benzene, diphenylmethane, phenylphenol, and diaryl-ethers and alkanes. At low conversions, phenols and sesquimers arose in comparable molar proportions, whereas toluene yield was quite small. At higher conversions, phenols and toluene were comparable, with the sesquimers correspondingly smaller. This behavior appeared somewhat insensitive to temperature, rather dependent only on conversion.

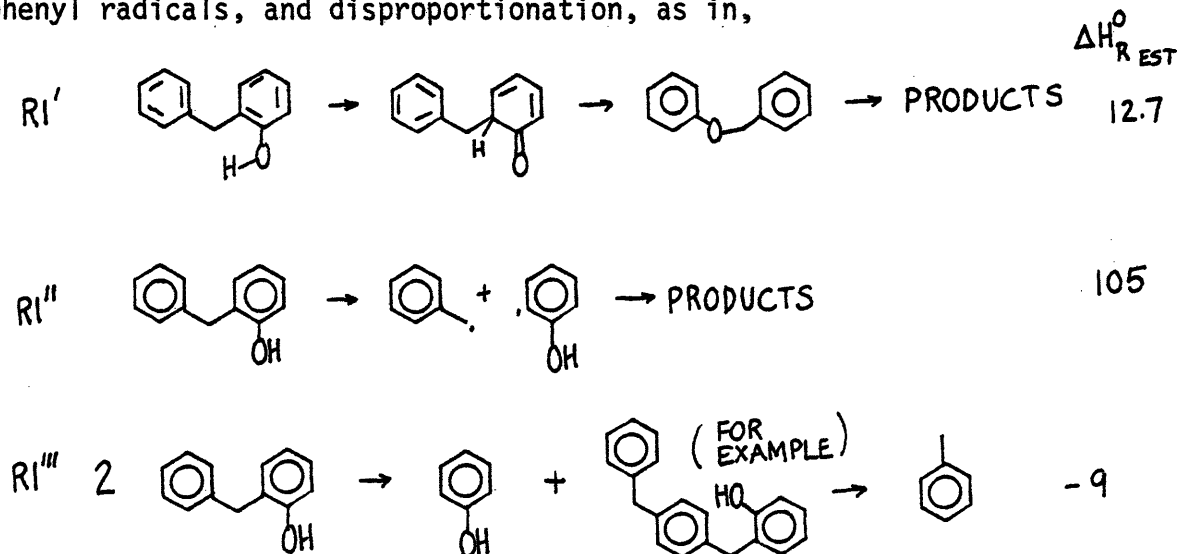
These results suggested that phenol and sesquimers arose as the primary observable products, whereas toluene was formed through secondary degradation of the sesquimers. The pathway for OHD degradation was thus noted as:



where the hydrogen balance, not decisively delineated, was satisfied in the appearance of the hydrogen deficient polymers and diaryl species detected. Mechanistically at least three competing pathways arise,



these involving intramolecular rearrangement to benzylphenylether (BPE), followed by ether degradation, direct radical scission to benzylic and phenyl radicals, and disproportionation, as in,



With regard to pathway R1', benzylphenylether (BPE) pyrolysis has been previously established to yield phenol, toluene, and benzyl phenol<sup>79</sup> (OHD,PHD,MHD). The degradation has been postulated to occur by both free radical and pericyclic routes. With regard to R1'', these data suggest that the benzylic radical generated by fission selectively condensed, yielding sesquimers, which later yielded toluene; however, the same results would imply that the hydroxyphenyl radical preferentially abstracted hydrogen to yield phenol. The disproportionation pathway R1''' is based on analogous toluene disproportionation reactions; it is also cogent to note that the reaction of two benzenes to biphenyl is well known, and is essentially thermoneutral.

Of the pathways R1', R1'' and R1''', the experimental OHD pyrolysis Arrhenius parameters  $(\log_{10}A, E^*) = (9.6, 43.4)$  accord best with pathway R1' and R1'''. The rearrangement would be expected to proceed through an ordered transition state, reflected in the low  $\log_{10}A$  observed.

In pathway R1'', with bond fission likely rate determining, the transition state would likely be loose, with  $\log_{10} A > 13.5$  and  $E^*$  more closely resembling the bond strength  $\sim 105$  kcal/mol. The disproportionation R''' should be strictly second order, and occur with  $\log_{10} A < 13.5$ . As noted above, the estimated net enthalpy of reaction is  $-9$  kcal/mol, and thus a favorable thermodynamic driving force exists. Although the mechanistic details of R1''' are not as readily discerned as those of R1', pathway R1''' represents a very plausible scheme.

Previous pyrolyses of diphenylmethanes and BPE are relevant here. With regard to the former substrate, Benjamin, et al.<sup>78</sup>, have pyrolysed both the o- and p- hydroxydiphenylmethane (OHD, PHD) isomers in tetralin at 400C. The ortho isomer yielded phenol and toluene exclusively, whereas the para isomer produced predominantly these, but also traces of benzene and p-cresol. Further, the ortho-isomer was more reactive than the para isomer at 400C, where single run conversion data yield apparent first order rate constants  $-\log_{10} k_o = 4.21$  and  $-\log_{10} k_p = 4.53$ . The product spectra are in accord with the results obtained here. Most significantly, the products from OHD were toluene and phenol, as reported here, and not benzene and o-cresol. Further, PHD yielded predominantly phenol and toluene, with only small proportions of benzene and p-cresol. The presence of tetralin resulted in production of only single ring aromatics, as sesquimers or polymers were not reported. This would be expected, as tetralin is well known to be an effective hydrogen donor, and could cap moieties subject to condensation reactions in neat pyrolyses. This effect of tetralin does not allow discrimination between mechanisms R1' and R1'', as tetralin could cap the BPE pyrolysis products or the initial radicals of R1'' equally well.

The second order disproportionation would be expected to be disfavored by tetralin dilution, yet continue to yield sesquimers. That sesquimers were not reported for pyrolysis in tetralin suggests that pathway R1'' may operate in parallel with but not to the exclusion of R1' for neat pyrolysis. The greater reactivity of OHD relative to PHD accords with pathway R1', where the hydroxy substituent is in a position to more readily allow concerted benzylic shift; such a shift would be more difficult or stepwise for the para isomer; the hydroxy substituent may in fact be more activating in the ortho position, and thus the rate differences might be explained in terms of electronic activation. However, the pyrolyses of non-hydroxylic diphenylmethanes suggest that the hydroxylic substituent may in fact actively participate in the degradation mechanism.

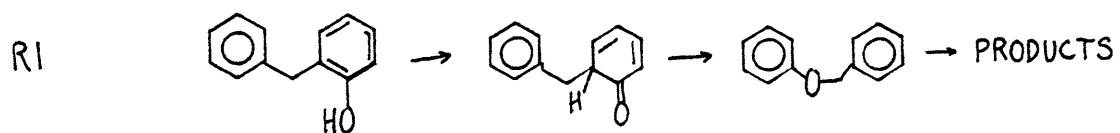
Diphenylmethanes have been pyrolysed by a number of investigators, who each found the substrate essentially unreactive. Benjamin, et al.<sup>78</sup>, have found diphenylmethane, triphenylmethane, and tritolylmethane stable in tetralin at 400C for 18 hours. Of these, tritolylmethane should have electronic features similar to para hydroxydiphenylmethane, since hydroxy and methyl substituents are both  $\ddot{X}$  or electron donating substituents. However, whereas PHD reacts at 400C, the tritolylmethane was stable. Kayima, et al.<sup>79</sup>, report diphenylmethane to undergo only 1.7% conversion at 450C and 30 min. holding time, yielding an apparent first order rate constant  $-\log_{10}k_{450} = 5.02$ , which was orders of magnitude below  $-\log_{10}k_{450} = 3.45$  found here for OHD. Similarly, Sweeting and Wilshire<sup>88</sup> found diphenylmethane essentially unreacted at 700C and an estimated 24 second holding time, with very small amounts

of toluene, benzene and fluorene reported. Thus, the hydroxylic substituent exerts overwhelming influence on diphenylmethane reactivity.

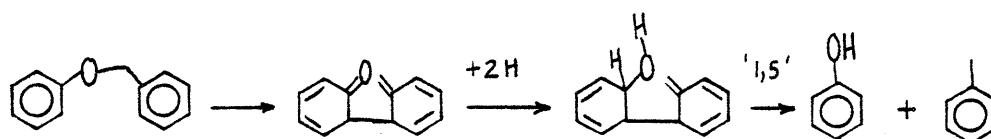
A pyrolysis of BPE in tetralin at 400C<sup>79</sup> resulted in complete substrate conversion and the appearance of toluene, phenol, and benzylphenol (o,m,p -hydroxydiphenylmethane) in molar yields of 61%, 66% and 27%, respectively. Pyrolyses at 320C also produced these same products. Significantly, BPE pyrolysis produced OHD or an isomer, the formal reverse of reaction R1', Similarly, Savinykh, et al.<sup>81</sup>, determined a BPE pyrolysis product spectrum consisting of toluene, phenol, benzene, benzaldehyde, dibenzyl, diphenylmethane, benzophenone, and OHD and PHD. This product spectrum is quite similar to that reported here for OHD pyrolysis.

To summarize, the literature suggests that the hydroxyl substituent not only exerts considerable pyrolysis activation, but may also actively participate in the reaction mechanism. Further, the pyrolysis product spectrum of BPE is quite similar to that reported here for OHD, and in fact includes OHD. These observations coupled with the Arrhenius parameters determined in the present investigation suggest that pathway R1', initiated by intramolecular rearrangement, may describe the mechanistic features of OHD pyrolysis. Hence, the BPE intermediate likely degrades to phenol and toluene precursors, the former yielding phenol directly, the latter yielding higher molecular weight materials as primary observables, which can in turn degrade to toluene. Such a

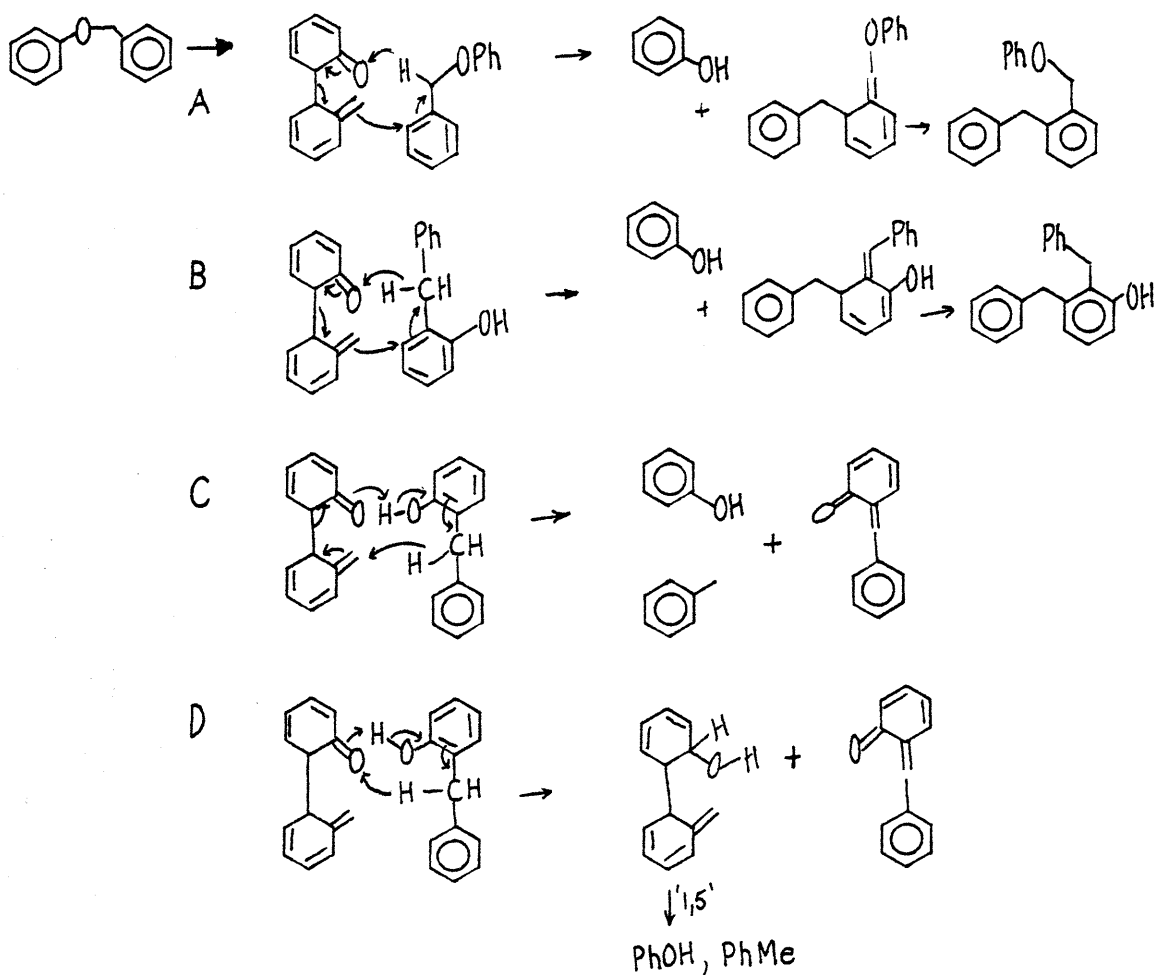
pathway might be represented as:



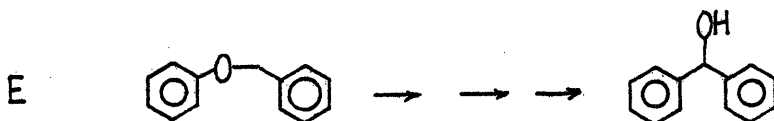
where the benzylphenyl ether can degrade via pathways similar to those proposed by Virk<sup>166</sup>,



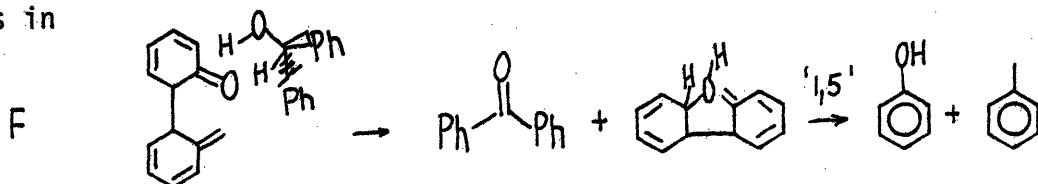
for BPE pyrolysis in an hydrogen donating solvent, or by



in the absence of external hydrogen, as in the present investigation. Further, a rather involved and energetic isomerization of BPE could yield diphenylmethanol, i.e.



which could serve as a facile hydrogen donor to yield benzophenone, as in



It is cogent to note that benzophenone was reported from BPE pyrolysis by Savinykh, et al.<sup>81</sup>,

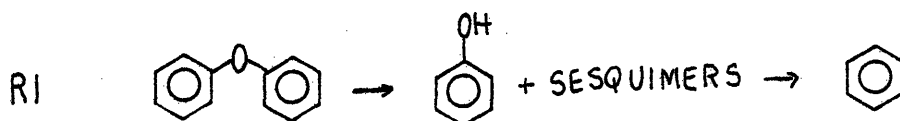
Hence, OHD rearrangement to BPE followed by ether reversion is consistent with results obtained here and reported in the literature. Consider the speculative pathways for pyrolysis in the absence of external hydrogen, as effected in the present investigation. These are pathways R1, A,B,C,D,E and F. Pathways A and B rationalize primary production of phenol and sesquimers, with little toluene produced. Reversion of the sesquimers could then yield further phenol, diphenylmethane, toluene and other polymeric species. Pathways C and D provide for less facile stoichiometric production of phenol and toluene, along with hydrogen deficient polymeric precursors. Hence, higher temperatures and substrate conversions could promote toluene production through A,B,C, and D, with coincident sesquimer

loss to heavier polymeric species. Pathways E and F provide examples of alternative pathways to toluene and phenol again with hydrogen donation from substrate isomers, specifically diphenylmethanol dehydrogenation to benzophenone for E and F.

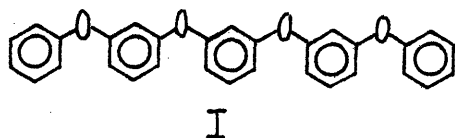
Overall, the obscure nature of the triaromatic and polymeric species has precluded decisive delineation of OHD reaction pathways. However, the results obtained here and in the literature are well rationalized by a mechanistic pathway of the type R1', with conceivable mechanistic steps R1, A,B,C,D,E and F. These lettered steps further explain some features of neat BPE pyrolysis hitherto not well rationalized by pericyclic formalism. An equally plausible and likely mechanistic interpretation of OHD pyrolysis is represented by pathway R1'', the disproportionation reaction. The details of this mechanism are not clear, but are likely analogous to toluene disproportionation to benzene and xylene and biphenyl formation from benzene. Additional kinetic information, such as determination of reaction order and solvent effects, would be useful in ascertaining the relative contributions of R1' and R1''.

### Phenylether

Phenol, benzene and apparent sesquimers were the major products from phenylether pyrolysis, the former two products approaching stoichimetric proportions only at high substrate conversions. The phenylether product spectra were thus analogous to those previously described for OHD pyrolyses. Phenylether pyrolyses at 400 and 450C and at times to 4 hours effected no substrate conversion; apparent first order Arrhenius parameters determined over the temperature range 500-587C,  $(\log_{10}A, E^*) = (14.8, 72.1)$  further reflect the thermal stability of the substrate. The overall pathway earlier ascribed to phenylether pyrolysis was:



The literature provides some framework for comparison. Kayima, et al.<sup>79</sup>, have pyrolyzed phenylether at 450C for 30 and 120 minutes. They do not report pyrolysis products, and indicate only 2% substrate conversion. Benjamin, et al.<sup>78</sup>, have pyrolysed chains of phenylethers, as in structure I

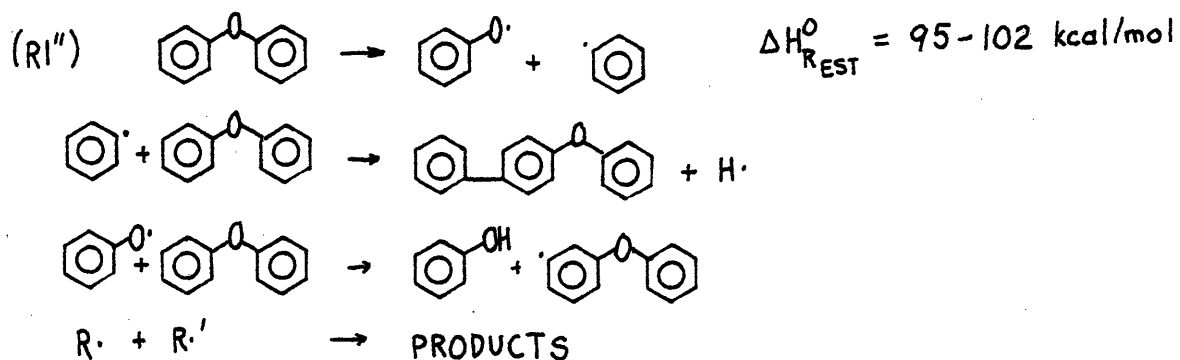


and report no conversion at 400C for 18 hours holding time. The ether will react at 970-1175C, as reported by Ingold and Lossing<sup>82</sup>.



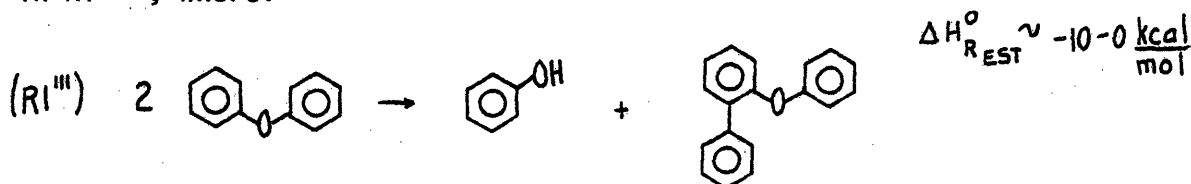
The pyrolysis products included hydrogen, carbon, acetylene, ethylene, CO, butadiene, benzene, biphenyl and trace amounts of phenol. These products are clearly indicative of aromatic ring disruption and secondary pyrolyses further demonstrating the refractory nature of the substrate. In 1938, Starokadonskaya<sup>83</sup>, determined an activation energy of 85 kcal/mol for the first order decomposition of phenylether. The ether was unconverted at 440C, even at 60 hr reaction time. Thus, the literature generally accord well with the notion of high temperature, relatively slow degradation of phenylether.

The high activation energies determined here and in the literature suggest that the radical reactions may be important. Thus, pathway R1 could occur via reactions of the type:



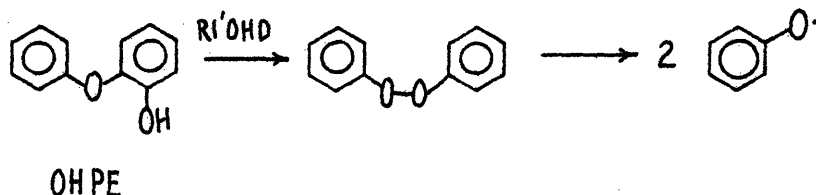
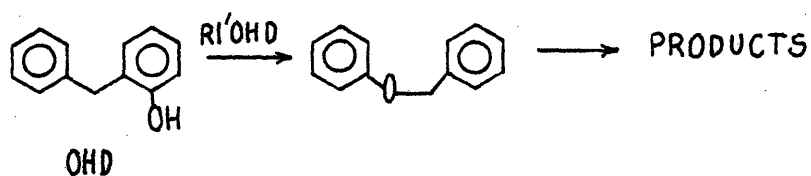
The activation energies determined here and in the literature are roughly 15-25 kcal/mol lower than the phenylether bond strength, which indicates that a free radical mechanism must be more complex than simple fission as a rate determining step. For example, a free radical chain or other complex behavior could lower the apparent first order activation energy.

Alternatively, disproportionation pathways of the type previously described for OHD pyrolysis could be important in phenylether pyrolysis. These may be envisioned to yield phenol and sesquimers directly, as in R1''', where:



Further degradation of the primary sesquimer products could produce the benzene and additional phenol detected.

The possible phenylether pyrolysis mechanisms presented thus far are completely analogous to R1'' and R1''' for OHD, where the ortho-hydroxy substituent was not actively involved in a mechanistic step. However, it is relevant to consider the OHD isomerization pathway R1' applied to an analogous orthohydroxy phenylether (OHPE) substrate as well. As illustrated here, this pathway is not favorable due to the generation of a peroxide in the first step.



Thus, while it is reasonable that an orthohydroxy substituent could enhance free radical reactivity, it is unlikely that an OHPE substrate (as found in lignin) would degrade by a pathway similar to R1' proposed for OHD.

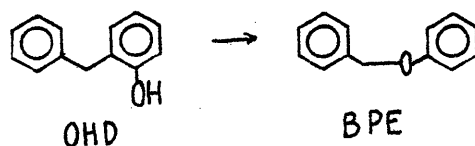
In summary, phenylether pyrolysis yielded phenol, benzene and apparent sesquimers as products; these are completely analogous to the pyrolysis products of OHD. However of the mechanistic possibilities R1', R1'' and R1''' for OHD pyrolysis, only R1'' and R1''' are likely for phenylether pyrolysis. Further experimental characterization of the apparent sesquimers, determination of overall reaction order, and investigation of solvent effects are needed to discriminate between these latter mechanistic possibilities.

Biphenyl, Biphenol

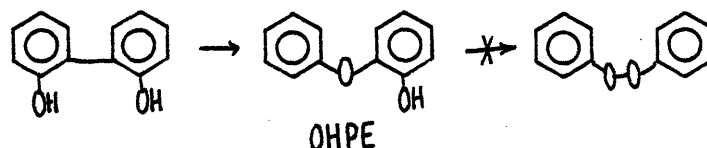
The most refractory substrates pyrolysed were biphenyl and biphenol, the former suffering only slight conversion at 587C. Biphenol was only pyrolysed at 500C, but was completely stable as well. For the case where biphenyl degradation occurred, the only measureable product was benzene; higher molecular weight materials dictated by hydrogen balance went undetected in the present analysis. A first order rate constant  $k=10^{-3.82} \text{s}^{-1}$  was determined based on benzene appearance at 587C.

Literature references also report the linkage quite stable. Ingold and Lossing<sup>82</sup> decomposed biphenyl from 1300-1500C; and detected product spectra consisting of hydrogen, carbon, acetylene, ethylene, butadiene, and benzene. However, the same authors have also pyrolysed benzene from 1350-1450C, and obtained a similar product spectrum. Thus, this high temperature biphenyl pyrolysis likely represents aromatic ring opening reactions either in addition to or to the exclusion of direct biphenyl cleavage to two radicals.

Since neither biphenyl or biphenol were reactive at 500C, the data do not allow estimation of the effect of orthohydroxy substitution in biaryl reactivity. Analogous to the effect of orthohydroxy substitution on diphenylmethane reactivity, an enhancement of biphenyl cleavage might have been expected. Just as orthohydroxy substitution on the diphenylmethane backbone introduced the possibility of intramolecular rearrangements, i.e.



the same type of rearrangement is formally possible for biphenol, as in



However, whereas OHD rearrangement generated a reactive BPE molecule, rearrangement of biphenol generates a less labile OHPE molecule.

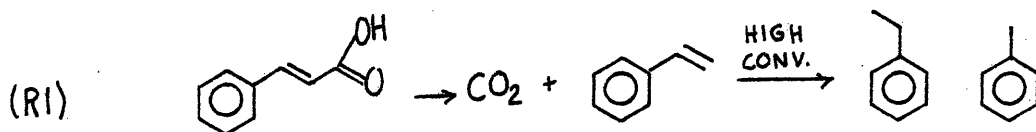
As discussed in the previous section, phenylether degrades slowly and possibly by a free radical cleavage pathway, and facile reaction of OHPE by pathways of the type presented for OHD is unlikely. Thus, the possibility of intramolecular rearrangement should do little to enhance overall biphenol reactivity relative to biphenyl.

In summary, the biaryl linkage appears quite stable and likely degrades only at high temperatures. The data do not show an overwhelming enhancement of the rate of cleavage due to hydroxy substitution, although the effect has not truly been tested. Rearrangement reactions of the type possible for OHD lead to rather stable phenylether moieties, and thus hydroxy substitution will likely not enhance cleavage significantly.

## Cinnamic Acid

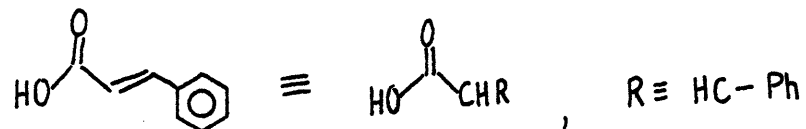
Pyrolysis of cinnamic acid yielded  $\text{CO}_2$  and styrene as stoichiometric major products, with only minor amounts of dimers, toluene and ethylbenzene. This contrasts with cinnamic alcohol and aldehyde pyrolyses, where dimer formation was a major reaction. At the higher temperatures, secondary styrene degradation produced toluene and ethylbenzene, the ratio  $\text{CO}_2/(\text{Styrene} + \text{toluene} + \text{ethylbenzene})$  essentially unity at all conversions attained. Further, each mol of decomposed acid yielded essentially one mol of  $\text{CO}_2$ , the ratio  $\text{CO}_2/(\text{CA}_0 - \text{CA}) = 1.047 \pm 0.4$  for all conversions. The rather large standard deviation demonstrates the experimental difficulties inherent in both  $\text{CO}_2$  sampling procedures and acid chromatography.

These observations suggested one major primary pathway for cinnamic acid pyrolyses, namely:

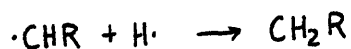
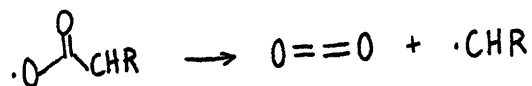
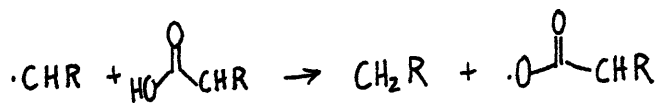
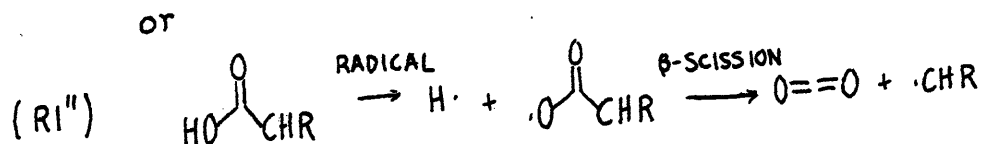
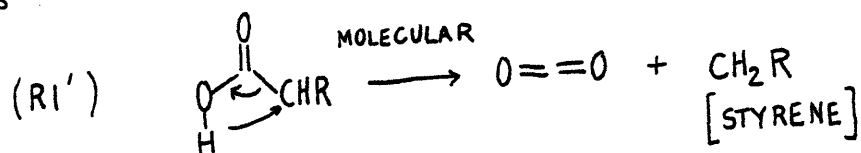


where at higher conversions the styrene suffered secondary degradation to toluene and ethylbenzene, completely analogous to behavior previously reported for styrene from phenethylphenylether. Mechanistic interpretation of cinnamic acid pyrolysis is difficult, but the Arrhenius parameters  $(\log_{10} A, E^*) = (8.0 \pm 1.8, 31.0 \pm 5.0)$  determined for pathway R1 are relevant. The low values for  $\log_{10} A$  and  $E^*$  suggest that direct bond fission as a rate determining step was unlikely. This would

indicate then that either a radical chain or molecular rearrangement account for the acid pyrolysis. In this regard, it is convenient to visualize the acid with reference to the carbonyl moiety, as in



Just as acetone pyrolysis has been postulated to proceed via either a radical chain or molecular elimination to ketene, acid pyrolysis can be visualized as a similar pyrolysis to  $\text{CO}_2$ , in this case stable and isolable. Hence, likely mechanistic features for R1 can be visualized as



Both mechanisms could be consistent with the observed activation parameters, as the unimolecular rearrangement would be expected to proceed with a negative entropy of activation, and a large chain

length could considerably reduce apparent  $\log_{10}A$  and  $E^*$ . The  $\log_{10}A$  determined is rather low for a unimolecular rearrangement, but falls within the commonly observed values when the standard deviation of the regressed  $E^*$  is considered.

Both of  $R1'$  and  $R1''$  seem capable of explaining the observed data. The reaction fit first order kinetics to conversion as high as 70-80%, outside the range likely for pseudo-first order kinetics. The unimolecular rearrangement of the type  $R1'$  would be strictly first order, but a suitable choice of chain termination steps would predict first order kinetics from  $R1''$  as well. In this case, ester formation by combination of  $RCH\cdot$  and  $\cdot O-CO-CHR$  radicals would yield first order kinetics, combination of  $2RCH\cdot$  radicals  $3/2$  order, and peroxide formation  $1/2$  order kinetics. The data do not allow unequivocal discrimination between mechanisms  $R1'$  and  $R1''$ , both depicting decarboxylation, the major pathway in cinnamic acid pyrolysis.

### Ferulic Acid

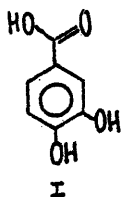
Ferulic acid pyrolysis was studied in an effort to examine the effect of guaiacyl substitution on side chain reactivity. For comparison with  $CO_2$  release from cinnamic acid,  $CO_2$  yields from ferulic acid were monitored with time and temperature of pyrolysis.



Liquid phase product spectra were not analysed. In every case studied, initial rates of  $\text{CO}_2$  release were much faster than those for cinnamic acid. For example,  $k_1^{\text{FA}}/k_1^{\text{C.A}}$  attained values of about 20, 10, and 8 at 250, 300 and 350C, respectively. In fact, ferulic acid readily decarboxylated at 200C, whereas cinnamic acid was stable. These data suggest that the principal result of guaiacyl activation was to reduce the overall energy of activation for R1. These results are similar to those previously reported for benzaldehyde and vanillin, where  $k^{\text{VAN}}/k^{\text{BA}} \sim 10-20$ .

A previous pyrolysis of ferulic acid has been performed by Juntgen and vanHeek,<sup>112</sup> who heated the substrate at a rate of 5.6 C/min and measured the volume of  $\text{CO}_2$  produced. These workers reported significant  $\text{CO}_2$  evolution as low as 175C, with a maximum rate at 225C. These results accord with the present results noting  $\text{CO}_2$  evolution as low as 200C. Further, the rate parameters reported by these workers,  $(\log_{10} A(\text{s}^{-1}), E^*(\text{kcal/mol})) = (9.8, 27.7)$  yield  $-\log_{10} k(\text{s}^{-1}) = 3.05$  at 200C, in accord with the present results of  $-\log_{10} k_{200\text{C}} = 3.30$ . The rate constants determined here fall short of those predicted by Juntgen and van Heek at higher temperatures, due to an apparent lower activation energy. However, as the maximum evolution of  $\text{CO}_2$  was at 225C for Juntgen and van Heek, it is reasonable that the lower temperature data should agree best. These investigators have further pyrolysed protocatechuic acid, I, which also decarboxylated readily, with maximal rate at 250C when heated at

5.8C/min.



This behavior is also similar to that previously noted for benzaldehyde, vanillin, and cinnamaldehyde decarbonylation. In comparison of the pairs vanillin - benzaldehyde and ferulic-cinnamic acid, the extreme activation due to guaiacyl activation is apparent. Further comparison of benzaldehyde-cinnamaldehyde and ferulic-protocatechuic acid reveals that styrene-type conjugation has a much less marked effect, as in both cases the conjugated aldehyde or acid pyrolysed only slightly more readily than did the acid or aldehyde directly bonded to the aromatic ring.

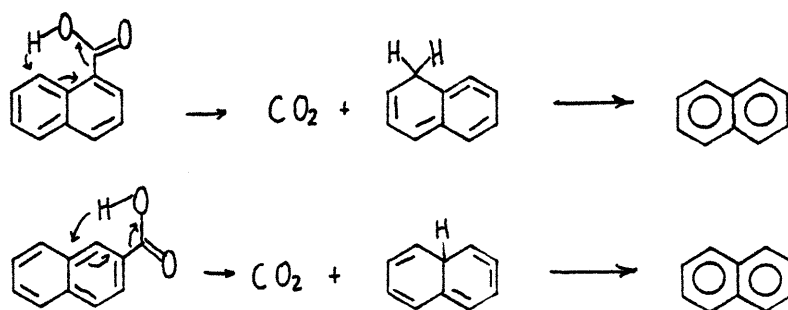
Ferulic acid thus further demonstrates an effect of guaiacyl activation on the reactions of lignin side chain models. Carbon dioxide evolution was faster from ferulic acid than from cinnamic acid due to an apparent reduction in the activation energy for pathway R1 for acid pyrolysis.

### Napthoic Acids

Pyrolysis of 1- and 2- naphthoic acids resulted in rather facile elimination of CO<sub>2</sub>, with the former substrate reacting more readily but with less thermal activation than the latter. It was suggested that these differences in pyrolysis rate were likely due to stereochemical or electronic effects. That is, apparently 1-naphthoic

acid had access to a pathway not available to the 2-napthoic acid isomer.

Consistent with these results is the notion of a unimolecular rearrangement pathway for 1-napthoic acid which is sterically less favored for 2-napthoic acid, as in:



where the intermediate allene undergoes hydrogen shift to readily regenerate the naphthalene. The initial hydrogen shift in each pathway is likely much easier for 1-napthoic acid relative to the 2-napthoic acid isomer. In fact, a free radical pathway is likely to compete favorably in 2-napthoic acid pyrolysis. Both isomers undergo decarboxylation and should serve as typical sites for CO<sub>2</sub> release in lignin and lignite humic acids.

### 10.1.2 Thermochemical-Kinetic Comparison



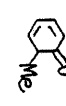
The purpose of the present section is to consider the experimental kinetic parameters in light of the constraints and dictates of thermodynamics. Although not often fully appreciated, thermodynamics and kinetics are indeed interrelated disciplines, perhaps best exemplified by the concept of dynamic thermodynamic equilibrium; at equilibrium, any one of the forward and reverse kinetic constants and equilibrium constant can be determined from the other two. Further, it is clear that thermodynamics specifies a lower bound on the activation energy of an elementary endothermic reaction, which must be greater than the corresponding enthalpy of reaction. These thermodynamic considerations constitute the material of the present section.

Table 10.1.1 is a list of pertinent thermochemical parameters for each reaction pathway determined in the present investigation; where relevant, postulated mechanistic intermediates have been included, and thus introduce additional steps to the pathways. Included in Table 10.1.1 are the enthalpy and entropy of each reaction, estimated by the techniques presented by Benson<sup>169</sup>. The technique is based on the additivity of group properties, where the atomic features of a given molecule sum to the whole molecular property. Whenever possible, integral molecules were used for comparison, but frequent reference to the atomic group property table of Benson was required. For example, guaiacol can be considered as the formal superposition of a phenol and

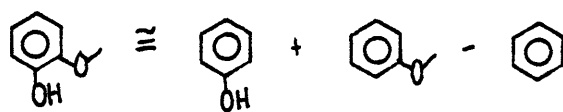
Table 10.1.1 Summary of Thermochemical Parameters for Model Pathways

Substrate	Pathway	$\Delta H_R^0$ (kcal/mol)	$\Delta S_R^0$ (cal/molK)	$E_F^*$ (kcal/mol)	$\log_{10} A_F$ ( $s^{-1}$ )	$E_R^*$ (kcal/mol)	$\log_{10} A_R$ ( $s^{-1}$ or $1/mol \cdot s$ )
PPE	PPE $\rightarrow$ PhOH+St	10.5	33.8	45.0	11.1	35.9	5.9
G	G $\rightarrow$ Q+CH <sub>4</sub>	13.1	(6.22)	43.7	10.9	31.9	(11.7)
	G $\rightarrow$ CAT+CH <sub>4</sub> -H <sub>2</sub>	-23.	130.8	43.7	10.9	-	-
AN	G $\rightarrow$ PhOH+CO+H <sub>2</sub>	11.5	56.5	47.4	11.5	-	-
	AN $\rightarrow$ PhOH+CH <sub>4</sub> -H <sub>2</sub>	-23.	4.9	54.7	13.0	-	-
	AN $\rightarrow$ PhH+CO+H <sub>2</sub>	11.4	56.5	61.0	14.5	-	-
VE	AN $\rightarrow$ oCR	-12.7	-0.7	40.5	7.9	53.2	8.05
	VE $\rightarrow$ G+CH <sub>4</sub> -H <sub>2</sub>	-23.1	2.2	55.9	13.9	-	-
	VE $\rightarrow$ PhOH+CH <sub>4</sub> +CO	-11.6	58.7	58.4	14.1	-	-
	VE $\rightarrow$ AN+CO+H <sub>2</sub>	11.4	56.5	60.7	14.8	-	-
	VE $\rightarrow$ oCR+CO+H <sub>2</sub>	-13	55.8	49.2	11.2	53.2	4.46
SAL	SAL $\rightarrow$ QM+H <sub>2</sub> O	(16.7)	(16.7)	33.4	13.4	(18.0)	(11.9)
BA	BA $\rightarrow$ PhH+CO	2.3	25.5	41.5	9.5	40.5	6.10
VA	VA $\rightarrow$ G+CO	2.3	25.5	38.5	10.2	37.5	6.80
AP	AP $\rightarrow$ TOL+CO	7.6	30.5	56.4	10.9	50.1	6.41
CAD	AP $\rightarrow$ PhH+CO+CH <sub>4</sub> -H <sub>2</sub>	-2.5	31.5	50.5	9.6	-	-
	CAD $\rightarrow$ St+CO	3.12	31.91	48.2	12.1	46.4	7.3
CAL	CAL $\rightarrow$ CAD+H <sub>2</sub>	-23.43	14.22	21.8	4.22	-	-
OHD	CAL $\rightarrow$ AB+H <sub>2</sub> O-H <sub>2</sub>	-53.25	73.53	16.7	1.4	-	-
	CAL $\rightarrow$ St+MeOH-H <sub>2</sub>	-41.91	47.54	24.7	3.4	-	-
	OHD $\rightarrow$ BPE	12.7	.75	43.4	9.6	30.7	9.44

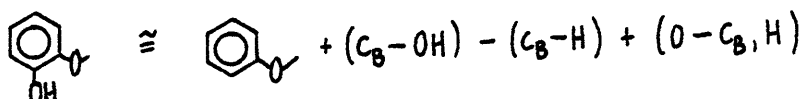
Table 10.1.1 Summary of Thermochemical Parameters for Model Pathways (cont'd)

Substrate	Pathway	$\Delta H_R^{\circ}$ (kcal/mol)	$\Delta S_R^{\circ}$ (cal/molK)	$E_F^*$ (kcal/mol)	$\log_{10} A_F$ (s <sup>-1</sup> )	$E_R^*$ (kcal/mol)	$\log_{10} A_R$ (s <sup>-1</sup> or 1/mol s)
OHD	OHD → TOL+PhOH-H <sub>2</sub>	-5.7	53.65	43.4	9.6	-	-
PE	PE → PhOH+PhH-H <sub>2</sub>	6.8	22.0	72.1	14.8	-	-
BP	BP → 2PhH-H <sub>2</sub>	-3.92	3.5	X	X	X	X
BPhOH	BPhOH → 2PhOH-H <sub>2</sub>	-3.92	3.5	X	X	X	X
	BPhOH → OHPE	-10.72	-18.5	X	X	X	X
CA	CA → St+CO <sub>2</sub>	0.07	50.22	31.0	8.0	-	-
FA	FA → VG+CO <sub>2</sub>	0.07	50.22	19.8	5.2	-	-
1NA	1NA → N+CO <sub>2</sub>	6.95	60.6	24.0	4.5	-	-
2NA	2NA → N+CO <sub>2</sub>	6.95	60.6	36.5	7.9	-	-
G	G → 	(11.07)	(-25.38)	47.4	11.5	(36.33)	(17.0)
VE	VE → 	(-4.33)	(-12.44)	49.2	11.2	(53.53)	(13.9)
AN	AN → 	(-8.85)	(-23.26)	40.5	7.9	(49.4)	(13.0)

anisole, minus



or



a benzene molecule to calculate group properties. On the other hand, guaiacol can be calculated from a base of anisole by adding and subtracting appropriate atomic group properties; a value  $\Delta H_f^0 = -61$  kcal/mol was obtained for guaiacol by either method. The same techniques were used to obtain  $\Delta H_f^0$  and  $\Delta S_f^0$  for every molecular species studied or postulated, the results listed in Table 10.1.2. While many of the thermochemical parameters are calculated with only the uncertainty inherent in the Benson tables, certain group properties, particularly those for the cinnamyl alcohol derivatives, quinone and quinonemethide, were not listed. Values for these groups were estimated by analogy to other isoelectronic or atomic groups listed, and are subject to considerable uncertainty. With reference to Table 10.2.1 and .2 those values considered most uncertain are listed in parentheses. Returning to Table 10.1.1 the individual molecular values of  $\Delta H_f^0$  and  $\Delta S_f^0$  were combined to yield  $\Delta H_R^0$  and  $\Delta S_R^0$  for each pathway listed.






The experimental Arrhenius parameters are listed in Table 10.1.1 as well. These provide the data for the first thermodynamic-kinetic

Table 10.1.2 Thermochemical Parameters For Model Molecular Species

		$\Delta H_f^0$	$\Delta S_f^0$		$\Delta H_f^0$	$\Delta S_f^0$	
PPE		1.65	123.78	AN		-18.0	86.2
PhOH		-23.1	75.1	OCR		-30.7	85.5
St		35.22	82.5	VE		-55.8	108.1
EB		7.12	86.2	SAL		-65.4	83.6
PhH		19.8	64.3	QM		(9.1)	(55.2)
G		-61	97	H <sub>2</sub> O	-	-57.8	45.1
Q		(-30.0)	(58.7)	BA		-8.9	86
CH <sub>4</sub>	-	-17.9	44.5	VA		-89.7	118.7
CAT		-66.1	214.5	AP		-22.0	93.3
H <sub>2</sub>	-	0	31.2	CAD		5.7	76.3
CO	-	-26.4	47.2	CAL		29.13	93.2

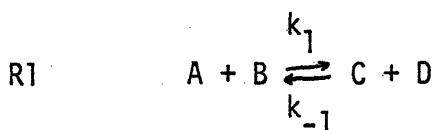


Table 10.1.2 Thermochemical Parameters For Model Molecular Species (cont'd)

	$\Delta H_f^0$	$\Delta S_f^0$	NA	$\Delta H_f^0$	$\Delta S_f^0$
AB	33.68	90.5		-64.9	71
MeOH	-48.0	57.3	N	36.1	80.5
OHD	-5.41	129.3	CO <sub>2</sub>	-94.05	51.1
BPE	7.29	130	CH <sub>2</sub> O	-26.0	52.3
PE	-10.1	86.2	TOL	+12	76.6
BP	43.52	93.9	MTC	-49.3	-
BPhOH	-42.3	115.5	DIMETHIDE	(48.84)	(48.74)
OHPE	-53	97		(-2.48)	(98.95)
CA	-58.9	83.4	HCl	-22.0	44.6
FA	-139.7	116.1		(-26.85)	(62.94)
VG	-45.6	115.2		(-60.13)	(95.66)
				(-49.93)	(71.62)

comparison, that of the  $E^*$  and  $\Delta H_R^0$  for each pathway. As evidenced in Table 10.1.1 and dictated by transition state theory, the activation energy for each pathway was in excess of the reaction enthalpy change. Thus, each pathway conforms to this first constraint imposed by thermodynamics.

However, the mechanistic insights and assertions of section 10.1.1 are subject to further examination. In particular the elementary reactions of Table 10.1.1 are easily associated with an equilibrium reverse reaction. For those forward reactions where a mechanism was postulated, the implied reverse reaction mechanism must be consistent. Hence, the reverse reaction Arrhenius parameters must accord with the implied reverse reaction mechanism. As developed here, the forward reaction Arrhenius parameters and thermochemical parameters ( $\Delta H_R^0$ ,  $\Delta S_R^0$ ) provide the necessary information to determine these reverse parameters. Consider the elementary reaction,



At equilibrium,  $dA/dt = dB/dt = dC/dt = dD/dt = 0$ , or

$$\text{(I)} \quad k_1 AB = k_{-1} CD \Rightarrow \frac{k_1}{k_{-1}} = \frac{CD}{AB} = K_1$$

$$\text{(II)} \quad \text{where} \quad -\log_{10} K_1(\text{atm}) = + \frac{\Delta G_R^0}{\theta} = \frac{\Delta H_R^0}{\theta} - \frac{\Delta S_R^0}{2.303R}$$

This equilibrium  $K_1$  is based on the standard state of 1 atm and ideal gas; transformation to the normal kinetic concentration units is considered below. Combining I and II

$$\log_{10} K_1(\text{atm}) = \log_{10} k_1 - \log_{10} k_{-1}, \text{ or}$$

$$\text{(III)} \log_{10} A_{-1} = \log_{10} A_1 - \Delta S_R^0 / (2.303R)$$

$$\text{(IV)} E_{-1}^* = E_1^* - \Delta H_R^0$$

Thus, the reverse activation parameters are determined upon specification of the thermodynamic and forward reaction parameters. When there is no mol change in the reaction, the forward and reverse reactions are of the same order and the Arrhenius parameters for each have the same units. Further, first order parameters are concentration independent and the Arrhenius parameters are thus independent of standard states. However, when there is non-zero mol change,  $\Delta n \neq 0$ , the Arrhenius parameters for forward and reverse rates will have different units and will depend on the standard state specification. For the purpose of this work, it is most convenient to transform pressure units to concentration units, as this provides facile comparison to the standard literature references. In this case,

$$\text{(V)} \quad \text{a) } E_C = E_p + \Delta nRT \quad ; \quad \text{b) } A_C = A_p (R'T)^{\Delta n} e^{\Delta n}$$

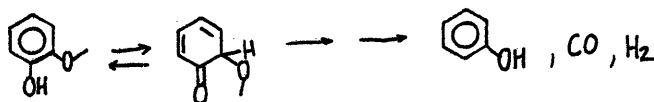
where  $E_p$  and  $A_p$  are determined from III and IV. In Va, R will conveniently assume a value of 0.001987 kcal/mol-K, where in Vb  $R' = 0.08206$  l-atm/molK. Reverse reaction Arrhenius parameters were calculated in this manner for the relevant pathways of Table 10.1.1 for a reference temperature of 400C; only reactions where a molecular or otherwise elementary reaction mechanism has been postulated are

considered. These reverse parameters are also presented in Table 10.1.1.

As detailed in section 10.1.1, the reverse ene cycloaddition reaction parameters calculated from the PPE forward and thermochemical parameters are  $(\log_{10}A, E^*) = (5.9, 35.9)$ . These reverse Arrhenius parameters agree quite well with those commonly encountered in cycloaddition reactions,<sup>170,171</sup> and the  $\log_{10}A \sim 6$  is particularly characteristic of concerted cycloaddition.

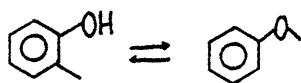
Estimated thermochemistry for the demethanation of guaiacol to the diquinone and methane yielded reverse addition parameters  $(\log_{10}A, E^*) = (11.7, 31.9)$ . These parameters are indicative of a loss of entropy in attaining the addition transition state, although a  $\log_{10}A$  value of 11.7 does not unequivocally imply a concerted molecular addition. However, as noted above, the estimation of  $\Delta H_f^0$  and  $\Delta S_f^0$ , particularly the latter, for the quinonemethide was with considerable uncertainty. Group values for Cd-(CO)(H) and others, especially with regard to the entropic terms, cannot be found directly in the literature. Thus, these reverse parameters are presented as suggestive, and are extremely tentative. As an example of the propagation of this uncertainty,  $\log_{10}A$  would have arisen as  $\sim 8.7$  and  $6.5$  for  $\Delta S_R^0 = 20$  and  $30$  e.u. respectively.

With regard to guaiacol pathway R2, formation of phenol, CO and H<sub>2</sub> has been envisioned to occur via a mechanism initiated by 1,7 sigmatropic hydrogen shift, i.e.,

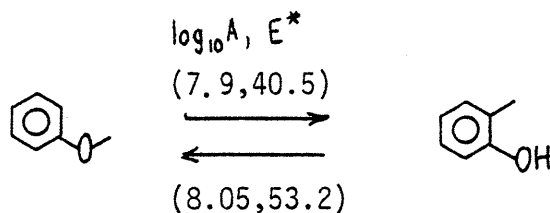


Although estimation of the thermochemical properties of the conjugated carbonyl is with considerable uncertainty, reverse hydrogen shift Arrhenius parameters arose as  $(\log_{10} A, E^*) = (17.0, 36.3)$ . The high  $\log_{10} A$  arises because of the unusually low estimate for  $\Delta S_R^0$  in Table 10.1.1 in turn arising due to uncertainty in the estimate of the quinone properties.

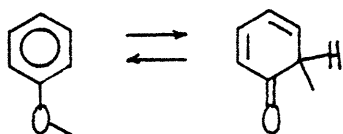
The forward parameters for anisole isomerization to o-cresol yielded parameters of  $(\log_{10} A, E^*) = (8.05, 53.2)$  for the reaction:



These values suggest that while the formation of anisole from o-cresol is considerably more activated than the reverse, both paths proceed through entropically similar transition states. That is,



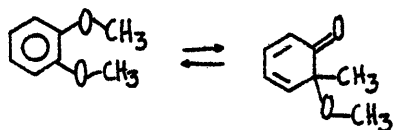
The actual mechanism for anisole isomerization has been visualized as step-wise or simultaneous methyl and hydrogen migration, where the above analysis more properly corresponds to the latter case. For a step-wise mechanism, anisole isomerization is likely limited by disruption of the ring aromaticity, generating a carbonyl as:



Parameters for the reverse methyl shift have been estimated as  $(\log_{10} A, E^*)$

= (13,49.4), indicative of a modestly tight transition state. As noted above for guaiacol, estimation of ring carbonyl properties is clouded by considerable uncertainty.

Similarly, veratrole pyrolysis to o-cresol in a step-wise



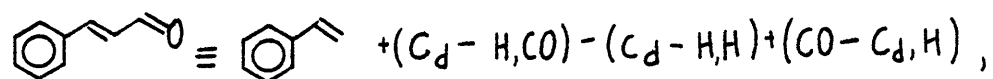
manner yielded reverse methyl shift parameters of  $(\log_{10}A_1E^*) = (13.9, 53.6)$ . These are in substantial agreement with those noted for anisole.

The Arrhenius parameters for forward saligenol dehydration yielded reverse water addition parameters of  $(\log_{10}A, E^*) = (11.9, 18.0)$ . While these parameters appear reasonable, the uncertainty involved in the estimation of the quinonemethide thermochemical properties renders detailed interpretation difficult. The endothermic dehydration (estimated) yielded a rather low reverse water addition activation energy, while the reaction entropy change yielded a modestly 'tight' reverse transition state A factor of  $\log_{10}A \sim 12$ .

The experimental Arrhenius and estimated thermochemical parameters for benzaldehyde and vanillin pyrolyses yielded quite reasonable reverse parameters. These cheletropic addition parameters arose as  $(\log_{10}A, E^*) = (6.10, 40.5)$  and  $(6.80, 37.5)$  for benzaldehyde and vanillin, respectively. The low values for  $\log_{10}A \sim 6.5 \pm 0.5$  are consistent with the tight transition state likely for non-linear cheletropic addition. It is cogent to note that the thermochemical

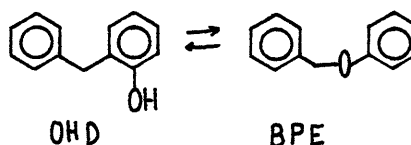
properties of benzaldehyde, benzene and CO are well documented in the literature, and that those for vanillin and guaiacol can be readily obtained by superposition of the properties of phenol, anisole, benzene and benzaldehyde.

Similarly, estimation of cinnamaldehyde properties as



yields, in combination with the forward decarbonylation parameters,  $(\log_{10} A, E^*) = (7.3, 46.4)$  for reverse cheletropic addition. These parameters are quite analagous to those noted above for reverse cheletropic CO addition to benzene and guaiacol. Upon consideration of the sensitivity of these calculations to uncertainty in the thermochemical estimates, the reverse CO addition entropic parameters for cinnamaldehyde are essentially identical to those for benzaldehyde and vanillin. Since  $\Delta H_R^\circ$  is virtually identical for the latter pair, the lower  $E^*$  for addition to form vanillin is considered real, in accord with the postulated inductive effect of guaiacol substitution.

At least two different mechanistic interpretations of OHD pyrolysis are equally plausible, these being the isomerization to BPE and the disproportionation reaction to phenol and sesquimers. Whereas the details of the latter mechanism are unclear, the former rearrangement is readily included in the present discussion. The isomerization of OHD to BPE, namely:



is net endothermic by about 12.7 kcal/mol and near isentropic ( $\Delta S_R^\circ \sim 0.75$ ). These combine with the forward Arrhenius parameters to yield back parameters of  $(\log_{10} A, E^*) = (9.4, 30.7)$ . Hence, the back reaction to OHD appears more facile by about 12.7 kcal/mol, over 4 orders of magnitude in rate at 400C,  $\theta^{-1} = 0.325$ . Overall BPE reactivity is also much faster than that of OHD, evidenced best in comparison of literature BPE conversion and the present OHD pyrolyses (cf chapter 8.0). The net isentropic reaction yielded near equal forward and reverse  $\log_{10} A$  values, consistent with the notion of benzylic or hydrogen sigmatropic migration.

In summary, the group additivity concept of Benson has been used to compare the experimental kinetic parameters with the constraints and dictates of thermodynamics. The principle of microscopic reversibility has been used to compare forward reaction rates and mechanisms with implied reverse rates and mechanisms. In many cases the comparisons were consistent and informative, most notably in the decarbonylation reactions of benzaldehyde, vanillin, and cinnamaldehyde. The thermochemical parameters for these reactions are either well documented or easily estimated by superposition, and thus provide a basis for critical comparison. On the other hand, thermochemical data for the diquinones, quinonemethide and other conjugated carbonyls are virtually nonexistent, and the additive group properties could be estimated only by analogy. These comparisons were correspondingly less informative, showing extreme sensitivity to the estimated parameters. In all, the present thermochemical



comparison emphasizes that both experimental and theoretical aspects of the present investigation are subject to considerable refinement.

## 10.2 Simulation Predictions

Previous discussion has focused upon the results and implications of the experimental model compound pyrolyses. It is the purpose of the present section to consider the mathematical superposition of these, namely the whole-lignin simulation model predictions. The model predictions were described in terms of gas, liquid, phenolic and carbonaceous residue product fractions in Chapter 9. The same organizational strategy will be used in the present section, where overall fraction and individual product yields will be compared to experimental lignin pyrolyses reported in the literature. Discussion will begin with a description of the literature citations which allow relevant comparisons. This will be followed by a consideration of the overall fraction yields, which will be compared to both the literature yields and theoretical maximum limits. Individual product yields will be described next, followed by a consideration of the limitations and merits of the simulation.

### 10.2.1 Relevant Literature for Comparison

Quantitative comparison of the simulation results with previous experimental pyrolyses is difficult because the latter have employed a wide range of lignin types, lignin isolation methods, and pyrolysis reactor configurations. For example, many previous pyrolyses have been of the destructive distillation type, while others were DTA/DTG studies; still others have been effected in reactors designed to emphasize primary reactions, where volatile products either diffused or were swept from the pyrolysis zone.

Table 10.2.1 is a grid depicting the areas where the items predicted by the model are relevantly compared with the literature. The four major product fractions have been delineated in terms of overall and constituent component yields; the carbonaceous residue fraction contains a subheading labeled kinetics, where the time dependency of overall lignin pyrolysis is examined. The grid contains six columns, representing the model prediction and six sets of literature references. The six literature reference sets include: 1) the collected reports of Table 4.1, 2) the tar yields of Table 4.4, 3) the data of Iatridis and Gavalas<sup>26</sup>, 4) the data of Kirshbaum<sup>41</sup>, 5) the data of Domburg<sup>39</sup>, and 6) the DTA/DTG data of Domburg and Sergeeva<sup>129</sup>. A plus indicates that information relevant for comparison with the simulation was reported, whereas the 'x' indicates that no relevant comparison was possible.

The model provides entries for each of the grid points save CO<sub>2</sub> yield, which was included in Table 10.2.1 because CO<sub>2</sub> is readily incorporated into the model and has been reported by a number of previous workers. The collected investigations of Table 4.1 provide detailed accounts of gas and aqueous distillate overall and component yields. This reference set also provides relevant information regarding overall phenolic and char yield. Because of the lack of detailed temperature-time information, and since many of these investigations were destructive distillations, the grid entries for this column are best considered as asymptotic ultimate yields.

Item	Model Prediction	Collected Authors Table 4.1	Collected Author Table 4.4	Iatridis and Gavaias <sup>26</sup>	Kirshbaum <sup>41</sup>	Domburg <sup>39</sup>	Domburg and Sergeeva <sup>129</sup>
Gas Fraction							
Overall	+	+	X	+	+	X	X
CH <sub>4</sub>	+	+	X	+	X	X	X
CO	+	+	X	+	X	X	X
CO <sub>2</sub>	X	+	X	+	X	X	X
Liquid Fraction							
Overall	+	+	X	X	X	X	X
H <sub>2</sub> O	+	+	X	X	X	X	X
MeOH	+	+	X	+	X	X	X
Phenolics							
Overall	+	+	+	+	+	+	X
Individual Phenols	+	X	X	+	+	+	X
Carbonaceous Residue							
Overall	+	+	X	+	+	X	X
Kinetics	+	X	X	+	X	+	+

+ relevant information provided

Table 10.2.1

X no relevant comparison possible  
Literature references relevant for comparison  
with simulation predictions

The collected investigations of Table 4.4 provide information regarding the overall yield of phenolic materials from lignin pyrolyses. These entries are also best considered as long time ultimate yields. This reference set will provide no other points for comparison.

The data of Iatridis and Gavalas<sup>26</sup> provide grid entries for all save overall aqueous distillate and water yields. The data were obtained in a reactor designed to emphasize primary reactions, and detailed temperature-time information was provided. Thus, comparison of kinetic results is relevant. However, since primary reactions were emphasized in the experiments, guaiacol yields should be higher and catechol yields lower than those predicted by the model; a lower methane yield might also be expected based on this point.

Kirshbaum<sup>41</sup> provides grid entries for overall gas & losses yield, overall phenolics, and overall carbonaceous residue yield. The one additional entry is for individual phenol yield, where detailed phenolic product spectra are presented as a function of pyrolysis temperature. The exact temperature time history is unclear, and these data will be considered as ultimate yields.

Another detailed description of phenolic product spectra is provided by Domburg, et al.<sup>39</sup>, who pyrolysed lignins to 475C. Gas and liquid yields are not included, although DTA/DTG information is provided. The final reference is that of Domburg and Sergeeva<sup>129</sup>, who provide DTA/DTG information for comparison.

In summary, while the literature provides a wealth of information regarding lignin thermolyses, that relevant for comparison to the simulation is diffuse. That is, the six reference sets of Table 10.2.1 are collectively needed to examine aspects of each model prediction. Experimental lignins, lignin isolation methods, and pyrolysis reactors have varied, and no one experimental pyrolysis was at reactor conditions implied by the batch simulation. Thus, quantitative comparisons will need be considered with certain reservation. Overall, however, the simulation predictions and experimental pyrolyses provide much information for meaningful comparison.

#### 10.2.2 Overall Product Fraction Yields

The discussion of Chapter 9 has described the yields of each individual pyrolysis product. The overall product fraction yields, however, arise as the summation of each individual product. That is, whereas overall yields are measured directly and then quantitatively characterized in experimental pyrolyses, the individual constituent products sum to the overall fraction yield in the simulation. This summation is considered here. The products have been divided into four product fractions, a gas, aqueous distillate, phenolic and carbonaceous residue fraction.

Since only CO and CH<sub>4</sub> were accounted in the simulation, these two sum to the overall gas fraction. In fact, CO and CH<sub>4</sub> are by far the prevalent constituents in the lignin off-gas. A minor component CO<sub>2</sub> will be discussed as well, even though it was not included in the simulation model. The aqueous distillate will be composed of

water and methanol only, since acetone, acetic acid, and other minor liquid products were not included in the simulation. The phenolic fraction will be considered as the molar sum of all single ring phenols, even though many of these are complex. Thus, this overall yield might correspond best to the overall tar yield reported in pyrolysis experiments. Finally, as was described in Chapter 9, the carbonaceous residue fraction is composed of all multiple ring aromatic units.

A summary of the product yields predicted by the simulation and reported in the literature is presented as Table 10.2.2. This grid is completely analogous to Table 10.2.1, only entries denoting the potential for fruitful comparison have been replaced by entries for representative quantitative yields.

#### Gas Evolution

The predicted overall gas fraction rose steadily with increasing time and temperature and achieved a value of about 15% of lignin, by weight, at 600C. This compares favorably with the data of Table 4.1, where gas yields ranged from about 10-20%. Iatridis and Gavalas report an overall yield as high as 23% at 650C, but this included 7.2% CO<sub>2</sub>. As discussed below, this rather high CO<sub>2</sub> content may be due to lignin structural modifications induced by the lignin isolation method. If CO<sub>2</sub> is not considered as part of the product yield, then the overall yield drops to 16%, in good agreement with both the simulation and the data of Table 4.1. Additionally, Kirshbaum reports a gas and losses yield of ~5% at 250C and ~18% at 600C.

Item	Model Prediction	Collected Authors: Table 4.1	Collected Authors: Table 4.4	LITERATURE	Latridis and Gavaias <sup>26</sup>	Kirschbaum <sup>41</sup>	Domburg <sup>39</sup>
Gas							Domburg <sup>39</sup>
Fraction							Domburg <sup>39</sup>
Overall yields	15% @ 600C	10-20%, 15% mean	X		23% max including CO <sub>2</sub>	5% @ 250C, 18% @ 600C gases and losses	Domburg <sup>39</sup>
CH <sub>4</sub>	6% @ 600C	7% based on mean overall yield of 15%	X		4.8% @ 650C	X	and Sergeeva <sup>129</sup>
CO	9% @ 600C	7% based on overall mean of 15%	X		9.2% @ 650C	X	
CO <sub>2</sub>	X not included in simulation	1.5%	X		near 6%, all temperatures	X	
Liquid Fraction							
Overall	6% maximum	overall mean 15%	X		X	X	
H <sub>2</sub> O	6% maximum	12-15%	X		X	X	
MeOH	0.1% maximum	0.2-1.0%	X		3% @ 650C	X	
Phenolics							
Overall	Sum of single ring phenols as function of time 7-80%, include complex phenols	3-30%	1.3-14%		0.3-3.0%, 400-650C	3.3-14.5% @ 75C	0.2% @ 250C, 14% @ 500C
Individual Detailed Yields of Individual Phenols as a function of time and temperature		X	X		only guaiacols and phenols	detailed yields of 20+ different phenols	detailed yields of 20+ different phenols
Carbonaceous Residue							
Overall	Ultimate residue yield from 0.385 @ 600C to 0.914 @ 300C	40-60% yield of char	X		weight loss of 53% @ 600C	Char yield of 91% @ 250C, 26% @ 600C	X
Kinetics	multiple ring aromatics as function of time, ultimate yields as function of temperature	X	X		weight loss for 400-600C as in function of time	X	DTA/DTG experiments yield E kcal/mol 26-30

Table 10.2.2: Quantitative simulation literature comparison grid.

DTA/DTG experiments  
yield E  
kcal/mol  
18-38



The theoretically maximum overall gas yield should be a function of temperature. Idealized limits can be estimated at high and low temperatures. At low temperatures, gas release from methoxyphenols should be prevalently methane, and assuming  $1\text{CH}_4/\text{OMe}$ , a maximum methane yield of  $\sim 9\%$  arises. Further, assuming an ideal release of one CO per side chain, a low temperature CO maximum of  $\sim 15\%$  arises. Thus, a low temperature total gas yield, on a weight per cent basis, of  $\sim 24\%$  can be calculated assuming  $\text{CH}_4$  and CO are the major constituents of the lignin off-gas. On the other hand, at high temperatures the methoxyphenol gas release selectivity will shift toward CO evolution, and thus two mols of CO will be produced from each aromatic unit in the present idealization. Hence, an overall gas yield, composed entirely of CO, of about 30% by weight arises.

In short, the overall gas yields predicted by the simulation model are in good agreement with the literature. The calculated upper limits for gas release assume 100% conversion of idealized substrates and may be slightly high. However, both the simulation predictions and literature reports are well within these bounds.

#### Aqueous Distillate

The simulation predicted an overall distillate yield of about 6% based on the sum of water and methanol yields. This value is generally lower than those reported by the grid reference Table 4.1, where distillate yields of about 15% are reported. Since water is by far the prevalent component of the overall aqueous distillate fraction, a theoretical maximum yield of water is relevant. Assuming

the release of one  $H_2O$  mol per 3-carbon side chain, an ideal maximum of about 10% is calculated. Since methanol, acetic acid and acetone account for at most about 3% of the lignin yield, the literature report is still at least 2% higher than this ideal maximum; the reports are often much higher (cf. Table 4.1). Further, all lignin side chains do not yield one mol of water, as evidenced by the pyrolysis product spectra of cinnamaldehyde and cinnamylalcohol. The latter substrate yielded water in about 4% yield. As discussed in greater detail below, physically associated water either existing with the plant lignin or introduced by lignin isolation may yield the seemingly high distillate yields. Another likely source is the carbohydrate impurity invariably present in lignin preparations. Of course, the possibility of additional 'chemical' water precursors cannot be unequivocally dismissed, but was not suggested in the experimental portion of the present investigation.

### Phenolics

The predicted overall yield of single ring phenols ranged from 7-80%, on a molar or moiety basis. Equivalently, up to 80% of the lignin aromatic units were transformed into single ring aromatics for simulation pyrolysis to 600C and 7s. Included in this single ring phenol yield are substantial amounts of complex phenols, such as coniferaldehyde and guaiacyl vinyl ketone (termed guaiacyl acrolein in the present investigation). These are not often reported as single ring phenols in experimental pyrolyses, presumably due to GC analysis difficulties.

The reported experimental overall phenolic yields were about 3-30% for the collected authors of Table 4.1, 1.3-14% for the collected authors of Table 4.4, only 0.3-3% for Iatridis and Gavalas, 3.3-14.5% for Kirshbaum, and 0.2-14% for Domburg. These were lower than the simulation prediction for two likely reasons. The first is that the complex phenols which surely existed in the tar fraction were not likely identified. It is cogent to note that tar yields in excess of 50% have been reported<sup>71</sup>. The second explanation is that the simulation model has rather unrealistically suppressed bimolecular condensation and polymerization reactions, which effected a higher yield of single ring phenols. For example, condensation reactions of cinnamaldehyde side chains will likely occur, although to an extent reduced from that observed for the neat cinnamaldehyde pyrolysis substrate. The 'low concentration' approximation is one limiting idealization, useful for development of the simulation. Refinement of the model could account for condensation-type reactions.

#### Carbonaceous Residue

The simulation predicted carbonaceous residue yields of about 40% at 600C and 7s and about 91% at 300C and  $10^4$ s, which compare favorably with the literature. The authors of Table 4.1 report char yields generally of the order 40-60% of lignin. Iatridis and Gavalas report a weight loss of ~20% and 53% at 400 and 600C, respectively. Rephrased, the char yields should correspond to ~80% and 47% at these respective temperatures. Kirshbaum reports a char yield of 91% at 250C and only 26% at 600C. As will be

developed below, the time variation of the predicted weight loss coincides quite well with the experimental data of Iatridis and Gavalas. In short, the operational definition of residue as multiple ring aromatics yields carbonaceous residue yields that are in good accord with the experimental literature.

The overall product fraction yields are in substantial agreement with the literature. Gas and carbonaceous residue yields compare quantitatively, whereas liquid and phenolic yields are in less precise accord. The predicted liquid yields fell short by a factor of about 2 or 3, reflecting likely uncertainty in both of the simulation and the experiments. Similarly, it is not clear that the experimentally reported phenols represent all single ring phenols produced in lignin pyrolysis. Combining this possibility with a likely underprediction of condensation reactions at least qualitatively explains the greater simulation yield of phenols relative to those reported in the literature.

### 10.2.3. Individual Product Yields

#### Gas Evolution

The simulation model accounted for methane, CO, and hydrogen, and is readily upgraded to include CO<sub>2</sub> release. Discussion commences with consideration of the former product.



The simulation predicted methane yields of 0.05%, 6.2%, 5.9 % and 6.1% at (300C,10<sup>4</sup>s )(400C,10<sup>4</sup>s), (500C,100s) and (600C,7s), respectively. The time dependency of the methane yield at each temperature is detailed in Figure 9.1 and Appendix 9.1. Comparison with the literature is difficult, since the exact conditions of pyrolysis time and temperature have not always been reported. However, Iatridis and Gavalas<sup>26</sup> have studied the pyrolysis of a Kraft lignin at 400-650C, and report 0.52% yield of methane at 400C and 60-120s. The present simulation predicts 0.18% at 400C and 100s, rather good agreement considering both the likely uncertainty in the simulation as well as the established variations in experimental lignin pyrolyses. Table 4.1 lists other gas yields for comparison; those studies reporting gas composition did not list overall yield. However, as most total gas yields fall between 10 and 20%, estimates of individual component yields are apparent. Assuming 15% gas yields, the lignin methane

yields listed in Table 4.1 correspond to 5.6% and 7.2 %.

These were likely obtained from DTA or destructive distillation processes, and thus correspond quite well to the ultimate yield of 6.2% at 400C and  $10^4$  s. Of course, these comparisons are qualitative, since the exact nature of these latter pyrolyses has not been well described.

At 500C and 100s, the simulation predicted a methane yield of 5.9 %, whereas at 600C and 7s, a yield of 6.1% was predicted. For comparison, Iatridis and Gavalas report 2.21% at 500 and 60s, and a 1.3% yield at 600 and 10s. The latter compares directly with the 600C simulation, whereas the simulation predicts a  $\text{CH}_4$  yield of 5.1% at 500C and 60s. Thus, in all cases the model overpredicted methane yield as compared to the data of Iatridis and Gavalas. Although Kraft pulping is known to reduce the overall lignin methoxyl content, this is likely a contributing, but not dominant factor in the experimental-simulation discrepancy. Rather, the predominant effect likely concerns reactor engineering. The pyrolyser of Iatridis and Gavalas was designed to emphasize primary reactions, such that primary products could leave the 'reaction zone'. Outside of this zone, the gas contents were maintained below 100C, restricting secondary pyrolysis. On the other hand, the simulation models a batch reactor, where primary products are capable of secondary degradation. Thus, in the simulation, guaiacols were subjected to extensive secondary pyrolyses, yielding catechols and methane. In the experimental work, a portion of the guaiacols were likely volatilized and swept from the reaction zone, precluding secondary methane formation. This point is to be developed further below, yet deserves brief anticipation here. At 500C and 60s, the model predicts

about 17.3% single ring catechols. This corresponds to at least 2.2% methane release from guaiacol precursors, close to the difference in the experimental results and model predictions. Further, the model predicted only 0.04% guaiacol at 500C and 60s, whereas the experimental work yielded 0.98% guaiacol. Thus, the 0.25% and 1.9% yields of catechol and methyl catechol, respectively, predicted by the model accord reasonably well. In short, secondary pyrolyses likely explain the predictions of both the greater yield of methane and lower yields of guaiacols, when compared against the higher temperature experimental work.

Overall, methane yields are in general agreement with those previously reported from experimental pyrolyses. The yields are of the same order of magnitude, yet absolute discrepancies exist. These are well explained in terms of secondary guaiacol pyrolyses, more severe at higher temperatures.

#### CO

The simulation predicted CO evolution in yields of 0.037%, 3.5%, 4.4% and 9% at (300C,10<sup>4</sup>s), (400C,10<sup>4</sup>s), (500C,60s) and (600C,7s), respectively. The ratio CO/CH<sub>4</sub> was greater than one at low temperatures and low conversion, whereas the ratio was less than one at moderate temperatures and conversions; at higher temperatures the ratio again exceeded unity. These results were interpreted in terms of dual sites for CO release, namely, the lignin carbonyls and methoxyphenols. Cinnamaldehyde units initially present in the lignin substrate yield CO readily in the early stages of pyrolysis, whereas initial guaiacols and guaiacols generated from ether reversion release greater amounts of methane at modest conversions. The acrolein-type carbonyls

generated by ether reversion degrade rather slowly at these conditions, and low temperature guaiacol degradation selectivity favors demethanation. Thus, the off-gas from moderate lignin pyrolysis is dominated by  $\text{CH}_4$ . On the other hand, the high activation energies for acrolein decarbonylation and guaiacyl demethoxylation result in larger proportions of CO from high temperature pyrolyses.

As was the case with methane, simulation CO yields generally exceeded those reported by Iatridis and Gavalas. For example, these workers report 1.2%, 2.05%, 2.65% and 9.2% at (400C,120s), (500C,60s), (600C,10s) and (650C,120s), respectively. The latter data set aligns with model predictions at 600C and 7s, whereas model predictions for (400C,100s) and (500C,60s) were 0.22% and 4.4 % , respectively. The experimental  $\text{CO}/\text{CH}_4$  ratio varied from about 2.3 at 400C, 0.88 at 500C and 1.8 at 600C, in general accord with the model behavior described above. Other literature citations, noted in Table 4.1, are also in substantial agreement with the model predictions.

In summary, model predictions for CO evolution are in general accord with the literature experimental studies. Detailed quantitative comparison is difficult, since experimental lignins, reactors, and reaction conditions vary widely. In fact, considerable variation exists in the literature product spectra, offering, at best, ranges for product yields. That the CO yields agree within an order of magnitude thus seems reasonable.



$\text{CO}_2$ 

The present system of model equations does not provide for  $\text{CO}_2$  release, although ferulic acid, humic acid, and lactone groups present in the lignin in modest amounts serve as facile  $\text{CO}_2$  precursors. Evidence for this is provided in the work of Iatridis and Gavalas<sup>26</sup>, who obtained considerable  $\text{CO}_2$ , as much as 6% at 400C, from the precipitated Kraft lignin. Other workers<sup>28,38</sup> report yields of  $\text{CO}_2$  closer to 1-2%, from HCL and hydrolysis lignins, respectively. Kraft pulping effects an introduction of carboxylic acid units into the lignin macromolecule, which might explain the higher yields of  $\text{CO}_2$  reported by Iatridis and Gavalas. Further, this logic would support the hypothesis of acid or lactonic precursors for  $\text{CO}_2$  release. As the experimental section of the present investigation included ferulic and cinnamic acid pyrolyses, inclusion of these into the reaction model requires only an accurate assessment of the proportion of the acid sites in the substrate lignin.

Overall, the simulation predictions of gas release are in substantial accord with the experimental pyrolyses reported in the literature. Methane and CO are well predicted, and further constitute a vast proportion of the experimental product gases. Pathways for  $\text{CO}_2$  release have not been included, but should be readily incorporated into revisions of the simulation model. Other possible pathways for  $\text{CO}_2$  formation include shift reactions, carbohydrate impurities, and lignin modification reactions, which have not been investigated.

### Liquid Products

#### H<sub>2</sub>O

The simulation provides for water formation predominantly through saligenol dehydration, although cinnamyl alcohol side chains provide less important precursors. The ultimate yields were rather modest, amounting to 0.05%, 5.3%, 4.4%, and 4.4% at (300C,10<sup>4</sup>s), (400C,10<sup>4</sup>s), (500C,10<sup>2</sup>s) and (600C,7s), respectively. Thus, the simulation would seem to predict ultimate yields of H<sub>2</sub>O at about 6%.

Absolute determination of experimental water yields have not often been effected, yet Table 4.1 presents total aqueous distillate yields of 8.7-30%, averaging about 15%. As water is the major component of these distillates, and methanol, acetone and acetic acid comprise from .3-2%, .1-1% and .1-1% respectively, a likely average H<sub>2</sub>O yield is about 12-13%. This yield is significantly in excess of the 6% simulation prediction, which suggests alternative origins for H<sub>2</sub>O formation in lignin; the rapidity of saligenol dehydration precludes possible kinetic limitations. The alternative water precursors are likely of two types, physically adsorbed water or saturated hydroxyls. It is quite likely that some water is associated with lignin in a physical sense, which would appear as product water as low as 100C. The water could be either biological in origin or introduced in extraction or pulping methods. The large variations in distillate yields of Table 4.1 suggest that isolation methods and lignin type affect the ultimate yield of water attained. This is likely in part due to chemical modification of the lignin structure, but may also be due to variable amounts of associated physical water introduced. With regard to

saturated hydroxylic water precursors, formal hydroxyl cleavage would produce two water molecules from guaiacylglycerol- $\beta$ -ethers, and thus increase net water formation from lignin. This would not double lignin water, however, as the  $\alpha$ -oxygen in  $\beta$ -ethers can also be etherified or a carbonyl moiety. To elucidate this problem, pyrolyses of substituted PPE units, which include  $\alpha$ -hydroxy and  $\beta$ -methylol substituents, must be effected. This would provide the best evidence as to the primary or secondary nature of water release, the latter proceeding through saligenol intermediates.

#### MeOH

An ultimate methanol yield of only about 0.1% is predicted by the simulation model. This yield is substantially less than the yields reported by Iatridis and Gavalas, on the order 2%, and by those studies listed in Table 4.1, where yields range from 0.28 - 1.5%. The reasons for the smaller methanol predictions are not clear, and could be due to kinetic limitations or alternative lignin pathways. With regard to the former, the simulation reaction to methanol is through degradation of cinnamyl alcohol side chains. The reaction was minor, but significant, and was subject to considerable experimental uncertainty. An increase in the rate constant for this reaction could improve the selectivity to methanol in model predictions. Alternatively, other methanol forming reaction pathways not delineated in the model compound pyrolyses may operate in whole-lignin pyrolysis. An obvious possibility arises in the methoxyphenol units, where formal demethoxylation could result in methanol formation. However the experimental results obtained here, as well as reports from the literature<sup>91,96</sup>,

indicate that methanol formation from methoxyphenols is not significant. This may be an area for further experimental investigation. Other possible methanol precursors include cinnamaldehyde and saturated primary methylol groups, where hydrogenation of the former and cracking of both could formally produce methanol. However, such reactions were not experimentally observed and thus depict a need for further research.

High temperature pyrolyses of formaldehyde indicate reaction to CO and H<sub>2</sub>, and have been modelled as such in the simulation model. However, in many experimental pyrolyses, volatiles are capable of diffusing from the reaction zone, generally quenching reactivity. A further possibility of formaldehyde hydrogenation to methanol at the lower temperatures must thus be considered. Again, unequivocal discussion of such a reaction awaits experimental investigation.

A more subtle possibility for an alternative methanol precursor arises in consideration of the simulation description of the unreacted lignin substrate. Rather surprisingly, the model predicts the existence of about 7% single ring aromatic units before pyrolysis. These arise because the Freudenberg structure depicts both free phenolic methoxyphenol as well as cinnamaldehyde and hydroxyacetone 3-carbon side chain aromatic ring substituents. Thus, the statistical matching of all possible methoxyphenols with all possible 3-carbon side chains will predict single ring phenols. This is not unreasonable, as lignification need not effect 100% incorporation of all cinnamyl alcohol precursors into branching and multiple ring bonding formations. As lignification conversion rises, it is reasonable to envision steric

hindrance and/or viscosity effects which might 'trap' unreacted monomer alcohols. The same single ring alcohols could have experienced prior or even later radical exchange reactions, generating the aldehyde and ketone moieties depicted in the Freudenberg structure. However, even though the Freudenberg structure includes few unperturbed cinnamyl alcohol side chains (Unit 14c), the same logic rationalizing the existence of single ring cinnamaldehydes and hydroxyacetones might be applied to suggest the presence of greater numbers of single ring cinnamyl alcohols. In fact, the alcohols need not be single ring, as methoxyphenol etherification should affect the side chain little. Indeed, as the cinnamyl alcohols are the sole starting monomers of lignification, any lignification conversion of less than 100% should result in substantial amounts of free cinnamyl alcohol side chains. Hence, as the initial simulation conditions were based on the Freudenberg structure, the existence of additional free alcohol side chains in the real lignins could explain the underprediction of methanol yield relative to experimental lignin pyrolyses. Of course, this explanation is rather speculative, verification of which is dependent on further characterization of actual lignins.

In short, the simulation model seems to underpredict methanol yield when compared to previous experimental lignin pyrolyses. Rationalization for this behavior is rather weak, and thus provides an area for further investigation.

#### Phenolic Products

As evidenced in Appendix 9.1 the simulation model faithfully predicts most of the 30+ phenols detected in the previous experimental

pyrolyses. The model also predicts other products not hitherto delineated in the literature. Overall, product yields are close to or within the rather generous band of yields reported in the literature, yet specific instances of departure arise. Most of these concern the issue of secondary pyrolyses, often suppressed in the experimental studies. The simulation prediction of phenols will be discussed by phenol type, where literature comparisons and generalizations are most facilitated.

### Guaiacols

Guaiacols arise in lignin pyrolysis through the simultaneous degradation of the 3-carbon chain and ether reversions of the methoxyphenol. Thus, the products coniferaldehyde, guaiacylacrolein, eugenol, propylguaiacol, vinylguaiacol, ethylguaiacol, methyl guaiacol and guaiacol represent various stages of the 3-carbon chain degradation. At 400C and 100s, the ratios (coniferaldehyde: vinylguaiacol: methylguaiacol: guaiacol) were (.68: .13: .088: .011), whereas at 500s, the proportions were (.096: .020: .26: .034) and at 1000s, (.000125: .000218: .03: .0039). The data at 1000s reflect not only 3-carbon chain degradation of the aldehyde, but also the secondary pyrolyses of guaiacol to catechol, discussed below. Thus, each of the guaiacol products attain maximal proportions at some point in the pyrolysis, as each is both formed and degraded during lignin pyrolysis.

The literature is in reasonable accord with these product relationships. For example, Kirshbaum, et al.<sup>41</sup>, provide a comprehensive product spectra for pyrolysis of an aspen alkali lignin. At 250C, guaiacol was obtained in 0.005% yield, and this yield increased to

about 0.8% at 500C. Pyrolysis at 500 and 600C yielded less guaiacol, likely due to secondary pyrolysis. For comparison, catechol was not detected at 250C, and monotonically increased in yield to 0.9% at 600C. Similar behavior was reported for other products, where vinylguaiacol, methylguaiacol, propylguaiacol, syringol, methylsyringol, ethylsyringol, propylsyringol, eugenol, isoeugenols, vinylsyringol, vanillin, and syringaldehyde all attained maximal concentrations. In contrast, phenols, xlenols, methylcatechol and ethylcatechol all increased with pyrolysis temperature monotonically. Another report by Kirshbaum<sup>42</sup> reported similar maximal proportions of guaiacols and syringols.

In contrast to the above results, however, Iatridis and Gavalas<sup>26</sup> report only phenols and guaiacols from pyrolysis of a Kraft lignin. As noted in relation to methane yields, the reactor system employed by Iatridis and Gavalas was designed to emphasize primary reactions. Thus, once formed, guaiacol compounds likely were removed from the reaction zone and quenched from further pyrolysis.

Detailed quantitative yield comparison is difficult due to the wide ranging and poorly described experimental pyrolysis conditions. Further, many of the most complete experimental product spectra are from the Russian laboratories, where use of aspen wood lignins is prevalent. This wood type incorporates more sinapyl alcohol monomers into the lignin macromolecule, and thus syringol (DMP) and substituted syringols arise in substantial yields with pyrolysis. Kirshbaum, et al.<sup>41</sup>, report (vinylguaiacol: methylguaiacol: guaiacol)= (0.03:.1:.1) at 300C, whereas the yields from the simulation model align as (.0037:.02:.0029). At 400C, the experimental data align

as (.1:.9:.6), where the simulation predicts (.128:.087:.011) at 100s and (.02:.26:.034) at 500s. Thus, the model predictions are lower than those determined by Kirshbaum, et al., but are generally within an order of magnitude. As discussed below, the prediction catechol yields are higher than the experimental, compensating for the lower guaiacol yields. Additionally, the Kirshbaum, et al., data are of the DTA type, and the exact temperature-time sequence is unclear. Further, the yields of guaiacols vary widely from one experiment to another, and often the model prediction will be quite close to certain experiments. For example, at 500C and 30s holding time, the model predicts methylguaiacol in yield of .53%, whereas Iatridis and Gavalas obtained .4% at 500C and 30s. Thus, the model describes the features of lignin pyrolysis well, and is within about an order of magnitude of the previous experimental pyrolyses. The experimental results vary in such a manner so as to be more generous than discriminate, concerning model-experimental match, and thus experiments more carefully designed to conform to the model conditions are needed to critically test its validity. Further, the model is as yet incomplete, as a small number of important compound studies and model refinements are desirable. With regard to the remaining other guaiacols predicted by the model, notable among these are guaiacyl acrolein, coniferaldehyde, and the eugenols. Only the more exhaustive investigations have reported the latter two,<sup>38,39,41,34</sup> whereas the acrolein is not generally reported. The acrolein arises from saligenol dehydration of  $\beta$ -ethers suffering PPE reversions, and thus is produced in significant proportions. The guaiacyl acrolein was not directly



studied here, and has been modelled as a hybrid moiety with regard to kinetics, cinnamaldehyde with regard to products. Thus, further examination of this compound is warranted, as this would surely sharpen model predictions. Even though the guaiacyl acrolein has not been experimentally reported, it is likely a real intermediate and product in lignin pyrolysis.

The compound might be so retentive so as to elude G.C. elution, and thus not be reported. Hence, the simulation is suggestive of an experimental probe designed at checking for this compound, either through G.C. coinjection or G.C.-M.S. conjunction studies. Precedent in fact exists in the literature, in that many compounds reported by one team of investigators have remained undetected by others. Iatridis and Gavalas, for example, do not even report syringols, catechols, or vinylguaiacols. Further, Table 4.5 lists at least 9 phenols that have been reported by only one investigation, whereas at least 15 or more investigations have been referenced. Thus, the phenolic product spectra is not unequivocally established, and guaiacyl acrolein, and indeed many other single ring aromatics, may well be present.

#### Syringols (2,6-dimethoxyphenols)

The initial conditions imposed upon the present simulation reflect those of a spruce lignin, which incorporates relatively few sinapyl alcohol units. Thus, the present simulation results will not align with those pyrolyses involving aspen wood lignins. Future application of the model might be directed to aspen wood lignins, as this would involve only a change in the initial concentration vector of the methoxyphenols, with slight implications toward the 3-carbon side

chain vector.

Quantitative comparison of syringol yields with the literature is fruitful in only a few instances, as experimental yields range from absent<sup>26,39</sup> to dominant<sup>39,41</sup>. Pyrogallol, clearly characteristic of sinapyl units, was obtained in 0.05% at 600C and 7s simulation time. Kirshbaum, et al.<sup>41</sup>, report less than 0.2 % at 475C. Methyl syringol was predicted in yields of about 0.02% at 400C and 100s, whereas experimental yields from spruce lignins range from 0-0.1%. In short, the simulation reactions of sinapyl units were in reasonable accord with those reported in the literature. These reactions were not of prime interest here, however, and await both further experimental investigation and simulation adjustments.

#### Catechols

Rather substantial amounts of catechols are predicted by the simulation model. The catechols are clearly secondary products, most selectively favored at lower temperatures and longer holding times. These conditions are optimal for catechol production since guaiacol demethoxylation to phenols is more strongly thermally activated, and thus favored at higher temperatures. Thus, the yields of catechol and methylcatechol increased dramatically with increasing temperature and holding time, whereas the vinyl catechols increased more slowly, and would attain maximal proportions, due to secondary 3-carbon chain degradation.

Quantitative comparison with the literature is possible in few instances. Kirshbaum, et al.<sup>41</sup>, reported catechol yields of 0.07, 0.05, and 0.9 at 400,500 and 600C, respectively, comparing favorably

with the ultimate yields of 0.2, 0.38, and 0.86 predicted by the model at the same temperatures. However, in contrast to the model predictions, these workers report methylcatechol yields just slightly below the catechol yields; the model consistently predicted methylcatechol/catechol ratios  $> 1$ , as a consequence of the present distribution observed for secondary styrene pyrolyses. Further, vinylcatechol was not reported. These data are not representative of the remaining experimental literature, however, as Domburg, et al.<sup>39</sup>, have pyrolysed an alkali spruce lignin to 475C and report catechol and methyl catechol yields of 0.8% and 1.1%, respectively. These yields are within a factor of 2-3 with the model predictions at 500C. Further variation in the literature is exemplified by the report of Iatridis and Gavalas<sup>26</sup>, who do not even list catechols as products from the pyrolysis of a Kraft lignin. This is rather surprising, as a modest but significant reaction in Kraft pulping is liquid phase demethylation of methoxyl groups; this yields catechol units to the extent of about 0.2/MeO. Thus, the experimental investigations report significantly different catechol yields, again likely due to variations in lignin type, lignin isolation and pyrolysis reactor conditions.

#### Phenols

Phenols are reported in most experimental lignin pyrolyses, and thus comparison with the previous literature is relevant. Domburg, et al.<sup>39</sup>, report yields of simple phenol of .1% from both alkali and HCL spruce lignin pyrolysis at 475C. These compare well with the simulation predictions of 0.067% at 400C and .16% at 500C. The same

investigators report cresols in .5% yield at 475C, whereas the simulation predicts 0.55% at 400C and 1.3% at 500C; this is reasonable but less exact agreement. Kirshbaum, et al.<sup>41</sup>, report phenol yields of 0.05, 0.1, and 0.1 at 400, 500 and 600C, respectively. The corresponding model predictions are 0.067, 0.16 and 0.39. Iatridis and Gavalas<sup>26</sup> report phenol yields of 0.1, 0.1, and 0.06 at (400C,120s), (500C,60s) and (600C,10s) respectively. For comparison, the model predicts 0.0013% at 400C and 100s, .11% at 500C and 60s, and .39% at 600C and 7s. These comparisons would suggest that relative to the data of Iatridis and Gavalas, the model predicts phenol formation with an apparently excessive energy of activation. However, the higher temperature discrepancies between model and experiment likely involve the previously discussed secondary reaction deviations. That is, the apparatus of Iatridis and Gavalas was designed to emphasize primary reactions, whereas the simulation depicts secondary phenol formation from guaiacols. In summary, however, the agreement between previous experiments and the simulation model is reasonably good, all predicting phenol yields on the order 0.1%.

With regard to the prediction of overall phenolics (guaiacols, syringols, etc.), the accuracy of simulation is uncertain. Much of the uncertainty arises from the wide range of lignin types, isolation methods and reactor configurations employed in experimental studies. These provide a rather generous band for comparison with model predictions. Thus, in most cases the predictions and experimental data differed by a factor of 2-10. Other deviations, such as those related to guaiacol, catechol, and syringol, are well explained by

inherent model-experimental differences. In other words, the deviations between model and experiment was no greater than the deviations among experiments.

Additional uncertainty surely arises from the parameters which comprise the model. Most have been measured in the experimental phase of this investigation, yet important exceptions exist. For example, no direct model of the guaiacyl acrolein unit has been studied, rather, this moiety has been depicted as a hybrid unit kinetically, a cinnamaldehyde unit with regard to product spectra. Further refinement of the  $\beta$ -ether models is in order, as well as more detailed investigation into the nature of guaiacyl activation of 3-carbon side chain reactivities. These are but a few of the semi-infinite refinements which must be applied to the simulation model to effect a sharpening of phenolic distribution predictions.

In short, considering the present level of model sophistication, the agreement between experimental and simulation data is quite encouraging.

#### Carbonaceous Residue

The kinetics implied by the time variation of the simulation yield of multiple ring aromatic units have been previously compared with the literature. Kinetic parameters obtained from 'long time' simulation runs are in substantial agreement with those obtained from non-isothermal DTA/DTG investigations. However, a more relevant experimental comparison is provided by the data of Iatridis and Gavalas<sup>26</sup>, who have pyrolysed a Kraft lignin at well defined temperatures and holding times. These workers report lignin weight loss

data as a function of pyrolysis time and temperature. These data compared favorably with the simulation predictions in two ways. In the first, rate constants implied by simulation and experimental weight loss, at similar pyrolysis times and temperatures, were within about 0.5 order of magnitude, often much closer. In the second, the simulation weight loss curves aligned reasonably well with the experimental weight loss curves, with a modest underprediction at low temperatures and overprediction at high temperatures.

Even though the simulation model has differed from the data of Iatridis and Gavalas with regard to product spectra, it is quite reasonable that the global kinetics should accord. The differences in product spectra can be attributed to secondary simulation pyrolyses not possible in the apparatus of Iatridis and Gavalas. The secondary pyrolyses alter predominantly only the yields of CO, CH<sub>4</sub>, guaiacol, catechol and phenols, the latter two derived from guaiacol. Thus, overall lignin weight loss should be substantially unaffected. That is, weight loss is recorded once guaiacol is volatilized, and secondary guaiacol reactions are irrelevant to global kinetics. Further, all gas release or other weight loss from non-volatile lignin moieties should be identical for the reactor system described by the model and that used by Iatridis and Gavalas. Non-volatile lignin moieties should experience a complete temperature-time program in even the experimental apparatus. Thus, the differences in the reactor systems used by Iatridis and Gavalas and that implied by the simulation model should cause no real discrepancies in overall lignin weight loss.

On the other hand, the differences in model and experimental lignin substrates could explain the slight model overprediction at high temperature and underprediction at low temperatures. The substrate employed by Iatridis and Gavalas was a Douglas fir precipitated Kraft lignin. As detailed in Section 3.2.3, Kraft pulping can alter the chemical nature of lignin substantially. One result of pulping is an increase in internal condensations, arising due to cleavage of aromatic unit bond linkages. Thus, as evidenced in Figure 3.11, reactive  $\alpha$ - and  $\beta$ -ether linkages can be transformed into less reactive diphenyl-methane, ethane, and ethylene linkages. A further result of Kraft pulping is the introduction of carboxylic acid units, as evidenced by structures 2, 4, and 14 in Figure 3.11. Thus, the low temperature reactivity of a Kraft lignin might be expected to be greater than its protolignin counterpart because of facile  $\text{CO}_2$  evolution. At higher temperatures and/or conversions, however, the reactivity of the Kraft lignin should be less, since diphenyl-methanes, ethanes, and ethylenes units have replaced the more reactive protolignin  $\alpha$ - and  $\beta$ -ethers.

These assertions are reasonably well supported by the data of Iatridis and Gavalas. At 400C and 120s, a  $\text{CO}_2$  yield of 5.9% was reported. By contrast, methane and CO were only 0.52 and 1.2%, respectively. The model did not predict  $\text{CO}_2$  formation at this or any other temperature. As reflected in Figure 9.2, this  $\text{CO}_2$  yield is of the magnitude of the simulation underprediction at 400C and 120s. However, at 600C and 10s, the experimental  $\text{CO}_2$  yield was only 4.1%; this agrees well with the notion of a finite number of

easily decarboxylated acid sites. Thus, the  $\text{CO}_2$  yield is reasonably constant with pyrolysis temperature and should not compensate for the intrinsic reactivity loss due to the introduction of diphenylmethane units. Hence, as evidenced in Figure 9.2, model weight loss predictions at 600C were in excess of those reported by Iatridis and Gavalas.

By way of summary, the simulation can describe the essential features of lignin pyrolysis, and further accords reasonably well with previous experimental lignin pyrolyses. The major gases, methane and carbon monoxide were both well predicted by the model. Carbon dioxide and other trace gases were not described, but are readily incorporated into the model. Predictions of negative hydrogen yield suggest that light volatile yields may be somewhat over-predicted. Consistent with this is the likelihood of coking and condensation reactions in actual lignin pyrolyses, which have not been incorporated into the present version of the model. Water and methanol were predicted with only modest success, the former shy by a factor of 2-3, the latter off by as much as an order of magnitude. The water deviation is considered reasonable, as physical water likely exists in the native lignin or is introduced in isolation methods. The methanol deviation is more serious, and suggests a point for further research. Methanol formation kinetics from cinnamyl alcohol were rather uncertain, and this could account for part of the discrepancy. Further, alternative pathways for methanol may exist, these through additional precursor degradation or complex secondary interactions. The previous experimental phenolic product spectra were well described by the simulation model, those



major deviations arising well rationalized by inherent differences in reactor configurations and substrate variations. Speculative chemical structures for important constitutional moieties of the carbonaceous residue have been presented, based on the kinetic implications of the model compound studies as well as possible condensation-coking reactions of intermediate products. An operational definition of lignin conversion based on the yields of multiple ring aromatic units has provided kinetic parameters in excellent accord with the experimental data presented by Iatridis and Gavalas<sup>26</sup>. Thus, an overall description of lignin thermolysis is well depicted by the simulation.

Several limitations of the model need be described here. Chemically, the model thus far is based on estimated rate data for guaiacylacrolein and acetone moieties. These estimated data have been based on analogous pyrolyses of acetophenone and cinnamaldehyde for the former, and acetone for the latter. Further, Arrhenius parameters for certain reactions have been based on actual experimental data at 400C, with an activation energy or  $\log_{10}A$  factor calculated by impressing an analogous  $\log_{10}A$  or  $E^*$  respectively. Such is the case for phenetole and BPE pyrolyses, where kinetic data scanning temperature ranges are scarce. Thus, although most of the kinetic parameters input to the simulation are based on the experimental part of this investigation, several future pyrolyses arise for further predictive sharpening.

Similarly, the model compounds selected to mimic the elements

of lignin pyrolysis are subject to considerable sophistication. For example, whereas PPE modelled the essential  $\beta$ -ether backbone, a further pyrolysis might include  $\alpha$ -hydroxylic and  $\beta$ -methylol substitution effects. It would be further useful to more carefully investigate the effects of guaiacyl substitution on 3-carbon chain reactivity, as every lignin aromatic unit is comprised of both 3-carbon chains and methoxyphenol units.

Mathematically, the model must be expanded to include the effects of catalysts and solvents on model compound reactions. In this regard, more sophisticated numerical integration techniques may be required. The current solution method is a fourth order Runge-Kutta technique, which gives very accurate results over most conditions studied with very reasonable step sizes. For example, certain individual equations of the simulation set are easily solved analytically, and the analytical and numerical solutions converge to significant figures well beyond those implied from the model compound pyrolyses as well as simulation goals. On the other hand, at very high temperatures, where the various rate constants can differ by many orders of magnitude, the equations become unstable for certain compounds at high levels of conversion. Thus, anticipating even greater rate constant deviations incurred by catalysis, numerical techniques for 'stiff' systems of equations should be incorporated.

The model is comprised of fundamental rate parameters, and as such should be applicable to a wider range of lignins and reaction operating conditions than strictly empirical correlations. For

example, application to hardwood lignins can be effected by rather straightforward modification of the initial concentration vectors. Alternatively, the effect of a given catalyst on the rate of a current or new reaction pathway could be introduced to the simulation as its effect on reaction rate constants. Thus, the fundamental nature of the simulation model should permit its use over a wide range of conditions of interest.

The reasonable agreement of model predictions with previous experimental lignin pyrolyses suggests that the present approach to describing the features of lignin thermolysis is valid. The approach approximates whole lignin moieties as discrete model compounds, and then describes whole lignin and whole lignin pyrolysis as a statistical superposition of these discrete compounds. Although incomplete, the present set of model compounds pyrolyses combine with the present analytical interpretation of lignin reactivity to yield encouraging results.

### 10.3 Optimization and Modification Strategies

As evidenced in the discussion of section 10.2, the present fundamental description of lignin thermolysis accurately depicts many of the important features of whole-lignin pyrolysis. The implied elucidation of the origins and pathways for the formation of individual pyrolysis products allows an assessment of the likely effects of catalysts, solvents, and reactor operating conditions. Thus, strategies for optimization and modification of lignin pyrolysis arise. This section will consider some of the philosophical features and logic of these strategies, whereas detailed experimental studies are required to formulate exact recipes for optimization. The strategies are presented here with an aim toward increasing the yields and selectivities of desired relative to undesired pyrolysis products. Of course, an exact definition of a desired product will vary from process to process.

#### Water Release

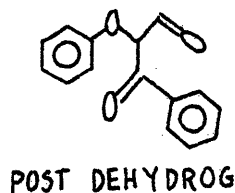
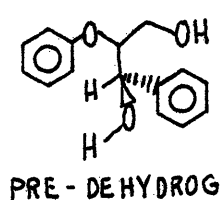
Lignin, like coal, is carbon rich and hydrogen poor relative to most desired thermolysis products; lignin also contains substantial amounts of oxygen. The thermal processing of lignin to useful products is generally attended by the release of large quantities of water. However, this rejection of oxygen as  $H_2O$  must be considered detrimental since the substrate is already H-poor. Thus, increasing the reactivity of desired reactions relative to water formation is required. The present interpretation of water formation as arising through dehydration of saligenol units suggests

that deceleration of water formation, rather than acceleration of desired reactions, be attempted. That is, saligenol dehydration is so fast that enhancement of competitive reactions is likely infeasible.

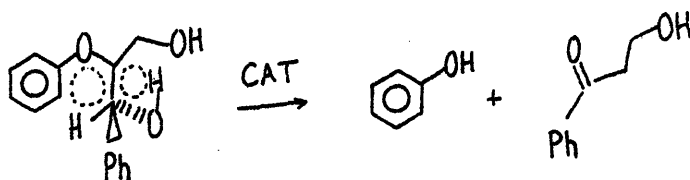
Given the formation of saligenol units, pyrolysis in an atmosphere of steam might be one way of suppressing water release. The dehydration is net endothermic by about 17 kcal/mol (cf10.1), and thus low temperatures and high steam pressures could impose equilibrium limitations. Another strategy might be to disrupt the hydrogen bonding of saligenol moieties, as this bonding undoubtedly contributes to the ease of dehydration. This might be effected by the actions of solvents, for example.

Another direction for modification might be to reduce the formation of saligenol-type water precursors, thus indirectly suppressing water formation. The present analysis suggests that the reversion of a guaiacyl-glycerol -  $\beta$  - ether unit results in the essentially instantaneous generation of one mol of water, through the short-lived saligenol intermediate. Hence, direct acceleration of the thermal PPE pathway would only further increase the apparent rate of water formation. Rather, an alternative strategy might be catalytic dehydrogenation of saturated hydroxyls to carbonyls, which could suffer further decarbonylation reactions. In fact, dehydrogenation of both  $\alpha$  ( benzylic ) and  $\gamma$  hydroxyls would remove the  $\alpha$  - hydrogen mechanistically involved in ether reversion, and could hinder the formation of single ring phenols

as well as water. This point is further illustrated here, where the  $\alpha$  hydrogen is removed in dehydrogenation of the guaiacyl-glycerol-



$\beta$ -ether. Relevant are the studies of Domburg, et al.<sup>75</sup>, who have shown that the carbonyl  $\beta$  ethers are more thermally stable than their hydroxylic analogues. An ideal catalyst would not only prevent water formation, but would also accelerate overall lignin activity. For example, if ether reversion and  $\alpha$ -hydroxylic dehydrogenation could be effected in one step, such that an ethylbenzene rather than styrene moiety is generated with concomitant formation of an  $\alpha$  carbonyl, then both goals would be realized. Water formation would be less favorable, but the hydrogen would remain with the substrate. The goal of such a catalyst can be schematicized as:



Alternatively, a catalyst which could selectively dehydrogenate the  $\gamma$ -hydroxyl, or selectively rehydrogenate the  $\alpha$ -carbonyl would prevent saligenol-type dehydration and allow for ether reversion.

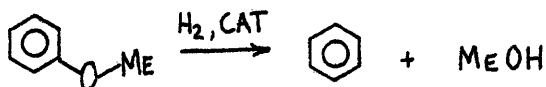
### Gas Evolution:

The reactions of the lignin methoxyphenol units produce both methane and carbon monoxide, the former with consumption and the latter with release of hydrogen. The methane is favored at low temperatures, whereas CO and H<sub>2</sub> are favored at high temperatures. The reactions of the lignin side chains will produce primarily CO, proceeding through the decarbonylation of cinnamaldehyde and thermally activated ( high E\* ) guaiacyl acrolein units. Thus, low temperatures and long time pyrolyses favor CH<sub>4</sub>, while CO and H<sub>2</sub> are selectively favored at high temperatures. Hence, pyrolytic evolution of synthetic natural gas or synthesis gas could be optimized with respect to temperature alone. Further, acceleration of the reversion of lignin interunit linkages would enhance overall gas release, as these reversions generate both reactive guaiacols from veratroles and additional carbonyls. The relative insensitivity of guaiacyl demethanation to substituent group effects suggest that catalysis of demethanation may be difficult, whereas the strong effect of guaiacyl substitution on decarbonylation suggests that further catalysis might be useful.

### Methanol:

With further regard to methoxyphenol reactivity, demethylation, isomerization and demethoxylation were all competitive. The latter pathway resulted in the formation of CO and H<sub>2</sub>, and not methanol. This is hardly surprising, in fact, as the aromatic Ph-OMe bond strength is approximately 101 kcal/mol, and rupture of this bond should be extremely disfavored at the temperatures of interest here and in most lignin pyrolyses. However, each lignin aromatic unit

contains about one methoxyl group, on average, and a potential methanol yield approaching 20% of lignin by weight is suggested. The nominal methanol yields from experimental lignin pyrolyses are on the order 0.3 ~ 3.0 %, and likely arise from degradation of the 3-carbon side chains. Complete utilization of the methoxyphenols could thus result in a large enhancement of methanol yields, and merits further study. Pyrolysis at elevated temperatures would favor formal demethoxylation by direct bond scission, which would occur with an activation energy at least as large as the bond strength. However, not only would the methoxy radical formed be prone to isomerization and decomposition to formaldehyde, but also detrimental would be the extensive demethylation occurring during the rise to the elevated temperature. An ideal catalyst would accelerate the low temperature hydrocracking reaction to methanol and aromatic, represented here for anisole:

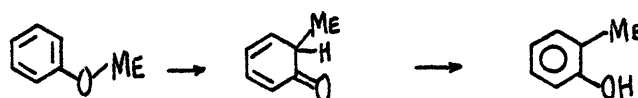


### Phenols and Liquefaction

As the production of methane from methoxyphenols requires the addition of external hydrogen, lignin liquefaction with an aim toward producing phenols and cresols would be enhanced by a reduced selectivity toward demethanation. The negligible effects of substituents on guaiacol demethanation activity suggests that catalysis or anti-catalysis of demethanation might be futile. Acceleration of preferred



pathways to cresols thus arises as the likely modification action. Anisole and veratrole both underwent rearrangement reactions to cresol, CO and H<sub>2</sub> evolution accompanying for the latter substrate. These pathways were not detected for guaiacols, due likely to the enhanced rate of concerted demethanation. The rearrangements were envisioned to initiate through a methyl shift, as in:



The isomerizations have the virtue of producing essentially unreactive cresols from methoxyl groups, and allow the substrate to retain hydrogen. The rearrangement is net exothermic by about 13 kcal/mol, and should be thermodynamically favored at lower temperatures; higher temperature destructive distillations could favor the reverse isomerization of cresols to anisoles or substituted anisoles, which could undergo further demethoxylations or demethanation reactions rejecting CH<sub>4</sub>, CO and H<sub>2</sub> from the liquefaction material. Thus, an ideal liquefaction catalyst might promote the low temperature isomerization of methoxyphenols to cresols, which would effect a decrease in hydrogen consumption.

Other miscellaneous areas for catalytic study are suggested by the model pathways as well. The biphenyl and phenyl ether linkages were essentially inert for pyrolysis to 600C, and the diphenylmethane linkage only moderately reactive. Thus, complete degradation of lignin

to single ring aromatics at moderate temperatures would require acceleration of the cleavage of these linkages. Another aspect for catalytic study deals with the large oxygen content of lignin. Lewis acids are well known to catalyze various pericyclic reactions, principally by altering the energy levels and coefficients of the controlling frontier molecular orbitals.<sup>176</sup> These Lewis acids commonly coordinate with carbonyl moieties, which are prevalent in lignin. Hence, catalysis by Lewis acids may represent an area for meaningful research.

In summary, the strategies for thermolysis optimization and modification are speculative in detail, but are firmly based on the implications of the lignin model pathways in design. In fact, since study of the effects of catalysis and solvents on the model pathways was not part of the experimental portion of the present research, the dismissal of potential strategies is far more certain than are the likely effects of promising modifications. For example, direct deceleration of saligenol dehydration should be extremely difficult, and acceleration of PPE reversion could enhance the apparent rate of water formation. Overall, the model experiments have provided rationalization for the origins of and pathways for the evolution of lignin thermolysis products; by difference, certain desired pathways have been found kinetically insignificant. A simulation model such as that developed here will allow the effects of catalysts, solvents, and reactor operating conditions to be tested on simple models and then applied to whole-lignin thermolyses. Thus, a continuation of

fundamental pathway research in parallel with appropriate and selected whole-lignin test experiments should provide meaningful insights and strategies for the modification of lignin thermolyses toward the production of useful products.

## 11.0 Conclusions

The major conclusions from the present investigation arise from the efficacy of the fundamental model pathway description of whole-lignin thermolysis. Thus, the collected significance of the lignin analysis, model experiments and simulation development will be considered as opposed to the details associated with each. For clarity, the conclusions are presented in an itemized fashion, with the more important aspects listed first.

### 11.1 Model Compound Pyrolyses Describe Features of Whole-Lignin Pyrolysis

The product spectra of whole-lignin pyrolyses are well interpreted in terms of the model compound thermolysis products. The methoxyphenol models rationalize the evolution of methane, carbon monoxide, and hydrogen, the latter two products favored at higher temperatures. Carbon monoxide is also readily produced in the degradation of many 3-carbon side chain models. These side chain models have also produced water and methanol, both constituents of the whole-lignin aqueous distillate fraction. The phenolic portions of whole-lignin pyrolysis product spectra are well rationalized by both methoxyphenol and 3-carbon side chain model degradation products. The former model products accord with guaiacols, syringols, catechols and phenols observed, whereas the latter models explain the various types of para substitution of these found in whole-lignin products. The carbonaceous residue is likely comprised of both unreacted lignin and methoxyphenol and 3-carbon side chain condensation products.

## 11.2 Fundamental Description of Lignin Thermolysis in Accord with Experimental Pyrolyses.

The present investigation has combined a statistical interpretation of the unreacted lignin substrate, the substrate pyrolysis, and the pyrolysis products with experimental model compound results to form a whole-lignin thermolysis simulation model. The simulation predictions were often in excellent quantitative agreement with previous experimental pyrolyses. The model strengths are in the prediction of overall gas, methane, carbon monoxide, individual phenol and carbonaceous residue yields. The time variation of the latter accords well with experimental kinetics and weight loss studies. Areas where the model is in fair agreement with the literature are the prediction of overall aqueous distillate, water, and overall phenol yields. The discord of the latter predictions is likely due to differences in lignin types, lignin isolation methods, and operational definitions of yield between the model and experiments as well as model inadequacies. The model consistently underpredicted methanol yields. The simulation did not include pathways for acetone, acetic acid, and  $\text{CO}_2$ , although the latter is readily included for carboxylic acid containing substrates. Pathways for acetone and acetic acid were not observed, and require further experimental and theoretical study. Overall, the simulation model is in good agreement with whole lignin thermolyses, especially encouraging for an early version subject to considerable refinement and sophistication. This agreement lends credence to the present fundamental experimental approach toward discerning lignin pyrolysis pathways and mechanisms, and further supports the present theoretical analysis of the lignin substrate and

pyrolysis.

### 11.3 Pericyclic Pathways in Lignin Thermolyses

Hitherto not mentioned in previous lignin pyrolysis literature, reaction pathways of the type termed pericyclic are suggested by the present analysis. The more likely examples of these pericyclic or concerted reactions are: 1) retroene reversion of  $\beta$ -ethers, 2) group transfer demethanation of guaiacols and dehydration of saligenol moieties, 3) sigmatropic shift of anisoles to cresol 4) cheletropic or geminal group transfer extrusion of CO from benzaldehyde, vanillin, and cinnamaldehyde, and 5) Diels-Alder cycloadditions for cinnamaldehyde and cinnamyl alcohol side chain units. Less certain, but yet plausible pericyclic pathways are: 6) isomerization of orthohydroxydiphenylmethanes to benzyl phenyl ether moieties, 7) sigmatropic and retroene steps in demethoxylation of guaiacols and veratroles, and 8) cyclo addition reactions for orthodiquinone and its adducts. The molecular topology of lignin is well suited for these and other pericyclic reactions. Thus, overall reactivity is likely comprised of both pericyclic and free radical components.

### 11.4. Aromatic Methoxyl Reactions

The present analyses suggest that the principal reactions of the lignin methoxyphenol groups are demethylation, isomerization, and demethoxylation; the latter reaction yields CO and H<sub>2</sub>, and not MeOH, as isolable products. While this is in agreement with previous

Russian pyrolyses of anisole, guaiacol and other methoxyphenol models, this contrasts with the popular designation of the aromatic methoxyl group as a precursor to pyrolytic methanol. Rather, methanol likely arises through degradation of cinnamyl alcohol 3-carbon side chains. That is, while hardwood lignins generally produce more methanol than softwood lignins, the extra methanol is often attributed to demethoxylation of the additional dimethoxylated sinapyl alcohol monomers. In fact, the dimethoxylated monomers may exert steric blocking effects, resulting in fewer interunit linkages involving 3-carbon side chains. Thus, hardwoods likely contain additional cinnamyl alcohol side chains which account for the extra methanol. However, the aromatic methoxyl does represent a potential source for methanol, and should be the subject of further experimental inquiry.

#### 11.5 Modifications of Lignin Thermolyses

The present description of whole-lignin thermolysis allows the formulation of strategies for modification of process conditions toward more optimal product spectra. Catalysis of the prevalent  $\beta$ -ether linkages would be beneficial in that reactive guaiacols are generated from less reactive veratroles, and that sites for CO release through decarbonylation are produced; the same catalysis would be detrimental in that ether reversion results in essentially instantaneous water formation. Water formation is one of the major limitations preventing economic pyrolyses of lignin and biomass. This suggests that low temperature catalysis be aimed toward either preventing the formation of reactive saligenol units or accelerating desired reactions

relative to  $\beta$ -ether reversion.

Similarly, the elucidation of the origins and pathways of the formation of lignin pyrolysis products has allowed delineation of strategies for optimal production of each.

Overall, this fundamental description of lignin pyrolysis is in good accord with previous experimental investigations. As the approach is rather novel, every facet of whole-lignin thermolysis could necessarily not be explored. Rather, the conclusions of the present investigation should encourage further fundamental research of this and an expanded type.



## 12.0 Suggestions for Future Research

Since the present attempt at description of whole-lignin pyrolysis has used a rather novel, almost pioneering approach, a compromise between breadth and depth of coverage was necessary. This balance is reflected primarily in the experimental model compound studies, although the simulation model provides ample opportunity for future research. Thus, the areas listed for future research will be of two general types, namely those dealing with further refinement of the work executed here, as well as additional studies suggested by the present results.

### 12.1 Whole Lignin Thermolyses

While the literature provides ample previous lignin pyrolyses for general comparison with the present simulation model, detailed comparison is difficult because of the wide range of lignins, lignin isolation methods, and pyrolysis reactors employed; further, none of these provide an exact match with the conditions of the present version of the simulation. A carefully designed whole-lignin pyrolysis experiment would thus be useful. To coincide best with the model, the experiments should be isothermal batch pyrolyses of milled-wood spruce lignins. The pyrolyses should be effected at well defined time intervals to allow kinetic description. Further, GC and GC-MS analyses should anticipate the production of more complex single ring phenols, typically, coniferaldehyde or guaiacylacrolein types. Of course, further development of the simulation model should

permit comparison with less rigorously defined pyrolyses.

### 12.2 Additional Simulation Trials

The present simulation model can be readily applied to different types of lignin. For example, simulation of an aspen wood pyrolysis should involve only major readjustment of the initial methoxyphenol vectors and minor changes in the 3-carbon side chain vector. Simulation of a Kraft lignin need only account for the higher proportions of diphenyl-methane, ethane and ethylene linkages and the introduction of carboxylic acid groups. In short, the statistical interpretation of lignin and its pyrolysis allows for facile perturbations about the base Freudenberg structure.

### 12.3 Refinement of Model Compound Studies

As the present investigation utilized a rather novel approach for the description of whole-lignin pyrolysis, certain aspects of the individual model compound pyrolyses were necessarily left undelineated. That is, this investigation was aimed at a thorough examination of a large number of model compounds rather than an exhaustive study of only one. The most important issue to be resolved is the apparent non-closure of the hydrogen balance in the guaiacol pathway to catechol and methane. The present explanations listed in sections 7 and 10 need be investigated. Pertinent experiments might be aimed at trapping the postulated o-diquinone moiety. Pyrolysis in the presence of an activated dienophile could be one technique to isolate this compound.

Similar approaches have been quite successful in isolating the analogous o-quinonemethide from saligenol pyrolyses. The use of IR and NMR spectroscopy and mass spectrometry would be particularly relevant here. For example, a low pressure pyrolysis reactor equipped for on-line spectroscopy could provide direct evidence as to the existence of the diquinone intermediate. Characterization of the coke obtained in guaiacol pyrolysis could yield further insight into this area. Additional research should also be aimed at a better characterization of the cinnamyl alcohol and cinnamaldehyde pyrolysis product spectra. Particularly obscure is the chemical nature of the apparent dimers. Similarly, the apparent sesquimers from OHD and phenyl ether pyrolysis are in need of more quantitative characterization. Higher molecular weight materials in general represent an area of weakness in the present investigation. In short, the pyrolysis reactions of the model compounds studied here are surely not exhaustively delineated, and further study of each is merited.

#### 12.4 Additional Model Compound Studies

While the previous section considered the limitations of the present model compound pyrolysis experiments, this section will consider the limitations of the models themselves. That is, the lignin moiety models employed here have depicted many essential features of lignin pyrolysis, but are subject to considerable sophistication. The most obvious additional lignin moiety in need of experimental investigation is the guaiacyl acrolein side chain. Thus, pyrolysis of guaiacyl vinyl ketone is suggested. This lignin moiety was not

directly modelled here, and likely arises in substantial proportions during lignin pyrolysis (cf 10.2). Pyrolysis of substituted  $\beta$ -ethers should yield further meaningful insight, as PPE depicted only the essential  $\beta$ -ether chain. The model for pyrolysis should include both  $\alpha$ -hydroxy and  $\beta$ -methylol substitutions; guaiacyl-glycerol- $\beta$ -ether itself represents the ideal model compound. The effect of guaiacyl substitution on 3-carbon side chain reactivity also need be better defined, preferentially by comparing the pyrolyses of conifer-aldehyde and coniferylalcohol with those of cinnamaldehyde and cinnamyl alcohol. In the limit of infinite model refinement all possible lignin models should actually contain guaiacyl substitution, including those depicting the reactivities of the interunit linkages. The present simulation has incorporated styrene or vinyl guaiacol reactivity as observed in the secondary reaction in PPE pyrolyses. Thus, primary pyrolyses of neat styrene and vinyl guaiacol would be useful. Finally, the present simulation model suppresses the importance of bimolecular and coking reactions. Although not a realistic depiction of lignin, pyrolyses of model compound blends could provide some insight into the interactions of lignin moieties.

### 12.5 Mathematical Refinement of Simulation Model

The mathematics of the simulation model are also subject to further refinement. The present equations become unstable at very high temperatures unless an unreasonably small Runge-Kutta step size is used. Anticipating greater difficulties when simulating catalytic effects, the integration algorithm should be revised to allow for

'stiff' systems of equations. Further, rate parameters should be modified to handle the possible kinetic effects of catalysis. The model should also be revised to include condensation, coking and other bimolecular reactions, as these are likely significant in whole-lignin thermolysis.

### 12.6 Modification of Whole-Lignin as Suggested by Model Results

As suggested above, model compound studies could be an effective method of probing the effects of catalysts, solvents, and other additives on whole-lignin thermolysis. Early studies might be aimed at effecting guaiacyl-glycerol- $\beta$ -ether cleavage to ethylbenzene and carbonyl moieties rather than to styrene and hydroxylic moieties; this action should suppress water formation. Catalysis of desired but thermally insignificant reactions, such as methanol formation from methoxyphenols, could be another meaningful area for further research. In short, the present approach allows for a fundamental rationalization and prediction of the effects of actions taken to modify lignin pyrolysis.

### 12.7 Expansion of Reactor Capabilities

While the present reactor system provides for the rapid acquisition of meaningful pyrolysis data, certain limitations are apparent. Extremely high temperature and/or low residence time data are unavailable, due to apparatus and heat transfer limitations. Thus, the development of a flow reactor would be desirable,

preferably with on-line GC and spectroscopic capabilities. This would allow for the accrual of low residence time and high temperature pyrolysis data, as well as provide for detection of possible reaction intermediate species.

In summary, rather than unequivocally describing every aspect of lignin thermolysis, the present investigation has provided an encouraging framework for further research. A fundamental description of lignin thermolysis appears quite valid, and thus continuation of model compound and whole-lignin pyrolysis experiments, the latter often suggested by the former, should yield meaningful scientific insights.

### 13.0 References

1. Hottel, H. C. and Howard, J. B., New Energy Technology, MIT Press, Cambridge, Ma (1971)
2. Energy Alternatives: A Comparative Analysis, Report prepared by Science and Public Policy Program at the University of Oklahoma, Stock #041-001-00025-4, U. S. Gov't Printing Office, Wash., D.C. (1975)
3. Brink, D. L., Applied Polymer Symposium, No. 28, 1377-91 (1976)
4. Freudenberg, K.; Neish, A. C., Constitution and Biosynthesis of Lignin, Springer-Verlag, New York (1968)
5. Harkin, J. M., in Battersby and Taylor, Oxidative Coupling of Phenols, Marcel-Dekker (1967)
6. Sarkanen, K. V., Ludwig, C. H., ed., Lignins Occurrence, Formation Structure and Reaction, Wiley Interscience, New York (1975)
7. Pearl, I. A., The Chemistry of Lignin, Marcel Dekker, Inc., New York (1967)
8. vanKrevelen, D. W., Coal, Elsevier Publishing Co., Amsterdam (1961)
9. Flaig, W., Chemistry of Humic Substances in Relation to Coalification, in Coal Science, Advances in Chemistry Series, ACS, Wash., D. C. (1966)
10. Given, P. H., Fuel, 39, 147 (1960), Fuel 40, 427 (1961)
11. Raj, S., Acs Div. of Fuel Chem. preprints, 24, (3), 251 (1979)
12. Hayatsu, R., et al., Nature, 278, 41 (1979); Fuel, 57, (9), 541 (1978)
13. Stephens, J. F., Fuel 58, 489 (1979)
14. Wender, I., ACS Div. Fuel Chem. preprints, 20 (4) 16 (1975)
15. Hill, G. and Lyon, L., Ind. Eng. Chem., 54 (6), 30-9 (1962)
16. Brown, J. K. et al., Fuel, Lond. (1960), 39, 79 and 87
17. Montgomery, R. S. and Holly, E. D., Fuel, Lond., 39, 323 (1960)
18. Lai, in Sarkanen, K. V. and C. H. Ludwig, Lignins, Wiley, New York (1975)

19. Wenzyl ; H.F.J., The Chemical Technology of Wood, Academic Press, New York (1970)
20. Rydholm, S.A., Pulping Processes, Interscience Publishers, London (1965)
21. Marton, in Sarkanen and Ludwig, ed., Lignins, Wiley, New York, (1975)
22. Glennie; in Sarkanen and Ludwig, ed., Lignins, Wiley, New York, (1975)
23. Heuser, E. ; Skioldebrand, C., Z. angew. Chem., I, 32, 41 (1919)
- 24a. Klason, P; Haindenstam, G.v.; Norlin, E., Z. angew Chem., 22, 1205 (1909)
- b. Klason, P; Haindenstam, G.v.; Norlin, E., Z. angew Chem, 23, 1522 (1910)
- c. Klason, P; Haindenstam, G.v.; Norlin, E., ArkivKemi. Mineral, Geol., 3 no. 1 (1907)
- d. Klason, P.; Haindenstam, G.v.; Norlin, E., ArkivKemi. Mineral. Geol., 3 no. 10 (1908)
25. Gladkova, N. Ya.; Sokolova, N. A.,; Levin, E. D., Khim. Ispol'z Lignina, 434 (1974)
26. Iatridis, B. and Gavalas, G. R., Ind. Eng. Chem. Prod. Res. Dev., 18(2), 127 (1979)
27. Mikulich, S. M.; Mikulich, A. S., Svoistva Strukt. Gazov, Zhidk, Tverd. Tel, 52-65 (1975)
28. Zaitsev, V. M.; Piyalkin, V. N.; Tysganoo, E. A., Gidroly Lesokhim. Prom. no. 3:10 (1975)
29. Goheen and Henderson in Allan, G. G.; Matilla, T., op. cit. 30
30. Allan, G. G.; Mattila, T., in Sarkanen, K. V. and Ludwig, C. H., Lignins Occurrence, Formation, Structure and Reactions, Wiley Interscience, New York (1971)
31. Szelenyi, G., Gomory, A., Brennstoff-Chem. 9, 72 (1928)
32. Heuser, E.; Brotz, A., Papier-Fabrik., 23, Fest-und Ausland-Heft, 69 (1925)



33. Brauns, F. E., Chemistry of Lignin, Academic Press, Inc., New York, 1952 p 581
34. Phillips, M., J. Am. Chem. Soc., 51, 2420 (1929)
35. Bridger, G. L., Ind. Eng. Chem., 30, 1174 (1938)
36. Karrer, P., Organic Chemistry, Elsevier Publ. Co., Inc., New York, 1947 p 168
37. Morgan, J. Soc. Chem. Ind., 51, 67T, (1932)
38. Domburg, G. E.; et al., Khim, Drev. no. 5, 64 (1976)
39. Domburg, E. E., et al. Thermal Analysis of Lignin in Thermal Analysis Vol. 3 Proc. 3rd ICTA Davos (1971) pp 327-40  
Burkhaeuser, Basel 1972
40. Panasyuk, L. V.; Travleeva, L. V.; Panasyuk, V. G., Khim. Drev. 1:301 (1968)
41. Kirshbaum, I. Z.; Domburg, G. E., Sergeeva, V. N. Khim. Drev. no. 4, 96 (1976)
42. Kirshbaum, I. Z.; Domburg, G. E., Izv. Akad. NaukLatv. 55R no. 2, 43 (1970)
43. Vorher, W.; Schweers, W. H. M., G. Appl. Polymer Sci. (Appl. Polymer Symp) no. 28, 277 (1975)
44. Faix, O.; Schweers, W.; Holzforschung 29, no. 6,224 (1975)
45. Goldstein, J. S., Applied Polymer Symposium, No. 28, 259 (1975)
46. Hellwig, K. C., et al., Production of Phenols from Lignin, TAPPI annual meeting, New York (1969)
47. Rachinskii, A. V.; Levin, E. D., Izv. Vuz. Lesnoi, Zh. 17(1), 111 (1974)
48. Gillet, A; Urlings, J., Chim & Ind. (Paris), 68, 55 (1952)
49. Panasyuk, V. G.; Maksimenko, N. S., Gidroliz. iLesokhim. Prom. 11, no. 1, 16-17 (1958)
50. Skrigan, A. I., et. al., Trudy Inst. Lesokhoz. Problem Akad. Nauk Latv. S. S. R. 16, 109-17 (1958)

51. Suuberg, E. M., Sc.D. Thesis, M.I.T., August 1977
52. Prosinski, S.; Czechowski, Z.; Kielczewski, M., Koks. Smola. Gaz. 15, no. 11, 322 (1970)
53. Hagglund, E., Arkiv. for Kemi, Min. och Geol., 7, 1 (1918)
54. Phillips, M.; Goss, M. J., Ind. Eng. Chem., 24, 1436 (1932)
55. Fisher, F.; Schrader, H., Ges. Abhandl. Kenntnis Kohle, 5, 106 (1922)
56. Tropsch, H., Ges. Abhandl. Kenntnis Kohle, 6, 293 (1921)
57. Picteti, A.; Gaulis, M., Helv. Chim. Acta, 6, 627 (1923)
58. Fletcher, T. L.; Harris, E. E., Tappi, 35, 536 (1952)
59. Kurth, E. E.; Ervin, H. O.; Kroll, R. L., J. Am. Chem. Soc., 58, 571 (1955)
- 60a. Shimaboto, T., et. al., J. Japan Forestry Soc., 32, 43, 47, 75 (1950)
  - b. Shimaboto, T.; Minami, K.; Kadama, T., J. Japan Forestry Soc., 34, 77 (1952)
  - c. Shimaboto, T.; Minami, K.; Sakai, H., J. Japan Forestry Soc., 33, 12 (1951)
61. Panasyuk, V. G., Zhurn. prikl. Khim., 34, 1409, 1605 (1958)
62. Fletcher, T. L.; Harris, E. E., J. Am. Chem. Soc., 69, 3144 (1947)
63. Morozov, E. F., Gidroliz, Lesokhim. Prom. 23, no. 7, 15 (1970)
64. Sergeeva, V. N.; Mozheiko, L. N., Trudy ILP i KhD AN Latv. SSR, 6, 29 (1959)
65. Gracheve, E. V.; Levin, E. D. Izv. Vuz. Lesnoi. Zh. 19, no. 2, 108 (1976)
66. Panasyuk, V. G., Zh. Prikl. Khim, 30 598 (1957)
67. Sukhanovskii, S. I., et al., Khim. Perab. Zashch. Drev., 87 (1964)

68. Akhmina, E. I., et al., Khim, Tekhnol. Topl. Prod. Ego. Pererab, 12 (1965)
69. Sukhanovskii, S. I., et al., Sb. Tr. Vses, Nauch. Issled. Inst. Gidroliz. Sulifitno Spirt. Prom., 13, 274 (1965)
70. Reznikov, V. M.; Morozov. E. E., Khim Pererab. Drev., 22, 10 (1966)
71. Domburg, G. E.; Kirshbaums, I.; Sergeeva, V. N., Khim. Drev., 7, 51 (1971)
72. Panasyuk, V. G., Zhur. Priklad Khim. 30.598-603 (1957)
73. Panasyuk, V. G., Zhur. Priklad Khim. 30, 1049-56 (1957)
74. Gladkova, N. Ya., Levin, E. D., KhimDrev. no. 1, 101 (1975)
75. Domburg, G. E., Thermal Analysis, 2 Proc. 4th ICTA, Budapest (1974)
76. Savinykh, V. I., et al., Khim. Drev., 5, 100 (1975)
77. Kislitsyn, A. N., et al., Khim Drev., 9, 131 (1971)
78. Benjamin, B. M. et al., Fuel, 57, 270 (1978)
79. Kayima, Y., et al., ACS Div. of Full Chem. preprints, 24 (2), 116 (1979)
80. Miller, R. E. and Stein, S. E., ACS Div. of Full Chem. preprints, 24 (3), 271 (1979)
81. Savinykh, V. I., et al., Khim. Drev., 3, 91 (1976)
82. Ingold, K. V. and Lossing, F. P., Can. J. of Chem., 31, 30-41 (1953)
83. Starokadonskaya, E., J. Applied Chem. (USSR) 11:646 (1938)
84. Collins, C. J., et al., Fuel, 56, 107 (1977)
85. Domburg, G. E., Rossinskaya, G. A., Dobelev, G. V., Khim Drev., 4, 87 (1975)
86. Sato, Y., et al., J. Japan Petrol. Inst., 21 (2), 110 (1978)
87. Brower, K. R., Fuel, 56, 245 (1977)

88. Sweeting, J. W. and J. F. K. Wilshire, *Aua. J. Chem.*, 15 89 (1962)
89. Domburg, G. E., Rossinskaya, G. A.; Dobele, G. V., *Khim. Drev.*, 5, 103 (1975)
90. Domburg, G. E., ; Sergeeva, V. N.; Zheibe, G. A., *J. Therm. Anal.* 2 (4), 419 (1970)
91. Shaposhnikov, Uy. K. and Kosyukova, L. V., *Khim. Pererabotka Drev.*, Ref. Inform., no. 3, 6-9 (1965)
92. Kravchenko, M. I.; Kiprianov, A. I.; Korotov, S. Ya; *Nauch. Tr. Leningrad Lesotekh. Akad.*, 135 (2), 60-4 (1970)
93. Kiprianov, A. I. and Kravchenko, M. I., *Izv. Vyssh. Ucheb. Zaved.*, *Les Zh.* 15 (5), p 121-5 (1972)
94. Kislitsyn, A. N. ; Rodionova, Z. M.; Savinykh, V. I.; Ill'ina, E.I.; Abakhumov, G. A., *Sb. Tr., T sent. Nauch - Issled. Prockt. Inst. Lesokhim. Prom.*, no. 22, p 4-16 (1971)
95. Friedlin, L. Kh; Balandin, A. A.; Nazarova, N. M.; *Izvest. Akad. Nauk S.S.S.R., Otdel Khim. Nauk*, no. 1, 102-9 (1949)
96. Obolentsev, R. D., *J. Gen. Chem. (U.S.S.R.)* 16, 1959-70 (1946)
97. Kislitsyn, A. N., et al., *Zh. Prikl. Khim (Leningrad)* 45 (2), 384 (1972)
98. Smith, R. E. and Hinshelwood, C. N., *Proc. Roy. Soc., (London) A*, 175, 131-142 (1940)
99. Domburg, G. E.; Sergeeva, V. N.; Zheibe, G. A.; *Khim. Drev.*, 7 59 (1971)
100. Kislitsyn, A. N.; et.al., *Khim. Drev.*, 9, 125 (1971)
101. Sprengling, G. R., *J. Am. Chem. Soc.*, 74, 2937 (1952)
102. Gardner, P. D., et al., *J. Am. Chem. Soc.*, 81, 5515 (1959)
103. Cavitt, S. B., et al., *J. Org. Chem.*, 27; 1211 (1962)
104. Sliwa, M., et al., *Bull. Soc. Chim. Fr.*, (5-6, Pt.2), 958 (1974)
105. Brugidou, J. and H. Christol, *Bull. Soc. Chim.*, (1966), p 1974
106. Ropiteau, P. and P. Maitte, *Bull Soc. Chim.*, (1969), p 1715

107. Wakselman, M. and M. Vilkas, C. R. Acad. Sci., 258, 1526 (1964)
108. Curreen, J. I. et al., J. Chem. Soc., (1943) p 472
109. Capelin, B. C., et al., Microchemical Journal, 19, 229 (1974)
110. Hinshelwood, C. N., and W. K. Hutchison, Proc. Roy. Soc., Ser A, 111, 245 (1926)
111. Wolf, T. and M. Rosie, Anal. Chem. 39, 725 (1967)
112. Juntgen, H.; vanHeek, K. H., Fuel, 47, 103 (1968)
113. Phillips, M., Science, 73, 568 (1931)
114. Karrer, P.; Boddington-Wiger, B., Helv. Chim. Acta, 6, 817 (1923)
115. Fuchs, W., Ber., 60, 957 (1927)
116. Fierz-David, H. E.; Hannig, M., Helv. Chim. Acta, 8, 900 (1925)
117. Phillips, M., J. Am. Chem. Soc., 53, 768 (1931)
118. Freudenberg, K., Adam, K.; Ber., 74B, 387 (1941)
119. Sergeeva, V. N.; Surgna, Ya. A., Trudy ILD i KhD AN Latv SSR, 21, 107 (1960)
120. Sergeeva, V. N., Khim. Drev. 1, 253 (1968)
121. Goheen, D. W., "Hydrogenation of Lignin by the Noguchi Process," in Lignin Structure and Reactions, Advan. Chem. Ser., 59, 205 (1966)
122. Erdmann, J., Ann., 138, 1 (1866)
123. Heuser, E.; Winsvold, A., Cellulosechem, 2, 113 (1921)
124. Heuser, E.; Winsvold, A., Cellulosechem, 4, 49, 62 (1923)
125. Heuser, E.; Winsvold, A., Chem. Ber., 56, 902 (1923)
126. Panasyuk, L. V.; Panasyuk, V. G., Izv. Vyssh. Ucheb. Saved. Lesnoi Zhur. 11 (3), 116 (1968)
127. Chudakov, M. I., Sukhanovskii, S. I., Trudy Leningrad. Lesotekh. Akad. no. 75, 121-31 (1956) Referat Zhur., Khim no. 4, 440 (1957)
128. Domburg, G. E., et al., Khim. Drev. no. 5, 73 (1976)

129. Domburg, G. E.; Sergeeva, V. N., J. Thermal, Anal. 1, 53 (1969)
130. Stamm, A. J., Ind. Eng. Chem., 48, 413 (1956)
131. Solomon, B., et. al., Cellulose Chemistry and Technology, 1, 601 (1967)
132. Koshik, M. et al., Holzforschung and Holzverwertung, 20, 15 (1968)
133. Domburg, G. E.; Sergeeva, V. N., Isv. ANLatv SSR. Ser. Khim 5, 620 (1967)
134. Andersen, C. C., Kgl. Norske, Videnskab. Sebskabs. Forh, (1951) 23, 32, 130
135. Domburg, G. E.; Sergeeva, V. N. Izv. ANLatv SSR. Ser. Khim 5, 624 (1967)
136. Domburg, G. E.; Sergeeva, V. N.; Salna, L. Ya.; Izv. AN Latv. SSR Ser. khim 4, 509 (1967)
137. Domburg, G. E., et al.; Khim. Drev. 15, 94 (1974)
138. Domburg, G. E.; Sergeeva, V. N.; Popov, A. N., Khim. Drev. 6, 133 (1970)
139. Modavskii, B.L.; Vainshtein, S. M., Khim. Tverd. Topl., 6, 656 (1935)
140. Hachihama, Y.; Jodai, S.; Vmezw, M., Kogyo Kagaku Zasshi, 43, 127 (1940)
141. Freudenberg, K. et al., Ber., 74 B, 171 (1941)
142. Hachihama, Y.; Jodai, S., Kogyo Kagaku Zasshi, 44, 773 (1941)
143. Hachihama, Y.; Jodai, S., Kogyo Kagaku Zasshi, 45, 302 (1942)
144. Takahashi, T.; Matsuda, T., J. Soc. Text Cellul. Ind. Jap., 1, 656 (1945)
145. Harris, E. E.; Saemen, J. F.; Bergstrom, C. B.; Ind. Eng. Chem., 41, 2063 (1949)
146. Giesen, J., U. S. Patent 2,774,795, Dec. 18, 1956
147. Giesen, J., Swiss Patent 318, 446, Feb. 28, 1957.

148. Oshima, M.; Maeda, Y.; Kashima, K., German Patent 1,115, 737 Oct. 26, 1961
149. Sakakibara, A.; Araki, T.; Mokuzai Gokkaishi, 7, 19 (1961)
150. Ploetz, T., et al., German Patent 1,142,853, Jan. 31, 1963
151. Sakakibara, A., Japanese Patent 26,668, Dec. 28, 1963
152. Rieche, A.; Redinger, L.; Lindenhayn, K., Monatschr. Deut. Akad. Wiss. Berlin 6(6), 430 (1964)
153. Oshima, M.; Maeda, Y.; Kashima, K., U. S. Patent 3,223,698, Dec. 14, 1965
154. Oshima, M.; et al., Bull. Chem. Soc. Jap., 39 (12), 2750, 2755 (1966)
155. Bronovitskii, V. E.; Kalinskaya, L., UzbKhim. Zh., 11 (2), 31 (1967)
156. Bronovitskii, V. E., et al., Vzb. Khim. Zh., 12 (3), 71 (1968)
157. Lapai, A. P.; Safonov, V. F.; Nazarova, N. I., Izo. Nauch. Issled Inst. Nefte-Vglekhim, 1969 (11), Pt. 1, 81.
158. Schweers, W., Holzforschung, 23 (1), 5 (1969)
159. Benigni, J. D.; Goldstein, I. S., J. Polym. Sci. C36, 477 (1971)
160. Bronovitskii, V. E.; Kalinskaya, L. L.; Ikramova, D. R., Gidroliz Lesokhim. Prom., 24 (8), 14 (1971)
161. Bronovitskii, V. E., Kalinskaya, L. L.; Khim. Prir. Soedin., 8 (1), 106 (1972)
162. San John, L.; Dobrev, S. T., Tsellyul. Khartiya, 4 (4), 22
163. El-Saied, Houssni, J. Appl. Chem. Biotechnol., 27, 443 (1977)
164. Mademov, S. and D. N. Khydyrov, Zhurnal Obshchei Khimii, 32 (5), 1427 (1962)
165. Ekpenyong, I. A., Dept. of Chem. Eng., MIT, personal communication
166. Virk, P. S., Fuel, 58, 149 (1979)
167. Frey, H. M., and Walsh, R., Chem. Rev., 69 103 (1969)

168. Klein, R., Scheer, M. D., Schoen, L. J., J. Am. Chem. Soc., 78, 50 (1956)
169. Benson, S. W., Thermochemical Kinetics, Wiley, New York (1968)  
Benson, S. W., et al., Chem. Rev., 69 279 (1969)
170. Woodward, R. B. and Hoffmann, R., The Conservation of Orbital Symmetry, Verlag Chemie, Academic Press, Germany (1971)
171. Mock, W. L. in Pericyclic Reactions Volume II, A. P. Marchand and R. E. Lehr, Editors, Academic Press, New York (1977)
172. Clarke, S. C. and Johnson, B. L., Tetrahedron, 27, 3555-61 (1971)
173. Breslow, R., et al., J. Am. Chem. Soc., 87 (6) 1326 (1965);  
Breslow, R., et al., J. Am. Chem. Soc., 87 (6) 1320 (1965)
174. Rice, F. O. and W. D. Walters, J. Amer. Chem. Soc., 63, 1701 (1941)
175. Froment, G. F. and K. B. Bischoff, Chemical Reactor Analysis and Design, Wiley, (1979)
176. Fleming, I., Frontier Orbitals and Organic Chemical Reactions, Wiley, London (1976)
177. Sauer, J., Angew. Chem. internat. Edit., 6 (1), 14 (1967)
178. Dulong, L., Makromol. Chem., 76, 119 (1964)
179. Bjorkman, A, Nature, 174, 1057 (1954); Svensk Papperstid, 59, 477 (1956)
180. Yu, K. C., S. B. Thesis, MIT, June, 1980



## LIST OF APPENDICES

Appendix No.		Page
6.1	G. C. details for each model compound experiment	642
7.1	Model compound pyrolysis product spectra: a) Mol fractions b) G. C. areas	645
7.2	Summary of experimental kinetic parameters	759
9.1	Tables of simulation predictions	765

Appendix 6.1 Experimental GC details for each model compound pyrolysis.

<u>PRODUCT</u>	<u>a<sub>i</sub></u>	<u>GAS ANALYSIS</u> <u>G C CONDITIONS</u>
CO	1.1	Silica gel, porapak Q, molecular sieve, Porapak P, Q, room temperature
CH <sub>4</sub>	1.3	
N <sub>2</sub>	1.0	
CO <sub>2</sub>	1.0	

<u>PRODUCT</u>	<u>a<sub>i</sub></u>	<u>LIQUID ANALYSIS</u> <u>SUBSTRATE, CONDITIONS</u>
PhOH	1.0	Guaiacol, Anisole Substrates Porapak P, oven at 230 C
G	0.85	
Cat	1.5	Veratrole Substrate OV17, 70-250 C @ 12 C/min
PhH	1.04	
Tol	0.022	
An	0.843	
oCr	1.0	
An	0.96	
PhOH	1	
G	0.96	
VE	0.58	
Cat	0.36	
PhH	2.0	isoeugenol substrate OV 17, FID detector, over @ 150C
Tol	1.5	
Xyl	0.96	
oCr	1.0	
dimer	0.3	
propenyl catechol	1	
propenyl phenol	1	
isoeugenol	1	
guaiacol	1	
phenol	1	
catechol	1	2,6-DMP substrate OV17 @ 180C
guaiacol	1	
catechol	1	cinn acid OV17 70-250 @ 12/min
methoxycatechol	6	
pyrogallol	-	
2,6-DMP	0.95	
toluene	2.5	
EB	1.7	
ST	2.0	
CA	3.5	
dim	3	

Appendix 6.1 Experimental GC details for each model compound  
pyrolysis (cont'd)

<u>PRODUCT</u>	<u>a<sub>i</sub></u>	LIQUID ANALYSIS SUBSTRATE, G C CONDITIONS
H <sub>2</sub> O	1	CAL substrate
MeOH	1	Por Q 150 C
CH <sub>3</sub> CHO	1	
CH <sub>2</sub> O	1	
EtOH	1	
MeCL <sub>2</sub>	1	
MeCL <sub>2</sub>	1	CAL substrate
T	SEE PPE	OV17 100-250 C @ 12/min
EB		
ST		
AB		
PhOH		
Cr		CAL substrate
6.2		OV17 100-250 C @ 12/min
7.0		
CAD		
CAL		
DIM		
PhH	3.1	PPE substrate
To1	2.5	OV17 70-250 C @ 12/min
EB	1.7	
St	2.0	
PhOH	2.7	
PE	1.7	
DPM	0.63	
	2.0	
BB	7.0	
PhPHOH	2.0	
BPE	2.0	
PPE	0.87	
DIM	2.0	
PPE S=0	0.87	
PPE 0.245	0.78	
PPE 0.492	0.75	
PPE 1.48	0.62	
PPE 4.92	0.55	
PPE 9.8	0.55	

Appendix 6.1 Experimental GC details for each model compound  
pyrolysis (cont'd)

<u>PRODUCT</u>	<u>a<sub>i</sub></u>	<u>LIQUID ANALYSIS SUBSTRATE, GC CONDITIONS</u>
Saligenol	3.12	Saligenol substrate
oCr	1.18	10& UCW-982 100-150 @ 12C/min
Toluene	1.0	
Toluene	1.0	Saligenol substrate
H <sub>2</sub> O	4.17	PorP 100-250 @ 12min
Benzene	2.3	Phenylether Substrate
Phenol	3	OV1 750-157 @ 12/min
Phenylether	1	FID detector
Sesquimers	1.1	
PhH	1.35	OHD substrate
Tol	1	OV17 70-250 @ 12/min
PhOH	0.64	
OHD	0.71	
PhH	2.3	Biphenyl Substrate
BP	1.14	OV17 50-150 @ 12/min.
	NA CO <sub>2</sub> only FA gas only	
PhH	1.126	BA substrate
PhOH	1	
BA	1	
dimer	1	
G	1	Van Substrate, TCD detector
PhOH	1	OV17 @ 200C
Cat	1	
Van	1.09	
G	1	Van Substrate, FID detector
PhOH	1	OV17 @ 150C
Cat	1	
Van	0.86	
PhH	1.8	Acetophenone substrate
Tol	1.3	
Xyl	1.3	PorP 200-240 @ 12/min
PhOH	1	FID
BA	1	OV17 70-250 @ 12/min
AP	1	TCD
PhH	SEE PPE	OV17 70-250 @ 12/min TCD
Tol		PorP 200-240 @ 12/min FID
EB		Cinnamaldehyde Substrate
ST		
PhOH		
oCr		
CAD		
D		

## Appendix 7.1 Model Compound Pyrolysis Product Spectra

PRODUCT YIELDS: PPE (E PPE)																		
T	E <sub>0</sub>	S	t	(M)	E <sub>0</sub>	E <sub>0</sub> -E	B/E <sub>0</sub>	T/E <sub>0</sub>	EB/E <sub>0</sub>	St/E <sub>0</sub>	P/E <sub>0</sub>	P/(E <sub>0</sub> -E)	St/(E <sub>0</sub> -E)	Ei/(E <sub>0</sub> -E)	E/E <sub>0</sub>	-lnE/E <sub>0</sub>	H/C	O/C
325	0.15	0	15	96.5	0.982	0.0176	0	0	2.71-4	9.03-3	0.028	1.53	0.503	0.518	0.982	0.018		
			30	99.9	0.975	0.025	0	1.88-3	1.39-3	0.0129	0.0332	1.27	0.495	0.620	0.974	0.026		
			45	98.5	0.975	0.025	0	1.93-3	1.37-3	0.0125	0.034	1.34	0.496	0.627	0.975	0.026		
			90	100.2	0.961	0.040	0	4.25-3	5.19-3	0.0175	0.0521	1.25	0.420	0.647	0.958	0.0425		
			115	105.0	0.9492	0.057	0	3.21-3	8.09-3	0.016	0.072	1.20	0.265	0.453	0.940	0.062		
350	0.25	0	10	98.6	0.980	0.0197	0	1.46-4	8.25-3	0.0129	0.0260	1.29	0.639	0.687	0.980	0.020		
			10	97.8	0.978	0.0215	0	1.48-4	4.76-4	0.0129	0.0291	1.33	0.587	0.676	0.978	0.022		
			20	99.5	0.966	0.035	0	4.76-3	1.83-3	0.022	0.414	1.15	0.606	0.789	0.964	0.037		
			20	99.2	0.965	0.036	0	4.14-3	1.80-3	0.022	0.045	1.20	0.589	0.748	0.963	0.038		
			30	100.6	0.966	0.035	0	4.11-3	2.52-3	0.0194	0.0424	1.17	0.534	0.717	0.964	0.037		
			30	100.2	0.965	0.035	0	4.35-3	2.52-3	0.0194	0.0425	1.18	0.537	0.727	0.964	0.037		
			40	100.6	0.948	0.054	0	8.11-3	0	0.0316	0.0675	1.19	0.555	0.698	0.943	0.059		
			40	99.9	0.941	0.060	0	7.30-3	4.96-3	0.0298	0.0700	1.25	0.466	0.659	0.936	0.066		
			50	99.4	0.933	0.062	0	0.0211	0.0107	0.0386	0.0600	0.897	0.577	1.05	0.933	0.069		
			50	100.2	0.932	0.068	0	0.0191	0.0130	0.0483	0.0611	0.835	0.659	1.10	0.927	0.076		
400	0.083	0	5	98.2	0.9127	0.0857	0	5.69-3	8.39-3	0.0701	0.1052	1.12	0.7467	0.8967	0.9061	0.986	1.017	0.081
			10	99.3	0.8115	0.1885	0	0.0246	0.0567	0.1183	0.2563	1.10	0.5093	0.8594	0.7677	0.2643	1.040	0.082
			15	102.4	0.769	0.246	0	0.0455	0.0923	0.1313	0.3146	0.9824	0.4100	0.8400	0.6798	0.3859	1.040	0.078
			25	99.6	0.693	0.303	0	0.061	0.162	0.147	0.481	1.10	0.337	0.846	0.583	0.575	1.160	0.0818
400	0.25	0	5	99.8	0.943	0.0567	0	0.011	4.41-3	0.040	0.064	1.06	0.661	0.914	0.940	0.062	1.022	0.078
			10	99.4	0.861	0.138	1.97-3	0.032	0.019	0.084	0.175	1.09	0.520	0.846	0.839	0.175	1.029	0.081
			15	100.9	0.829	0.177	2.49-3	0.045	0.024	0.101	0.227	1.06	0.472	0.808	0.787	0.240	1.028	0.081
			20	101.4	0.766	0.243	0.0102	0.082	0.051	0.114	0.326	1.03	0.361	0.813	0.683	0.381	1.038	0.078
			25	101.8	0.714	0.297	0.0165	0.114	0.077	0.124	0.476	1.02	0.298	0.796	0.584	0.538	1.041	0.0786
400	0.25	0	5	99.8	0.940	0.061	0	0	1.97-3	0.039	0.084	1.3	0.601	0.632	0.935	0.067	1.002	0.0978
			10	101.5	0.798	0.212	0	0.0572	0.0492	0.101	0.284	1.07	0.380	0.780	0.734	0.309	1.037	0.0826
			15	101.9	0.844	0.160	0	0.0413	0.0201	0.110	0.178	0.940	0.583	0.907	0.811	0.210	1.022	0.0700
			20	101.9	0.713	0.302	0	0.0964	0.0993	0.117	0.463	1.09	0.275	0.737	0.576	0.551	1.044	0.0853
			25	101.8	0.666	0.350	0	0.124	0.152	0.110	0.575	1.10	0.209	0.733	0.47	0.744	1.353	0.0856
400	0.75	0	4	106.4	0.937	0.0775	0	0.065	0.0307	0.0786	0.226	0.881	0.307	0.779	0.917	0.0663	1.020	0.0771
			8	105.3	0.815	0.209	0.028	0.065	0.0307	0.0786	0.226	0.881	0.307	0.779	0.917	0.0663	1.020	0.0771
			12	109.3	0.830	0.210	4.93-3	0.0615	0.0289	0.0639	0.231	0.915	0.253	0.629	0.747	0.292	1.023	0.082
			16	108.6	0.737	0.313	0.0176	0.1262	0.0624	0.0733	0.381	0.897	0.172	0.658	0.575	0.553	1.032	0.0795
400	0.83	0	5	100.8	0.940	0.061	0	0.0160	3.85-3	0.0500	0.0544	0.834	0.766	1.07	0.935	0.068	1.021	0.0635
			10	104.1	0.859	0.154	2.70-3	0.0431	0.0175	0.0664	0.1805	1.01	0.370	0.723	0.821	0.198	1.022	0.0820
			15	106.9	0.794	0.130	7.81-2	0.0793	0.0291	0.0718	0.291	0.96	0.237	0.654	0.596	0.350	1.025	0.0823
			20	106.7	0.754	0.287	0.012	0.108	0.061	0.070	0.365	0.959	0.185	0.653	0.620	0.431	1.031	0.0800
400	1.66	0	5	103.5	0.938	0.069	0	0.0172	6.07-3	0.047	0.061	0.830	0.640	0.958	0.927	0.0761	1.021	0.0664
			10	107.2	0.790	0.247	6.40-3	0.0835	0.0481	0.061	0.304	0.971	0.194	0.653	0.687	0.375	1.028	0.0836
			15	109.2	0.748	0.306	0.0105	0.1113	0.0781	0.0495	0.380	0.928	0.121	0.609	0.591	0.526	1.036	0.0835
			20	111.9	0.704	0.378	0.0193	0.1561	0.1036	0.0483	0.454	0.846	0.0898	0.6093	0.463	0.771	1.044	0.0800
			25	115.6	0.675	0.445	0.024	0.178	0.145	0.0415	0.504	0.764	0.063	0.589	0.341	1.08	1.053	0.0789

PRODUCT YIELDS: PPE (E PPE)

T	E <sub>0</sub>	S	t	(M)	E <sub>0</sub>	E-E	B/E <sub>0</sub>	T/E <sub>0</sub>	EB/E <sub>0</sub>	St/E <sub>0</sub>	P/E <sub>0</sub>	P/(E <sub>0</sub> -E)	St/(E <sub>0</sub> -E)	Et/(E <sub>0</sub> -E)	E/E <sub>0</sub>	-lnE/E <sub>0</sub>	H/C	O/C
400	0.25	0.245	5	98.23	0.950	0.0493	0	0.010	0.0161	0.0270	0.0513	0.9908	0.5197	1.02	0.948	0.0532	1.058	0.071
			10	99.1	0.868	0.132	1.02-3	0.0282	0.0635	0.0527	0.154	1.02	0.347	0.957	0.848	0.165	1.072	0.0744
			15	99.4	0.775	0.225	2.02-3	0.0527	0.143	0.066	0.305	1.05	0.227	0.910	0.709	0.343	1.083	0.0776
			20	99.5	0.762	0.240	4.15-3	0.060	0.188	0.050	0.315	1.0	0.158	0.959	0.685	0.378	1.099	0.0736
			25	100.1	0.745	0.259	6.16-3	0.072	0.176	0.067	0.348	1.0	0.193	0.924	0.652	0.427	1.085	0.0745
	0.25	0.492	5	107.5	0.955	0.053	0	7.27-3	8.73-3	0.027	0.050	0.891	0.487	0.773	0.944	0.058	1.039	0.0782
			10	98.93	0.910	0.0828	0	0.0160	0.0155	0.0531	0.095	1.04	0.584	0.931	0.909	0.095	1.036	0.0768
			15	99.45	0.860	0.135	1.36-3	0.0291	0.0547	0.0640	0.157	1.00	0.409	0.953	0.843	0.170	1.062	0.0741
			20	99.9	0.808	0.195	2.84-3	0.046	0.119	0.054	0.244	1.01	0.226	0.922	0.759	0.276	1.082	0.0757
			25	99.8	0.756	0.247	5.75-3	0.064	0.192	0.039	0.331	1.01	0.121	0.923	0.674	0.395	1.10	0.0754
	0.25	1.48	5	104.4	0.920	0.057	0	8.02-3	8.53-3	0.0374	0.0543	0.870	0.599	0.864	0.938	0.065	1.005	0.0740
			10	98.8	0.887	0.100	0	0.0167	0.0250	0.0616	0.120	1.07	0.547	0.919	0.888	0.119	1.042	0.0784
			15	99.6	0.815	0.147	0	0.035	0.033	0.088	0.193	1.07	0.488	0.866	0.820	0.198	1.036	0.0805
			20	100.2	0.747	0.183	2.03-3	0.056	0.058	0.101	0.250	1.02	0.412	0.886	0.756	0.280	1.047	0.078
			25	101.0	0.695	0.232	4.52-3	0.084	0.098	0.102	0.337	1.01	0.305	0.861	0.666	0.407	1.049	0.0789
	0.25	1.48	5	99.5	0.951	0.048	0	6.93-3	0.0138	0.0308	0.0485	0.954	0.607	1.01	0.9487	0.0521	1.047	0.0698
			10	99.4	0.877	0.124	0	0.0184	0.0530	0.0624	0.146	1.03	0.440	0.943	0.858	0.153	1.061	0.0756
			15	100.4	0.800	0.205	0	0.0331	0.1017	0.0767	0.280	1.09	0.299	0.825	0.744	0.296	1.064	0.0820
			20	100.3	0.749	0.257	0	0.0543	0.166	0.0705	0.368	1.07	0.205	0.848	0.657	0.420	1.078	0.0808
			25	102.1	0.756	0.259	0	0.0476	0.187	0.0612	0.337	0.982	0.179	0.802	0.657	0.420	1.086	0.0725
	0.25	4.92	5	103.1	0.975	0.081	0	8.92-3	5.28-3	0.0226	0.0890	0.376	0.880	1.47	0.907	0.0260	1.052	0.0307
			10	97.7	0.873	0.081	0	0.0253	5.28-3	0.0689	0.0890	0.9564	0.741	1.07	0.907	0.0977	1.027	0.0682
			15	98.28	0.855	0.114	0	0.0353	0.0842	0.0213	0.1280	0.9595	0.155	0.926	0.867	0.143	1.110	0.0689
			20	98.2	0.817	0.179	0	0.040	0.140	0.022	0.239	1.09	0.101	0.926	0.781	0.247	1.106	0.0792
			25	98.6	0.758	0.224	0.022	9.24-3	0.0185	0.0291	0.0253	0.609	0.702	0.926	0.705	0.350	1.139	0.0630
	0.25	9.8	5	100	0.958	0.0397	0	0.0187	0.0664	0.0363	0.0643	0.6854	0.387	1.37	0.959	0.042	1.062	0.0462
			10	100	0.898	0.0843	0	0.0409	0.127	0.0544	0.236	1.04	0.387	1.29	0.906	0.099	1.113	0.0485
			15	98.34	0.597	0.136	0	0.0494	0.105	0.047	0.185	0.965	0.239	0.977	0.772	0.259	1.094	0.0747
			20	98.2	0.773	0.148	0	0.0592	0.119	0.052	0.306	1.16	0.197	0.874	0.736	0.307	1.082	0.0692
			25	97.4	0.565	0.149	0	1.75-3	3.20-3	0.0104	0.343	0.356	1.08	0.874	0.903	9.67-3	1.082	0.0845
350	0.25	1.48	20	101.4	0.9893	9.52-3	0	3.10-3	5.16-3	0.0171	4.01-3	0.266	1.13	1.59	0.989	0.0152	1.082	0.0845
			30	100.4	0.978	0.0208	0	4.07-3	5.79-3	0.0209	0.0112	0.528	0.9799	1.44	0.987	0.0215	1.082	0.0845
			42	97.9	0.951	0.458	0	6.51-3	9.104	0.0255	0.0539	1.12	0.506	1.44	0.987	0.0215	1.082	0.0845
			50	97.7	0.947	0.0461	0	6.28-3	9.05-3	0.0267	0.0563	1.16	0.549	0.865	0.987	0.0215	1.082	0.0845

## PRODUCT YIELDS: PPE (E PPE)

T	E <sub>0</sub>	S	t	(M)	E <sub>0</sub>	E <sub>0</sub> -E	B/E <sub>0</sub>	T/E <sub>0</sub>	EB/E <sub>0</sub>	ST/E <sub>0</sub>	PhE <sub>0</sub>	Rh(E <sub>0</sub> -E)	St(E <sub>0</sub> -E)	Et(E <sub>0</sub> -E)	E/E <sub>0</sub> - lnE/E <sub>0</sub>	H/C	O/C
350	0.25	4.92	10	108.7	0.976	0.0245	0	2.89-3	6.95-3	0.0138	0.0161	0.6397	0.557	0.941	0.975	0.0255	
			20	100	0.976	0.0210	0	3.82-3	9.82-3	0.0137	0.0152	0.706	0.457	1.27	0.979	0.0217	
			30	99.8	0.970	0.0251	0	4.80-3	9.80-3	0.192	0.0176	0.680	0.740	1.30	0.974	0.0263	
			40	102.3	0.975	0.0216	0	5.30-3	0.0159	0.0175	4.16-3	0.188	0.791	1.75	0.978	0.0224	
			50	126.6	0.918	0.0723	0	7.46-3	0.0203	0.0215	0.0342	0.4342	0.624	0.624	0.921	0.0820	
450	0.25	1.48	2.5	98.3	0.878	0.119	0	0.023	0.040	0.075	0.134	0.996	0.553	1.02	0.865	0.145	
			3	99.4	0.832	0.168	1.91-3	0.040	0.083	0.085	0.187	0.926	0.423	1.04	0.798	0.226	
			4	99.2	0.757	0.235	4.07-3	0.081	0.112	0.178	0.242	0.777	0.573	1.21	0.689	0.372	
			5	98.5	0.651	0.342	0.0177	0.120	0.326	0.073	0.514	0.978	0.138	1.02	0.474	0.746	
			6	98.8	0.643	0.352	0.0188	0.134	0.307	0.095	0.530	0.968	0.173	1.01	0.453	0.793	
450	0.25	4.92	2.5	101.4	0.880	0.055	0	0.011	0.043	0.039	0.030	0.479	0.613	1.48	0.936	0.065	
			3	100	0.822	0.121	0	0.025	0.107	0.054	0.106	0.718	0.369	1.26	0.852	0.160	
			4	99.8	0.778	0.182	0	0.045	0.120	0.096	0.201	0.856	0.408	1.11	0.766	0.267	
			5	101	0.721	0.280	0	0.093	0.144	0.148	0.347	0.894	0.383	1.48	0.612	0.491	
			6	100.4	0.661	0.280	0	0.096	0.259	0.0999	0.365	0.859	0.235	1.07	0.576	0.552	
400	0.83	1.48	5	96.2	0.884	0.080	0	8.42-3	5.91-3	0.0363	0.135	1.49	0.402	0.560	0.906	0.095	
			10	97.8	0.783	0.144	0	0.026	0.0385	0.0496	0.252	1.37	0.270	0.621	0.817	0.203	
			15	99.3	0.700	0.200	2.47-3	0.065	0.068	0.058	0.356	1.24	0.203	0.676	0.714	0.336	
			20	99.7	0.709	0.207	2.68-3	0.058	0.124	0.024	0.351	1.20	0.083	0.715	0.708	0.345	
			25	100.2	0.637	0.229	4.44-3	0.080	0.153	0.032	0.413	1.15	0.089	0.751	0.640	0.446	
400	0.25	4.92	5	99.8	0.930	0.070	0	0.013	0.034	0.048	0.054	0.723	0.641	1.26	0.925	0.078	
			10	99.5	0.938	0.060	0	8.06-3	0.041	0.022	0.056	0.876	0.350	1.11	0.936	0.066	
			16	98.4	0.817	0.175	0	0.0324	0.136	0.027	0.235	1.10	0.127	0.912	0.786	0.241	
			20	98.6	0.794	0.200	0	0.0422	0.183	0.0128	0.268	1.06	0.051	0.942	0.748	0.291	
			25	96.0	0.904	0.379	5.67-3	0.383	0.196	4.94-3	0.273	0.65	0.0118	1.40	0.581	0.544	
400	0.083	14.8	15	94.6	0.603	0.233	0	9.60-3	0.030	0.0142	0.755	1.95	0.0368	1.40	0.614	0.488	
			20	95.4	0.632	0.232	0	0.027	0.073	0.021	0.648	1.76	0.056	0.313	0.632	0.458	
			25	95.8	0.645	0.195	0	0.022	0.074	0.028	0.496	1.64	0.092	0.426	0.698	0.360	
450	0.25	0	2	97.9	0.90	0.073	0	0.0133	3.45-3	0.697	0.049	1.19	0.604	0.811	0.919	0.0844	
			3	99.3	0.91	0.0998	0	0.0187	5.83-3	0.086	0.106	0.962	0.781	1.00	0.890	0.116	
			4	99.6	0.792	0.212	6.19-3	0.051	0.0442	0.139	0.278	1.04	0.520	0.897	0.733	0.311	
			6	100	0.754	0.244	0.012	0.082	0.033	0.172	0.318	0.982	0.532	0.925	0.676	0.391	
			7	100.2	0.745	0.259	0.021	0.099	0.036	0.177	0.322	0.928	0.510	0.953	0.654	0.427	
			10	103.6	0.695	0.314	0.027	0.124	0.062	0.186	0.389	0.860	0.411	0.882	0.548	0.601	
500	0.75	0	1	102.9	0.771	0.251	0.0187	0.091	0.029	0.156	0.285	0.877	0.478	0.904	0.675	0.394	
			2	104.5	0.751	0.281	0.0227	0.109	0.0425	0.139	0.326	0.871	0.370	0.836	0.626	0.469	
			2.5	104.5	0.648	0.397	0.0556	0.216	0.0973	0.144	0.525	0.855	0.233	0.835	0.386	0.952	
			3	105	0.597	0.457	0.075	0.280	0.151	0.122	0.643	0.839	0.160	0.820	0.234	1.45	

PRODUCT YIELDS: PPE (E PPE)

T	E <sub>0</sub>	S	t	(M)	E <sub>0</sub>	E-E	B/E <sub>0</sub>	T/E <sub>0</sub>	EB/E <sub>0</sub>	St/E <sub>0</sub>	P/E <sub>0</sub>	P/(E <sub>0</sub> -E)	St/(E <sub>0</sub> -E)	Et/(E <sub>0</sub> -E)	E/E <sub>0</sub>	-InE/E <sub>0</sub>	H/C	O/C
550	0.75	0	30	101.4	0.972	0.0293	0	6.69-3	1.27-3	0.022	0.027	0.888	0.717	0.981	0.9698	0.0306		
			45	101.1	0.839	0.167	5.93-3	0.0517	0.0153	0.118	0.181	0.910	0.591	0.958	0.8010	0.2218		
			60	103.1	0.646	0.384	0.051	0.198	0.087	0.192	0.512	0.862	0.323	0.888	0.406	0.902		
			75	101.6	0.525	0.497	0.126	0.442	0.234	0.130	0.758	0.800	0.137	0.983	0.0524	2.95		
			90	100.4	0.517	0.496	0.124	0.399	0.217	0.267	0.774	0.807	0.278	1.05	0.040	3.22		
500	0.25	0	2	98.5	0.801	0.224	0.010	0.069	0.027	0.153	0.287	1.03	0.553	0.936	0.722	0.325		
			3	100.1	0.644	0.357	0.035	0.161	0.070	0.253	0.528	0.952	0.467	0.937	0.446	0.808		
			5	100.6	0.874	0.450	0.066	0.201	0.113	0.160	0.412	0.799	0.311	1.05	0.484	0.724		
			7	99.3	0.506	0.487	0.117	0.383	0.257	0.202	0.869	0.903	0.209	0.995	0.0375	3.28		
			2.5	98.1	0.973	0.020	0	3.39-	4.62-4	0.0172	0.0206	0.9980	0.833	1.02	0.9794	0.021		
			5	97.5	0.949	0.049	0	8.01-3	2.11-3	0.0358	0.0580	1.13	0.6999	0.8976	0.9486	0.053		
			7.5	98.2	0.921	0.077	1.30-3	0.0135	5.10-3	0.0554	0.0912	1.10	0.665	0.9035	0.9167	0.0870		
			10.33	98.9	0.896	0.103	1.79-3	0.0223	0.010	0.0748	0.117	1.02	0.651	0.9476	0.8851	0.122		
			30	100.7	0.771	0.191	6.48-3	0.070	0.0467	0.110	0.231	0.9311	0.445	0.942	0.752	0.285		
			6	99.5	0.931	0.066	0	6.34-3	3.44-3	0.056	0.073	1.04	0.787	0.926	0.929	0.0732		
			8	99.5	0.912	0.088	0	0.0112	6.38-3	0.067	0.103	1.07	0.696	0.881	0.904	0.1013		
			10	99.6	0.882	0.106	0	0.0166	8.28-3	0.0794	0.129	1.08	0.661	0.868	0.880	0.128		
			2	101.2	0.981	0.0187	0	3.06-3	7.14-4	0.0138	0.0184	0.9626	0.7220	0.9198	0.9809	0.0193		
			4	100.7	0.941	0.054	0	0.0120	3.72-3	0.0373	0.0563	0.9748	0.6456	0.9178	0.9422	0.595		
			6	100.6	0.899	0.106	0	0.0271	8.67-3	0.0657	0.117	0.989	0.557	0.8598	0.8819	0.1257		
			30	96.53	0.9922	7.44-3	0	0	2.02-4	6.22-3	9.57-3	1.21	0.7857	0.8111	0.9920	7.94-3		
			30	98.04	0.9920	7.85-3	0	0	4.45-4	1.34-4	6.20-3	0.0153	1.42	0.575	0.628	0.9892	0.0108	
			30	96.84	0.9887	0.0107	0	0	3.24-4	5.88-3	0.0432	1.82	0.247	0.261	0.976	0.0241		
			30	95.3	0.975	0.0232	0	0	0	0	0	0	0.918	0.918	0.996	3.93-3		
			60	98.6	0.9996	3.92-3	0	0	0	360-3	4.28-3	1.09	0.492	0.557	0.991	9.26-3		
			50	101.0	0.9914	9.14-3	0	0	5.96-4	4.53-3	0.0121	1.31	0.974	1.21	0.969	0.0314		
			60	100.4	0.975	0.0302	0	0	7.33-3	0.0301	0.0236	0.762	0.974	0.638	0.986	0.0140		
			60	96.93	0.986	0.0137	0	6.16-4	9.58-4	7.33-3	0.0196	1.40	0.525	0.137	0.975	0.0255		
			75	94.97	0.951	0.024	0	0.16-4	7.15-4	2.74-3	0.049	1.941	0.109	0.294	0.968	0.0322		
			75	96.15	0.967	0.031	0	5.16-4	1.30-3	7.49-3	0.055	1.75	0.236	0.236	0.995	4.60-3		
			90	110.1	0.996	4.58-3	0	1.23-4	9.07-4	0.0109	0.0267	1.37	0.558	0.68	0.980	0.0197		
			90	96.92	0.980	0.0192	0	1.44-3	9.07-4	0.0109	0.0267	1.37	0.558	0.68	0.980	0.0197		
			90	97.3	0.991	8.47-3	0	0	0	5.78-3	0.0116	1.36	0.677	0.68	0.991	8.58-3		
			90	96.8	0.973	0.0265	0	0	4.88-4	7.07-3	0.0473	1.74	0.260	0.277	0.973	0.0276		
			90	97.9	0.966	0.033	0	1.55-3	2.81-3	0.0108	0.052	1.53	0.318	0.467	0.966	0.0344		
			110	99.04	0.9810	0.0190	0	8.33-4	1.50-3	8.80-3	0.0262	1.37	0.454	0.574	0.981	0.0196		
			180	99.9	0.968	0.0323	0	2.58-3	4.45-3	0.0111	0.0455	1.36	0.331	0.542	0.967	0.034		
			240	97.0	0.976	0.0233	0	2.22-3	1.63-3	0.0121	0.035	1.46	0.507	0.575	0.976	0.024		
			240	96.7	0.974	0.0247	0	2.22-3	2.35-3	0.0115	0.036	1.42	0.453	0.633	0.975	0.026		
			240	96.6	0.9753	0.023	0	0	9.95-4	0.0113	0.036	1.53	0.478	0.520	0.976	0.024		





MOL FRACTIONS: PPE

RT	COMPOUND	50 Min.	T=450, PPE <sub>0</sub> =0.25, S=0										T=500, PPE <sub>0</sub> =0.75, S=0					T=550, PPE <sub>0</sub> =0.75, S=0	
			2	3	4	6	7	10	1	1.5	2	2.5	3	30s	45s				
0.74	BE	0	0	0	4.9-3	9.0-3	0.016	0.019	0	0.0144	0.0171	0.036	0.045	0	0				
1.11	TO	0.0197	0.0178	0.012	0.017	0.04	0.062	0.074	0.086	0	0.0704	0.0818	0.140	0.167	0	6.5-3			
1.67	EB	0.010	0.0121	3.1-3	5.3-3	0.035	0.025	0.027	0.043	0	0.022	0.0319	0.063	0.090	0	1.23-3			
2.14	ST	0.036	0.045	0.044	0.078	0.110	0.130	0.132	0.129	0	0.12	0.1041	0.093	0.073	0	0.021			
3.60	Ph	0.056	0.056	0.087	0.096	0.22	0.24	0.24	0.27	0	0.22	0.245	0.34	0.384	0	0.026			
6.99	BP	0	0	0	0	0	0	0	0	0	0	310-3	3.33-3	3.46-3	0	0			
8.80	PE	0	0	3.0-5	0	2.5-4	4.7-4	1.7-4	7.2-4	0	5.18-4	1.07-3	1.97-3	2.43-3	0	0			
9.20	PPM	0	0	7.0-5	1.4-4	8.8-4	1.5-3	1.3-3	8.8-4	0	5.86-4	9.77-4	2.01-3	2.70-3	0	3.21-5			
9.70	PT	0	0	0	1.77-4	0	3.3-4	8.8-4	0	3.72-4	7.75-4	2.90-3	3.46-3	0	0				
10.02	BB	3.16-4	3.03-4	4.0-4	6.0-4	4.7-3	9.3-3	1.3-2	1.7-2	0	0.0151	0.0196	0.0354	0.0431	0	3.75-4			
10.60	PP	0	0	0	2.0-4	0	5.0-4	1.5-3	0	4.46-4	7.75-4	6.23-0	4.06-3	0	4.77-4				
11.21	BPE	2.27-3	2.76-3	8.0-4	2.0-3	5.0-3	6.6-3	6.8-3	0.018	0	0.016	0.023	0.028	0.027	0	1.56-3			
11.79	PPE	0.871	0.864	0.827	0.81	0.58	0.51	0.486	0.381	0	0.52	0.47	0.25	0.14	1.0	0.9426			
12+	DIW	0	0	0	0	0	0	0	0	0	2.88-3	3.45-3	2.17-3	0.015	0	0			

## MOL FRACTIONS: PPE

T=400, PPE <sub>0</sub> =0.083, S=0		T=400, PPE <sub>0</sub> =0.25, S=0					T=400, PPE <sub>0</sub> =0.75, S=0								
RT	COMPOUND	5 Min.	10	15	20	25	5	10	15	20	25	4	8	12	16
0.74	BE	0	0	0	3.11-3	0	0	1.71-3	2.06-3	7.79-3	0.0118	0	0.023	4.09-3	0.0130
1.11	TO	5.2-3	0.02	0.035	6.65-3	0.042	0.0102	0.0274	0.0373	0.063	0.0813	0.015	0.053	0.051	0.093
1.67	EB	7.66-3	0.046	0.071	0.032	0.112	4.16-3	0.016	0.020	0.039	0.055	4.34-3	0.025	0.024	0.046
2.17	ST	0.064	0.096	0.101	0.092	0.102	0.0375	0.072	0.0833	0.0875	0.0885	0.041	0.064	0.053	0.054
3.60	Ph	0.0960	0.208	0.242	0.21	0.333	0.0601	0.151	0.188	0.2494	0.304	0.070	0.184	0.192	0.281
6.99	BP	0	0	0	0	0	0	0	0	0	0	0	0	0	0
8.80	PE	0	0	0.0173	0	0	0	0	0	2.23-4	2.95-4	0	0	0	3.28-4
9.20	DPM	0	0	0	0	0	0	1.82-4	2.91-4	6.62-4	9.03-4	5.25-5	3.86-4	5.50-4	1.16-3
9.70	PT	0	0	4.68-4	0	8.11-4	0	0	0	3.67-4	5.43-4	0	4.21-4	6.91-4	1.54-3
10.02	BB	0	0	3.52-3	3.26-3	3.62-3	5.50-4	2.89-3	5.97-3	0.0125	0.0164	1.35-3	9.18-3	0.011	0.019
10.60	PP	0	1.69-3	7.15-4	0	7.49-4	0	0	0	0	0	0	0	0	3.51-4
11.21	BPE	0	4.27-3	5.39-3	5.15-3	7.49-3	1.10-3	4.39-3	9.62-3	0.0135	0.0195	3.99-3	0.027	0.034	0.050
11.79	PPE	0.827	0.623	0.523	0.65	0.39	0.8863	0.723	0.652	0.523	0.417	0.86	0.606	0.620	0.424
12+	DIM	0	0	0	0	0	0	0	0	0	0	8.44-3	6.50-3	9.95-3	0.0116

MOL FRACTIONS: PPE

		T=400, PPE <sub>0</sub> =0.83, S=0					T=400, PPE <sub>0</sub> =1.06, S=0				
RT	COMPOUND	5 Min.	10	15	20	25	5	10	15	20	25
0.74	BE	0	2.32-3	6.20-3	9.01-3	6.20-3	0	5.06-3	7.84-3	0.0136	0.016
1.11	TO	0.0150	0.037	0.063	0.0813	0.0722	0.0161	0.066	0.0833	0.11	0.12
1.67	EB	3.62-3	0.015	0.031	0.046	0.047	5.69-3	0.038	0.0584	0.073	0.098
2.17	ST	0.047	0.057	0.057	0.053	0.051	0.044	0.048	0.037	0.034	0.029
3.60	Ph	0.0512	0.155	0.231	0.275	0.248	0.0570	0.24	0.284	0.32	0.34
6.99	BP	0	0	0	0	0	0	0	0	0	0
8.80	PE	0	0	0	0	0	0	0	0	0	0
9.20	DPM	0	2.99-4	6.59-4	1.03-3	1.25-3	0	5.09-4	8.74-4	1.52-3	1.48-3
9.70	PT	0	0	8.54-4	1.38-3	1.63-3	0	9.22-4	1.39-3	2.27-3	2.26-3
10.02	BB	0	6.54-3	0.013	0.017	0.016	1.46-3	0.0132	0.0156	0.0213	0.0184
10.60	PP	0	0	0	0	0	0	0	0	0	0
11.21	BPE	3.76-3	0.0184	0.042	0.048	0.051	7.17-3	0.0449	0.0542	0.052	0.051
11.79	PPE	0.879	0.705	0.554	0.467	0.501	0.869	0.543	0.442	0.326	0.230
12+	DIM	0	0	0	0	0	0	0	0.0121	0.042	0.087



## MOL FRACTIONS: PPE

T=400, PPE<sub>0</sub>=0.25, S=0.245

	5	10	15	20	25
0	8.85-4	2.03-3	3.16-3	4.59-3	
9.57-3	0.0245	0.0408	0.046	0.054	
0.0153	0.0551	0.111	0.143	0.131	
0.0256	0.0457	0.0511	0.038	0.050	
0.0488	0.134	0.236	0.240	0.259	
0	0	0	0	1.65-3	
0	0	0	0	0	
0	0	0	0	0	
0	0	0	0	0	
0	0	0	0	3.26-4	
0	1.01-3	2.07-3	2.26-3	3.51-3	
0	0	0	0	0	
0	2.21-3	5.55-3	5.32-3	8.76-3	
0.9008	0.736	0.5495	0.522	0.486	
0	0	0	0	0	



MOL FRACTIONS: PPE

RT	COMPOUND	(T=400, PPE <sub>0</sub> =0.25, S=4.92) T=400, PPE <sub>0</sub> =0.25, S=9.8					T=400, PPE <sub>0</sub> =0.25, S=1.48					T=400, PPE <sub>0</sub> =0.25, S=0				
		25 Min.	5 Min.	10	15	20	25	5	10	15	20	25	5	10	15	
0.74	BE	0.0165	0	0	0	0	0	0	0	0	0	0	0	0		
1.11	TO	0.0355	8.85-3	0.0168	0.0244	0.0382	0.0335	4.2303	0.0110	0.0193	0.0311	0.0274	0	0.0457	0.0348	
1.67	EB	0.20	0.0177	0.0597	0.0761	0.0814	0.0674	8.42-3	0.317	0.0595	0.096	0.108	1.86-3	0.0393	0.0170	
2.17	ST	0	0.0279	0.0326	0.0325	0.0362	0.0295	0.019	0.0374	0.0449	0.040	0.0355	0.0365	0.0806	0.0930	
3.60	Ph	0.1972	0.0242	0.0578	0.141	0.143	0.173	0.096	0.0871	0.1636	0.211	0.1948	0.0787	0.227	0.150	
6.99	BP	0	0	0	0	0	0	0	0	0	0	0	0	0		
8.80	PE	0	0	0	0	0	0	0	0	0	0	0	0	5.44-5		
9.20	OPM	0	0	0	0	0	0	0	0	0	0	0	0	2.98-4	3.02-4	
9.70	PT	0	0	0	0	0	0	0	0	0	0	0	0	1.99-4	1.51-4	
10.02	BB	0	0	0	0	0	0	0	0	0	0	0.0119	1.99-4	3.21-4	6.87-3	
10.60	PP	0	0	0	0	0	0	0	0	0	0	0	0	3.21-4	6.87-3	
11.21	BPPE	0	0	0	0	0	0	0	0	0	0	0	0	6.01-3	0	
11.79	PPE	0.5343	0.9184	0.8141	0.461	0.6247	0.476	6.55-4	2.03-3	5.53-3	7.95-3	4.87-3	2.03-3	0	0.0130	
12+	DIM	0.0151	0	0.0178	0.256	0.0751	0.280	0.9378	0.8308	0.7040	0.6107	0.6152	0.8794	0.15859	0.6840	



MOL FRACTIONS: PPE

RT COMPOUND	T=400, PPE <sub>0</sub> =0.83, S=1.48					T=400, PPE <sub>0</sub> =0.25, S=4.92					T=400, PPE <sub>0</sub> =0.083, S=14.76				
	20	Min	25	5	10	16	20	25	15	20	25	15	20	25	
0.74 BE	1.90-3	2.83-3	0	0	0	0	0	5.13-3	0	0	0	0	0	0	
1.11 TO	0.041	0.0513	0.0118	7.56-3	0.0265	0.0335	0.0346	5.79-3	0.0137	0.0171	0.0346	5.79-3	0.0137	0.0171	
1.67 EB	0.088	0.0978	0.0316	0.0382	0.111	0.145	0.177	0.0182	0.046	0.048	0.177	0.0182	0.046	0.048	
2.14 ST	0.0171	0.0203	0.0446	0.0210	0.0222	0.0102	4.47-3	8.58-3	0.013	0.018	4.47-3	8.58-3	0.013	0.018	
3.60 Ph	0.249	0.263	0.0505	0.0525	0.1920	0.213	0.247	0.455	0.41	0.32	0.247	0.455	0.41	0.32	
6.99 BP	0	0	0	0	0	0	0	0	0	0	0	0	0	0	
8.80 PE	0	0	0	0	0	0	0	0	0	0	0	0	0	0	
9.20 DPM	0	0	0	0	0	0	0	0	0	0	0	0	0	0	
9.70 PT	1.66-3	2.19-3	0	0	0	0	0	0	0	0	0	0	0	0	
10.02 BB	8.76-4	1.50-3	0	0	0	0	0	0	0	0	0	0	0	0	
10.60 PP	0	0	0	0	0	0	0	0	0	0	0	0	0	0	
11.21 BPE	0.0114	0.0143	0	6.39-4	7.76-4	2.15-3	0	0	0	0	2.15-3	0	0	0	
11.79 PPE	0.5021	0.4081	0.8598	0.8776	0.6423	0.594	0.525	0.37	0.40	0.45	0.525	0.37	0.40	0.45	
12+ DIM	0.066	0.1162	0	0	0	0	0	0	0	0.036	0	0	0	0.036	

RT	COMPOUND	MOL FRACTIONS: PPE																	
		T=400, PPE <sub>0</sub> =0.25, S=0.492		T=400, PPE <sub>0</sub> =0.25, S=1.48		T=400, PPE <sub>0</sub> =0.25, S=4.92		T=400, PPE <sub>0</sub> =0.25, S=1.48		T=400, PPE <sub>0</sub> =0.25, S=4.92									
		5	10	15	20	25	5	10	15	20	25	5	10	15	20	5	10	15	20
0.74	BE	0	0	1.17-3	2.30-3	4.35-3	0	0	0	1.52-3	3.14-3	0	0	0	0	0	0	0	0
1.11	TO	6.94-3	0.0146	0.025	0.0372	0.0485	7.38-3	0.0149	0.0282	0.042	0.0582	8.69-3	0.0221	0.0302	0.0330	0.0221	0.0302	0.0330	0.0330
1.67	EB	8.33-3	0.0141	0.047	0.096	0.145	7.85-3	0.0222	0.0273	0.043	0.0678	6.13-3	4.61-3	0.0720	0.1145	0.0678	0.0720	0.1145	0.1145
2.17	ST	0.026	0.0484	0.055	0.044	0.0298	0.0344	0.0546	0.0715	0.0752	0.0708	0.022	0.0602	0.0182	0.0180	0.0602	0.0182	0.0180	0.0180
3.60	Ph	0.0476	0.0865	0.135	0.1974	0.250	0.050	0.1064	0.1571	0.187	0.234	9.39-3	0.0777	0.1095	0.1952	0.0777	0.1095	0.1952	0.1952
6.99	BP	0	0	0	0	1.54-3	0	0	0	0	0	0	0	0	0	0	0	0	0
8.80	PE	0	0	0	0	4.35-4	9.35-3	0	0	0	4.407-3	0	0	0	0	0	0	0	0
9.20	DPH	0	0	0	1.67-4	0	0	0	0	0	0	0	0	0	0	0	0	0	0
9.70	PT	0	0	0	0	0	0	0	0	0	0	0	0	0	0	0	0	0	0
10.02	BB	0	3.08-4	1.16-3	1.94-3	2.39-3	0	0	1.22-3	1.79-3	2.10-3	0	0	0	0	0	0	0	0
10.60	PP	0	0	0	0	0	0	0	0	0	0	0	0	0	0	0	0	0	0
11.21	BPE	0	1.82-3	3.48-3	6.9-3	7.07-3	0	1.92-3	6.12-3	0.0102	0.0146	1.80-3	0	0	0	0	0	0	0
11.79	PPE	0.9012	0.8274	0.7253	0.6137	0.5096	0.8624	0.7872	0.6686	0.5649	0.4626	0.9495	0.7915	0.7411	0.6350	0.7915	0.7411	0.6350	0.6350
12+	DIM	9.47-3	6.78-3	4.64-3	0	0	0.0268	0.0104	0.0376	0.0723	0.081	0	0.0389	0.0261	0	0.0389	0.0261	0	0





## MOL FRACTIONS: GUAIACOL

$G_0$	T	t	P/ $G_0$	C/ $G_0$	G/ $G_0$	$CH_4/G_0$	$CO/G_0$
0.45	250	40	4.45-4	4.46-3	0.9955	-	-
		60	4.45-4	6.64-3	0.9929	-	-
		80	4.46-4	5.66-3	0.9939	-	-
		100	4.46-4	7.54-3	0.9920	-	-
0.45	300	10	0	4.91-4	0.9995	-	-
		20	1.50-4	2.99-3	0.9968	-	-
		30	2.72-4	6.03-3	0.9937	-	-
		40	3.42-4	6.75-3	0.9930	-	-
0.45	450	0.5	0	0	1	0	0
		0.5	0	0	1	-	-
		1	3.40-4	1.34-2	0.9862	8.79-3	4.71-4
		1	0	0	1	-	-
		1.5	1.19-3	1.97-2	0.9791	1.83-2	8.46-3
		1.5	0	0	1	-	-
		2	3.49-2	0.181	0.7839	7.69-2	1.16-2
		2	3.60-2	0.342	0.6620	-	-
		2.5	4.68-2	0.297	0.6559	6.79-2	9.06-3
		2.5	5.21-2	.690	0.2571	-	-
		0.25	0	0	1	-	-
		0.5	0	0	1	-	-
0.45	500	0.75	6.58-4	1.19-2	0.9874	-	-
		1	1.16-2	1.26-1	0.8674	-	-
		0.17	0	0	1	-	-
		0.33	0	0	1	-	-
0.45	525	0.67	3.09-3	5.43-2	0.9426	-	-
		0.83	1.08-2	1.54-1	0.8355	-	-

MOL FRACTIONS: GUAIACOL

$G_0$	T	t	$P/G_0$	$C/G_0$	$G/G_0$	$CH_4/G_0$	$CO/G_0$	$-\ln G/G_0$
0.45	350	4	5.57-4	1.36-2	0.9858	9.24-3	-	1.43-2
		8	2.40-3	2.47-2	0.9729	1.66-2	4.03-3	2.75-2
		2	0	0	1	0	0	0
		4	5.97-4	3.63-3	0.9958	6.32-3	2.65-3	0.00424
		6	1.23-3	1.21-2	0.9867	1.39-2	3.20-3	0.0134
		8	2.37-3	1.18-2	0.9858	1.96-2	2.89-3	0.0143
		10	3.28-3	1.78-2	0.9789	2.63-2	3.20-3	0.0213
		12	3.24-3	2.35-2	0.9733	2.24-2	4.56-3	0.0271
0.75	300	16	5.89-3	3.24-2	0.9617	3.07-2	4.48-3	0.039
		20	8.39-3	4.74-2	0.9444	3.46-2	4.03-3	0.0572
		2	0	8.21-3	0.9918	2.75-3	1.61-3	0.00823
		4	4.18-4	8.61-3	0.9910	1.03-2	2.88-3	0.009041
		6	1.14-3	1.06-2	0.9883	1.75-2	3.50-3	0.0118
		8	1.86-3	1.55-2	0.9826	1.58-2	3.24-3	0.0176
		10	6.66-3	1.71-2	0.9763	2.3-2	3.14-3	0.0240
		2	0	0	1	0	0	0
1.05	350	4	1.63-4	5.24-4	0.9993	8.16-4	9.85-4	6.87-4
		6	1.60-3	1.36-3	0.9970	1.39-3	9.48-4	2.96-3
		8	3.57-3	1.25-3	0.9905	1.19-2	1.46-3	1.0-2
		10	4.87-3	1.19-2	0.9844	1.59-2	1.12-3	1.57-2
		2	0	1.99-3	0.9980	1.12-3	7.09-4	2.00-3
		4	2.75-4	2.04-3	0.9977	6.18-3	1.36-3	2.31-3
		6	9.76-4	7.28-3	0.9917	8.32-3	1.63-3	8.33-3
		8	2.24-3	9.96-3	0.9878	9.45-3	1.38-3	0.0123
		10	1.82-3	1.59-2	0.9823	1.35-2	1.99-3	0.0179
		4	1.16-3	3.80-3	0.9950	-	-	7.63-3
		8	5.72-3	1.20-2	0.9882	-	-	0.0119
		12	9.23-3	1.87-2	0.9720	-	-	0.0284
1.50	350	16	1.14-2	2.56-2	0.9630	-	-	0.0377
		20	1.41-2	2.78-2	0.9580	-	-	0.043

## MOL FRACTIONS: GUAIACOL

G <sub>0</sub>	T	t	P/G <sub>0</sub>	C/G <sub>0</sub>	G/G <sub>0</sub>	CH <sub>4</sub> /G <sub>0</sub>	CO/G <sub>0</sub>	-1nG/G <sub>0</sub>
3	350	4	1.27-3	3.93-3	0.9948	-	-	5.21-3
		8	3.39-3	7.96-3	0.9886	-	-	0.0115
		12	5.45-3	1.47-2	0.9799	-	-	0.0203
		16	1.02-2	2.02-2	0.9698	-	-	0.0307
		20	1.33-2	2.93-2	0.9574	-	-	0.0435
3	350	2	6.55-6	-	1	0	-	0
		4	5.21-4	2.67-3	0.9968	3.82-3	2.57-4	3.20-3
		6	4.07-4	1.66-3	0.9979	3.79-3	3.46-4	2.10-3
		8	4.11-4	3.14-3	0.9965	6.86-3	3.01-4	3.56-3
		10	1.66-3	6.83-3	0.9915	7.09-3	3.75-4	5.01-3
		5	5.7 -4	4.10-3	0.9953	2.68-3	3.54-3	
		10	1.68-3	9.02-3	0.9893	1.05-3	5.12-3	
		15	5.09-3	1.57-2	0.9792	1.65-2	4.11-3	
		20	7.94-3	2.99-2	0.9662	2.81-2	5.39-3	
		25	1.02-2	4.32-2	0.9446	3.83-2	3.84-3	
		5	7.48-4	1.94-3	0.9973	2.20-3	1.22-3	
		10	3.14-3	1.03-2	0.9860	1.20-2	3.79-3	
		15	9.43-3	1.61-2	0.9747	1.93-2	3.37-3	
		20	1.09-3	1.82-2	0.9712	1.87-2	2.56-3	
		25	1.03-2	1.87-2	0.9710	1.59-2	2.44-3	
		5	0	0	1	0	-	
		10	2.28-3	2.34-3	0.9959	2.42-3	5.32-4	
		15	5.81-4	-	0.9994	5.55-4	0	
		20	5.44-3	4.55-3	0.9900	6.90-3	1.44-3	
		20	2.96-3	4.92-3	0.9921	3.93-3	6.30-4	
		20	4.20-3	4.74-3	0.9911	5.42-3	1.44-3	

MOL FRACTIONS: GUAIACOL

$G_0$	T	t	P/ $G_0$	C/ $G_0$	g/ $G_0$	CH <sub>4</sub> / $G_0$	CO/ $G_0$	-1ng/ $G_0$
0.45	400	1.25	0	1.22-2	0.9878	0	0	
		2	3.50-3	2.28-2	0.9737	2.3502	8.80-3	
		3	1.01-2	4.56-2	0.9442	4.16-2	9.45-3	
		4	2.60-2	9.46-2	0.8795	5.60-2	9.22-3	
		5	2.87-2	9.61-2	0.8751	6.30-2	9.61-3	



## MOL FRACTIONS: DMP

DMP <sub>0</sub>	T	t	CH <sub>4</sub> /DMP	CO/DMP <sub>0</sub>	G/DMP <sub>0</sub>	C/DMP <sub>0</sub>	MC/DMP <sub>0</sub>	DMP/DMP <sub>0</sub>	-lnDMP/DMP <sub>0</sub>
0.37	400	2	4.05-3	2.33-3	1.80-3	8.72-3	0.0208	0.9687	0.0318
		4	2.72-2	5.43-3	9.76-3	0.0620	0.1506	0.7776	0.2515
		2	-	-	7.96-4	2.66-3	2.88-2	0.9677	0.0328
		4	-	-	2.66-3	2.25-2	1.27-1	0.8479	0.1650
		5	-	-	1.13-2	4.60-2	0.2810	0.6677	0.4039
		6	-	-	1.58-2	6.85-2	0.2702	0.6456	0.4376
		7	-	-	1.42-2	7.36-2	0.2740	0.6381	0.4492
0.37	500	2	-	-	2.55-2	6.21-2	0.7986	0.1138	2.173
		3	-	-	1.85-2	1.22-2	0.9463	2.31-2	3.77
		4	-	-	2.54-2	0	0.8098	0.1648	1.80
		4.5	-	-	1.69-2	0	0.9513	3.17-2	3.45
		5	-	-	9.39-3	0	0.9742	1.64-2	4.11
0.37	300	5	-	-	0	0	0	1	0
		10	-	-	0	0	0	1	0
		15	-	-	0	0	4.26-3	0.9957	4.31-3
		12.5	-	-	0	0	0	1	0
		5	5.95-5	0	0	0	3.47-3	0.9965	3.47-3
		10	1.70-4	0	1.58-4	1.58-4	4.10-3	0.9956	4.42-3
		15	2.08-4	0	2.42-4	3.63-4	4.35-3	0.9950	4.97-3
		20	3.94-4	0	4.78-4	3.58-4	9.31-3	0.9899	0.0102
		30	6.04-4	0	4.20-4	7.88-4	8.83-3	0.9900	0.0101
		5.5	6.30-4	0	0	0	4.14-3	0.9959	4.11-3
		10	1.64-3	0	4.34-4	1.56-3	0.0438	0.9542	0.0469
		15	3.02-3	0	6.77-4	2.57-3	8.67-3	0.9881	0.0120
0.35	350	20	4.67-3	0	8.32-4	2.50-3	0.0384	0.9582	0.0427
		25	4.35-3	0	9.38-4	2.25-3	0.0165	0.9803	0.0199
		4	7.6-4	2.82-4	9.04-4	-	0	0.9991	9.00-4
		8	3.14-3	6.02-4	2.65-3	-	3.97-3	0.9933	6.72-3
		12	5.2-3	7.86-4	3.22-3	-	3.27-2	0.9640	3.67-2
		16	1.07-2	1.22-3	3.48-3	-	1.12-2	0.9848	1.53-2
		20	1.22-2	1.38-3	6.70-3	-	1.52-2	0.9782	2.20-2
0.37	350	2	1.47-4	7.97-4	2.09-4	1.25-3	3.75-3	0.9948	5.23-3
		5	3.56-3	1.91-3	1.13-3	4.01-3	7.41-3	0.9874	0.0126
		7	5.48-3	2.29-3	2.78-3	8.68-3	9.72-3	0.9788	0.0214
		10	1.12-3	1.13-3	3.43-3	0.0250	0.0442	0.9274	0.0754
		15	3.15-2	3.57-3	0.013-2	0.495	0.0998	0.8376	0.177
		20	6.09-2	5.17-3	9.78-3	0.0213	0.0881	0.8808	0.127
		2	0	3.15-3	0	0	0	1	0
		4	2.93-4	2.34-3	1.27-3	0	4.99-3	0.9937	6.32-3
		6	8.26-4	0	0	0	7.25-4	0.9992	8.00-4
		8	4.92-3	3.23-3	4.95-4	0	5.95-3	0.9935	6.52-3
		10	2.75-3	1.99-3	3.85-3	0	4.25-2	0.9537	4.74-2
		5	8.43-3	0	1.49-3	2.67-3	5.60-3	0.9902	9.81-3
0.37	375	10	4.98-3	0	-	-	-	-	-
		15	3.14-2	6.55-4	4.95-3	0.0285	0.174	0.792	0.233
		20	2.03-2	2.37-4	4.65-3	0.0250	0.0423	0.9280	0.0747
		3	7.59-3	2.76-3	1.26-3	5.39-3	6.90-3	0.9864	0.0136
		6	1.38-2	2.61-3	2.84-3	0.0126	0.0175	0.9669	0.0336
		9	1.50-2	1.99-3	0	0.0246	0.0448	0.9305	0.0720



## MOL FRACTIONS: ANISOLE

A <sub>0</sub>	T	t	CO/A <sub>0</sub>	CH <sub>4</sub> /A <sub>0</sub>	B	T	AN	Ph	oCr	-lnA/A <sub>0</sub>
1.57	344	5.25	0	3.14-5	0	0	0.9986	1.36-3	0	1.36-3
		10	-	-	0	0	1.0	0	0	0
		15	0	8.02-5	0	0	0.9983	1.67-3	0	1.67-3
		20	0	9.48-5	0	0	0.9975	2.50-3	0	2.50-3
		25	0	1.21-4	0	6.62-5	0.9967	3.19-3	0	3.26-3
370	5	0	1.26-4	0	0	0.9977	1.93-3	3.31-4	2.26-3	
		10	5.13-4	7.29-4	8.52-5	6.30-5	0.9944	2.46-3	2.89-3	5.52-3
		15	5.30-4	7.76-4	9.04-5	6.68-5	0.9950	2.39-3	2.55-3	5.11-3
		20	9.06-4	1.47-3	3.49-4	2.06-4	0.9896	3.65-3	6.15-3	0.0104
		25	-	1.13-3	2.58-4	1.52-4	0.9931	2.73-3	3.80-3	0.0070
406	5	0	4.0-5	1.33-3	6.88-4	0.9873	0.0107	0	0.0128	
		10	6.59-4	5.71-3	1.66-3	1.88-3	0.9781	0.0139	4.45-3	0.0221
		15	3.16-3	8.32-3	4.87-3	5.02-3	0.9525	0.0300	7.51-3	0.0486
		20	5.36-3	1.15-2	2.24-3	4.14-3	0.9499	0.0351	8.63-3	0.0514
		25	1.54-2	3.33-2	0.0111	0.0108	0.9252	0.0409	0.0121	0.0777
434	4	8.25-3	1.33-2	0.0166	6.34-3	0.9116	0.0530	0.0124	0.0925	
		8	0.0147	0.0204	0.0353	0.0134	0.8680	0.0685	0.0149	0.1416
		12	0.0148	0.0193	0.036	0.0142	0.8467	0.0794	0.0236	0.166
		16	0.0213	0.0246	0.057	0.024	0.802	0.0972	0.0203	0.2206
		20	0.0183	0.0210	0.0796	0.0255	0.7467	0.1257	0.0225	0.2921
465	3	0.0145	0.0205	0.0388	0.0105	0.8241	0.0984	0.0282	0.1935	
		6	0.0242	0.0323	0.123	0.023	0.654	0.164	0.0373	0.425
		9	0.0503	0.0706	0.166	0.023	0.551	0.214	0.0467	0.596
		12	0.0554	0.0781	0.173	0.022	0.517	0.237	0.050	0.659
		15	0.0249	0.0391	0.186	0.026	0.466	0.274	0.0487	0.765
490	3	0.0178	0.0336	0.172	0.021	0.531	0.241	0.036	0.633	
		6.5	0.0360	0.0674	0.247	0.057	0.305	0.350	0.041	1.19
		9	0.0153	0.0414	0.266	0.063	0.212	0.407	0.052	1.55
		12	0.0151	0.0438	0.322	0.056	0.092	0.485	0.046	2.39
		15	0.0267	0.0667	0.322	0.071	0.107	0.470	0.029	2.23

## MOL FRACTIONS: ANISOLE

$A_0$	T	t	$H_2/A_0$	$CO/A_0$	$CH_4/A_0$	$B/A_0$	$T/A_0$	$A/A_0$	$P/A_0$	$\sigma Cr/A_0$	$-lnA/A_0$
0.46	450	2	0	3.24-3	3.76-3	0	0	0.9869	0.01314	0	0.0132
		4	0	2.85-3	3.53-3	1.17-3	4.56-4	0.9705	0.027	7.89-4	0.030
		4	3.18-3	1.17-2	1.34-2	1.66-2	2.22-3	0.9019	0.0691	1.01-2	0.103
		6	3.11-3	1.20-3	1.67-2	1.46-2	2.02-3	0.9159	0.0612	9.23-3	0.0878
		8	5.13-3	2.21-3	2.56-2	3.21-2	6.81-3	0.8548	0.0948	0.0116	0.157
		8	7.13-3	2.66-2	2.55-2	7.89-2	1.30-2	0.7484	0.1450	1.49-2	0.29
		10	8.61-3	3.01-2	3.15-2	5.47-2	9.29-3	0.7903	0.1287	0.0170	0.24
		12	8.50-3	3.65-2	3.36-2	1.16-1	1.97-2	0.6555	0.1885	1.89-2	0.423
		16	6.60-3	2.89-2	2.59-2	1.25-1	2.28-2	0.6199	0.2130	1.89-2	0.48
		20	4.52-3	3.07-2	2.98-2	1.39-1	3.09-2	0.5848	0.1850	1.64-2	0.54
0.77	450	2	3.05-3	4.78-3	5.66-3	5.29-3	1.14-3	0.9562	0.0314	5.92-3	0.045
		4	2.95-3	1.04-2	1.31-2	2.41-2	3.58-3	0.8810	0.0744	1.69-2	0.127
		6	5.83-3	1.77-2	1.88-2	5.14-2	8.53-3	0.8075	0.1223	1.03-2	0.214
		8	3.26-3	1.81-2	1.88-2	7.85-2	2.44-2	0.7463	0.1320	1.92-2	0.293
		10	5.77-3	2.28-2	2.25-2	9.12-2	1.74-2	0.7223	0.1510	1.72-2	0.33
1.08	450	2	-	1.41-3	8.13-4	3.90-4	-	0.9896	0.0100	1.30-3	0.010
		4	2.47-3	5.34-3	7.96-3	5.81-3	1.01-3	0.9506	0.0345	8.61-3	0.051
		6	2.66-3	8.16-3	1.16-2	1.30-2	2.82-3	0.9253	0.0437	1.53-2	0.078
		8	4.57-3	2.21-2	2.78-2	3.51-2	6.82-3	0.8516	0.0820	2.45-2	0.161
		10	8.38-3	2.42-2	2.88-2	3.87-2	6.78-3	0.8400	0.0880	2.70-2	0.174
1.54	450	2	7.18-4	2.22-3	3.68-3	2.91-3	7.94-4	0.9661	0.0228	7.33-3	0.0344
		4	2.22-3	7.86-3	1.03-2	2.37-2	6.81-3	0.8844	0.0711	1.40-2	0.123
		6	1.74-3	9.39-3	1.17-2	4.43-2	5.57-3	0.8107	0.1020	3.72-2	0.210
		8	1.96-3	1.14-2	1.41-2	5.08-2	9.51-3	0.7926	0.1080	3.87-2	0.232
		10	2.15-3	1.52-2	1.97-2	7.34-2	1.67-2	0.7443	0.1290	3.71-2	0.295
3.08	450	2	4.82-4	1.14-3	2.05-3	2.22-3	3.86-4	0.9079	0.0177	8.81-3	0.0967
		4	1.37-3	5.01-3	7.36-3	2.22-3	5.83-3	0.8745	0.0645	3.29-2	0.134
		6	7.60-4	2.74-3	3.03-3	2.85-2	7.83-3	0.8484	0.1029	1.25-2	0.164
		8	6.30-4	6.89-3	1.20-2	5.77-2	2.28-2	0.7743	0.1100	3.52-2	0.256
		10.5	2.66-3	2.25-2	4.87-2	6.61-2	2.87-2	0.7478	0.1170	3.98-2	0.291
		25	6.10-4	1.94-3	1.88-3	1.64-1	1.25-2	0.5678	0.2269	2.90-2	
0.43	340	5	1.47-4	3.54-4	4.23-4	3.94-2	2.91-3	0.8524	0.0895	1.57-2	
$V_r=10.6$		10	3.23-4	9.39-4	8.91-4	3.54-2	3.10-3	0.8021	0.1393	2.01-2	
		15	4.00-4	1.56-3	1.44-3	1.09-1	1.41-2	0.6914	0.1667	1.92-2	
		20	3.87-4	1.27-3	1.19-3	9.23-2	9.30-3	0.6834	0.1857	2.93-2	
0.46	550	2				4.31-1	2.43-2	0.0540	0.4783	1.33-2	
		6				4.64-1	2.25-2	0.0000	0.5025	1.10-2	
		3				3.63-1	2.74-2	0.0176	0.4629	1.29-1	
		5				4.48-1	1.91-2	0.0009	0.5232	9.50-3	
		4				0.428	0.0231	0.0167	0.5248	7.03-3	

MOL FRACTIONS: VERATROLE

Vo	T	t	CO/VO	CH <sub>4</sub> VO	MeOH	B	ToI	Xy <sup>I</sup> <sub>I</sub>	Xy <sup>I</sup> <sub>II</sub>	An	Ph	OCr	G	V	C	D
(0.33	425)															
		12	-	-	0.046	0.046	0.068	0.00297	0.00180	0.0975	0.0311	0.072	0.144	0.384	0.073	0.010
	375	10	-	-	0.0021	0	0.00279	0	9.88-5	0.00107	0.00159	0	0.0114	0.9810	0	0
		15	-	-	0.00145	0	0.00635	0	2.22-4	0.00314	0.00366	0.00231	0.027	0.956	0	0
		20	-	-	0.00287	0	0.00462	0	2.25-4	0.00345	0.00449	0.00297	0.0294	0.9520	0	0
		25	-	-	0.0121	0	0.00958	3.54-4	0	0.00698	0.00535	0.00526	0.0443	0.916	0	0
		30	-	-	0.0123	0	0	0.00511	3.35-4	0.00699	0.00614	0.00242	0.0338	0.927	0	0
	350	5	1.95-3	0	0.00268	0	0	0	0	0	0	0	0	0.9973	0	0
		10	3.49-3	2.51-3	0.00258	0	0	0	0	0	0	0	0	0.9974	0	0
		15	4.14-3	4.45-3	0.00287	0	0	0	0.00336	1.84-4	3.57-4	0	0.00173	0.9945	0	0
		20	4.09-3	5.23-3	0.00245	0	0	0	0	1.71-4	5.44-4	0	0	0.9968	0	0
		25	5.03-3	6.91-3	0.00232	0	0	5.29-4	0	3.21-4	6.24-4	0	0.00326	0.9929	0	1.10-5

MOL FRACTIONS: VERATROLE																
Vo	T	t	CO/V <sub>0</sub>	CH <sub>4</sub> /V <sub>0</sub>	MeOH	B	Tol	Xy <sup>1</sup> I	Xy <sup>1</sup> II	An	Ph	oCr	G	V	C	D
0.33	550	2	0.030	0.049	0.0773	0	0.0314	0	0.0038	0.12	0.13	0.27	0	0.0752	0.214	0.0748
	3	0.186	0.300	0.083	0	0.0381	0	0.0099	0.123	0.214	0.297	0	0.0012	0.204	0.0294	
	4	0.145	0.215	0.0767	0.0303	0.0438	0	0.0083	0.069	0.253	0.312	0	0.00251	0.166	0.0390	
	5	0.132	0.213	0.1598	0	0.035	0	0.0038	0.058	0.248	0.316	0	0.00353	0.147	0.028	
	6	0.153	0.254	0.0960	0	0.030	0	0.0005	0.069	0.260	0.337	0	0.00030	0.133	0.069	
0.33	500	805	-	-	0.021	0	0.011	0.000621	0	0.0322	0.0079	0.0113	0.102	0.720	0.090	0.00492
	1005	-	-	-	0.0458	0.052	0.033	0.0028	0.00323	0.16	0.078	0.048	0.16	0.31	0.095	0.0114
	2.5	0.135	0.23	0.0977	0.0331	0.0635	0.00442	0.00362	0.134	0.161	0.262	0	0.0556	0.167	0.018	
	4	0.122	0.205	0.147	0	0.0181	0.00118	0.108	0.206	0.340	0	0	0	0.180	0	
	6	0.128	0.196	0.179	0	0.011	0.00147	0.043	0.224	0.395	0	0	0	0.147	0	
	8	0.179	0.28	0.160	0	0.013	0.00159	0.043	0.254	0.344	0	0	0	0.181	0.00452	
	10	0.15	0.24	0.064	0.034	0.050	0.00714	0.00635	0.064	0.320	0.325	0	0	0.120	0.00992	
0.33	450	1.5	-	-	0.00692	0	0.00372	0	0.00228	0.00193	0	0.0127	0.961	0	0.120	0.00992
	2	-	-	-	0.0155	0	0.00496	0.00023	0.00699	0.00423	0.00376	0.037	0.927	0	0	0.0113
	2.5	-	-	-	0.00781	0	0.0179	0.00167	0	0.0282	0.00746	0.0224	0.118	0.779	0.0178	0
	3	0.0411	0.0699	0.0128	0	0.0112	0	0.00152	0.0292	0.0322	0.0194	0.1194	0.6882	0.0794	0.00662	
	7.5	0.130	0.2168	0.043	0.0245	0.0327	0.0027	0.00096	0.133	0.117	0.082	0.141	0.308	0.112	0.00409	
	10	0.1057	0.189	0.064	0	0.0373	0.00420	0.00570	0.138	0.148	0.112	0.119	0.230	0.127	0.0141	
	12	0.1161	0.223	0.066	0	0.0388	0.000178	0.00261	0.163	0.214	0.174	0.079	0.086	0.161	0.024	
	15	0.1049	0.193	0.070	0.002630	0.0406	0.00179	0.00197	0.157	0.239	0.243	0	0.022	0.186	0.0364	
0.33	400	4	7.84-3	0.0131	0.00351	0	0.00113	5.3E-5	7.78-4	9.02-4	0	0.00644	0.9871	0	0	
	8	0.010	0.0202	0.0269	0	0	0.00163	1.68-4	1.63-3	2.06-3	0.00120	0.0145	0.9519	0	0	
	12	0.5317	0.0609	0.00516	0	0.003170	4.42-4	6.83-3	6.44-3	0.00368	0.0383	0.9360	0	0	0	
	16	0.0423	0.0735	0.0102	0	0	0.00150	7.96-4	0.0157	0.0051	0.0646	0.8876	0	0	0	
	20	0.0534	0.0893	0.0144	0	0.0120	0.00964	9.64-4	0.0336	0.0374	0.0145	0.0947	0.7915	0	0	
	4	-	-	0.00721	0	0.0123	0	8.84-4	0.0102	0.00509	0.00775	0.056	0.901	0	0	
	6	-	-	0.0193	0	0.0195	0	0.00154	0.0282	0.00956	0.0150	0.0862	0.824	0	0.0031	
	8	-	-	0.0186	0	0.041	0.00218	0.00119	0.0548	0.0234	0.0431	0.1333	0.641	0	0.036	0.00551
	10	-	-	0.0156	0.0596	0.062	0.00438	0.00191	0.0814	0.0222	0.0585	0.16	0.46	0	0.072	0.00443

## MOL FRACTIONS: SALIGENOL

T	S <sub>0</sub> (mol/l)	t	H <sub>2</sub> O/HBA <sub>0</sub>	oCR/HBA <sub>0</sub>	HBA/HBA <sub>0</sub>	[H <sub>2</sub> O/HBA <sub>0</sub> - (H <sub>2</sub> O/HBA <sub>0</sub> ) <sub>0</sub> ]	1 - $\frac{\text{HBA}}{\text{HBA}_0}$	-ln HBA/HBA <sub>0</sub>
200	1.25	.5	0.24	5.28-3	0.560	-	0.44	0.58
200	1.25	1	0.13.8	1.62-3	0.839	-	0.161	0.18
200	1.25	3	0.263	7.07-3	0.349	-	0.651	1.05
225	0.265	1	0.691	1.38-3	0.9741	0	0.026	0.026
225	0.243	2	1.08	0.0112	0.276	0.36	0.72	1.29
225	0.252	2.5	1.24	7.22-3	0.022	0.52	0.978	3.82
225	0.28	3	2.17	4.89-3	1.28-3	1.41	0.9987	6.66
175	0.292	3	0.805	3.21-3	1.11	0.085	0	0.104
175	0.268	6	0.962	3.33-3	0.397	0.24	0.603	0.923
175	0.238	9	1.24	7.38-3	0.541	0.52	0.46	0.614
175	0.278	12	1.14	9.89-3	0.264	0.42	0.74	1.33
175	0.302	18	1.23	9.13-3	0.188	0.51	0.81	1.67

## BENZALDEHYDE PRODUCT SPECTRA: MOL PERCENT

Vr	T	BA <sub>0</sub>	t	CO/BA <sub>0</sub>	B/BA <sub>0</sub>	P/BA <sub>0</sub>	BA/BA <sub>0</sub>	D/BA <sub>0</sub>
10.6	400	0.47	6	tr	0	0	0	0
				tr	0	0	0	0
			8	5.80-2	6.03-2	2.38-2	0.9342	3.11-3
				5.54-2	5.10-2	2.61-3	0.9464	0
			10	2.34-3	6.75-2	2.91-2	0.9033	0
				5.34-3	-	-	-	-
				4.04-2	2.99-2	2.84-3	0.9673	0
			15	3.96-2	3.24-2	2.53-3	0.9650	0
				6.80-2	6.04-2	4.02-3	0.9356	0
				6.31-2	6.60-2	4.04-3	0.9241	5.74-3
			20	7.24-2	9.16-2	5.71-3	0.9026	0
				-	7.87-2	4.85-3	0.9164	0
			25	0.1680	0.1890	0.0236	0.7871	0
				0.155	0.175	0.0241	0.8013	0
			30.5	0.311	0.331	0.0381	0.6310	0
				0.300	0.418	0.0437	0.5378	0
			17	0.135	0.138	0.0149	0.8462	0
-	0.149	0.0154		0.8357	0			
0.6	400	0.164	7	4.48-3	0.0152	5.71-4	0.7353	.25
				-	5.65-3	5.77-4	0.8493	.144
0.6	400	.492	9	2.43-2	0.0152	0	0.9811	3.66-3
				2.0-2	3.30-2	1.82-3	0.9652	0
0.6	400	.492	4	-	1.96-2	0	0.9570	2.10-2
				1.89-2	1.83-2	9.09-4	0.9808	0
0.6	400	.492	6	-	1.76-2	0	0.9576	2.47-2
				2.46-2	6.14-2	1.20-3	0.9373	0
0.6	400	.492	8	-	6.90-2	3.90-3	0.9160	1.13-2
				2.95-2	7.02-2	0	0.9298	0
0.6	400	.492	10	-	8.53-2	7.12-3	0.9023	0
				5.46-2	1.34-1	7.94-3	0.8350	2.14-3
0.6	400	1.64	12	-	1.34-1	6.25-3	0.8593	1.54-4
				1.84-2	9.25-2	2.47-2	0.8809	1.95-3
0.6	400	1.64	6	-	5.27-2	8.23-3	0.9391	0
				2.11-2	1.09-1	3.30-2	0.8417	1.57-2
0.6	400	1.64	8	-	8.33-2	1.65-2	0.9002	0
				2.81-2	1.09-1	2.98-2	0.8584	2.58-3
0.6	400	1.64	10	-	1.36-1	3.18-2	0.8299	2.52-3
				3.36-2	1.85-1	4.40-2	0.7689	2.05-3
0.6	400	1.64	12	-	1.73-1	3.17-2	0.7928	2.00-3
				2.79-3	1.96-3	5.96-4	0.9930	4.48-3
0.6	400	1.64	3	2.10-3	0.0235	0.0187	0.9225	0.0352
				-	0.0232	0.0197	0.9222	0.0347
0.6	400	1.64	7	2.98-2	0.0379	0.0184	0.9377	6.01-3
				-	0.0510	0.0165	0.9271	5.40-3



## BENZALDEHYDE PRODUCT SPECTRA: MOL PERCENT

Vr	T	BA <sub>0</sub>	t	CO/BA <sub>0</sub>	B/BA <sub>0</sub>	P/BA <sub>0</sub>	BA/BA <sub>0</sub>	D/BA <sub>0</sub>	
(0.6	400	1.64)	11	2.57-2	0.097	0.0606	0.8370	5.53-3	
				-	0.120	0.058	0.817	5.87-3	
		3.28	4	1.55-2	5.82-2	2.04-2	0.9208	5.47-4	
				-	5.32-2	1.98-2	0.9252	1.69-3	
			6	1.72-2	1.39-1	5.51-2	0.8057	0	
				-	1.53-1	6.02-2	0.7592	2.77-2	
			5	4.08-2	2.50-3	1.18-3	0.9741	0.0222	
				-	3.03-3	1.36-3	0.9741	0.0215	
			7	1.65-2	0.0148	0.0108	0.9457	0.0285	
				-	0.0139	9.83-3	0.9513	0.0250	
			9	2.10-2	0.1931	0.1219	0.6810	3.98-3	
	-	0.176	0.115	0.6981	0.011				
0.6	350	0.49	10	-	0	3.04-2	0.657	0.313	
				-	0	0	0.9670	3.30-2	
			20	-	0	3.27-2	0.9673	0	
				-	0	1.55-2	0.9694	1.51-2	
			30	-	0	0	0.9960	4.03-3	
				-	0	6.69-3	0.9803	1.26-2	
			50	-	-	-	-	-	
				-	0.0130	0.0117	0.9676	7.74-3	
			60	-	0	0	0.9469	5.31-2	
				-	0	0	0.9895	1.04-2	
			450	0.49	4	0	0.1091	0.0172	0.8737
	-	7.15-2			1.33-2	0.9152	0		
6	8.25-2	0.248			6	0.7350	1.69-2		
	-	0			0	1	0		
8	7.65-3	0.4474			0	0.5526	0		
	-	0.6621			3.57-2	0.2995	2.75-3		
10	7.38-2	0.6621			3.87-2	0.2956	3.65-3		
	-	0.3605			4.58-2	0.5936	0		
12	9.06-2	0.3567			1.90-2	0.6244	0		
	-	0.6337			1.07-2	0.3556	0		
500	0.49	3			7.71-2	0.6337	1.07-2	0.3556	0
			-	0.5666	1.23-2	0.4211	0		
		4	8.75-2	0.6454	9.57-3	0.3450	0		
			-	0.5779	1.51-3	0.4206	0		
		5	8.94-2	0.7226	2.28-2	0.1644	0		
			-	0.7900	2.56-2	0.1764	8.65-3		
		6	7.80-2	0.8289	0	0.1710	4.61-4		
			-	0.7920	2.38-2	0.1808	3.32-3		
		550	0.49	3	8.36-2	0.5940	1.52-2	0.3903	4.45-4
					-	0.6107	1.38-2	0.3750	4.69-4
				3.5	8.32-2	0.7970	2.18-2	0.1806	5.87-4
	-	0.8310	1.63-2	0.1378	1.49-2				

## BENZALDEHYDE PRODUCT SPECTRA: MOL PERCENT

Vr	T	BA <sub>0</sub>	t	CO/BA <sub>0</sub>	B/BA <sub>0</sub>	P/BA <sub>0</sub>	BA/BA <sub>0</sub>	D/BA <sub>0</sub>
(0.6	500	0.49)	4	8.15-2	0.8346	1.55-2	0.1478	2.15-3
				-	0.8336	2.08-2	0.1414	4.25-3
			4.5	7.24-2	0.8860	1.82-2	9.48-2	9.68-4
				-	0.8746	2.17-2	0.1016	2.07-3
			5	7.02-2	0.8992	2.41-2	7.67-2	0
0.6	570	0.49		-	0.9063	1.96-2	7.40-2	0
			3	0.0768	0.8024	1.18-2	0.1858	0
				-	0.8131	1.22-2	0.1747	0
			3.5	0.1113	0.8588	1.46-2	0.1266	0
				-	0.8943	1.50-2	9.07-2	0
			4	5.28-2	0.8845	3.60-2	7.95-2	0
				-	0.8846	3.99-2	7.55-2	0
			4.5	0.0754	0.9363	1.78-2	4.58-2	0
				-	0.9283	1.92-2	5-25-2	0
			5	0.1051	0.9473	2.92-2	2.34-2	0
	-	0.9490	2.78-2	2.32-2	0			



MOL FRACTIONS: VANILLIN

T, C	t, min	g/V <sub>0</sub>	C/V <sub>0</sub>	V/V <sub>0</sub>	DHB/V <sub>0</sub>	P/V <sub>0</sub>	CO/V <sub>0</sub>	CH <sub>4</sub> /V <sub>0</sub>
(350)	20	6.03-1	1.01-1	0.1970	9.95-2	0	-	-
	4	1.00-3	0	0.9989	0	0	5.18-3	0
	8	3.50-2	7.30-3	0.9577	0	0	2.47-2	2.30-3
	12	7.76-2	6.75-3	0.9156	0	0	2.79-2	3.21-3
	16	3.29-1	4.40-2	0.5750	5.29-2	0	6.96-2	1.13-2
	20	3.26-1	4.87-2	0.5550	7.01-2	0	7.38-2	1.36-2
	7	4.16-2	0	0.9583	0	0	6.15-2	5.85-3
	8	1.161-2	0	0.9839	0	0	1.83-2	0
	10	9.40-2	4.72-3	0.9051	0	0	3.37-2	6.87-4
	12	1.67-1	1.80-2	0.7650	6.70-2	0	1.34-1	1.00-2
	3	1.24-2	0	0.9875	0	0	-	-
	6	5.05-2	1.22-3	0.9345	1.38-2	0	-	-
	12	6.01-1	1.07-1	0.2420	5.01-2	0	-	-
	15	7.75-1	5.54-2	0.1006	6.89-2	0	-	-
	375							

## MOL FRACTIONS: ACETEPHENONE

AP <sub>0</sub>	T,C	t,min	CO/AP <sub>0</sub>	CH <sub>4</sub> /AP <sub>0</sub>	B	T	X	P	BA	AP	-lnAP/AP <sub>0</sub>
1.42	550	3	-	-	8.47-3	3.17-3	9.66-4	1.77-4	0	0.9872	0.0129
V <sub>r</sub> =0.6 k		3	-	-	8.43-3	4.41-3	1.85-3	6.79-4	0	0.9846	0.0155
		4	-	-	-	-	-	-	-	-	-
		4	-	-	-	-	-	-	-	-	-
		6	-	-	0.0551	0.0184	0.0105	0	0	0.9160	0.0877
		6	-	-	0.0493	0.0191	0.0122	0	0	0.9193	0.0842
		8	-	-	-	-	-	-	-	-	-
		8	-	-	0.124	0.0897	0.0659	0	0	0.7201	0.3283
		10	-	-	-	-	-	-	-	-	-
		10	-	-	-	-	-	-	-	-	-
		12	-	-	0.2215	0.0922	0.0625	4.60-3	0	0.6192	0.4793
		12	-	-	0.248	0.088	0.6605	5.25-3	0	0.5978	0.5145
		4	8.18-4	3.59-5	0	0	0	0	0	1	0
1.42	400	8	1.53-3	3.08-4	8.45-4	0	5.55-4	0	0	0.9986	1.40-3
V <sub>r</sub> =0.6		12	2.42-3	4.74-4	4.29-3	2.64-4	3.29-3	2.06-3	0	0.9901	9.95-3
		16	5.15-3	4.73-3	6.61-3	4.49-4	5.56-3	4.73-3	0	0.9827	0.0175
		20	6.32-3	5.25-4	7.02-3	4.50-4	6.18-3	4.65-3	0	0.9817	0.0185
1.42	500	3	4.52-3	1.24-3	3.56-3	3.28-4	0.0225	0	0	0.9736	0.0268
V <sub>r</sub> =0.6		6	8.45-3	3.22-3	-	-	-	-	-	-	-
		9	3.19-3	1.44-3	0.0118	3.33-3	2.14-3	1.15-3	0	0.9816	0.0185
		12	0.0282	6.77-3	0.154	0.0444	0.0369	0.0131	0	0.7514	0.2858

MOL FRACTIONS: ACETOPHENONE

AP <sub>0</sub>	T, C	t, min	B	T	X	P	BA	AP	-ln AP/AP <sub>0</sub>	
0.43 V <sub>r</sub> =0.6	500	5	0	0	0.0175	0	1.92-4	0.9805	0.0196	
		5	0	0.026	0.0143	6.49-3	0	0.9534	0.0478	
		10	0.012	5.41-3	2.93-3	0	3.00-5	0.9799	0.0203	
		10	0.014	4.54-3	2.64-3	1.07-3	2.28-4	0.9779	0.0223	
		15	0	0	2.63-3	0	0	0.9974	2.63-3	
		15	0	4.70-3	4.25-3	2.06-3	1.39-3	0.9876	0.0125	
		20	0	0	0	0	0	1	0	
		20	0	0	0	0	0	1	0	
		25	-	-	-	-	-	-	-	-
		25	-	-	-	-	-	-	-	-
		25	-	-	-	-	-	-	-	-
		0.43 V <sub>r</sub> =0.6	550	3	4.27-3	1.00-3	0	6.41-4	0	0.9941
3	4.89-3			1.17-3	5.71-4	0	0	0.9934	6.66-3	
4	0.123			3.27-3	1.06-3	1.54-4	0	0.9832	0.0169	
4	8.71-3			3.28-3	7.26-4	6.61-4	3.72-4	0.9863	0.0138	
6	0.023			7.72-3	2.60-3	1.06-3	1.06-3	0.9647	0.0360	
6	0.025			7.93-3	2.59-3	1.13-3	3.00-4	0.9632	0.0375	
8	0.050			0.020	3.58-3	5.35-4	6.38-5	0.9258	0.0771	
8	0.049			0.020	3.03-3	4.28-4	0	0.9272	0.0755	
10	0.0556			0.028	0.0122	3.45-4	0	0.9040	0.101	
10	0.076			0.029	0.010	2.09-3	0	0.8827	0.125	
12	0.095			0.0386	0.0147	3.41-3	7.88-5	0.8482	0.165	
12	0.092			0.037	0.015	3.01-3	0	0.8535	0.158	
0.143 V <sub>r</sub> =0.6	550	4	0	0	0.0194	0	0	0.9806	0.0196	
		4	-	-	-	-	-	-	-	
		6	-	-	-	-	-	-	-	
		6	-	-	-	-	-	-	-	
		8	0.0447	0.020	0.0172	0	0	0.9181	0.0855	
		8	0.044	0.023	0.014	0	3.59-4	0.9180	0.0856	
0.143mol/1	550	10	0.0681	0.0314	0	0	0.9005	0.1048		
		10	0.0817	0.0361	8.27-3	0	0.8739	0.1348		
		12	0.0876	0.0324	0.0219	0	0.8580	0.1531		
		12	0.0841	0.0346	0.0200	0	0.8613	0.1493		
		12	-	-	-	-	-	-	-	
		12	-	-	-	-	-	-	-	

## MOL FRACTIONS: ACETEPHENONE

AP <sub>0</sub>	T.C	t, min	CO/AP <sub>0</sub>	CH <sub>4</sub> /AP <sub>0</sub>	B	T	X	P	BA	AP	-lnAP/AP <sub>0</sub>	CO/BTX
0.0404	400	10	1.26-4	1.45-4	1.25-4	5.01-5	0	4.35-4	0	0.9994	6.11-4	0.72
V <sub>r</sub> =10.6		10	6.13-5	1.32-4	2.50-4	0	0	4.81-5	0	0.9997	2.98-4	0.25
		15	-	-	-	-	-	-	-	-	-	-
		15	-	-	-	-	-	-	-	-	-	-
		20	-	-	-	-	-	-	-	-	-	-
		20	-	-	-	-	-	-	-	-	-	-
		25	2.58-3	1.44-3	6.32-4	3.47-4	0	6.77-4	0	0.9983	1.67-3	2.63
		25	-	-	1.99-3	2.56-4	0	2.22-4	0	0.9975	2.47-3	-
		30	5.22-4	2.11-4	0	3.99-4	0	5.37-4	0	0.9991	9.37-4	1.31
		30	3.69-4	1.96-4	-	-	-	-	-	-	-	-
.404	500	6	2.90-3	1.49-3	2.13-3	3.61-4	1.78-4	1.78-4	0	0.9971	2.86-3	1.09
V <sub>r</sub> =10.6		6	2.77-3	1.42-3	1.22-3	4.37-4	3.58-4	3.00-4	1.36-4	0.9975	2.45-3	1.37
		12	3.59-3	2.26-3	5.04-3	1.79-3	9.48-4	5.05-4	0	0.9917	8.32-3	0.46
		12	9.65-3	3.76-3	-	-	-	-	-	-	-	-
		24	0.0149	6.35-3	0.0157	5.88-3	2.40-3	0	0	0.9760	0.0243	0.62
		24	0.020	8.67-3	0.0179	4.98-3	3.13-3	3.97-4	0	0.9736	0.0268	0.77
		30	0.069	0.027	0.033	0.012	3.72-3	1.27-3	0	0.9502	0.0511	1.42
		30	0.062	0.025	0.035	0.0135	4.23-3	1.11-3	0	0.9465	0.0550	1.18
		40	0.031	0.013	0.013	4.45-3	1.65-3	6.93-4	1.42-4	0.9801	0.0200	1.62
.43	400	15	4.25-3	.339-4	0	0	0	4.24-5	5.82-4	0.9938	6.25-4	-
V <sub>r</sub> =0.6		15	-	-	-	-	-	-	-	-	-	-
		20	7.08-3	4.65-4	0	5.43-5	0	0	1.47-4	0.9998	2.01-4	-
		20	-	-	8.27-3	1.47-4	5.33-5	2.92-4	1.15-3	0.9975	2.47-3	-
		25	5.38-3	4.71-4	0	0	1.78-4	6.17-4	1.11-3	0.9981	1.91-3	-
		25	-	-	0	0	0	4.54-4	6.63-4	0.9989	1.12-3	-
		30	5.25-3	8.21-5	0	2.77-4	0	0	0	0.9997	2.77-4	-
		30	-	-	-	-	-	-	-	-	-	-
		35	5.18-3	1.69-4	0	0	0	1.17-3	4.93-4	0.9983	1.67-3	-
		35	-	-	0	3.52-4	0	2.34-4	6.08-4	0.9988	1.19-3	-

MOL FRACTIONS: ACETEPHENONE

AP <sub>o</sub>	T, C	t, min	CO/AP <sub>o</sub>	CH <sub>4</sub> /AP <sub>o</sub>	B	T	X	P	BA	AP	-1nAP/AP <sub>o</sub>	CO/BTX
.404 V <sub>r</sub> =10.6	550	6	0.0511	0.0223	0.0150	6.18-3	1.96-3	2.19-4	0	0.9766	0.0237	2.21
		6	0.0511	0.0223	0.0142	6.39-3	1.04-3	1.35-4	9.45-5	0.9781	0.0222	2.36
		8	-	-	0.0148	7.01-3	1.89-3	1.60-4	0	0.9761	0.0242	
		8	-	-	0.0205	9.45-3	2.13-3	1.07-4	0	0.9678	0.0328	
		10	0.033	0.015	0.0120	4.79-3	1.57-3	4.03-4	0	0.9812	0.0190	1.80
		10	0.032	0.015	0.0124	4.30-3	1.58-3	2.55-4	0	0.9814	0.0187	1.75
		12	0.0850	0.036	0.034	0.016	3.45-3	0	0	0.9473	0.0542	1.59
		12	0.0840	0.036	0.0393	0.0176	4.04-3	2.20-4	0	0.9389	0.6030	1.38
		16	0.0954	0.0411	0.0502	0.0214	3.98-3	1.26-4	0	0.9243	0.0788	1.26
		16	0.0940	0.0401	0.0364	0.0174	3.03-3	2.46-4	0	0.9428	0.059	1.65
1.42 V <sub>r</sub> =0.6	400	26.5	4.51-3	7.93-4	2.82-3	1.45-4	1.39-3	1.12-3	0	0.9945	5.49-3	1.04
		26.5	-	-	2.32-3	1.15-4	9.42-4	1.51.3	0	0.9951	4.89-3	
		35	8.54-3	1.91-3	5.86-3	0	1.97-3	2.54-3	0	0.9896	0.0104	1.09
		35	-	-	5.88-3	4.27-4	1.84-3	2.36-3	0	0.9895	0.0106	
		56	0.0153	7.61-3	0.0146	1.38-3	5.03-3	4.34-3	0	0.9746	0.0260	0.73
		56	-	-	0.0167	1.57-3	5.85-3	4.60-3	0	0.9712	0.0292	
		68	0.0136	0.0192	0.0109	1.18-3	4.08-3	2.99-3	0	0.9808	0.0193	0.80
		68	-	-	0.0133	1.29-3	4.61-3	3.36-3	0	0.9774	0.0228	
		83	0.0255	0.0271	0.0447	7.84-3	0.0207	5.45-3	0	0.9213	0.0820	0.177
		83	-	-	0.036	6.72-3	0.0180	5.17-3	0	0.9342	0.0681	
1.42 V <sub>r</sub> =0.6 K	550	6	0.0273	0.0125	0.079	0.026	0.012	0.012	0	0.8716	0.137	
		6	-	-	0.072	0.024	0.011	1.23-3	0	0.8915	0.115	
		9	0.0201	0.016	0.155	0.056	0.032	7.37-4	0	0.7568	0.279	
		9	-	-	0.161	0.057	0.032	2.01-4	0	0.7490	0.289	
		10	9.01-3	0.012	0.247	0.105	0.057	3.56-4	0	0.5914	0.525	
		10	-	-	0.256	0.089	0.052	3.35-4	0	0.602	0.507	
		15	0.0122	0.0165	0.331	0.116	0.058	9.07-5	0	0.494	0.705	
		15	-	-	0.340	0.117	0.060	1.25-4	0	0.483	0.728	
		20	8.72-3	0.0177	0.391	0.167	0.098	0	0	0.343	0.107	
		20	-	-	0.415	0.148	0.094	4.52-4	0	0.343	1.07	



## MOL FRACTIONS: ACETOPHENONE

AP <sub>0</sub>	T, C	t, min	B	T	X	ST	AN	BA	Cr	AP	BP	PE, DPM	DIM	-lnAP/AP <sub>0</sub>
0.43	550	3	1.72-2	7.22-3	2.17-3	1.58-3	9.03-4	5.55-4	7.78-4	0.9446	7.47-4	1.61-3	0.0226	0.0570
V <sub>r</sub>		3	1.190-2	8.12-3	2.28-3	1.48-3	7.93-4	4.06-4	4.87-4	0.9390	5.03-4	1.44-3	0.0264	0.0629
r <sub>k</sub>		6	6.27-2	2.96-2	1.21-2	4.59-3	2.82-3	1.58-3	1.48-3	0.8136	1.30-2	1.89-2	3.96-2	0.206
		6	6.34-2	2.92-2	1.18-2	4.55-3	2.81-3	1.59-3	1.82-3	0.8086	1.07-2	1.72-2	4.83-2	0.213
		9	2.41-2	1.02-2	5.59-3	2.76-3	1.48-3	8.73-4	2.33-4	0.9300	1.02-3	2.47-3	0.0212	0.073
		9	2.74-2	1.99-2	1.09-2	5.27-3	3.10-3	1.82-3	7.19-4	0.8669	2.06-3	6.17-3	0.0358	0.143
		12	0.119	5.89-2	2.73-2	7.94-3	3.16-3	1.73-3	2.07-3	0.6769	0.0127	0.0306	0.0599	0.390
		12	0.105	5.33-2	2.54-2	7.48-3	2.96-3	1.62-3	2.05-3	0.6741	0.0155	0.0424	0.0700	0.394
		13	0.120	6.17-2	3.11-2	8.15-3	3.30-3	1.85-3	1.18-3	0.6728	8.08-3	0.0255	0.076	0.396
		13	0.110	5.67-2	2.09-2	7.59-3	3.16-3	3.29-4	7.29-4	0.6643	0.0153	0.0371	0.076	0.409
0.43	500	5	3.30-3	1.56-4	8.42-4	9.57-4	4.79-4	3.19-4	0	0.9888	0	0	5.14-3	0.011
V <sub>r</sub>		5	0	0	2.97-4	8.92-4	1.69-4	0	0	0.9420	0	0	5.67-2	0.060
r <sub>k</sub>		10	8.87-3	1.99-3	6.37-4	8.81-4	3.95-4	4.74-5	1.81-4	0.9774	0	0	9.57-3	0.023
		10	8.53-3	1.89-3	6.01-4	7.55-4	2.65-4	0	0	0.9811	0	0	6.83-3	0.019
		15	2.20-3	4.27-4	8.44-3	8.54-3	1.33-3	0	0	0.9563	0	0	2.28-2	0.045
		20	0	0	0	3.15-3	3.72-3	0	0	0.9326	0	0	6.05-2	0.070
		20	0	1.33-2	0	2.90-3	2.69-3	5.0-3	4.73-4	0.7734	0	4.26-2	0.16	0.257
		25	1.33=2	4.39-3	6.58-3	4.46-3	2.79-3	4.31-4	0	0.7839	0	8.45-2	9.98-2	0.243
		25	1.70-2	4.93-3	3.52-3	1.76-3	1.26-3	5.6-3	2.82-2	0.8955	0	0	6.76-2	0.11
0.43	450	10	8.2-4	3.17-4	3.74-4	7.65-4	2.69-4	8.79-4	0	0.9903	0	0	6.23-3	9.75-3
V <sub>r</sub>		10	6.72-4	2.51-4	3.76-4	8.47-4	2.13-4	9.86-4	0	0.9898	0	0	6.88-3	0.102
r <sub>k</sub>		20	3.03-3	6.32-4	5.96-4	8.67-4	4.97-4	1.13-4	7.22-4	0.9848	0	1.28-4	8.4-3	0.015
		20	2.10-3	6.16-4	5.35-4	8.52-4	4.87-4	1.05-3	0	0.9832	0	1.38-4	1.10-2	0.015
		25	2.27-3	6.29-4	6.12-4	7.69-4	4.81-4	2.13-4	3.26-4	0.9735	0	2.48-4	2.09-2	0.027
		25	3.46-3	8.76-4	6.30-4	8.31-4	5.03-4	1.61-4	4.52-4	0.9824	0	5.19-4	1.06-2	0.018
		30	3.27-3	8.18-4	8.35-4	1.02-3	5.73-4	2.11-4	0	0.9841	0	0	8.68-3	0.016
		30	3.03-3	8.20-4	8.20-4	9.95-4	5.6104	2.22-4	3.90-4	0.9840	0	0	9.13-3	0.016
		40	9.19-3	1.87-3	1.68-3	1.54-3	2.69-4	1.31-4	1.21-4	0.9731	0	0	1.21-2	0.027
		40	4.59-3	1.29-3	1.58-3	1.24-3	7.45-4	1.49-4	0	0.9776	0	0	1.28-2	0.023
0.43	400	20	0	1.16-4	7.71-5	5.05-4	5.61-4	0	0	0.9741	0	0	0.0246	0.026
V <sub>r</sub>		20	4.13-4	1.60-4	6.43-5	4.69-4	5.45-4	0	0	0.9785	0	0	0.0199	0.022

MOL FRACTIONS: ACETOPHENONE

AP <sub>0</sub>	T,C t,min	B	T	X	ST	AN	BA	Cr	AP	BP	PE,DPM	DIM	-1mAP/AP <sub>0</sub>
(0.43	400												
V=0.6)													
	40	0	8.99-5	1.06-4	4.88-4	6.46-4	0	0	0.9888	0	0	9.84-3	0.011
	40	4.48-4	8.96-5	4.77-5	1.76-3	2.08-3	0	0	0.9758	0	0	1.98-2	0.0245
	60	4.26-3	8.16-4	6.51-3	3.12-3	8.03-3	6.51-4	0	0.8917	0	2.95-4	8.46-2	0.115
	60	3.16-3	7.82-4	1.71-3	1.95-3	9.06-3	1.22-3	0	0.8724	0	1.09-3	0.11	0.137
	80	4.81-3	9.20-4	1.25-3	2.06-3	6.24-3	5.87-4	0	0.9252	0	8.59-4	0.0581	0.078
	80	3.51-3	8.80-4	1.20-3	2.04-3	5.37-3	0	0	0.9241	0	1.12-3	0.0618	0.079
	40	1.58-3	1.33-3	1.41-3	1.41-3	7.45-4	1.10-3	0	0.9811	0	0	0.0113	0.0191
	40	1.66-3	1.41-3	1.46-3	1.46-3	7.94-4	1.46-4	8.65-4	0.9917	0	0	5.00-4	8.33-3



T(°C)	MOL FRACTIONS: CINNAMYL ALCOHOL												
	350	350	350	350	350	350	350	350	350	350	350		
t(min)	1	1.5	2	2.5	3	3	3	5	7	7	9	11	11
H <sub>2</sub> /CAL <sub>o</sub>	-	-	-	-	-	-	-	-	-	-	-	-	-
CO/CAL <sub>o</sub>	-	-	-	-	-	0	-	0	0.011	-	0.013	0.029	-
CH <sub>4</sub> /CAL <sub>o</sub>	-	-	-	-	-	-	-	-	-	-	-	-	-
C <sub>2</sub> H <sub>2</sub> /CAL <sub>o</sub>	-	-	-	-	-	-	-	-	-	-	-	-	-
H <sub>2</sub> O	-	-	-	-	-	-	-	-	-	-	-	-	-
MeOH	-	-	-	-	-	-	-	-	-	-	-	-	-
CH <sub>3</sub> CHO	-	-	-	-	-	-	-	-	-	-	-	-	-
EtOH	-	-	-	-	-	-	-	-	-	-	-	-	-
CH <sub>2</sub> O	-	-	-	-	-	-	-	-	-	-	-	-	-
T	0	0	0	0	0	0	0	0	0	0	0	0.026	4.2-3
EB	0	0	0	0	0	0	0	0	0	0	0	4.48-3	8.25-3
ST	0	0	0	0	0	0	0	0	0	0	0	3.56-3	7.15-3
AB	0	0	1.43-4	1.07-3	0	3.71-3	7.61-3	5.42-4	5.27-4	0.011	1.12-3	0.047	0.056
Ph	0	6.22-4	6.41-4	1.92-3	5.4-3	0.027	0.030	0.010	0.028	0.014	0.078	0.11	0.12
Cr	0	0	0	0	0	6.48-3	7.16-3	7.59-3	4.96-3	0.015	2.6-3	4.6-3	6.15-3
6.2	0	6.88-4	5.17-4	1.51-3	1.94-4	4.63-3	9.61-3	0.015	0.014	0.023	0.021	0.035	0.037
7.0	9.76-4	2.26-3	2.37-3	3.73-3	6.36-3	8.65-3	0.015	0.033	0.023	0.023	0.031	0.047	0.051
CAD	0	0	0	5.82-3	0.026	0	0.084	0.098	0.064	0.064	0.21	0.21	0.23
CAL	0.9990	0.9964	0.924	0.951	0.941	0.920	0.80	0.71	0.82	0.82	0.47	0.26	0.22
DTM	0	0	0.072	0.034	0.021	0.030	0.054	0.096	0.039	0.039	0.15	0.25	0.24
CAL <sub>o</sub>	1.2						0.35						



MOL FRACTIONS: CINNAMALDEHYDE

CAD <sub>0</sub>	T, C	t, min	CO/CAD <sub>0</sub>	B	T	EB	ST	Ph+OCR	6.49	6.80	7.36	CAD	D1	D2
(V <sub>r</sub> =10.6)														
		15	0.096	0	2.27-3	7.12-4	3.83-3	0.046	0	0	0	0.771	6.01-3	0.170
		21	-	6.04-3	0.071	0.024	0.016	0.204	0	0	0	0.143	0.035	0.5
		21	-	0.0744	0.107	0.015	0.030	0.23	0	0	0	0.091	0.021	0.43
		25	0.11	0	2.59-3	5.03-3	8.28-3	0.093	0	0	0	0.461	0.030	0.39
		25	0.19	2.77-3	2.27-3	5.12-3	0.011	0.094	0	0	0	0.462	0.0262	0.39
		28	-	9.31-3	0.113	0.037	0.020	0.22	0	0	0	0.072	0.037	0.50
		28	-	0	0.065	0.020	0.0126	0.184	0	0	0	0.052	0.034	0.64

## MOL FRACTIONS: CINNAMALDEHYDE

CAD <sub>0</sub>	mo/l	T,C	t,min	CO/CAD <sub>0</sub>	B	T	EB	ST	Ph+Cr	CAD	D
0.67		450	2	5.10-2	0.013	0.18	0.070	0.080	0.067	0.520	0.069
			2	-	0.019	0.21	0.076	0.085	0.10	0.511	0
			3	-	-	-	-	-	-	-	-
			3	-	-	-	-	-	-	-	-
			3.5	6.20-2	0.0240	0.38	0.14	0.0811	0.0734	0.222	0.0792
			3.5	-	0.0192	0.38	0.14	0.0835	0.071	0.217	0.0930
			4	7.70-2	0.0340	0.54	0.25	0.076	-	0.045	0.049
			4	-	0	0.60	0	0.067	0.14	0.11	0.081
			5	7.10-2	0.023	0.59	0.31	0.032	0.035	0.00079	0.00985
			5	-	0.028	0.57	0.30	0.035	0.038	0.019	0.012
0.67		400	3	0.041	0.0095	0.053	0.013	0.031	0.060	0.7760	0.057
			3	-	0.0097	0.058	0.016	0.039	0.066	0.7539	0.058
			4	0.046	0	0.014	0.0039	0.012	0.018	0.9191	0.033
			4	-	0	0.014	0.00046	0.013	0.021	0.9144	0.037
			6	0.066	0	0.54	0.21	0.049	0.12	0.0265	0.0564
			6	-	0.037	0.55	0.21	0.058	0.098	0.033	0.013
1.21		400	2	4.90-3	0	2.33-4	0	8.35-4	8.35-3	0.9906	0
			4	0.0233	0.026	0.18	0.064	0.058	0.175	0.50	0
			6	0.067	0.040	0.46	0.19	0.046	0.20	0.059	0
			8	0.098	0.039	0.50	0.21	0.030	0.144	0.081	0
1.21		350	2	9.9-4	0	0	0	0	2.6-3	0.9974	0
			4	4.8-3	0	2.9-4	0	9.9-4	6.0-3	0.9927	0
			8	1.2-2	2.9-3	7.3-3	2.1-3	6.9-3	0.051	0.9297	0
			6	1.80-2	1.2-3	2.6-3	7.5-4	4.4-3	0.031	0.9602	0
			10	1.50-2	7.3-3	2.0-2	5.7-3	0.012	0.144	0.8110	0
1.21		300	3	-	0	0	0	0	2.9-3	0.9971	0
			6	-	0	0	0	0	3.0-3	0.9970	0
			9	-	0	0	0	0	4.5-3	0.9955	0
			12	-	0	0	0	1.80-4	4.1-4	0.9994	0
			15	-	0	0	0	2.60-4	7.4-3	0.9923	0

MOL FRACTIONS: CINNAMALDEHYDE

CAD <sub>0</sub>	T, C	t, min	CO/CAD <sub>0</sub>	B	T	EB	ST	Ph+Cr	6.49	6.80	7.36	CAD	D1	D2
0.67	300	20	-	3.38-4	0	0	3.38-4	0.0303	0	0	0	0.9023	5.53-3	0.0612
		20	-	0	0	0	2.47-4	0.0344	0	0	0	0.9493	2.21-4	0.0159
		40	-	0	3.45-4	1.11-4	9.98-4	0.0254	0	0	0	0.9089	9.85.4	0.0632
		40	-	0	2.98-4	1.06-4	9.78-4	0.0233	0	0	0	0.8969	1.00-3	0.0775
		60	-	0	1.74-3	3.04-4	5.06-3	0.077	0	0	0	0.6137	0.0419	0.2510
		60	-	0	1.91-3	3.38-4	4.85-3	0.0904	0	0	0	0.5387	0.0353	0.313
		80	-	0	0.0246	5.27-3	4.35-3	0.169	0	0	0	0.4380	0.0210	0.309
		80	-	0	3.78-3	1.05-3	1.30-3	0.094	0	0	0	0.2690	0.0260	0.590
0.67	250	40	-	0	0	0	0	3.17-3	0	0	0	0.9958	0	9.98-4
		120	-	0	0	0	8.37-5	0.0214	0	0	0	0.9633	0	0.0153
		120	-	0	0	0	1.04-4	0.040	0	0	0	0.9363	0	0.0236
		150	-	0	0	0	9.73-5	0.020	0	0	0	0.9670	0	0.0133
		150	-	0	0	0	8.32-5	0.012	0	0	0	0.9748	0	0.0131



MOL FRACTIONS: CINNAMALDEHYDE

CAD <sub>0</sub> ,mol/l	T,C	t,min	CO/CAD <sub>0</sub>	B	T	EB	ST	Ph+Cr	CAD	D
1.21	250	5	-	0	0	0	0	1.9-3	0.9981	0
		10	-	0	0	0	0	2.1-3	0.9979	0
		15	-	0	0	0	0	1.9-3	0.9981	0
		20	-	0	0	0	0	2.5-3	0.9975	0
		25	-	0	0	0	0	3.1-3	0.9969	0
0.67	250	40	-	0	3.8-4	0	0	1.6-3	0.9980	0
		40	-	0	0	0	0	3.0-3	0.9970	0
		70	-	0	0	0	0	3.6-3	0.9964	0
		70	-	0	0	0	0	4.0-3	0.9960	0

MOL FRACTIONS: CINNAMALDEHYDE

CAD <sub>0</sub>	T, C	t, min	CO/CAD <sub>0</sub>	B	T	EB	ST	Ph+oCR	6.49	6.80	7.36	CAD	D1	D2
2.64	400	2	-	0	1.71-3	4.11-4	3.77-3	0.0299	4.46-3	0.0302	0	0.8239	0	0.106
		3	-	3.58-3	0.0475	0.0182	9.59-3	0.1044	0	0.0106	0	0.180	0.068	0.558
		4	-	0	0.0821	0.0324	0.0115	0.0484	0.0552	0	4.52-3	0.059	0.113	0.594
		6	-	5.97-3	0.1673	0.1043	0.0109	0.025	0.0131	0.0151	3.93-4	0.0203	0.167	0.471
		8	-	0.010	0.21	0.11	0.019	0.024	7.17-3	7.49-3	7.00-4	0.0211	0.185	0.41
		2	-	0	4.93-4	0	0	5.68-3	5.93-3	1.51-4	0.0289	0.9457	0	0.0131
		3	-	2.14-3	0.029	0.0102	0.0145	0.0920	2.93-3	0.0116	0	0.4122	0.0484	0.377
		4	-	4.90-3	0.0946	0.0394	0.0244	0.138	2.49-3	5.87-3	0	0.1545	0.0595	0.476
		6	-	0	0.172	0.072	0	0.048	0	0.0457	0.0145	0.0186	0.137	0.492
		8	-	9.37-3	0.198	0.105	0.016	0.025	0.011	0.012	2.42-4	0.019	0.186	0.42
0.40	400	2	-	0	0	2.08-3	0.016	0.025	0.016	2.43-3	0.0424	0.776	0	0.120
		3	-	0	0.0130	1.69-3	0.020	0.046	0.037	5.82-4	0.0231	0.721	0.0119	0.125
		4	-	0	0.0449	0.0141	0.0265	0.045	0.0461	9.31-3	0.0214	0.353	0.045	0.395
		6	-	0	0	0.133	0.0554	0.128	0	0.0752	4.58-3	0.154	0.067	0.383
		8	-	0	0	0.241	0.100	0.076	0	0	0.0555	0.123	0	0.40
		2	-	0	0	1.25-3	2.65-3	0.0495	0.0338	0	0.0132	0.8914	0	8.09-3
		3	-	0	0	0	0	0.0947	0.0485	0	0.0338	0.7513	0	0.0718
		4	-	0	3.55-3	0.0127	0.0448	0.194	0	0.118	0.0119	0.4391	0.011	0.165
		6	-	0	0	0	0.071	0.168	0	0.130	0.0145	0.424	0.034	0.160
		8	-	0	0.019	0	0.093	0	0	0	1.86-3	0.137	0.280	0.468
0.40	350	7	-	0	9.26-4	1.97-4	3.24-3	0.0198	0	0	0.8914	0	0.0841	
		7	-	0	1.16-3	3.18-4	3.23-3	0.021	0	0	0.8738	0	0.101	
		10	-	4.51-3	0.0338	0.010	0.021	0.182	0	0	0.315	0.0175	0.416	
		10	-	2.60-3	0.023	6.51-3	0.0142	0.187	0	0	0.284	0.0170	0.464	
		14	-	0	0.022	8.86-3	0.0133	0.160	0	0	0.337	0.0253	0.434	
		14	-	0	0.021	7.70-3	0.0119	0.204	0	0	0.339	0.0189	0.397	
		15	-	0	0	0	4.0-3	0.052	0	0	0.801	6.76-3	0.132	
		15	0.054	9.64-4	2.59-3	7.51-4	0	0	0	0	0	0	0	0

V<sub>r</sub>=10.6

MOL FRACTIONS: CINNAMYL ALCOHOL

T(°C)	300	300	300	300	300
t(min)	5	10	15	21	25
H <sub>2</sub> /CAL <sub>0</sub>	0	0	0	0	0
CO/CAL <sub>0</sub>	0	2.95-3	5.04-3	5.77-3	8.08-3
CH <sub>4</sub> /CAL <sub>0</sub>	0	0	0	0	0
C <sub>2</sub> H <sub>2</sub> /CAL <sub>0</sub>	0	0	0	0	0
H <sub>2</sub> O	7.92-3	0.646	0.051	0.070	0.067
MeOH	1.33-4	1.35-3	2.31-3	3.00-3	4.37-3
Acetaldehyde	0	1.87-4	1.82-4	2.72-4	4.09-4
EtOH	0	0	0	0	0
CH <sub>2</sub> O	0	0	0	0	0
T	0	0	0	0	0
EB	0	0	0	0	0
ST	0	0	0	0	0
AB	0	2.46-3	6.69-3	6.52-3	8.56-3
Ph	3.41-3	0.017	0.028	0.033	0.044
Cr	0	0	1.39-3	1.88-3	1.93-3
6.2	2.43-3	0	6.18-3	3.08-3	0.011
7.0	1.65-3	7.95-3	0.013	0.0152	0.018
CAD	8.51-3	0.043	0.060	0.083	0.098
CAL	0.973	0.82	0.703	0.72	0.63
D	2.92-3	0.064	0.129	0.060	0.12
CAL <sub>0</sub>					

MOL FRACTIONS: CINNAMYL ALCOHOL

T(°C)	400	400	400	400	400	400	400
t(min)	4	4	6	8	8	10	12
H <sub>2</sub> /CAL <sub>0</sub>	0	-	0	2.70-3	-	0	4.21-3
CO/CAL <sub>0</sub>	0.034	-	0.070	0.076	-	0.12	0.113
CH <sub>4</sub> /CAL <sub>0</sub>	1.19-4	-	2.87-4	1.96-4	-	7.54-4	7.45-4
C <sub>2</sub> H <sub>2</sub> /CAL <sub>0</sub>	0	-	0	1.16-3	-	2.32-3	2.35-3
H <sub>2</sub> O	0.031	0.033	0.041	0.037	0.032	0.028	0.042
MeOH	3.09-3	3.57-3	6.65-3	6.58-3	5.67-3	6.20-3	0.016
Acetaldehyde	6.50-4	7.47-4	2.13-3	2.39-3	2.67-3	2.55-3	4.83-3
EtOH	0	0	3.20-4	4.47-4	3.86-4	4.74-4	1.04-3
CH <sub>2</sub> O	0	0	0	0	0	0	0
T	0	0	0.012	0.011	7.59-3	0.013	0.023
EB	0	0	4.21-3	4.74-3	3.96-3	8.33-3	0.012
ST	2.05-3	2.04-3	9.83-3	9.12-3	7.26-3	7.40-3	0.011
AB	0.017	0.017	0.029	0.029	0.024	0.034	0.038
Ph	0.045	0.045	0.050	0.050	0.057	0.099	0.093
Cr	4.03-3	4.02-3	5.62-3	5.62-3	5.28-3	0.010	0.010
6.2	0.032	0.032	0.056	0.062	0.069	0.10	0.092
7.0	0.067	0.066	0.12	0.14	0.16	0.18	0.17
CAD	0.14	0.14	0.13	0.13	0.13	0.11	0.095
CAL	0.59	0.59	0.34	0.32	0.35	0.15	0.20
D	0.060	0.060	0.18	0.17	0.13	0.21	0.18
CAL <sub>0</sub>	0.39						

MOL FRACTIONS: CINNAMYL ALCOHOL

T(°C)	350	350	350	350	350
t(min)	4	8	12	16	20
H <sub>2</sub> /CAL <sub>0</sub>	0	0	0	0	0
CO/CAL <sub>0</sub>	3.02-3	0.0125	0.0224	0.034	0.049
CH <sub>4</sub> /CAL <sub>0</sub>	0	0	0	1.17-4	1.53-4
C <sub>2</sub> H <sub>2</sub> /CAL <sub>0</sub>	0	0	0	0	5.96-4
H <sub>2</sub> O	0.053	0.021	0.052	0.052	0.054
MeOH	2.39-3	3.42-4	4.29-3	6.53-3	7.07-3
Acetaldehyde	3.35-4	0	7.35-4	1.24-3	1.75-3
EtOH	0	0	0	0	0
CH <sub>2</sub> O	0	0	0	0	0
T	0	0	0	0	0
EB	0	0	0	0	0
ST	0	0	5.58-4	1.41-3	1.39-3
AB	6.94-3	0	0.013	0.024	0.020
Ph	0.023	0.015	0.041	0.073	0.064
Cr	3.07-3	3.65-3	3.71-3	5.47-3	5.56-3
6.2	7.60-3	0.017	0.028	0.046	0.048
7.0	0.015	0.033	0.060	0.072	0.095
CAD	0.049	0.13	0.14	0.15	0.13
CAL	0.796	0.74	0.62	0.46	0.34
D	0.044	0.038	0.035	0.10	0.23
CAL <sub>0</sub>					

MOL FRACTIONS: OHD													
T(°C)	t(min)	B	T	P	DPM	10.3	10.7	11.3	11.9	OHD	13.5	17.5	19.8
400	0	0	0	0	0	0	0	2.68-3	2.68-3	0.9973	0	0	0
	15	0	0	0.183	8.95-4	0	0	9.43-4	9.43-4	0.76	0	0	0.055
	30	0	5.33-3	0.190	8.77-4	0	0	9.81-4	9.81-4	0.66	0	2.12-3	0.14
450	50	2.79-3	0.0198	0.163	1.37-3	0	0	6.23-4	6.23-4	0.647	0	4.69-3	0.161
	80	6.14-3	0.075	0.259	2.40-3	3.59-4	0	3.48-2	3.48-3	0.645	0	6.94-3	2.02-3
	5	0	0.0183	0.129	1.11-3	0	0	0	7.57-4	0.787	0	1.40-3	0.062
500	10	6.51-3	0.092	0.235	3.50-3	0	0	6.24-4	7.64-4	0.588	0	9.76-3	0.064
	16	3	0.153	0.276	4.44-3	0	0	1.79-4	7.77-4	0.491	0	0.019	0.055
	20	365.3	0.221	0.264	4.73-3	5.85-4	0	2.25-4	7.01-4	0.441	0	0.021	0.042
500	26	5.44-3	0.246	0.284	5.93-3	7.64-4	0	2.9-4	1.47-3	0.378	0.013	0.010	0.030
	3	0	0.133	0.158	1.34-3	2.75-4	8.66-5	2.9-4	7.43-4	0.634	0	0.010	0.0611
	6	0.011	0.32	0.29	8.46-3	6.66-4	4.82-4	1.03-3	2.06-3	0.299	9.65-3	0.052	9.64-3
550	9	0.035	0.39	0.34	8.46-3	6.66-4	4.82-4	1.67-3	3.92-3	0.12	0.043	0.045	2.25-3
	12	0	0.40	0.38	7.89-3	8.65-4	1.21-4	1.21-3	3.07-3	0.13	8.04-3	0.051	0
	2	9.05-3	0.30	0.29	8.65-4	1.72-3	1.16-4	4.67-4	1.11-3	0.314	8.04-3	0.058	0.011
500	3	0.038	0.44	0.33	8.65-4	1.44-3	1.15-3	1.39-3	1.97-3	0.056	0.028	0.072	0.013
	4	0.032	0.45	0.35	9.01-4	1.44-3	1.24-3	1.44-3	2.20-3	0.051	0.038	0.057	3.40-3
	5	0.070	0.46	0.36	9.01-4	2.00-3	2.00-3	1.95-3	1.55-3	0.016	0.024	0.042	5.44-3
500	6	0.091	0.45	0.34	8.02-4	8.02-4	2.26-3	2.26-3	1.30-3	9.52-3	0.023	0.038	5.45-3
	10+	0	0.395	0.396	8.56-4	6.68-4	6.68-4	1.49-3	3.34-3	0.125	0.0117	3.18-3	0.046
	15+	0.034	0.434	0.296	8.56-4	2.59-4	2.59-4	9.79-4	2.59-3	0.279	2.25-3	0.033	2.82-3
					0.020	9.85-4	7.88-4	1.71-3	3.09-3	0.088	0.014	0.048	3.49-3

MOL FRACTIONS: PHENYL ETHER

T(°C)	t	B	Ph	PE	tr
500	90	0	2.91-2	0.9695	1.51-3
	90	0	2.30-2	0.9723	4.73-3
	90	0	2.72-2	0.9692	3.57-3
	120	0	1.60-2	0.9840	0
	120	0	1.85-2	0.9814	1.01-4
	150	0	1.80-2	0.9770	4.92-3
	150	0	2.11-2	0.9787	1.41-4
	550	10	0	2.46-2	0.9754
10		0	3.33-2	0.9667	0
20		0	2.26-2	0.9774	0
20		0	2.07-2	0.9793	0
20		0	4.50-2	0.9520	3.04-3
40		1.73-2	5.32-2	0.9258	3.60-3
50		2.53-2	7.21-2	0.8973	5.25-3
60		0	8.47-2	0.9117	3.55-3
80		6.69-2	0.146	0.7582	2.88-2
80		9.31-2	0.161	0.7126	3.32-2
100		9.95-2	0.145	0.7267	2.90-2
100		0.103	0.154	0.705	3.70-2
20		0	4.54-2	0.9506	4.06-3
40		2.60-2	5.34-2	0.9150	5.70-3
40		0	5.47-2	0.9428	2.47-3
570		7	0	3.24-2	0.9676
	10	0	2.40-2	0.9710	4.53-3
	10	0	3.36-2	0.9644	2.02-3
	15	2.96-2	8.33-2	0.8730	1.40-2
	15	2.81-2	8.13-2	0.8767	1.39-2
587	4	0	2.20-2	0.4757	2.27-3
	8.5	8.36-2	0.167	0.7304	1.92-2
	11	6.32-2	0.147	0.7642	2.58-2
	12	5.97-2	0.109	0.8180	1.36-2
	16	0.128	0.171	0.6745	2.64-2
	6.5	0	5.84-2	0.9406	1.01-3
	6.5	1.46-2	6.11-2	0.9241	1.86-4
	8	0	0.119	0.8813	0
	8	0	0.246	0.7544	0
	14	0	0.1420	0.858	0
	14	7.78-2	0.145	0.777	0
	14	7.84-2	0.155	0.766	2.11-4
	4	5.52-3	1.18-2	0.9773	5.33-3

MOL FRACTIONS: BP,BPL

T		t	B	BP
587	BP	6	0.0252	0.9748
		13.5	0.1075	0.8925
		15	0.1004	0.8996
		18	0.1911	0.8089
		23	0.1625	0.8374
550	BP	4-8 minutes, no reaction		
400	BP	2-10 minutes, no reaction		
500	BPL	5-25+ minutes, no reaction		



MOL FRACTIONS: CA

T	t	CO <sub>2</sub> /CA <sub>0</sub>	T	EB	ST	9.4	CA	DIMERS	Z <sub>i</sub> , T, EB, ST	CA <sub>0</sub> (mol/l)	Y <sub>ST</sub>	Y	X	Y <sub>CO<sub>2</sub></sub>
400	2.5	0.437	0.027	0.011	0.233	0	0.729	0	0.271	0.455	0.86	1	0.271	1.61
	3	0.500	8.20-3	0.012	0.236	3.41-3	0.715	0.026	0.256	0.34	0.83	1	0.285	1.75
	4	-	8.92-3	0.049	0.457	5.98-3	0.453	0.027	0.515	0.165	0.84	0.94	0.55	0.91
	5	0.674	0.0251	0.097	0.367	0.0172	0.460	0.034	0.49	0.225	0.68	0.91	0.54	1.25
	6	0.831	0.037	0.138	0.506	0	0.266	0.052	0.681	0.173	0.69	1	0.73	1.13
	4	0.092	0	0	0.217	0	0.783	0	0.217	0.19	1	1	0.217	0.42
	6	-	2.9-3	0	0.263	2.67-3	0.717	0.016	0.270	0.20	0.93	0.94	0.283	0.65
	10	-	9.12-3	0	0.352	3.59-3	0.613	0.022	0.360	0.23	0.91	0.93	0.39	1.03
	12	0.23	7.11-3	0.072	0.473	2.67-3	0.376	0.069	0.552	0.275	0.76	0.88	0.62	0.37
	2	0.0241	-	-	0.0175	-	0.9825	-	-	0.33	1	1	0.0175	1.37
	4	0.101	-	-	0.0711	-	0.9289	-	-	0.240	1	1	0.0711	1.42
	6	0.18	-	-	0.1331	-	0.8689	-	-	0.249	1.02	1.02	0.1311	1.37
	8	0.29	-	-	0.207	-	0.793	-	-	0.235	1	1	0.207	1.40
	10	0.36	-	-	0.567	-	0.433	-	-	0.295	1	1	0.567	0.63
300	5	0.081	0	0	0	0	1.0	0	0	0.111	1	1	0.12	0.56
	10	0.067	0	0	0.12	0	0.88	0	0.12	0.19	1	1	0.13	1.04
	10	0.135	0	0	0.13	0	0.87	0	0.13	0.32	1	1	0.2	0.65
	15	0.131	0	4.33-3	0.12	0	0.80	0	0.20	0.182	0.6	0.62	0.36	0.80
	20	0.287	0	3.21-3	0.356	0	0.641	0	0.359	0.153	0.99	1.00	0.23	1.4
	25	0	0	1.83-3	0.231	0	0.767	0	0.232	0.217	0.99	1.0	0.23	1.4
	25	0.333	0	4.45-4	0.228	0	0.772	0	0.228	0.256	1	1.02	0.23	1.4
	3	0.033	-	-	3.59-3	0	0.9964	-	-	0.244	0.99	1	0.0036	9.1
	6	0.097	-	-	-	-	-	-	-	0.197	1	1	0.0754	1.6
	9	0.12	-	-	0.0754	-	0.9246	-	-	0.244	1	1	0.082	1.77
	12	0.145	-	-	0.0818	-	0.9182	-	-	0.177	1	1	0.14	1.2
	15	0.168	-	-	0.1395	-	0.8605	-	-	0.188	1	1	-	-

$\Sigma = T+EB+ST$

$Y_{ST} = [ST/CA_0] / [1.-CA/CA_0]$

$Y = [\Sigma/CA_0] / [1.-CA/CA_0]$

$X = 1.-CA/CA_0$

$Y_{CO_2} = CO_2/CA_0 / [1.-CA/CA_0]$

MOL FRACTIONS: FERULIC ACID

T(°C)	t	CO <sub>2</sub> /FA <sub>0</sub>
200	4	0.635
	8	0.183
	12	0.321
	16	0.260
	20	0.332
	24	0.426
250	1	0.0345
	2	0.109
	3	0.156
	4	0.129
	5	0.432
	7	0.465
	300	3
6		0.393
9		0.441
12.5		0.424
15		0.418
350	2	0.375
	4	0.409
	6	0.444
	8	0.461
	10	0.334
250	5	0.309
	10	0.395
	12.5	0.293
	15	0.414
	20	0.428

<u>MOL FRACTIONS: NAPTHOIC ACID (NA)</u>				
T(°C)	CO <sub>2</sub> /1-NA <sub>0</sub>	t	CO <sub>2</sub> /2-NA <sub>0</sub>	
400	0.783	3	0.053	
	0.148	5	0.047	
	0.125	6	0.047	
	0.286	8	0.041	
	0.262	10	0.044	
	0.41	12	0.070	
	0.213	14	0.094	
	0.470	16	0.143	
	0.354	18	0.097	
	0.548	20	0.120	
	0.25	6	0.12	
	0.40	7	0.07	
	0.23	7	0.036	
	0.37	9	0.15	
	0.39	11	0.15	
	0.58	13	0.12	
	0.42	14	0.081	
	0.57	25	0.15	
	0.020	2	-	
	0.071	4	-	
	0.28	5	-	
	350	0.051	3	0.022
		0.079	5	0.029
		0.10	9	0.035
		0.096	10	0.033
0.094		13	0.040	
0.23		15	0.0793	
0.148		17	0.029	
0.176		20	0.054	
0.202		22	0.32	
0.24		25	0.047	

MOL FRACTIONS: NA

T	CO <sub>2</sub> /1-NA <sub>0</sub>	t	CO <sub>2</sub> /2-NA <sub>0</sub>
450	0.54	1	0.045
	0.260	2	0.090
	0.292	3	0.103
	0.395	4	0.222
	0.354	5	0.131
	0.547	6	0.247
	0.677	7	0.20
	0.587	8	0.41
	-	10	0.398
	-	12	0.267

## G. C. AREAS: PPE

T=300C, PPE=0.25M, S=0

RT	COMPOUND	30 Minutes		60 minutes		75 minutes	
0.74	BE	0	0	0	0	0	0
1.11	TO	0	0	0	0	0	0.0132
1.67	EB	0	9.9-3	0.012	0	0.006	0.019
2.17	ST	0.16	0.26	0.0053	0.013	0.13	0.048
3.16		0	0	0.21	0.20	0	0.312
3.60	Ph	0.40	0.34	0.44	1.25	0.16	0.71
6.99	BP	0	0	0	0	0	0
8.80	PE	0	0	0	0	0	0
9.20	DPM	0	0	0	0	0	0
9.70	PT	0	0	0	0	0	0
10.02	BB	0	0	0	0	0	0
10.60	PP	0	0	0	0	0	0
11.21	BPE	0	0	0	0	0.004	0.0037
11.79	PPE	8.14	82.9	67.0	66.4	51.0	84.0
12+	DIM	0	0	0	0	0	0
				71.1	96.1	44.0	62.0
				67.4	67.4	0	0





G. C. AREAS: PPE		(T=350, PPE=0.25, S=0)				T=500, PPE=0.75, S=0			
RT	COMPOUND	40 Min	50	1	1.5	2	2.5	3	
0.74	BE	0	0	0	0.55	0.64	1.59	1.92	
1.11	TO	0.2	0.17	0.55	0.47	0	3.33	3.8	
1.67	EB	0	0.17	0.42	0.47	0	1.52	2.18	
2.17	ST	0.97	0.85	1.25	1.5	0	6.92	6.04	
3.16		0	0.016	0.15	0	0	0.088	0.10	
3.60	Ph	1.76	1.98	1.67	1.6	0	11.2	12.11	
6.99	BP	0	0	0	0	0	0	0.18	
8.80	PE	0	0	0	0	0	0.036	0.073	
9.20	DPM	0	0.003	0	0	0	0.11	0.18	
9.70	PT	0	0	0	0	0	0.022	0.045	
10.02	BB	0.020	0.02	0.011	0.010	0	0.89	1.14	
10.60	PP	0	0	0	0	0	0.026	0.045	
11.21	BPPE	0.13	0.11	0.079	0.091	0	0.97	1.35	
11.79	PPE	58.1	54.5	60.65	57.0	73.4	61.0	54.0	
12+	DIM	0	0	0	0	0	0.17	0.20	
							0.15	1.0	



G. C. AREAS: PPE														
T=350, PPE <sub>0</sub> = 0.25, S=4.92:A														
RT	COMPOUND	10	20	30	40	50	10	20	30	42	50	T=450, PPE <sub>0</sub> = 0.25, S=4.92 :A		
		Min.										2.5	3	4
0.74	BE	0	0	0	0	0	0	0	0	0	0	0	0	0
1.11	TO	0.013	0.019	0.022	0.024	0.039	0.023	0.042	0.055	0.088	0.083	0.049	0.14	0.22
1.67	EB	0.20	0.25	0.22	0.26	0.31	0.14	0.181	0.193	0.285	0.254	0.425	1.03	1.02
2.17	ST	0.078	0.061	0.11	0.099	0.14	0.171	0.29	0.352	0.447	0.44	0.21	0.38	0.59
3.16		0.091	0.089	0.096	0.095	0.10	0.063	0.064	0.065	0.077	0.090	0.092	0.11	0.096
3.60	Ph	0.077	0.19	0.086	0.13	0.30	0.048	0.116	0.220	0.833	0.85	0.248	0.74	1.16
6.99	BP	0	0	0	0	0	0	0	0	0	0	0	0	0
8.80	PE	0	0	0	0	0	0	0	0	0	0	0	0	0
9.20	DPM	0	0	0	0	0	0	0	0	0	0	0	0	0
9.70	PT	0	0	0	0	0	0	0	0	0	0	0	0	0
10.02	BB	0	0	0	0	0	0	0	0	0	0	0	0	0
10.60	PP	0.034	0	0	0	0	0	0	0	0	0	0	0	0
11.21	BPE	0	0	0	0	0.26	0	0	0	0	0	0	0	0.027
11.79	PPE	20.07	22.22	20.4	20.2	22.0	52.75	54.07	53.49	52.05	50.9	18.4	21.79	17.26
12+	DIM	0	0	0	0	0	0	0	0	0	0	0.41	0.462	0.32
Tet	TET	62.13	64.84	60.37	60.71	62.92	42.84	42.7	42.82	43.78	44.32	58.03	58.9	57.93
6.1	NAP	0	0	0	0	0	0	0	0	0	0	0	10.96	0
9.65	IMP	0.74	0.68	0.59	0.77	0.76	0.16	0.14	0.135	0.108	0.169	0.48	0.624	0.48

G. C. AREAS: PPE  
T=400C, PPE<sub>0</sub>=0.083, S=0

RT	COMPOUND	5 Min.	10	15	20	25	5	10	15	20	25
0.74	BE	0	0	tr	0.023	0	0	0.057	0.069	0.287	0.504
1.11	TO	0.092	0.303	0.51	0.062	0.54	0.40	0.14	1.55	2.87	4.31
1.67	EB	0.20	1.03	1.52	0.443	2.12	0.24	0.96	1.22	2.63	4.27
2.17	ST	1.42	1.82	1.83	1.07	1.64	1.84	3.76	4.33	5.0	5.87
3.16		0	0.018	0.0082	0	0.025	0	0.058	0.101	0.16	0.296
3.60	Ph	1.81	3.36	3.75	2.08	4.54	2.51	6.66	8.32	12.13	17.18
6.99	BP	0	0	0	0	0	0	0	0	0	0
8.80	PE	0	0	0.17	0	0	0	0	0	0.015	0.023
9.20	DPM	0	0	0	0	0	0	0.030	0.048	0.12	0.19
9.70	PT	0	0	8.5-3	0	0.013	0	0	0	0.021	0.036
10.02	BB	0	0	0.064	0.038	0.058	0.027	0.150	0.31	0.714	1.09
10.60	PP	0	0.032	0.013	0	0.012	0	0	0	0	0
11.21	8PE	0	0.081	0.098	0.060	0.12	0.054	0.228	0.50	0.769	1.29
11.79	PPE	36.7	23.61	19.01	15.11	12.7	86.94	75.15	67.74	59.81	55.31
12+	DIM	0	0	0	0	0	0	0	0	0	0

.T=400, PPE<sub>0</sub>=0.25, S=0

G. C. AREAS: PPE		T=400, PPE <sub>0</sub> =0.83, S=0									
T=400, PPE <sub>0</sub> =0.75, S=0		T=400, PPE <sub>0</sub> =0.83, S=0									
RT	COMPOUND	4 Min.	8	12	16	5	10	15	20	25	
0.74	BE	0	0.79	0.13	0.48	0	0.071	0.23	0.32	0.22	
1.11	TO	0.54	2.20	1.99	4.25	0.48	1.40	2.87	3.58	3.20	
1.67	EB	0.23	1.54	1.38	3.1	0.17	0.86	2.08	2.95	3.03	
2.17	ST	1.85	3.34	2.63	3.1	1.87	2.72	3.27	2.91	2.85	
3.16		0	0.076	0.093	0.22	0	0.049	0.14	0.18	0.16	
3.60	Ph	2.67	8.19	8.05	13.65	1.74	6.27	11.28	12.80	11.7	
6.99	BP	0	0	0	0	0	0	0	0	0	
8.80	PE	0	0	0	0.022	0	0	0	0	0	
9.20	DPM	7.5-3	0.064	0.086	0.21	0	0.045	0.12	0.18	0.22	
9.70	PT	0	0.022	0.034	0.088	0	0	0.049	0.076	0.090	
10.02	BB	0.061	0.48	0.54	1.07	0	0.31	0.74	0.91	0.91	
10.60	PP	0	0	0	0.020	0	0	0	0	0	
11.21	BPE	0.18	1.40	1.69	2.88	0.15	0.92	2.39	2.62	2.85	
11.79	PPE	77.1	63.4	60.8	48.4	70.18	66.9	63.6	51.4	55.5	
12+	DIM	0.38	0.34	0.49	0.66	0	0	0	0	0	

G. C. AREAS: PPE

T=400, PPE<sub>0</sub>=0.83, S=1.48

T=400, PPE<sub>0</sub>=0.25, S=4.92

T=400, PPE<sub>0</sub>=0.0033, S=14.76

RT	COMPOUND	5 Min.	10	15	20	25	5	10	16	20	25	15	20	25
0.74	BE	0	0	0.024	0.028	0.045	0	0	0	0	0.037	0	0	0
1.11	TO	0.089	0.28	0.79	0.74	1.01	0.078	0.046	0.21	0.29	0.31	0.0281	0.078	0.92
1.67	EB	0.17	0.69	1.29	2.43	2.91	0.46	0.492	1.45	2.0	2.48	0.13	0.382	0.38
2.17	ST	0.48	0.67	0.88	0.39	0.50	0.37	0.16	0.22	0.11	0.050	0.052	0.091	0.12
3.16		0.50	0.57	0.60	0.54	0.59	0.082	0.091	0.12	0.11	0.12	0.87	0.85	0.77
3.60	Ph	1.59	2.95	4.67	4.9	5.57	0.465	0.45	1.73	2.07	2.46	2.35	2.48	1.83
6.99	BP	0	0	0	0	0	0	0	0	0	0	0	0	0
8.80	PE	0	0	0	0	0	0	0	0	0	0	0	0	0
9.20	DPM	0	0	0	0	0	0	0	0	0	0	0	0	0
9.70	PT	0	0	0.044	0.038	0.054	0	0	0	0	0	0	0	0
10.02	88	0	0	0.028	0.020	0.037	0	0	0	0	0	0	0	0
10.60	PP	0	0	0	0	0	0	0	0	0	0	0	0	0
11.21	BPE	0	0.076	0.28	0.26	0.352	0	0	6.33-3	8.40-3	2.40-2	0	0	0
11.79	PPE	38.9	35.7	35.19	37.1	32.52	25.99	24.4	23.28	23.51	21.48	4.47	5.70	6.05
12+	DIM	0	0.69	1.65	1.5	2.86	0	0	0	0	0	0	0	0.24
Tet	TET	46.2	53.46	49.59	49.88	46.9	71.25	54.41	59.46	58.29	58.48	74.8	71.64	76.5
6.1	NAP	0	0	0	0	0	0	8.67	11.1	11.88	13.1	0	0	0
9.65	IMP	0.055	0.056	0.298	0.24	0.43	0.61	0.35	0.56	0.49	0.43	0.074	0.097	0.082

G. C. AREAS: PPE  
T=400, PPE<sub>0</sub>=0.25, S=1.48

RT	COMPOUND	5 Min.	10	15	20	25
0.74	BE	0.0	0	0	0	0
1.11	TO	0.094	0.220	0.40	0.69	0.631
1.67	EB	0.275	0.957	1.81	3.11	3.66
2.17	ST	0.524	0.958	1.16	1.12	1.02
3.16		0.011	0	0	0	0
3.60	Ph	0.700	1.90	3.60	4.98	4.77
6.99	BP	0	0	0	0	0
8.80	PE	0	0	0	0	0
9.20	DPM	0	0	0	0	0
9.70	PT	0	0	0	0	0.341
10.02	BB	0	0	0.071	0.067	0.056
10.60	PP	0	0	0.0084	0.0067	0.0070
11.21	BPE	0.0182	0.052	0.143	0.22	0.14
11.79	PPE	52.1	42.6	36.4	33.8	35.4
12+	DIM	0	0	0	0	0
Tet	TET	40.1	40.66	40.0	38.8	40.2
6.1	NAP	0	0	0	0	0
9.65	IMP	0.705	0.661	0.513	0.45	0.341

G. C. AREAS: PPE

T=400, PPE<sub>0</sub>=0.25, S=0.245

T=400, PPE<sub>0</sub>=0.25, S=0.492

T=400, PPE<sub>0</sub>=0.25, S=1.48

RT	COMPOUND	5 Min.	10	15	20	25	5	10	15	20	25	5	10	15
0.74	BE	0	0.022	0.057	0.093	0.142	0	0	0.026	0.056	0.115	0	0	0
1.11	TO	0.26	0.754	1.42	1.67	2.06	0.17	0.38	0.69	1.12	1.59	0.11	0.23	0.48
1.67	EB	0.61	2.50	5.68	7.68	7.41	0.30	0.54	1.89	4.25	6.99	0.25	0.58	0.76
2.17	ST	0.87	1.76	2.22	1.74	2.40	0.81	1.57	1.90	1.64	1.22	0.64	1.05	1.52
3.16		0	0.044	0.0187	0.0165	0.0478	0	0	0.069	0.042	0.061	0.069	0.08	0.086
3.60	Ph	1.41	4.38	8.72	9.34	10.56	1.24	2.39	3.97	6.33	8.72	0.85	1.80	2.9
6.99	BP	0	0	0	0	0.079	0	0	0	0	0.063	0	0	0
8.80	PE	0	0	0	0	0	0	0	0	0	0.021	0.205	0	0
9.20	DPM	0	0	0	0	0	0	0	0	0.020	0	0	0	0
9.70	PT	0	0	0	0	0.0156	0	0	0	0	0	0	0	0
10.02	BB	0	0.039	0.090	0.103	0.168	0	0.010	0.040	0.073	0.098	0	0	0.026
10.60	PP	0	0	0	0	0	0	0	0	0	0	0	0	0
11.21	BPE	0	0.085	0.241	0.243	0.420	0	0.059	0.12	0.26	0.29	0	0.037	0.13
11.79	PPE	78.16	72.45	61.0	60.85	59.5	74	72	67	62.0	56.0	52.0	49.0	46.0
12+	DIM	0	0	0	0	0	0.29	0.22	0.16	0	0	0.5	0.2	0.8
Tet	TET	11.4	8.06	6.12	4.78	5.20	18.42	19.05	14.66	14.15	12.54	42.07	43.98	43.64
6.1	NAP	0	4.05	5.75	7.94	7.39	0	0	5.17	7.26	9.56	0	0	0
9.65	IMP	0.036	0.063	0.0170	0.0193	0.154	0.12	0.15	0.13	0.075	0.086	0.090	0.21	0.15

G. C. AREAS: PPE													
(T=400, PPE <sub>0</sub> =0.25, S=1.48) T=400, PPE <sub>0</sub> =0.25, S=492													
RT	COMPOUND	20 Min.	25	5	10	15	20	25	5	10	15	20	25
0.74	BE	0.023	0.050	0	0	0	0	0.12	0	0	0	0	0
1.11	TO	0.79	1.15	0.054	0.15	0.213	0.205	0.32	0.045	0.077	0.13	0.149	0.182
1.67	EB	1.26	2.05	0.056	0.2	0.9	1.2	2.8	0.387	0.641	0.84	0.854	0.799
2.17	ST	1.77	1.75	0.17	0.51	0.16	0.14	0	0.130	0.163	0.20	0.213	0.190
3.16		0.094	0.083	0.088	0.11	0.093	0.077	0.086	0.113	0.105	0.093	0.108	0.091
3.60	Ph	3.80	4.97	0.172	0.67	0.93	1.4	2.0	0.25	0.40	0.89	0.87	1.10
6.99	BP	0	0	0	0	0	0	0	0	0	0	0	0
8.80	PE	0	0.13	0	0	0	0	0	0	0	0	0	0
9.20	DPM	0	0	0	0	0	0	0	0	0	0	0	0
9.70	PT	0	0	0	0	0	0	0	0	0	0	0	0
10.02	BB	0.042	0.052	0	0	0	0	0	0	0	0	0	0
10.60	PP	0	0	0	0	0	0	0	0	0	0	0	0
11.21	BPE	0.24	0.36	0.014	0	0	0	0	0	0	0	0	0
11.79	PPE	43.0	37.0	26.94	24.52	23.85	18.11	22.0	15.65	14.88	10.35	13.45	9.77
12+	DIN	1.7	2.0	0	0.33	0.23	0	0.17	0	0.089	1.63	0.442	1.80
Tet	TET	44.96	44.36	70.41	71.01	72.05	74.65	71.41	82.46	81.42	83.5	80.89	82.88
6.1	NAP	0	0	0	0	0	0	0	0	0	0	0	0
9.65	IMP	0.11	0.114	0.20	0.15	0.05	0.03	0.026	0.0298	0.029	0	0.0267	0.0245

RT	COMPOUND	T=400, PPE <sub>0</sub> =1.66, S=0										T=550, PPE <sub>0</sub> =0.75, S=0											
		5 Min.	10	15	20	25	30	45	60	75	90	120	5 Min.	10	15	20	25	30	45	60	75	90	120
0.74	BE	0	0.17	0.31	0.58	0.64	0	0	0.16	1.38	2.52	2.76	0	0.17	0.31	0.58	0.64	0	0	0.16	1.38	2.52	2.76
1.11	TO	0.54	2.75	4.08	5.61	6.12	0	0.24	1.73	6.68	11.03	11.04	0.54	2.75	4.08	5.61	6.12	0	0.24	1.73	6.68	11.03	11.04
1.67	EB	0.28	2.34	4.21	5.72	7.13	0	0.067	0.75	4.34	8.58	8.85	0.28	2.34	4.21	5.72	7.13	0	0.067	0.75	4.34	8.58	8.85
2.17	ST	1.83	2.48	2.29	2.22	1.80	0	0.97	4.92	8.08	4.03	9.30	1.83	2.48	2.29	2.22	1.80	0	0.97	4.92	8.08	4.03	9.30
3.16		0	0.13	0.16	0.21	0.12	0	0	0.015	0.16	0.27	0.13	0	0.13	0.16	0.21	0.12	0	0	0.015	0.16	0.27	0.13
3.60	Ph	2.03	10.53	14.83	18.27	17.9	0	1.03	6.46	18.41	20.15	22.83	2.03	10.53	14.83	18.27	17.9	0	1.03	6.46	18.41	20.15	22.83
6.99	BP	0	0	0	0	0	0	0	0	0.15	0.53	0.012	0	0	0	0	0	0	0	0	0.15	0.53	0.012
8.80	PE	0	0	0	0	0	0	0	0.013	0.12	0.20	0.16	0	0	0	0	0	0	0	0.013	0.12	0.20	0.16
9.20	DPH	0	0.094	0.17	0.32	0.29	0	4.7-3	0.052	0.30	0.52	0.43	0	0.094	0.17	0.32	0.29	0	4.7-3	0.052	0.30	0.52	0.43
9.70	PT	0	0.048	0.085	0.15	0.14	0	0	4.0-3	0.094	0.25	0.16	0	0.048	0.085	0.15	0.14	0	0	4.0-3	0.094	0.25	0.16
10.02	BB	0.061	0.69	0.951	1.41	1.14	0	0.0173	0.35	2.20	1.6	1.40	0.061	0.69	0.951	1.41	1.14	0	0.0173	0.35	2.20	1.6	1.40
10.60	PP	0	0	0	0	0	0	0.022	0.015	0.32	0.63	0.56	0	0	0	0	0	0	0.022	0.015	0.32	0.63	0.56
11.21	BPPE	0.30	3.34	3.32	3.44	3.17	0	0.072	0.36	1.20	1.49	1.48	0.30	3.34	3.32	3.44	3.17	0	0.072	0.36	1.20	1.49	1.48
11.79	PPE	72.7	56.6	54.14	43.19	28.54	100	87.0	67.0	34.2	3.29	2.78	72.7	56.6	54.14	43.19	28.54	100	87.0	67.0	34.2	3.29	2.78
12+	DIM	0	0	0.74	2.79	5.4	0	0	0	0	0	0	0	0	0.74	2.79	5.4	0	0	0	0	0	0





G. C. AREAS: GUAIACOL

G <sub>0</sub>	T	t	N <sub>2</sub>	CO	CH <sub>4</sub>	P	G	C
0.45	250	40	141014	2934	-			
		60	120086	2165	-			
		80	148459	3179	-			
		100	105577	2078	-			
	300	10						
		20						
		30						
		40						
	450	5	131326	76	-			
		1	117524	3496	1286			
		1.5	132432	5759	5237			
		2	82102	5360	32622			
		2.5	84009	3775	26514			
		0.5						
		1						
		1.5						
		2						
		2.5						
	500	0.25	126049	0	0			
		0.5	139774	3808	188			
		0.75	118919	5745	4192			
		1	90817	6234	22754			
	525	0.17	155779	0	0			
		0.33	127743	0	0			
		0.67	115085	6529	11851			
		0.83	79929	8156	28400			

- analysis not performed



mol fraction reported directly utilizing integrator software

G. C. AREAS: GUAIACOL

G <sub>o</sub>	T	t	N <sub>2</sub>	CO	CH <sub>4</sub>	P	G	C
0.45	400	1.25	118143	3473	578	0	313467	0
		2	111490	4742	6544	0	255613	837
		3	93262	4409	12652	1727	240620	5144
		4	98648	4474	23710	2196	226930	10089
		5	93995	4534	27611	4768	231642	13941
0.75		1	114972	2744	0	0	412630	0
		2	113752	4993	3478	0	255613	837
		3	98458	5906	18603	1727	240620	5144
		4	75963	4451	24195	2196	226930	10089
		5	78446	4237	30643	4768	231642	13941
1.5		1	123451	3844	329	0	412630	0
		2	109016	4482	4590	161	434258	867
		3	84247	4288	15358	686	307071	2484
		4	75658	3918	23609	1552	257570	6565
		5	75840	4586	36413	6650	548144	35674

G. C. AREAS: GUAIACOL

G <sub>0</sub>	T	t	N <sub>2</sub>	CO	CH <sub>4</sub>	P	G	C
3	350	2	CO, CH <sub>4</sub>	1.39	0	0.00449	80.63	0
		4		1.6	6.75	0.0371	83.41	0.126
		6		2.15	8.42	0.0121	35.02	0.0332
		8		1.87	12.3	0.0102	29.04	0.05191
		10	N <sub>2</sub>	2.33	16.8	0.0517	36.22	0.1414
		5						
		10						
		15						
		20						
		25						
		5	221168	2597	3965			
		10	167033	6077	16292			
		15	173179	5610	27304			
		20	150420	3694	22952			
		25	175156	4112	22589			
		5						
		10						
		15						
		20						
		20						
		20						
		1	112814	4645	0	0	151018	1788
		2	114820	4803	855	0	54497	1214
		3	97652	5531	2903	429	213153	6626
		4	112142	6185	5319	804	241396	8479
		5	106723	6144	11713	1255	129552	9199

G. C. AREAS: GUAIACOL									
G	T	t	N <sub>2</sub>	CO	CH <sub>4</sub>	P	G	C	
0.45	350	4	144426	5801	1731	0.0147	29.47	0.2314	
		8	134301	4227	4203	0.0628	29.94	0.4313	
		2		0	0	0	21.38	0	
		4	CO, CH <sub>4</sub>	2.47	0.427	0.0104	20.44	0.0423	
		6		2.98	2.0	0.0238	22.49	0.1573	
		8	N <sub>2</sub>	2.69	2.63	0.0509	24.88	0.1695	
		10		2.98	4.13	0.0898	31.48	0.3246	
		12	115158	4891	6543	0.0585	20.67	0.283	
		16	100430	4159	8299	0.137	26.3	0.502	
		20	104271	3904	10934	0.192	25.38	0.722	
0.75	350	2	97.2	2.441	0.338	0	38.34	0.18	
		4	93.56	4.19	2.25	0.0142	39.46	0.1943	
		6	90.56	4.92	4.31	0.0389	39.77	0.243	
		8	90.02	4.53	5.42	0.0587	36.36	0.325	
		10	86.98	4.24	8.78	0.211	36.37	0.362	
1.05	350	2		1.52	0	0	28.15	0	
		4		2.14	1.5	0.0054	38.85	0.0116	
		6	CO, CH <sub>4</sub>	2.06	2.56	0.0404	29.64	0.0230	
		8		3.16	5.78	0.0969	31.59	0.1153	
		10	N <sub>2</sub>	2.44	6.36	0.125	29.66	0.1843	
1.50	350	2	97.47	2.15	0.290	0	43.1	0.0488	
		4	93.24	3.93	2.78	0.0103	43.7	0.0516	
		6	90.01	4.57	5.41	0.0375	44.9	0.187	
		8	89.39	3.83	6.72	0.0790	40.9	0.426	
		10	84.46	5.23	10.28	0.0731	46.4	0.234	
		4		-	-	0.0459	46.4	0.1005	
		8		-	-	0.1787	36.12	0.251	
		12		-	-	0.6951	86.1	0.94	
		16		-	-	0.866	85.9	1.29	
		20		-	-	0.4662	37.19	0.613	

G. C. AREAS: GUAIACOL

G <sub>0</sub>	T	t	N <sub>2</sub>	CO	CH <sub>4</sub>	P	G	C
3	350	4	-	-	-	0.0407	37.54	0.0840
		8	-	-	-	0.1045	35.88	0.164
		12	-	-	-	0.1517	32.06	0.272
		16	-	-	-	0.352	39.92	0.471
		20	-	-	-	0.4192	35.42	0.614

## G. C. AREAS: 2,6-DIMETHOXYPHENOL (DMP)

DMP <sub>o</sub>	T	t	N <sub>2</sub>	CH <sub>4</sub>	CO	G	C	MC	DMP
0.37	400	2	69.1	6.06	4.31	0.25	1.21	0.48	134.4
		4	45.5	26.8	6.6	1.47	9.34	3.78	117.1
		6	35.0	34.7	5.2	2.28	11.22	9.36	69.1
		8	28.8	37.0	4.8	3.04	11.28	8.96	42.6
		2	-	-	-	605	1995	3650	735007
		4	-	-	-	0.073	0.617	0.579	23.21
		5	-	-	-	0.610	2.16	2.53	36.07
		6	-	-	-	0.1979	0.856	0.563	8.07
		7	-	-	-	0.118	0.611	0.379	5.30
		0.37	500	2	-	-	-	0.278	0.6774
3	-			-	-	0.111	0.073	0.947	0.139
4	-			-	-	0.0145	0	0.0770	0.0940
4.5	-			-	-	0.04	0	0.375	0.075
5	-			-	-	0.074	0	1.28	0.129
0.37	300	5	-	-	-	0	0	0	1
		10	-	-	-	0	0	0	1
		15	-	-	-	0	0	8.77-3	12.29
		20	-	-	-	35679	0	18795	1968047
		12.5	-	-	-	0	0	0	1
		5	76.85	0.099	0	0	0	0.0975	168.0
		10	78.14	0.288	0	0.03	0.03	0.13	189.6
		15	77.33	0.348	0	0.04	0.06	0.12	164.6
		20	76.71	0.654	0	0.08	0.06	0.26	165.8
		30	75.65	0.99	0	0.08	0.15	0.28	188.4
0.37	325	5.5	56.4	0.77	0	0	0	0.33	476.0
		10	5.44	0.193	0	0.025	0.09	0.42	54.88
		15	73.2	4.79	0	0.15	0.57	0.32	218.9
		20	54.4	5.5	0	0.2	0.6	1.54	230.4
		25	57.2	5.39	0	0.3	0.72	0.88	313.6
0.35	350	4	135577	681	299	158	0	0	183485
		8	159695	3309	751	508	-	127	200404
		12	133217	4575	818	568	-	96.3	178773
		16	149452	10551	1433	721	-	406	214140
		20	109025	8762	1177	1422	-	538	218904
0.37		2	82.6	0.263	1.76	0.04	0.24	0.12	190.8
		5	74.9	5.78	3.82	0.22	0.78	0.24	192.0
		7	71.8	8.52	4.4	0.48	1.5	0.28	169.1
		10	79.2	1.92	2.4	0.28	2.04	0.6	75.6
		15	46.2	31.44	4.4	1.92	7.2	2.42	121.9
		20	31.9	42.0	4.4	1.68	3.66	2.52	151.2
		2	44552	0	1137	0	0	0	451314
		4	83594	168	1589	500	0	327	410612

G. C. AREAS: DMP

DMP <sub>o</sub>	T	t	N <sub>2</sub>	CH <sub>4</sub>	CO	G	C	MC	DMP
(0.37	350)	6	65175	369	439	0	0	132	1147939
		8	60787	2049	1592	166	0	333	351044
		10	39800	640	749	94	0	173	24516
		5	48.8	8.91	3.08	0.7	1.26	0.44	466.5
		10	72.5	7.81	2.0	-	-	-	-
		15	32.2	22	2.97	1.2	6.9	7.04	192.0
		20	19	8.36	1.53	0.95	5.1	1.44	189.3
	375	3	36.8	6.05	2.72	0.35	1.5	0.32	274.4
		6	34	10.12	2.38	0.7	3.12	0.72	238.1
		9	22.4	7.28	1.19	-	6.0	1.82	226.6
		12	22.6	20.13	2.38	2.5	9.12	18.92	143.52
		15	9.88	7.48	1.36	1.6	8.4	9.54	100.8





## G. C. AREAS: ANISOLE

A <sub>0</sub>	T	t	A <sub>H<sub>2</sub></sub>	N <sub>2</sub>	CO	CH <sub>4</sub>	B	T	A	P	oCr
0.46	450	2	0	28533	935	918	0	0	718605	8134	0
		4	0	31896	922	964	653	288	664562	15759	459
		4	38	40704	4834	4673	0.804	0.107	43.53	3.34	0.49
		6	21	23548	2871	3360	9371	1867	916239	51995	7848
		8	55	37382	8380	8198	8610	2062	280784	26455	3243
		8	63	30114	8113	6573	2.59	0.43	24.6	4.76	0.49
		10	55	22252	6782	5994	10378	1989	183530	25395	3362
		12	98	39284	14545	11315	3.50	0.592	19.72	5.67	0.60
		16	102	52722	15492	11705	2.76	0.503	13.7	4.72	0.417
		20	41	30920	9616	7887	3.55	0.79	14.9	5.71	0.53
0.77	450	2	79	52962	4006	4285	0.17	0.036	30.1	0.99	0.19
		4	82	56849	10009	10604	0.75	0.11	27.2	2.3	0.52
		6	108	39868	11892	10698	0.56	0.093	8.84	1.34	0.11
		8	65	40774	12492	10882	2.35	0.731	22.4	3.94	0.58
		10	88	31216	12035	10010	2.19	0.42	17.35	3.63	0.412
1.08	450	2	0	42289	1411	687	124	0	384293	3318	512
		4	33	19993	2504	3181	855	176	170944	5283	1322
		6	45	25249	4830	5842	1791	438	155945	6256	2192
		8	17	5554	2902	3085	5808	1272	172183	14085	4214
		10	85	15153	8647	8725	5436	1076	144483	12863	3892
1.54	450	2	34	48407	3631	5091	0.117	0.032	38.7	0.92	0.294
		4	82	37725	10022	11144	0.672	0.193	25.12	2.02	0.397
		6	74	43413	13772	14576	1.77	0.221	32.3	4.07	1.48
		8	69	36040	13932	14556	2.15	0.403	33.6	4.59	1.64
		10	43	20467	10539	11539	2.27	0.515	22.85	3.97	1.14
3.08	450	2	40	42439	3278	4977	0.0604	0.011	27.6	0.504	0.251
		4	102	37957	12868	15970	0.721	0.19	28.3	2.09	1.06
		6	80	53815	9963	9342	0.072	0.026	2.15	0.261	0.032
		8	25	20291	9442	13870	1.97	0.78	26.4	3.76	1.20
		10	49	9415	14342	26224	2.51	1.09	28.4	4.47	1.51
0.43	450	25	178	10413	19654	16159	63725	5535	270487	91851	11734
		5	370	91209	31423	31808	13505	1128	357839	31956	5632
		10	337	37787	34562	27771	6546	648	181415	26783	3867
		15	458	41456	62956	49049	43401	6354	337823	69212	7969
		20	496	46370	57533	45464	29126	3332	263836	60932	9608

## G. C. AREAS: ANISOLE

A <sub>0</sub>	T	t	H <sub>2</sub>	N <sub>2</sub>	CH <sub>4</sub>	CO	B	T	A	P	OCR
1.57	344	5.25	0.01	76.3	0.065	0	0	0	207.2	0.24	-
		10	0	82.32	0	0	0	0	0	0	-
		15	0.01	75.24	0.163	0	0	0	216.3	0.308	-
		20	0.006	76.68	0.195	0	0	0	218.4	0.465	-
		25	0.005	75.12	0.245	0	0	0.0125	204	0.555	-
1.57	370	5	0.02	76.08	0.26	5.92	0	0	213	0.35	0.06
		10	0.045	72.48	1.43	6.89	0.015	0.0125	214.2	0.45	0.53
		15	0.04	72.84	1.53	6.96	0.015	0.0125	202.0	0.413	0.44
		20	0.0425	70.56	2.80	7.61	0.06	0.04	208.3	0.653	1.1
		25	0.0425	72.6	2.21	5.40	0.045	0.03	212.0	0.495	0.69
1.57	406	5	0.055	72	7.24	5.13	0.3	0.175	272.4	2.5	-
		10	0.050	70.6	10.14	6.56	0.345	0.44	248.2	3.0	0.96
		15	0.04	54.2	11.7	9.55	1.07	1.24	255.2	6.84	1.71
		20	0.07	51.24	15.0	12.42	0.48	1	248.6	7.8	1.92
		25	0.1	35.2	28.9	19.0	2.25	2.46	229.0	8.6	2.54
1.57	434	4	0.0875	41.0	13.92	13.6	2.32	1.0	155.8	7.7	1.8
		8	0.025	10.6	5.54	5.7	6.0	2.56	180.5	12.1	2.64
		12	0.0725	34.7	17.3	18.9	6.12	2.72	175.7	14.	4.16
		16	0.035	12.5	7.97	9.44	9.84	4.70	170.9	17.6	3.68
		20	0.0725	32.16	17.4	21.11	12.12	4.38	139.1	19.9	3.57
1.57	465	3	0.09	35.8	18.85	19.04	6.55	2.0	170.4	17.3	4.96
		6	0.068	28.1	23.78	23.94	19.6	4.06	128.0	27.2	6.21
		9	0.08	16.1	29.0	26.79	25.2	3.92	102.6	33.8	7.38
		12	0.075	14.66	29.3	26.79	27.2	3.98	99.6	38.8	8.20
		15	0.053	25.32	25.8	22.2	29.4	4.62	90.0	45.0	8.0
1.57	490	3	0.053	30.02	26.7	19.8	25.2	3.5	95.3	36.7	5.44
		6.5	0.040	17.8	31.6	22.2	37.0	9.66	55.9	54.6	6.4
		9	0.020	25.1	27.6	14.5	39.0	10.36	38.0	62.0	8
		12	0.020	25.1	29.3	14.4	46.0	9.07	16.0	72.0	6.79
		15	0.019	17.62	31.2	16.8	47.2	11.76	19.2	71.4	4.4

## G. C. AREAS: ANISOLE

A <sub>0</sub>	T	t	H <sub>2</sub>	N <sub>2</sub>	CO	CH <sub>4</sub>	B	T	A	P	oCR	
0.46	550	3	-	-	-	-	293516	18718	45253	339191	9394	
		6	-	-	-	-	150690	8248	274	169694	3707	
		4	-	-	-	-	-	129928	11077	7783	172439	48203
		5	-	-	-	-	-	315279	15191	744	383318	6970
		4	-	-	-	-	-	199220	12100	9532	253793	3400
0.46	350	5	-	-	-	-	0	0	674799	20620	0	
		11	-	-	-	-	0	0	455602	5310	0	
		15	-	-	-	-	-	0	0	48801	678	0
		20	-	-	-	-	-	0	0	500390	8391	0
		25	-	-	-	-	-	0	0	467795	26468	0

G. C. AREAS: VERBTROLE

T	t	N <sub>2</sub>	CO	CH <sub>4</sub>	MeOH	MeCl <sub>2</sub> <sub>I</sub>	MeCl <sub>2</sub> <sub>II</sub>	B	TOL	Xy <sup>1</sup> <sub>I</sub>	Xy <sup>1</sup> <sub>II</sub>	An	Ph	cCr	G	Ver	Cat	Dim
550	2	61.8	16.1	22.1	0.442	96.5	84.7	0	0.21	0	0.04	1.22	1.34	2.74	0	1.30	5.95	2.5
	3	20.7	33.5	45.8	0.375	97.1	88.8	0	0.21	0	0.085	1.06	1.77	2.45	0	9.27	4.69	0.81
	4	26.0	32.8	41.2	0.39	96.3	87.5	0.14	0.23	0	0.08	0.66	2.34	3.12	0	0.060	4.04	0.92
	5	26.9	30.9	42.2	0.86	96.4	88.4	0	0.17	0	0.039	0.60	2.45	2.86	0	0.0044	3.14	1.96
	6	23.8	31.7	44.5	0.442	96.6	89.0	0	0.32	0.073	0.04	0.61	2.21	0.34	0	4.58	10.85	0.71
	80s	-	-	-	1.46	88.02	27.4	0	0.32	0.13	0.15	7.3	3.49	3.49	2.16	7.41	24.1	11.7
500	2.5	25.8	30.5	43.7	0.59	96.0	86.4	0.18	0.46	0.050	0.041	1.52	1.75	2.85	0	1.04	5.03	0.65
	4	28.0	29.8	42.2	0.40	96.3	93.6	0	0	0.10	0.0065	0.595	1.09	1.8	0	0	2.64	0
	6	28.1	31.4	40.6	0.45	95.0	94.5	0	0	0.057	0.00598	0.222	1.12	1.98	0	0	2.05	0
	8	21.7	33.9	44.4	0.32	97.3	96.4	0	0	0.054	0.0066	0.18	1.01	1.37	0	0	2.0	0.06
	10	24.6	32	43.4	0.29	96.4	90.2	0.14	0.28	0.063	0.056	0.56	2.71	2.75	0	0	2.83	0.28
	1.5	-	-	-	1.11	99.36	64.55	0	0	0.08	0	0.049	0.041	0	0.273	34.21	0	0.78
450	2	-	-	-	1.05	93.42	29.36	0	0	0.22	0.01	1.18	0.18	0.16	1.64	68.09	0	0
	2.5	-	-	-	0.48	96.65	31.64	0	0.48	0.07	0	0.31	0.30	0.90	4.95	54.	2.0	0
	3	53.4	19.1	27.5	0.26	98.7	54.9	0	0.17	0	0.036	0.69	0.73	0.44	2.82	26.9	5.0	0.5
	7.5	26.8	30.4	42.8	0.65	96.6	69.7	0.27	0.48	0.052	0.022	3.05	2.57	1.81	3.24	11.7	6.83	0.3
	10	30.2	27.8	42	0.76	96.0	74.8	0	0.46	0.081	0.11	2.66	2.74	2.07	2.30	7.36	6.55	0.87
	12	27.4	27.7	45	0.59	95.3	79.9	0	0.39	0.028	0.041	2.57	3.08	2.63	1.24	2.23	6.76	1.2
400	15	30	27.4	42.6	0.42	96.2	85.7	0.013	0.29	0.020	0.022	1.75	2.56	2.60	0	0.40	5.54	1.3
	4	85.835	86	8.31	0.094	99.43	52.0	0	0	0.033	0.0028	0.0227	0.0253	0	0.19	47.71	0	0
	8	80.9	7.04	12.1	0.75	98.41	51.5	0	0	0.050	0.0051	0.0495	0.06	0.035	0.44	47.88	0	0
	12	58.0	16.0	26.0	0.183	99.12	45.44	0	0.069	0	0.015	0.232	0.21	0.12	3.50	52.61	0	0
	16	52.4	19.3	28.3	0.17	99.23	64.5	0	0	0.034	0.018	0.33	0.34	0.11	1.46	33.2	0	0
	20	47.1	21.9	31.0	0.40	98.21	51.3	0	0.23	0.029	0.029	1.01	1.08	0.42	2.85	39.42	0	0
425	4	-	-	-	0.45	97.2	32.13	0	0.34	0	0.038	0.44	0.28	0.44	2.40	64.1	0	0
	6	-	-	-	0.51	95.7	53.1	0	0.38	0	0.047	0.68	0.28	0.44	2.63	41.6	0	0.3
	8	-	-	-	0.61	97.2	44.3	0	0.813	0.068	0.037	1.71	0.70	1.29	4.16	33.1	3.0	0.55
	10	-	-	-	2.22	86.64	40.57	1.11	1.59	0.17	0.674	3.16	0.83	0.83	2.18	6.03	29.8	7.41
	12	-	-	-	0.19	96.2	23.7	1.6	2.04	0.14	0.085	4.6	1.41	1.41	3.24	6.78	30.0	9.24
	15	-	-	-	0.30	96.2	12.1	0	0.083	0	0.046	0.050	0.071	0.071	0	0.53	75.5	0
375	15	-	-	-	0.32	97.8	32.3	0	0.22	0	0.012	0.17	0.19	0.12	1.46	85.7	0	0
	20	-	-	-	0.73	96.7	32.7	0	0.111	0	0.014	0.14	1.03	0.14	1.03	61.2	0	0
	25	-	-	-	0.48	97.2	42.3	0	0.26	0.015	0	0.30	0.22	0.22	1.88	64.3	0	0
	30	-	-	-	0.48	99.3	58.85	0	0	0.183	0.012	0.25	0.21	0.083	1.39	55.0	0	0
	5	98.3	1.7	0	0.054	99.3	58.85	0	0	0	0	0	0	0	0	41.13	0	0
	10	95.3	2.9	1.8	0.072	98.4	50.59	0	0	0	0.0097	0.0053	0	0	0	49.37	0	0
350	15	93.6	3.4	3.1	0.75	99.11	52.42	0	0	0	0	0.0059	0.0099	0	0.050	47.48	0	0
	20	93.1	3.32	3.6	0.093	99.01	43.09	0	0	0	0	0.0059	0.018	0	0	56.86	0	0
	25	91.4	4.0	4.7	0.059	99.53	52.23	0	0	0.015	0	0.0091	0.017	0	0.0924	46.61	0	0.001

## G. C. AREAS: SALIGENOL

T(°C)	S <sub>0</sub> (mol)	t(min)	T <sub>1</sub>	oCR	HBA	H <sub>2</sub> O	T <sub>2</sub>
200	7.50-4	0	5.18	0.37	23.19	0.13	1.08
200	7.50-4	0.5	8.41	0.60	23.93	3.80	4.80
200	7.50-4	1	3.60	0.079	15.44	2.65	5.01
200	7.50-4	3	33.87	3.24	60.38	4.56	4.53
225	1.59-4	1	4.80	0.019	5.07	3.39	6.05
225	1.46-4	2	5.42	0.16	1.49	6.13	7.61
225	1.51-4	2.5	4.22	0.083	0.0936	4.64	4.87
225	1.68-4	3	2.97	0.044	0.0043	46.17	3.31
175	1.75-4	3	4.25	0.043	5.61	4.37	6.08
175	1.61-4	6	7.45	0.072	3.25	7.13	9.02
175	1.43-4	9	6.31	0.12	3.33	5.72	6.34
175	1.67-4	12	6.21	0.185	1.87	8.28	8.50
175	1.81-4	18	5.77	0.172	1.34	8.54	7.51

## G. C. AREAS: BENZALDEHYDE

Vr	T	BA <sub>0</sub>	t	H <sub>2</sub>	N <sub>2</sub>	CO	B	P	BA	D
10.6	400	0.47	6	0	91.54	7.17	-	-	-	-
			8	0	94.06	5.94	-	-	-	-
			10	0.032	62.04	37.51	3.17	0.1418	55.59	0.185
				0.035	63.11	36.45	2.57	0.1481	53.68	0
				0.0051	97.52	2.38	0.238	0.1154	3.58	0
				0	94.57	5.26	-	-	-	-
				0.022	70.35	29.62	1.43	0.153	51.92	0
				0.0187	70.79	29.19	1.54	0.135	51.64	0
			15	0.0352	58.52	41.44	2.94	0.212	51.18	0
			20	0.0311	60.32	39.65	3.58	0.246	56.33	0.35
				0.046	56.87	42.9	2.21	0.155	24.49	0
				0.043	58.2	41.6	1.86	0.129	24.32	0
			25	0.0481	36.3	63.65	10.39	1.46	48.61	0
			30	0.0432	38.21	61.74	10.6	1.65	54.73	0
				0.055	46.53	52.98	1.28	0.134	7.81	0
				-	-	-	1.59	0.1722	7.57	0
			30.5	0.0522	23.56	76.39	17.32	2.25	37.17	0
				0.0513	24.25	75.70	15.65	2.31	28.4	0
			17	0.051	41.23	58.19	4.55	0.55	31.2	0
				0.049	44.18	55.27	6.39	0.7424	40.33	0
0.6	400	0.164	7	-	98.41	1.59	0.87	0.11	14.7	2.5
				-	-	-	0.236	0	12.88	4.36
			9	-	91.95	8.05	0.0642	0	4.67	0.0174
0.6	400	0.492	4	0.020	82.17	17.81	0.583	0.0361	19.18	0
				-	-	-	0.211	0	10.32	0.227
			6	-	82.72	17.0	0.243	0.0136	14.68	0
				-	-	-	0.237	0	14.48	0.374
			8	-	78.99	21.01	1.122	0.267	19.27	0
				-	-	-	1.028	0.0654	15.36	0.1899
			10	0.030	75.99	24.2	0.607	0	9.05	0
				-	-	-	0.575	0.054	6.88	0

## G. C. AREAS: BENZALDEHYDE

Vr	T	BA <sub>0</sub>	t	H <sub>2</sub>	N <sub>2</sub>	CO	B	P	BA	D
(0.6	400	0.492)	12	0.028	62.8	37.17	2.07	0.138	14.84	0.0371
					-	-	2.33	0.122	16.75	0.00330
0.6	400	1.64	4	-	62.83	36.94	0.86	0.33	26.65	0
					-	-	1.45	0.503	35.9	0
			6	-	60.04	39.96	2.89	0.867	30.96	0.0686
					-	-	1.08	0.190	21.67	0
			8	-	56.74	43.26	2.83	0.96	24.47	0.457
					-	-	1.57	0.35	19.08	0
			10	-	49.67	50.33	1.77	0.543	15.64	0.0470
					-	-	2.13	0.562	14.65	0.0444
			12	-	45.18	54.82	3.23	0.865	15.1	0.0402
					-	-	3.14	0.647	16.15	0.0408
			3	-	72.12	7.77	0.070	0.024	39.96	0.179
			5	-	93.31	6.69	0.108	0.066	48.6	0.362
					-	-	0.083	0.069	41.3	1.80
			7	-	56.84	43.16	0.95	0.85	41.9	1.6
					-	-	0.952	0.91	42.5	1.6
			9	-	48.15	51.85	1.01	0.55	28.1	0.18
					-	-	1.51	0.55	30.9	0.18
			11	-	51.9	48.1	1.79	1.26	17.4	0.115
					-	-	2.30	1.25	17.68	0.127
		3.28	4	-	47.18	52.82	2.41	0.951	42.89	0.0255
					-	-	2.02	0.848	39.51	0.0722
			6	-	44.67	55.33	3.32	1.48	21.63	0
					-	-	4.60	2.04	25.71	0.938
			8	-	35.43	64.57	7.44	4.20	24.36	1.41
					-	-	8.14	4.67	22.38	3.72
			10	-	18.22	81.78	16.02	8.43	13.34	7.3
					-	-	17.48	7.13	11.03	0.624
			12	-	24.15	75.85	8.89	3.65	15.58	0.718
					-	-	10.5	4.42	16.94	0.192



G. C. AREAS: BENZALDEHYDE

Vr	T	BA <sub>0</sub>	t	H <sub>2</sub>	N <sub>2</sub>	CO	B	P	BA	D
(0.6	400	3.28)	5	-	75.89	24.11	0.151	0.08	66.3	1.51
			6	-	-	-	0.1882	0.095	68.02	1.5
			7	-	45.56	54.44	0.74	0.61	53.01	1.6
			9	-	-	-	0.69	0.55	53.21	1.4
			11	-	39.64	60.3	3.67	2.57	14.36	0.084
			11	-	-	-	4.25	3.13	18.98	0.298
			10	-	52.97	47.03	3.27	3.36	33.55	3.63
0.6	350	0.49	10	-	-	-	5.06	5.35	33.48	4.09
			20	-	-	-	0	0.044	0.949	0.452
			30	-	-	-	0	0	1.35	0.046
			50	-	-	-	0	0.17	5.03	0
			60	-	-	-	0	0.238	14.92	0.2331
			4	-	-	-	0	0	14.34	0.058
			6	-	-	-	0	0.0772	11.32	0.145
			8	-	-	-	0	0	0	0
0.6	450	0.49	4	-	-	-	0.1237	0.125	10.35	0.0828
			6	-	-	-	0	0	1.73	0.097
			10	-	-	-	0	0	1.71	0.0181
			12	-	-	-	0.0793	0.0141	0.7147	0
			3	-	-	-	0.0526	0.011	0.7577	0
			8	-	52.78	47.18	0.209	0	0.6964	0.016
			10	-	-	-	0	0	0.0824	0
			12	-	92.34	7.66	0.2139	0	0.2972	0
			3	-	-	-	0	0	0.3491	0
			4	-	55.54	44.43	9.03	0.548	4.60	0.0422
			6	-	-	-	8.88	0.584	4.46	0.055
			8	-	50.46	49.54	0.2454	0.0351	0.4546	0
			10	-	-	-	0.2325	0.014	0.458	0
0.6	500	0.49	3	-	54.45	45.5	10.66	0.2023	6.73	0
			4	-	-	-	10.12	0.2476	8.46	0

## G. C. AREAS: BENZALDEHYDE

Vr	T	BA <sub>0</sub>	t	H <sub>2</sub>	N <sub>2</sub>	CO	B	P	BA	D
(0.6	500	0.49)	4	0.060	51.31	48.63	13.97	0.2331	8.40	0
			5	0.073	50.75	49.17	11.04	0.0325	9.04	0
			6	0.070	54.14	45.79	10.59	0.3752	2.71	0
							10.47	0.381	2.63	0.120
							15.98	0	3.70	0.01
							18.66	0.6317	4.792	0.088
0.6	550	0.49	3	0.045	52.45	47.5	15.91	0.4593	11.76	0.0134
			3.5	0.067	52.56	47.37	17.27	0.44	11.93	0.013
			4	0.074	53.08	46.85	16.91	0.521	4.31	0.014
			4.5	0.054	56.01	43.93	17.64	0.390	3.29	0.356
			5	0.089	56.70	43.13	24.15	0.5042	4.81	0.07
							27.88	0.781	5.32	0.16
							19.53	0.452	2.35	0.024
							18.82	0.525	2.46	0.05
							17.42	0.525	1.67	0
							18.17	0.443	1.67	0
0.6	570	0.49	3		51.47	40.53	10.92	0.18	2.85	0.05
			3.5		43.29	54.61	10.69	0.18	2.58	0
			4		63.61	36.39	13.35	0.256	2.21	0
			4.5		55.05	44.95	15.86	0.299	1.81	0
							13.62	0.624	1.38	0
							10.78	0.547	1.04	0
							10.46	0.224	0.576	0
							9.58	0.223	0.610	0
			5		46.76	53.24	12.01	0.4164	0.335	0
							12.01	0.3963	0.330	0

## G. C. AREAS: VANILLIN

$V_0$ , mol	$V_r$ , cm <sup>3</sup>	T, C	t, min	G	C	V	DHB	P	N <sub>2</sub>	CO	CH <sub>4</sub>
8.83-4	3.5	400	1	0	0	1.0	0	0	-	-	-
8.06-4	3.5		2	1.2	0	81.6	0	0	-	-	-
1.01-3	3.5		4	8.4	0.64	85.8	1.8	0	-	-	-
9.76-4	3.5		6	23.76	1.6	15.36	2.52	0	-	-	-
9.32-4	3.5		8	25.92	1.92	7.04	3.2	0	-	-	-
9.78-4	3.5		10	12.48	0.96	4	1.28	0	-	-	-
1.53-3	0.6		2	1.56	0.36	84.24	0	0	-	-	-
8.03-4	0.6		4	12.64	1.92	22.4	1.33	0	-	-	-
1.00-3	0.6		6	-	-	-	-	0	-	-	-
1.35-3	0.6		8	16.0	2.4	16.1	3.42	0	-	-	-
1.41-4	0.6		3	0.526	0.056	1.30	0	0	-	-	-
1.65-4	0.6		4	0.622	0.104	0.0898	0	0	-	-	-
1.65-4	0.6		6	2.36	0.210	0	0	0.109	-	-	-
1.53-4	0.6		8	1.50	0.026	0	0	0	-	-	-
1.79-4	0.6		10	1.56	0.093	0	0	0.248	-	-	-
1.42-4	0.6	500	1	0.9785	0.0273	4.174	0	0	-	-	-
1.89-4	0.6		2	1.091	0.6612	tr	0	0.4162	-	-	-
2.18-4	0.6		3	0.1113	0.4431	0	0	0.3795	-	-	-
1.60-4	0.6		4	0	0.9957	0	0	0.9486	-	-	-
2.25-4	0.6		5	0.0585	2.271	0	0	1.57	-	-	-
1.37-3	3.5	300	5	0.16	0	292.6	1	0	-	-	-
7.01-4	0.6		5	0.12	0.045	51.24	0	0	-	-	-
1.59-3	0.6		10	0.12	0.045	59.84	0	0	-	-	-
1.17-3	0.6		15	0.3	0.060	60.72	0	0	-	-	-
1.34-3	0.6		20	0.28	0.062	80.1	0	0	-	-	-
1.24-3	3.5		25	2.7	0.160	160.0	0	0	-	-	-
1.64-3	0.6		30	1.17	0.180	77.0	0	0	-	-	-
1.78-4	0.6		8	0	0	12.98	0	0	-	-	-
1.74-4	0.6		12	0	0	6.62	0	0	-	-	-
1.63-4	0.6		20.5	0.2893	0.0474	2.56	0	0	-	-	-
1.82-4	0.6		25	0.252	0.0225	13.8	0	0	-	-	-
1.74-4	0.6		26	0.046	0.0098	0.878	0	0	-	-	-

## G. C. AREAS: VANILLIN

$V_0, \text{mol}$	$V_r, \text{cm}^3$	T, C	$t_r, \text{min}$	G	C	V	DHB	P	$N_2$	CO	$CH_4$
1.15-3	3.5	350	4	1.2	0.08	173.9	0.5	0	-	-	-
8.91-4	0.6		4	1.56	0.42	58.0	0	0	-	-	-
1.13-3	3.5		8	7.2	0.24	144.0	1.62	0	-	-	-
9.58-4	0.6		8	4.24	1.08	51.2	0.38	0	-	-	-
1.34-3	0.6		12	8.08	1.56	45.2	0.76	0	-	-	-
8.41-4	0.6		15	15.04	2.64	9.62	2.63	0	-	-	-
8.84-4	0.6		20	17.28	2.88	5.18	2.85	0	-	-	-
3.41-3	10.6		4	663	0	611403	0	0	90040	3360	0
3.36-3	10.6		8	15770	3277	395200	0	0	112596	19733	1554
3.43-3	10.6		12	8428	733	91204	0	0	55571	11261	1096
3.24-3	10.6		16	57123	7641	91641	9193	0	39317	18754	2579
3.47-3	10.6		20	47871	7158	74728	10287	0	17869	9669	1511
1.22-3	10.6		6	0	0	100	0	0	18799	368	0
1.20-3	10.6		7	3705	0	78216	0	0	25391	3968	319
1.52-3	10.6		8	1640	0	92169	0	0	10582	623	0
1.49-3	10.6		10	4806	222	42050	0	0	33266	2944	61
9.04-4	10.6		12	18749	1922	78466	7527	0	6431	1646	104
9.67-4	3.5	375	3	2.04	0	148.4	0	0	-	-	-
1.26-3	3.5		6	6.6	0.16	112.0	1.8	0	-	-	-
1.06-3	3.5		12	28.8	5.12	10.64	2.4	0	-	-	-
1.15-3	3.5		15	26.9	1.92	3.2	2.4	0	-	-	-

## C. G. AREAS: ACETOPHENONE

AP <sub>0</sub> mol/l	T.C.	t, min	N <sub>2</sub>	CO	CH <sub>4</sub>	B	T	X	P	BA	AP
1.42	550	3	-	-	-	0.133	0.069	0.021	0.005	0	27.9
V <sub>r</sub> =0.6		3	-	-	-	0.138	0.100	0.042	0.020	0	29.0
		4	-	-	-	-	-	-	-	-	-
		4	-	-	-	-	-	-	-	-	-
		6	-	-	-	0.578	0.267	0.153	0	0	17.3
		6	-	-	-	0.495	0.266	0.170	0	0	16.6
		8	-	-	-	-	-	-	-	-	-
		8	-	-	-	0.139	0.139	0.102	0	0	1.45
		10	-	-	-	-	-	-	-	-	-
		10	-	-	-	-	-	-	-	-	-
		12	-	-	-	7.22	4.16	2.82	0.27	0	36.33
		12	-	-	-	6.96	3.43	2.35	0.27	0	30.19
		12	-	-	-	0	0	0	0	0	1
1.42	400	4	97.4	2.53	0.094	0	0	0.022	0	0	51.5
V <sub>r</sub> =0.6		8	94.6	4.61	0.783	0.0242	0	0.091	0	0	35.6
		12	91.8	7.04	1.17	0.0857	0.0073	0.182	0.074	0	41.8
		16	85.0	13.9	1.08	0.1562	0.0147	0.187	0.201	0	38.6
		20	82.2	16.5	1.16	0.1534	0.0136	0.853	0.183	0	50.2
		3	85.0	12.2	2.84	0.102	0.013	0.051	0	0	-
1.42	500	6	73.8	19.8	6.39	0.336	0.092	0.086	0	0	51.4
V <sub>r</sub> =0.6		9	87.7	8.9	3.40	0.342	0.134	0.086	0.06	0	28.6
		12	48.1	43.1	8.75	3.26	1.30	1.08	0.50	0	-

## G. C. AREAS: ACETOPHENONE

AP <sub>0</sub> mol/l	T, C	t, min	B	T	X	ST	AN	BA	Cr	AP	BP	PE, PPM	DIM		
0.43 V <sub>r</sub> =0.6	550	3	0.24	0.13	0.052	0.038	0.026	0.008	0.014	24.01	0.019	0.041	0.58		
		3	0.29	0.16	0.06	0.039	0.025	0.0064	0.0096	26.0	0.014	0.040	0.74		
		6	0.69	0.42	0.23	0.087	0.064	0.018	0.021	16.3	0.26	0.38	0.80		
		6	0.81	0.48	0.26	0.10	0.074	0.021	0.030	18.8	0.25	0.40	1.12		
		9	0.40	0.22	0.16	0.079	0.051	0.015	0.005	28.2	0.031	0.075	0.644		
		9	0.42	0.26	0.19	0.092	0.065	0.019	0.0094	16.0	0.038	0.114	0.661		
		12	2.0	1.28	0.79	0.23	0.110	0.03	0.045	20.8	0.39	0.94	1.84		
		12	1.63	1.07	0.68	0.20	0.095	0.026	0.041	19.1	0.44	1.22	1.99		
		13	0.69	0.46	0.31	0.081	0.040	0.011	0.0088	7.68	0.085	0.27	0.70		
		13	0.84	0.56	0.38	0.10	0.050	0.0026	0.0072	9.26	0.213	0.52	1.06		
		5	0.10	0.061	0.044	0.05	0.030	0.020	0	54.7	0	0	0.285		
		5	0	0	0.012	0.036	0.0082	0	0	40.3	0	0	2.42		
		0.43 V <sub>r</sub> =0.6	500	10	0.38	0.11	0.047	0.065	0.035	0.0021	0.010	76.4	0	0	0.75
10	0.42			0.12	0.50	0.064	0.027	0	0	88.1	0	0	0.71		
15	0.18			0.050	0.42	0.21	0.047	0	0	15.8	0	0	0.31		
15	-			0.03	0.79	0.80	0.15	0	0	94.8	0	0	2.26		
20	0			0	0	0.012	0.127	0	0	3.76	0	0	0.244		
20	0			0.031	0	0.0090	0.010	0.0093	0.0011	2.54	0	0.14	0.524		
25	0.33			0.14	0.28	0.19	0.139	0.01	0	35.32	0	3.81	4.5		
25	0.56			0.21	0.20	0.10	0.086	0.19	0.12	53.8	0	0	4.06		
0.43 V <sub>r</sub> =0.6	450			10	0.028	0.014	0.022	0.045	0.019	0.031	0	61.7	0	0	0.39
				10	0.029	0.014	0.620	0.063	0.019	0.044	0	77.9	0	0	0.542
				20	0.13	0.035	0.044	0.064	0.044	0.0050	0.04	76.97	0	0.010	2.68
				20	0.10	0.038	0.044	0.070	0.048	0.052	0	85.6	0	0.012	0.96
				25	0.074	0.027	0.035	0.044	0.033	0.0073	0.014	59.0	0	0.014	1.27
		25	0.15	0.049	0.047	0.062	0.045	0.0072	0	77.6	0	0.041	0.84		
		30	0.18	0.058	0.079	0.096	0.065	0.012	0.032	98.5	0	0	0.87		
		30	0.12	0.042	0.056	0.068	0.046	0.0091	0.020	71.2	0	0	0.66		
		40	0.38	0.10	0.12	0.11	0.023	0.0056	0.0065	73.4	0	0	0.91		
		40	0.14	0.051	0.083	0.065	0.047	0.0047	0	53.3	0	0	0.711		
		20	0	0.0062	0.0055	0.036	0.048	0	0	76.6	0	0	1.86		
		0.43	400	20	0	0	0	0.036	0.048	0	0	76.6	0	0	1.86
				20	0	0	0	0.036	0.048	0	0	76.6	0	0	1.86

G. C. AREAS: ACETOPHENONE

AP <sub>0</sub> mol/l	T.C	t, min.	N <sub>2</sub>	CO	CH <sub>4</sub>	B	T	X	P	BA	AP
0.404	550	6	61.3	28.2	10.4	0.332	0.189	0.060	0.0087	-	38.8
V <sub>r</sub> =10.6		6	61.4	28.2	10.4	0.335	0.208	0.034	0.0057	0.004	41.4
		8	-	-	-	0.401	0.263	0.071	0.0078	-	47.6
		8	-	-	-	0.578	0.368	0.083	0.0054	-	49.0
		10	71.0	20.9	8.08	0.365	0.201	0.066	0.022	-	53.5
		10	71.7	20.3	7.91	0.393	0.180	0.069	0.0145	-	55.8
		12	49.1	37.5	13.3	1.14	0.735	0.162	-	-	57.8
		12	49.3	37.2	13.4	1.39	0.86	0.198	0.014	-	59.8
		16	46.1	39.5	14.4	1.994	1.18	0.219	0.009	-	66.1
		16	46.5	39.1	14.2	1.44	0.955	0.166	0.0175	-	67.1

G. C. AREAS: ACETOPHENONE

AP <sub>0</sub> mol/l	T, C	t, min	B	T	X	ST	AN	BA	Cr	AP	BP	PE, DPM	DIM
V <sub>r</sub> = 0.6	(400)	20	0.022	0.011	0.0059	0.043	0.06	0	0	95.1	0	0	1.93
		40	0	0.0047	0.0074	0.034	0.054	0	0	73.0	0	0	0.73
		40	0.024	0.0062	0.0044	0.0162	0.23	0	0	95.3	0	0	1.94
		60	0.19	0.047	0.5	0.24	0.74	0.03	0	72.5	0	0.024	6.88
		60	0.15	0.048	0.14	0.16	0.89	0.06	0	75.6	0	0.095	6.93
		80	0.19	0.047	0.085	0.14	0.51	0.024	0	66.7	0	0.062	4.19
		80	0.17	0.055	0.10	0.17	0.54	0	0	81.5	0	0.10	5.45
		40	0.078	0.085	0.12	0.12	0.076	0.0056	0	88.3	0	0	1.01
		40	0.073	0.080	0.11	0.11	0.072	0.0066	0.049	79.3	0	0	0.04



## G. C. AREAS: ACETOPHENONE

AP <sub>0</sub> mol/l	T.C	t, min.	N <sub>2</sub>	CO	CH <sub>4</sub>	B	T	X	P	BA	AP
0.404	400	10	99.8	0.113	0.11	0.0066	0.00366	0	0.0413	0	94.86
V <sub>r</sub> =10.6		10	99.8	0.55	0.10	0.013	0	0	0.0045	0	95.53
		15	-	-	-	-	-	-	-	-	-
		15	-	-	-	-	-	-	-	-	-
		20	-	-	-	-	-	-	-	-	-
		20	-	-	-	-	-	-	-	-	-
		25	96.7	2.24	1.06	0.025	0.019	0	0.0482	0	71.05
		25	-	-	-	0.0793	0.0141	0	0.0159	0	71.47
		30	99.4	0.466	0.160	-	0.020	0	0.035	0	65.1
		30	99.5	0.330	0.148	-	-	-	-	-	-
0.404	500	6	96.41	2.51	1.09	0.0691	0.0162	0.008	0.0104	0	58.12
V <sub>r</sub> =10.6		6	96.6	2.40	1.04	0.0450	0.0223	0.0183	0.0199	0.0094	66.2
		12	95.3	3.07	1.64	0.146	0.0718	0.038	0.0263	0	51.07
		12	89.6	7.77	2.56	-	-	-	-	-	-
		24	84.5	11.3	4.08	0.246	0.1275	0.0519	0	0	27.49
		24	80.1	14.4	5.28	0.376	0.1497	0.091	0.015	0	36.8
		30	54.7	33.8	11.42	1.37	0.671	0.213	0.095	0	70.8
		30	57.1	32.0	10.87	1.34	0.72	0.226	0.077	0	65.8
		40	72.7	20.1	7.22	0.55	0.262	0.0974	0.053	0.0109	75.0
		40	71.4	19.3	9.31	0.51	0.237	0.0894	0.059	0	71.7
0.43	400	15	95.2	3.85	0.26	0	0	0	1.18-3	1.16-2	27.8
V <sub>r</sub> =0.6		15	-	-	-	0	0	0.0127	7.77-3	5.61-2	-
		20	93.4	6.30	0.35	0	2.2-3	0	0	7.77-2	52.7
		20	-	-	-	2.44-2	5.91-3	2.18-3	1.55-2	6.09-2	53.0
		25	94.8	4.86	0.36	0	0	4.82-3	2.17-2	3.90-2	35.11
		25	-	-	-	0	0	0	1.65-2	2.41-2	36.3
		30	95.2	4.76	0.063	0	8.46-3	0	0	0	39.7
		30	-	-	-	0	0	0	0	0	-
		35	95.2	4.70	0.13	0	0	0	3.29-2	1.38-2	27.96
		35	-	-	-	0	7.34-3	0	6.43-3	1.67-2	27.43

G. C. AREAS: ACETOPHENONE

AP <sub>0</sub> mol/l	T.C	t, min	N <sub>2</sub>	CO	CH <sub>4</sub>	B	T	X	P	BA	AP	
0.43 V <sub>r</sub> =0.6	500	5	-	-	-	0	0	0.0096	0	0.00137	0.699	
		5	-	-	-	0	0.138	0.0076	0.0045	0	0.661	
		10	-	-	-	0	0.111	0.060	0	0.0008	26.13	
		10	-	-	-	0.174	0.098	0.057	0.030	0.0064	27.44	
		15	-	-	-	0.212	0	0.011	0	0	5.43	
		15	-	-	-	0	0	0.019	0.012	0.0081	5.74	
		20	-	-	-	0	0.021	0	0	0	0.599	
		20	-	-	-	0	0	0	0	0	0.06	
		25	-	-	-	0	0	0.0193	0	0	0	0
		25	-	-	-	0	0	0	0	0	0	0
		25	-	-	-	0	0	0	0	0	0	0
		0.43 V <sub>r</sub> =0.6	550	3	-	-	-	0	0	0	0.030	0
3	-			-	-	0.111	0.0361	0	0	0	47.5	
3	-			-	-	0.130	0.643	0.021	0	0	47.5	
4	-			-	-	0.310	0.114	0.037	0.007	0	44.6	
4	-			-	-	0.234	0.122	0.027	0.032	0.018	47.7	
6	-			-	-	0.623	0.291	0.098	0.052	0.052	47.3	
6	-			-	-	0.644	0.285	0.093	0.053	0.014	45.0	
8	-			-	-	1.34	0.762	0.134	0.026	0.0031	45.0	
8	-			-	-	1.41	0.790	0.12	0.022	0	47.7	
10	-			-	-	0.983	0.684	0.30	0.011	0	28.8	
10	-			-	-	1.41	0.75	0.26	0.07	0	29.5	
12	-			-	-	2.01	1.13	0.43	0.13	0.003	32.3	
0.143 V <sub>r</sub> =0.6	550	12	-	-	-	1.86	1.04	0.42	0.11	0	31.2	
		4	-	-	-	0	0	0.018	0	0	1.18	
		4	-	-	-	0	0	0	0	0	0	
		6	-	-	-	0	0	0	0	0	0	
		6	-	-	-	0	0	0	0	0	0	
		8	-	-	-	0	0	0	0	0	0	
		8	-	-	-	8078	6017	4302	0	0	298679	0
		8	-	-	-	0.482	0.35	0.209	0	0.007	17.91	
		10	-	-	-	0.58	0.37	0	0	0	13.8	
		10	-	-	-	0.784	0.48	0.11	0	0	15.1	
		12	-	-	-	0.664	0.34	0.23	0	0	11.7	
		12	-	-	-	0.667	0.38	0.22	0	0	12.3	

## G. C. AREAS: CINNAMALDEHYDE

CAD <sub>0</sub>	T,C	t,min	B	T	EB	ST	Ph+oCr	6.49	6.80	7.36	CAD	D1	D2
0.67	300	20	0.022	0	0	0.022	1.97	0	0	0	58.7	0.36	3.24
	300	20	0	0	0	0.019	2.64	0	0	0	72.9	0.017	1.22
		40	0	0.027	0.0085	0.078	1.99	0	0	0	71.05	0.077	3.62
		40	0	0.025	0.0089	0.082	1.95	0	0	0	75.2	0.084	6.50
		60	0	0.086	0.37	0.25	3.80	0	0	0	30.8	2.07	12.4
		60	0.040	0.13	0.023	0.33	6.15	0	0	0	37.6	2.38	16.26
		80	0	0.56	0.12	0.099	3.84	0	0	0	10.6	0.47	6.65
		80	0	0.18	0.05	0.062	4.50	0	0	0	13.5	1.22	23.8
0.67	250	40	0	0	0	0	0.27	0	0	0	84.8	0	0.085
		120	0	0	0	0.0058	1.48	0	0	0	66.74	0	1.06
		120	0	0	0	0.0081	3.12	0	0	0	73.0	0	1.84
		150	0	0	0	0.0063	1.27	0	0	0	62.6	0	0.901
		150	0	0	0	0.0068	0.98	0	0	0	79.7	0	1.07

G. C. AREAS: CINNAMALDEHYDE

CAD <sub>0</sub>	T, C	t, min	N <sub>2</sub>	CO	B	T	EB	ST	PH+OCR	6.49	6.80	7.36	CHD	D1	D2
(1.40 400)	15	68.54	31.5	0.034	0.093	0.027	0.144	1.87	0	0	0	28.8	0.243	4.77	
	15	43.61	38.0	0	0.102	0.032	0.172	2.06	0	0	0	34.63	0.27	7.72	
	25	39.66	35.9	0	0.45	0.17	0.28	3.13	0	0	0	15.6	1.02	13.2	
	25	30.1	52.5	0.099	0.523	0.183	0.39	3.16	0	0	0	16.51	0.94	13.8	

## G. C. AREAS: CINNAMALDEHYDE

CAD <sub>0</sub>	T,C	t,min	N <sub>2</sub>	CO	B	T	EB	ST	Ph+Cr	6.49	6.80	7.36	CHD	D1	D2
2.64	400	2	-	-	0	0.15	0.036	0.33	2.6	0.39	2.64	0	72.1	0	9.24
		3	-	-	0.25	3.32	1.27	0.67	7.3	0	0.74	0	12.6	4.75	39.0
		4	-	-	0	3.27	1.29	0.46	1.93	2.2	0	0.18	2.35	4.5	23.6
		6	-	-	0.273	7.65	4.77	0.5	1.13	0.60	0.69	0.018	0.93	2.24	21.6
		8	-	-	0.64	12.85	6.52	1.16	1.47	0.44	0.46	0.043	1.30	2.24	25.2
1.32	400	2	-	-	0	0.049	0	0	0.057	0.59	0.015	2.87	93.98	0	1.32
		3	-	-	0.168	2.25	- .80	1.14	7.22	0.23	0.91	0	32.34	3.8	29.6
		4	-	-	0.275	5.31	2.21	1.37	7.74	0.14	0.33	0	8.67	3.34	26.7
		6	-	-	0	4.26	1.77	0	1.2	0	1.13	0.36	0.46	3.38	12.2
		8	-	-	0.54	11.43	6.05	0.93	1.43	0.66	0.72	0.014	1.12	10.7	24.0
0.40	400	2	-	-	0	0	0.086	0.66	1.03	0.66	0.10	1.75	32.02	0	4.93
		3	-	-	0	0.47	0.061	0.72	1.68	1.32	0.021	0.833	26	0.43	4.52
		4	-	-	0	1.95	0.61	1.15	1.95	2.0	0.404	0.93	15.31	1.95	17.2
		6	-	-	0	0	1.54	0.63	1.48	0	0.87	0.053	1.78	0.78	4.4
		8	-	-	0	0	1.39	0.58	0.44	0	0	0.32	0.71	0	2.33
0.13	400	2	-	-	0	0	0.017	0.036	0.673	0.46	0	0.18	12.12	0	0.11
		3	-	-	0	0	0	0	1.09	0.56	0	0.39	8.68	0	0.83
		4	-	-	0	0.019	0.068	0.24	3.05	0	0.63	0.064	2.35	0.052	0.89
		6	-	-	0	0	0	0.21	1.69	0	0.39	0.043	1.26	0.10	0.47
		8	-	-	0	0.014	0	0.070	0.104	0	0	0.0014	0.103	0.21	0.351
1.40	350	7	-	-	0	0.016	0.0034	0.056	0.348	0	0	0	15.4	0	1.45
		7	-	-	0	0.023	0.0062	0.064	0.41	0	0	0	17.3	0	2.0
		10	-	-	0.072	0.54	0.16	0.33	2.91	0	0	0	5.02	0.282	6.64
		10	-	-	0.044	0.388	0.11	0.24	3.18	0	0	0	4.80	0.288	7.85
		14	-	-	0	0.17	0.070	0.11	1.26	0	0	0	2.67	0.20	3.43
		14	-	-	0	0.23	0.084	0.13	2.22	0	0	0	3.70	0.21	4.34
		21	-	-	0.055	0.65	0.22	0.15	1.87	0	0	0	1.30	0.32	4.55
		21	-	-	0.651	0.94	0.13	0.26	2.03	0	0	0	0.80	0.18	3.76
		28	-	-	0.089	1.08	0.35	0.19	2.08	0	0	0	0.69	0.35	4.74
		28	-	-	0	0.88	0.29	0.18	2.64	0	0	0	0.75	0.484	9.09

G. C. AREAS: CINNAMALDEHYDE

CAD <sub>o</sub>	T, C	t, min	N <sub>2</sub>	CO	B	T	EB	ST	Ph+oCR	CAD	D
(1.21	250)	15	-	-	0	0	0	0	0.10	51.3	0
		20	-	-	0	0	0	0	0.083	33.2	0
		25	-	-	0	0	0	0	0.124	39.9	0
		40	-	-	0	0.011	0	0	0.046	28.61	0
0.67	250	40	-	-	0	0	0	0	0.076	25.4	0
		70	-	-	0	0	0	0	0.133	36.9	0
		70	-	-	0	0	0	0	0.173	42.8	0

## G. C. AREAS: CINNAMALDEHYDE

CAD <sub>0</sub>	T,C	t,min	N <sub>2</sub>	CO	B	T	EB	ST	Ph+oCr	CAD	D
0.67	450	2	40.7	30.8	0.124	1.75	0.66	0.76	0.64	4.89	0.66
		2	-	-	0.145	1.59	0.58	0.65	0.77	3.91	0
		3	-	-	0	0	0.03	0.080	0.015	0.05	0
		3	-	-	0	0.082	0	0.084	0.004	0.823	0
		3.5	52.1	47.9	0.38	5.85	2.22	1.26	1.14	3.45	1.23
		3.5	-	-	0.214	4.21	1.54	0.93	0.79	2.42	1.03
		4	46.9	53.1	0.28	4.42	2.02	0.62	0.04	0.37	0.4
		4	-	-	0	3.35	0	0.37	0.79	0.60	0.45
		5	48.4	50.6	0.46	11.92	6.35	0.642	0.72	0.016	0.20
		5	-	-	0.54	11.0	5.76	0.67	0.73	0.36	0.24
0.67	400	3	62.6	37.5	0.220	1.23	0.31	0.714	1.38	17.96	1.33
		3	-	-	0.174	1.04	0.28	0.692	1.19	13.5	1.03
		4	59.7	40.3	0	0.386	0.104	0.312	0.492	24.6	0.872
		4	-	-	0	0.336	0.011	0.351	0.502	22	0.896
		6	50.3	49.1	0	3.53	1.38	0.323	0.787	0.174	0.37
		6	-	-	0.224	3.31	1.25	0.348	0.59	0.196	0.08
1.21	400	2	88.4	11.5	0	0.012	0	0.043	0.43	51.0	0
		4	62.1	37.8	0.16	1.11	0.397	0.36	1.08	3.05	0
		6	59.0	40.8	0.31	3.53	1.46	0.35	1.56	0.45	0
		8	61.2	37.9	0.19	2.46	1.02	0.15	0.71	0.40	0
1.21	350	2	97.4	2.60	0	0	0	0	0.133	50.4	0
		4	88.6	11.32	0	0.013	0	0.0447	0.272	45.0	0
		8	67.8	32.2	0.12	0.30	0.085	0.284	2.11	38.3	0
		6	76.2	23.8	0.039	0.083	0.024	0.141	0.985	30.7	0
		10	71.7	28.3	0.141	0.39	0.11	0.225	2.77	15.6	0
1.21	300	3	-	-	0	0	0	0	0.109	36.9	0
		6	-	-	0	0	0	0	0.162	53.2	0
		9	-	-	0	0	0	0	0.211	47.0	0
		12	-	-	0	0	0	6.18-3	0.014	34.1	0
		15	-	-	0	0	0	1.28-2	0.362	48.6	0
1.21	250	5	-	-	0	0	0	0	0.088	46.5	0
		10	-	-	0	0	0	0	0.080	37.6	0

GC AREAS: CINNAMYL ALCOHOL

T(°C)	350								
t(min)	1	1.5	2	2.5	3	3	5	7	7
H <sub>2</sub>	-	-	-	-	-	-	-	-	-
N <sub>2</sub>	-	-	-	-	-	10.0	100	87.85	-
CO	-	-	-	-	-	-	0	7.72	-
H <sub>2</sub> +N <sub>2</sub> +CO	-	-	-	-	-	-	-	-	-
CH <sub>4</sub>	-	-	-	-	-	-	-	-	-
C <sub>2</sub> H <sub>2</sub>	-	-	-	-	-	-	-	-	-
H <sub>2</sub> O	-	-	-	-	-	-	-	-	-
MeOH	-	-	-	-	-	-	-	-	-
CH <sub>3</sub> CHO	-	-	-	-	-	-	-	-	-
EtOH	-	-	-	-	-	-	-	-	-
CH <sub>2</sub> O	-	-	-	-	-	-	-	-	-
MeCl <sub>2</sub> I	-	-	-	-	-	-	-	-	-
MeCl <sub>2</sub> II	-	-	-	-	-	-	-	-	-
T	0	0	0	0	0	0	0	0	0
EB	0	0	0	0	0	0	0	0	0
ST	0	0	0	0	0	0	0	0.17	0.015
AB	0	0	0.008	0.060	0	0.12	0.17	0.341	0.29
Ph	0	0.028	0.036	0.108	0.056	0.89	0.68	0.89	0.74
Cr	0	0	0	0	0	0.21	0.16	0.16	0.21
6.2	0	0.031	0.029	0.085	0.002	0.15	0.17	0.45	0.42
7.0	0.045	0.102	0.133	0.21	0.065	0.28	0.33	0.74	0.9
CAD	0	0	0	0.384	0.271	0	1.7	1.9	2.4
CAL	46.0	44.9	51.8	53.5	9.77	29.7	17.9	26.5	20
DIM	0	0	4.06	1.89	0.213	0.97	1.31	1.25	2.66
CAL <sub>0</sub>	1.2	1.2	1.2	1.2	1.2	0.39	0.39	0.39	0.39



GC AREAS: CINNAMYL ALCOHOL

T(°C)	350		
t(min)	9	11	11
H <sub>2</sub>	-	-	-
N <sub>2</sub>	1.51	73.3	-
CO	0.16	17.9	-
H <sub>2</sub> N <sub>2</sub> +CO	-	-	-
CH <sub>4</sub>	-	-	-
H <sub>2</sub> O	-	-	-
MeOH	-	-	-
CH <sub>3</sub> CHO	-	-	-
EtOH	-	-	-
CH <sub>2</sub> O	-	-	-
MeCl <sub>2</sub> I	-	-	-
MeCl <sub>2</sub> II	-	-	-
T	0	0.076	0.45
EB	0	0.15	0.078
ST	0.023	0.13	0.062
AB	0.622	1.02	0.81
Ph	1.63	2.2	1.9
Cr	0.053	0.11	0.08
6.2	0.42	0.68	0.601
7.0	0.64	0.92	0.81
CAD	4.25	4.2	3.64
CAL	9.73	4.0	4.5
DIM	3.01	4.55	4.31
CAL <sub>o</sub>	0.39	0.39	0.39

## G C AREAS: CINNAMYL ALCOHOL

T(°C)		350	H <sub>2</sub> O QUENCH			
t(min)		5	7	9	11	13
H <sub>2</sub>		0.0110	0	0.0185	0	0
N <sub>2</sub>	5.6	96.21	95.91	94.08	93.96	97.84
CO		3.73	4.09	5.90	6.04	2.16
H <sub>2</sub> +N <sub>2</sub> +CO		-	-	-	-	-
CH <sub>4</sub>		-	-	-	-	-
C <sub>2</sub> H <sub>2</sub>	Por	-	-	-	-	-
H <sub>2</sub> O	Q	2.25	1.63	2.22	1.82	1.57
MeOH		0.094	0.10	0.09	0.089	0.031
CH <sub>3</sub> CHO		-	-	-	-	-
EtOH	Por	-	-	-	-	-
CH <sub>2</sub> O	Q	-	-	-	-	-
MeCl <sub>2</sub> I		97.61	98.25	97.63	98.06	98.4
MeCl <sub>2</sub> II		62.75	71.48	70.54	70.84	63.21
T		0	0	0	0.013	0
EB		0	0	0	0	0
ST		0	0.011	0.012	0.025	0
AB		0.007	0.32	0.25	0.42	0
Ph		0.44	1.05	0.78	1.9	0.56
Cr	OV17	0	0	0.11	0.099	0.053
6.2		0.13	0.30	0.35	0.43	0.66
7.0		0.43	0.54	0.99	0	0.30
CAD		1.55	3.42	3.18	4.99	1.62
CAL		27.8	19.72	21.01	18.02	27.6
DIM		1.62	2.4	1.85	2.16	0.93
CAL <sub>0</sub>	=	0.39				

G C AREAS: CINNAMYL ALCOHOL

T(°C)	350	AIR COOL						
t(min)	4	6	8	8	10	10	12	12
H <sub>2</sub>	0	0	0		0	-	0	-
N <sub>2</sub> 5.6	95.75	98.85	97.21	-	84.74	-	93.9	-
CO	4.09	0.872	2.79	-	15.3	-	6.1	-
H <sub>2</sub> +N <sub>2</sub> +CO	-	-	-	-	-	-	-	-
CH <sub>4</sub>	-	-	-	-	-	-	-	-
C <sub>2</sub> H <sub>2</sub> Por	-	-	-	-	-	-	-	-
H <sub>2</sub> O Q	2.57	1.12	1.48	-	1.12	-	1.16	-
MeOH	0.10	0.023	0.075	-	0.13	-	0.10	-
CH <sub>3</sub> CHO	-	-	-	-	0	-	-	-
EtOH Por	-	-	-	-	0	-	-	-
CH <sub>2</sub> O Q	-	-	-	-	0	-	-	-
MeCL <sub>2</sub> I	97.3	98.82	98.4	-	98.7	-	98.61	-
MeCL <sub>2</sub> II	64.8	65.41	77.1	71.6	83.27	78.2	71.94	51.5
T	0	0	0	0	0.081	0.06	0	0.021
EB	0	0	0	0.012	0.019	0.013	0	0.005
ST	0	0	0.017	0.012	0.062	0.049	0.022	0.030
AB	0.28	0	0.37	4.26	0.65	0.62	0.44	0.62
Ph	0.92	0.44	1.20	1.26	2.1	2.43	1.48	2.41
Cr OV17	0.085	0	0.053	0.087	0.085	0.12	0.047	0.16
6.2	0.19	0.12	0.38	0.36	0.79	0.98	0.45	0.7
7.0	0.43	0.20	0.72	0.72	0.96	1.25	0.74	1.2
CAD	2.71	1.17	4.1	3.97	4.16	5.3	4.19	7.7
CAL	25.02	27.3	15.73	15.38	4.86	6.64	13.87	21.48
DIM	4.7	1.2	2.13	2.13	2.14	3.2	4.7	3.7
CAL <sub>0</sub> =	0.39							

## G. C. AREAS: CINNAMYL ALCOHOL

T(°C)	400 - - - - -						
t(min)	4	4	6	8	8	10	12
H <sub>2</sub>	0	-	0	0.0431	-	0	0.0564
N <sub>2</sub>	78.06	-	58.79	61.25	-	51.0	51.5
CO	21.94	-	34.32	38.71	-	49.0	48.5
H <sub>2</sub> +N <sub>2</sub> +CO	93.33	-	92.61	93.86	-	91.06	91.2
CH <sub>4</sub>	0.062	-	0.12	0.0805	-	0.25	0.25
C <sub>2</sub> H <sub>2</sub>	0	-	0	0.475	-	0.77	0.79
H <sub>2</sub> O	1.9	2.02	1.65	1.4	-	0.77	0.81
MeOH	0.19	0.22	0.27	0.25	-	0.17	0.20
CH <sub>3</sub> CHO	0.04	0.046	0.086	0.091	-	0.07	0.093
EtOH	0	0	0.013	0.017	-	0.013	0.020
CH <sub>2</sub> O	0	0	0	0	-	0	0
MeCl <sub>2</sub> I	97.85	97.69	97.95	98.22	-	98.96	98.9
MeCl <sub>2</sub> II	55.2	-	68.77	70.82	67.56	78.1	83.46
T	0	-	0.33	0.30	0.23	0.29	0.38
EB	0	-	0.12	0.13	0.12	0.18	0.20
ST	.071	-	0.28	0.25	0.22	0.16	0.18
AB	0.60	-	0.83	0.80	0.74	0.73	0.61
Ph	1.56	-	1.7	1.69	1.72	2.15	1.52
Cr	0.14	-	0.16	0.15	0.16	0.22	0.17
6.2	1.12	-	1.6	1.71	2.09	2.18	1.5
7.0	2.31	-	3.3	3.94	4.72	3.9	2.8
CAD	5.02	-	3.7	3.47	4.05	2.4	1.55
CAL	20.5	-	9.7	8.85	10.7	3.17	3.3
DIM	2.09	-	5.1	4.6	4.04	4.5	2.9
CAL <sub>o</sub>	0.39						

G. C. AREAS: CINNAMYL ALCOHOL

T(°C)	500		450					
t(min)	5	5	3	4	5	6	7	7
H <sub>2</sub>	0	-	0	0	0	0.074	0.0543	-
N <sub>2</sub>	65.8	-	52.14	43.1	64.1	45.2	39.41	-
CO	31.3	-	47.9	56.92	35.9	54.8	60.54	-
H <sub>2</sub> N <sub>2</sub> +CO	93.74	-	93.73	94.71	94.94	93.4	89.97	-
CH <sub>4</sub>	1.2	-	0.34	0.36	0.33	0.65	0.86	-
C <sub>2</sub> H <sub>2</sub>	0	-	0	0	0	0	0	-
H <sub>2</sub> O	0.30	0.33	0.66	0.97	0.74	0.72	0.63	0.72
MEoH	0.30	0.32	0.20	0.29	0.19	0.33	0.30	0.36
CH <sub>3</sub> CHO	0.042	0.046	0.081	0.14	0.099	0.16	0.14	0.17
EtOH	0.055	0.072	0	0.022	0	0.036	0.04	0.046
CH <sub>2</sub> O	0	0	0	0	0	0	0	0
MeCl <sub>2</sub> <sup>I</sup>	99.3	99.21	98.99	98.6	98.95	98.73	98.9	98.7
MeCl <sub>2</sub> <sup>II</sup>	92.7	-	79.74	77.15	81.08	79.46	76.8	-
T	1.58	-	0.51	1.38	2.16	1.13	1.91	-
EB	0.89	-	0.21	0.76	0.89	0.754	1.32	-
ST	0	-	0.39	0.76	0.44	0.53	0.71	-
AB	0	-	1.2	1.17	1.09	0.91	1.21	-
Ph	0.27	-	2.6	2.75	2.5	1.85	2.24	-
Cr	0	-	0.18	0.25	0.15	0.18	0.24	-
6.2	0.47	-	1.83	0.24	1.08	1.82	2.11	-
7.0	1.47	-	1.75	2.7	1.6	3.38	4.13	-
CAD	0.11	-	2.48	1.81	1.13	1.36	1.21	-
CAL	0.091	-	4.43	2.63	0.5	2.05	1.63	-
DIM	2.4	-	3.47	4.74	6.3	5.2	5.44	-
CAL <sub>o</sub>			0.39					

G.C. AREAS: CINNAMYL ALCOHOL

T(°C)	500 - - - - -							
t(min)	1	1	2	2	3	3	4	4
H <sub>2</sub>	0	-	0.0652	-	-	-	0.028	-
N <sub>2</sub>	95.74	-	54.9	-	-	-	66.4	-
CO	4.3	-	43.5	-	-	-	30.2	-
H <sub>2</sub> +N <sub>2</sub> +CO	100	-	93.54	-	-	-	83.1	-
CH <sub>4</sub>	0	-	0.2	-	-	-	1.9	-
C <sub>2</sub> H <sub>2</sub>	0	-	0	-	-	-	2.92	-
H <sub>2</sub> O	0.68	0.69	0.38	0.51	0.42	0.36	0.32	0.29
MeOH	0.053	0.0686	0.28	0.26	0.31	0.28	0.30	0.34
CH <sub>3</sub> CHO	0.020	0.030	0.11	0.11	0.11	0.096	0.068	0.078
EtOH	0	0	0.036	0.045	0.067	0.067	0.086	0.066
CH <sub>2</sub> O	0.0053	0.0044	0.0066	0	0.0074	0	0.014	0
MeCl <sub>2</sub> I	99.22	99.19	99.15	99.06	99.07	99.78	99.19	99.2
MeCl <sub>2</sub> II	62.41	-	87.69	-	89.02	-	92.14	-
T	0	-	0.31	-	1.64	-	1.57	-
EB	0	-	0	-	0.94	-	0.89	-
ST	0	-	0.20	-	0	-	0	-
AB	0.022	-	0.33	-	0	-	0	-
Ph	0.30	-	0.33	-	0.57	-	0.36	-
Cr	0.037	-	0.031	-	0.038	-	0	-
6.2	0.40	-	0.56	-	0.51	-	0.46	-
7.0	0.89	-	1.83	-	3.04	-	1.27	-
CAD	0.97	-	0.38	-	0.35	-	0.14	-
CAL	33.9	-	1.89	-	0.10	-	0.099	-
DIM	0.281	-	1.9	-	3.73	-	3.0	-
CAL <sub>o</sub>	1.2	-						

G. C. AREAS: CINNAMYL ALCOHOL

T(°C)	300				
t(min)	5	10	15	21	25
H <sub>2</sub>	0	0	0	0	0
N <sub>2</sub>	97.82	97.63	93.64	95.41	93.69
CO	0	2.4	3.93	4.59	6.31
H <sub>2</sub> +N <sub>2</sub> +CO	99.0	98.73	98.87	100	100
CH <sub>4</sub>	0	0	0	0	0
C <sub>2</sub> H <sub>2</sub>	0	0	0	0	0
H <sub>2</sub> O	0.55	2.3	3.08	2.56	2.47
MeOH	0.0092	0.068	0.14	0.11	0.16
CH <sub>3</sub> CHO	0	0.0094	0.011	0.010	0.015
EtOH	0	0	0	0	0
CH <sub>2</sub> O	0	0	0	0	0
MeCl <sub>2</sub> I	99.42	97.58	96.75	97.3	97.32
MeCl <sub>2</sub> II	58.89	65.99	62.02	73.15	71.4
T	0	0	0	0	0
EB	0	0	0	0	0
ST	0	0	0	0	0
AB	0	0.0837	0.26	0.18	0.23
Ph	0.14	0.59	1.07	0.92	1.19
Cr	0	0	0.054	0.052	0.052
6.2	0.10	0	0.24	0.085	0.30
7.0	0.068	0.27	0.52	0.42	0.48
CAD	0.35	1.47	2.33	2.3	2.66
CAL	32.35	27.8	27.3	20.01	16.9
DIM	0.12	2.16	5	1.6	3.13
CAL <sub>0</sub>					

## G. C. AREAS: CINNAMYL ALCOHOL

T(°C)	350	-----			
t(min)	4	8	12	16	20
H <sub>2</sub>	0	0	0	0	0
N <sub>2</sub>	97.54	90.5	84.24	78.03	71.08
CO	2.46	9.5	15.76	21.97	28.92
H <sub>2</sub> +N <sub>2</sub> +CO	98.3	96.5	96.4	92.08	92.52
CH <sub>4</sub>	0	0	0	0.06	0.072
C <sub>2</sub> H <sub>2</sub>	0	0	0	0	0.28
H <sub>2</sub> O	2.2	0.78	1.7	1.42	1.45
MeOH	0.10	0.013	0.14	0.18	0.19
CH <sub>3</sub> CHO	0.014	0	0.024	0.034	0.047
EtOH	0	0	0	0	0
CH <sub>2</sub> O	0	0	0	0	0
MeCl <sub>2</sub> I	97.66	99.2	98.13	98.34	98.29
MeCl <sub>2</sub> II	70.66	69.3	75.33	78.35	78.94
T	0	0	0	0	0
EB	0	0	0	0	0
ST	0	0	0.014	0.031	0.030
AB	0.21	0	0.33	0.52	0.43
Ph	0.69	0.39	1.02	1.61	1.39
Cr	0.093	0.097	0.093	0.12	0.12
6.2	0.23	0.46	0.70	1.0	1.04
7.0	0.45	0.87	1.5	1.57	2.06
CAD	1.49	3.43	3.45	3.39	2.88
CAL	24.1	19.74	15.6	10.03	7.25
DIM	1.32	1.02	0.881	2.24	4.91
CAL <sub>0</sub>					



## G. C. AREAS: ORTHOHYDROXYDIPHENYLMETHANE (OHD)

T(°C)	OHD <sub>0</sub>	t(min)	B	T	P	DPM	10.3	10.7	11.3	11.9	OHD	13.5	17.5	19.8
400	0.27	0	0	0	0	0	0	0	0	0.16	59.73	0	0	0
		15	0	0	2.23	0.0241	0	0	0	0.0254	14.14	0	0	1.23
		30	0	0.074	4.12	0.042	0	0	0	0.047	21.81	0	0	5.62
		50	0.048	0.461	5.91	0.11	0	0	0	0.050	35.82	0	0.0841	10.72
		80	0.11	1.81	9.79	0.20	0.030	0	0.0123	0.29	37.15	0	0.48	0.14
450	0.27	5	0	0.252	2.78	0.053	0	0	0	0.036	25.9	0	0.055	2.45
		10	0.064	1.22	4.87	0.16	0	0	0	0.035	18.6	0	0.37	2.44
		16	0	3.20	9.03	0.32	0	0	0.045	0.056	24.4	0	1.12	3.30
		20	0.0962	7.86	14.7	0.58	0.084	0	0.022	0.086	37.4	0	2.14	4.32
		26	0.13	7.92	14.3	0.66	0.085	0	0.025	0.163	29.0	1.0	3.3	2.80
500	0.27	3	0	5.21	9.64	0.18	0.037	0	0.039	0.10	59.0	0	1.16	6.82
		6	0.34	14.0	19.5	1.27	0.10	0.013	0.154	0.31	31.0	1.0	6.41	1.2
		9	1.18	17.5	24.2	2.71	0.141	0.075	0.26	0.61	12.7	4.6	5.8	0.29
		12	0	6.0	8.95	0.871	0.045	0.012	0.063	0.16	4.73	0.65	2.20	0
		2	0.35	15.7	23.5	1.42	0.31	0.021	0.084	0.20	39.0	1	8.72	1.6
550	0.84	3	1.7	26.4	31.6	3.41	0.30	0.24	0.29	0.41	8.02	3.97	12.36	2.28
		4	1.01	18.8	22.8	3.05	0.21	0.18	0.21	0.32	5.15	3.81	6.89	0.41
		5	3.01	26.4	32.2	5.02	0.18	0.40	0.39	0.31	2.27	3.36	6.93	0.9
		6	3.89	25.8	31.0	7.60	0.16	0.45	0.45	0.26	1.31	3.11	6.20	0.9
500	0.27	10+	0	6.51	10.2	1.0	0.054	0.038	0.085	0.19	4.89	0.46	0.15	2.16
		5+	0	8.35	10.34	0.624	0.066	0.020	0.076	0.20	14.9	0.12	2.13	0.18
		15+	1.11	19.2	24.3	3.08	0.15	0.12	0.26	0.47	9.3	1.47	6.01	0.44

## G. C. AREAS: PHENYL ETHER

T(°C)	PE <sub>0</sub> (mol/l)	t(min)	B	Ph	PE	TRIMERS
400	0.32	2-10	NO REACTION			
500	0.32	90	0	0.502	50.1	0.0707
		90	0	0.242	44.8	0
		90	0	0.258	41.9	0.192
		120	0	0.355	45.0	0.199
		120	0	0.367	39.2	0.131
		150	0	0.292	46.5	4.33-3
		150	0	0.298	41.4	5.42-3
550	0.32	2-8	NO REACTION			
		10	0	0.201	23.9	0
		10	0	0.277	24.1	0
		20	0	0.125	16.3	0
		20	0	0.106	15.5	0
		20	0	5501	349155	1013
		50	5940	12989	484773	2578
		60	0	6358	205296	726
		80	0.770	1.29	20.1	0.692
		80	1.62	2.15	28.52	1.21
		100	1.14	1.27	19.17	0.696
		100	1.48	1.69	23.2	1.11
		20	0	8136	511236	1986
		40	4404	6931	356594	2021
		40	0	3448	178190	424
		80	0	4539	269166	1323
570	0.32	7	0	2.74-2	2.46	0
		10	0	3.07-2	3.73	1.74-2
		10	0	4.33-2	3.73	7.11-3
		15	0.387	0.8349	26.3	0.3838
		15	0.345	0.7665	24.8	0.3571
587	0.32	4	0	0.333	44.3	0.0935
		8.5	1.69	2.59	34.0	0.811
		11	0.975	1.73	27.1	0.832
		12	0.798	1.11	25.2	0.381
		16	1.48	1.51	17.9	0.636
587	0.32	6.5	0	0.539	26.03	0.0253
		6.5	0.209	0.673	30.5	5.57-3
		8	0	0.333	7.42	0
		8	0	0.439	4.05	0
		14	0	1.46	26.5	0
		14	1.28	1.84	29.5	0
		14	1.48	2.25	33.3	9.18-3
		4	0.1414	0.2321	57.6	0.286

## G. C. AREAS: BIPHENYL, BIPHENOL

T		$S_0$ (mol)	t	B	BP
587	BP	2.96-4	6	0.432	34.9
		2.72-4	13.5	2.58	44.73
		2.22-4	15	2.93	54.8
		3.48-4	18	3.50	31.0
		3.97-4	23	3.80	40.9
550	BP	4-8 minutes, no reaction			
400	BP	2-10 minutes, no reaction			
500	BPL	5-25+ minutes, no reaction			



G. C. AREAS: FERULIC ACID

T	FA <sub>o</sub> (mol)	t	A <sub>N<sub>2</sub></sub>	A <sub>CO<sub>2</sub></sub>	A <sub>CH<sub>4</sub></sub>	A <sub>CO</sub>	Vr
200	2.41-4	4	90.0	9.69	-	-	3.47
	3.21-4	8	70.3	29.0	-	-	
	1.95-4	12	69.2	30.5	-	-	
	2.97-4	16	64.8	35.2	-	-	
	2.32-4	20	64.4	34.8	-	-	
	1.65-4	24	66.4	32.9	-	-	
250	5.59-5	1	92.3	7.57	-	-	0.6
	9.40-5	2	69.2	29.8	-	-	
	9.71-5	3	61.0	39.0	-	-	
	9.37-5	4	66.0	33.5	-	-	
	1.56-4	5	67.2	31.9	-	-	
	2.71-4	7	52.6	46.7	-	-	
300	5.14-4	3	33.3	13.9	-	-	3.47
	4.04-4	6	33.3	13.9	-	-	
	3.28-4	9	35.2	13.6	-	-	
	4.11-4	12.5	31.4	14.5	0.06	0.171	
	3.40-4	15	35.5	13.6	-	-	
350	3.47-4	2	37.1	12.7	0	0.19	
	3.57-4	4	34.6	13.5	0.083	0.19	
	4.60-4	6	27.5	15.0	0.083	0.20	
	3.26-4	8	34.6	13.7	0.25	0.24	
	4.29-4	10	34.6	13.1	0.22	0.29	
250	2.68-4	5	41.3	9.1	-	-	
	3.88-4	10	34.9	14.1	-	-	
	5.95-4	12.5	31.4	14.5	-	-	
	3.78-4	15	33.6	14.0	-	-	
	3.40-4	20	34.6	13.3	-	-	

G. C. AREAS: NA

T(°C)	1-NA <sub>0</sub>	N <sub>2</sub>	CO <sub>2</sub>	t	2-NA <sub>0</sub>	N <sub>2</sub>	CO <sub>2</sub>	V <sub>r</sub> =0.6cm <sup>3</sup>	
400	1.01-4	75.9	24.11	3	9.05-5	83.95	16.1		
	1.34-4	55.6	44.4	5	1.21-4	81.5	18.5		
	1.37-4	52.3	40.7	6	1.37-4	79.6	20.4		
	1.12-4	43.7	56.3	8	1.43-4	80.8	19.2		
	1.51-4	38.6	61.4	10	1.66-4	77.4	22.6		
	9.32-5	39.4	60.6	12	1.61-4	68.9	31.1		
	1.08-4	52.0	48.0	14	1.32-4	66.7	33.4		
	9.65-5	35.4	64.6	16	1.08-4	60.8	37.6		
	1.11-4	38.8	61.2	18	1.65-4	60.9	39.1		
	9.21-5	33.0	67.0	20	1.98-4	51.2	48.8		
	5.19-5	65.9	34.1	6	8.32-5	71.3	28.7		
	6.64-5	48.7	51.3	7	1.12-4	76.0	24.0		
	1.42-4	43.2	56.8	7	2.57-4	72.9	27.1		
	8.22-5	45.2	54.8	9	1.21-4	57.7	42.3		
	8.42-5	43.0	57.0	11	1.09-4	60.3	39.7		
	6.45-5	39.8	60.2	13	1.15-4	64.9	35.1		
	9.50-5	38.5	61.5	14	1.59-4	66.0	34.0		
	9.70-5	31.3	68.8	25	1.33-4	55.3	44.7		
	2.21-4	85.2	14.8	2	-	-	-		
	2.18-4	61.7	38.3	4	-	-	-		
	7.41-5	54.5	66.2	5	-	-	-		
	350	7.26-5	87.1	12.9	3	1.15-4	88.4	8.79	
		4.94-5	86.5	13.5	5	1.09-4	86.0	11.0	
		6.48-5	78.1	20.3	9	1.20-4	85.7	14.4	
		6.88-5	79.0	21.0	10	1.04-4	87.9	12.1	
9.75-5		73.1	26.9	13	1.09-4	85.1	14.9		
5.02-5		68.5	31.5	15	7.91-5	79.6	20.1		
8.32-5		64.8	32.1	17	1.46-4	85.5	14.5		
7.06-5		60.52	30.2	20	9.68-5	82.6	17.4		
9.18-5		57.3	48.7	22	1.37-4	85.0	15.0		
5.72-5		64.7	35.3	25	1.00-4	84.1	15.9		
450	7.81-5	85.4	14.6	1	8.66-5	86.6	13.4		
	7.26-5	56.9	43.1	2	7.78-5	78.0	22.0		
	6.10-5	58.3	41.7	3	2.09-4	53.5	46.5		
	4.65-5	56.7	41.7	4	6.21-5	64.3	35.7		
	1.60-4	41.3	58.7	5	1.64-4	53.8	46.2		
	7.59-5	37.5	62.5	6	1.22-4	45.3	54.6		
	4.78-5	43.5	56.5	7	1.16-4	51.8	48.2		
	4.96-5	38.0	44.4	8	7.61-5	44.5	55.4		

## Appendix 7.2. Summary of Model Compound Kinetic Data

Substrate	Reaction	So(mol/l)	T,C	$\log_{10}k(s^{-1})$	S=mol T/ mol S <sub>0</sub>		
PPE	R1:PPE → Ph+St E*=45.0±2.7 $\log_{10}A=11.1 \pm .9$	.25	300	5.97	0		
		.25	325	5.17	0		
		.25	350	4.67	0		
		.083	400	3.41	0		
		.25	400	3.41	0		
		.25	400	3.27	0		
		.75	400	3.23	0		
		.83	400	3.47	0		
		1.16	400	3.13	0		
		.25	450	2.72	0		
		.25	500	1.67	0		
		.75	500	1.79	0		
		.75	550	.865			
		.25	400	3.49	.245		
		.25	400	3.55	.492		
		.25	400	3.55	1.48		
		.25	400	3.48	1.48		
		.25	400	3.58	4.92		
		.25	400	3.67	9.8		
		OHD	R1:OHD → TOL+Ph E*=43.4±1.4 $\log_{10}A=9.6 \pm 0.4$	.25	350	4.72	1.48
.25	350			4.72	4.92		
.25	450			2.47	1.48		
.25	450			2.62	4.92		
.27	400			4.51	0		
.27	450			3.45	0		
.27	500			2.74	0		
.84	550			1.91	0		
PE	R1:PE → Ph+B E*=72.1±4.8 $\log_{10}A=14.8 \pm 1.3$			0.32	500	5.64	0
				0.32	550	4.47	0
		.32	570	3.86	0		
		.32	587	3.61	0		
BP	R1:BP → 2B	.49	587	3.82	0		

Note: E\* [=] kcal/mol  
A [=] s<sup>-1</sup>

SUBSTRATE: GUAIACOL

$G_0$ (mol/l)	T(C)	$-\log_{10}k(s^{-1})$		
		R1: $G \rightarrow C+CH_4$	R2: $G \rightarrow P+CO$	R0: $G \rightarrow PRODUCTS$
.45	250	5.93	7.15	5.90
.45	300	6.68	6.80	5.65
.45 -3.0	350	4.45	5.10	4.36
.45	400	3.2	3.8	3.10
.45	450	2.15	3.12	2.11
.45	450	2.08	2.78	2.00
.45	500	1.86	3.16	1.84
.45	525	1.10	2.88	1.09

$E^*$ $\log_{10}A$		
	43.7±1.4	47.4±1.6
	10.9±0.5	11.5±0.5

SUBSTRATE: ISOEUGENOL

$I_0$	T(C)	$-\log_{10}k(s^{-1})$	
		R1: $I \rightarrow PC+CH_4$	R2: $I \rightarrow PP+CO$
.33	300	5.68	-
.31	350	4.23	4.93
.33	400	3.24	3.73

$E^*$ $\log_{10}A$		
	4.29±2.5	46.2
	10.8±.88	11.3

SUBSTRATE: 2,6-DIMETHOXYPHENOL

$DMP_0$	T(C)	$-\log_{10}k(s^{-1})$	
		R1: $DMP \rightarrow MC+CH_4$	R2: $DMP \rightarrow G+CO$
0.37	300	5.41	6.02
.37	325	5.21	5.59
.37	350	4.41	5.32
.37	375	3.98	4.30
.37	400	3.01	3.4
.37	500	1.88	2.98

$E^*$ $\log_{10}A$		
	42.2±6.0	45.5±7.6
	10.4±2.1	11.1±2.7



## SUBSTRATE: VANILLIN

$VA_0$	T(C)	R1:V $\rightarrow$ DHB+CH <sub>4</sub>	(carbonyl) R1: $\rightarrow$ G+CO
.2	300	6.00	4.03,4.61,4.93
.2	350	4.09	3.33
.2	375	3.52	2.68
.2	400	3.47	2.42
E*		47.3 $\pm$ 8.6	38.5 $\pm$ 5.9
log <sub>10</sub> A		12.2 $\pm$ 3.0	10.2 $\pm$ 2.1

## SUBSTRATE: VERATROLE

VE <sub>0</sub>	T(C)	R3:VE $\rightarrow$ G+CH <sub>4</sub>	R3 <sup>1</sup> :VE $\rightarrow$ Ph+CO+CH <sub>4</sub>	R4:VE $\rightarrow$ AN+CO	R5:VE $\rightarrow$ OC+CO	R0:VE $\rightarrow$ PRODUCTS
0.33	350	5.67	-	6.71		5.63
.33	375	4.62	5.60	5.28	5.50	4.46
.33	400	4.02	4.81	4.48	5.03	3.81
.33	425	3.53	4.23	3.78	3.85	3.18
.33	450	2.87	3.51	3.53	3.53	2.65
.33	500	(2.39)	(2.91)	2.4	2.94	1.98
.33	550	-	(2.66)	(2.70)	(2.35)	-
E*	55.9 $\pm$ 4.03	58.4 $\pm$ 2.8	60.1 $\pm$ 5.73	49.2 $\pm$ 7.05		
log <sub>10</sub> A	13.9 $\pm$ 1.32	14.1 $\pm$ 0.9	14.8 $\pm$ 1.83	11.2 $\pm$ 2.2		

## SUBSTRATE ANISOLE

AN <sub>0</sub>	T	R3:AN $\rightarrow$ PH+CH <sub>4</sub>	R4:AN $\rightarrow$ B+CO	R5:AN $\rightarrow$ OC	R0:AN $\rightarrow$ PRODUCTS
1.57	344	(5.81)	-	-	-
1.57	370	.552	6.59	5.47	5.22
1.57	406	4.57	5.17	5.02	4.27
1.57	434	4.14	4.21	4.97	3.70
1.57	465	3.12	3.43	3.78	2.87
1.57	490	27	2.85	3.47	2.30
.46	550	(2.2)	2.15	3.0	1.30
.46	450	3.66	3.82	4.47	3.18
.77	450	3.40	3.86	4.48	3.16
1.08	450	3.70	4.19	4.38	3.43
1.54	450	3.38	3.91	4.24	3.15
3.08	450	3.44 <sub>±</sub>	3.96	4.18	3.23 <sub>±</sub>
ALL	450	3.50 <sub>±</sub> .14	3.95 <sub>±</sub> .15	4.35 <sub>±</sub> .14	3.24 <sub>±</sub> .12
E*	54.7 $\pm$ 3.06	61.0 $\pm$ 3.99	40.5 $\pm$ 4.9		
log <sub>10</sub> A	13.0 $\pm$ .94	14.5 $\pm$ 1.21	7.9 $\pm$ 1.5		

## SUBSTRATE: CINNAMYL ALCOHOL

CAL <sub>0</sub>	T	CAL → CAD	CAL → DIM	CAL → PHENOLS	CAL → H <sub>2</sub> O	CAL → MeOH	CAL → PRODUCTS
.39	300	4.14	4.10	4.52	(4.35)	5.54	3.45
.39	350	2.28	3.78	4.26	4.35	5.23	3.03
.39	400	2.90	3.00	3.86	4.23	4.65	2.37
.39	450				3.52	4.03	
1.2	500				16.7	3.56	
E*		26.8			1.4	24.7	
log <sub>10</sub> A		4.22				3.4	

## SUBSTRATE: SALIGENOL

## SUBSTRATE: BENZALDEHYDE

SAL <sub>0</sub>	T	SAL → H <sub>2</sub> O	BA <sub>0</sub>	T	R1:BA → B+CO)
.23-12	175	2.79	.49	350	5.36
	200	2.22	.16-3.3	400	3.60(4x), 3.75
	225	1.20	.49	450	2.28, 3.10
E*		33.4	.49	500	2.29, 2.20
log <sub>10</sub> A		13.4	.49	550	1.91, 1.54
			E*		41.5±2.77
			log <sub>10</sub> A		9.5±.85

## SUBSTRATE: ACETOPHENONE

AP <sub>0</sub>	T	AP → CO	AP → CH <sub>4</sub>	AP → B	AP → TOL	AP → DIM	AP → PRODUCTS
0.46	400						
		CONVERSION VERY SMALL, NO ACCURATE ESTIMATES					
0.46	450	5.43	5.92	5.66	6.15	5.20	4.95
0.46	500	4.70	5.05	4.86	5.26	4.34	3.78
0.46	550	3.71	4.06	3.78	4.05	4.00	3.03
E*				50.5	5.64±7.6	32.7	52.1±4.11
log <sub>10</sub> A				9.6	10.9±2.1	4.8	10.9±11.7

## SUBSTRATE: CINNAMALDEHYDE

CAD <sub>0</sub>	T	R1:CAD → St+CO	R3:CAD → DIM	R2:CAD → Phenols	R0:CAD → PRODUCTS
.67,1.21	250	7.95	5.55	5.95	5.35
.67,1.21	300	6.30	4.08	4.77	3.52
.4,1.21	350	4.78	3.44	3.6	2.68
.13-2.64	400	3.48	2.28	2.78	2.02
E*		48.2±1.1	33.7±3.07	34.5±1.0	35.4±4.55
log <sub>10</sub> A		12.1±.4	8.60±1.14	8.5±0.4	9.67±1.69

## SUBSTRATE: CINNAMMIC ACID

CA <sub>0</sub>	T	R1:CA → St+CO <sub>2</sub>
.5	300	3.78
	350	3.06
	400	2.00
E*		31.0±5.0
log <sub>10</sub> A		8.0±1.8

## SUBSTRATE: FERULIC ACID

FA <sub>0</sub>	T	R1:FA → VG+CO <sub>2</sub>
.5	200	3.30
	250	2.70
	300	2.60
	350	1.90

## SUBSTRATE: NAPTHOIC ACID

NA <sub>0</sub>	T	R1:1-NA → N+CO <sub>2</sub>	R1:2-NA → N+CO <sub>2</sub>
.1	350	3.81	4.82
	400	3.36	4.20
	450	2.65	3.05

TIME	INTERVAL	TEMP(C)	
0.00000	0	0.10000	2 300.0
0.00000	0	0.10000	2 300.0
PRODUCT	YIELD(WT%)		
PHENOL	0.00000	0	
CRESOLS	0.00000	0	
ETHYLPHENOL	0.00000	0	
PROPYLPHENOL	0.00000	0	
GUAIACOL	0.00000	0	
METHYLGUAIACOL	0.00000	0	
ETHYLGUAIACOL	0.00000	0	
PROPYLGUAIACOL	0.00000	0	
EUGENOL	0.00000	0	
VINYLGUAIACOL	0.00000	0	
CONIFERALDEHYDE	0.20160	1	
PROPIOVANILLONE	0.00000	0	
CATECHOL	0.00000	0	
METHYLCATECHOL	0.00000	0	
ETHYLCATECHOL	0.00000	0	
3,4-DIHYDROXYCINNAMALDEHYDE	0.00000	0	
VINYLCATECHOL	0.00000	0	
ALLYLCATECHOL	0.00000	0	
SYRINGOL	0.00000	0	
METHYLSYRINGOL	0.00000	0	
ETHYLSYRINGOL	0.00000	0	
PROPYLSYRINGOL	0.00000	0	
VINYLSYRINGOL	0.00000	0	
ALLYLSYRINGOL	0.00000	0	
SYRINGALDEHYDE	0.00000	0	
PROPIOSYRINGONE	0.00000	0	
METHOXYCATECHOL	0.00000	0	
METHANE	0.00000	0	
CARBON MONOXIDE	0.00000	0	
WATER	0.00000	0	
CARBON DIOXIDE	0.00000	0	
HYDROGEN	0.00000	0	
METHANOL	0.00000	0	
GUAIACYL ACRROLEIN	0.00000	0	
SINAPYL ACRROLEIN	0.00000	0	
HYDROXYPHENYL ACRROLEIN	0.00000	0	
SINAPYL ALDEHYDE	0.26570	-1	
COUMARALDEHYDE	0.22440	0	
PYROGALLOL	0.00000	0	
3,4-DIHYDROXYPHENYLACROLEIN	0.00000	0	
SINGLE RINGS, MULTIPLE RINGS, AND SINGLES+			
LIGHTS ON MOL FRACTION BASIS			
SINGLE RING AROMATICS	0.71200	-1	
MULTIPLE RING AROMATICS	0.92760	0	
SINGLE RINGS AND LIGHTS	0.71200	-1	

Appendix 9.1 Tables of simulation predictions.

TIME	INTERVAL	TEMP(C)	
0.10000	4	0.10000	2 300.0
0.10000	4	0.10000	2 300.0
PRODUCT	YIELD(WTZ)		
PHENOL	0.16000 -4		
CRESOLS	0.12660 -3		
ETHYLPHENOL	0.96050 -4		
PROPYLPHENOL	0.16090 -3		
GUAIACOL	0.15700 -3		
METHYLGUAIACOL	0.12030 -2		
ETHYLGUAIACOL	0.89040 -3		
PROPYLGUAIACOL	0.14610 -2		
EUGENOL	0.14430 -2		
VINYLGUAIACOL	0.58240 -2		
CONIFERALDEHYDE	0.16480 1		
PROPIOVANILLONE	0.00000 0		
CATECHOL	0.23670 -6		
METHYLCATECHOL	0.18370 -5		
ETHYLCATECHOL	0.13740 -5		
3,4-DIHYDROXYCINNAMALDEHYDE	0.25800 -2		
VINYLCATECHOL	0.91050 -5		
ALLYLCATECHOL	0.22440 -5		
SYRINGOL	0.25000 -5		
METHYLSYRINGOL	0.18780 -4		
ETHYLSYRINGOL	0.13670 -4		
PROPYLSYRINGOL	0.22120 -4		
VINYLSYRINGOL	0.89590 -4		
ALLYLSYRINGOL	0.21890 -4		
SYRINGALDEHYDE	0.00000 0		
PROPIOSYRINGONE	0.00000 0		
METHOXYCATECHOL	0.36310 -8		
METHANE	0.51780 -2		
CARBON MONOXIDE	0.58530 -2		
WATER	0.43560 -2		
CARBON DIOXIDE	0.00000 0		
HYDROGEN	-0.15730 -3		
METHANOL	0.74330 -4		
GUAIACYL ACROLEIN	0.12420 -1		
SINAPYL ACROLEIN	0.18610 -3		
HYDROXYPHENYL ACROLEIN	0.13880 -2		
SINAPYL ALDEHYDE	0.24680 -1		
COUMARALDEHYDE	0.18410 0		
PYROGALLOL	0.27320 -11		
3,4-DIHYDROXYPHENYLACROLEIN	0.19440 -4		
SINGLE RINGS, MULTIPLE RINGS, AND SINGLES+			
LIGHTS ON MOL FRACTION BASIS			
SINGLE RING AROMATICS	0.73640 -1		
MULTIPLE RING AROMATICS	0.92550 0		
SINGLE RINGS AND LIGHTS	0.88940 -1		

TIME	INTERVAL	TEMP(C)	
0.2000D	4	0.1000D	2 300.0
0.2000D	4	0.1000D	2 300.0
PRODUCT	YIELD(WTZ)		
PHENOL	0.4996D	-4	
CRESOLS	0.3949D	-3	
ETHYLPHENOL	0.3000D	-3	
PROPYLPHENOL	0.5090D	-3	
GUAIACOL	0.4886D	-3	
METHYLGUAIACOL	0.3741D	-2	
ETHYLGUAIACOL	0.2771D	-2	
PROPYLGUAIACOL	0.4606D	-2	
EUGENOL	0.4550D	-2	
VINYLGUAIACOL	0.7827D	-2	
CONIFERALDEHYDE	0.1364D	1	
PROPIOVANILLONE	0.0000D	0	
CATECHOL	0.1463D	-5	
METHYLCATECHOL	0.1135D	-4	
ETHYLCATECHOL	0.8490D	-5	
3,4-DIHYDROXYCINNAMALDEHYDE	0.4242D	-2	
VINYLCATECHOL	0.2431D	-4	
ALLYLCATECHOL	0.1405D	-4	
SYRINGOL	0.8640D	-5	
METHYLSYRINGOL	0.6484D	-4	
ETHYLSYRINGOL	0.4723D	-4	
PROPYLSYRINGOL	0.7743D	-4	
VINYLSYRINGOL	0.1337D	-3	
ALLYLSYRINGOL	0.7664D	-4	
SYRINGALDEHYDE	0.0000D	0	
PROPIOSYRINGONE	0.0000D	0	
METHOXYCATECHOL	0.2380D	-7	
METHANE	0.1044D	-1	
CARBON MONOXIDE	0.1088D	-1	
WATER	0.9335D	-2	
CARBON DIOXIDE	0.0000D	0	
HYDROGEN	0.1104D	-3	
METHANOL	0.2308D	-3	
GUAIACYL ACROLEIN	0.2519D	-1	
SINAPYL ACROLEIN	0.4192D	-3	
HYDROXYPHENYL ACROLEIN	0.2826D	-2	
SINAPYL ALDEHYDE	0.2270D	-1	
COUMARALDEHYDE	0.1530D	0	
PYROGALLOL	0.3510D	-10	
3,4-DIHYDROXYPHENYLACROLEIN	0.7835D	-4	
SINGLE RINGS, MULTIPLE RINGS, AND SINGLES+			
LIGHTS ON MOL FRACTION BASIS			
SINGLE RING AROMATICS	0.7602D	-1	
MULTIPLE RING AROMATICS	0.9238D	0	
SINGLE RINGS AND LIGHTS	0.1070D	0	

TIME	INTERVAL	TEMP(C)	
0.3000D	4	0.1000D	2 300.0
0.3000D	4	0.1000D	2 300.0
PRODUCT	YIELD(WT%)		
PHENOL	0.8948D	-4	
CRESOLS	0.7074D	-3	
ETHYLPHENOL	0.5372D	-3	
PROPYLPHENOL	0.9354D	-3	
GUAIACOL	0.8718D	-3	
METHYLGUAIACOL	0.6675D	-2	
ETHYLGUAIACOL	0.4943D	-2	
PROPYLGUAIACOL	0.8432D	-2	
EUGENOL	0.8331D	-2	
VINYLGUAIACOL	0.8074D	-2	
CONIFERALDEHYDE	0.1142D	1	
PROPIOVANILLONE	0.0000D	0	
CATECHOL	0.3889D	-5	
METHYLCATECHOL	0.3016D	-4	
ETHYLCATECHOL	0.2257D	-4	
3,4-DIHYDROXYCINNAMALDEHYDE	0.5289D	-2	
VINYLCATECHOL	0.3736D	-4	
ALLYLCATECHOL	0.3832D	-4	
SYRINGOL	0.1683D	-4	
METHYLSYRINGOL	0.1263D	-3	
ETHYLSYRINGOL	0.9201D	-4	
PROPYLSYRINGOL	0.1548D	-3	
VINYLSYRINGOL	0.1506D	-3	
ALLYLSYRINGOL	0.1532D	-3	
SYRINGALDEHYDE	0.0000D	0	
PROPIOSYRINGONE	0.0000D	0	
METHOXYCATECHOL	0.6673D	-7	
METHANE	0.1578D	-1	
CARBON MONOXIDE	0.1528D	-1	
WATER	0.1460D	-1	
CARBON DIOXIDE	0.0000D	0	
HYDROGEN	0.5246D	-3	
METHANOL	0.4169D	-3	
GUAIACYL ACROLEIN	0.3830D	-1	
SINAPYL ACROLEIN	0.6957D	-3	
HYDROXYPHENYL ACROLEIN	0.4312D	-2	
SINAPYL ALDEHYDE	0.2074D	-1	
COUMARALDEHYDE	0.1285D	0	
PYROGALLOL	0.1452D	-9	
3,4-DIHYDROXYPHENYLACROLEIN	0.1774D	-3	
SINGLE RINGS, MULTIPLE RINGS, AND SINGLES+			
LIGHTS ON MOL FRACTION BASIS			
SINGLE RING AROMATICS	0.7834D	-1	
MULTIPLE RING AROMATICS	0.9224D	0	
SINGLE RINGS AND LIGHTS	0.1249D	0	



TIME	INTERVAL	TEMP(C)	
0.4000D	4	0.1000D	2 300.0
0.4000D	4	0.1000D	2 300.0
PRODUCT	YIELD(WTZ)		
PHENOL			0.1288D -3
CRESOLS			0.1018D -2
ETHYLPHENOL			0.7734D -3
PROPYLPHENOL			0.1395D -2
GUAIACOL			0.1251D -2
METHYLGUAIACOL			0.9576D -2
ETHYLGUAIACOL			0.7090D -2
PROPYLGUAIACOL			0.1253D -1
EUGENOL			0.1238D -1
VINYLGUAIACOL			0.7581D -2
CONIFERALDEHYDE			0.9648D 0
PROPIOVANILLONE			0.0000D 0
CATECHOL			0.7399D -5
METHYLCATECHOL			0.5739D -4
ETHYLCATECHOL			0.4293D -4
3,4-DIHYDROXYCINNAMALDEHYDE			0.5929D -2
VINYLCATECHOL			0.4652D -4
ALLYLCATECHOL			0.7553D -4
SYRINGOL			0.2603D -4
METHYLSYRINGOL			0.1954D -3
ETHYLSYRINGOL			0.1423D -3
PROPYLSYRINGOL			0.2480D -3
VINYLSYRINGOL			0.1524D -3
ALLYLSYRINGOL			0.2454D -3
SYRINGALDEHYDE			0.0000D 0
PROPIOSYRINGONE			0.0000D 0
METHOXYCATECHOL			0.1331D -6
METHANE			0.2120D -1
CARBON MONOXIDE			0.1919D -1
WATER			0.1999D -1
CARBON DIOXIDE			0.0000D 0
HYDROGEN			0.9781D -3
METHANOL			0.6118D -3
GUAIACYL ACRROLEIN			0.5169D -1
SINAPYL ACRROLEIN			0.1012D -2
HYDROXYPHENYL ACRROLEIN			0.5841D -2
SINAPYL ALDEHYDE			0.1889D -1
COUMARALDEHYDE			0.1090D 0
PYROGALLOL			0.3805D -9
3,4-DIHYDROXYPHENYLACROLEIN			0.3176D -3
SINGLE RINGS, MULTIPLE RINGS, AND SINGLES+			
LIGHTS ON MOL FRACTION BASIS			
SINGLE RING AROMATICS			0.8059D -1
MULTIPLE RING AROMATICS			0.9210D 0
SINGLE RINGS AND LIGHTS			0.1426D 0

TIME	INTERVAL	TEMP(C)	
0.5000D	4	0.1000D	2 300.0
0.5000D	4	0.1000D	2 300.0
PRODUCT	YIELD(WT%)		
PHENOL		0.1657D	-3
CRESOLS		0.1310D	-2
ETHYLPHENOL		0.9950D	-3
PROPYLPHENOL		0.1870D	-2
GUAIACOL		0.1603D	-2
METHYLGUAIACOL		0.1227D	-1
ETHYLGUAIACOL		0.9087D	-2
PROPYLGUAIACOL		0.1673D	-1
EUGENOL		0.1653D	-1
VINYLGUAIACOL		0.6837D	-2
CONIFERALDEHYDE		0.8238D	0
PROPIOVANILLONE		0.0000D	0
CATECHOL		0.1179D	-4
METHYLCATECHOL		0.9143D	-4
ETHYLCATECHOL		0.6842D	-4
3,4-DIHYDROXYCINNAMALDEHYDE		0.6295D	-2
VINYLCATECHOL		0.5217D	-4
ALLYLCATECHOL		0.1254D	-3
SYRINGOL		0.3559D	-4
METHYLSYRINGOL		0.2671D	-3
ETHYLSYRINGOL		0.1945D	-3
PROPYLSYRINGOL		0.3532D	-3
VINYLSYRINGOL		0.1467D	-3
ALLYLSYRINGOL		0.3496D	-3
SYRINGALDEHYDE		0.0000D	0
PROPIOSYRINGONE		0.0000D	0
METHOXYCATECHOL		0.2217D	-6
METHANE		0.2669D	-1
CARRON MONOXIDE		0.2272D	-1
WATER		0.2546D	-1
CARBON DIOXIDE		0.0000D	0
HYDROGEN		0.1430D	-2
METHANOL		0.8075D	-3
GUAIACYL ACRYLEIN		0.6535D	-1
SINAPYL ACRYLEIN		0.1365D	-2
HYDROXYPHENYL ACRYLEIN		0.7412D	-2
SINAPYL ALDEHYDE		0.1721D	-1
COUMARALDEHYDE		0.9343D	-1
PYROGALLOL		0.7824D	-9
3,4-DIHYDROXYPHENYLACRYLEIN		0.4993D	-3
SINGLE RINGS, MULTIPLE RINGS, AND SINGLES+			
LIGHTS ON MOL FRACTION BASIS			
SINGLE RING AROMATICS		0.8278D	-1
MULTIPLE RING AROMATICS		0.9198D	0
SINGLE RINGS AND LIGHTS		0.1599D	0

TIME	INTERVAL	TEMP(C)	
0.6000D	4	0.1000D	2 300.0
0.6000D	4	0.1000D	2 300.0
PRODUCT	YIELD(WTZ)		
PHENOL	0.1994D	-3	
CRESOLS	0.1577D	-2	
ETHYLPHENOL	0.1197D	-2	
PROPYLPHENOL	0.2350D	-2	
GUAIACOL	0.1921D	-2	
METHYLGUAIACOL	0.1471D	-1	
ETHYLGUAIACOL	0.1089D	-1	
PROPYLGUAIACOL	0.2095D	-1	
EUGENOL	0.2070D	-1	
VINYLGUAIACOL	0.6065D	-2	
CONIFERALDEHYDE	0.7110D	0	
PROPIOVANILLONE	0.0000D	0	
CATECHOL	0.1689D	-4	
METHYLCATECHOL	0.1310D	-3	
ETHYLCATECHOL	0.9799D	-4	
3,4-DIHYDROXYCINNAMALDEHYDE	0.6490D	-2	
VINYLCATECHOL	0.5528D	-4	
ALLYLCATECHOL	0.1876D	-3	
SYRINGOL	0.4515D	-4	
METHYLSYRINGOL	0.3389D	-3	
ETHYLSYRINGOL	0.2468D	-3	
PROPYLSYRINGOL	0.4680D	-3	
VINYLSYRINGOL	0.1377D	-3	
ALLYLSYRINGOL	0.4633D	-3	
SYRINGALDEHYDE	0.0000D	0	
PROPIOSYRINGONE	0.0000D	0	
METHOXYCATECHOL	0.3304D	-6	
METHANE	0.3225D	-1	
CARBON MONOXIDE	0.2596D	-1	
WATER	0.3097D	-1	
CARBON DIOXIDE	0.0000D	0	
HYDROGEN	0.1859D	-2	
METHANOL	0.1000D	-2	
GUAIACYL ACRYLEIN	0.7923D	-1	
SINAPYL ACRYLEIN	0.1752D	-2	
HYDROXYPHENYL ACRYLEIN	0.9019D	-2	
SINAPYL ALDEHYDE	0.1572D	-1	
COUMARALDEHYDE	0.8093D	-1	
PYROGALLOL	0.1385D	-8	
3,4-DIHYDROXYPHENYLACRYLEIN	0.7233D	-3	
SINGLE RINGS, MULTIPLE RINGS, AND SINGLES+			
LIGHTS ON MOL FRACTION BASIS			
SINGLE RING AROMATICS	0.8493D	-1	
MULTIPLE RING AROMATICS	0.9186D	0	
SINGLE RINGS AND LIGHTS	0.1770D	0	

TIME	INTERVAL	TEMP(C)	
0.7000D	4	0.1000D	2 300.0
0.7000D	4	0.1000D	2 300.0
PRODUCT	YIELD(WTZ)		
PHENOL	0.2299D	-3	
CRESOLS	0.1818D	-2	
ETHYLPHENOL	0.1380D	-2	
PROPYLPHENOL	0.2833D	-2	
GUAIACOL	0.2208D	-2	
METHYLGUAIACOL	0.1691D	-1	
ETHYLGUAIACOL	0.1252D	-1	
PROPYLGUAIACOL	0.2517D	-1	
EUGENOL	0.2487D	-1	
VINYLGUAIACOL	0.5354D	-2	
CONIFERALDEHYDE	0.6199D	0	
PROPIOVANILLONE	0.0000D	0	
CATECHOL	0.2254D	-4	
METHYLCATECHOL	0.1749D	-3	
ETHYLCATECHOL	0.1308D	-3	
3,4-DIHYDROXYCINNAMALDEHYDE	0.6574D	-2	
VINYLCATECHOL	0.5670D	-4	
ALLYLCATECHOL	0.2618D	-3	
SYRINGOL	0.5452D	-4	
METHYLSYRINGOL	0.4092D	-3	
ETHYLSYRINGOL	0.2980D	-3	
PROPYLSYRINGOL	0.5909D	-3	
VINYLSYRINGOL	0.1278D	-3	
ALLYLSYRINGOL	0.5849D	-3	
SYRINGALDEHYDE	0.0000D	0	
PROPIOSYRINGONE	0.0000D	0	
METHOXYCATECHOL	0.4573D	-6	
METHANE	0.3788D	-1	
CARBON MONOXIDE	0.2897D	-1	
WATER	0.3653D	-1	
CARBON DIOXIDE	0.0000D	0	
HYDROGEN	0.2261D	-2	
METHANOL	0.1189D	-2	
GUAIACYL ACRYLEIN	0.9335D	-1	
SINAPYL ACRYLEIN	0.2169D	-2	
HYDROXYPHENYL ACRYLEIN	0.1066D	-1	
SINAPYL ALDEHYDE	0.1440D	-1	
COUMARALDEHYDE	0.7081D	-1	
PYROGALLOL	0.2216D	-8	
3,4-DIHYDROXYPHENYLACRYLEIN	0.9900D	-3	
SINGLE RINGS, MULTIPLE RINGS, AND SINGLES+			
LIGHTS ON MOL FRACTION BASIS			
SINGLE RING AROMATICS	0.8702D	-1	
MULTIPLE RING AROMATICS	0.9173D	0	
SINGLE RINGS AND LIGHTS	0.1938D	0	

TIME	INTERVAL	TEMP(C)	
0.8000D	4	0.1000D	2 300.0
0.8000D	4	0.1000D	2 300.0
PRODUCT	YIELD(WTZ)		
PHENOL	0.2576D	-3	
CRESOLS	0.2036D	-2	
ETHYLPHENOL	0.1546D	-2	
PROPYLPHENOL	0.3316D	-2	
GUAIACOL	0.2464D	-2	
METHYLGUAIACOL	0.1887D	-1	
ETHYLGUAIACOL	0.1397D	-1	
PROPYLGUAIACOL	0.2936D	-1	
EUGENOL	0.2900D	-1	
VINYLGUAIACOL	0.4737D	-2	
CONIFERALDEHYDE	0.5464D	0	
PROPIOVANILLONE	0.0000D	0	
CATECHOL	0.2865D	-4	
METHYLCATECHOL	0.2222D	-3	
ETHYLCATECHOL	0.1662D	-3	
3,4-DIHYDROXYCINNAMALDEHYDE	0.6597D	-2	
VINYLCATECHOL	0.5711D	-4	
ALLYLCATECHOL	0.3477D	-3	
SYRINGOL	0.6361D	-4	
METHYLSYRINGOL	0.4774D	-3	
ETHYLSYRINGOL	0.3477D	-3	
PROPYLSYRINGOL	0.7204D	-3	
VINYLSYRINGOL	0.1181D	-3	
ALLYLSYRINGOL	0.7131D	-3	
SYRINGALDEHYDE	0.0000D	0	
PROPIOSYRINGONE	0.0000D	0	
METHOXYCATECHOL	0.6010D	-6	
METHANE	0.4356D	-1	
CARBON MONOXIDE	0.3179D	-1	
WATER	0.4211D	-1	
CARBON DIOXIDE	0.0000D	0	
HYDROGEN	0.2635D	-2	
METHANOL	0.1374D	-2	
GUAIACYL ACROLEIN	0.1076D	0	
SINAPYL ACROLEIN	0.2614D	-2	
HYDROXYPHENYL ACROLEIN	0.1234D	-1	
SINAPYL ALDEHYDE	0.1327D	-1	
COUMARALDEHYDE	0.6264D	-1	
PYROGALLOL	0.3302D	-8	
3,4-DIHYDROXYPHENYLACROLEIN	0.1300D	-2	
SINGLE RINGS, MULTIPLE RINGS, AND SINGLES+			
LIGHTS ON MOL FRACTION BASIS			
SINGLE RING AROMATICS	0.8907D	-1	
MULTIPLE RING AROMATICS	0.9161D	0	
SINGLE RINGS AND LIGHTS	0.2105D	0	

TIME	INTERVAL	TEMP(C)	
0.9000D	4	0.1000D	2 300.0
0.9000D	4	0.1000D	2 300.0
PRODUCT	YIELD(WTZ)		
PHENOL	0.2825D	-3	
CRESOLS	0.2234D	-2	
ETHYLPHENOL	0.1697D	-2	
PROPYLPHENOL	0.3798D	-2	
GUAIACOL	0.2693D	-2	
METHYLGUAIACOL	0.2063D	-1	
ETHYLGUAIACOL	0.1528D	-1	
PROPYLGUAIACOL	0.3350D	-1	
EUGENOL	0.3310D	-1	
VINYLGUAIACOL	0.4215D	-2	
CONIFERALDEHYDE	0.4869D	0	
PROPIOVANILLONE	0.0000D	0	
CATECHOL	0.3511D	-4	
METHYLCATECHOL	0.2725D	-3	
ETHYLCATECHOL	0.2038D	-3	
3,4-DIHYDROXYCINNAMALDEHYDE	0.6593D	-2	
VINYLCATECHOL	0.5699D	-4	
ALLYLCATECHOL	0.4449D	-3	
SYRINGOL	0.7233D	-4	
METHYLSYRINGOL	0.5432D	-3	
ETHYLSYRINGOL	0.3955D	-3	
PROPYLSYRINGOL	0.8554D	-3	
VINYLSYRINGOL	0.1094D	-3	
ALLYLSYRINGOL	0.8466D	-3	
SYRINGALDEHYDE	0.0000D	0	
PROPIOSYRINGONE	0.0000D	0	
METHOXYCATECHOL	0.7599D	-6	
METHANE	0.4929D	-1	
CARBON MONOXIDE	0.3446D	-1	
WATER	0.4770D	-1	
CARBON DIOXIDE	0.0000D	0	
HYDROGEN	0.2980D	-2	
METHANOL	0.1554D	-2	
GUAIACYL ACRYLEIN	0.1221D	0	
SINAPYL ACRYLEIN	0.3086D	-2	
HYDROXYPHENYL ACRYLEIN	0.1405D	-1	
SINAPYL ALDEHYDE	0.1230D	-1	
COUMARALDEHYDE	0.5601D	-1	
PYROGALLOL	0.4664D	-8	
3,4-DIHYDROXYPHENYLACRYLEIN	0.1654D	-2	
SINGLE RINGS, MULTIPLE RINGS, AND SINGLES+			
LIGHTS ON MOL FRACTION BASIS			
SINGLE RING AROMATICS	0.9104D	-1	
MULTIPLE RING AROMATICS	0.9150D	0	
SINGLE RINGS AND LIGHTS	0.2270D	0	

TIME	INTERVAL	TEMP(C)		
0.1000D	5	0.1000D	2	300.0
0.1000D	5	0.1000D	2	300.0
PRODUCT	YIELD(WTZ)			
PHENOL				0.3055D -3
CRESOLS				0.2415D -2
ETHYLPHENOL				0.1834D -2
PROPYLPHENOL				0.4277D -2
GUAIACOL				0.2903D -2
METHYLGUAIACOL				0.2223D -1
ETHYLGUAIACOL				0.1646D -1
PROPYLGUAIACOL				0.3761D -1
EUGENOL				0.3715D -1
VINYLGUAIACOL				0.3780D -2
CONIFERALDEHYDE				0.4384D 0
PROPIOVANILLONE				0.0000D 0
CATECHOL				0.4192D -4
METHYLCATECHOL				0.3253D -3
ETHYLCATECHOL				0.2433D -3
3,4-DIHYDROXYCINNAMALDEHYDE				0.6577D -2
VINYLCATECHOL				0.5662D -4
ALLYLCATECHOL				0.5533D -3
SYRINGOL				0.8077D -4
METHYLSYRINGOL				0.6064D -3
ETHYLSYRINGOL				0.4416D -3
PROPYLSYRINGOL				0.9949D -3
VINYLSYRINGOL				0.1016D -3
ALLYLSYRINGOL				0.9847D -3
SYRINGALDEHYDE				0.0000D 0
PROPIOSYRINGONE				0.0000D 0
METHOXYCATECHOL				0.9334D -6
METHANE				0.5508D -1
CARBON MONOXIDE				0.3703D -1
WATER				0.5331D -1
CARBON DIOXIDE				0.0000D 0
HYDROGEN				0.3296D -2
METHANOL				0.1730D -2
GUAIACYL ACROLEIN				0.1368D 0
SINAPYL ACROLEIN				0.3581D -2
HYDROXYPHENYL ACROLEIN				0.1579D -1
SINAPYL ALDEHYDE				0.1148D -1
COUMARALDEHYDE				0.5060D -1
PYROGALLOL				0.6330D -8
3,4-DIHYDROXYPHENYLACROLEIN				0.2052D -2
SINGLE RINGS, MULTIPLE RINGS, AND SINGLES+				
LIGHTS ON MOL FRACTION BASIS				
SINGLE RING AROMATICS				0.9297D -1
MULTIPLE RING AROMATICS				0.9139D 0
SINGLE RINGS AND LIGHTS				0.2434D 0

:UDD:MK:PROD

TIME	INTERVAL	TEMP(C)	
0.0000D	0	0.1000D	2 400.0
0.0000D	0	0.1000D	2 400.0
PRODUCT	YIELD(WTZ)		
PHENOL	0.0000D 0		
CRESOLS	0.0000D 0		
ETHYLPHENOL	0.0000D 0		
PROPYLPHENOL	0.0000D 0		
GUAIACOL	0.0000D 0		
METHYLGUAIACOL	0.0000D 0		
ETHYLGUAIACOL	0.0000D 0		
PROPYLGUAIACOL	0.0000D 0		
EUGENOL	0.0000D 0		
VINYLGUAIACOL	0.0000D 0		
CONIFERALDEHYDE	0.2016D 1		
PROPIOVANILLONE	0.0000D 0		
CATECHOL	0.0000D 0		
METHYLCATECHOL	0.0000D 0		
ETHYLCATECHOL	0.0000D 0		
3,4-DIHYDROXYCINNAMALDEHYDE	0.0000D 0		
VINYLCATECHOL	0.0000D 0		
ALLYLCATECHOL	0.0000D 0		
SYRINGOL	0.0000D 0		
METHYLSYRINGOL	0.0000D 0		
ETHYLSYRINGOL	0.0000D 0		
PROPYLSYRINGOL	0.0000D 0		
VINYLSYRINGOL	0.0000D 0		
ALLYLSYRINGOL	0.0000D 0		
SYRINGALDEHYDE	0.0000D 0		
PROPIOSYRINGONE	0.0000D 0		
METHOXYCATECHOL	0.0000D 0		
METHANE	0.0000D 0		
CARBON MONOXIDE	0.0000D 0		
WATER	0.0000D 0		
CARBON DIOXIDE	0.0000D 0		
HYDROGEN	0.0000D 0		
METHANOL	0.0000D 0		
GUAIACYL ACROLEIN	0.0000D 0		
SINAPYL ACROLEIN	0.0000D 0		
HYDROXYPHENYL ACROLEIN	0.0000D 0		
SINAPYL ALDEHYDE	0.2657D -1		
COUMARALDEHYDE	0.2244D 0		
PYROGALLOL	0.0000D 0		
3,4-DIHYDROXYPHENYLACROLEIN	0.0000D 0		
SINGLE RINGS, MULTIPLE RINGS, AND SINGLES+			
LIGHTS ON MOL FRACTION BASIS			
SINGLE RING AROMATICS	0.7120D -1		
MULTIPLE RING AROMATICS	0.9276D 0		
SINGLE RINGS AND LIGHTS	0.7120D -1		



TIME	INTERVAL	TEMP(C)		
0.1000D	2	0.1000D	2	400.0
0.1000D	2	0.1000D	2	400.0
PRODUCT	YIELD(WTZ)			
PHENOL				0.2416D -4
CRESOLS				0.1927D -3
ETHYLPHENOL				0.1450D -3
PROPYLPHENOL				0.5695D -4
GUAIACOL				0.2344D -3
METHYLGUAIACOL				0.1810D -2
ETHYLGUAIACOL				0.1329D -2
PROPYLGUAIACOL				0.5112D -3
EUGENOL				0.5050D -3
VINYLGUAIACOL				0.4160D -1
CONIFERALDEHYDE				0.1742D 1
PROPIOVANILLONE				0.0000D 0
CATECHOL				0.1052D -5
METHYLCATECHOL				0.8230D -5
ETHYLCATECHOL				0.6104D -5
3,4-DIHYDROXYCINNAMALDEHYDE				0.8121D -2
VINYLCATECHOL				0.1937D -3
ALLYLCATECHOL				0.2337D -5
SYRINGOL				0.4156D -5
METHYLSYRINGOL				0.3146D -4
ETHYLSYRINGOL				0.2272D -4
PROPYLSYRINGOL				0.8617D -5
VINYLSYRINGOL				0.7128D -3
ALLYLSYRINGOL				0.8529D -5
SYRINGALDEHYDE				0.0000D 0
PROPIOSYRINGONE				0.0000D 0
METHOXYCATECHOL				0.1714D -7
METHANE				0.1683D -1
CARBON MONOXIDE				0.3146D -1
WATER				0.1402D -1
CARBON DIOXIDE				0.0000D 0
HYDROGEN				-0.1354D -2
METHANOL				0.7295D -4
GUAIACYL ACROLEIN				0.4456D -1
SINAPYL ACROLEIN				0.7434D -3
HYDROXYPHENYL ACROLEIN				0.5039D -2
SINAPYL ALDEHYDE				0.2906D -1
COUMARALDEHYDE				0.1970D 0
PYROGALLOL				0.3785D -10
3,4-DIHYDROXYPHENYLACROLEIN				0.2077D -3
SINGLE RINGS, MULTIPLE RINGS, AND SINGLES+				
LIGHTS ON MOL FRACTION BASIS				
SINGLE RING AROMATICS				0.7727D -1
MULTIPLE RING AROMATICS				0.9218D 0
SINGLE RINGS AND LIGHTS				0.1383D 0

TIME	INTERVAL	TEMP(C)		
0.2000D	2	0.1000D	2	400.0
0.2000D	2	0.1000D	2	400.0
PRODUCT	YIELD(WTZ)			
PHENOL	0.9031D	-4		
CRESOLS	0.7173D	-3		
ETHYLPHENOL	0.5423D	-3		
PROPYLPHENOL	0.2192D	-3		
GUAIACOL	0.8630D	-3		
METHYLGUAIACOL	0.6639D	-2		
ETHYLGUAIACOL	0.4894D	-2		
PROPYLGUAIACOL	0.1938D	-2		
EUGENOL	0.1914D	-2		
VINYLGUAIACOL	0.7254D	-1		
CONIFERALDEHYDE	0.1518D	1		
PROPIOVANILLONE	0.0000D	0		
CATECHOL	0.7662D	-5		
METHYLCATECHOL	0.5971D	-4		
ETHYLCATECHOL	0.4447D	-4		
3,4-DIHYDROXYCINNAMALDEHYDE	0.1400D	-1		
VINYLCATECHOL	0.6679D	-3		
ALLYLCATECHOL	0.1752D	-4		
SYRINGOL	0.1806D	-4		
METHYLSYRINGOL	0.1362D	-3		
ETHYLSYRINGOL	0.9876D	-4		
PROPYLSYRINGOL	0.3856D	-4		
VINYLSYRINGOL	0.1467D	-2		
ALLYLSYRINGOL	0.3816D	-4		
SYRINGALDEHYDE	0.0000D	0		
PROPIOSYRINGONE	0.0000D	0		
METHOXYCATECHOL	0.1382D	-6		
METHANE	0.3411D	-1		
CARBON MONOXIDE	0.5929D	-1		
WATER	0.2829D	-1		
CARBON DIOXIDE	0.0000D	0		
HYDROGEN	-0.2302D	-2		
METHANOL	0.2700D	-3		
GUAIACYL ACROLEIN	0.9117D	-1		
SINAPYL ACROLEIN	0.1796D	-2		
HYDROXYPHENYL ACROLEIN	0.1047D	-1		
SINAPYL ALDEHYDE	0.2989D	-1		
COUMARALDEHYDE	0.1742D	0		
PYROGALLOL	0.5916D	-9		
3,4-DIHYDROXYPHENYLACROLEIN	0.8408D	-3		
SINGLE RINGS, MULTIPLE RINGS, AND SINGLES+				
LIGHTS ON MOL FRACTION BASIS				
SINGLE RING AROMATICS	0.8304D	-1		
MULTIPLE RING AROMATICS	0.9166D	0		
SINGLE RINGS AND LIGHTS	0.2027D	0		

TIME	INTERVAL	TEMP (C)	
0.3000D	2	0.1000D	2 400.0
0.3000D	2	0.1000D	2 400.0
PRODUCT	YIELD(WT%)		
PHENOL	0.1899D	-3	
CRESOLS	0.1506D	-2	
ETHYLPHENOL	0.1140D	-2	
PROPYLPHENOL	0.4733D	-3	
GUAIACOL	0.1788D	-2	
METHYLGUAIACOL	0.1374D	-1	
ETHYLGUAIACOL	0.1014D	-1	
PROPYLGUAIACOL	0.4125D	-2	
EUGENOL	0.4075D	-2	
VINYLGUAIACOL	0.9490D	-1	
CONIFERALDEHYDE	0.1335D	1	
PROPIOVANILLONE	0.0000D	0	
CATECHOL	0.2361D	-4	
METHYLCATECHOL	0.1837D	-3	
ETHYLCATECHOL	0.1370D	-3	
3,4-DIHYDROXYCINNAMALDEHYDE	0.1830D	-1	
VINYLCATECHOL	0.1299D	-2	
ALLYLCATECHOL	0.5547D	-4	
SYRINGOL	0.4239D	-4	
METHYLSYRINGOL	0.3191D	-3	
ETHYLSYRINGOL	0.2317D	-3	
PROPYLSYRINGOL	0.9294D	-4	
VINYLSYRINGOL	0.2173D	-2	
ALLYLSYRINGOL	0.9199D	-4	
SYRINGALDEHYDE	0.0000D	0	
PROPIOSYRINGONE	0.0000D	0	
METHOXYCATECHOL	0.4632D	-6	
METHANE	0.5179D	-1	
CARBON MONOXIDE	0.8429D	-1	
WATER	0.4278D	-1	
CARBON DIOXIDE	0.0000D	0	
HYDROGEN	-0.2940D	-2	
METHANOL	0.5625D	-3	
GUAIACYL ACROLEIN	0.1394D	0	
SINAPYL ACROLEIN	0.3110D	-2	
HYDROXYPHENYL ACROLEIN	0.1624D	-1	
SINAPYL ALDEHYDE	0.2977D	-1	
COUMARALDEHYDE	0.1554D	0	
PYROGALLOL	0.2908D	-8	
3,4-DIHYDROXYPHENYLACROLEIN	0.1912D	-2	
SINGLE RINGS, MULTIPLE RINGS, AND SINGLES+			
LIGHTS ON MOL FRACTION BASIS			
SINGLE RING AROMATICS	0.8850D	-1	
MULTIPLE RING AROMATICS	0.9121D	0	
SINGLE RINGS AND LIGHTS	0.2650D	0	

TIME	INTERVAL	TEMP(C)	
0.4000D	2	0.1000D	2 400.0
0.4000D	2	0.1000D	2 400.0
PRODUCT	YIELD(WTZ)		
PHENOL	0.3156D	-3	
CRESOLS	0.2501D	-2	
ETHYLPHENOL	0.1894D	-2	
PROPYLPHENOL	0.8058D	-3	
GUAIACOL	0.2931D	-2	
METHYLGUAIACOL	0.2250D	-1	
ETHYLGUAIACOL	0.1661D	-1	
PROPYLGUAIACOL	0.6924D	-2	
EUGENOL	0.6841D	-2	
VINYLGUAIACOL	0.1106D	0	
CONIFERALDEHYDE	0.1185D	1	
PROPIOVANILLONE	0.0000D	0	
CATECHOL	0.5123D	-4	
METHYLCATECHOL	0.3983D	-3	
ETHYLCATECHOL	0.2972D	-3	
3,4-DIHYDROXYCINNAMALDEHYDE	0.2151D	-1	
VINYLCATECHOL	0.2004D	-2	
ALLYLCATECHOL	0.1233D	-3	
SYRINGOL	0.7655D	-4	
METHYLSYRINGOL	0.5759D	-3	
ETHYLSYRINGOL	0.4184D	-3	
PROPYLSYRINGOL	0.1719D	-3	
VINYLSYRINGOL	0.2790D	-2	
ALLYLSYRINGOL	0.1702D	-3	
SYRINGALDEHYDE	0.0000D	0	
PROPIOSYRINGONE	0.0000D	0	
METHOXYCATECHOL	0.1079D	-5	
METHANE	0.6981D	-1	
CARBON MONOXIDE	0.1071D	0	
WATER	0.5741D	-1	
CARBON DIOXIDE	0.0000D	0	
HYDROGEN	-0.3349D	-2	
METHANOL	0.9273D	-3	
GUAIACYL ACRYLEIN	0.1891D	0	
SINAPYL ACRYLEIN	0.4646D	-2	
HYDROXYPHENYL ACRYLEIN	0.2233D	-1	
SINAPYL ALDEHYDE	0.2911D	-1	
COUMARALDEHYDE	0.1399D	0	
PYROGALLOL	0.8873D	-8	
3,4-DIHYDROXYPHENYLACRYLEIN	0.3432D	-2	
SINGLE RINGS, MULTIPLE RINGS, AND SINGLES+			
LIGHTS ON MOL FRACTION BASIS			
SINGLE RING AROMATICS	0.9368D	-1	
MULTIPLE RING AROMATICS	0.9082D	0	
SINGLE RINGS AND LIGHTS	0.3256D	0	

TIME	INTERVAL	TEMP(C)	
0.5000D	2	0.1000D	2 400.0
0.5000D	2	0.1000D	2 400.0
PRODUCT	YIELD(WTZ)		
PHENOL	0.4610D	-3	
CRESOLS	0.3653D	-2	
ETHYLPHENOL	0.2767D	-2	
PROPYLPHENOL	0.1204D	-2	
GUAIACOL	0.4223D	-2	
METHYLGUAIACOL	0.3241D	-1	
ETHYLGUAIACOL	0.2394D	-1	
PROPYLGUAIACOL	0.1020D	-1	
EUGENOL	0.1008D	-1	
VINYLGUAIACOL	0.1210D	0	
CONIFERALDEHYDE	0.1061D	1	
PROPIOVANILLONE	0.0000D	0	
CATECHOL	0.9175D	-4	
METHYLCATECHOL	0.7132D	-3	
ETHYLCATECHOL	0.5324D	-3	
3,4-DIHYDROXYCINNAMALDEHYDE	0.2394D	-1	
VINYLCATECHOL	0.2726D	-2	
ALLYLCATECHOL	0.2258D	-3	
SYRINGOL	0.1193D	-3	
METHYLSYRINGOL	0.8972D	-3	
ETHYLSYRINGOL	0.6519D	-3	
PROPYLSYRINGOL	0.2739D	-3	
VINYLSYRINGOL	0.3301D	-2	
ALLYLSYRINGOL	0.2711D	-3	
SYRINGALDEHYDE	0.0000D	0	
PROPIOSYRINGONE	0.0000D	0	
METHOXYCATECHOL	0.2053D	-5	
METHANE	0.8813D	-1	
CARBON MONOXIDE	0.1281D	0	
WATER	0.7217D	-1	
CARBON DIOXIDE	0.0000D	0	
HYDROGEN	-0.3592D	-2	
METHANOL	0.1345D	-2	
GUAIACYL ACROLEIN	0.2396D	0	
SINAPYL ACROLEIN	0.6368D	-2	
HYDROXYPHENYL ACROLEIN	0.2869D	-1	
SINAPYL ALDEHYDE	0.2819D	-1	
COUMARALDEHYDE	0.1270D	0	
PYROGALLOL	0.2085D	-7	
3,4-DIHYDROXYPHENYLACROLEIN	0.5408D	-2	
SINGLE RINGS, MULTIPLE RINGS, AND SINGLES+			
LIGHTS ON MOL FRACTION BASIS			
SINGLE RING AROMATICS	0.9855D	-1	
MULTIPLE RING AROMATICS	0.9046D	0	
SINGLE RINGS AND LIGHTS	0.3847D	0	

TIME	INTERVAL	TEMP(C)	
0.6000D	2	0.1000D	2 400.0
0.6000D	2	0.1000D	2 400.0
PRODUCT	YIELD(WTZ)		
PHENOL	0.6213D	-3	
CRESOLS	0.4920D	-2	
ETHYLPHENOL	0.3729D	-2	
PROPYLPHENOL	0.1656D	-2	
GUAIACOL	0.5614D	-2	
METHYLGUAIACOL	0.4306D	-1	
ETHYLGUAIACOL	0.3183D	-1	
PROPYLGUAIACOL	0.1384D	-1	
EUGENOL	0.1368D	-1	
VINYLGUAIACOL	0.1273D	0	
CONIFERALDEHYDE	0.9580D	0	
PROPIOVANILLONE	0.0000D	0	
CATECHOL	0.1457D	-3	
METHYLCATECHOL	0.1132D	-2	
ETHYLCATECHOL	0.8456D	-3	
3,4-DIHYDROXYCINNAMALDEHYDE	0.2583D	-1	
VINYLCATECHOL	0.3427D	-2	
ALLYLCATECHOL	0.3660D	-3	
SYRINGOL	0.1691D	-3	
METHYLSYRINGOL	0.1271D	-2	
ETHYLSYRINGOL	0.9242D	-3	
PROPYLSYRINGOL	0.3964D	-3	
VINYLSYRINGOL	0.3704D	-2	
ALLYLSYRINGOL	0.3923D	-3	
SYRINGALDEHYDE	0.0000D	0	
PROPIOSYRINGONE	0.0000D	0	
METHOXYCATECHOL	0.3437D	-5	
METHANE	0.1068D	0	
CARBON MONOXIDE	0.1477D	0	
WATER	0.8699D	-1	
CARBON DIOXIDE	0.0000D	0	
HYDROGEN	-0.3722D	-2	
METHANOL	0.1801D	-2	
GUAIACYL ACRROLEIN	0.2910D	0	
SINAPYL ACRROLEIN	0.8246D	-2	
HYDROXYPHENYL ACRROLEIN	0.3532D	-1	
SINAPYL ALDEHYDE	0.2715D	-1	
COUMARALDEHYDE	0.1163D	0	
PYROGALLOL	0.4148D	-7	
3,4-DIHYDROXYPHENYLACRROLEIN	0.7845D	-2	
SINGLE RINGS, MULTIPLE RINGS, AND SINGLES+			
LIGHTS ON MOL FRACTION BASIS			
SINGLE RING AROMATICS	0.1032D	0	
MULTIPLE RING AROMATICS	0.9016D	0	
SINGLE RINGS AND LIGHTS	0.4427D	0	

TIME	INTERVAL	TEMP(C)	
0.7000D	2	0.1000D	2 400.0
0.7000D	2	0.1000D	2 400.0
PRODUCT	YIELD(WT%)		
PHENOL	0.7922D	-3	
CRESOLS	0.6272D	-2	
ETHYLPHENOL	0.4754D	-2	
PROPYLPHENOL	0.2151D	-2	
GUAIACOL	0.7061D	-2	
METHYLGUAIACOL	0.5415D	-1	
ETHYLGUAIACOL	0.4002D	-1	
PROPYLGUAIACOL	0.1774D	-1	
EUGENOL	0.1753D	-1	
VINYLGUAIACOL	0.1305D	0	
CONIFERALDEHYDE	0.8711D	0	
PROPIOVANILLONE	0.0000D	0	
CATECHOL	0.2133D	-3	
METHYLCATECHOL	0.1657D	-2	
ETHYLCATECHOL	0.1237D	-2	
3,4-DIHYDROXYCINNAMALDEHYDE	0.2733D	-1	
VINYLCATECHOL	0.4088D	-2	
ALLYLCATECHOL	0.5459D	-3	
SYRINGOL	0.2245D	-3	
METHYLSYRINGOL	0.1687D	-2	
ETHYLSYRINGOL	0.1227D	-2	
PROPYLSYRINGOL	0.5362D	-3	
VINYLSYRINGOL	0.4008D	-2	
ALLYLSYRINGOL	0.5307D	-3	
SYRINGALDEHYDE	0.0000D	0	
PROPIOSYRINGONE	0.0000D	0	
METHOXYCATECHOL	0.5263D	-5	
METHANE	0.1256D	0	
CARBON MONOXIDE	0.1661D	0	
WATER	0.1019D	0	
CARBON DIOXIDE	0.0000D	0	
HYDROGEN	-0.3784D	-2	
METHANOL	0.2282D	-2	
GUAIACYL ACRYLEIN	0.3428D	0	
SINAPYL ACRYLEIN	0.1025D	-1	
HYDROXYPHENYL ACRYLEIN	0.4218D	-1	
SINAPYL ALDEHYDE	0.2606D	-1	
COUMARALDEHYDE	0.1072D	0	
PYROGALLOL	0.7358D	-7	
3,4-DIHYDROXYPHENYLACRYLEIN	0.1076D	-1	
SINGLE RINGS, MULTIPLE RINGS, AND SINGLES+			
LIGHTS ON MOL FRACTION BASIS			
SINGLE RING AROMATICS	0.1075D	0	
MULTIPLE RING AROMATICS	0.8988D	0	
SINGLE RINGS AND LIGHTS	0.4996D	0	

TIME	INTERVAL	TEMP(C)	
0.8000D	2	0.1000D	2 400.0
0.8000D	2	0.1000D	2 400.0
PRODUCT	YIELD(WTZ)		
PHENOL	0.9703D	-3	
CRESOLS	0.7680D	-2	
ETHYLPHENOL	0.5825D	-2	
PROPYLPHENOL	0.2680D	-2	
GUAIACOL	0.8536D	-2	
METHYLGUAIACOL	0.6544D	-1	
ETHYLGUAIACOL	0.4839D	-1	
PROPYLGUAIACOL	0.2181D	-1	
EUGENOL	0.2155D	-1	
VINYLGUAIACOL	0.1313D	0	
CONIFERALDEHYDE	0.7976D	0	
PROPIOVANILLONE	0.0000D	0	
CATECHOL	0.2939D	-3	
METHYLCATECHOL	0.2283D	-2	
ETHYLCATECHOL	0.1705D	-2	
3,4-DIHYDROXYCINNAMALDEHYDE	0.2853D	-1	
VINYLCATECHOL	0.4690D	-2	
ALLYLCATECHOL	0.7651D	-3	
SYRINGOL	0.2839D	-3	
METHYLSYRINGOL	0.2134D	-2	
ETHYLSYRINGOL	0.1552D	-2	
PROPYLSYRINGOL	0.6899D	-3	
VINYLSYRINGOL	0.4221D	-2	
ALLYLSYRINGOL	0.6828D	-3	
SYRINGALDEHYDE	0.0000D	0	
PROPIOSYRINGONE	0.0000D	0	
METHOXYCATECHOL	0.7555D	-5	
METHANE	0.1446D	0	
CARBON MONOXIDE	0.1837D	0	
WATER	0.1168D	0	
CARBON DIOXIDE	0.0000D	0	
HYDROGEN	-0.3807D	-2	
METHANOL	0.2777D	-2	
GUAIACYL ACROLEIN	0.3949D	0	
SINAPYL ACROLEIN	0.1236D	-1	
HYDROXYPHENYL ACROLEIN	0.4924D	-1	
SINAPYL ALDEHYDE	0.2497D	-1	
COUMARALDEHYDE	0.9945D	-1	
PYROGALLOL	0.1200D	-6	
3,4-DIHYDROXYPHENYLACROLEIN	0.1412D	-1	
SINGLE RINGS, MULTIPLE RINGS, AND SINGLES+			
LIGHTS ON MOL FRACTION BASIS			
SINGLE RING AROMATICS	0.1116D	0	
MULTIPLE RING AROMATICS	0.8963D	0	
SINGLE RINGS AND LIGHTS	0.5556D	0	



TIME	INTERVAL	TEMP(C)	
0.90000	2	0.10000	2 400.0
0.90000	2	0.10000	2 400.0
PRODUCT	YIELD(WT%)		
PHENOL	0.11530	-2	
CRESOLS	0.91270	-2	
ETHYLPHENOL	0.69200	-2	
PROPYLPHENOL	0.32340	-2	
GUAIACOL	0.10010	-1	
METHYLGUAIACOL	0.76750	-1	
ETHYLGUAIACOL	0.56740	-1	
PROPYLGUAIACOL	0.25970	-1	
EUGENOL	0.25660	-1	
VINYLGUAIACOL	0.13040	0	
CONIFERALDEHYDE	0.73420	0	
PROPIOVANILLONE	0.00000	0	
CATECHOL	0.38730	-3	
METHYLCATECHOL	0.30090	-2	
ETHYLCATECHOL	0.22480	-2	
3,4-DIHYDROXYCINNAMALDEHYDE	0.29510	-1	
VINYLCATECHOL	0.52350	-2	
ALLYLCATECHOL	0.10240	-2	
SYRINGOL	0.34660	-3	
METHYLSYRINGOL	0.26050	-2	
ETHYLSYRINGOL	0.18940	-2	
PROPYLSYRINGOL	0.85520	-3	
VINYLSYRINGOL	0.43640	-2	
ALLYLSYRINGOL	0.84650	-3	
SYRINGALDEHYDE	0.00000	0	
PROPIOSYRINGONE	0.00000	0	
METHOXYCATECHOL	0.10310	-4	
METHANE	0.16380	0	
CARBON MONOXIDE	0.20030	0	
WATER	0.13160	0	
CARBON DIOXIDE	0.00000	0	
HYDROGEN	-0.38140	-2	
METHANOL	0.32800	-2	
GUAIACYL ACROLEIN	0.44730	0	
SINAPYL ACROLEIN	0.14580	-1	
HYDROXYPHENYL ACROLEIN	0.56520	-1	
SINAPYL ALDEHYDE	0.23920	-1	
COUMARALDEHYDE	0.92760	-1	
PYROGALLOL	0.18360	-6	
3,4-DIHYDROXYPHENYLACROLEIN	0.17980	-1	
SINGLE RINGS, MULTIPLE RINGS, AND SINGLES+			
LIGHTS ON MOL FRACTION BASIS			
SINGLE RING AROMATICS	0.11550	0	
MULTIPLE RING AROMATICS	0.89400	0	
SINGLE RINGS AND LIGHTS	0.61070	0	

TIME	INTERVAL	TEMP(C)	
0.10000	3	0.10000	2 400.0
0.10000	3	0.10000	2 400.0
PRODUCT	YIELD(WTZ)		
PHENOL	0.13380	-2	
CRESOLS	0.10590	-1	
ETHYLPHENOL	0.80290	-2	
PROPYLPHENOL	0.38060	-2	
GUAIACOL	0.11460	-1	
METHYLGUAIACOL	0.87900	-1	
ETHYLGUAIACOL	0.64990	-1	
PROPYLGUAIACOL	0.30180	-1	
EUGENOL	0.29820	-1	
VINYLGUAIACOL	0.12820	0	
CONIFERALDEHYDE	0.67910	0	
PROPIOVANILLONE	0.00000	0	
CATECHOL	0.49240	-3	
METHYLCATECHOL	0.38240	-2	
ETHYLCATECHOL	0.28570	-2	
3,4-DIHYDROXYCINNAMALDEHYDE	0.30290	-1	
VINYLCATECHOL	0.57090	-2	
ALLYLCATECHOL	0.13200	-2	
SYRINGOL	0.41070	-3	
METHYLSYRINGOL	0.30870	-2	
ETHYLSYRINGOL	0.22440	-2	
PROPYLSYRINGOL	0.10280	-2	
VINYLSYRINGOL	0.44360	-2	
ALLYLSYRINGOL	0.10170	-2	
SYRINGALDEHYDE	0.00000	0	
PROPIOSYRINGONE	0.00000	0	
METHOXYCATECHOL	0.13540	-4	
METHANE	0.18320	0	
CARBON MONOXIDE	0.21640	0	
WATER	0.14660	0	
CARBON DIOXIDE	0.00000	0	
HYDROGEN	-0.38360	-2	
METHANOL	0.37840	-2	
GUAIACYL ACROLEIN	0.50010	0	
SINAPYL ACROLEIN	0.16850	-1	
HYDROXYPHENYL ACROLEIN	0.64000	-1	
SINAPYL ALDEHYDE	0.22890	-1	
COUMARALDEHYDE	0.86910	-1	
PYROGALLOL	0.26710	-6	
3,4-DIHYDROXYPHENYLACROLEIN	0.22310	-1	
SINGLE RINGS, MULTIPLE RINGS, AND SINGLES+			
LIGHTS ON MOL FRACTION BASIS			
SINGLE RING AROMATICS	0.11910	0	
MULTIPLE RING AROMATICS	0.89210	0	
SINGLE RINGS AND LIGHTS	0.66520	0	

TIME	INTERVAL	TEMP(C)	
0.2000D	3	0.1000D	2 400.0
0.2000D	3	0.1000D	2 400.0
PRODUCT	YIELD(WT%)		
PHENOL	0.3076D	-2	
CRESOLS	0.2435D	-1	
ETHYLPHENOL	0.1846D	-1	
PROPYLPHENOL	0.9602D	-2	
GUAIACOL	0.2324D	-1	
METHYLGUAIACOL	0.1782D	0	
ETHYLGUAIACOL	0.1317D	0	
PROPYLGUAIACOL	0.6711D	-1	
EUGENOL	0.6631D	-1	
VINYLGUAIACOL	0.8381D	-1	
CONIFERALDEHYDE	0.3502D	0	
PROPIOVANILLONE	0.0000D	0	
CATECHOL	0.2028D	-2	
METHYLCATECHOL	0.1575D	-1	
ETHYLCATECHOL	0.1176D	-1	
3,4-DIHYDROXYCINNAMALDEHYDE	0.3173D	-1	
VINYLCATECHOL	0.7584D	-2	
ALLYLCATECHOL	0.5966D	-2	
SYRINGOL	0.1009D	-2	
METHYLSYRINGOL	0.7587D	-2	
ETHYLSYRINGOL	0.5517D	-2	
PROPYLSYRINGOL	0.2772D	-2	
VINYLSYRINGOL	0.3517D	-2	
ALLYLSYRINGOL	0.2743D	-2	
SYRINGALDEHYDE	0.0000D	0	
PROPIOSYRINGONE	0.0000D	0	
METHOXYCATECHOL	0.6743D	-4	
METHANE	0.3813D	0	
CARBON MONOXIDE	0.3531D	0	
WATER	0.2935D	0	
CARBON DIOXIDE	0.0000D	0	
HYDROGEN	-0.6579D	-2	
METHANOL	0.8210D	-2	
GUAIACYL ACROLEIN	0.1008D	1	
SINAPYL ACROLEIN	0.4120D	-1	
HYDROXYPHENYL ACROLEIN	0.1464D	0	
SINAPYL ALDEHYDE	0.1431D	-1	
COUMARALDEHYDE	0.5084D	-1	
PYROGALLOL	0.2678D	-5	
3,4-DIHYDROXYPHENYLACROLEIN	0.9136D	-1	
SINGLE RINGS, MULTIPLE RINGS, AND SINGLES+			
LIGHTS ON MOL FRACTION BASIS			
SINGLE RING AROMATICS	0.1471D	0	
MULTIPLE RING AROMATICS	0.8785D	0	
SINGLE RINGS AND LIGHTS	0.1177D	1	

TIME	INTERVAL	TEMP(C)	
0.3000D	3	0.1000D	2 400.0
0.3000D	3	0.1000D	2 400.0
PRODUCT	YIELD(WTZ)		
PHENOL	0.4425D	-2	
CRESOLS	0.3504D	-1	
ETHYLPHENOL	0.2656D	-1	
PROPYLPHENOL	0.1457D	-1	
GUAIACOL	0.2965D	-1	
METHYLGUAIACOL	0.2274D	0	
ETHYLGUAIACOL	0.1681D	0	
PROPYLGUAIACOL	0.9032D	-1	
EUGENOL	0.8923D	-1	
VINYLGUAIACOL	0.4828D	-1	
CONIFERALDEHYDE	0.1981D	0	
PROPIOVANILLONE	0.0000D	0	
CATECHOL	0.4002D	-2	
METHYLCATECHOL	0.3109D	-1	
ETHYLCATECHOL	0.2322D	-1	
3,4-DIHYDROXYCINNAMALDEHYDE	0.2777D	-1	
VINYLCATECHOL	0.6758D	-2	
ALLYLCATECHOL	0.1242D	-1	
SYRINGOL	0.1404D	-2	
METHYLSYRINGOL	0.1055D	-1	
ETHYLSYRINGOL	0.7671D	-2	
PROPYLSYRINGOL	0.4065D	-2	
VINYLSYRINGOL	0.2209D	-2	
ALLYLSYRINGOL	0.4024D	-2	
SYRINGALDEHYDE	0.0000D	0	
PROPIOSYRINGONE	0.0000D	0	
METHOXYCATECHOL	0.1446D	-3	
METHANE	0.5801D	0	
CARBON MONOXIDE	0.4651D	0	
WATER	0.4360D	0	
CARBON DIOXIDE	0.0000D	0	
HYDROGEN	-0.1437D	-1	
METHANOL	0.1123D	-1	
GUAIACYL ACRYLEIN	0.1463D	1	
SINAPYL ACRYLEIN	0.6515D	-1	
HYDROXYPHENYL ACRYLEIN	0.2394D	0	
SINAPYL ALDEHYDE	0.8823D	-2	
COUMARALDEHYDE	0.3243D	-1	
PYROGALLOL	0.8837D	-5	
3,4-DIHYDROXYPHENYLACRYLEIN	0.2050D	0	
SINGLE RINGS, MULTIPLE RINGS, AND SINGLES+			
LIGHTS ON MOL FRACTION BASIS			
SINGLE RING AROMATICS	0.1662D	0	
MULTIPLE RING AROMATICS	0.8688D	0	
SINGLE RINGS AND LIGHTS	0.1644D	1	

TIME	INTERVAL	TEMP(C)	
0.4000D	3	0.1000D	2 400.0
0.4000D	3	0.1000D	2 400.0
PRODUCT	YIELD(WT%)		
PHENOL	0.5464D	-2	
CRESOLS	0.4329D	-1	
ETHYLPHENOL	0.3280D	-1	
PROPYLPHENOL	0.1883D	-1	
GUAIACOL	0.3267D	-1	
METHYLGUAIACOL	0.2507D	0	
ETHYLGUAIACOL	0.1852D	0	
PROPYLGUAIACOL	0.1042D	0	
EUGENOL	0.1029D	0	
VINYLGUAIACOL	0.2923D	-1	
CONIFERALDEHYDE	0.1279D	0	
PROPIOVANILLONE	0.0000D	0	
CATECHOL	0.6073D	-2	
METHYLCATECHOL	0.4720D	-1	
ETHYLCATECHOL	0.3523D	-1	
3,4-DIHYDROXYCINNAMALDEHYDE	0.2469D	-1	
VINYLCATECHOL	0.5633D	-2	
ALLYLCATECHOL	0.1972D	-1	
SYRINGOL	0.1635D	-2	
METHYLSYRINGOL	0.1230D	-1	
ETHYLSYRINGOL	0.8938D	-2	
PROPYLSYRINGOL	0.4957D	-2	
VINYLSYRINGOL	0.1413D	-2	
ALLYLSYRINGOL	0.4906D	-2	
SYRINGALDEHYDE	0.0000D	0	
PROPIOSYRINGONE	0.0000D	0	
METHOXYCATECHOL	0.2289D	-3	
METHANE	0.7746D	0	
CARBON MONOXIDE	0.5643D	0	
WATER	0.5750D	0	
CARBON DIOXIDE	0.0000D	0	
HYDROGEN	-0.2497D	-1	
METHANOL	0.1336D	-1	
GUAIACYL ACRYLEIN	0.1860D	1	
SINAPYL ACRYLEIN	0.8759D	-1	
HYDROXYPHENYL ACRYLEIN	0.3411D	0	
SINAPYL ALDEHYDE	0.6023D	-2	
COUMARALDEHYDE	0.2346D	-1	
PYROGALLOL	0.1914D	-4	
3,4-DIHYDROXYPHENYLACRYLEIN	0.3590D	0	
SINGLE RINGS, MULTIPLE RINGS, AND SINGLEST+ LIGHTS ON MOL FRACTION BASIS			
SINGLE RING AROMATICS	0.1820D	0	
MULTIPLE RING AROMATICS	0.8592D	0	
SINGLE RINGS AND LIGHTS	0.2084D	1	

TIME	INTERVAL	TEMP(C)		
0.5000D	3	0.1000D	2	400.0
0.5000D	3	0.1000D	2	400.0
PRODUCT	YIELD(WTZ)			
PHENOL	0.6337D	-2		
CRESOLS	0.5022D	-1		
ETHYLPHENOL	0.3802D	-1		
PROPYLPHENOL	0.2278D	-1		
GUAIACOL	0.3404D	-1		
METHYLGUAIACOL	0.2613D	0		
ETHYLGUAIACOL	0.1929D	0		
PROPYLGUAIACOL	0.1132D	0		
EUGENOL	0.1119D	0		
VINYLGUAIACOL	0.2020D	-1		
CONIFERALDEHYDE	0.9645D	-1		
PROPIOVANILLONE	0.0000D	0		
CATECHOL	0.8155D	-2		
METHYLCATECHOL	0.6340D	-1		
ETHYLCATECHOL	0.4730D	-1		
3,4-DIHYDROXYCINNAMALDEHYDE	0.2400D	-1		
VINYLCATECHOL	0.5019D	-2		
ALLYLCATECHOL	0.2763D	-1		
SYRINGOL	0.1781D	-2		
METHYLSYRINGOL	0.1340D	-1		
ETHYLSYRINGOL	0.9729D	-2		
PROPYLSYRINGOL	0.5631D	-2		
VINYLSYRINGOL	0.1021D	-2		
ALLYLSYRINGOL	0.5574D	-2		
SYRINGALDEHYDE	0.0000D	0		
PROPIOSYRINGONE	0.0000D	0		
METHOXYCATECHOL	0.3139D	-3		
METHANE	0.9635D	0		
CARBON MONOXIDE	0.6562D	0		
WATER	0.7112D	0		
CARBON DIOXIDE	0.0000D	0		
HYDROGEN	-0.3660D	-1		
METHANOL	0.1506D	-1		
GUAIACYL ACROLEIN	0.2206D	1		
SINAPYL ACROLEIN	0.1086D	0		
HYDROXYPHENYL ACROLEIN	0.4505D	0		
SINAPYL ALDEHYDE	0.4747D	-2		
COUMARALDEHYDE	0.1969D	-1		
PYROGALLOL	0.3364D	-4		
3,4-DIHYDROXYPHENYLACROLEIN	0.5489D	0		
SINGLE RINGS, MULTIPLE RINGS, AND SINGLES+				
LIGHTS ON MOL FRACTION BASIS				
SINGLE RING AROMATICS	0.1965D	0		
MULTIPLE RING AROMATICS	0.8492D	0		
SINGLE RINGS AND LIGHTS	0.2506D	1		

TIME	INTERVAL	TEMP(C)	
0.60000	3	0.10000	2 400.0
0.60000	3	0.10000	2 400.0
PRODUCT	YIELD(WT%)		
PHENOL	0.71330	-2	
CRESOLS	0.56540	-1	
ETHYLPHENOL	0.42810	-1	
PROPYLPHENOL	0.26670	-1	
GUAIACOL	0.34630	-1	
METHYLGUAIACOL	0.26590	0	
ETHYLGUAIACOL	0.19630	0	
PROPYLGUAIACOL	0.11980	0	
EUGENOL	0.11840	0	
VINYLGUAIACOL	0.16050	-1	
CONIFERALDEHYDE	0.81290	-1	
PROPIOVANILLONE	0.00000	0	
CATECHOL	0.10250	-1	
METHYLCATECHOL	0.79700	-1	
ETHYLCATECHOL	0.59450	-1	
3,4-DIHYDROXYCINNAMALDEHYDE	0.24990	-1	
VINYLCATECHOL	0.49250	-2	
ALLYLCATECHOL	0.36120	-1	
SYRINGOL	0.18830	-2	
METHYLSYRINGOL	0.14170	-1	
ETHYLSYRINGOL	0.10290	-1	
PROPYLSYRINGOL	0.61930	-2	
VINYLSYRINGOL	0.84300	-3	
ALLYLSYRINGOL	0.61300	-2	
SYRINGALDEHYDE	0.00000	0	
PROPIOSYRINGONE	0.00000	0	
METHOXYCATECHOL	0.39840	-3	
METHANE	0.11460	1	
CARBON MONOXIDE	0.74330	0	
WATER	0.84520	0	
CARBON DIOXIDE	0.00000	0	
HYDROGEN	-0.48360	-1	
METHANOL	0.16560	-1	
GUAIACYL ACRYLEIN	0.25080	1	
SINAPYL ACRYLEIN	0.12830	0	
HYDROXYPHENYL ACRYLEIN	0.56650	0	
SINAPYL ALDEHYDE	0.41590	-2	
COUMARALDEHYDE	0.18370	-1	
PYROGALLOL	0.52450	-4	
3,4-DIHYDROXYPHENYLACRYLEIN	0.77080	0	
SINGLE RINGS, MULTIPLE RINGS, AND SINGLES+			
LIGHTS ON MOL FRACTION BASIS			
SINGLE RING AROMATICS	0.21050	0	
MULTIPLE RING AROMATICS	0.83910	0	
SINGLE RINGS AND LIGHTS	0.29130	1	

TIME	INTERVAL	TEMP(C)	
0.7000D	3	0.1000D	2 400.0
0.7000D	3	0.1000D	2 400.0
PRODUCT	YIELD(WTZ)		
PHENOL	0.7904D	-2	
CRESOLS	0.6271D	-1	
ETHYLPHENOL	0.4744D	-1	
PROPYLPHENOL	0.3060D	-1	
GUAIACOL	0.3487D	-1	
METHYLGUAIACOL	0.2680D	0	
ETHYLGUAIACOL	0.1977D	0	
PROPYLGUAIACOL	0.1249D	0	
EUGENOL	0.1234D	0	
VINYLGUAIACOL	0.1400D	-1	
CONIFERALDEHYDE	0.7263D	-1	
PROPIOVANILLONE	0.0000D	0	
CATECHOL	0.1237D	-1	
METHYLCATECHOL	0.9631D	-1	
ETHYLCATECHOL	0.7177D	-1	
3,4-DIHYDROXYCINNAMALDEHYDE	0.2676D	-1	
VINYLCATECHOL	0.5151D	-2	
ALLYLCATECHOL	0.4515D	-1	
SYRINGOL	0.1965D	-2	
METHYLSYRINGOL	0.1480D	-1	
ETHYLSYRINGOL	0.1074D	-1	
PROPYLSYRINGOL	0.6692D	-2	
VINYLSYRINGOL	0.7621D	-3	
ALLYLSYRINGOL	0.6623D	-2	
SYRINGALDEHYDE	0.0000D	0	
PROPIOSYRINGONE	0.0000D	0	
METHOXYCATECHOL	0.4828D	-3	
METHANE	0.1322D	1	
CARBON MONOXIDE	0.8270D	0	
WATER	0.9767D	0	
CARBON DIOXIDE	0.0000D	0	
HYDROGEN	-0.5991D	-1	
METHANOL	0.1796D	-1	
GUAIACYL ACROLEIN	0.2769D	1	
SINAPYL ACROLEIN	0.1468D	0	
HYDROXYPHENYL ACROLEIN	0.6885D	0	
SINAPYL ALDEHYDE	0.3850D	-2	
COUMARALDEHYDE	0.1806D	-1	
PYROGALLOL	0.7573D	-4	
3,4-DIHYDROXYPHENYLACROLEIN	0.1021D	1	
SINGLE RINGS, MULTIPLE RINGS, AND SINGLES+			
LIGHTS ON MOL FRACTION BASIS			
SINGLE RING AROMATICS	0.2242D	0	
MULTIPLE RING AROMATICS	0.8284D	0	
SINGLE RINGS AND LIGHTS	0.3308D	1	



TIME	INTERVAL	TEMP(C)	
0.8000D	3	0.1000D	2 400.0
0.8000D	3	0.1000D	2 400.0
PRODUCT	YIELD(WTZ)		
PHENOL	0.8671D	-2	
CRESOLS	0.4883D	-1	
ETHYLPHENOL	0.5204D	-1	
PROPYLPHENOL	0.3461D	-1	
GUAIACOL	0.3494D	-1	
METHYLGUAIACOL	0.2686D	0	
ETHYLGUAIACOL	0.1980D	0	
PROPYLGUAIACOL	0.1290D	0	
EUGENOL	0.1275D	0	
VINYLGUAIACOL	0.1282D	-1	
CONIFERALDEHYDE	0.6660D	-1	
PROPIOVANILLONE	0.0000D	0	
CATECHOL	0.1453D	-1	
METHYLCATECHOL	0.1132D	0	
ETHYLCATECHOL	0.8430D	-1	
3,4-DIHYDROXYCINNAMALDEHYDE	0.2877D	-1	
VINYLCATECHOL	0.5530D	-2	
ALLYLCATECHOL	0.5467D	-1	
SYRINGOL	0.2036D	-2	
METHYLSYRINGOL	0.1534D	-1	
ETHYLSYRINGOL	0.1113D	-1	
PROPYLSYRINGOL	0.7148D	-2	
VINYLSYRINGOL	0.7217D	-3	
ALLYLSYRINGOL	0.7075D	-2	
SYRINGALDEHYDE	0.0000D	0	
PROPIOSYRINGONE	0.0000D	0	
METHOXYCATECHOL	0.5670D	-3	
METHANE	0.1492D	1	
CARBON MONOXIDE	0.9081D	0	
WATER	0.1106D	1	
CARBON DIOXIDE	0.0000D	0	
HYDROGEN	-0.7117D	-1	
METHANOL	0.1927D	-1	
GUAIACYL ACROLEIN	0.2997D	1	
SINAPYL ACROLEIN	0.1643D	0	
HYDROXYPHENYL ACROLEIN	0.8157D	0	
SINAPYL ALDEHYDE	0.3651D	-2	
COUMARALDEHYDE	0.1813D	-1	
PYROGALLOL	0.1036D	-3	
3,4-DIHYDROXYPHENYLACROLEIN	0.1294D	1	
SINGLE RINGS, MULTIPLE RINGS, AND SINGLES+			
LIGHTS ON MOL FRACTION BASIS			
SINGLE RING AROMATICS	0.2378D	0	
MULTIPLE RING AROMATICS	0.8176D	0	
SINGLE RINGS AND LIGHTS	0.3692D	1	

TIME	INTERVAL	TEMP(C)		
0.9000D	3	0.1000D	2	400.0
0.9000D	3	0.1000D	2	400.0
PRODUCT	YIELD(WTZ)			
PHENOL				0.9444D -2
CRESOLS				0.7495D -1
ETHYLPHENOL				0.5668D -1
PROPYLPHENOL				0.3870D -1
GUAIACOL				0.3490D -1
METHYLGUAIACOL				0.2683D 0
ETHYLGUAIACOL				0.1978D 0
PROPYLGUAIACOL				0.1323D 0
EUGENOL				0.1308D 0
VINYLGUAIACOL				0.1199D -1
CONIFERALDEHYDE				0.6172D -1
PROPIOVANILLONE				0.0000D 0
CATECHOL				0.1675D -1
METHYLCATECHOL				0.1304D 0
ETHYLCATECHOL				0.9717D -1
3,4-DIHYDROXYCINNAMALDEHYDE				0.3076D -1
VINYLCATECHOL				0.5969D -2
ALLYLCATECHOL				0.6470D -1
SYRINGOL				0.2097D -2
METHYLSYRINGOL				0.1581D -1
ETHYLSYRINGOL				0.1146D -1
PROPYLSYRINGOL				0.7562D -2
VINYLSYRINGOL				0.6964D -3
ALLYLSYRINGOL				0.7484D -2
SYRINGALDEHYDE				0.0000D 0
PROPIOSYRINGONE				0.0000D 0
METHOXYCATECHOL				0.6511D -3
METHANE				0.1657D 1
CARBON MONOXIDE				0.9861D 0
WATER				0.1232D 1
CARBON DIOXIDE				0.0000D 0
HYDROGEN				-0.8205D -1
METHANOL				0.2055D -1
GUAIACYL ACROLEIN				0.3193D 1
SINAPYL ACROLEIN				0.1805D 0
HYDROXYPHENYL ACROLEIN				0.9475D 0
SINAPYL ALDEHYDE				0.3490D -2
COUMARALDEHYDE				0.1832D -1
PYROGALLOL				0.1363D -3
3,4-DIHYDROXYPHENYLACROLEIN				0.1591D 1
SINGLE RINGS, MULTIPLE RINGS, AND SINGLES+				
LIGHTS ON MOL FRACTION BASIS				
SINGLE RING AROMATICS				0.2513D 0
MULTIPLE RING AROMATICS				0.8068D 0
SINGLE RINGS AND LIGHTS				0.4065D 1

TIME	INTERVAL	TEMP(C)		
0.10000	4	0.10000	2	400.0
0.10000	4	0.10000	2	400.0
PRODUCT	YIELD(WT%)			
PHENOL				0.10220 -1
CRESOLS				0.81200 -1
ETHYLPHENOL				0.61360 -1
PROPYLPHENOL				0.42860 -1
GUAIACOL				0.34770 -1
METHYLGUAIACOL				0.26760 0
ETHYLGUAIACOL				0.19720 0
PROPYLGUAIACOL				0.13490 0
EUGENOL				0.13330 0
VINYLGUAIACOL				0.11320 -1
CONIFERALDEHYDE				0.57420 -1
PROPIOVANILLONE				0.00000 0
CATECHOL				0.19000 -1
METHYLCATECHOL				0.14810 0
ETHYLCATECHOL				0.11030 0
3,4-DIHYDROXYCINNAMALDEHYDE				0.32580 -1
VINYLCATECHOL				0.64140 -2
ALLYLCATECHOL				0.75100 -1
SYRINGOL				0.21540 -2
METHYLSYRINGOL				0.16250 -1
ETHYLSYRINGOL				0.11780 -1
PROPYLSYRINGOL				0.79480 -2
VINYLSYRINGOL				0.67750 -3
ALLYLSYRINGOL				0.78670 -2
SYRINGALDEHYDE				0.00000 0
PROPIOSYRINGONE				0.00000 0
METHOXYCATECHOL				0.73440 -3
METHANE				0.18160 1
CARBON MONOXIDE				0.10620 1
WATER				0.13570 1
CARBON DIOXIDE				0.00000 0
HYDROGEN				-0.92560 -1
METHANOL				0.21790 -1
GUAIACYL ACRYLEIN				0.33580 1
SINAPYL ACRYLEIN				0.19570 0
HYDROXYPHENYL ACRYLEIN				0.10830 1
SINAPYL ALDEHYDE				0.33470 -2
COUMARALDEHYDE				0.18510 -1
PYROGALLOL				0.17380 -3
3,4-DIHYDROXYPHENYLACRYLEIN				0.19060 1
SINGLE RINGS, MULTIPLE RINGS, AND SINGLES+				
LIGHTS ON MOL FRACTION BASIS				
SINGLE RING AROMATICS				0.26460 0
MULTIPLE RING AROMATICS				0.79580 0
SINGLE RINGS AND LIGHTS				0.44290 1

TIME	INTERVAL	TEMP(C)	
0.2000D	4	0.1000D	2 400.0
0.2000D	4	0.1000D	2 400.0
PRODUCT	YIELD(WTZ)		
PHENOL	0.1828D	-1	
CRESOLS	0.1456D	0	
ETHYLPHENOL	0.1097D	0	
PROPYLPHENOL	0.8570D	-1	
GUAIACOL	0.3135D	-1	
METHYLGUAIACOL	0.2419D	0	
ETHYLGUAIACOL	0.1778D	0	
PROPYLGUAIACOL	0.1360D	0	
EUGENOL	0.1344D	0	
VINYLGUAIACOL	0.6790D	-2	
CONIFERALDEHYDE	0.2880D	-1	
PROPIOVANILLONE	0.0000D	0	
CATECHOL	0.4321D	-1	
METHYLCATECHOL	0.3376D	0	
ETHYLCATECHOL	0.2507D	0	
3,4-DIHYDROXYCINNAMALDEHYDE	0.4123D	-1	
VINYLCATECHOL	0.9705D	-2	
ALLYLCATECHOL	0.1910D	0	
SYRINGOL	0.2442D	-2	
METHYLSYRINGOL	0.1847D	-1	
ETHYLSYRINGOL	0.1335D	-1	
PROPYLSYRINGOL	0.1007D	-1	
VINYLSYRINGOL	0.5110D	-3	
ALLYLSYRINGOL	0.9971D	-2	
SYRINGALDEHYDE	0.0000D	0	
PROPIOSYRINGONE	0.0000D	0	
METHOXYCATECHOL	0.1475D	-2	
METHANE	0.3133D	1	
CARBON MONOXIDE	0.1702D	1	
WATER	0.2454D	1	
CARBON DIOXIDE	0.0000D	0	
HYDROGEN	-0.1785D	0	
METHANOL	0.3226D	-1	
GUAIACYL ACROLEIN	0.3918D	1	
SINAPYL ACROLEIN	0.2872D	0	
HYDROXYPHENYL ACROLEIN	0.2505D	1	
SINAPYL ALDEHYDE	0.2111D	-2	
COUMARALDEHYDE	0.1842D	-1	
PYROGALLOL	0.8164D	-3	
3,4-DIHYDROXYPHENYLACROLEIN	0.5608D	1	
SINGLE RINGS, MULTIPLE RINGS, AND SINGLES+			
LIGHTS ON MOL FRACTION BASIS			
SINGLE RING AROMATICS	0.3885D	0	
MULTIPLE RING AROMATICS	0.6863D	0	
SINGLE RINGS AND LIGHTS	0.7532D	1	

TIME	INTERVAL	TEMP(C)		
0.3000D	4	0.1000D	2	400.0
0.3000D	4	0.1000D	2	400.0
PRODUCT	YIELD(WTZ)			
PHENOL		0.2627D		-1
CRESOLS		0.2097D		0
ETHYLPHENOL		0.1577D		0
PROPYLPHENOL		0.1253D		0
GUAIACOL		0.2618D		-1
METHYLGUAIACOL		0.2024D		0
ETHYLGUAIACOL		0.1484D		0
PROPYLGUAIACOL		0.1156D		0
EUGENOL		0.1142D		0
VINYLGUAIACOL		0.4187D		-2
CONIFERALDEHYDE		0.1455D		-1
PROPIOVANILLONE		0.0000D		0
CATECHOL		0.6809D		-1
METHYLCATECHOL		0.5332D		0
ETHYLCATECHOL		0.3951D		0
3,4-DIHYDROXYCINNAMALDEHYDE		0.3930D		-1
VINYLCATECHOL		0.1129D		-1
ALLYLCATECHOL		0.3061D		0
SYRINGOL		0.2363D		-2
METHYLSYRINGOL		0.1791D		-1
ETHYLSYRINGOL		0.1292D		-1
PROPYLSYRINGOL		0.9918D		-2
VINYLSYRINGOL		0.3652D		-3
ALLYLSYRINGOL		0.9817D		-2
SYRINGALDEHYDE		0.0000D		0
PROPIOSYRINGONE		0.0000D		0
METHOXYCATECHOL		0.1929D		-2
METHANE		0.4066D		1
CARBON MONOXIDE		0.2176D		1
WATER		0.3294D		1
CARBON DIOXIDE		0.0000D		0
HYDROGEN		-0.2383D		0
METHANOL		0.4001D		-1
GUAIACYL ACROLEIN		0.3482D		1
SINAPYL ACROLEIN		0.2957D		0
HYDROXYPHENYL ACROLEIN		0.3832D		1
SINAPYL ALDEHYDE		0.1236D		-2
COUMARALDEHYDE		0.1601D		-1
PYROGALLOL		0.1874D		-2
3,4-DIHYDROXYPHENYLACROLEIN		0.9405D		1
SINGLE RINGS, MULTIPLE RINGS, AND SINGLES+				
LIGHTS ON MOL FRACTION BASIS				
SINGLE RING AROMATICS		0.4917D		0
MULTIPLE RING AROMATICS		0.5897D		0
SINGLE RINGS AND LIGHTS		0.9829D		1

TIME	INTERVAL	TEMP(C)	
0.4000D	4	0.1000D	2 400.0
0.4000D	4	0.1000D	2 400.0
PRODUCT	YIELD(WTZ)		
PHENOL			0.3376D -1
CRESOLS			0.2699D 0
ETHYLPHENOL			0.2027D 0
PROPYLPHENOL			0.1584D 0
GUAIACOL			0.2094D -1
METHYLGUAIACOL			0.1621D 0
ETHYLGUAIACOL			0.1187D 0
PROPYLGUAIACOL			0.9089D -1
EUGENOL			0.8980D -1
VINYLGUAIACOL			0.2634D -2
CONIFERALDEHYDE			0.7372D -2
PROPIOVANILLONE			0.0000D 0
CATECHOL			0.9182D -1
METHYLCATECHOL			0.7202D 0
ETHYLCATECHOL			0.5329D 0
3,4-DIHYDROXYCINNAMALDEHYDE			0.3357D -1
VINYLCATECHOL			0.1198D -1
ALLYLCATECHOL			0.4060D 0
SYRINGOL			0.2092D -2
METHYLSYRINGOL			0.1588D -1
ETHYLSYRINGOL			0.1143D -1
PROPYLSYRINGOL			0.8632D -2
VINYLSYRINGOL			0.2542D -3
ALLYLSYRINGOL			0.8543D -2
SYRINGALDEHYDE			0.0000D 0
PROPIOSYRINGONE			0.0000D 0
METHOXYCATECHOL			0.2083D -2
METHANE			0.4730D 1
CARBON MONOXIDE			0.2532D 1
WATER			0.3918D 1
CARBON DIOXIDE			0.0000D 0
HYDROGEN			-0.2800D 0
METHANOL			0.4573D -1
GUAIACYL ACRROLEIN			0.2782D 1
SINAPYL ACRROLEIN			0.2614D 0
HYDROXYPHENYL ACRROLEIN			0.4919D 1
SINAPYL ALDEHYDE			0.6928D -3
COUMARALDEHYDE			0.1304D -1
PYROGALLOL			0.3192D -2
3,4-DIHYDROXYPHENYLACRROLEIN			0.1267D 2
SINGLE RINGS, MULTIPLE RINGS, AND SINGLES+			
LIGHTS ON MOL FRACTION BASIS			
SINGLE RING AROMATICS			0.5735D 0
MULTIPLE RING AROMATICS			0.5113D 0
SINGLE RINGS AND LIGHTS			0.1152D 2

TIME	INTERVAL	TEMP(C)	
0.5000	4	0.1000	2 400.0
0.5000	4	0.1000	2 400.0
PRODUCT	YIELD(WTZ)		
PHENOL	0.4067	-1	
CRESOLS	0.3255	0	
ETHYLPHENOL	0.2441	0	
PROPYLPHENOL	0.1845	0	
GUAIACOL	0.1632	-1	
METHYLGUAIACOL	0.1265	0	
ETHYLGUAIACOL	0.9251	-1	
PROPYLGUAIACOL	0.6850	-1	
EUGENOL	0.6768	-1	
VINYLGUAIACOL	0.1688	-2	
CONIFERALDEHYDE	0.3746	-2	
PROPIOVANILLONE	0.0000	0	
CATECHOL	0.1138	0	
METHYLCATECHOL	0.8935	0	
ETHYLCATECHOL	0.6600	0	
3,4-DIHYDROXYCINNAMALDEHYDE	0.2712	-1	
VINYLCATECHOL	0.1220	-1	
ALLYLCATECHOL	0.4864	0	
SYRINGOL	0.1750	-2	
METHYLSYRINGOL	0.1330	-1	
ETHYLSYRINGOL	0.9562	-2	
PROPYLSYRINGOL	0.6982	-2	
VINYLSYRINGOL	0.1748	-3	
ALLYLSYRINGOL	0.6911	-2	
SYRINGALDEHYDE	0.0000	0	
PROPIOSYRINGONE	0.0000	0	
METHOXYCATECHOL	0.2016	-2	
METHANE	0.5204	1	
CARBON MONOXIDE	0.2805	1	
WATER	0.4374	1	
CARBON DIOXIDE	0.0000	0	
HYDROGEN	-0.3092	0	
METHANOL	0.4994	-1	
GUAIACYL ACROLEIN	0.2107	1	
SINAPYL ACROLEIN	0.2126	0	
HYDROXYPHENYL ACROLEIN	0.5760	1	
SINAPYL ALDEHYDE	0.3779	-3	
COUMARALDEHYDE	0.1024	-1	
PYROGALLOL	0.4627	-2	
3,4-DIHYDROXYPHENYLACROLEIN	0.1526	2	
SINGLE RINGS, MULTIPLE RINGS, AND SINGLES+			
LIGHTS ON MOL FRACTION BASIS			
SINGLE RING AROMATICS	0.6368	0	
MULTIPLE RING AROMATICS	0.4507	0	
SINGLE RINGS AND LIGHTS	0.1276	2	

TIME	INTERVAL	TEMP(C)		
0.60000	4	0.10000	2	400.0
0.60000	4	0.10000	2	400.0
PRODUCT				YIELD(WTZ)
PHENOL				0.46960 -1
CRESOLS				0.37630 0
ETHYLPHENOL				0.28180 0
PROPYLPHENOL				0.20460 0
GUAIACOL				0.12500 -1
METHYLGUAIACOL				0.96990 -1
ETHYLGUAIACOL				0.70840 -1
PROPYLGUAIACOL				0.50370 -1
EUGENOL				0.49770 -1
VINYLGUAIACOL				0.10980 -2
CONIFERALDEHYDE				0.19070 -2
PROPIOVANILLONE				0.00000 0
CATECHOL				0.13390 0
METHYLCATECHOL				0.10520 1
ETHYLCATECHOL				0.77660 0
3,4-DIHYDROXYCINNAMALDEHYDE				0.21210 -1
VINYLCATECHOL				0.12200 -1
ALLYLCATECHOL				0.54970 0
SYRINGOL				0.14090 -2
METHYLSYRINGOL				0.10720 -1
ETHYLSYRINGOL				0.77020 -2
PROPYLSYRINGOL				0.54010 -2
VINYLSYRINGOL				0.11960 -3
ALLYLSYRINGOL				0.53450 -2
SYRINGALDEHYDE				0.00000 0
PROPIOSYRINGONE				0.00000 0
METHOXYCATECHOL				0.18170 -2
METHANE				0.55430 1
CARBON MONOXIDE				0.30180 1
WATER				0.47050 1
CARBON DIOXIDE				0.00000 0
HYDROGEN				-0.32970 0
METHANOL				0.53050 -1
GUAIACYL ACRYLEIN				0.15470 1
SINAPYL ACRYLEIN				0.16420 0
HYDROXYPHENYL ACRYLEIN				0.63770 1
SINAPYL ALDEHYDE				0.20230 -3
COUMARALDEHYDE				0.78580 -2
PYROGALLOL				0.60660 -2
3,4-DIHYDROXYPHENYLACRYLEIN				0.17210 2
SINGLE RINGS, MULTIPLE RINGS, AND SINGLES+				
LIGHTS ON MOL FRACTION BASIS				
SINGLE RING AROMATICS				0.68470 0
MULTIPLE RING AROMATICS				0.40480 0
SINGLE RINGS AND LIGHTS				0.13670 2



TIME	INTERVAL	TEMP(C)	
0.7000D	4	0.1000D	2 400.0
0.7000D	4	0.1000D	2 400.0
PRODUCT	YIELD(WTZ)		
PHENOL	0.5275D	-1	
CRESOLS	0.4232D	0	
ETHYLPHENOL	0.3166D	0	
PROPYLPHENOL	0.2196D	0	
GUAIACOL	0.9449D	-2	
METHYLGUAIACOL	0.7343D	-1	
ETHYLGUAIACOL	0.5356D	-1	
PROPYLGUAIACOL	0.3639D	-1	
EUGENOL	0.3596D	-1	
VINYLGUAIACOL	0.7231D	-3	
CONIFERALDEHYDE	0.9714D	-3	
PROPIOVANILLONE	0.0000D	0	
CATECHOL	0.1522D	0	
METHYLCATECHOL	0.1198D	1	
ETHYLCATECHOL	0.8832D	0	
3,4-DIHYDROXYCINNAMALDEHYDE	0.1625D	-1	
VINYLCATECHOL	0.1208D	-1	
ALLYLCATECHOL	0.5972D	0	
SYRINGOL	0.1105D	-2	
METHYLSYRINGOL	0.8420D	-2	
ETHYLSYRINGOL	0.6041D	-2	
PROPYLSYRINGOL	0.4048D	-2	
VINYLSYRINGOL	0.8173D	-4	
ALLYLSYRINGOL	0.4006D	-2	
SYRINGALDEHYDE	0.0000D	0	
PROPIOSYRINGONE	0.0000D	0	
METHOXYCATECHOL	0.1559D	-2	
METHANE	0.5787D	1	
CARBON MONOXIDE	0.3188D	1	
WATER	0.4944D	1	
CARBON DIOXIDE	0.0000D	0	
HYDROGEN	-0.3443D	0	
METHANOL	0.5534D	-1	
GUAIACYL ACROLEIN	0.1114D	1	
SINAPYL ACROLEIN	0.1226D	0	
HYDROXYPHENYL ACROLEIN	0.6819D	1	
SINAPYL ALDEHYDE	0.1069D	-3	
COUMARALDEHYDE	0.5948D	-2	
PYROGALLOL	0.7445D	-2	
3,4-DIHYDROXYPHENYLACROLEIN	0.1864D	2	
SINGLE RINGS, MULTIPLE RINGS, AND SINGLES+			
LIGHTS ON MOL FRACTION BASIS			
SINGLE RING AROMATICS	0.7206D	0	
MULTIPLE RING AROMATICS	0.3707D	0	
SINGLE RINGS AND LIGHTS	0.1435D	2	

TIME	INTERVAL	TEMP(C)		
0.8000D	4	0.1000D	2	400.0
0.8000D	4	0.1000D	2	400.0
PRODUCT	YIELD(WTZ)			
PHENOL				0.5810D -1
CRESOLS				0.4664D 0
ETHYLPHENOL				0.3487D 0
PROPYLPHENOL				0.2307D 0
GUAIACOL				0.7081D -2
METHYLGUAIACOL				0.5506D -1
ETHYLGUAIACOL				0.4014D -1
PROPYLGUAIACOL				0.2602D -1
EUGENOL				0.2571D -1
VINYLGUAIACOL				0.4812D -3
CONIFERALDEHYDE				0.4952D -3
PROPIOVANILLONE				0.0000D 0
CATECHOL				0.1691D 0
METHYLCATECHOL				0.1332D 1
ETHYLCATECHOL				0.9813D 0
3,4-DIHYDROXYCINNAMALDEHYDE				0.1228D -1
VINYLCATECHOL				0.1192D -1
ALLYLCATECHOL				0.6331D 0
SYRINGOL				0.8509D -3
METHYLSYRINGOL				0.6486D -2
ETHYLSYRINGOL				0.4651D -2
PROPYLSYRINGOL				0.2973D -2
VINYLSYRINGOL				0.5587D -4
ALLYLSYRINGOL				0.2942D -2
SYRINGALDEHYDE				0.0000D 0
PROPIOSYRINGONE				0.0000D 0
METHOXYCATECHOL				0.1291D -2
METHANE				0.5964D 1
CARBON MONOXIDE				0.3327D 1
WATER				0.5116D 1
CARBON DIOXIDE				0.0000D 0
HYDROGEN				-0.3546D 0
METHANOL				0.5702D -1
GUAIACYL ACROLEIN				0.7915D 0
SINAPYL ACROLEIN				0.8949D -1
HYDROXYPHENYL ACROLEIN				0.7123D 1
SINAPYL ALDEHYDE				0.5599D -4
COUMARALDEHYDE				0.4456D -2
PYROGALLOL				0.8736D -2
3,4-DIHYDROXYPHENYLACROLEIN				0.1963D 2
SINGLE RINGS, MULTIPLE RINGS, AND SINGLES+				
LIGHTS ON MOL FRACTION BASIS				
SINGLE RING AROMATICS				0.7471D 0
MULTIPLE RING AROMATICS				0.3455D 0
SINGLE RINGS AND LIGHTS				0.1486D 2

TIME	INTERVAL	TEMP(C)		
0.90000	4	0.10000	2	400.0
0.90000	4	0.10000	2	400.0
PRODUCT			YIELD(WTZ)	
PHENOL			0.63080	-1
CRESOLS			0.50680	0
ETHYLPHENOL			0.37870	0
PROPYLPHENOL			0.23920	0
GUAIACOL			0.52700	-2
METHYLGUAIACOL			0.41010	-1
ETHYLGUAIACOL			0.29880	-1
PROPYLGUAIACOL			0.18490	-1
EUGENOL			0.18260	-1
VINYLGUAIACOL			0.32300	-3
CONIFERALDEHYDE			0.25260	-3
PROPIOVANILLONE			0.00000	0
CATECHOL			0.18480	0
METHYLCATECHOL			0.14560	1
ETHYLCATECHOL			0.10720	1
3,4-DIHYDROXYCINNAMALDEHYDE			0.91990	-2
VINYLCATECHOL			0.11740	-1
ALLYLCATECHOL			0.66030	0
SYRINGOL			0.64560	-3
METHYLSYRINGOL			0.49240	-2
ETHYLSYRINGOL			0.35290	-2
PROPYLSYRINGOL			0.21530	-2
VINYLSYRINGOL			0.38230	-4
ALLYLSYRINGOL			0.21310	-2
SYRINGALDEHYDE			0.00000	0
PROPIOSYRINGONE			0.00000	0
METHOXYCATECHOL			0.10410	-2
METHANE			0.60920	1
CARBON MONOXIDE			0.34450	1
WATER			0.52400	1
CARBON DIOXIDE			0.00000	0
HYDROGEN			-0.36210	0
METHANOL			0.58260	-1
GUAIACYL ACROLEIN			0.55780	0
SINAPYL ACROLEIN			0.64290	-1
HYDROXYPHENYL ACROLEIN			0.73230	1
SINAPYL ALDEHYDE			0.29120	-4
COUMARALDEHYDE			0.33160	-2
PYROGALLOL			0.99260	-2
3,4-DIHYDROXYPHENYLACROLEIN			0.20310	2
SINGLE RINGS, MULTIPLE RINGS, AND SINGLES+				
LIGHTS ON MOL FRACTION BASIS				
SINGLE RING AROMATICS			0.76670	0
MULTIPLE RING AROMATICS			0.32720	0
SINGLE RINGS AND LIGHTS			0.15240	2

TIME	INTERVAL	TEMP(C)	
0.1000D	5	0.1000D	2 400.0
0.1000D	5	0.1000D	2 400.0
PRODUCT	YIELD(WTZ)		
PHENOL	0.6777D	-1	
CRESOLS	0.5448D	0	
ETHYLPHENOL	0.4067D	0	
PROPYLPHENOL	0.2451D	0	
GUAIACOL	0.3898D	-2	
METHYLGUAIACOL	0.3035D	-1	
ETHYLGUAIACOL	0.2209D	-1	
PROPYLGUAIACOL	0.1304D	-1	
EUGENOL	0.1289D	-1	
VINYLGUAIACOL	0.2180D	-3	
CONIFERALDEHYDE	0.1288D	-3	
PROPIOVANILLONE	0.0000D	0	
CATECHOL	0.1994D	0	
METHYLCATECHOL	0.1573D	1	
ETHYLCATECHOL	0.1157D	1	
3,4-DIHYDROXYCINNAMALDEHYDE	0.6844D	-2	
VINYLCATECHOL	0.1157D	-1	
ALLYLCATECHOL	0.6798D	0	
SYRINGOL	0.4845D	-3	
METHYLSYRINGOL	0.3698D	-2	
ETHYLSYRINGOL	0.2648D	-2	
PROPYLSYRINGOL	0.1541D	-2	
VINYLSYRINGOL	0.2619D	-4	
ALLYLSYRINGOL	0.1526D	-2	
SYRINGALDEHYDE	0.0000D	0	
PROPIOSYRINGONE	0.0000D	0	
METHOXYCATECHOL	0.8227D	-3	
METHANE	0.6187D	1	
CARBON MONOXIDE	0.3547D	1	
WATER	0.5329D	1	
CARBON DIOXIDE	0.0000D	0	
HYDROGEN	-0.3677D	0	
METHANOL	0.5917D	-1	
GUAIACYL ACROLEIN	0.3905D	0	
SINAPYL ACROLEIN	0.4568D	-1	
HYDROXYPHENYL ACROLEIN	0.7448D	1	
SINAPYL ALDEHYDE	0.1506D	-4	
COUMARALDEHYDE	0.2456D	-2	
PYROGALLOL	0.1102D	-1	
3,4-DIHYDROXYPHENYLACROLEIN	0.2075D	2	
SINGLE RINGS, MULTIPLE RINGS, AND SINGLES+			
LIGHTS ON MOL FRACTION BASIS			
SINGLE RING AROMATICS	0.7811D	0	
MULTIPLE RING AROMATICS	0.3137D	0	
SINGLE RINGS AND LIGHTS	0.1554D	2	

TIME	INTERVAL	TEMP(C)	
0.00000	0	0.10000	0 500.0
0.00000	0	0.10000	0 500.0
PRODUCT	YIELD(WTZ)		
PHENOL	0.00000	0	
CRESOLS	0.00000	0	
ETHYLPHENOL	0.00000	0	
PROPYLPHENOL	0.00000	0	
GUAIACOL	0.00000	0	
METHYLGUAIACOL	0.00000	0	
ETHYLGUAIACOL	0.00000	0	
PROPYLGUAIACOL	0.00000	0	
EUGENOL	0.00000	0	
VINYLGUAIACOL	0.00000	0	
CONIFERALDEHYDE	0.20160	1	
PROPIOVANILLONE	0.00000	0	
CATECHOL	0.00000	0	
METHYLCATECHOL	0.00000	0	
ETHYLCATECHOL	0.00000	0	
3,4-DIHYDROXYCINNAMALDEHYDE	0.00000	0	
VINYLCATECHOL	0.00000	0	
ALLYLCATECHOL	0.00000	0	
SYRINGOL	0.00000	0	
METHYLSYRINGOL	0.00000	0	
ETHYLSYRINGOL	0.00000	0	
PROPYLSYRINGOL	0.00000	0	
VINYLSYRINGOL	0.00000	0	
ALLYLSYRINGOL	0.00000	0	
SYRINGALDEHYDE	0.00000	0	
PROPIOSYRINGONE	0.00000	0	
METHOXYCATECHOL	0.00000	0	
METHANE	0.00000	0	
CARBON MONOXIDE	0.00000	0	
WATER	0.00000	0	
CARBON DIOXIDE	0.00000	0	
HYDROGEN	0.00000	0	
METHANOL	0.00000	0	
GUAIACYL ACRYLALDEHYDE	0.00000	0	
SINAPYL ACRYLALDEHYDE	0.00000	0	
HYDROXYPHENYL ACRYLALDEHYDE	0.00000	0	
SINAPYL ALDEHYDE	0.26570	-1	
COUMARALDEHYDE	0.22440	0	
PYROGALLOL	0.00000	0	
3,4-DIHYDROXYPHENYLACRYLALDEHYDE	0.00000	0	
SINGLE RINGS, MULTIPLE RINGS, AND SINGLES+ LIGHTS ON MOL FRACTION BASIS			
SINGLE RING AROMATICS	0.71200	-1	
MULTIPLE RING AROMATICS	0.92760	0	
SINGLE RINGS AND LIGHTS	0.71200	-1	

TIME	INTERVAL	TEMP(C)	
0.1010D	2	0.1000D 0	500.0
0.1010D	2	0.1000D 0	500.0
PRODUCT	YIELD(WTZ)		
PHENOL	0.1405D	-1	
CRESOLS	0.1117D	0	
ETHYLPHENOL	0.8431D	-1	
PROPYLPHENOL	0.1257D	-1	
GUAIACOL	0.5388D	-1	
METHYLGUAIACOL	0.4150D	0	
ETHYLGUAIACOL	0.3054D	0	
PROPYLGUAIACOL	0.4459D	-1	
EUGENOL	0.4406D	-1	
VINYLGUAIACOL	0.4286D	0	
CONIFERALDEHYDE	0.1723D	0	
PROPIOVANILLONE	0.0000D	0	
CATECHOL	0.1906D	-1	
METHYLCATECHOL	0.1487D	0	
ETHYLCATECHOL	0.1106D	0	
3,4-DIHYDROXYCINNAMALDEHYDE	0.6330D	-1	
VINYLCATECHOL	0.1572D	0	
ALLYLCATECHOL	0.1607D	-1	
SYRINGOL	0.3125D	-2	
METHYLSYRINGOL	0.2359D	-1	
ETHYLSYRINGOL	0.1708D	-1	
PROPYLSYRINGOL	0.2459D	-2	
VINYLSYRINGOL	0.2401D	-1	
ALLYLSYRINGOL	0.2434D	-2	
SYRINGALDEHYDE	0.0000D	0	
PROPIOSYRINGONE	0.0000D	0	
METHOXYCATECHOL	0.7598D	-3	
METHANE	0.1478D	1	
CARBON MONOXIDE	0.1459D	1	
WATER	0.1000D	1	
CARBON DIOXIDE	0.0000D	0	
HYDROGEN	-0.8963D	-1	
METHANOL	0.1402D	-1	
GUAIACYL ACRYLEIN	0.3016D	1	
SINAPYL ACRYLEIN	0.1646D	0	
HYDROXYPHENYL ACRYLEIN	0.8625D	0	
SINAPYL ALDEHYDE	0.9401D	-2	
COUMARALDEHYDE	0.4927D	-1	
PYROGALLUL	0.1155D	-3	
3,4-DIHYDROXYPHENYLACRYLEIN	0.1108D	1	
SINGLE RINGS, MULTIPLE RINGS, AND SINGLES+			
LIGHTS ON MOL FRACTION BASIS			
SINGLE RING AROMATICS	0.2376D	0	
MULTIPLE RING AROMATICS	0.7967D	0	
SINGLE RINGS AND LIGHTS	0.4099D	1	

TIME	INTERVAL	TEMP(C)	
0.2010D	2	0.1000D	0 500.0
0.2010D	2	0.1000D	0 500.0
PRODUCT	YIELD(WTZ)		
PHENOL	0.3349D	-1	
CRESOLS	0.2666D	0	
ETHYLPHENOL	0.2010D	0	
PROPYLPHENOL	0.3494D	-1	
GUAIACOL	0.6912D	-1	
METHYLGUAIACOL	0.5330D	0	
ETHYLGUAIACOL	0.3919D	0	
PROPYLGUAIACOL	0.6673D	-1	
EUGENOL	0.6592D	-1	
VINYLGUAIACOL	0.2317D	0	
CONIFERALDEHYDE	0.1063D	0	
PROPIOVANILLONE	0.0000D	0	
CATECHOL	0.5980D	-1	
METHYLCATECHOL	0.4671D	0	
ETHYLCATECHOL	0.3470D	0	
3,4-DIHYDROXYCINNAMALDEHYDE	0.9551D	-1	
VINYLCATECHOL	0.2079D	0	
ALLYLCATECHOL	0.5880D	-1	
SYRINGOL	0.4851D	-2	
METHYLSYRINGOL	0.3667D	-1	
ETHYLSYRINGOL	0.2652D	-1	
PROPYLSYRINGOL	0.4452D	-2	
VINYLSYRINGOL	0.1572D	-1	
ALLYLSYRINGOL	0.4407D	-2	
SYRINGALDEHYDE	0.0000D	0	
PROPIOSYRINGONE	0.0000D	0	
METHOXYCATECHOL	0.2296D	-2	
METHANE	0.2649D	1	
CARBON MONOXIDE	0.2341D	1	
WATER	0.1781D	1	
CARBON DIOXIDE	0.0000D	0	
HYDROGEN	-0.1503D	0	
METHANOL	0.2815D	-1	
GUAIACYL ACROLEIN	0.3935D	1	
SINAPYL ACROLEIN	0.2599D	0	
HYDROXYPHENYL ACROLEIN	0.2091D	1	
SINAPYL ALDEHYDE	0.7020D	-2	
COUMARALDEHYDE	0.5649D	-1	
PYROGALLOL	0.7978D	-3	
3,4-DIHYDROXYPHENYLACROLEIN	0.3536D	1	
SINGLE RINGS, MULTIPLE RINGS, AND SINGLES+			
LIGHTS ON MOL FRACTION BASIS			
SINGLE RING AROMATICS	0.3406D	0	
MULTIPLE RING AROMATICS	0.7293D	0	
SINGLE RINGS AND LIGHTS	0.6990D	1	

TIME	INTERVAL	TEMP(C)	
0.3010D	2	0.1000D	0 500.0
0.3010D	2	0.1000D	0 500.0
PRODUCT	YIELD(WTZ)		
PHENOL	0.5384D	-1	
CRESOLS	0.4291D	0	
ETHYLPHENOL	0.3232D	0	
PROPYLPHENOL	0.5919D	-1	
GUAIACOL	0.6804D	-1	
METHYLGUAIACOL	0.5252D	0	
ETHYLGUAIACOL	0.3858D	0	
PROPYL GUAIACOL	0.6922D	-1	
EUGENOL	0.6839D	-1	
VINYLGUAIACOL	0.1438D	0	
CONIFERALDEHYDE	0.6271D	-1	
PROPIOVANILLONE	0.0000D	0	
CATECHOL	0.1076D	0	
METHYLCATECHOL	0.8413D	0	
ETHYLCATECHOL	0.6244D	0	
3,4-DIHYDROXYCINNAMALDEHYDE	0.1030D	0	
VINYLCATECHOL	0.2358D	0	
ALLYLCATECHOL	0.1115D	0	
SYRINGOL	0.5430D	-2	
METHYLSYRINGOL	0.4108D	-1	
ETHYLSYRINGOL	0.2968D	-1	
PROPYLSYRINGOL	0.5251D	-2	
VINYLSYRINGOL	0.1108D	-1	
ALLYLSYRINGOL	0.5198D	-2	
SYRINGALDEHYDE	0.0000D	0	
PROPIOSYRINGONE	0.0000D	0	
METHOXYCATECHOL	0.3683D	-2	
METHANE	0.3538D	1	
CARBON MONOXIDE	0.3048D	1	
WATER	0.2399D	1	
CARBON DIOXIDE	0.0000D	0	
HYDROGEN	-0.1938D	0	
METHANOL	0.3950D	-1	
GUAIACYL ACROLEIN	0.3851D	1	
SINAPYL ACROLEIN	0.2891D	0	
HYDROXYPHENYL ACROLEIN	0.3342D	1	
SINAPYL ALDEHYDE	0.4708D	-2	
COUMARALDEHYDE	0.5443D	-1	
PYROGALLOL	0.2182D	-2	
3,4-DIHYDROXYPHENYLACROLEIN	0.6324D	1	
SINGLE RINGS, MULTIPLE RINGS, AND SINGLES+			
LIGHTS ON MOL FRACTION BASIS			
SINGLE RING AROMATICS	0.4311D	0	
MULTIPLE RING AROMATICS	0.6667D	0	
SINGLE RINGS AND LIGHTS	0.9262D	1	



TIME	INTERVAL	TEMP(C)	
0.4010D	2	0.1000D	0 500.0
0.4010D	2	0.1000D	0 500.0
PRODUCT	YIELD(WTZ)		
PHENOL	0.7366D	-1	
CRESOLS	0.5875D	0	
ETHYLPHENOL	0.4422D	0	
PROPYLPHENOL	0.8191D	-1	
GUAIACOL	0.6068D	-1	
METHYLGUAIACOL	0.4689D	0	
ETHYLGUAIACOL	0.3441D	0	
PROPYLGUAIACOL	0.6244D	-1	
EUGENOL	0.6169D	-1	
VINYLGUAIACOL	0.9169D	-1	
CONIFERALDEHYDE	0.3636D	-1	
PROPIOVANILLONE	0.0000D	0	
CATECHOL	0.1567D	0	
METHYLCATECHOL	0.1227D	1	
ETHYLCATECHOL	0.9095D	0	
3,4-DIHYDROXYCINNAMALDEHYDE	0.9755D	-1	
VINYLCATECHOL	0.2456D	0	
ALLYLCATECHOL	0.1643D	0	
SYRINGOL	0.5312D	-2	
METHYLSYRINGOL	0.4023D	-1	
ETHYLSYRINGOL	0.2904D	-1	
PROPYLSYRINGOL	0.5196D	-2	
VINYLSYRINGOL	0.7755D	-2	
ALLYLSYRINGOL	0.5143D	-2	
SYRINGALDEHYDE	0.0000D	0	
PROPIOSYRINGONE	0.0000D	0	
METHOXYCATECHOL	0.4610D	-2	
METHANE	0.4211D	1	
CARBON MONOXIDE	0.3613D	1	
WATER	0.2889D	1	
CARBON DIOXIDE	0.0000D	0	
HYDROGEN	-0.2252D	0	
METHANOL	0.4849D	-1	
GUAIACYL ACROLEIN	0.3348D	1	
SINAPYL ACROLEIN	0.2758D	0	
HYDROXYPHENYL ACROLEIN	0.4458D	1	
SINAPYL ALDEHYDE	0.2995D	-2	
COUMARALDEHYDE	0.4841D	-1	
PYROGALLOL	0.4161D	-2	
3,4-DIHYDROXYPHENYLACROLEIN	0.8982D	1	
SINGLE RINGS, MULTIPLE RINGS, AND SINGLES+			
LIGHTS ON MOL FRACTION BASIS			
SINGLE RING AROMATICS	0.5078D	0	
MULTIPLE RING AROMATICS	0.6109D	0	
SINGLE RINGS AND LIGHTS	0.1104D	2	

TIME	INTERVAL	TEMP(C)	
0.5010D	2	0.1000D	0 500.0
0.5010D	2	0.1000D	0 500.0
PRODUCT			YIELD(WTZ)
PHENOL			0.9213D -1
CREOLS			0.7354D 0
ETHYLPHENOL			0.5529D 0
PROPYLPHENOL			0.1018D 0
GUAIACOL			0.5124D -1
METHYLGUAIACOL			0.3962D 0
ETHYLGUAIACOL			0.2905D 0
PROPYLGUAIACOL			0.5236D -1
EUGENOL			0.5173D -1
VINYLGUAIACOL			0.5897D -1
CONIFERALDEHYDE			0.2091D -1
PROPIOVANILLONE			0.0000D 0
CATECHOL			0.2041D 0
METHYLCATECHOL			0.1598D 1
ETHYLCATECHOL			0.1184D 1
3,4-DIHYDROXYCINNAMALDEHYDE			0.8647D -1
VINYLCATECHOL			0.2436D 0
ALLYLCATECHOL			0.2124D 0
SYRINGOL			0.4806D -2
METHYLSYRINGOL			0.3642D -1
ETHYLSYRINGOL			0.2626D -1
PROPYLSYRINGOL			0.4669D -2
VINYLSYRINGOL			0.5344D -2
ALLYLSYRINGOL			0.4621D -2
SYRINGALDEHYDE			0.0000D 0
PROPIOSYRINGONE			0.0000D 0
METHOXYCATECHOL			0.5029D -2
METHANE			0.4717D 1
CARBON MONOXIDE			0.4068D 1
WATER			0.3278D 1
CARBON DIOXIDE			0.0000D 0
HYDROGEN			-0.2477D 0
METHANOL			0.5555D -1
GUAIACYL ACROLEIN			0.2733D 1
SINAPYL ACROLEIN			0.2412D 0
HYDROXYPHENYL ACROLEIN			0.5390D 1
SINAPYL ALDEHYDE			0.1845D -2
COUMARALDEHYDE			0.4123D -1
PYROGALLOL			0.6538D -2
3,4-DIHYDROXYPHENYLACROLEIN			0.1130D 2
SINGLE RINGS, MULTIPLE RINGS, AND SINGLES+			
LIGHTS ON MOL FRACTION BASIS			
SINGLE RING AROMATICS			0.5713D 0
MULTIPLE RING AROMATICS			0.5628D 0
SINGLE RINGS AND LIGHTS			0.1244D 2

TIME	INTERVAL	TEMP(C)		
0.6010D	2	0.1000D	0	500.0
0.6010D	2	0.1000D	0	500.0
PRODUCT	YIELD(WTZ)			
PHENOL			0.1089D	0
CRESOLS			0.8696D	0
ETHYLPHENOL			0.6534D	0
PROPYLPHENOL			0.1183D	0
GUAIACOL			0.4176D	-1
METHYLGUAIACOL			0.3231D	0
ETHYLGUAIACOL			0.2367D	0
PROPYLGUAIACOL			0.4200D	-1
EUGENOL			0.4149D	-1
VINYLGUAIACOL			0.3822D	-1
CONFERALDEHYDE			0.1195D	-1
PROPIOVANILLONE			0.0000D	0
CATECHOL			0.2479D	0
METHYLCATECHOL			0.1943D	1
ETHYLCATECHOL			0.1439D	1
3,4-DIHYDROXYCINNAMALDEHYDE			0.7369D	-1
VINYLCATECHOL			0.2353D	0
ALLYLCATECHOL			0.2540D	0
SYRINGOL			0.4128D	-2
METHYLSYRINGOL			0.3131D	-1
ETHYLSYRINGOL			0.2256D	-1
PROPYLSYRINGOL			0.3947D	-2
VINYLSYRINGOL			0.3651D	-2
ALLYLSYRINGOL			0.3907D	-2
SYRINGALDEHYDE			0.0000D	0
PROPIOSYRINGONE			0.0000D	0
METHOXYCATECHOL			0.5023D	-2
METHANE			0.5098D	1
CARBON MONOXIDE			0.4437D	1
WATER			0.3589D	1
CARBON DIOXIDE			0.0000D	0
HYDROGEN			-0.2638D	0
METHANOL			0.6111D	-1
GUAIACYL ACRYLEIN			0.2143D	1
SINAPYL ACRYLEIN			0.1993D	0
HYDROXYPHENYL ACRYLEIN			0.6128D	1
SINAPYL ALDEHYDE			0.1112D	-2
COUMARALDEHYDE			0.3417D	-1
PYROGALLOL			0.9104D	-2
3,4-DIHYDROXYPHENYLACRYLEIN			0.1322D	2
SINGLE RINGS, MULTIPLE RINGS, AND SINGLES+				
LIGHTS ON MOL FRACTION BASIS				
SINGLE RING AROMATICS			0.6230D	0
MULTIPLE RING AROMATICS			0.5225D	0
SINGLE RINGS AND LIGHTS			0.1354D	2

TIME	INTERVAL	TEMP(C)		
0.7010D	2	0.1000D	0	500.0
0.7010D	2	0.1000D	0	500.0
PRODUCT	YIELD(WT%)			
PHENOL				0.1238D 0
CRESOLS				0.9899D 0
ETHYLPHENOL				0.7433D 0
PROPYLPHENOL				0.1318D 0
GUAIACOL				0.3320D -1
METHYLGUAIACOL				0.2571D 0
ETHYLGUAIACOL				0.1882D 0
PROPYLGUAIACOL				0.3269D -1
EUGENOL				0.3230D -1
VINYLGUAIACOL				0.2496D -1
CONIFERALDEHYDE				0.6802D -2
PROPIOVANILLONE				0.0000D 0
CATECHOL				0.2879D 0
METHYLCATECHOL				0.2258D 1
ETHYLCATECHOL				0.1670D 1
3,4-DIHYDROXYCINNAMALDEHYDE				0.6126D -1
VINYLCATECHOL				0.2244D 0
ALLYLCATECHOL				0.2888D 0
SYRINGOL				0.3422D -2
METHYLSYRINGOL				0.2597D -1
ETHYLSYRINGOL				0.1870D -1
PROPYLSYRINGOL				0.3203D -2
VINYLSYRINGOL				0.2485D -2
ALLYLSYRINGOL				0.3170D -2
SYRINGALDEHYDE				0.0000D 0
PROPIOSYRINGONE				0.0000D 0
METHOXYCATECHOL				0.4720D -2
METHANE				0.5385D 1
CARBON MONOXIDE				0.4740D 1
WATER				0.3840D 1
CARBON DIOXIDE				0.0000D 0
HYDROGEN				-0.2753D 0
METHANOL				0.6547D -1
GUAIACYL ACRYLEIN				0.1635D 1
SINAPYL ACRYLEIN				0.1586D 0
HYDROXYPHENYL ACRYLEIN				0.6690D 1
SINAPYL ALDEHYDE				0.6596D -3
COUMARALDEHYDE				0.2783D -1
PYROGALLOL				0.1170D -1
3,4-DIHYDROXYPHENYLACRYLEIN				0.1473D 2
SINGLE RINGS, MULTIPLE RINGS, AND SINGLES+				
LIGHTS ON MOL FRACTION BASIS				
SINGLE RING AROMATICS				0.6646D 0
MULTIPLE RING AROMATICS				0.4889D 0
SINGLE RINGS AND LIGHTS				0.1442D 2

TIME	INTERVAL	TEMP(C)	
0.8010D	2	0.1000D	0 500.0
0.8010D	2	0.1000D	0 500.0
PRODUCT	YIELD(WTZ)		
PHENOL	0.1372D	0	
CRESOLS	0.1098D	1	
ETHYLPHENOL	0.8236D	0	
PROPYLPHENOL	0.1426D	0	
GUAIACOL	0.2594D	-1	
METHYLGUAIACOL	0.2010D	0	
ETHYLGUAIACOL	0.1470D	0	
PROPYLGUAIACOL	0.2493D	-1	
EUGENOL	0.2463D	-1	
VINYLGUAIACOL	0.1645D	-1	
CONIFERALDEHYDE	0.3857D	-2	
PROPIOVANILLONE	0.0000D	0	
CATECHOL	0.3238D	0	
METHYLCATECHOL	0.2542D	1	
ETHYLCATECHOL	0.1879D	1	
3,4-DIHYDROXYCINNAMALDEHYDE	0.5001D	-1	
VINYLCATECHOL	0.2130D	0	
ALLYLCATECHOL	0.3171D	0	
SYRINGOL	0.2762D	-2	
METHYLSYRINGOL	0.2098D	-1	
ETHYLSYRINGOL	0.1509D	-1	
PROPYLSYRINGOL	0.2524D	-2	
VINYLSYRINGOL	0.1692D	-2	
ALLYLSYRINGOL	0.2498D	-2	
SYRINGALDEHYDE	0.0000D	0	
PROPYOSYRINGONE	0.0000D	0	
METHOXYCATECHOL	0.4241D	-2	
METHANE	0.5600D	1	
CARBON MONOXIDE	0.4991D	1	
WATER	0.4043D	1	
CARBON DIOXIDE	0.0000D	0	
HYDROGEN	-0.2835D	0	
METHANOL	0.6888D	-1	
GUAIACYL ACRYLEIN	0.1225D	1	
SINAPYL ACRYLEIN	0.1227D	0	
HYDROXYPHENYL ACRYLEIN	0.7107D	1	
SINAPYL ALDEHYDE	0.3864D	-3	
COUMARALDEHYDE	0.2238D	-1	
PYROGALLOL	0.1422D	-1	
3,4-DIHYDROXYPHENYLACRYLEIN	0.1588D	2	
SINGLE RINGS, MULTIPLE RINGS, AND SINGLES+			
LIGHTS ON MOL FRACTION BASIS			
SINGLE RING AROMATICS	0.6977D	0	
MULTIPLE RING AROMATICS	0.4611D	0	
SINGLE RINGS AND LIGHTS	0.1512D	2	

TIME	INTERVAL	TEMP(C)	
0.9010D	2	0.1000D 0	500.0
0.9010D	2	0.1000D 0	500.0
PRODUCT	YIELD(WTZ)		
PHENOL	0.1492D	0	
CRESOLS	0.1195D	1	
ETHYLPHENOL	0.8958D	0	
PROPYLPHENOL	0.1511D	0	
GUAIACOL	0.1999D	-1	
METHYLGUAIACOL	0.1550D	0	
ETHYLGUAIACOL	0.1133D	0	
PROPYLGUAIACOL	0.1873D	-1	
EUGENOL	0.1850D	-1	
VINYLGUAIACOL	0.1093D	-1	
CONIFERALDEHYDE	0.2182D	-2	
PROPTOVANILLONE	0.0000D	0	
CATECHOL	0.3562D	0	
METHYLCATECHOL	0.2798D	1	
ETHYLCATECHOL	0.2067D	1	
3,4-DIHYDROXYCINNAMALDEHYDE	0.4039D	-1	
VINYLCATECHOL	0.2020D	0	
ALLYLCATECHOL	0.3399D	0	
SYRINGOL	0.2185D	-2	
METHYLSYRINGOL	0.1661D	-1	
ETHYLSYRINGOL	0.1194D	-1	
PROPYLSYRINGOL	0.1946D	-2	
VINYLSYRINGOL	0.1155D	-2	
ALLYLSYRINGOL	0.1926D	-2	
SYRINGALDEHYDE	0.0000D	0	
PROPIOSYRINGONE	0.0000D	0	
METHOXYCATECHOL	0.3686D	-2	
METHANE	0.5762D	1	
CARBON MONOXIDE	0.5204D	1	
WATER	0.4209D	1	
CARBON DIOXIDE	0.0000D	0	
HYDROGEN	-0.2892D	0	
METHANOL	0.7155D	-1	
GUAIACYL ACROLEIN	0.9043D	0	
SINAPYL ACROLEIN	0.9301D	-1	
HYDROXYPHENYL ACROLEIN	0.7404D	1	
SINAPYL ALDEHYDE	0.2244D	-3	
COUMARALDEHYDE	0.1787D	-1	
PYROGALLOL	0.1658D	-1	
3,4-DIHYDROXYPHENYLACROLEIN	0.1674D	2	
SINGLE RINGS, MULTIPLE RINGS, AND SINGLES+ LIGHTS ON MOL. FRACTION BASIS			
SINGLE RING AROMATICS	0.7241D	0	
MULTIPLE RING AROMATICS	0.4384D	0	
SINGLE RINGS AND LIGHTS	0.1568D	2	

TIME	INTERVAL	TEMP(C)		
0.1001D	3	0.1000D	0	500.0
0.1001D	3	0.1000D	0	500.0
PRODUCT			YIELD(WTZ)	
PHENOL			0.1601D	0
CRESOLS			0.1282D	1
ETHYLPHENOL			0.9608D	0
PROPYLPHENOL			0.1578D	0
GUAIACOL			0.1525D	-1
METHYLGUAIACOL			0.1183D	0
ETHYLGUAIACOL			0.8644D	-1
PROPYLGUAIACOL			0.1391D	-1
EUGENOL			0.1374D	-1
VINYLGUAIACOL			0.7327D	-2
CONIFERALDEHYDE			0.1232D	-2
PROPIOVANILLONE			0.0000D	0
CATECHOL			0.3853D	0
METHYLCATECHOL			0.3029D	1
ETHYLCATECHOL			0.2236D	1
3,4-DIHYDROXYCINNAMALDEHYDE			0.3233D	-1
VINYLCATECHOL			0.1920D	0
ALLYLCATECHOL			0.3580D	0
SYRINGOL			0.1702D	-2
METHYLSYRINGOL			0.1294D	-1
ETHYLSYRINGOL			0.9301D	-2
PROPYLSYRINGOL			0.1476D	-2
VINYLSYRINGOL			0.7901D	-3
ALLYLSYRINGOL			0.1461D	-2
SYRINGALDEHYDE			0.0000D	0
PROPIOSYRINGONE			0.0000D	0
METHOXYCATECHOL			0.3119D	-2
METHANE			0.5884D	1
CARBON MONOXIDE			0.5386D	1
WATER			0.4345D	1
CARBON DIOXIDE			0.0000D	0
HYDROGEN			-0.2931D	0
METHANOL			0.7365D	-1
GUAIACYL ACROLEIN			0.6607D	0
SINAPYL ACROLEIN			0.6938D	-1
HYDROXYPHENYL ACROLEIN			0.7607D	1
SINAPYL ALDEHYDE			0.1293D	-3
COUMARALDEHYDE			0.1418D	-1
PYROGALLOL			0.1876D	-1
3,4-DIHYDROXYPHENYLACROLEIN			0.1734D	2
SINGLE RINGS, MULTIPLE RINGS, AND SINGLES+				
LIGHTS ON MOL FRACTION BASIS				
SINGLE RING AROMATICS			0.7448D	0
MULTIPLE RING AROMATICS			0.4198D	0
SINGLE RINGS AND LIGHTS			0.1614D	2

TIME	INTERVAL	TEMP(C)	
0.0000	0	0.5000	-2 600.0
0.0000	0	0.5000	-2 600.0
PRODUCT	YIELD(WTZ)		
PHENOL	0.0000	0	
CRESOLS	0.0000	0	
ETHYLPHENOL	0.0000	0	
PROPYLPHENOL	0.0000	0	
GUAIACOL	0.0000	0	
METHYLGUAIACOL	0.0000	0	
ETHYLGUAIACOL	0.0000	0	
PROPYLGUAIACOL	0.0000	0	
EUGENOL	0.0000	0	
VINYLGUAIACOL	0.0000	0	
CONIFERALDEHYDE	0.2016	1	
PROPIOVANILLONE	0.0000	0	
CATECHOL	0.0000	0	
METHYLCATECHOL	0.0000	0	
ETHYLCATECHOL	0.0000	0	
3,4-DIHYDROXYCINNAMALDEHYDE	0.0000	0	
VINYLCATECHOL	0.0000	0	
ALLYLCATECHOL	0.0000	0	
SYRINGOL	0.0000	0	
METHYLSYRINGOL	0.0000	0	
ETHYLSYRINGOL	0.0000	0	
PROPYLSYRINGOL	0.0000	0	
VINYLSYRINGOL	0.0000	0	
ALLYLSYRINGOL	0.0000	0	
SYRINGALDEHYDE	0.0000	0	
PROPIOSYRINGONE	0.0000	0	
METHOXYCATECHOL	0.0000	0	
METHANE	0.0000	0	
CARBON MONOXIDE	0.0000	0	
WATER	0.0000	0	
CARBON DIOXIDE	0.0000	0	
HYDROGEN	0.0000	0	
METHANOL	0.0000	0	
GUAIACYL ACROLEIN	0.0000	0	
SINAPYL ACROLEIN	0.0000	0	
HYDROXYPHENYL ACROLEIN	0.0000	0	
SINAPYL ALDEHYDE	0.2657	-1	
COUMARALDEHYDE	0.2244	0	
PYROGALLOL	0.0000	0	
3,4-DIHYDROXYPHENYLACROLEIN	0.0000	0	
SINGLE RINGS, MULTIPLE RINGS, AND SINGLES+			
LIGHTS ON MOL FRACTION BASIS			
SINGLE RING AROMATICS	0.7120	-1	
MULTIPLE RING AROMATICS	0.9276	0	
SINGLE RINGS AND LIGHTS	0.7120	-1	



TIME	INTERVAL	TEMP(C)	
0.1005D	1	0.5000D -2	600.0
0.1005D	1	0.5000D -2	600.0
PRODUCT	YIELD(WTZ)		
PHENOL	0.3984D	-1	
CRESOLS	0.3217D	0	
ETHYLPHENOL	0.2391D	0	
PROPYLPHENOL	0.1656D	-1	
GUAIACOL	0.4706D	-1	
METHYLGUAIACOL	0.3682D	0	
ETHYLGUAIACOL	0.2668D	0	
PROPYLGUAIACOL	0.1810D	-1	
EUGENOL	0.1788D	-1	
VINYLGUAIACOL	0.7756D	0	
CONIFERALDEHYDE	0.6461D	-1	
PROPIOVANILLONE	0.0000D	0	
CATECHOL	0.6852D	-1	
METHYLCATECHOL	0.5430D	0	
ETHYLCATECHOL	0.3975D	0	
3,4-DIHYDROXYCINNAMALDEHYDE	0.9772D	-1	
VINYLCATECHOL	0.1171D	1	
ALLYLCATECHOL	0.2685D	-1	
SYRINGOL	0.3556D	-2	
METHYLSYRINGOL	0.2727D	-1	
ETHYLSYRINGOL	0.1943D	-1	
PROPYLSYRINGOL	0.1300D	-2	
VINYLSYRINGOL	0.5662D	-1	
ALLYLSYRINGOL	0.1287D	-2	
SYRINGALDEHYDE	0.0000D	0	
PROPIOSYRINGONE	0.0000D	0	
METHOXYCATECHOL	0.2486D	-2	
METHANE	0.3739D	1	
CARBON MONOXIDE	0.3765D	1	
WATER	0.2293D	1	
CARBON DIOXIDE	0.0000D	0	
HYDROGEN	-0.2605D	0	
METHANOL	0.1848D	-1	
GUAIACYL ACROLEIN	0.3708D	1	
SINAPYL ACROLEIN	0.2636D	0	
HYDROXYPHENYL ACROLEIN	0.3443D	1	
SINAPYL ALDEHYDE	0.4594D	-2	
COUMARALDEHYDE	0.5999D	-1	
PYROGALLOL	0.1353D	-2	
3,4-DIHYDROXYPHENYLACROLEIN	0.5608D	1	
SINGLE RINGS, MULTIPLE RINGS, AND SINGLES+			
LIGHTS ON MOL FRACTION BASIS			
SINGLE RING AROMATICS	0.4255D	0	
MULTIPLE RING AROMATICS	0.6126D	0	
SINGLE RINGS AND LIGHTS	0.9980D	1	

TIME	INTERVAL	TEMP(C)	
0.2005D	1	0.5000D -2	600.0
0.2005D	1	0.5000D -2	600.0
PRODUCT	YIELD(WTZ)		
PHENOL			0.1096D 0
CRESOLS			0.8837D 0
ETHYLPHENOL			0.6578D 0
PROPYLPHENOL			0.4940D -1
GUAIACOL			0.3658D -1
METHYLGUAIACOL			0.2858D 0
ETHYLGUAIACOL			0.2074D 0
PROPYLGUAIACOL			0.1526D -1
EUGENOL			0.1508D -1
VINYLGUAIACOL			0.3062D 0
CONIFERALDEHYDE			0.2020D -1
PROPIOVANILLONE			0.0000D 0
CATECHOL			0.2192D 0
METHYLCATECHOL			0.1734D 1
ETHYLCATECHOL			0.1272D 1
3,4-DIHYDROXYCINNAMALDEHYDE			0.1257D 0
VINYLCATECHOL			0.1903D 1
ALLYLCATECHOL			0.9313D -1
SYRINGOL			0.3283D -2
METHYLSYRINGOL			0.2514D -1
ETHYLSYRINGOL			0.1795D -1
PROPYLSYRINGOL			0.1302D -2
VINYLSYRINGOL			0.2656D -1
ALLYLSYRINGOL			0.1289D -2
SYRINGALDEHYDE			0.0000D 0
PROPIOSYRINGONE			0.0000D 0
METHOXYCATECHOL			0.4524D -2
METHANE			0.5223D 1
CARBON MONOXIDE			0.5611D 1
WATER			0.3388D 1
CARBON DIOXIDE			0.0000D 0
HYDROGEN			-0.3170D 0
METHANOL			0.4247D -1
GUAIACYL ACROLEIN			0.1905D 1
SINAPYL ACROLEIN			0.1609D 0
HYDROXYPHENYL ACROLEIN			0.6258D 1
SINAPYL ALDEHYDE			0.1706D -2
COUMARALDEHYDE			0.6637D -1
PYROGALLOL			0.8037D -2
3,4-DIHYDROXYPHENYLACROLEIN			0.1185D 2
SINGLE RINGS, MULTIPLE RINGS, AND SINGLES+			
LIGHTS ON MOL FRACTION BASIS			
SINGLE RING AROMATICS			0.6166D 0
MULTIPLE RING AROMATICS			0.4730D 0
SINGLE RINGS AND LIGHTS			0.1456D 2

TIME	INTERVAL	TEMP(C)		
0.3005D	1	0.5000D -2	600.0	
0.3005D	1	0.5000D -2	600.0	
PRODUCT			YIELD(WTZ)	
PHENOL			0.1831D	0
CRESOLS			0.1477D	1
ETHYLPHENOL			0.1100D	1
PROPYLPHENOL			0.7847D	-1
GUAIACOL			0.1933D	-1
METHYLGUAIACOL			0.1510D	0
ETHYLGUAIACOL			0.1096D	0
PROPYLGUAIACOL			0.7663D	-2
EUGENOL			0.7571D	-2
VINYLGUAIACOL			0.1014D	0
CONIFERALDEHYDE			0.4999D	-2
PROPIOVANILLONE			0.0000D	0
CATECHOL			0.3877D	0
METHYLCATECHOL			0.3067D	1
ETHYLCATECHOL			0.2250D	1
3,4-DIHYDROXYCINNAMALDEHYDE			0.1041D	0
VINYLCATECHOL			0.2110D	1
ALLYLCATECHOL			0.1566D	0
SYRINGOL			0.1876D	-2
METHYLSYRINGOL			0.1436D	-1
ETHYLSYRINGOL			0.1026D	-1
PROPYLSYRINGOL			0.7070D	-3
VINYLSYRINGOL			0.9508D	-2
ALLYLSYRINGOL			0.6998D	-3
SYRINGALDEHYDE			0.0000D	0
PROPIOSYRINGONE			0.0000D	0
METHOXYCATECHOL			0.3826D	-2
METHANE			0.5771D	1
CARBON MONOXIDE			0.6778D	1
WATER			0.3921D	1
CARBON DIOXIDE			0.0000D	0
HYDROGEN			-0.3103D	0
METHANOL			0.6209D	-1
GUAIACYL ACROLEIN			0.7124D	0
SINAPYL ACROLEIN			0.6505D	-1
HYDROXYPHENYL ACROLEIN			0.7404D	1
SINAPYL ALDEHYDE			0.4564D	-3
COUMARALDEHYDE			0.5195D	-1
PYROGALLOL			0.1812D	-1
3,4-DIHYDROXYPHENYLACROLEIN			0.1484D	2
SINGLE RINGS, MULTIPLE RINGS, AND SINGLES+				
LIGHTS ON MOL FRACTION BASIS				
SINGLE RING AROMATICS			0.7187D	0
MULTIPLE RING AROMATICS			0.4126D	0
SINGLE RINGS AND LIGHTS			0.1694D	2

TIME	INTERVAL	TEMP(C)		
0.4005D	1	0.5000D -2	600.0	
0.4005D	1	0.5000D -2	600.0	
PRODUCT	YIELD(WTZ)			
PHENOL			0.2492D	0
CRESOLS			0.2009D	1
ETHYLPHENOL			0.1496D	1
PROPYLPHENOL			0.9879D	-1
GUAIACOL			0.8417D	-2
METHYLGUAIACOL			0.6572D	-1
ETHYLGUAIACOL			0.4773D	-1
PROPYLGUAIACOL			0.3087D	-2
EUGENOL			0.3050D	-2
VINYLGUAIACOL			0.2956D	-1
CONIFERALDEHYDE			0.1092D	-2
PROPIOVANILLONE			0.0000D	0
CATECHOL			0.5414D	0
METHYLCATECHOL			0.4282D	1
ETHYLCATECHOL			0.3142D	1
3,4-DIHYDROXYCINNAMALDEHYDE			0.7292D	-1
VINYLCATECHOL			0.1972D	1
ALLYLCATECHOL			0.2023D	0
SYRINGOL			0.8504D	-3
METHYLSYRINGOL			0.6509D	-2
ETHYLSYRINGOL			0.4650D	-2
PROPYLSYRINGOL			0.2966D	-3
VINYLSYRINGOL			0.2885D	-2
ALLYLSYRINGOL			0.2935D	-3
SYRINGALDEHYDE			0.0000D	0
PROPIOSYRINGONE			0.0000D	0
METHOXYCATECHOL			0.2290D	-2
METHANE			0.5968D	1
CARBON MONOXIDE			0.7580D	1
WATER			0.4184D	1
CARBON DIOXIDE			0.0000D	0
HYDROGEN			-0.2906D	0
METHANOL			0.7596D	-1
GUAIACYL ACRYLALDEHYDE			0.2344D	0
SINAPYL ACRYLALDEHYDE			0.2228D	-1
HYDROXYPHENYL ACRYLALDEHYDE			0.7612D	1
SINAPYL ALDEHYDE			0.1038D	-3
COUMARALDEHYDE			0.3545D	-1
PYROGALLOL			0.2809D	-1
3,4-DIHYDROXYPHENYLACRYLALDEHYDE			0.1566D	2
SINGLE RINGS, MULTIPLE RINGS, AND SINGLES+ LIGHTS ON MOL FRACTION BASIS				
SINGLE RING AROMATICS			0.7697D	0
MULTIPLE RING AROMATICS			0.3907D	0
SINGLE RINGS AND LIGHTS			0.1829D	2

TIME	INTERVAL	TEMP(C)	
0.5005D	1	0.5000D -2	600.0
0.5005D	1	0.5000D -2	600.0
PRODUCT	YIELD(WT%)		
PHENOL	0.3051D		0
CRESOLS	0.2460D		1
ETHYLPHENOL	0.1831D		1
PROPYLPHENOL	0.1118D		0
GUAIACOL	0.3261D		-2
METHYLGUAIACOL	0.2547D		-1
ETHYLGUAIACOL	0.1848D		-1
PROPYLGUAIACOL	0.1105D		-2
EUGENOL	0.1092D		-2
VINYLGUAIACOL	0.8022D		-2
CONIFERALDEHYDE	0.2204D		-3
PROPIOVANILLONE	0.0000D		0
CATECHOL	0.6705D		0
METHYLCATECHOL	0.5305D		1
ETHYLCATECHOL	0.3890D		1
3,4-DIHYDROXYCINNAMALDEHYDE	0.4706D		-1
VINYLCATECHOL	0.1711D		1
ALLYLCATECHOL	0.2315D		0
SYRINGOL	0.3365D		-3
METHYLSYRINGOL	0.2577D		-2
ETHYLSYRINGOL	0.1839D		-2
PROPYLSYRINGOL	0.1085D		-3
VINYLSYRINGOL	0.8000D		-3
ALLYLSYRINGOL	0.1074D		-3
SYRINGALDEHYDE	0.0000D		0
PROPIOSYRINGONE	0.0000D		0
METHOXYCATECHOL	0.1125D		-2
METHANE	0.6037D		1
CARBON MONOXIDE	0.8178D		1
WATER	0.4320D		1
CARBON DIOXIDE	0.0000D		0
HYDROGEN	-0.2729D		0
METHANOL	0.8504D		-1
GUAIACYL ACROLEIN	0.7220D		-1
SINAPYL ACROLEIN	0.7011D		-2
HYDROXYPHENYL ACROLEIN	0.7409D		1
SINAPYL ALDEHYDE	0.2140D		-4
COUMARALDEHYDE	0.2261D		-1
PYROGALLOL	0.3642D		-1
3,4-DIHYDROXYPHENYLACROLEIN	0.1542D		2
SINGLE RINGS, MULTIPLE RINGS, AND SINGLES+			
LIGHTS ON MOL FRACTION BASIS			
SINGLE RING AROMATICS	0.7948D		0
MULTIPLE RING AROMATICS	0.3846D		0
SINGLE RINGS AND LIGHTS	0.1914D		2

TIME	INTERVAL	TEMP(C)	
0.6005D	1	0.5000D -2	600.0
0.6005D	1	0.5000D -2	600.0
PRODUCT	YIELD(WTZ)		
PHENOL			0.3511D 0
CRESOLS			0.2834D 1
ETHYLPHENOL			0.2107D 1
PROPYLPHENOL			0.1197D 0
GUAIACOL			0.1171D -2
METHYLGUAIACOL			0.9155D -2
ETHYLGUAIACOL			0.6636D -2
PROPYLGUAIACOL			0.3694D -3
EUGENOL			0.3649D -3
VINYLGUAIACOL			0.2107D -2
CONIFERALDEHYDE			0.4216D -4
PROPIOVANILLONE			0.0000D 0
CATECHOL			0.7761D 0
METHYLCATECHOL			0.6146D 1
ETHYLCATECHOL			0.4501D 1
3,4-DIHYDROXYCINNAMALDEHYDE			0.2902D -1
VINYLCATECHOL			0.1448D 1
ALLYLCATECHOL			0.2494D 0
SYRINGOL			0.1221D -3
METHYLSYRINGOL			0.9356D -3
ETHYLSYRINGOL			0.6671D -3
PROPYLSYRINGOL			0.3661D -4
VINYLSYRINGOL			0.2123D -3
ALLYLSYRINGOL			0.3624D -4
SYRINGALDEHYDE			0.0000D 0
PROPIOSYRINGONE			0.0000D 0
METHOXYCATECHOL			0.4867D -3
METHANE			0.6062D 1
CARBON MONOXIDE			0.8652D 1
WATER			0.4394D 1
CARBON DIOXIDE			0.0000D 0
HYDROGEN			-0.2603D 0
METHANOL			0.9072D -1
GUAIACYL ACRROLEIN			0.2140D -1
SINAPYL ACRROLEIN			0.2099D -2
HYDROXYPHENYL ACRROLEIN			0.7038D 1
SINAPYL ALDEHYDE			0.4136D -5
COUMARALDEHYDE			0.1387D -1
PYROGALLOL			0.4299D -1
3,4-DIHYDROXYPHENYLACROLEIN			0.1473D 2
SINGLE RINGS, MULTIPLE RINGS, AND SINGLES+			
LIGHTS ON MOL FRACTION BASIS			
SINGLE RING AROMATICS			0.8066D 0
MULTIPLE RING AROMATICS			0.3839D 0
SINGLE RINGS AND LIGHTS			0.1974D 2

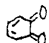
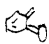
TIME	INTERVAL	TEMP(C)		
0.7005D	1	0.5000D -2	600.0	
0.7005D	1	0.3000D -2	600.0	
PRODUCT			YIELD(WTZ)	
PHENOL			0.3893D	0
CRESOLS			0.3146D	1
ETHYLPHENOL			0.2336D	1
PROPYLPHENOL			0.1244D	0
GUAIACOL			0.3996D	-3
METHYLGUAIACOL			0.3127D	-2
ETHYLGUAIACOL			0.2264D	-2
PROPYLGUAIACOL			0.1181D	-3
EUGENOL			0.1167D	-3
VINYLGUAIACOL			0.5484D	-3
CONIFERALDEHYDE			0.7756D	-5
PROPIOVANILLONE			0.0000D	0
CATECHOL			0.8630D	0
METHYLCATECHOL			0.6841D	1
ETHYLCATECHOL			0.5005D	1
3,4-DIHYDROXYCINNAMALDEHYDE			0.1740D	-1
VINYLCATECHOL			0.1228D	1
ALLYLCATECHOL			0.2599D	0
SYRINGOL			0.4182D	-4
METHYLSYRINGOL			0.3208D	-3
ETHYLSYRINGOL			0.2285D	-3
PROPYLSYRINGOL			0.1175D	-4
VINYLSYRINGOL			0.5546D	-4
ALLYLSYRINGOL			0.1163D	-4
SYRINGALDEHYDE			0.0000D	0
PROPIOSYRINGONE			0.0000D	0
METHOXYCATECHOL			0.1935D	-3
METHANE			0.6070D	1
CARBON MONOXIDE			0.9052D	1
WATER			0.4438D	1
CARBON DIOXIDE			0.0000D	0
HYDROGEN			-0.2520D	0
METHANOL			0.9416D	-1
GUAIACYL ACRYLEIN			0.6187D	-2
SINAPYL ACRYLEIN			0.6093D	-3
HYDROXYPHENYL ACRYLEIN			0.6612D	1
SINAPYL ALDEHYDE			0.7638D	-6
COUMARALDEHYDE			0.8289D	-2
PYROGALLOL			0.4820D	-1
3,4-DIHYDROXYPHENYLACRYLEIN			0.1368D	2
SINGLE RINGS, MULTIPLE RINGS, AND SINGLES+				
LIGHTS ON MOL FRACTION BASIS				
SINGLE RING AROMATICS			0.8123D	0
MULTIPLE RING AROMATICS			0.3845D	0
SINGLE RINGS AND LIGHTS			0.2021D	2

## NOMENCLATURE, SYMBOLS USED:

A, AN	Anisole
AB	Allylbenzene
AP	Acetophenone
BA	Benzaldehyde
BB, DPE	Bibenzyl, Diphenylethane
BP	Biphenyl
BPE	Benzyl Phenyl Ether
BPhOH	Biphenol
CA	Cinnamic Acid
CAD	Cinnamaldehyde
CAL	Cinnamyl Alcohol
CAT, C	Catechol
CR	Cresols
DHB	Dihydroxybenzaldehyde
DIM	Dimers
DMP, 2,6-DMP	2,6-Dimethoxyphenol
DPM	Diphenylmethane
EB	Ethylbenzene
FA	Ferulic Acid
GUA, G	Guaiacol
I, ISO	Isoeugenol
MC	Methoxycatechol
MeOH	Methanol
N	Napthalene
1-NA	1-Napthoic Acid
2-NA	2- Napthoic Acid
oCr, oC, oCR, OC	ortho-cresol
OHD	orthohydroxydiphenylmethane
OHPE	orthohydroxyphenylether
PC	propenylcatechol
PE	phenyl ether
PHD	parahydroxydiphenylmethane
PhH, B, Be	Benzene



## NOMENCLATURE(cont.)

PhOH, Ph, P	Phenol
PP	propenylphenol
PP, PhPhOH	phenylphenol
PPE, E	Phenethyl Phenyl Ether
PT	phenyltoluene
Q , 	o-diquinone
QM, 	quinonemethide
S	mol tetralin/ mol PPE
SAL	Saligenol
SESQ, TRI	Sesquimers, triaromatics
St, ST	Styrene
Tet, T	Tetralin
Tol, TOL, TO	Toluene
⊖	0.004576xT , T in K
VA, VAN	Vanillin
VE	Veratrole
VG	Vinylguaiacol
xy1	xylene
-OMe, -O'	-OCH <sub>3</sub>